

**Ongoing Face Recognition
Vendor Test (FRVT)**
Part 1: Verification

Patrick Grother
Mei Ngan
Kayee Hanaoka
*Information Access Division
Information Technology Laboratory*

This publication is available free of charge from:
<https://www.nist.gov/programs-projects/face-recognition-vendor-test-frvt-ongoing>

2020/09/08

ACKNOWLEDGMENTS

The authors are grateful to staff in the NIST Biometrics Research Laboratory for infrastructure supporting rapid evaluation of algorithms.

DISCLAIMER

Specific hardware and software products identified in this report were used in order to perform the evaluations described in this document. In no case does identification of any commercial product, trade name, or vendor, imply recommendation or endorsement by the National Institute of Standards and Technology, nor does it imply that the products and equipment identified are necessarily the best available for the purpose.

INSTITUTIONAL REVIEW BOARD

The National Institute of Standards and Technology's Research Protections Office reviewed the protocol for this project and determined it is not human subjects research as defined in Department of Commerce Regulations, 15 CFR 27, also known as the Common Rule for the Protection of Human Subjects (45 CFR 46, Subpart A).

FRVT STATUS

This report is a draft NIST Interagency Report, and is open for comment. It is the nineteenth edition of the report since the first was published in June 2017. Prior editions of this report are maintained on the FRVT [website](#), and may contain useful information about older algorithms and datasets no longer used in FRVT.

FRVT remains open: All [four tracks](#) of the FRVT are open to new algorithm submissions.

Changes since July 27, 2020:

- ▷ We have introduced per-algorithm report sheets. These are HTML documents linked from the accuracy tables in this report (i.e. Table 16) and on the FRVT 1:1 [homepage](#). The sheets contain interactive graphics allowing, for example, mouseover exploration of FNMR(T) and FMR(T). Some of their content had previously appeared in this document.
- ▷ This report adds results for algorithms from six new developers. ACI Software, Bresee Technology, Fiberhome Telecommunication Technologies, Imageware Systems, Oz Forensics, and Pensees.
- ▷ The report includes results for thirteen developers who have previously submitted algorithms: Canon Information Technology (Beijing), Cyberlink, Dahua Technology, Gorilla Technology, ID3 Technology, Intel Research Group, iQIYI Inc, Momentum Digital, Netbridge Technology, Tech5 SA, Shenzhen AiMall Tech, Vigilant Solutions, and VisionLabs.
- ▷ We have retired results for nine algorithms per our policy to only list results for two algorithms per developer. Results for retired algorithms appear in prior versions of this report in the [archive](#).

Changes since May 18, 2020:

- ▷ The report is the first FRVT update since the pandemic closed it from March to June 2020.
- ▷ This report includes results for algorithms from nine new developers: GeoVision Inc, Su Zhou NaZhi-TianDi Intelligent Technology, YooniK, AYF Technology, PXL Vision AG, Yuan High-Tech Development, Beihang University-ERCACAT, ICM Airport Technics, and Staqu Technologies
- ▷ This report includes results for algorithms from 15 returning developers Acer Incorporated, Antheus Technologia, Chosun University, Chunghwa Telecom, Idemia, Moontime Smart Technology, Neurotechnology, Guangzhou Pixel Solutions, Panasonic R+D Center Singapore, Rank One Computing, Scanovate, Shanghai Universiy - Shanghai Film Academy, Synesis, Trueface.ai, and Veridas Digital Authentication Solutions
- ▷ We have retired results for ten algorithms per our policy to only list results for two algorithms per developer. Results for retired algorithms appear in prior versions of this report in the [archive](#).
- ▷ We separated timing and other resource consumption from the main participation table. The new Table 10 includes template generation durations for four kinds of images, not just mugshots.
- ▷ We have published a separate report, [NIST Interagency Report 8311](#) on accuracy of pre-pandemic algorithms on subjects wearing face masks. We plan to track improvements in accuracy on masked images going forward. In particular, we invite submission of algorithms that can detect whether a person is wearing a mask, extract features from the full face or the exposed periocular region, and do appropriate comparison. We do not intend to evaluate algorithms that assume 100% of images will be of masked individuals.

Changes since March 25, 2020:

- ▷ The report is a maintenance release - it does not add any new algorithms, and FRVT has been closed to new algorithms since mid March 2020.
- ▷ We modified the primary accuracy summary, Table 16, as follows:
 - ▷ For visa images, the column for FNMR at FMR = 0.0001 has been removed. The visa images are so highly controlled that the error rates for the most accurate algorithms are dominated by false rejection of very young children and by the presence of a few noisy greyscale images. For now, two visa columns remain: FNMR at FMR= 10^{-6} and, for matched covariates, FNMR at FMR= 10^{-4} .
 - ▷ We have inserted a new column labelled “BORDER” giving accuracy for comparison of moderately poor webcam border-crossing photos that exhibit pose variations, poor compression, and low contrast due to strong background illumination. The accuracies are the worst from all cooperative image datasets used in FRVT.
- ▷ Accordingly, we updated the failure-to-template rates in Table 21.
- ▷ We withdrew a figure showing how false matches are concentrated in certain visa images used in cross-comparison, because it didn't attempt to include demographic information.

Changes since February 27, 2020:

- ▷ The report adds results algorithms from two new developers: Beijing Alleyes Technology, and the Chinese University of Hong Kong. Results for newly submitted algorithms from two other developers will appear in the next report.
- ▷ The report adds results for algorithms from thirteen returning developers: ASUSTek Computer, Aware, Cyberlink Corp, Gorilla Technology, Innovative Technology, Kakao Enterprise, Lomonosov Moscow State University, Panasonic R+D Center Singapore, Shenzhen AiMall Technology, Shenzhen Intellifusion Technologies, Synology, Tech5 SA, and Via Technologies.
- ▷ Per policy to only list results for two algorithms per developer, we have dropped results for algorithms from Aware, Cyberlink, Gorilla Technology, Kakao Enterprise, Lomonosov Moscow State University, Panasonic R+D Center Singapore, and Tech5 SA.

Changes since January 20, 2020:

- ▷ The report adds results for five new developers: Ability Enterprise (Andro Video), Chosun University, Fujitsu Research and Development Center, University of Coimbra, and Xforward AI Technology.
- ▷ The report adds results for algorithms from six returning developers: AlphaSSTG, Incode Technologies, Kneron, Shanghai Jiao Tong University, Vocord, and X-Laboratory.
- ▷ We have corrected template comparison timing numbers for algorithms submitted September 2019 to January 2020. The values reported previously were slower due to a software bug.
- ▷ We have dropped results for algorithms from Vocord and Incode per policy to only list results for two algorithms per developer.
- ▷ The [FRVT 1:1 homepage](#) has been updated with latest accuracy results.
- ▷ The [FRVT 1:N homepage](#) now includes an update to the September 2019 NIST Interagency Report 8271. The new report adds results for one-to-many search algorithms submitted to NIST from June 2019 to January 2020.

Changes since January 6, 2020:

- ▷ Section 2 has been updated to better describe the Visa and Border images. The caption for Table 16 has been updated to better relate the accuracy values to particular image comparisons.
- ▷ The report adds results for five new developers: Acer, Advance.AI, Expasoft, Netbridge Technology, and Videmo Intelligent Videoanalyse.
- ▷ The report adds results for algorithms from 7 returning developers: China Electronics Import-Export Corp, Intel Research Group, ITMO University, Neurotechnology, N-Tech Lab, Rokid, and VisionLabs.
- ▷ We have dropped results from this edition of the report per policy to only list results for two algorithms per developer: N-Tech Lab, Neurotechnology, ITMO, Visionlabs, and CEIEC.
- ▷ The [FRVT homepage](#) has been updated with latest accuracy results.

Changes since November 11, 2019:

- ▷ Table 10 has been updated to include runtime memory usage. This is the first time such a quantity has been reported. The value is the peak size of the resident set size logged during enrollment of single images.
- ▷ We have migrated summary results table to a new platform that supports sortable tables:
<https://pages.nist.gov/frvt/html/frvt11.html>
- ▷ The report adds results for four new developers: Antheus Technologia, BioID Technologies SA, Canon Information Tech. (Beijing), Samsung S1 (listed in the tables as S1), and Taiwan AI Labs.
- ▷ The report adds results for algorithms from 13 returning developers: Anke Investments, Chunghwa Telecom, Deepglint, Institute of Information Technologies, iQIYI, Kneron, Ping An Technology, Paravision, KanKan Ai, Rokid Corporation, Shanghai Universiy - Shanghai Film Academy, Veridas Digital Authentication Solutions, and Videometrics Technology.
- ▷ We have dropped results from this edition of the report per policy to only list results for two algorithms per developer: remarkai-000, veridas-001, sensetime-001, iit-000, anke-003, and everai-002. Results for these are available in prior editions of this report linked from the FRVT page.
- ▷ We issued [NIST Interagency Report 8280: FRVT Part 3: Demographics](#) on 2019-12-19. It includes results for many of the algorithms covered by this report.

Changes since October 16, 2019:

- ▷ The report adds results for ten new developers: Ai-Union Technology, ASUSTek Computer, DiDi ChuXing Technology, Innovative Technology, Luxand, MVision, Pyramid Cyber Security + Forensic, Scanovate, Shenzhen AiMall Tech, and TUPU Technology.
- ▷ The report adds results for 12 returning developers: CTBC Bank Glory Gorilla Technology Guangzhou Pixel Solutions Imagus Technology Incode Technologies Lomonosov Moscow State University Rank One Computing Samtech InfoNet Shanghai Ulucu Electronics Technology Synesis, and Winsense.
- ▷ We have dropped results from this edition of the report per policy to only list results for two algorithms per developer: glory-000, gorilla-002, incode-003, rankone-006, and synesis-004.
- ▷ Results for five recently submitted algorithms will appear in the next report.

Changes since September 11, 2019:

- ▷ The report adds results for five new participants: Awidit Systems (Awiros), Momenmtum Digital (Sertis), Trueface AI, Shanghai Jiao Tong University, and X-Laboratory.

- ▷ The report adds results for five new algorithms from returning developers: Cyberlink, Hengrui AI Technology, Idemia, Panasonic R+D Singapore, and Tevian. This causes three algorithm, to be de-listed from the report per policy to list results for two algorithms per developer.

Changes since July 31 2019:

- ▷ The HTML table on the [FRVT 1:1 homepage](#) has been updated to include a column for cross-domain Visa-Border verification. Results for this new dataset appeared in the July 29 report under the name "CrossEV" - these are now renamed "Visa-Border".
- ▷ The [FRVT 1:1 homepage](#) lists algorithms according to lowest mean rank accuracy:

$$\begin{aligned} &\text{Rank(FNMR}_{\text{VISA}} \text{ at FMR = 0.000001}) + \\ &\text{Rank(FNMR}_{\text{VISA-BORDER}} \text{ at FMR = 0.000001}) + \\ &\text{Rank(FNMR}_{\text{MUGSHOT}} \text{ at FMR = 0.00001 after 14 years}) + \\ &\text{Rank(FNMR}_{\text{WILD}} \text{ at FMR = 0.00001}) \end{aligned}$$

This ordering rewards high accuracy across all datasets.
- ▷ The main results in Table 16 is now in landscape format to accomodate extra columns for the Visa-Border set, and mugshot comparisons after at least 12 years.
- ▷ The report adds results for nine new participants: Alpha SSTG, Intel Research, ULSee, Chungwa Telecon, iSAP Solution, Rokid, Shenzhen EI Networks, CSA Intellicloud, Shenzhen Intellifusion Technologies.
- ▷ The reports adds results for six new algorithms from returning developers: Innovatrics, Dahua Technology, Tech5 SA, Intellivision, Nodeflux and Imperial College, London. One algorithm, from Imperial has been retired, per policy to list results for two algorithms per developer.
- ▷ The cross-country false match rate heatmaps have been replotted to reveal more structure by listing countries by region instead of alphabetically.
- ▷ The next version of this report will be posted around October 18, 2019.

Changes since July 3 2019:

- ▷ The HTML table on the [FRVT 1:1 homepage](#) has been updated to list the 20 most accurate developers rather than algorithms, choosing the most accurate algorithm from each developer based on visa and mugshot results. Also, the algorithms are ordered in terms of lowest mean rank across mugshot, visa and wild datasets, rewarding broad accuracy over a good result on one particular dataset.
- ▷ This report includes results for a new dataset - see the column labelled "visa-border" in Table 5. It compares a new set of high quality visa-like portraits with a set webcam border-crossing photos that exhibit moderately poor pose variations and background illumination. The two new sets are described in sections 2.3 and 2.4. The comparisons are "cross-domain" in that the algorithm must compare "visa" and "wild" images. Results for other algorithms will be added in future reports as they become available.
- ▷ This report adds results for algorithms from 9 developers submitted in early July 2019. These are from 3DiVi, Camvi, EverAI-Paravision, Facesoft, Farbar (F8), Institute of Information Technologies, Shanghai U. Film Academy, Via Technologies, and Ulucu Electronics Tech. Six of these are new participants.
- ▷ Several other algorithms have been submitted and are being evaluated. Results will be released in the next report, scheduled for September 5. That report will include results for new datasets.
- ▷ Older algorithms from Everai, Camvi and 3DiVi, have been retired, per the policy to list only two algorithms per developer.

Changes since June 20 2019:

- ▷ This report adds results for algorithms from 18 developers submitted in early June 2019. These are from CTBC Bank, Deep Glint, Thales Cogent, Ever AI Paravision, Gorilla Technology, Imagus, Incode, Kneron, N-Tech Lab, Neurotechnology, Notiontag Technologies, Star Hybrid, Videonetics, Vigilant Solutions, Winsense, Anke Investments, CEIEC, and DSK. Nine of these are new participants.

- ▷ Several other algorithms have been submitted and are being evaluated. Results will be released in the next report, scheduled for August 1.
- ▷ Older algorithms from Everai, Thales Cogent, Gorilla Technology, Incode, Neurotechnology, N-Tech Lab and Vigilant Solutions have been retired, per the policy to list only two algorithms per developer.

Changes since April 2019:

- ▷ This report adds results for nine algorithms from nine developers submitted in early June 2019. These are from Tencent Deepsea, Hengrui, Kedacom, Moontime, Guangzhou Pixel, Rank One Computing, Synesis, Sensetime and Vocord.
- ▷ Another 23 algorithms have been submitted and are being evaluated. Results will be released in the next report, scheduled for July 3.
- ▷ Older algorithms for Rank One, Synesis, and Vocord have been retired, per the policy to list only two algorithms per developer.

Changes since February 2019:

- ▷ This report adds results for 49 algorithms from 42 developers submitted in early March 2019.
- ▷ This report omits results for algorithms that we retired. We retired for three reasons: 1. The developer submitted a new algorithm, and we only list two. 2. The algorithm needs a GPU, and we no longer allow GPU-based algorithms. 3. Inoperable algorithms.
- ▷ Previous results for retired algorithms are available in older editions of this report linked [here](#).
- ▷ The mugshot database used from February 2017 to January 2019 has been replaced with an extract of the mugshot database documented in NIST Interagency Report 8238, November 2018. The new mugshot set is described in section [2.5](#) and is adopted because:
 - ▷▷ It has much better identity label integrity, so that false non-match rates are substantially lower than those reported in FRVT 1:1 reports to date - see Figure [49](#).
 - ▷▷ It includes images collected over a 17 year period such that ageing can be much better characterized - - see Figure [181](#).
- ▷ Using the new mugshot database, Figure [181](#) shows accuracy for four demographic groups identified in the biographic metadata that accompanies the data: black females, black males, white females and white males.
- ▷ The report adds Figure [13](#) with results for the twenty human-difficult pairs used in the May 2018 paper *Face recognition accuracy of forensic examiners, superrecognizers, and face recognition algorithms* by Phillips et al. [[1](#)].
- ▷ The report uses an update to the wild image database that corrects some ground truth labels.
- ▷ Some results for the child exploitation database are not complete. They are typically updated less frequently than for other image sets.

Contents

| | |
|--|-----------|
| ACKNOWLEDGMENTS | 1 |
| DISCLAIMER | 1 |
| INSTITUTIONAL REVIEW BOARD | 1 |
| 1 METRICS | 30 |
| 1.1 CORE ACCURACY | 30 |
| 2 DATASETS | 31 |
| 2.1 CHILD EXPLOITATION IMAGES | 31 |
| 2.2 VISA IMAGES | 31 |
| 2.3 APPLICATION IMAGES | 31 |
| 2.4 BORDER CROSSING IMAGES | 32 |
| 2.5 MUGSHOT IMAGES | 32 |
| 2.6 WILD IMAGES | 32 |
| 3 RESULTS | 33 |
| 3.1 TEST GOALS | 33 |
| 3.2 TEST DESIGN | 33 |
| 3.3 FAILURE TO ENROLL | 36 |
| 3.4 RECOGNITION ACCURACY | 41 |
| 3.5 GENUINE DISTRIBUTION STABILITY | 186 |
| 3.5.1 EFFECT OF BIRTH PLACE ON THE GENUINE DISTRIBUTION | 186 |
| 3.5.2 EFFECT OF AGEING | 207 |
| 3.5.3 EFFECT OF AGE ON GENUINE SUBJECTS | 222 |
| 3.6 IMPOSTOR DISTRIBUTION STABILITY | 244 |
| 3.6.1 EFFECT OF BIRTH PLACE ON THE IMPOSTOR DISTRIBUTION | 244 |
| 3.6.2 EFFECT OF AGE ON IMPOSTORS | 248 |

List of Tables

| | |
|-------------------------------------|----|
| 1 PARTICIPANT INFORMATION | 12 |
| 2 PARTICIPANT INFORMATION | 13 |
| 3 PARTICIPANT INFORMATION | 14 |
| 4 PARTICIPANT INFORMATION | 15 |
| 5 ALGORITHM SUMMARY | 16 |
| 6 ALGORITHM SUMMARY | 17 |
| 7 ALGORITHM SUMMARY | 18 |
| 8 ALGORITHM SUMMARY | 19 |
| 9 ALGORITHM SUMMARY | 20 |
| 10 ALGORITHM SUMMARY | 21 |
| 11 FALSE NON-MATCH RATE | 22 |
| 12 FALSE NON-MATCH RATE | 23 |
| 13 FALSE NON-MATCH RATE | 24 |
| 14 FALSE NON-MATCH RATE | 25 |
| 15 FALSE NON-MATCH RATE | 26 |
| 16 FALSE NON-MATCH RATE | 27 |
| 17 FAILURE TO ENROL RATES | 36 |
| 18 FAILURE TO ENROL RATES | 37 |
| 19 FAILURE TO ENROL RATES | 38 |
| 20 FAILURE TO ENROL RATES | 39 |

| | |
|-------------------------------------|----|
| 21 FAILURE TO ENROL RATES | 40 |
|-------------------------------------|----|

List of Figures

| | |
|--|----|
| 1 PERFORMANCE SUMMARY: FNMR VS. TEMPLATE SIZE TRADEOFF | 28 |
| 2 PERFORMANCE SUMMARY: FNMR VS. TEMPLATE TIME TRADEOFF | 29 |
| 3 EXAMPLE IMAGES | 33 |
| (A) VISA | 33 |
| (B) MUGSHOT | 33 |
| (C) WILD | 33 |
| (D) BORDER | 33 |
| 4 PERFORMANCE ON 20 HUMAN-DIFFICULT PAIRS | 42 |
| 5 PERFORMANCE ON 20 HUMAN-DIFFICULT PAIRS | 43 |
| 6 PERFORMANCE ON 20 HUMAN-DIFFICULT PAIRS | 44 |
| 7 PERFORMANCE ON 20 HUMAN-DIFFICULT PAIRS | 45 |
| 8 PERFORMANCE ON 20 HUMAN-DIFFICULT PAIRS | 46 |
| 9 PERFORMANCE ON 20 HUMAN-DIFFICULT PAIRS | 47 |
| 10 PERFORMANCE ON 20 HUMAN-DIFFICULT PAIRS | 48 |
| 11 PERFORMANCE ON 20 HUMAN-DIFFICULT PAIRS | 49 |
| 12 PERFORMANCE ON 20 HUMAN-DIFFICULT PAIRS | 50 |
| 13 PERFORMANCE ON 20 HUMAN-DIFFICULT PAIRS | 51 |
| 14 ERROR TRADEOFF CHARACTERISTIC: VISA IMAGES | 52 |
| 15 ERROR TRADEOFF CHARACTERISTIC: VISA IMAGES | 53 |
| 16 ERROR TRADEOFF CHARACTERISTIC: VISA IMAGES | 54 |
| 17 ERROR TRADEOFF CHARACTERISTIC: VISA IMAGES | 55 |
| 18 ERROR TRADEOFF CHARACTERISTIC: VISA IMAGES | 56 |
| 19 ERROR TRADEOFF CHARACTERISTIC: VISA IMAGES | 57 |
| 20 ERROR TRADEOFF CHARACTERISTIC: VISA IMAGES | 58 |
| 21 ERROR TRADEOFF CHARACTERISTIC: VISA IMAGES | 59 |
| 22 ERROR TRADEOFF CHARACTERISTIC: VISA IMAGES | 60 |
| 23 ERROR TRADEOFF CHARACTERISTIC: VISA IMAGES | 61 |
| 24 ERROR TRADEOFF CHARACTERISTIC: VISA IMAGES | 62 |
| 25 ERROR TRADEOFF CHARACTERISTIC: VISA IMAGES | 63 |
| 26 ERROR TRADEOFF CHARACTERISTIC: VISA IMAGES | 64 |
| 27 ERROR TRADEOFF CHARACTERISTIC: VISA IMAGES | 65 |
| 28 ERROR TRADEOFF CHARACTERISTIC: VISA IMAGES | 66 |
| 29 ERROR TRADEOFF CHARACTERISTIC: VISA IMAGES | 67 |
| 30 ERROR TRADEOFF CHARACTERISTIC: VISA IMAGES | 68 |
| 31 ERROR TRADEOFF CHARACTERISTIC: VISA IMAGES | 69 |
| 32 ERROR TRADEOFF CHARACTERISTIC: VISA IMAGES | 70 |
| 33 ERROR TRADEOFF CHARACTERISTIC: VISA IMAGES | 71 |
| 34 ERROR TRADEOFF CHARACTERISTIC: VISA IMAGES | 72 |
| 35 ERROR TRADEOFF CHARACTERISTIC: VISA IMAGES | 73 |
| 36 ERROR TRADEOFF CHARACTERISTIC: VISA IMAGES | 74 |
| 37 ERROR TRADEOFF CHARACTERISTIC: VISA IMAGES | 75 |
| 38 ERROR TRADEOFF CHARACTERISTIC: MUGSHOT IMAGES | 76 |
| 39 ERROR TRADEOFF CHARACTERISTIC: MUGSHOT IMAGES | 77 |
| 40 ERROR TRADEOFF CHARACTERISTIC: MUGSHOT IMAGES | 78 |
| 41 ERROR TRADEOFF CHARACTERISTIC: MUGSHOT IMAGES | 79 |
| 42 ERROR TRADEOFF CHARACTERISTIC: MUGSHOT IMAGES | 80 |
| 43 ERROR TRADEOFF CHARACTERISTIC: MUGSHOT IMAGES | 81 |
| 44 ERROR TRADEOFF CHARACTERISTIC: MUGSHOT IMAGES | 82 |
| 45 ERROR TRADEOFF CHARACTERISTIC: MUGSHOT IMAGES | 83 |
| 46 ERROR TRADEOFF CHARACTERISTIC: MUGSHOT IMAGES | 84 |
| 47 ERROR TRADEOFF CHARACTERISTIC: MUGSHOT IMAGES | 85 |

| | | |
|-----|---|-----|
| 48 | ERROR TRADEOFF CHARACTERISTIC: MUGSHOT IMAGES | 86 |
| 49 | ERROR TRADEOFF CHARACTERISTIC: MUGSHOT IMAGES | 87 |
| 50 | ERROR TRADEOFF CHARACTERISTIC: WILD IMAGES | 88 |
| 51 | ERROR TRADEOFF CHARACTERISTIC: WILD IMAGES | 89 |
| 52 | ERROR TRADEOFF CHARACTERISTIC: WILD IMAGES | 90 |
| 53 | ERROR TRADEOFF CHARACTERISTIC: WILD IMAGES | 91 |
| 54 | ERROR TRADEOFF CHARACTERISTIC: WILD IMAGES | 92 |
| 55 | ERROR TRADEOFF CHARACTERISTIC: WILD IMAGES | 93 |
| 56 | ERROR TRADEOFF CHARACTERISTIC: WILD IMAGES | 94 |
| 57 | ERROR TRADEOFF CHARACTERISTIC: WILD IMAGES | 95 |
| 58 | ERROR TRADEOFF CHARACTERISTIC: WILD IMAGES | 96 |
| 59 | ERROR TRADEOFF CHARACTERISTIC: WILD IMAGES | 97 |
| 60 | ERROR TRADEOFF CHARACTERISTICS: CHILD EXPLOITATION IMAGES | 98 |
| 61 | ERROR TRADEOFF CHARACTERISTICS: CHILD EXPLOITATION IMAGES | 99 |
| 62 | ERROR TRADEOFF CHARACTERISTICS: CHILD EXPLOITATION IMAGES | 100 |
| 63 | ERROR TRADEOFF CHARACTERISTICS: CHILD EXPLOITATION IMAGES | 101 |
| 64 | CMC CHARACTERISTICS: CHILD EXPLOITATION IMAGES | 102 |
| 65 | CMC CHARACTERISTICS: CHILD EXPLOITATION IMAGES | 103 |
| 66 | CMC CHARACTERISTICS: CHILD EXPLOITATION IMAGES | 104 |
| 67 | CMC CHARACTERISTICS: CHILD EXPLOITATION IMAGES | 105 |
| 68 | CMC CHARACTERISTICS: CHILD EXPLOITATION IMAGES | 106 |
| 69 | FALSE MATCH RATES WITHIN AND ACROSS DEMOGRAPHIC GROUPS | 107 |
| 70 | FALSE MATCH RATES WITHIN AND ACROSS DEMOGRAPHIC GROUPS | 108 |
| 71 | FALSE MATCH RATES WITHIN AND ACROSS DEMOGRAPHIC GROUPS | 109 |
| 72 | FALSE MATCH RATES WITHIN AND ACROSS DEMOGRAPHIC GROUPS | 110 |
| 73 | FALSE MATCH RATES WITHIN AND ACROSS DEMOGRAPHIC GROUPS | 111 |
| 74 | FALSE MATCH RATES WITHIN AND ACROSS DEMOGRAPHIC GROUPS | 112 |
| 75 | FALSE MATCH RATES WITHIN AND ACROSS DEMOGRAPHIC GROUPS | 113 |
| 76 | FALSE MATCH RATES WITHIN AND ACROSS DEMOGRAPHIC GROUPS | 114 |
| 77 | FALSE MATCH RATES WITHIN AND ACROSS DEMOGRAPHIC GROUPS | 115 |
| 78 | FALSE MATCH RATES WITHIN AND ACROSS DEMOGRAPHIC GROUPS | 116 |
| 79 | FALSE MATCH RATES WITHIN AND ACROSS DEMOGRAPHIC GROUPS | 117 |
| 80 | FALSE MATCH RATES WITHIN AND ACROSS DEMOGRAPHIC GROUPS | 118 |
| 81 | SEX AND RACE EFFECTS: MUGSHOT IMAGES | 119 |
| 82 | SEX AND RACE EFFECTS: MUGSHOT IMAGES | 120 |
| 83 | SEX AND RACE EFFECTS: MUGSHOT IMAGES | 121 |
| 84 | SEX AND RACE EFFECTS: MUGSHOT IMAGES | 122 |
| 85 | SEX AND RACE EFFECTS: MUGSHOT IMAGES | 123 |
| 86 | SEX AND RACE EFFECTS: MUGSHOT IMAGES | 124 |
| 87 | SEX AND RACE EFFECTS: MUGSHOT IMAGES | 125 |
| 88 | SEX AND RACE EFFECTS: MUGSHOT IMAGES | 126 |
| 89 | SEX AND RACE EFFECTS: MUGSHOT IMAGES | 127 |
| 90 | SEX AND RACE EFFECTS: MUGSHOT IMAGES | 128 |
| 91 | SEX AND RACE EFFECTS: MUGSHOT IMAGES | 129 |
| 92 | SEX AND RACE EFFECTS: MUGSHOT IMAGES | 130 |
| 93 | SEX EFFECTS: VISA IMAGES | 131 |
| 94 | SEX EFFECTS: VISA IMAGES | 132 |
| 95 | SEX EFFECTS: VISA IMAGES | 133 |
| 96 | SEX EFFECTS: VISA IMAGES | 134 |
| 97 | SEX EFFECTS: VISA IMAGES | 135 |
| 98 | SEX EFFECTS: VISA IMAGES | 136 |
| 99 | SEX EFFECTS: VISA IMAGES | 137 |
| 100 | SEX EFFECTS: VISA IMAGES | 138 |
| 101 | SEX EFFECTS: VISA IMAGES | 139 |
| 102 | SEX EFFECTS: VISA IMAGES | 140 |
| 103 | SEX EFFECTS: VISA IMAGES | 141 |
| 104 | SEX EFFECTS: VISA IMAGES | 142 |

| | | |
|-----|--|-----|
| 105 | SEX EFFECTS: VISA IMAGES | 143 |
| 106 | SEX EFFECTS: VISA IMAGES | 144 |
| 107 | SEX EFFECTS: VISA IMAGES | 145 |
| 108 | SEX EFFECTS: VISA IMAGES | 146 |
| 109 | SEX EFFECTS: VISA IMAGES | 147 |
| 110 | SEX EFFECTS: VISA IMAGES | 148 |
| 111 | SEX EFFECTS: VISA IMAGES | 149 |
| 112 | FALSE MATCH RATE CALIBRATION: MUGSHOT IMAGES | 150 |
| 113 | FALSE MATCH RATE CALIBRATION: MUGSHOT IMAGES | 151 |
| 114 | FALSE MATCH RATE CALIBRATION: MUGSHOT IMAGES | 152 |
| 115 | FALSE MATCH RATE CALIBRATION: MUGSHOT IMAGES | 153 |
| 116 | FALSE MATCH RATE CALIBRATION: MUGSHOT IMAGES | 154 |
| 117 | FALSE MATCH RATE CALIBRATION: MUGSHOT IMAGES | 155 |
| 118 | FALSE MATCH RATE CALIBRATION: MUGSHOT IMAGES | 156 |
| 119 | FALSE MATCH RATE CALIBRATION: MUGSHOT IMAGES | 157 |
| 120 | FALSE MATCH RATE CALIBRATION: MUGSHOT IMAGES | 158 |
| 121 | FALSE MATCH RATE CALIBRATION: MUGSHOT IMAGES | 159 |
| 122 | FALSE MATCH RATE CALIBRATION: MUGSHOT IMAGES | 160 |
| 123 | FALSE MATCH RATE CALIBRATION: MUGSHOT IMAGES | 161 |
| 124 | FALSE MATCH RATE CALIBRATION: VISA IMAGES | 162 |
| 125 | FALSE MATCH RATE CALIBRATION: VISA IMAGES | 163 |
| 126 | FALSE MATCH RATE CALIBRATION: VISA IMAGES | 164 |
| 127 | FALSE MATCH RATE CALIBRATION: VISA IMAGES | 165 |
| 128 | FALSE MATCH RATE CALIBRATION: VISA IMAGES | 166 |
| 129 | FALSE MATCH RATE CALIBRATION: VISA IMAGES | 167 |
| 130 | FALSE MATCH RATE CALIBRATION: VISA IMAGES | 168 |
| 131 | FALSE MATCH RATE CALIBRATION: VISA IMAGES | 169 |
| 132 | FALSE MATCH RATE CALIBRATION: VISA IMAGES | 170 |
| 133 | FALSE MATCH RATE CALIBRATION: VISA IMAGES | 171 |
| 134 | FALSE MATCH RATE CALIBRATION: VISA IMAGES | 172 |
| 135 | FALSE MATCH RATE CALIBRATION: VISA IMAGES | 173 |
| 136 | FALSE MATCH RATE CALIBRATION: VISA IMAGES | 174 |
| 137 | FALSE MATCH RATE CALIBRATION: VISA IMAGES | 175 |
| 138 | FALSE MATCH RATE CALIBRATION: VISA IMAGES | 176 |
| 139 | FALSE MATCH RATE CALIBRATION: VISA IMAGES | 177 |
| 140 | FALSE MATCH RATE CALIBRATION: VISA IMAGES | 178 |
| 141 | FALSE MATCH RATE CALIBRATION: VISA IMAGES | 179 |
| 142 | FALSE MATCH RATE CALIBRATION: VISA IMAGES | 180 |
| 143 | FALSE MATCH RATE CALIBRATION: VISA IMAGES | 181 |
| 144 | FALSE MATCH RATE CALIBRATION: VISA IMAGES | 182 |
| 145 | FALSE MATCH RATE CALIBRATION: VISA IMAGES | 183 |
| 146 | FALSE MATCH RATE CALIBRATION: VISA IMAGES | 184 |
| 147 | FALSE MATCH RATE CALIBRATION: VISA IMAGES | 185 |
| 148 | EFFECT OF COUNTRY OF BIRTH ON FNMR | 187 |
| 149 | EFFECT OF COUNTRY OF BIRTH ON FNMR | 188 |
| 150 | EFFECT OF COUNTRY OF BIRTH ON FNMR | 189 |
| 151 | EFFECT OF COUNTRY OF BIRTH ON FNMR | 190 |
| 152 | EFFECT OF COUNTRY OF BIRTH ON FNMR | 191 |
| 153 | EFFECT OF COUNTRY OF BIRTH ON FNMR | 192 |
| 154 | EFFECT OF COUNTRY OF BIRTH ON FNMR | 193 |
| 155 | EFFECT OF COUNTRY OF BIRTH ON FNMR | 194 |
| 156 | EFFECT OF COUNTRY OF BIRTH ON FNMR | 195 |
| 157 | EFFECT OF COUNTRY OF BIRTH ON FNMR | 196 |
| 158 | EFFECT OF COUNTRY OF BIRTH ON FNMR | 197 |
| 159 | EFFECT OF COUNTRY OF BIRTH ON FNMR | 198 |
| 160 | EFFECT OF COUNTRY OF BIRTH ON FNMR | 199 |

| | | |
|-----|---|-----|
| 161 | EFFECT OF COUNTRY OF BIRTH ON FNMR | 200 |
| 162 | EFFECT OF COUNTRY OF BIRTH ON FNMR | 201 |
| 163 | EFFECT OF COUNTRY OF BIRTH ON FNMR | 202 |
| 164 | EFFECT OF COUNTRY OF BIRTH ON FNMR | 203 |
| 165 | EFFECT OF COUNTRY OF BIRTH ON FNMR | 204 |
| 166 | EFFECT OF COUNTRY OF BIRTH ON FNMR | 205 |
| 167 | EFFECT OF COUNTRY OF BIRTH ON FNMR | 206 |
| 168 | ERROR TRADEOFF CHARACTERISTIC: MUGSHOT IMAGES | 208 |
| 169 | ERROR TRADEOFF CHARACTERISTIC: MUGSHOT IMAGES | 209 |
| 170 | ERROR TRADEOFF CHARACTERISTIC: MUGSHOT IMAGES | 210 |
| 171 | ERROR TRADEOFF CHARACTERISTIC: MUGSHOT IMAGES | 211 |
| 172 | ERROR TRADEOFF CHARACTERISTIC: MUGSHOT IMAGES | 212 |
| 173 | ERROR TRADEOFF CHARACTERISTIC: MUGSHOT IMAGES | 213 |
| 174 | ERROR TRADEOFF CHARACTERISTIC: MUGSHOT IMAGES | 214 |
| 175 | ERROR TRADEOFF CHARACTERISTIC: MUGSHOT IMAGES | 215 |
| 176 | ERROR TRADEOFF CHARACTERISTIC: MUGSHOT IMAGES | 216 |
| 177 | ERROR TRADEOFF CHARACTERISTIC: MUGSHOT IMAGES | 217 |
| 178 | ERROR TRADEOFF CHARACTERISTIC: MUGSHOT IMAGES | 218 |
| 179 | ERROR TRADEOFF CHARACTERISTIC: MUGSHOT IMAGES | 219 |
| 180 | ERROR TRADEOFF CHARACTERISTIC: MUGSHOT IMAGES | 220 |
| 181 | ERROR TRADEOFF CHARACTERISTIC: MUGSHOT IMAGES | 221 |
| 182 | EFFECT OF SUBJECT AGE ON FNMR | 223 |
| 183 | EFFECT OF SUBJECT AGE ON FNMR | 224 |
| 184 | EFFECT OF SUBJECT AGE ON FNMR | 225 |
| 185 | EFFECT OF SUBJECT AGE ON FNMR | 226 |
| 186 | EFFECT OF SUBJECT AGE ON FNMR | 227 |
| 187 | EFFECT OF SUBJECT AGE ON FNMR | 228 |
| 188 | EFFECT OF SUBJECT AGE ON FNMR | 229 |
| 189 | EFFECT OF SUBJECT AGE ON FNMR | 230 |
| 190 | EFFECT OF SUBJECT AGE ON FNMR | 231 |
| 191 | EFFECT OF SUBJECT AGE ON FNMR | 232 |
| 192 | EFFECT OF SUBJECT AGE ON FNMR | 233 |
| 193 | EFFECT OF SUBJECT AGE ON FNMR | 234 |
| 194 | EFFECT OF SUBJECT AGE ON FNMR | 235 |
| 195 | EFFECT OF SUBJECT AGE ON FNMR | 236 |
| 196 | EFFECT OF SUBJECT AGE ON FNMR | 237 |
| 197 | EFFECT OF SUBJECT AGE ON FNMR | 238 |
| 198 | EFFECT OF SUBJECT AGE ON FNMR | 239 |
| 199 | EFFECT OF SUBJECT AGE ON FNMR | 240 |
| 200 | EFFECT OF SUBJECT AGE ON FNMR | 241 |
| 201 | EFFECT OF SUBJECT AGE ON FNMR | 242 |
| 202 | WORST CASE REGIONAL EFFECT FNMR | 245 |
| 203 | IMPOSTOR DISTRIBUTION SHIFTS FOR SELECT COUNTRY PAIRS | 247 |

| | Developer Name | Short Name | Seq. Num. | Validation Date |
|----|--|---------------------|-----------|-----------------|
| 1 | 3Divi | 3divi-003 | 003 | 2018-10-09 |
| 2 | 3Divi | 3divi-004 | 004 | 2019-07-22 |
| 3 | ACI Software | acisw-003 | 003 | 2020-08-03 |
| 4 | ADVANCE.AI | advance-002 | 002 | 2019-12-19 |
| 5 | ASUSTek Computer Inc | asusaics-000 | 000 | 2019-10-24 |
| 6 | ASUSTek Computer Inc | asusaics-001 | 001 | 2020-02-25 |
| 7 | AYF Technology | ayftech-001 | 001 | 2020-07-06 |
| 8 | Acer Incorporated | acer-000 | 000 | 2020-01-08 |
| 9 | Acer Incorporated | acer-001 | 001 | 2020-06-30 |
| 10 | Adera Global PTE | aderia-001 | 001 | 2019-06-17 |
| 11 | Ai First | aifirst-001 | 001 | 2019-11-21 |
| 12 | AiUnion Technology | aiunionface-000 | 000 | 2019-10-22 |
| 13 | Alchera Inc | alchera-000 | 000 | 2019-03-01 |
| 14 | Alchera Inc | alchera-001 | 001 | 2019-03-01 |
| 15 | Alivia / Innovation Sys | isystems-001 | 001 | 2018-06-12 |
| 16 | Alivia / Innovation Sys | isystems-002 | 002 | 2018-10-18 |
| 17 | AllGoVision | allgovision-000 | 000 | 2019-03-01 |
| 18 | AlphaSSTG | alphaface-001 | 001 | 2019-09-03 |
| 19 | AlphaSSTG | alphaface-002 | 002 | 2020-02-20 |
| 20 | Amplified Group | amplifiedgroup-001 | 001 | 2019-03-01 |
| 21 | Anke Investments | anke-004 | 004 | 2019-06-27 |
| 22 | Anke Investments | anke-005 | 005 | 2019-11-21 |
| 23 | Antheus Technologia | antheus-000 | 000 | 2019-12-05 |
| 24 | Antheus Technologia | antheus-001 | 001 | 2020-06-25 |
| 25 | AnyVision | anyvision-002 | 002 | 2018-01-31 |
| 26 | AnyVision | anyvision-004 | 004 | 2018-06-15 |
| 27 | Aware | aware-004 | 004 | 2019-03-01 |
| 28 | Aware | aware-005 | 005 | 2020-02-27 |
| 29 | Awudit Systems | awiros-001 | 001 | 2019-09-23 |
| 30 | Ayonix | ayonix-000 | 000 | 2017-06-22 |
| 31 | Beihang University-ERCACAT | ercacat-001 | 001 | 2020-07-06 |
| 32 | Beijing Alleyes Technology | alleyes-000 | 000 | 2020-03-09 |
| 33 | Beijing Vion Technology Inc | vion-000 | 000 | 2018-10-19 |
| 34 | BioID Technologies SA | bioidechswiss-000 | 000 | 2019-11-15 |
| 35 | BioID Technologies SA | bioidechswiss-001 | 001 | 2020-08-28 |
| 36 | Bitmain | bm-001 | 001 | 2018-10-17 |
| 37 | Bresee Technology | bresee-000 | 000 | 2020-08-07 |
| 38 | CSA IntelliCloud Technology | intellicloudai-001 | 001 | 2019-08-13 |
| 39 | CTBC Bank | ctbcbank-000 | 000 | 2019-06-28 |
| 40 | CTBC Bank | ctbcbank-001 | 001 | 2019-10-28 |
| 41 | Camvi Technologies | camvi-002 | 002 | 2018-10-19 |
| 42 | Camvi Technologies | camvi-004 | 004 | 2019-07-12 |
| 43 | Canon Information Technology (Beijing) | cib-000 | 000 | 2019-12-11 |
| 44 | Canon Information Technology (Beijing) | cib-001 | 001 | 2020-08-05 |
| 45 | China Electronics Import-Export Corp | ceiec-002 | 002 | 2019-06-12 |
| 46 | China Electronics Import-Export Corp | ceiec-003 | 003 | 2020-01-06 |
| 47 | China University of Petroleum | upc-001 | 001 | 2019-06-05 |
| 48 | Chinese University of Hong Kong | cuhkee-001 | 001 | 2020-03-18 |
| 49 | Chosun University | chosun-000 | 000 | 2020-02-12 |
| 50 | Chosun University | chosun-001 | 001 | 2020-07-01 |
| 51 | Chunghwa Telecom | chtface-002 | 002 | 2019-12-07 |
| 52 | Chunghwa Telecom | chtface-003 | 003 | 2020-06-24 |
| 53 | Cognitec Systems GmbH | cognitec-000 | 000 | 2018-10-19 |
| 54 | Cognitec Systems GmbH | cognitec-001 | 001 | 2019-03-01 |
| 55 | Cybercore | cybercore-000 | 000 | 2020-08-26 |
| 56 | Cyberextruder | cyberextruder-001 | 001 | 2017-08-02 |
| 57 | Cyberextruder | cyberextruder-002 | 002 | 2018-01-30 |
| 58 | Cyberlink Corp | cyberlink-004 | 004 | 2020-02-27 |
| 59 | Cyberlink Corp | cyberlink-005 | 005 | 2020-07-31 |
| 60 | DSK | dsk-000 | 000 | 2019-06-28 |
| 61 | Dahua Technology | dahua-004 | 004 | 2019-12-18 |
| 62 | Dahua Technology | dahua-005 | 005 | 2020-08-13 |
| 63 | Deepglint | deepglint-001 | 001 | 2019-06-21 |
| 64 | Deepglint | deepglint-002 | 002 | 2019-11-15 |
| 65 | Dermalog | dermalog-005 | 005 | 2018-02-02 |
| 66 | Dermalog | dermalog-006 | 006 | 2018-10-18 |
| 67 | DiDi ChuXing Technology | didiglobalface-001 | 001 | 2019-10-23 |
| 68 | Digital Barriers | digitalbarriers-002 | 002 | 2019-03-01 |
| 69 | Expasoft LLC | expasoft-000 | 000 | 2020-01-06 |
| 70 | FaceSoft | facesoft-000 | 000 | 2019-07-10 |

Table 1: Summary of participant information included in this report.

| | Developer Name | Short Name | Seq. Num. | Validation Date |
|-----|---|-----------------------------|-----------|-----------------|
| 71 | FarBar Inc | f8-001 | 001 | 2019-07-11 |
| 72 | Fujitsu Research and Development Center | fujitsulab-000 | 000 | 2020-02-04 |
| 73 | Gemalto Cogent | cogent-003 | 003 | 2019-03-01 |
| 74 | Gemalto Cogent | cogent-004 | 004 | 2019-06-14 |
| 75 | GeoVision Inc | geo-000 | 000 | 2020-06-29 |
| 76 | Glory | glory-001 | 001 | 2018-06-08 |
| 77 | Glory | glory-002 | 002 | 2019-11-12 |
| 78 | Gorilla Technology | gorilla-005 | 005 | 2020-03-11 |
| 79 | Gorilla Technology | gorilla-006 | 006 | 2020-07-31 |
| 80 | Guangzhou Pixel Solutions | pixelall-003 | 003 | 2019-10-15 |
| 81 | Guangzhou Pixel Solutions | pixelall-004 | 004 | 2020-07-02 |
| 82 | Hengrui AI Technology | hr-001 | 001 | 2019-06-04 |
| 83 | Hengrui AI Technology | hr-002 | 002 | 2019-10-08 |
| 84 | Hikvision Research Institute | hik-001 | 001 | 2019-03-01 |
| 85 | ID3 Technology | id3-004 | 004 | 2019-03-01 |
| 86 | ID3 Technology | id3-005 | 005 | 2020-08-04 |
| 87 | ITMO University | itmo-006 | 006 | 2019-03-01 |
| 88 | ITMO University | itmo-007 | 007 | 2020-01-06 |
| 89 | Idemia | idemia-005 | 005 | 2019-10-11 |
| 90 | Idemia | idemia-006 | 006 | 2020-07-06 |
| 91 | Imageware Systems | iws-000 | 000 | 2020-08-12 |
| 92 | Imagus Technology Pty | imagus-000 | 000 | 2019-06-19 |
| 93 | Imagus Technology Pty | imagus-001 | 001 | 2019-10-22 |
| 94 | Imperial College London | imperial-000 | 000 | 2019-03-01 |
| 95 | Imperial College London | imperial-002 | 002 | 2019-08-28 |
| 96 | Incode Technologies Inc | incode-006 | 006 | 2020-02-20 |
| 97 | Incode Technologies Inc | incode-007 | 007 | 2020-08-25 |
| 98 | Innovative Technology | innovativetechnologyltd-001 | 001 | 2019-10-22 |
| 99 | Innovative Technology | innovativetechnologyltd-002 | 002 | 2020-02-26 |
| 100 | Innovatrics | innovatrics-004 | 004 | 2018-10-19 |
| 101 | Innovatrics | innovatrics-006 | 006 | 2019-08-13 |
| 102 | Institute of Information Technologies | iit-001 | 001 | 2019-07-05 |
| 103 | Institute of Information Technologies | iit-002 | 002 | 2019-12-04 |
| 104 | Intel Research Group | intelresearch-001 | 001 | 2020-01-14 |
| 105 | Intel Research Group | intelresearch-002 | 002 | 2020-07-24 |
| 106 | Intellivision | intellivision-001 | 001 | 2017-10-10 |
| 107 | Intellivision | intellivision-002 | 002 | 2019-08-23 |
| 108 | Is It You | isityou-000 | 000 | 2017-06-26 |
| 109 | Kakao Enterprise | kakao-002 | 002 | 2019-06-19 |
| 110 | Kakao Enterprise | kakao-003 | 003 | 2020-02-26 |
| 111 | Kedacom International Pte | kedacom-000 | 000 | 2019-06-03 |
| 112 | Kneron Inc | kneron-003 | 003 | 2019-07-01 |
| 113 | Kneron Inc | kneron-005 | 005 | 2020-02-21 |
| 114 | Lomonosov Moscow State University | intsysmsu-001 | 001 | 2019-10-22 |
| 115 | Lomonosov Moscow State University | intsysmsu-002 | 002 | 2020-03-12 |
| 116 | Lookman Electroplast Industries | lookman-002 | 002 | 2018-06-13 |
| 117 | Lookman Electroplast Industries | lookman-004 | 004 | 2019-06-03 |
| 118 | Luxand Inc | luxand-000 | 000 | 2019-11-07 |
| 119 | MVision | mvision-001 | 001 | 2019-11-12 |
| 120 | Megvii/Face++ | megvii-001 | 001 | 2018-06-15 |
| 121 | Megvii/Face++ | megvii-002 | 002 | 2018-10-19 |
| 122 | MicroFocus | microfocus-001 | 001 | 2018-06-13 |
| 123 | MicroFocus | microfocus-002 | 002 | 2018-10-17 |
| 124 | Momentum Digital | sertis-000 | 000 | 2019-10-07 |
| 125 | Momentum Digital | sertis-001 | 001 | 2020-07-30 |
| 126 | Moontime Smart Technology | mt-000 | 000 | 2019-06-03 |
| 127 | Moontime Smart Technology | mt-002 | 002 | 2020-07-02 |
| 128 | N-Tech Lab | ntechlab-007 | 007 | 2019-06-25 |
| 129 | N-Tech Lab | ntechlab-008 | 008 | 2020-01-06 |
| 130 | Netbridge Technology Incoporation | netbridgegetech-001 | 001 | 2020-01-08 |
| 131 | Netbridge Technology Incoporation | netbridgegetech-002 | 002 | 2020-08-11 |
| 132 | Neurotechnology | neurotechnology-008 | 008 | 2020-01-08 |
| 133 | Neurotechnology | neurotechnology-009 | 009 | 2020-07-07 |
| 134 | Nodeflux | nodeflux-002 | 002 | 2019-08-13 |
| 135 | NotionTag Technologies Private Limited | notiontag-000 | 000 | 2019-06-12 |
| 136 | Oz Forensics LLC | oz-001 | 001 | 2020-07-29 |
| 137 | PXL Vision AG | pxl-001 | 001 | 2020-06-30 |
| 138 | Panasonic R+D Center Singapore | psl-003 | 003 | 2019-10-01 |
| 139 | Panasonic R+D Center Singapore | psl-005 | 005 | 2020-07-06 |
| 140 | Paravision (EverAI) | paravision | 003 | 2019-07-01 |

Table 2: Summary of participant information included in this report.

| | Developer Name | Short Name | Seq. Num. | Validation Date |
|-----|---|-----------------------|-----------|-----------------|
| 141 | Paravision (EverAI) | paravision-004 | 004 | 2019-12-11 |
| 142 | Pensees Pte | pensees-001 | 001 | 2020-08-17 |
| 143 | Pyramid Cyber Security + Forensic (P) | pyramid-000 | 000 | 2019-11-04 |
| 144 | Rank One Computing | rankone-008 | 008 | 2019-11-12 |
| 145 | Rank One Computing | rankone-009 | 009 | 2020-06-26 |
| 146 | Realnetworks Inc | realnetworks-002 | 002 | 2019-02-28 |
| 147 | Realnetworks Inc | realnetworks-003 | 003 | 2019-06-12 |
| 148 | Remark Holdings | remarkai-001 | 001 | 2019-03-01 |
| 149 | Remark Holdings | remarkai-002 | 002 | 2019-11-21 |
| 150 | Rokid Corporation | rokid-000 | 000 | 2019-08-01 |
| 151 | Rokid Corporation | rokid-001 | 001 | 2019-12-13 |
| 152 | Saffe | saffe-001 | 001 | 2018-10-19 |
| 153 | Saffe | saffe-002 | 002 | 2019-03-01 |
| 154 | Samsung S1 Corp | s1-001 | 001 | 2019-12-06 |
| 155 | Samtech InfoNet Limited | samtech-001 | 001 | 2019-10-15 |
| 156 | Satellite Innovation/Eocortex | eocortex-000 | 000 | 2020-08-26 |
| 157 | Scanovaate | scanovaate-001 | 001 | 2019-11-12 |
| 158 | Scanovaate | scanovaate-002 | 002 | 2020-06-26 |
| 159 | Sensetime Group | sensetime-002 | 002 | 2018-10-19 |
| 160 | Sensetime Group | sensetime-003 | 003 | 2019-06-04 |
| 161 | Shaman Software | shaman-000 | 000 | 2017-12-05 |
| 162 | Shaman Software | shaman-001 | 001 | 2018-01-13 |
| 163 | Shanghai Jiao Tong University | sjtu-001 | 001 | 2019-09-27 |
| 164 | Shanghai Jiao Tong University | sjtu-002 | 002 | 2020-02-12 |
| 165 | Shanghai Ulucu Electronics Technology | uluface-002 | 002 | 2019-07-10 |
| 166 | Shanghai Ulucu Electronics Technology | uluface-003 | 003 | 2019-11-12 |
| 167 | Shanghai University - Shanghai Film Academy | shu-002 | 002 | 2019-12-10 |
| 168 | Shanghai University - Shanghai Film Academy | shu-003 | 003 | 2020-06-24 |
| 169 | Shanghai Yitu Technology | yitu-003 | 003 | 2019-03-01 |
| 170 | Shenzhen AiMall Tech | aimall-002 | 002 | 2020-03-12 |
| 171 | Shenzhen AiMall Tech | aimall-003 | 003 | 2020-08-12 |
| 172 | Shenzhen EI Networks | einetworks-000 | 000 | 2019-08-13 |
| 173 | Shenzhen Inst Adv Integrated Tech CAS | siat-002 | 002 | 2018-06-13 |
| 174 | Shenzhen Inst Adv Integrated Tech CAS | siat-004 | 004 | 2019-03-01 |
| 175 | Shenzhen Intellifusion Technologies | intellifusion-001 | 001 | 2019-08-22 |
| 176 | Shenzhen Intellifusion Technologies | intellifusion-002 | 002 | 2020-03-18 |
| 177 | Smilart | smilart-002 | 002 | 2018-02-06 |
| 178 | Smilart | smilart-003 | 003 | 2018-06-18 |
| 179 | Staqu Technologies | st aqu-000 | 000 | 2020-07-15 |
| 180 | Star Hybrid Limited | starhybrid-001 | 001 | 2019-06-19 |
| 181 | Su Zhou NaZhiTianDi intelligent technology | nazhai-000 | 000 | 2020-06-25 |
| 182 | Synesis | synesis-006 | 006 | 2019-10-10 |
| 183 | Synesis | synesis-007 | 007 | 2020-06-24 |
| 184 | Synology Inc | synology-000 | 000 | 2019-10-23 |
| 185 | Synology Inc | synology-002 | 002 | 2020-08-20 |
| 186 | TUPU Technology | tuputech-000 | 000 | 2019-10-11 |
| 187 | Taiwan AI Labs | ailabs-001 | 001 | 2019-12-18 |
| 188 | Tech5 SA | tech5-004 | 004 | 2020-03-09 |
| 189 | Tech5 SA | tech5-005 | 005 | 2020-07-24 |
| 190 | Tencent Deepsea Lab | deepsea-001 | 001 | 2019-06-03 |
| 191 | Tevian | tevian-004 | 004 | 2019-03-01 |
| 192 | Tevian | tevian-005 | 005 | 2019-09-21 |
| 193 | TigerIT Americas LLC | tiger-002 | 002 | 2018-06-13 |
| 194 | TigerIT Americas LLC | tiger-003 | 003 | 2018-10-16 |
| 195 | TongYi Transportation Technology | tongyi-005 | 005 | 2019-06-12 |
| 196 | Toshiba | toshiba-002 | 002 | 2018-10-19 |
| 197 | Toshiba | toshiba-003 | 003 | 2019-03-01 |
| 198 | Trueface.ai | trueface-000 | 000 | 2019-10-08 |
| 199 | Trueface.ai | trueface-001 | 001 | 2020-07-20 |
| 200 | ULSee Inc | ulsee-001 | 001 | 2019-07-31 |
| 201 | Universidade de Coimbra | visteam-000 | 000 | 2020-01-14 |
| 202 | VCognition | vcog-002 | 002 | 2017-06-12 |
| 203 | Veridas Digital Authentication Solutions S.L. | veridas-003 | 003 | 2019-11-27 |
| 204 | Veridas Digital Authentication Solutions S.L. | veridas-004 | 004 | 2020-07-21 |
| 205 | Via Technologies Inc | via-000 | 000 | 2019-07-08 |
| 206 | Via Technologies Inc | via-001 | 001 | 2020-01-08 |
| 207 | Videmo Intelligent Videoanalyse | videmo-000 | 000 | 2019-12-19 |
| 208 | Videonetics Technology Pvt | videonetics-001 | 001 | 2019-06-19 |
| 209 | Videonetics Technology Pvt | videonetics-002 | 002 | 2019-11-21 |
| 210 | Vigilant Solutions | vigilantsolutions-007 | 007 | 2019-06-27 |

Table 3: Summary of participant information included in this report.

| | Developer Name | Short Name | Seq. Num. | Validation Date |
|-----|---------------------------------------|-----------------------|-----------|-----------------|
| 211 | Vigilant Solutions | vigilantsolutions-008 | 008 | 2020-08-03 |
| 212 | Visidon | vd-001 | 001 | 2019-02-26 |
| 213 | Vision-Box | visionbox-000 | 000 | 2019-02-26 |
| 214 | Vision-Box | visionbox-001 | 001 | 2019-03-01 |
| 215 | VisionLabs | visionlabs-008 | 008 | 2020-01-06 |
| 216 | VisionLabs | visionlabs-009 | 009 | 2020-07-27 |
| 217 | Vocord | vocord-007 | 007 | 2019-06-06 |
| 218 | Vocord | vocord-008 | 008 | 2020-01-031 |
| 219 | Winsense | winsense-000 | 000 | 2019-06-17 |
| 220 | Winsense | winsense-001 | 001 | 2019-10-16 |
| 221 | Xforward AI Technology | xforwardai-000 | 000 | 2020-02-06 |
| 222 | Xiamen Meiya Pico Information | meiya-001 | 001 | 2019-03-01 |
| 223 | YoomiK | yoonik-000 | 000 | 2020-06-24 |
| 224 | Yuan High-Tech Development | yuan-000 | 000 | 2020-06-30 |
| 225 | Zhuhai Yisheng Electronics Technology | yisheng-004 | 004 | 2018-06-12 |
| 226 | iQIYI Inc | iqface-000 | 000 | 2019-06-04 |
| 227 | iQIYI Inc | iqface-002 | 002 | 2020-07-30 |
| 228 | iSAP Solution Corporation | isap-001 | 001 | 2019-08-07 |

Table 4: Summary of participant information included in this report.

| | ALGORITHM | CONFIG | LIBRARY | TEMPLATE | | | | | | | | COMPARISON ⁴ | | |
|----|--------------------|---------|---------|---------------------|--------------------------|--------------------------|-------------------------|--------------------------|-------------------------|-----------------------------------|-------------------------------|-------------------------|------------------------|--|
| | | | | NAME | | DATA | DATA | MEMORY | SIZE | GENERATION TIME (ms) ⁴ | | | TIME (ns) ⁵ | |
| | | | | (KB) ¹ | (KB) ² | (MB) ³ | (B) | MUGSHOT | ISO | PHOTOJOURN. | WILD | GENUINE | IMPOSTOR | |
| 1 | 3divi-003 | 191636 | 55903 | ⁴³ 358 | ²¹¹ 4096 ± 0 | ¹³⁰ 650 ± 90 | ⁶¹ 409 ± 33 | ⁴⁶ 355 ± 73 | ⁶¹ 399 ± 33 | ²² 627 ± 11 | ²⁶ 623 ± 32 | | | |
| 2 | 3divi-004 | 263670 | 50794 | ⁵³ 430 | ¹¹³ 2048 ± 0 | ²¹⁷ 984 ± 131 | ¹⁵⁴ 746 ± 43 | ¹²⁸ 682 ± 71 | ¹⁵³ 729 ± 35 | ⁴⁰ 794 ± 35 | ⁴⁰ 801 ± 40 | | | |
| 3 | acer-000 | 109735 | 88323 | ⁶⁷ 478 | ¹⁰⁹ 2048 ± 0 | ²⁵ 222 ± 0 | ²⁷ 223 ± 1 | ²⁸ 229 ± 2 | ³¹ 241 ± 24 | ⁶⁴ 1065 ± 40 | ⁷³ 1109 ± 35 | | | |
| 4 | acer-001 | 36650 | 66086 | ⁴⁹ 417 | ³⁰ 512 ± 0 | ²³ 199 ± 0 | ²⁵ 198 ± 0 | ²⁶ 198 ± 0 | ²⁵ 198 ± 0 | ¹²⁶ 2453 ± 44 | ¹²⁷ 2461 ± 62 | | | |
| 5 | acisw-003 | 282029 | 35664 | ³⁵ 282 | ²²⁶ 18467 ± 8 | ²⁷ 232 ± 1 | ²² 187 ± 0 | ²⁵ 177 ± 7 | ²² 184 ± 0 | ²²⁵ 847908 ± 16757 | ²²⁵ 851850 ± 17018 | | | |
| 6 | aderu-001 | 0 | 79272 | ²⁶ 190 | ¹⁹⁴ 2560 ± 0 | ⁹ 97 ± 0 | - | - | - | ⁹⁸ 1604 ± 71 | ⁹⁹ 1649 ± 56 | | | |
| 7 | advance-002 | 257173 | 20434 | ³⁶ 295 | ⁷² 2048 ± 0 | ¹⁷⁸ 811 ± 2 | - | - | - | ⁵⁵ 987 ± 10 | ⁵⁴ 988 ± 45 | | | |
| 8 | aifirst-001 | 224157 | 808777 | ⁶⁸ 485 | ⁷¹ 2048 ± 0 | ¹⁰⁶ 587 ± 2 | ¹⁰⁴ 573 ± 2 | ⁹³ 571 ± 20 | ¹⁰⁹ 590 ± 1 | ⁷⁰ 1099 ± 14 | ⁷² 1087 ± 45 | | | |
| 9 | ailabs-001 | 1054663 | 49450 | ¹⁶⁹ 1252 | ⁸⁷ 2048 ± 0 | ¹³⁷ 664 ± 4 | ⁸⁹ 526 ± 1 | ⁷⁰ 491 ± 60 | ⁸⁶ 513 ± 2 | ²¹⁸ 104034 ± 661 | ²¹⁸ 103415 ± 722 | | | |
| 10 | aimall-002 | 370156 | 25210 | ¹⁹¹ 1576 | ¹¹⁹ 2048 ± 0 | ¹⁷¹ 776 ± 4 | ¹⁶¹ 775 ± 3 | ¹⁴⁸ 775 ± 4 | ¹⁶³ 774 ± 3 | ²¹⁶ 72811 ± 7399 | ²¹⁶ 71216 ± 6286 | | | |
| 11 | aimall-003 | 504324 | 171935 | ²⁰¹ 1913 | ⁴⁷ 1024 ± 0 | ¹³⁸ 662 ± 1 | ¹²⁸ 660 ± 1 | ¹¹⁶ 660 ± 2 | ¹²⁷ 661 ± 1 | ²¹⁰ 34565 ± 93 | ²¹¹ 34598 ± 118 | | | |
| 12 | aiunionface-000 | 241642 | 840295 | ⁴⁸ 402 | ¹¹⁵ 2048 ± 0 | ¹²⁵ 637 ± 13 | ¹⁰⁹ 592 ± 7 | ⁹⁷ 585 ± 15 | ¹¹² 598 ± 8 | ⁶⁵ 1072 ± 19 | ⁷¹ 1080 ± 47 | | | |
| 13 | alchera-000 | 258450 | 18848 | ⁹⁷ 614 | ⁹⁵ 2048 ± 0 | ¹⁰⁷ 587 ± 13 | ⁷⁶ 489 ± 8 | ⁶⁵ 473 ± 21 | ⁷⁴ 483 ± 7 | ¹⁴⁵ 3189 ± 32 | ¹⁴² 3031 ± 142 | | | |
| 14 | alchera-001 | 174013 | 18848 | ⁶⁶ 473 | ⁸⁸ 2048 ± 0 | ¹¹⁹ 627 ± 11 | ⁹¹ 527 ± 6 | ⁷⁸ 513 ± 21 | ⁹¹ 525 ± 7 | ¹⁴⁶ 3342 ± 81 | ¹⁴⁷ 3243 ± 47 | | | |
| 15 | alleyes-000 | 507636 | 997090 | ¹³⁴ 857 | ¹²³ 2048 ± 0 | ¹⁷⁴ 784 ± 1 | ¹⁷² 826 ± 2 | ¹⁶⁰ 823 ± 40 | ¹⁸³ 895 ± 2 | ⁸⁹ 1298 ± 34 | ⁹⁰ 1303 ± 51 | | | |
| 16 | allgovision-000 | 172509 | 155862 | ⁸⁷ 561 | ¹³⁷ 2048 ± 0 | ⁵⁵ 384 ± 8 | ⁵² 374 ± 11 | ⁵² 392 ± 26 | ⁵⁷ 383 ± 16 | ²⁰⁸ 29903 ± 406 | ²⁰⁹ 29735 ± 194 | | | |
| 17 | alphaface-001 | 259849 | 81636 | ⁸³ 527 | ¹⁰³ 2048 ± 0 | ¹¹⁴ 612 ± 1 | ¹¹⁷ 612 ± 1 | ¹⁰³ 613 ± 1 | ¹¹⁶ 615 ± 1 | ⁵⁸ 1008 ± 10 | ⁵⁸ 1002 ± 19 | | | |
| 18 | alphaface-002 | 768995 | 70692 | ¹⁸⁴ 1434 | ¹²⁴ 2048 ± 0 | ¹²⁰ 628 ± 2 | ¹²¹ 627 ± 1 | ³⁹ 326 ± 1 | ⁴⁴ 327 ± 1 | ⁴⁶ 945 ± 25 | ⁴⁸ 935 ± 17 | | | |
| 19 | amplifiedgroup-001 | 0 | 47053 | ⁹ 81 | ⁴⁰ 866 ± 2 | ⁶ 93 ± 0 | - | - | - | ²¹⁵ 57803 ± 4210 | ²¹⁵ 56365 ± 1196 | | | |
| 20 | anke-004 | 349388 | 410776 | ¹⁰⁴ 706 | ¹⁷³ 2056 ± 0 | ¹¹⁸ 625 ± 1 | ¹¹³ 599 ± 9 | ¹⁰⁶ 581 ± 2 | ²³ 633 ± 22 | ²⁷ 632 ± 34 | | | | |
| 21 | anke-005 | 328553 | 429160 | ¹⁶⁴ 1134 | ¹⁷⁵ 2056 ± 0 | ¹⁰⁸ 590 ± 2 | ¹⁰² 561 ± 2 | ⁸⁴ 535 ± 32 | ⁹⁶ 545 ± 1 | ²⁸ 685 ± 19 | ³¹ 687 ± 26 | | | |
| 22 | antheus-000 | 119453 | 41994 | ¹⁶ 116 | ³² 520 ± 0 | ¹¹ 109 ± 1 | ¹⁶ 159 ± 1 | ²⁴ 173 ± 14 | ¹⁴ 140 ± 1 | ¹⁷⁹ 6901 ± 268 | ¹⁷⁷ 6936 ± 103 | | | |
| 23 | antheus-001 | 119453 | 41962 | ¹⁷ 118 | ³³ 520 ± 0 | ¹³ 120 ± 1 | ²⁶ 204 ± 1 | ²⁷ 221 ± 20 | ²¹ 178 ± 1 | ¹⁷⁵ 6218 ± 47 | ¹⁷² 6216 ± 45 | | | |
| 24 | anyvision-002 | 662659 | 520039 | ⁶³ 468 | ⁴⁶ 1024 ± 0 | ²⁸ 248 ± 0 | ²⁴ 194 ± 0 | - | ²⁴ 190 ± 1 | ²¹⁷ 74069 ± 188 | ²¹⁷ 74019 ± 198 | | | |
| 25 | anyvision-004 | 401001 | 630797 | ¹⁶² 1102 | ⁴⁴ 1024 ± 0 | ⁵⁰ 355 ± 1 | ⁴⁷ 344 ± 1 | ⁵⁸ 425 ± 112 | ⁴⁸ 342 ± 1 | ¹¹¹ 1891 ± 51 | ¹⁰⁷ 1829 ± 85 | | | |
| 26 | asusaics-000 | 257418 | 245320 | ⁹⁵ 605 | ⁹⁹ 2048 ± 0 | ⁷⁸ 484 ± 13 | ⁶⁰ 407 ± 10 | ⁵³ 396 ± 18 | ⁶² 404 ± 7 | ¹⁶⁸ 5455 ± 78 | ¹⁶⁹ 5422 ± 112 | | | |
| 27 | asusaics-001 | 257418 | 245330 | ⁹⁰ 595 | ²¹⁵ 4096 ± 0 | ¹⁹¹ 842 ± 17 | ¹⁵⁷ 759 ± 7 | ¹⁴⁴ 747 ± 28 | ¹⁶⁰ 759 ± 10 | ¹⁸⁶ 8618 ± 42 | ¹⁸⁶ 8638 ± 136 | | | |
| 28 | aware-004 | 427829 | 28219 | ¹⁹⁸ 1820 | ¹⁸⁶ 2084 ± 0 | ²⁰² 900 ± 10 | ¹⁷⁸ 872 ± 11 | ¹⁶⁷ 872 ± 30 | ¹⁸⁰ 881 ± 33 | ⁸⁷ 1279 ± 50 | ⁸⁹ 1287 ± 100 | | | |
| 29 | aware-005 | 300017 | 26320 | ¹⁷¹ 1265 | ⁶³ 1572 ± 0 | ¹⁹⁸ 886 ± 23 | ¹⁷⁶ 861 ± 14 | ¹⁶⁵ 858 ± 151 | ¹⁸¹ 889 ± 45 | ⁹⁴ 1475 ± 63 | ⁹² 1427 ± 115 | | | |
| 30 | awirobs-001 | 15499 | 87480 | ¹² 88 | ¹⁹ 512 ± 0 | ⁸ 97 ± 6 | ⁶ 87 ± 6 | - | ⁶ 86 ± 7 | ⁶⁷ 1079 ± 44 | ⁶⁵ 1050 ± 45 | | | |
| 31 | ayftech-001 | 195423 | 43580 | ¹¹⁰ 731 | ²⁸ 512 ± 0 | ⁶⁴ 408 ± 23 | ⁴⁵ 339 ± 10 | ³⁸ 319 ± 18 | ⁴⁵ 336 ± 11 | ¹⁹ 615 ± 16 | ⁴⁴ 885 ± 44 | | | |
| 32 | ayonix-000 | 58505 | 5252 | ⁵ 69 | ⁴⁹ 1036 ± 0 | ² 18 ± 2 | ¹ 10 ± 1 | ⁴ 2 ± 4 | ¹ 10 ± 1 | ²¹ 621 ± 23 | ²⁵ 620 ± 26 | | | |
| 33 | bioditechswiss-000 | 758466 | 119955 | ¹⁵¹ 1039 | ¹⁰ 256 ± 0 | ¹²² 630 ± 2 | ¹¹⁴ 608 ± 1 | ¹⁰⁹ 629 ± 2 | ¹²¹ 630 ± 1 | ²⁰⁹ 34416 ± 137 | ²¹⁰ 34403 ± 126 | | | |
| 34 | bioditechswiss-001 | 1178769 | 120811 | ¹⁸⁶ 1455 | ¹⁸ 512 ± 0 | ²¹⁴ 966 ± 4 | ¹⁹² 954 ± 2 | ¹⁷⁹ 954 ± 6 | ¹⁹³ 980 ± 4 | ¹³⁴ 2610 ± 25 | ¹³⁴ 2624 ± 32 | | | |
| 35 | bm-001 | 287734 | 38076 | ¹⁹ 148 | ¹ 64 ± 0 | ⁶⁹ 444 ± 88 | ⁴⁰ 292 ± 25 | ²³ 173 ± 37 | ³⁸ 276 ± 71 | ¹¹⁰ 1887 ± 31 | ¹⁰⁹ 1877 ± 26 | | | |
| 36 | bresee-000 | 287880 | 22872 | ³⁸ 333 | ⁸⁶ 2048 ± 0 | ²²⁶ 1309 ± 1 | ¹⁹⁹ 1212 ± 1 | ¹⁸⁶ 1215 ± 0 | ¹⁹⁹ 1211 ± 1 | ²¹³ 45317 ± 228 | ²¹⁴ 48256 ± 425 | | | |
| 37 | camvi-002 | 236278 | 225285 | ¹¹¹ 737 | ⁴⁵ 1024 ± 0 | ¹⁴⁶ 677 ± 7 | ¹²² 628 ± 4 | ¹⁰⁷ 624 ± 7 | ¹²⁰ 627 ± 3 | ¹⁸ 612 ± 26 | ²⁰ 603 ± 20 | | | |
| 38 | camvi-004 | 280733 | 615819 | ¹⁴² 919 | ¹²⁹ 2048 ± 0 | ¹⁶⁸ 759 ± 10 | ¹⁵² 733 ± 3 | ¹⁴² 730 ± 10 | ¹⁵⁴ 731 ± 4 | ⁴⁷ 948 ± 40 | ⁵⁰ 963 ± 31 | | | |
| 39 | ceiec-002 | 269063 | 90975 | ⁵⁰ 426 | ⁸⁹ 2048 ± 0 | ¹¹⁵ 612 ± 17 | ¹⁰⁰ 557 ± 6 | ⁸⁹ 554 ± 21 | ¹⁰⁰ 555 ± 7 | ¹¹⁸ 2188 ± 57 | ¹²³ 2301 ± 56 | | | |
| 40 | ceiec-003 | 260371 | 88707 | ⁵² 430 | ⁹⁰ 2048 ± 0 | ¹⁸¹ 817 ± 4 | - | - | - | ¹²¹ 2256 ± 38 | ¹²¹ 2241 ± 54 | | | |
| 41 | chosun-000 | 167093 | 694 | ¹⁸ 136 | ⁸¹ 2048 ± 0 | ⁶⁸ 441 ± 1 | ⁵⁷ 402 ± 1 | ⁶ 9 ± 13 | ⁶⁰ 399 ± 1 | ⁵³ 983 ± 20 | ⁵³ 983 ± 29 | | | |
| 42 | chosun-001 | 765615 | 707 | ⁷⁰ 491 | ¹⁴¹ 2048 ± 0 | ¹⁷³ 783 ± 2 | ¹¹² 599 ± 1 | ⁹¹ 562 ± 31 | ¹⁰⁷ 589 ± 1 | ⁵⁶ 998 ± 25 | ⁶³ 1035 ± 11 | | | |
| 43 | chtface-002 | 363153 | 369529 | ¹⁶¹ 1100 | ¹⁰⁸ 2048 ± 0 | ¹⁰⁵ 584 ± 14 | ⁹⁴ 530 ± 9 | ⁸⁰ 521 ± 18 | ⁹³ 528 ± 7 | ¹²² 2264 ± 26 | ¹²⁰ 2234 ± 103 | | | |
| 44 | chtface-003 | 363153 | 369529 | ¹⁶⁵ 1178 | ¹⁴⁴ 2048 ± 0 | ¹¹⁰ 594 ± 16 | ⁹² 528 ± 7 | ⁸² 523 ± 19 | ⁹² 527 ± 7 | ¹¹⁴ 2110 ± 37 | ¹¹⁹ 2219 ± 65 | | | |

| Notes | | | | | | | | | | | | | |
|-------|---|--|--|--|--|--|--|--|--|--|--|--|--|
| 1 | The configuration size does not capture static data included in libraries. | | | | | | | | | | | | |
| 2 | The library size is the combined total of all files provided in the submission lib folder. These libraries e.g. OpenCV may or may not be installed on any end user's platform natively and would not need to be installed with the algorithm. | | | | | | | | | | | | |
| 4 | The memory usage is the peak resident set size reported by the ps system call during template generation. | | | | | | | | | | | | |
| 5 | The median template creation times are measured on Intel®Xeon®CPU E5-2630 v4 @ 2.20GHz processors. | | | | | | | | | | | | |
| 6 | The comparison durations, in nanoseconds, are estimated using std::chrono::high_resolution_clock which on the machine in (2) counts 1ns clock ticks. Precision is somewhat worse than that however. The ± value is the median absolute deviation times 1.48 for Normal consistency. | | | | | | | | | | | | |

| | ALGORITHM | CONFIG | LIBRARY | TEMPLATE | | | | | | | | COMPARISON ⁴ | | | | | | |
|----|-----------------------|---------|---------|----------|------|------|----------|------|-----------------------------------|-------------------|-------------------|-------------------------|------------------------|-----|-------------|-------------|-----------------|-------------------|
| | | | | NAME | DATA | DATA | MEMORY | SIZE | GENERATION TIME (ms) ⁴ | | | | TIME (ns) ⁵ | | | | | |
| | | | | | | | | | (KB) ¹ | (KB) ² | (MB) ³ | (B) | MUGSHOT | ISO | PHOTOJOURN. | WILD | GENUINE | IMPOSTOR |
| 45 | cib-000 | 340288 | 69515 | 86 | 557 | 122 | 2048 ± 0 | 219 | 993 ± 40 | 175 | 859 ± 21 | 164 | 845 ± 41 | 177 | 858 ± 22 | 205 | 24340 ± 60 | 205 25972 ± 97 |
| 46 | cib-001 | 436253 | 133766 | 129 | 836 | 112 | 2048 ± 0 | 132 | 651 ± 2 | 126 | 654 ± 2 | 124 | 674 ± 20 | 122 | 632 ± 2 | 158 | 3783 ± 38 | 155 3765 ± 37 |
| 47 | cogent-003 | 698290 | 40430 | 185 | 1445 | 41 | 1973 ± 0 | 210 | 952 ± 0 | - | - | - | - | - | - | 190 | 12496 ± 75 | 189 11822 ± 163 |
| 48 | cogent-004 | 722919 | 389164 | 154 | 1059 | 68 | 1983 ± 0 | 218 | 987 ± 50 | - | - | - | - | - | - | 196 | 15536 ± 75 | 196 15964 ± 708 |
| 49 | cognitec-000 | 474759 | 27371 | 72 | 495 | 160 | 2052 ± 0 | 26 | 224 ± 1 | - | - | - | - | - | - | 159 | 3835 ± 108 | 156 3782 ± 83 |
| 50 | cognitec-001 | 476809 | 27487 | 74 | 498 | 160 | 2052 ± 0 | 40 | 293 ± 17 | - | - | - | - | - | - | 163 | 4253 ± 59 | 161 4102 ± 167 |
| 51 | ctcbcbank-000 | 257208 | 599238 | 88 | 570 | 97 | 2048 ± 0 | 99 | 568 ± 43 | 80 | 498 ± 19 | - | - | 81 | 498 ± 15 | 151 | 3551 ± 87 | 163 4805 ± 209 |
| 52 | ctcbcbank-001 | 275511 | 599238 | 92 | 603 | 143 | 2048 ± 0 | 133 | 652 ± 35 | 111 | 595 ± 20 | - | - | 111 | 595 ± 17 | 160 | 3926 ± 45 | 159 3924 ± 56 |
| 53 | cuhkee-001 | 787853 | 74917 | 210 | 2515 | 161 | 2052 ± 0 | 215 | 977 ± 31 | - | - | - | - | - | 137 | 2719 ± 60 | 137 2783 ± 56 | |
| 54 | cybercore-000 | 86008 | 55441 | 29 | 200 | 27 | 512 ± 0 | 136 | 655 ± 3 | 71 | 475 ± 3 | 60 | 439 ± 26 | 72 | 459 ± 3 | 194 | 14800 ± 75 | 195 15757 ± 782 |
| 55 | cyberextruder-001 | 121211 | 13629 | 23 | 178 | 9 | 256 ± 0 | 201 | 893 ± 25 | 164 | 791 ± 17 | - | - | 161 | 765 ± 24 | 68 | 1083 ± 16 | 70 1079 ± 19 |
| 56 | cyberextruder-002 | 168909 | 13924 | 28 | 194 | 73 | 2048 ± 0 | 88 | 532 ± 6 | 83 | 505 ± 7 | 81 | 522 ± 25 | 88 | 515 ± 10 | 107 | 1803 ± 14 | 104 1779 ± 22 |
| 57 | cyberlink-004 | 340894 | 104662 | 152 | 1046 | 221 | 4140 ± 0 | 158 | 712 ± 1 | 145 | 713 ± 1 | 136 | 716 ± 1 | 145 | 716 ± 1 | 156 | 3693 ± 51 | 158 3898 ± 71 |
| 58 | cyberlink-005 | 341680 | 111358 | 150 | 1037 | 220 | 4140 ± 0 | 159 | 721 ± 1 | 149 | 724 ± 1 | 140 | 721 ± 1 | 150 | 720 ± 1 | 154 | 3680 ± 37 | 160 4021 ± 97 |
| 59 | dahua-004 | 832455 | 141070 | 220 | 4885 | 104 | 2048 ± 0 | 162 | 735 ± 3 | 153 | 738 ± 8 | 143 | 734 ± 4 | 155 | 734 ± 2 | 35 | 730 ± 25 | 33 707 ± 44 |
| 60 | dahua-005 | 1586899 | 169478 | 223 | 7360 | 214 | 4096 ± 0 | 227 | 1418 ± 34 | 201 | 1400 ± 8 | 188 | 1403 ± 10 | 201 | 1402 ± 10 | 50 | 957 ± 23 | 52 969 ± 19 |
| 61 | deepglint-001 | 569802 | 206788 | 141 | 917 | 208 | 4096 ± 0 | 160 | 721 ± 4 | 147 | 718 ± 1 | 135 | 715 ± 1 | 147 | 717 ± 1 | 155 | 3680 ± 35 | 152 3517 ± 182 |
| 62 | deepglint-002 | 459642 | 272878 | 194 | 1614 | 205 | 4096 ± 0 | 145 | 677 ± 2 | 137 | 675 ± 2 | 130 | 683 ± 2 | 128 | 661 ± 2 | 193 | 13633 ± 87 | 191 12905 ± 440 |
| 63 | deepsea-001 | 147497 | 336250 | 44 | 358 | 42 | 1024 ± 0 | 121 | 630 ± 7 | 119 | 619 ± 3 | 106 | 623 ± 8 | 119 | 625 ± 2 | 91 | 1401 ± 37 | 93 1467 ± 50 |
| 64 | dermalog-005 | 0 | 317687 | 42 | 357 | 2 | 128 ± 0 | 15 | 130 ± 11 | 11 | 121 ± 13 | 12 | 107 ± 21 | 9 | 122 ± 11 | 9 | 499 ± 22 | 10 500 ± 22 |
| 65 | dermalog-006 | 0 | 452387 | 147 | 970 | 3 | 128 ± 0 | 87 | 532 ± 12 | 90 | 526 ± 20 | 77 | 513 ± 27 | 94 | 529 ± 20 | 10 | 506 ± 23 | 7 459 ± 23 |
| 66 | didiglobalface-001 | 259849 | 70680 | 82 | 527 | 102 | 2048 ± 0 | 113 | 612 ± 1 | 115 | 612 ± 1 | 102 | 612 ± 1 | 114 | 612 ± 1 | 52 | 973 ± 20 | 55 988 ± 20 |
| 67 | digitalbarriers-002 | 83002 | 598577 | 203 | 1930 | 177 | 2056 ± 0 | 24 | 209 ± 11 | 20 | 180 ± 12 | 21 | 170 ± 15 | 23 | 184 ± 15 | 191 | 13409 ± 228 | 192 13267 ± 206 |
| 68 | dsk-000 | 11967 | 782905 | 31 | 252 | 21 | 512 ± 0 | 44 | 304 ± 47 | 12 | 131 ± 18 | 13 | 110 ± 40 | 15 | 143 ± 29 | 181 | 7152 ± 115 | 178 7134 ± 111 |
| 69 | einetworks-000 | 372608 | 219883 | 137 | 880 | 181 | 2056 ± 0 | 127 | 645 ± 3 | - | - | - | - | - | 164 | 4876 ± 66 | 164 5156 ± 77 | |
| 70 | eocortex-000 | 255937 | 59432 | 30 | 224 | 82 | 2048 ± 0 | 45 | 305 ± 22 | 32 | 238 ± 6 | - | - | 29 | 228 ± 6 | 45 | 923 ± 11 | 46 918 ± 11 |
| 71 | ercacat-001 | 811623 | 58012 | 215 | 2816 | 170 | 2052 ± 0 | 220 | 1052 ± 3 | 194 | 972 ± 2 | 181 | 989 ± 31 | 188 | 936 ± 2 | 130 | 2551 ± 62 | 128 2501 ± 81 |
| 72 | everai-paravision-003 | 539802 | 118876 | 168 | 1225 | 207 | 4096 ± 0 | 143 | 674 ± 4 | 136 | 673 ± 1 | 123 | 673 ± 2 | 136 | 672 ± 1 | 31 | 699 ± 20 | 35 713 ± 47 |
| 73 | expasoft-000 | 15341 | 240451 | 13 | 100 | 148 | 2048 ± 0 | 4 | 68 ± 0 | 47 | 72 ± 6 | 8 | 68 ± 0 | 46 | 70 ± 0 | 104 | 1779 ± 26 | 103 1757 ± 97 |
| 74 | f8-001 | 272977 | 19668 | 172 | 1276 | 85 | 2048 ± 0 | 180 | 822 ± 39 | - | - | - | - | - | 195 | 15262 ± 139 | 194 15277 ± 212 | |
| 75 | facesoft-000 | 370120 | 10612 | 120 | 796 | 154 | 2048 ± 0 | 144 | 675 ± 18 | 132 | 666 ± 2 | 118 | 666 ± 3 | 130 | 664 ± 2 | 120 | 2239 ± 28 | 122 2277 ± 96 |
| 76 | fujitsulab-000 | 0 | 205894 | 59 | 453 | 23 | 512 ± 0 | 65 | 419 ± 1 | 59 | 405 ± 1 | 54 | 399 ± 12 | 68 | 441 ± 1 | 153 | 3613 ± 37 | 153 3621 ± 29 |
| 77 | geo-000 | 114483 | 304983 | 33 | 279 | 96 | 2048 ± 0 | 192 | 851 ± 1 | 182 | 880 ± 3 | 125 | 675 ± 290 | 187 | 935 ± 1 | 219 | 137544 ± 6225 | 219 137925 ± 6548 |
| 78 | glory-001 | 0 | 144786 | 174 | 1331 | 65 | 1726 ± 0 | 59 | 393 ± 2 | 51 | 372 ± 5 | 48 | 367 ± 22 | 56 | 381 ± 3 | 188 | 9607 ± 128 | 188 9539 ± 182 |
| 79 | glory-002 | 0 | 385177 | 148 | 982 | 189 | 2106 ± 0 | 111 | 594 ± 3 | 99 | 553 ± 2 | 95 | 572 ± 7 | 104 | 575 ± 3 | 178 | 6787 ± 85 | 174 6551 ± 249 |
| 80 | gorilla-005 | 100684 | 1297614 | 99 | 629 | 192 | 2192 ± 0 | 61 | 407 ± 3 | 58 | 402 ± 2 | 55 | 407 ± 5 | 63 | 415 ± 4 | 135 | 2678 ± 42 | 136 2770 ± 112 |
| 81 | gorilla-006 | 172743 | 1318812 | 136 | 874 | 222 | 4240 ± 0 | 71 | 454 ± 3 | 68 | 445 ± 2 | 64 | 450 ± 5 | 71 | 456 ± 3 | 157 | 3755 ± 38 | 154 3737 ± 44 |
| 82 | hik-001 | 667866 | 9290 | 222 | 6597 | 57 | 1408 ± 0 | 131 | 651 ± 0 | 123 | 629 ± 1 | 110 | 629 ± 3 | 118 | 624 ± 1 | 8 | 488 ± 19 | 8 477 ± 22 |
| 83 | hr-001 | 346156 | 104483 | 198 | 1682 | 182 | 2057 ± 0 | 140 | 665 ± 3 | - | - | - | - | - | 197 | 17816 ± 260 | 197 17878 ± 464 | |
| 84 | hr-002 | 390059 | 327494 | 175 | 1337 | 183 | 2057 ± 0 | 204 | 908 ± 3 | - | - | - | - | - | 203 | 22530 ± 416 | 203 21651 ± 533 | |
| 85 | id3-004 | 171526 | 49725 | 96 | 613 | 12 | 264 ± 0 | 92 | 541 ± 11 | 84 | 510 ± 8 | 76 | 510 ± 21 | 85 | 513 ± 11 | 75 | 1135 ± 23 | 81 1156 ± 32 |
| 86 | id3-005 | 153439 | 22125 | 112 | 740 | 13 | 264 ± 0 | 77 | 479 ± 1 | 70 | 451 ± 0 | 63 | 446 ± 8 | 69 | 451 ± 1 | 174 | 6072 ± 35 | 171 6077 ± 38 |
| 87 | idemia-005 | 509824 | 116761 | 98 | 618 | 38 | 588 ± 0 | 83 | 514 ± 15 | 82 | 505 ± 3 | 72 | 494 ± 31 | 82 | 501 ± 4 | 177 | 6657 ± 54 | 175 6616 ± 53 |
| 88 | idemia-006 | 570566 | 115633 | 144 | 932 | 39 | 668 ± 0 | 148 | 679 ± 4 | 138 | 676 ± 2 | 121 | 671 ± 27 | 134 | 670 ± 2 | 165 | 5223 ± 80 | 165 5193 ± 72 |

Notes

- 1 The configuration size does not capture static data included in libraries.
- 2 The library size is the combined total of all files provided in the submission lib folder. These libraries e.g. OpenCV may or may not be installed on any end user's platform natively and would not need to be installed with the algorithm.
- 3 The memory usage is the peak resident set size reported by the ps system call during template generation.
- 4 The median template creation times are measured on Intel® Xeon® CPU E5-2630 v4 @ 2.20GHz processors.
- 5 The comparison durations, in nanoseconds, are estimated using std::chrono::high_resolution_clock which on the machine in (2) counts 1ns clock ticks. Precision is somewhat worse than that however. The ± value is the median absolute deviation times 1.48 for Normal consistency.

Table 6: Summary of algorithms and properties included in this report. The red superscripts give ranking for the quantity in that column.

| | ALGORITHM | CONFIG | LIBRARY | TEMPLATE | | | | | | | | COMPARISON ⁴ | | | |
|-----|-----------------------------|---------|---------|----------------------|--------------------------|--------------------------|-------------------------|--------------------------|--------------------------|-------------------------------|-------------------------------|-----------------------------------|----------|--|--|
| | | | | NAME | | DATA | | MEMORY | | SIZE | | GENERATION TIME (ms) ⁴ | | | |
| | | | | (KB) ¹ | (KB) ² | (MB) ³ | (B) | MUGSHOT | ISO | PHOTOJOURN. | WILD | GENUINE | IMPOSTOR | | |
| 89 | iit-001 | 269176 | 52055 | ¹¹⁷ 788 | ¹¹⁸ 2048 ± 0 | ¹⁵³ 699 ± 4 | ¹⁴² 697 ± 1 | ¹³² 697 ± 1 | ¹⁴¹ 697 ± 1 | ⁶³ 1060 ± 48 | ⁶⁸ 1074 ± 54 | | | | |
| 90 | iit-002 | 259579 | 52070 | ¹⁰⁹ 731 | ¹⁴⁰ 2048 ± 0 | ⁸⁴ 514 ± 1 | ⁸⁸ 523 ± 1 | ⁷⁹ 521 ± 2 | ⁹⁰ 523 ± 1 | ⁵⁹ 1023 ± 7 | ⁵⁹ 1011 ± 66 | | | | |
| 91 | imagus-000 | 183453 | 599571 | ⁶² 466 | ¹⁴⁶ 2048 ± 0 | ⁶⁶ 425 ± 24 | ⁶² 418 ± 22 | ⁵⁷ 421 ± 19 | ⁷⁰ 454 ± 15 | ⁷⁷ 1145 ± 25 | ¹⁰² 1718 ± 63 | | | | |
| 92 | imagus-001 | 282680 | 256875 | ¹²⁶ 826 | ¹¹⁴ 2048 ± 0 | ¹⁷⁷ 807 ± 29 | ¹⁶⁸ 799 ± 20 | ¹⁶² 836 ± 49 | ¹⁷¹ 805 ± 12 | ⁶⁰ 1045 ± 22 | ⁴⁷ 934 ± 45 | | | | |
| 93 | imperial-000 | 370120 | 10623 | ¹²¹ 796 | ¹¹¹ 2048 ± 0 | ¹⁴¹ 669 ± 1 | ¹³³ 668 ± 2 | ¹¹¹ 668 ± 2 | ¹³¹ 667 ± 1 | ¹¹⁶ 2130 ± 32 | ¹¹⁴ 2052 ± 100 | | | | |
| 94 | imperial-002 | 472327 | 16134 | ¹⁹⁹ 1826 | ⁷³ 2048 ± 0 | ¹⁰⁰ 569 ± 1 | ¹⁰³ 569 ± 1 | ⁹² 569 ± 1 | ¹⁰² 569 ± 1 | ¹²³ 2278 ± 90 | ¹¹³ 2131 ± 44 | | | | |
| 95 | incode-006 | 266095 | 63518 | ¹²⁴ 814 | ⁷⁷ 2048 ± 0 | ⁷⁶ 472 ± 1 | ⁷² 478 ± 0 | ⁶⁸ 479 ± 13 | ⁷⁹ 497 ± 1 | ¹⁰⁵ 1788 ± 41 | ¹⁰⁶ 1798 ± 59 | | | | |
| 96 | incode-007 | 266103 | 63524 | ¹²⁵ 818 | ¹¹⁶ 2048 ± 0 | ⁷⁵ 470 ± 1 | ⁷³ 480 ± 1 | ⁶⁷ 478 ± 13 | ⁸³ 504 ± 1 | ¹⁰⁶ 1799 ± 35 | ¹⁰⁵ 1789 ± 59 | | | | |
| 97 | innovativetechnologyltd-001 | 177232 | 335757 | ³⁹ 341 | ¹²⁰ 2048 ± 0 | ⁶⁷ 433 ± 7 | ⁶⁷ 439 ± 5 | ⁶² 445 ± 10 | ⁶⁶ 432 ± 6 | ¹⁰⁹ 1877 ± 42 | ¹¹⁰ 1924 ± 97 | | | | |
| 98 | innovativetechnologyltd-002 | 173939 | 372324 | ¹³⁹ 912 | ¹³⁰ 2048 ± 0 | ¹³⁷ 661 ± 2 | ¹⁰⁵ 573 ± 1 | ⁹⁰ 554 ± 21 | ¹⁰¹ 566 ± 2 | ¹⁰⁸ 1841 ± 50 | ¹⁰⁸ 1857 ± 59 | | | | |
| 99 | innovatrics-004 | 0 | 496988 | ¹⁷⁸ 1367 | ⁵² 1076 ± 0 | ⁵⁸ 391 ± 0 | ⁶⁹ 449 ± 1 | ⁴⁹ 383 ± 89 | ³⁷ 271 ± 1 | ¹⁸⁵ 8573 ± 274 | ¹⁸⁴ 7929 ± 244 | | | | |
| 100 | innovatrics-006 | 0 | 466269 | ¹⁶³ 1107 | ³⁴ 538 ± 0 | ¹⁸³ 820 ± 5 | ¹⁷⁷ 868 ± 4 | ¹⁵⁸ 815 ± 80 | ¹⁵¹ 726 ± 5 | ¹⁷² 5855 ± 204 | ¹⁶⁷ 5266 ± 118 | | | | |
| 101 | intellicloudai-001 | 220831 | 868246 | ¹⁰¹ 655 | ¹⁵¹ 2048 ± 0 | ⁷⁴ 468 ± 2 | ⁷⁴ 481 ± 2 | ⁶⁹ 482 ± 16 | ⁷³ 473 ± 2 | ⁶² 1056 ± 4 | ⁶⁶ 1051 ± 72 | | | | |
| 102 | intellifusion-001 | 271872 | 289387 | ¹¹³ 762 | ⁷⁹ 2048 ± 0 | ¹⁶⁹ 764 ± 38 | ¹⁴¹ 684 ± 32 | ¹¹³ 646 ± 41 | ¹³⁵ 671 ± 22 | ⁷¹ 1112 ± 28 | ⁷⁵ 1128 ± 41 | | | | |
| 103 | intellifusion-002 | 762731 | 385841 | ¹⁴⁵ 941 | ²⁰⁹ 4096 ± 0 | ²⁰⁸ 950 ± 2 | ¹⁹⁰ 942 ± 2 | ¹⁷¹ 884 ± 3 | ¹⁸² 892 ± 2 | ¹⁰² 1713 ± 57 | ¹⁰⁰ 1665 ± 87 | | | | |
| 104 | intellivision-001 | 43692 | 11649 | ⁷⁴ 74 | ¹⁷⁹ 2056 ± 0 | ³⁶ 62 ± 2 | ³⁴ 49 ± 1 | - | ³⁴ 47 ± 0 | ¹³² 2573 ± 91 | ¹³² 2544 ± 38 | | | | |
| 105 | intellivision-002 | 43692 | 14505 | ¹⁰ 81 | ¹⁷⁴ 2056 ± 0 | ⁴⁷ 322 ± 1 | ³⁸ 280 ± 1 | ¹⁵ 123 ± 88 | ³² 244 ± 0 | ¹⁹² 13525 ± 134 | ¹⁹⁰ 12782 ± 278 | | | | |
| 106 | intelresearch-001 | 353997 | 272602 | ¹⁸³ 1433 | ¹²⁷ 2048 ± 0 | ¹⁴⁹ 682 ± 4 | ¹³⁴ 671 ± 1 | ¹²⁰ 669 ± 10 | ¹³⁷ 676 ± 12 | ¹⁵² 3553 ± 57 | ¹⁵⁰ 3462 ± 161 | | | | |
| 107 | intelresearch-002 | 452850 | 86454 | ¹⁸⁰ 1420 | ¹⁰⁰ 2048 ± 0 | ¹⁵⁵ 707 ± 2 | ¹⁴⁴ 711 ± 4 | ¹³⁴ 709 ± 5 | ¹⁴² 708 ± 4 | ¹⁶² 4204 ± 91 | ¹⁶² 4153 ± 93 | | | | |
| 108 | intsyssmu-001 | 384409 | 172480 | ¹¹⁹ 789 | ¹⁰⁶ 2048 ± 0 | ¹¹⁶ 614 ± 2 | ¹¹⁶ 612 ± 2 | ¹⁰⁴ 613 ± 2 | ¹¹⁵ 613 ± 2 | ²⁰ 621 ± 8 | ²² 611 ± 31 | | | | |
| 109 | intsyssmu-002 | 765921 | 172298 | ¹¹⁶ 786 | ⁴⁸ 1024 ± 0 | ¹⁰⁹ 593 ± 1 | ¹⁰⁸ 592 ± 2 | ⁹⁹ 592 ± 1 | ¹¹⁰ 593 ± 1 | ¹³ 549 ± 25 | ¹⁵ 548 ± 29 | | | | |
| 110 | iqface-000 | 268819 | 596337 | ¹⁰³ 704 | ²²³ 4750 ± 32 | ⁸⁹ 538 ± 26 | ⁷⁵ 488 ± 1 | ⁷¹ 493 ± 1 | ⁷⁵ 487 ± 1 | ²²⁴ 636433 ± 38446 | ²²⁴ 632654 ± 85615 | | | | |
| 111 | iqface-002 | 268831 | 596337 | ¹⁰⁶ 717 | ²²⁴ 4763 ± 37 | ²²⁸ 3705 ± 11 | ²⁰² 3698 ± 7 | ¹⁸⁹ 3699 ± 11 | ²⁰² 3700 ± 11 | ²²³ 573908 ± 3063 | ²²³ 575909 ± 7068 | | | | |
| 112 | isap-001 | 99049 | 204201 | ¹ 18 | ²¹² 4096 ± 0 | ¹ 0 ± 0 | - | - | - | ⁴ 459 ± 17 | ⁶ 456 ± 11 | | | | |
| 113 | isityou-000 | 48010 | 36621 | ¹⁴ 110 | ²²⁷ 19200 ± 0 | ¹² 113 ± 5 | ⁸ 96 ± 18 | ¹⁷¹ 135 ± 68 | ¹⁰ 123 ± 41 | ²²¹ 237517 ± 1318 | ²²¹ 237374 ± 1279 | | | | |
| 114 | isystems-001 | 274621 | 639268 | ¹⁶⁰ 1091 | ⁷⁰ 2048 ± 0 | ³⁹ 291 ± 9 | ³⁵ 261 ± 6 | ³² 261 ± 15 | ³⁵ 261 ± 6 | ¹⁴ 557 ± 16 | ¹⁸ 564 ± 22 | | | | |
| 115 | isystems-002 | 358984 | 803389 | ¹⁹² 1595 | ¹²⁸ 2048 ± 0 | ¹⁸⁵ 822 ± 8 | ¹⁶² 789 ± 6 | ¹⁵¹ 787 ± 16 | ¹⁶⁴ 788 ± 7 | ³⁷ 749 ± 31 | ²⁸ 632 ± 28 | | | | |
| 116 | itmo-006 | 599187 | 96762 | ¹⁸⁸ 1489 | ¹⁹¹ 2121 ± 0 | ¹⁸⁰ 814 ± 1 | ¹⁷⁰ 807 ± 3 | ¹⁵⁷ 804 ± 6 | ¹⁷² 806 ± 3 | ²⁰⁷ 26154 ± 148 | ²⁰⁶ 26217 ± 260 | | | | |
| 117 | itmo-007 | 415979 | 245376 | ²⁰⁶ 2199 | ¹³⁴ 2048 ± 0 | ¹⁶³ 741 ± 2 | ¹⁶⁰ 769 ± 2 | ¹⁴⁹ 775 ± 26 | ¹⁵⁸ 750 ± 2 | ¹²⁹ 2551 ± 50 | ¹³¹ 2529 ± 80 | | | | |
| 118 | iws-000 | 30875 | 3063 | ⁸ 77 | ²² 512 ± 0 | ³⁴ 277 ± 5 | ²⁹ 226 ± 1 | - | ²⁸ 226 ± 4 | ⁵⁷ 999 ± 40 | ⁵⁷ 992 ± 22 | | | | |
| 119 | kakao-002 | 479406 | 33028 | ⁹³ 603 | ¹⁵⁶ 2048 ± 0 | ¹⁶⁴ 747 ± 6 | ¹⁴⁰ 681 ± 3 | ¹²² 672 ± 17 | ¹³⁸ 677 ± 3 | ¹⁰³ 1720 ± 62 | ¹⁰¹ 1715 ± 83 | | | | |
| 120 | kakao-003 | 414379 | 113944 | ¹⁹⁷ 1754 | ¹⁰⁷ 2048 ± 0 | ¹⁹⁷ 878 ± 3 | ¹⁸⁰ 879 ± 1 | ¹⁶⁸ 877 ± 2 | ¹⁷⁸ 877 ± 2 | ¹¹⁵ 2128 ± 34 | ¹¹⁷ 2134 ± 60 | | | | |
| 121 | kedacom-000 | 245292 | 37401 | ²²⁶ 23574 | ¹⁴ 292 ± 0 | ⁸¹ 506 ± 3 | ⁷⁷ 492 ± 1 | ¹ 1 ± 1 | ⁷⁸ 491 ± 2 | ²⁶ 684 ± 14 | ²⁹ 682 ± 16 | | | | |
| 122 | kneron-003 | 58366 | 1747 | ²⁴ 188 | ¹⁰⁵ 2048 ± 0 | ³⁶ 281 ± 3 | ³⁷ 276 ± 1 | - | ³⁹ 277 ± 1 | ¹⁶⁷ 5237 ± 63 | ¹⁶⁸ 5274 ± 99 | | | | |
| 123 | kneron-005 | 375374 | 13633 | ⁶⁰ 457 | ⁷⁸ 2048 ± 0 | ⁸⁶ 518 ± 2 | ⁸⁶ 514 ± 3 | ⁷⁵ 510 ± 5 | ⁸⁷ 514 ± 3 | ¹¹² 1922 ± 11 | ¹¹¹ 1926 ± 20 | | | | |
| 124 | lookman-002 | 138200 | 25410 | ²²⁴ 16518 | ³⁶ 548 ± 0 | ¹⁸ 173 ± 1 | ¹⁷ 160 ± 1 | ³ 1 ± 1 | ¹⁶ 158 ± 1 | ¹⁷ 610 ± 19 | ²³ 612 ± 22 | | | | |
| 125 | lookman-004 | 244775 | 37401 | ²²⁵ 23548 | ³⁵ 548 ± 0 | ⁸² 507 ± 5 | ⁷⁸ 494 ± 4 | ² 1 ± 1 | ⁷⁷ 490 ± 2 | ⁴³ 871 ± 29 | ⁴³ 878 ± 29 | | | | |
| 126 | luxand-000 | 0 | 57908 | ¹⁷⁷ 1366 | ⁵⁰ 1040 ± 0 | ⁶³ 407 ± 23 | ⁵⁶ 386 ± 14 | ⁵¹ 386 ± 29 | ⁴⁹ 344 ± 13 | ⁴² 828 ± 28 | ⁴² 828 ± 32 | | | | |
| 127 | megvii-001 | 1361523 | 16486 | ¹⁸¹ 1426 | ¹⁵⁰ 2048 ± 0 | ⁹³ 543 ± 0 | - | - | - | ¹⁶⁶ 5228 ± 32 | ¹⁶⁶ 5252 ± 60 | | | | |
| 128 | megvii-002 | 1809564 | 16491 | ²⁰⁰ 1879 | ²¹⁷ 4100 ± 0 | ¹²⁶ 644 ± 0 | - | - | - | ²¹⁴ 50630 ± 183 | ²¹³ 47591 ± 716 | | | | |
| 129 | meiya-001 | 280055 | 264913 | ⁷⁶ 507 | ¹⁵⁹ 2049 ± 0 | ¹¹⁷ 622 ± 12 | ¹⁰¹ 559 ± 7 | ⁸⁷ 541 ± 24 | ⁹⁰ 553 ± 8 | ¹⁸⁴ 8356 ± 615 | ¹⁸⁵ 8134 ± 97 | | | | |
| 130 | microfocus-001 | 104524 | 27242 | ²⁵ 190 | ⁷ 256 ± 0 | ³² 264 ± 18 | ²³ 188 ± 7 | ¹⁹ 144 ± 40 | ¹⁹ 170 ± 8 | ¹²¹⁵ ± 8 | ¹ 217 ± 10 | | | | |
| 131 | microfocus-002 | 96288 | 27362 | ²² 176 | ⁵ 256 ± 0 | ³⁰ 259 ± 18 | ²¹ 185 ± 7 | ¹⁸ 141 ± 36 | ¹⁸ 167 ± 8 | ² 337 ± 34 | ² 230 ± 25 | | | | |
| 132 | mt-000 | 372169 | 282036 | ¹⁵³ 1056 | ¹⁵⁸ 2049 ± 0 | ¹⁶¹ 724 ± 12 | ¹⁴⁶ 717 ± 2 | ¹³⁷ 717 ± 4 | ¹⁴⁶ 717 ± 2 | ¹⁰¹ 1678 ± 47 | ⁹⁸ 1614 ± 85 | | | | |

Notes

- 1 The configuration size does not capture static data included in libraries.
- 2 The library size is the combined total of all files provided in the submission lib folder. These libraries e.g. OpenCV may or may not be installed on any end user's platform natively and would not need to be installed with the algorithm.
- 3 The memory usage is the peak resident set size reported by the ps system call during template generation.
- 4 The median template creation times are measured on Intel® Xeon® CPU E5-2630 v4 @ 2.20GHz processors.
- 5 The comparison durations, in nanoseconds, are estimated using std::chrono::high_resolution_clock which on the machine in (2) counts 1ns clock ticks. Precision is somewhat worse than that however. The ± value is the median absolute deviation times 1.48 for Normal consistency.

Table 7: Summary of algorithms and properties included in this report. The red superscripts give ranking for the quantity in that column.

| ALGORITHM | | | CONFIG | LIBRARY | TEMPLATE | | | | | | COMPARISON ⁴ | |
|-----------|---------------------|-------------------|-------------------|---------------------|-------------------------|-------------------------|-----------------------------------|--------------------------|-------------------------|--------------------------------|--------------------------------|--|
| NAME | | | DATA | DATA | MEMORY | SIZE | GENERATION TIME (ms) ⁴ | | | TIME (ns) ⁵ | | |
| | (KB) ¹ | (KB) ² | (MB) ³ | (B) | MUGSHOT | ISO | PHOTOJOURN. | WILD | GENUINE | IMPOSTOR | | |
| 133 | mt-002 | 290753 | 145340 | ¹³⁰ 844 | ¹⁵⁷ 2049 ± 0 | ¹⁰¹ 573 ± 1 | ¹⁰⁷ 588 ± 4 | ⁹⁴ 571 ± 1 | ¹⁰³ 572 ± 1 | ¹⁸² 7205 ± 204 | ¹⁷⁹ 7211 ± 244 | |
| 134 | mvision-001 | 227502 | 149531 | ¹⁰⁷ 723 | ²⁵ 512 ± 0 | ¹⁵¹ 691 ± 21 | ¹²⁹ 661 ± 12 | ¹¹⁵ 657 ± 20 | ¹³² 669 ± 14 | ⁷⁴ 1123 ± 40 | ⁷⁹ 1154 ± 38 | |
| 135 | nazhiai-000 | 547484 | 16141 | ²¹³ 2716 | ¹²⁵ 2048 ± 0 | ¹⁵⁰ 683 ± 3 | ¹³⁹ 679 ± 1 | ¹²⁷ 678 ± 1 | ¹³⁹ 679 ± 1 | ¹¹⁹ 2230 ± 34 | ¹¹⁶ 2133 ± 81 | |
| 136 | netbridgetech-001 | 133108 | 205875 | ⁷⁷ 508 | ²⁰⁶ 4096 ± 0 | ⁵ 85 ± 1 | ⁷ 88 ± 0 | ¹⁰ 86 ± 3 | ⁷ 94 ± 1 | ¹⁸⁷ 9280 ± 74 | ¹⁸⁷ 9446 ± 512 | |
| 137 | netbridgetech-002 | 257687 | 49931 | ³⁷ 299 | ⁹³ 2048 ± 0 | ¹⁹⁰ 838 ± 6 | ¹⁷⁴ 843 ± 1 | ¹⁶³ 842 ± 7 | ¹⁷⁵ 849 ± 2 | ¹³⁹ 2893 ± 65 | ¹⁴³ 3050 ± 123 | |
| 138 | neurotechnology-008 | 119718 | 53462 | ¹⁰² 694 | ⁸ 256 ± 0 | ⁴⁹ 339 ± 0 | ⁴⁴ 337 ± 1 | ⁴¹ 337 ± 1 | ⁴⁷ 337 ± 1 | ⁵ 467 ± 19 | ⁹ 486 ± 26 | |
| 139 | neurotechnology-009 | 137515 | 53213 | ¹¹⁸ 789 | ⁶ 256 ± 0 | ⁵⁶ 388 ± 1 | ⁵⁵ 385 ± 1 | ⁵⁰ 385 ± 1 | ⁵⁸ 385 ± 1 | ¹¹ 513 ± 10 | ¹¹ 512 ± 16 | |
| 140 | nodeflux-002 | 774668 | 690213 | ⁶¹ 466 | ¹⁵² 2048 ± 0 | ¹⁵⁷ 708 ± 4 | ¹⁴³ 710 ± 3 | ¹³³ 705 ± 3 | ¹⁴⁴ 711 ± 3 | ¹⁴⁹ 3475 ± 62 | ¹⁴⁹ 3408 ± 143 | |
| 141 | notiontag-000 | 92753 | 406791 | ⁸¹ 525 | ³⁷ 584 ± 0 | ⁹² 548 ± 64 | ⁴³ 330 ± 20 | ³⁵ 269 ± 52 | ⁴² 302 ± 23 | ²¹² 44672 ± 269 | ²¹² 44593 ± 358 | |
| 142 | ntechlab-007 | 2509686 | 52474 | ²²¹ 5070 | ²⁰⁰ 3348 ± 0 | ¹⁷⁵ 792 ± 3 | ¹⁶³ 789 ± 1 | ¹⁵² 788 ± 2 | ¹⁶⁶ 791 ± 2 | ⁸² 1209 ± 59 | ⁸⁷ 1267 ± 65 | |
| 143 | ntechlab-008 | 1138002 | 52483 | ²¹² 2707 | ⁵⁶ 1300 ± 0 | ⁹⁸ 556 ± 1 | ⁹⁸ 550 ± 1 | ⁸⁸ 549 ± 1 | ⁹⁸ 550 ± 1 | ⁶⁹ 1095 ± 45 | ⁶⁴ 1049 ± 51 | |
| 144 | oz-001 | 303723 | 238311 | ¹⁴⁹ 1021 | ²¹⁹ 4125 ± 0 | ²²³ 1147 ± 3 | ¹⁹⁷ 1149 ± 3 | ¹⁸⁴ 1142 ± 11 | ¹⁹⁷ 1135 ± 4 | ²²⁰ 228011 ± 5455 | ²²⁰ 220746 ± 5572 | |
| 145 | paravision-004 | 556670 | 145440 | ¹⁹⁰ 1572 | ²⁰⁴ 4096 ± 0 | ¹⁸⁷ 829 ± 2 | ¹⁷³ 829 ± 1 | ¹⁶¹ 825 ± 2 | ¹⁷⁴ 829 ± 2 | ³⁶ 737 ± 31 | ³⁷ 718 ± 38 | |
| 146 | pensees-001 | 1619431 | 408932 | ²⁰² 1922 | ²²⁵ 8200 ± 0 | ²²¹ 1108 ± 3 | ¹⁹⁶ 1106 ± 3 | ¹⁸³ 1107 ± 3 | ¹⁹⁶ 1107 ± 3 | ¹⁴⁴ 3151 ± 34 | ¹⁴⁵ 3143 ± 25 | |
| 147 | pixelall-003 | 0 | 707030 | ¹³⁵ 865 | ¹⁹⁵ 2560 ± 0 | ¹⁵⁴ 699 ± 8 | ¹³³ 672 ± 6 | ¹²⁹ 678 ± 30 | ¹³³ 669 ± 4 | ⁸⁰ 1174 ± 28 | ⁷⁶ 1139 ± 68 | |
| 148 | pixelall-004 | 0 | 550919 | ⁸⁴ 529 | ¹⁹³ 2560 ± 0 | ⁷⁰ 451 ± 11 | ⁶³ 421 ± 7 | ⁶¹ 440 ± 28 | ⁶⁴ 425 ± 12 | ⁷⁶ 1139 ± 65 | ⁸³ 1186 ± 31 | |
| 149 | psl-003 | 1159643 | 1434859 | ²¹⁹ 3960 | ¹⁹⁰ 2120 ± 0 | ¹⁹⁴ 865 ± 3 | ¹⁷⁹ 879 ± 4 | ¹⁵³ 789 ± 12 | ¹⁶⁵ 790 ± 2 | ⁶¹ 1052 ± 14 | ⁶¹ 1025 ± 51 | |
| 150 | psl-005 | 774031 | 1560153 | ²⁰⁷ 2239 | ¹⁹⁹ 3144 ± 0 | ²⁰⁶ 922 ± 37 | ¹⁸⁵ 926 ± 13 | ¹⁷³ 924 ± 21 | ¹⁸⁵ 926 ± 7 | ³² 703 ± 32 | ³⁴ 708 ± 26 | |
| 151 | pxl-001 | 110116 | 78231 | ²⁰ 168 | ²⁹ 512 ± 0 | ¹⁰ 101 ± 5 | ⁵ 79 ± 3 | ⁹ 75 ± 6 | ⁵ 78 ± 3 | ¹⁷¹ 5598 ± 45 | ¹⁷⁰ 5590 ± 68 | |
| 152 | pyramid-000 | 372608 | 219883 | ¹²³ 804 | ¹⁷¹ 2056 ± 0 | ¹⁰⁴ 583 ± 2 | - | - | - | ¹⁸⁰ 7147 ± 59 | ¹⁸² 7586 ± 425 | |
| 153 | rankone-008 | 2 | 141234 | ⁶ 70 | ⁴ 165 ± 0 | ³³ 272 ± 3 | ³³ 251 ± 2 | ³¹ 253 ± 11 | ³⁴ 260 ± 7 | ³⁸ 750 ± 20 | ²⁴ 613 ± 23 | |
| 154 | rankone-009 | 0 | 107688 | ³ 41 | ¹¹ 260 ± 0 | ²¹ 179 ± 4 | ¹⁹ 163 ± 3 | ²² 172 ± 19 | ²⁰ 172 ± 8 | ³³ 710 ± 32 | ¹⁶ 552 ± 25 | |
| 155 | realnetworks-002 | 95328 | 107088 | ⁴⁰ 370 | ⁶⁷ 1848 ± 0 | ²⁹ 250 ± 2 | ³¹ 234 ± 4 | ²⁹ 234 ± 8 | ³⁰ 231 ± 3 | ⁸⁸ 1285 ± 17 | ⁸⁵ 1247 ± 42 | |
| 156 | realnetworks-003 | 95334 | 104498 | ⁴⁰ 345 | ⁶⁶ 1848 ± 0 | ²⁰ 177 ± 10 | ¹⁸ 162 ± 2 | ²⁰ 163 ± 6 | ¹⁷ 161 ± 2 | ⁹⁶ 1516 ± 29 | ⁹⁵ 1522 ± 60 | |
| 157 | remarkai-001 | 241857 | 868314 | ¹⁰⁸ 730 | ¹⁶⁵ 2052 ± 0 | ¹⁸⁸ 831 ± 6 | ¹⁶⁸ 794 ± 8 | ¹⁵⁰ 787 ± 15 | ¹⁶⁷ 793 ± 8 | ⁸⁴ 1229 ± 20 | ⁴¹ 805 ± 56 | |
| 158 | remarkai-002 | 224157 | 808777 | ⁵⁵ 443 | ⁹⁴ 2048 ± 0 | ²⁰⁹ 950 ± 6 | ¹⁹³ 968 ± 5 | ¹⁷⁶ 938 ± 24 | ¹⁹⁴ 997 ± 3 | ⁷² 1115 ± 25 | ⁶⁷ 1068 ± 54 | |
| 159 | rokid-000 | 258612 | 396624 | ¹⁶⁷ 1218 | ¹⁸⁰ 2056 ± 0 | ⁹⁴ 546 ± 3 | ⁸⁵ 514 ± 1 | ¹⁰⁰ 594 ± 15 | ⁸⁴ 511 ± 1 | ¹⁴⁸ 3457 ± 62 | ¹⁵¹ 3463 ± 77 | |
| 160 | rokid-001 | 641223 | 413733 | ¹⁵⁶ 1071 | ¹⁸⁴ 2060 ± 0 | ²⁰⁵ 911 ± 2 | ¹⁸³ 902 ± 2 | ¹⁶⁶ 858 ± 71 | ¹⁷⁶ 851 ± 1 | ¹⁴⁷ 3345 ± 50 | ¹⁴⁸ 3346 ± 149 | |
| 161 | s1-001 | 435491 | 844340 | ¹¹⁴ 772 | ¹⁸⁸ 2092 ± 0 | ¹¹² 605 ± 24 | ⁹³ 530 ± 10 | ⁸³ 523 ± 21 | ⁹⁵ 529 ± 5 | ⁹² 1428 ± 34 | ⁹¹ 1415 ± 85 | |
| 162 | saffe-001 | 85973 | 62488 | ²¹ 168 | ⁵⁵ 1280 ± 0 | ³⁵ 281 ± 1 | ¹⁴ 134 ± 1 | ¹¹ 98 ± 12 | ¹¹ 124 ± 1 | ⁸⁶ 1274 ± 19 | ⁸⁸ 1277 ± 26 | |
| 163 | saffe-002 | 260622 | 28285 | ¹³³ 855 | ¹³⁹ 2048 ± 0 | ¹⁸² 817 ± 11 | ¹⁶⁶ 794 ± 15 | ¹⁵⁴ 791 ± 31 | ¹⁷⁰ 802 ± 22 | ³⁴ 717 ± 7 | ³⁶ 714 ± 29 | |
| 164 | samtech-001 | 288082 | 219883 | ⁹⁴ 605 | ¹⁷⁶ 2056 ± 0 | ⁴¹ 294 ± 3 | - | - | - | ¹⁸³ 7694 ± 59 | ¹⁸³ 7678 ± 91 | |
| 165 | scanovate-001 | 257083 | 328532 | ⁹¹ 601 | ⁸³ 2048 ± 0 | ¹⁰² 577 ± 24 | - | - | - | ¹⁸⁹ 12054 ± 699 | ¹⁹³ 13795 ± 705 | |
| 166 | scanovate-002 | 256986 | 457227 | ¹³² 850 | ¹⁵³ 2048 ± 0 | ¹⁵² 696 ± 32 | ¹⁵⁰ 726 ± 25 | ¹³¹ 697 ± 31 | ¹⁴³ 710 ± 16 | ¹⁴² 3021 ± 38 | ¹⁴⁴ 3120 ± 163 | |
| 167 | sensetime-002 | 531783 | 7203 | ²⁰⁴ 2094 | ¹⁶⁸ 2052 ± 0 | ¹⁷⁶ 797 ± 3 | ¹⁴⁸ 718 ± 2 | ¹³⁹ 720 ± 7 | ¹⁴⁸ 717 ± 2 | ¹³⁶ 2713 ± 90 | ¹²⁴ 2301 ± 25 | |
| 168 | sensetime-003 | 787853 | 74950 | ²¹¹ 2519 | ¹⁶⁷ 2052 ± 0 | ²⁰³ 908 ± 4 | - | - | - | ¹²⁸ 2527 ± 65 | ¹⁴⁰ 3004 ± 174 | |
| 169 | sertis-000 | 265572 | 68770 | ⁵¹ 427 | ⁷⁶ 2048 ± 0 | ¹⁶⁶ 754 ± 0 | ¹⁵⁶ 755 ± 2 | ¹⁴⁶ 755 ± 2 | ¹⁵⁹ 752 ± 0 | ⁹⁵ 1497 ± 29 | ⁹⁷ 1582 ± 38 | |
| 170 | sertis-001 | 292591 | 68831 | ⁴⁶ 374 | ¹³⁵ 2048 ± 0 | ¹²⁴ 634 ± 1 | ¹²⁴ 633 ± 0 | ¹¹¹ 633 ± 1 | ¹²³ 634 ± 1 | ¹²⁵ 2449 ± 23 | ¹³⁵ 2685 ± 41 | |
| 171 | shaman-000 | 0 | 120033 | ⁷⁵ 507 | ²¹⁰ 4096 ± 0 | ¹³⁴ 653 ± 16 | ¹⁵⁸ 761 ± 76 | ¹¹² 639 ± 17 | ¹⁴⁰ 683 ± 37 | ³ 380 ± 25 | ⁴ 379 ± 31 | |
| 172 | shaman-001 | 0 | 174446 | ⁷⁵ 511 | ²⁰³ 4096 ± 0 | ⁴² 294 ± 2 | ⁴² 305 ± 9 | ⁵ 8 ± 11 | ⁴¹ 298 ± 6 | ²⁴ 635 ± 19 | ⁵ 441 ± 25 | |
| 173 | shu-002 | 731250 | 148309 | ¹³⁸ 890 | ²⁰² 4096 ± 0 | ¹⁶⁵ 751 ± 2 | ¹¹⁸ 618 ± 1 | ¹³⁸ 718 ± 8 | ¹⁴⁹ 719 ± 1 | ²²⁸ 2930763 ± 47355 | ²²⁸ 2929759 ± 39149 | |
| 174 | shu-003 | 428774 | 146940 | ⁷⁸ 511 | ¹²¹ 2048 ± 0 | ¹⁸⁴ 820 ± 6 | ¹⁶⁷ 798 ± 3 | ¹⁵⁶ 798 ± 7 | ¹⁶⁹ 799 ± 2 | ¹²⁷ 2506 ± 26 | ¹²⁹ 2512 ± 38 | |
| 175 | siat-002 | 486842 | 7738 | ²⁰⁸ 2434 | ¹⁶⁹ 2052 ± 0 | ¹⁰³ 579 ± 0 | ¹⁰⁶ 579 ± 8 | ⁹⁶ 577 ± 3 | ¹⁰⁵ 575 ± 1 | ³⁹ 769 ± 13 | ³⁸ 750 ± 13 | |
| 176 | siat-004 | 940063 | 6984 | ²¹⁸ 3860 | ²¹⁶ 4100 ± 0 | ¹⁴² 670 ± 0 | ¹³⁰ 662 ± 2 | ¹¹⁷ 663 ± 9 | ¹²⁹ 662 ± 3 | ¹⁶¹ 4013 ± 45 | ¹⁵⁷ 3782 ± 173 | |

Notes

- 1 The configuration size does not capture static data included in libraries.
- 2 The library size is the combined total of all files provided in the submission lib folder. These libraries e.g. OpenCV may or may not be installed on any end user's platform natively and would not need to be installed with the algorithm.
- 3 The memory usage is the peak resident set size reported by the ps system call during template generation.
- 4 The median template creation times are measured on Intel® Xeon® CPU E5-2630 v4 @ 2.20GHz processors.
- 5 The comparison durations, in nanoseconds, are estimated using std::chrono::high_resolution_clock which on the machine in (2) counts 1ns clock ticks. Precision is somewhat worse than that however. The ± value is the median absolute deviation times 1.48 for Normal consistency.

Table 8: Summary of algorithms and properties included in this report. The red superscripts give ranking for the quantity in that column.

| | ALGORITHM | CONFIG | LIBRARY | TEMPLATE | | | | | | | COMPARISON ⁴ | | | | | | | |
|-----|-----------------------|---------|---------|----------|------|----------|-----------|---------|-----------------------------------|-------------------|-------------------------|------------------------|------------|---------|-------------|----------------|-----------------|---------------------|
| | | | | NAME | DATA | DATA | MEMORY | SIZE | GENERATION TIME (ms) ⁴ | | | TIME (ns) ⁵ | | | | | | |
| | | | | | | | | | (KB) ¹ | (KB) ² | (MB) ³ | (B) | MUGSHOT | ISO | PHOTOJOURN. | WILD | GENUINE | IMPOSTOR |
| 177 | sjiu-001 | 347115 | 148322 | 54 | 438 | 74 | 2048 ± 0 | 129 | 650 ± 2 | 120 | 620 ± 1 | 105 | 615 ± 6 | 117 | 617 ± 1 | 227 | 2243804 ± 12751 | 227 2249915 ± 19380 |
| 178 | sjiu-002 | 446215 | 148306 | 85 | 538 | 142 | 2048 ± 0 | 189 | 835 ± 2 | 169 | 802 ± 3 | 155 | 794 ± 9 | 168 | 796 ± 1 | 226 | 2211198 ± 26052 | 226 2210428 ± 21877 |
| 179 | smilart-002 | 111826 | 87805 | 32 | 263 | 43 | 1024 ± 0 | 19 | 176 ± 16 | 9 | 112 ± 11 | 34 | 266 ± 158 | 50 | 349 ± 39 | 199 | 18784 ± 136 | 200 18795 ± 151 |
| 180 | smilart-003 | 67339 | 91670 | 27 | 192 | 20 | 512 ± 0 | 22 | 180 ± 12 | 18 | 139 ± 8 | 14 | 119 ± 22 | 13 | 136 ± 8 | 90 | 1395 ± 74 | 62 1027 ± 66 |
| 181 | staqu-000 | 879661 | 121058 | 155 | 1064 | 213 | 4096 ± 0 | 179 | 813 ± 25 | - | - | - | - | 40 | 2979 ± 31 | 141 | 3007 ± 75 | |
| 182 | starhybrid-001 | 100509 | 289356 | 131 | 845 | 98 | 2048 ± 0 | 52 | 358 ± 82 | 41 | 293 ± 22 | 36 | 298 ± 27 | 40 | 284 ± 19 | 66 | 1075 ± 51 | 69 1078 ± 53 |
| 183 | synesis-006 | 731941 | 21817 | 187 | 1472 | 218 | 4104 ± 0 | 96 | 549 ± 1 | 97 | 549 ± 0 | 98 | 588 ± 1 | 108 | 589 ± 1 | 30 | 697 ± 32 | 32 688 ± 31 |
| 184 | synesis-007 | 1442961 | 24145 | 209 | 2443 | 198 | 3080 ± 0 | 224 | 1215 ± 5 | 198 | 1196 ± 7 | 185 | 1204 ± 5 | 198 | 1202 ± 4 | 27 | 684 ± 32 | 30 686 ± 25 |
| 185 | synology-000 | 221021 | 25809 | 58 | 453 | 84 | 2048 ± 0 | 62 | 407 ± 14 | 48 | 344 ± 7 | 40 | 333 ± 17 | 51 | 349 ± 9 | 202 | 19720 ± 203 | 201 19767 ± 379 |
| 186 | synology-002 | 256713 | 25943 | 69 | 488 | 80 | 2048 ± 0 | 199 | 886 ± 4 | 181 | 879 ± 3 | 169 | 877 ± 4 | 179 | 878 ± 3 | 93 | 1466 ± 32 | 94 1496 ± 45 |
| 187 | tech5-004 | 2410272 | 118858 | 214 | 2733 | 15 | 321 ± 0 | 195 | 872 ± 2 | 184 | 926 ± 10 | 172 | 908 ± 4 | 191 | 944 ± 2 | 16 | 597 ± 13 | 19 592 ± 16 |
| 188 | tech5-005 | 1178769 | 120517 | 182 | 1426 | 24 | 512 ± 0 | 225 | 1272 ± 109 | 200 | 1239 ± 120 | 187 | 1252 ± 113 | 200 | 1289 ± 135 | 131 | 2573 ± 37 | 133 2545 ± 32 |
| 189 | tevian-004 | 863474 | 16544 | 115 | 774 | 101 | 2048 ± 0 | 80 | 506 ± 30 | 64 | 426 ± 25 | 43 | 352 ± 47 | 58 | 369 ± 24 | 6 | 474 ± 31 | 3 326 ± 20 |
| 190 | tevian-005 | 921043 | 16556 | 158 | 1083 | 136 | 2048 ± 0 | 123 | 633 ± 21 | 110 | 592 ± 15 | 101 | 600 ± 45 | 125 | 646 ± 1 | 18 | 568 ± 22 | 21 607 ± 35 |
| 191 | tiger-002 | 341638 | 178194 | 80 | 522 | 178 | 2056 ± 0 | 60 | 393 ± 20 | 54 | 378 ± 21 | 47 | 364 ± 42 | 58 | 387 ± 22 | 117 | 2135 ± 29 | 118 2137 ± 38 |
| 192 | tiger-003 | 426164 | 560292 | 105 | 708 | 172 | 2056 ± 0 | 72 | 458 ± 21 | 66 | 436 ± 21 | 56 | 421 ± 41 | 67 | 438 ± 22 | 113 | 2031 ± 35 | 113 2029 ± 38 |
| 193 | tongyi-005 | 1140701 | 138919 | 205 | 2121 | 187 | 2089 ± 0 | 17 | 165 ± 1 | - | - | - | - | - | 200 | 18924 ± 65 | 202 20158 ± 103 | |
| 194 | toshiba-002 | 813606 | 114260 | - | 61 | 1560 ± 0 | 91 | 541 ± 0 | - | - | - | - | - | 150 | 3521 ± 369 | 126 2449 ± 124 | | |
| 195 | toshiba-003 | 984125 | 114264 | 166 | 1197 | 62 | 1560 ± 0 | 90 | 540 ± 0 | 95 | 538 ± 2 | 170 | 882 ± 5 | 157 | 749 ± 4 | 124 | 2390 ± 41 | 125 2407 ± 81 |
| 196 | trueface-000 | 255123 | 796861 | 71 | 493 | 145 | 2048 ± 0 | 53 | 367 ± 8 | 49 | 356 ± 6 | 45 | 354 ± 11 | 52 | 355 ± 7 | 7 | 482 ± 13 | 14 528 ± 20 |
| 197 | trueface-001 | 255123 | 186754 | 100 | 638 | 16 | 500 ± 0 | 57 | 390 ± 1 | 50 | 358 ± 1 | 44 | 353 ± 6 | 53 | 355 ± 1 | 25 | 676 ± 26 | 17 558 ± 50 |
| 198 | tuputech-000 | 11476 | 17185 | 233 | 92 | 2048 ± 0 | 14 | 122 ± 4 | 10 | 114 ± 2 | - | - | 8 | 114 ± 3 | 204 | 23893 ± 406 | 204 25279 ± 406 | |
| 199 | ulsee-001 | 370519 | 57261 | - | 138 | 2048 ± 0 | 135 | 654 ± 2 | - | - | - | - | - | 173 | 6065 ± 94 | 173 6228 ± 77 | | |
| 200 | uluface-002 | 0 | 480761 | 159 | 1088 | 117 | 2048 ± 0 | 196 | 873 ± 42 | 171 | 825 ± 7 | 159 | 818 ± 13 | 173 | 825 ± 7 | 201 | 19207 ± 1114 | 199 18501 ± 274 |
| 201 | uluface-003 | 97357 | 529422 | 170 | 1264 | 197 | 3072 ± 0 | 213 | 965 ± 11 | 188 | 937 ± 7 | 175 | 934 ± 16 | 189 | 938 ± 6 | 206 | 26057 ± 195 | 208 26865 ± 566 |
| 202 | upc-001 | 0 | 89914 | 157 | 1077 | 51 | 1052 ± 0 | 97 | 551 ± 15 | 96 | 541 ± 5 | 86 | 539 ± 10 | 97 | 546 ± 6 | 143 | 3114 ± 44 | 146 3165 ± 97 |
| 203 | vcog-002 | 3229434 | 118946 | 216 | 3666 | 228 | 61504 ± 5 | 51 | 357 ± 25 | 39 | 289 ± 22 | 37 | 313 ± 43 | 43 | 307 ± 28 | 222 | 296154 ± 3077 | 222 296436 ± 4183 |
| 204 | vd-001 | 170262 | 44058 | 34 | 281 | 162 | 2052 ± 0 | 46 | 316 ± 6 | - | - | - | - | - | 85 | 1258 ± 38 | 78 1148 ± 109 | |
| 205 | veridas-003 | 293109 | 141587 | 64 | 469 | 110 | 2048 ± 0 | 200 | 890 ± 33 | 127 | 659 ± 16 | 108 | 628 ± 46 | 126 | 654 ± 16 | 169 | 5484 ± 42 | 180 7306 ± 410 |
| 206 | veridas-004 | 196585 | 160684 | 65 | 472 | 155 | 2048 ± 0 | 147 | 678 ± 22 | 87 | 522 ± 9 | 73 | 499 ± 29 | 89 | 520 ± 12 | 170 | 5516 ± 42 | 181 7425 ± 130 |
| 207 | via-000 | 124422 | 11151 | 146 | 964 | 131 | 2048 ± 0 | 156 | 707 ± 8 | 131 | 662 ± 1 | 129 | 682 ± 36 | 113 | 603 ± 2 | 51 | 966 ± 28 | 60 1021 ± 44 |
| 208 | via-001 | 370255 | 11151 | 196 | 1697 | 91 | 2048 ± 0 | 212 | 964 ± 3 | 187 | 934 ± 5 | 180 | 965 ± 36 | 184 | 918 ± 3 | 54 | 983 ± 31 | 56 989 ± 40 |
| 209 | videmo-000 | 139643 | 39470 | 47 | 390 | 149 | 2048 ± 0 | 16 | 142 ± 5 | 13 | 133 ± 3 | 16 | 132 ± 6 | 12 | 136 ± 4 | 51 | 513 ± 16 | 12 523 ± 38 |
| 210 | videonetics-001 | 30875 | 5963 | 4 | 61 | 17 | 512 ± 0 | 3 | 262 ± 3 | 28 | 226 ± 4 | - | - | 26 | 223 ± 4 | 78 | 1153 ± 38 | 77 1142 ± 65 |
| 211 | videonetics-002 | 121981 | 6289 | 15 | 115 | 164 | 2052 ± 0 | 37 | 282 ± 5 | 30 | 231 ± 3 | 85 | 536 ± 444 | 27 | 226 ± 0 | 83 | 1219 ± 57 | 86 1262 ± 56 |
| 212 | vigilantsolutions-007 | 255600 | 125715 | 140 | 912 | 60 | 1548 ± 0 | 79 | 493 ± 6 | 79 | 494 ± 3 | 74 | 499 ± 27 | 76 | 489 ± 3 | 41 | 803 ± 35 | 39 800 ± 40 |
| 213 | vigilantsolutions-008 | 441835 | 47824 | 122 | 802 | 59 | 1548 ± 0 | 128 | 647 ± 2 | 125 | 648 ± 1 | 114 | 652 ± 27 | 124 | 643 ± 2 | 44 | 889 ± 23 | 45 903 ± 44 |
| 214 | vion-000 | 228219 | 7533 | 73 | 498 | 163 | 2052 ± 0 | 48 | 333 ± 1 | 46 | 341 ± 1 | - | - | 46 | 337 ± 2 | 211 | 39839 ± 3561 | 207 26830 ± 2241 |
| 215 | visionbox-000 | 176501 | 190645 | 41 | 355 | 147 | 2048 ± 0 | 43 | 304 ± 7 | 34 | 252 ± 5 | 30 | 243 ± 12 | 33 | 250 ± 5 | 100 | 1648 ± 57 | 84 1192 ± 42 |
| 216 | visionbox-001 | 256869 | 190645 | 89 | 579 | 132 | 2048 ± 0 | 216 | 983 ± 7 | 186 | 933 ± 9 | 174 | 928 ± 20 | 186 | 932 ± 7 | 79 | 1161 ± 22 | 80 1154 ± 20 |
| 217 | visionlabs-008 | 706099 | 19705 | 57 | 446 | 26 | 512 ± 0 | 73 | 467 ± 1 | 65 | 434 ± 1 | 59 | 431 ± 10 | 65 | 431 ± 1 | 48 | 955 ± 23 | 49 962 ± 25 |
| 218 | visionlabs-009 | 706099 | 19862 | 56 | 444 | 31 | 513 ± 0 | 85 | 515 ± 41 | 81 | 498 ± 51 | 66 | 475 ± 40 | 80 | 497 ± 54 | 49 | 957 ± 28 | 51 965 ± 32 |
| 219 | visteam-000 | 32729 | 17740 | 11 | 83 | 58 | 1536 ± 0 | 79 | 67 ± 7 | 23 | 38 ± 4 | 7 | 27 ± 10 | 2 | 36 ± 4 | 176 | 6361 ± 87 | 176 6668 ± 277 |
| 220 | vocord-007 | 587489 | 344995 | 176 | 1352 | 64 | 1664 ± 0 | 172 | 780 ± 2 | 159 | 768 ± 2 | 147 | 765 ± 3 | 162 | 767 ± 2 | 133 | 2593 ± 83 | 130 2526 ± 59 |

Notes

- 1 The configuration size does not capture static data included in libraries.
- 2 The library size is the combined total of all files provided in the submission lib folder. These libraries e.g. OpenCV may or may not be installed on any end user's platform natively and would not need to be installed with the algorithm.
- 3 The memory usage is the peak resident set size reported by the ps system call during template generation.
- 4 The median template creation times are measured on Intel® Xeon® CPU E5-2630 v4 @ 2.20GHz processors.
- 5 The comparison durations, in nanoseconds, are estimated using std::chrono::high_resolution_clock which on the machine in (2) counts 1ns clock ticks. Precision is somewhat worse than that however. The ± value is the median absolute deviation times 1.48 for Normal consistency.

| | ALGORITHM | CONFIG | LIBRARY | TEMPLATE | | | | | | | COMPARISON ⁴ | | | | | | |
|-----|----------------|---------|---------|---------------------|-------------------------|-------------------------|-------------------------|-------------------------|-----------------------------------|---------------------------|---------------------------|------------------------|---------|-----|-------------|------|---------|
| | | | | NAME | DATA | DATA | MEMORY | SIZE | GENERATION TIME (ms) ⁴ | | | TIME (ns) ⁵ | | | | | |
| | | | | | | | | | (KB) ¹ | (KB) ² | (MB) ³ | (B) | MUGSHOT | ISO | PHOTOJOURN. | WILD | GENUINE |
| 221 | vocord-008 | 603867 | 345047 | ¹⁸⁹ 1559 | ¹⁹⁶ 2688 ± 0 | ²¹¹ 962 ± 2 | ¹⁹¹ 952 ± 2 | ¹⁷⁸ 949 ± 4 | ¹⁹² 953 ± 2 | ¹⁴¹ 3015 ± 50 | ¹³⁹ 2988 ± 62 | | | | | | |
| 222 | winsense-000 | 270819 | 32034 | ¹²⁷ 833 | ⁵³ 1280 ± 0 | ³⁸ 283 ± 1 | ³⁶ 262 ± 1 | ³³ 262 ± 4 | ³⁶ 265 ± 1 | ⁹⁷ 1551 ± 31 | ⁹⁶ 1532 ± 42 | | | | | | |
| 223 | winsense-001 | 264428 | 32035 | ¹⁴³ 922 | ⁵⁴ 1280 ± 0 | ¹⁷⁰ 766 ± 7 | ¹⁵¹ 729 ± 4 | ¹⁴¹ 726 ± 9 | ¹⁵² 727 ± 4 | ⁹⁹ 1631 ± 28 | ¹¹² 1964 ± 171 | | | | | | |
| 224 | xforwardai-000 | 242457 | 175556 | ¹⁷⁹ 1392 | ⁶⁹ 2048 ± 0 | ¹⁶⁷ 757 ± 6 | ¹⁵⁵ 753 ± 6 | ¹⁴⁵ 752 ± 1 | ¹⁵⁶ 747 ± 1 | ⁸¹ 1185 ± 44 | ⁸² 1157 ± 44 | | | | | | |
| 225 | yisheng-004 | 486351 | 38653 | ¹⁷³ 1279 | ²⁰¹ 3704 ± 0 | ⁵⁴ 378 ± 12 | ⁵³ 375 ± 14 | ⁴² 352 ± 16 | ⁵⁴ 367 ± 13 | ²⁹ 693 ± 137 | ¹³ 526 ± 34 | | | | | | |
| 226 | yitu-003 | 1525719 | 138919 | ²¹⁷ 3737 | ¹⁸⁵ 2082 ± 0 | ¹⁹² 860 ± 0 | - | - | - | ¹⁹⁸ 18305 ± 71 | ¹⁹⁸ 18286 ± 62 | | | | | | |
| 227 | yoonik-000 | 290414 | 206059 | ¹²⁸ 836 | ¹²⁶ 2048 ± 0 | ²⁰⁷ 941 ± 3 | ¹⁸⁹ 937 ± 4 | ¹⁷⁷ 939 ± 3 | ¹⁹⁰ 938 ± 2 | ⁷³ 1116 ± 34 | ⁷⁴ 1113 ± 54 | | | | | | |
| 228 | yuan-000 | 370472 | 331437 | ¹⁹³ 1605 | ¹³³ 2048 ± 0 | ²²² 1112 ± 6 | ¹⁹⁵ 1105 ± 3 | ¹⁸² 1106 ± 3 | ¹⁹⁵ 1106 ± 2 | ¹³⁸ 2777 ± 44 | ¹³⁸ 2937 ± 87 | | | | | | |

Notes

- 1 The configuration size does not capture static data included in libraries.
- 2 The library size is the combined total of all files provided in the submission lib folder. These libraries e.g. OpenCV may or may not be installed on any end user's platform natively and would not need to be installed with the algorithm.
- 4 The memory usage is the peak resident set size reported by the ps system call during template generation.
- 5 The median template creation times are measured on Intel® Xeon® CPU E5-2630 v4 @ 2.20GHz processors.
- 6 The comparison durations, in nanoseconds, are estimated using std::chrono::high_resolution_clock which on the machine in (2) counts 1ns clock ticks. Precision is somewhat worse than that however. The ± value is the median absolute deviation times 1.48 for Normal consistency.

Table 10: Summary of algorithms and properties included in this report. The red superscripts give ranking for the quantity in that column.

FNMR(T)

"False non-match rate"

FMR(T)

"False match rate"

| Algorithm | | FALSE NON-MATCH RATE (FNMR) | | | | | | | | | | | | | | | | | |
|-----------|--------------------|-----------------------------|-------|---------|---------------|-------------|--------|--------|--------|----------|-----|--------|-----|-----------------------------|-----|--------|-----|--------|----|
| | | CONSTRAINED, COOPERATIVE | | | | | | | | | | | | LESS CONSTRAINED, NON-COOP. | | | | | |
| Name | | ViSAMC | VISA | MUGSHOT | MUGSHOT12+YRS | VISA BORDER | BORDER | BORDER | WILD | CHILDEXP | | | | | | | | | |
| FMR | | 0.0001 | 1E-06 | 1E-05 | 1E-05 | 1E-06 | 1E-06 | 1E-05 | 0.0001 | 0.01 | | | | | | | | | |
| 1 | 3divi-003 | 0.0318 | 171 | 0.0588 | 169 | 0.0389 | 172 | 0.0639 | 170 | 0.0619 | 167 | 0.0928 | 127 | 0.0555 | 152 | 0.0867 | 166 | 0.5365 | 31 |
| 2 | 3divi-004 | 0.0095 | 78 | 0.0153 | 80 | 0.0097 | 91 | 0.0145 | 89 | 0.0175 | 90 | 0.0330 | 81 | 0.0242 | 106 | 0.0665 | 157 | 0.5025 | 24 |
| 3 | acer-000 | 0.1393 | 196 | 0.9075 | 223 | 0.9981 | 225 | - | | 1.0000 | 218 | 1.0000 | 211 | 0.9998 | 214 | 0.9841 | 220 | - | |
| 4 | acer-001 | 0.0294 | 166 | 0.0504 | 164 | 0.0240 | 160 | 0.0463 | 160 | 0.0436 | 156 | 0.0622 | 117 | 0.0360 | 132 | 0.0307 | 79 | - | |
| 5 | acisw-003 | 0.9682 | 229 | 0.9971 | 229 | 0.7892 | 220 | 0.8738 | 218 | 0.8752 | 211 | 0.8275 | 194 | 0.6698 | 203 | 0.4470 | 210 | - | |
| 6 | aderia-001 | 0.1021 | 193 | 0.1757 | 190 | 0.1823 | 199 | 0.2967 | 197 | 0.1714 | 185 | 0.6357 | 176 | 0.1127 | 168 | 0.1965 | 188 | 0.7202 | 57 |
| 7 | advance-002 | 0.0089 | 71 | 0.0137 | 71 | 0.0073 | 56 | 0.0115 | 59 | 0.0400 | 149 | 0.0722 | 123 | 0.0593 | 153 | 0.0498 | 143 | - | |
| 8 | aifirst-001 | 0.0119 | 100 | 0.0170 | 92 | 0.0084 | 75 | 0.0127 | 71 | 0.0131 | 63 | 0.0212 | 49 | 0.0138 | 54 | 0.0432 | 130 | 0.4301 | 16 |
| 9 | ailabs-001 | 0.0158 | 133 | 0.0276 | 140 | 0.0192 | 149 | 0.0317 | 145 | 0.0352 | 143 | 0.0608 | 113 | 0.0434 | 140 | 0.0338 | 106 | - | |
| 10 | aimall-002 | 0.0119 | 99 | 0.0167 | 88 | 0.0224 | 154 | 0.0411 | 155 | 0.0233 | 115 | 0.0373 | 93 | 0.0235 | 103 | 0.0327 | 97 | - | |
| 11 | aimall-003 | 0.0033 | 10 | 0.0041 | 7 | 0.0033 | 11 | 0.0035 | 4 | 0.0056 | 11 | 0.0109 | 15 | 0.0087 | 19 | 0.0312 | 86 | - | |
| 12 | aiunionface-000 | 0.0104 | 85 | 0.0154 | 83 | 0.0082 | 73 | 0.0122 | 64 | 0.0141 | 67 | 0.0243 | 59 | 0.0169 | 73 | 0.0306 | 77 | - | |
| 13 | alchera-000 | 0.0165 | 136 | 0.0243 | 128 | 0.0125 | 121 | 0.0186 | 114 | 0.0204 | 105 | 0.0349 | 88 | 0.0243 | 108 | 0.0370 | 116 | - | |
| 14 | alchera-001 | 0.0183 | 142 | 0.0299 | 142 | 0.0142 | 129 | 0.0234 | 128 | 0.0239 | 120 | 0.0388 | 95 | 0.0267 | 117 | 0.0372 | 117 | - | |
| 15 | alleyes-000 | 0.0058 | 38 | 0.0090 | 43 | 0.0055 | 32 | 0.0087 | 40 | 0.0068 | 17 | 0.0105 | 13 | 0.0076 | 11 | 0.0282 | 27 | - | |
| 16 | allgovision-000 | 0.0346 | 172 | 0.0527 | 166 | 0.0232 | 157 | 0.0339 | 147 | 0.0372 | 147 | 0.0620 | 116 | 0.0443 | 142 | 0.0607 | 153 | - | |
| 17 | alphaface-001 | 0.0065 | 48 | 0.0097 | 49 | 0.0039 | 18 | 0.0063 | 22 | 0.0083 | 30 | - | - | - | - | 0.0280 | 17 | - | |
| 18 | alphaface-002 | 0.0052 | 29 | 0.0075 | 29 | 0.0030 | 3 | 0.0044 | 8 | 1.0000 | 221 | 0.0115 | 18 | 0.0084 | 17 | 0.0279 | 14 | - | |
| 19 | amplifiedgroup-001 | 0.5034 | 216 | 0.5848 | 214 | 0.6973 | 215 | 0.8316 | 213 | 0.7807 | 205 | 0.7724 | 186 | 0.6354 | 200 | 0.4250 | 207 | - | |
| 20 | anke-004 | 0.0080 | 64 | 0.0154 | 82 | 0.0073 | 55 | 0.0112 | 57 | 0.0102 | 48 | 0.0178 | 41 | 0.0118 | 46 | 0.0288 | 46 | 0.3577 | 8 |
| 21 | anke-005 | 0.0070 | 55 | 0.0109 | 59 | 0.0059 | 42 | 0.0094 | 43 | 0.0105 | 49 | 0.0142 | 28 | 0.0102 | 32 | 0.0289 | 49 | 0.3337 | 6 |
| 22 | antheus-000 | 0.2564 | 203 | 0.3776 | 204 | 0.7240 | 216 | 0.8699 | 216 | 0.8899 | 212 | 0.9872 | 201 | 0.9483 | 208 | 0.7668 | 213 | 0.9233 | 78 |
| 23 | antheus-001 | 0.1311 | 194 | 0.2306 | 197 | 0.5113 | 208 | 0.6797 | 207 | 0.8748 | 210 | 0.9908 | 202 | 0.9649 | 210 | 0.7586 | 212 | - | |
| 24 | anyvision-002 | 0.0660 | 186 | 0.0898 | 181 | 0.0928 | 190 | 0.1512 | 186 | 0.0899 | 174 | 0.1191 | 139 | 0.0801 | 162 | 0.2227 | 192 | 0.6960 | 51 |
| 25 | anyvision-004 | 0.0267 | 163 | 0.0385 | 158 | 0.0258 | 163 | 0.0487 | 164 | 0.0234 | 117 | 0.0301 | 71 | 0.0191 | 88 | 0.0470 | 138 | 0.4633 | 19 |
| 26 | asusaics-000 | 0.0125 | 107 | 0.0209 | 108 | 0.0085 | 76 | 0.0134 | 79 | 0.0143 | 69 | 0.7189 | 181 | 0.0285 | 121 | 0.0295 | 61 | - | |
| 27 | asusaics-001 | 0.0125 | 108 | 0.0210 | 109 | 0.0085 | 78 | 0.0134 | 80 | 0.0143 | 70 | 0.7437 | 184 | 0.0289 | 122 | 0.0295 | 60 | - | |
| 28 | aware-004 | 0.0690 | 187 | 0.0949 | 185 | 0.0837 | 187 | 0.1436 | 185 | 0.1171 | 180 | 0.8137 | 191 | 0.1056 | 167 | 0.0516 | 145 | - | |
| 29 | aware-005 | 0.0457 | 176 | 0.0643 | 173 | 0.0603 | 181 | 0.1094 | 178 | 0.0613 | 165 | 0.1075 | 138 | 0.0491 | 147 | 0.0314 | 89 | - | |
| 30 | awiros-001 | 0.4044 | 209 | 0.4622 | 207 | 0.5530 | 209 | 0.6518 | 206 | 0.2008 | 187 | 0.1994 | 147 | 0.1386 | 172 | 0.5584 | 211 | - | |
| 31 | ayftech-001 | 0.0946 | 191 | 0.1941 | 194 | 0.2438 | 201 | 0.3625 | 198 | 0.1558 | 183 | 0.1589 | 144 | 0.0936 | 165 | 0.0785 | 162 | - | |
| 32 | ayonix-000 | 0.4351 | 212 | 0.4872 | 208 | 0.6150 | 212 | 0.7510 | 210 | 0.6557 | 201 | 0.6361 | 177 | 0.4981 | 196 | 0.3635 | 204 | 0.8434 | 69 |
| 33 | bioidtechswiss-000 | 0.0066 | 50 | 0.0082 | 38 | 0.0113 | 109 | 0.0225 | 125 | 0.0078 | 25 | 0.0139 | 26 | 0.0092 | 22 | 0.0278 | 11 | - | |
| 34 | bioidtechswiss-001 | 0.0054 | 32 | 0.0072 | 25 | 0.0069 | 52 | 0.0124 | 67 | 0.0060 | 13 | 0.0094 | 8 | 0.0065 | 5 | 0.0313 | 87 | - | |
| 35 | bm-001 | 0.7431 | 222 | 0.9494 | 226 | 0.9586 | 221 | 0.9843 | 219 | 0.9049 | 213 | 0.9021 | 198 | 0.8395 | 206 | 0.9935 | 221 | 0.8845 | 75 |
| 36 | bresee-000 | 0.8467 | 224 | 0.9472 | 224 | 0.9819 | 222 | 0.9903 | 220 | 0.9940 | 214 | 0.9919 | 203 | 0.9760 | 211 | 0.8992 | 217 | - | |
| 37 | camvi-002 | 0.0125 | 109 | 0.0221 | 116 | 0.0089 | 82 | 0.0145 | 91 | 0.0142 | 68 | 0.2650 | 155 | 0.0166 | 72 | 0.0288 | 44 | 0.5760 | 38 |
| 38 | camvi-004 | 0.0171 | 139 | 0.0316 | 146 | 0.0042 | 20 | 0.0049 | 15 | 0.0097 | 45 | 0.6636 | 178 | 0.0141 | 58 | 0.0284 | 34 | 0.5788 | 40 |
| 39 | ceiec-002 | 0.0161 | 135 | 0.0193 | 103 | 0.0122 | 118 | 0.0164 | 103 | 0.0270 | 127 | 0.0555 | 106 | 0.0472 | 145 | 0.0465 | 137 | 0.5156 | 28 |
| 40 | ceiec-003 | 0.0071 | 58 | 0.0107 | 57 | 0.0061 | 44 | 0.0079 | 33 | 0.0160 | 80 | 0.0316 | 73 | 0.0260 | 115 | 0.0308 | 83 | - | |
| 41 | chosun-000 | 0.8481 | 225 | 1.0000 | 230 | 1.0000 | 230 | - | | 1.0000 | 228 | 1.0000 | 227 | 1.0000 | 227 | 1.0000 | 229 | - | |
| 42 | chosun-001 | 0.0525 | 178 | 0.0936 | 183 | 0.0742 | 185 | 0.1263 | 182 | 0.0978 | 179 | 1.0000 | 217 | 0.9354 | 207 | 0.4446 | 209 | - | |
| 43 | chtface-002 | 0.0150 | 125 | 0.0268 | 136 | 0.0096 | 90 | 0.0140 | 85 | 0.0186 | 95 | 0.0320 | 75 | 0.0194 | 90 | 0.0306 | 78 | - | |
| 44 | chtface-003 | 0.0091 | 73 | 0.0146 | 76 | 0.0083 | 74 | 0.0128 | 73 | 0.0132 | 64 | 0.0220 | 53 | 0.0149 | 64 | 0.0301 | 71 | - | |

Table 11: FNMR is the proportion of mated comparisons below a threshold set to achieve the FMR given in the header on the fourth row. FMR is the proportion of impostor comparisons at or above that threshold. The light grey values give rank over all algorithms in that column. The pink columns use only same-sex impostors; others are selected regardless of demographics. The exception, in the green column, uses “matched-covariates” i.e. impostors of the same sex, age group, and country of birth. The second pink column includes effects of extended ageing. Missing entries for border, visa, mugshot and wild images generally mean the algorithm did not run to completion. For child exploitation, missing entries arise because NIST executes those runs only infrequently. The VISA columns compare images described in section 2.2. The MUGSHOT columns compare images described in section 2.5. The VISA-BORDER column compare images described in section 2.3 with those of section 2.4. The BORDER column compares images described in section 2.4. The WILD columns compare images described in section 2.6. The CHILD-EXPLOITATION columns compare images described in section 2.1.

| | Algorithm | FALSE NON-MATCH RATE (FNMR) | | | | | | | | | | | | LESS CONSTRAINED, NON-COOP. | | | | |
|-----|-----------------------|-----------------------------|--------|--------|---------|---------------|------------|--------|--------|--------|----------|--------|-----|-----------------------------|-----|--------|-----|-----------|
| | | CONSTRAINED, COOPERATIVE | | | | | | | | | | | | | | | | |
| | | Name | VISAMC | VISA | MUGSHOT | MUGSHOT12+YRS | VISABORDER | BORDER | BORDER | WILD | CHILDEXP | | | | | | | |
| FMR | | 0.0001 | 1E-06 | 1E-05 | 1E-05 | 1E-06 | 1E-06 | 1E-06 | 1E-05 | 0.0001 | 0.01 | | | | | | | |
| 45 | cib-000 | 0.0084 | 67 | 0.0156 | 85 | 0.0049 | 24 | 0.0051 | 17 | 0.0275 | 130 | 0.1371 | 142 | 0.0138 | 55 | 0.0294 | 59 | - |
| 46 | cib-001 | 0.0041 | 18 | 0.0061 | 19 | 0.0030 | 6 | 0.0041 | 7 | 0.0048 | 7 | 0.0578 | 108 | 0.0069 | 7 | 0.0279 | 13 | - |
| 47 | cogent-003 | 0.0091 | 72 | 0.0188 | 102 | 0.0098 | 93 | 0.0132 | 76 | 0.0187 | 96 | 0.0319 | 74 | 0.0224 | 101 | 0.0406 | 124 | - |
| 48 | cogent-004 | 0.0064 | 46 | 0.0116 | 63 | 0.0096 | 89 | 0.0134 | 81 | 0.0157 | 76 | 0.0325 | 79 | 0.0204 | 94 | 0.0379 | 119 | 0.7177 56 |
| 49 | cognitec-000 | 0.0116 | 96 | 0.0177 | 93 | 0.0118 | 114 | 0.0167 | 105 | 0.0285 | 133 | 0.9924 | 204 | 0.0435 | 141 | 0.0953 | 170 | 0.8365 68 |
| 50 | cognitec-001 | 0.0126 | 110 | 0.0185 | 100 | 0.0120 | 116 | 0.0168 | 106 | 0.0270 | 126 | 0.0554 | 105 | 0.0357 | 129 | 0.0598 | 152 | - |
| 51 | ctbcbank-000 | 0.0168 | 137 | 0.0250 | 132 | 0.0146 | 133 | 0.0224 | 124 | 0.0211 | 108 | 0.8964 | 197 | 0.3779 | 192 | 1.0000 | 228 | 0.8803 73 |
| 52 | ctbcbank-001 | 0.0155 | 128 | 0.0235 | 126 | 0.0148 | 138 | 0.0243 | 131 | 0.0207 | 106 | 0.9279 | 199 | 0.3469 | 190 | 1.0000 | 231 | - |
| 53 | cuhkee-001 | 0.0036 | 12 | 0.0045 | 10 | 0.0031 | 7 | 0.0046 | 10 | 0.0051 | 10 | 0.0095 | 10 | 0.0079 | 13 | 0.1492 | 182 | - |
| 54 | cybercore-000 | 0.0728 | 188 | 0.1110 | 188 | 0.1521 | 197 | 0.2375 | 196 | 0.1874 | 186 | 0.1907 | 146 | 0.1178 | 171 | 0.1191 | 177 | - |
| 55 | cyberextruder-001 | 0.1972 | 199 | 0.2547 | 198 | 0.4686 | 207 | 0.6387 | 205 | 0.3807 | 198 | 0.3806 | 164 | 0.2582 | 184 | 0.1747 | 185 | 0.7804 66 |
| 56 | cyberextruder-002 | 0.0811 | 189 | 0.1336 | 189 | 0.1465 | 196 | 0.2266 | 195 | 0.2086 | 189 | 1.0000 | 226 | 1.0000 | 226 | 0.1000 | 172 | 0.6105 42 |
| 57 | cyberlink-004 | 0.0074 | 63 | 0.0105 | 55 | 0.0068 | 50 | 0.0089 | 42 | 0.0094 | 42 | 0.0176 | 39 | 0.0117 | 45 | 0.0283 | 28 | - |
| 58 | cyberlink-005 | 0.0060 | 44 | 0.0092 | 45 | 0.0058 | 41 | 0.0067 | 25 | 0.0074 | 22 | 0.0146 | 32 | 0.0105 | 40 | 0.0283 | 31 | - |
| 59 | dahua-004 | 0.0045 | 23 | 0.0058 | 15 | 0.0036 | 15 | 0.0048 | 12 | 0.0051 | 8 | 0.0086 | 6 | 0.0070 | 8 | 0.0281 | 20 | - |
| 60 | dahua-005 | 0.0031 | 9 | 0.0046 | 12 | 0.0035 | 13 | 0.0049 | 16 | 0.0046 | 6 | 0.0076 | 2 | 0.0062 | 2 | 0.0277 | 9 | - |
| 61 | deepglint-001 | 0.0040 | 16 | 0.0062 | 22 | 0.0047 | 23 | 0.0067 | 24 | 0.0069 | 18 | 1.0000 | 215 | 1.0000 | 217 | 0.0278 | 10 | 0.4006 11 |
| 62 | deepglint-002 | 0.0016 | 2 | 0.0027 | 4 | 0.0032 | 9 | 0.0033 | 3 | 0.0043 | 3 | 0.0084 | 5 | 0.0077 | 12 | 0.0280 | 16 | 0.3422 7 |
| 63 | deepsea-001 | 0.0136 | 117 | 0.0215 | 112 | 0.0142 | 130 | 0.0214 | 121 | 0.0163 | 84 | 0.0250 | 60 | 0.0192 | 89 | 0.0347 | 107 | 0.5606 35 |
| 64 | dermalog-005 | 0.1526 | 198 | 0.1823 | 193 | 0.2580 | 202 | 0.4018 | 200 | - | | 0.2651 | 156 | 0.1585 | 174 | 0.0855 | 164 | 0.6842 48 |
| 65 | dermalog-006 | 0.0253 | 161 | 0.0369 | 155 | 0.0171 | 144 | 0.0283 | 139 | 0.0217 | 111 | 0.0358 | 91 | 0.0230 | 102 | 0.0623 | 155 | 0.5852 41 |
| 66 | didiglobalface-001 | 0.0055 | 34 | 0.0092 | 44 | 0.0030 | 4 | 0.0045 | 9 | 0.0088 | 35 | 0.0119 | 19 | 0.0085 | 18 | 0.0282 | 25 | 0.4270 14 |
| 67 | digitalbarriers-002 | 0.3360 | 206 | 0.3690 | 202 | 0.0877 | 189 | 0.1557 | 187 | 0.0971 | 178 | 0.0951 | 130 | 0.0497 | 148 | 0.0436 | 132 | - |
| 68 | dsk-000 | 0.1526 | 197 | 0.2169 | 195 | 0.3787 | 204 | 0.5426 | 203 | 0.3115 | 193 | 0.3089 | 160 | 0.1994 | 180 | 0.2201 | 190 | 0.7313 59 |
| 69 | einetworks-000 | 0.0099 | 80 | 0.0180 | 96 | 0.0088 | 81 | 0.0140 | 87 | 0.0130 | 61 | 0.0225 | 55 | 0.0147 | 63 | 0.0293 | 56 | - |
| 70 | eocortex-000 | 0.3485 | 207 | 0.6943 | 218 | 0.1122 | 194 | 0.1574 | 188 | 0.2155 | 190 | 0.2257 | 152 | 0.1606 | 176 | 0.2546 | 197 | - |
| 71 | ercacat-001 | 0.0036 | 13 | 0.0044 | 9 | 0.0033 | 10 | 0.0047 | 11 | 0.0106 | 50 | 0.0202 | 48 | 0.0184 | 82 | 0.0258 | 1 | - |
| 72 | paravision-003 | 0.0034 | 11 | 0.0050 | 13 | 0.0036 | 17 | 0.0052 | 19 | 0.0092 | 39 | 0.0193 | 46 | 0.0156 | 67 | 0.0278 | 12 | 0.2669 2 |
| 73 | expasoft-000 | 0.0427 | 174 | 0.0655 | 175 | 0.0239 | 159 | 0.0393 | 152 | 0.0673 | 169 | 0.8963 | 196 | 0.3832 | 193 | 0.0565 | 150 | - |
| 74 | f8-001 | 0.0249 | 160 | 0.0336 | 148 | 0.0178 | 146 | 0.0232 | 127 | 0.0303 | 138 | 0.0615 | 115 | 0.0408 | 137 | 0.0475 | 140 | 0.5272 29 |
| 75 | facesoft-000 | 0.0085 | 68 | 0.0112 | 62 | 0.0064 | 47 | 0.0107 | 52 | 0.0091 | 37 | 0.0171 | 37 | 0.0107 | 41 | 0.0275 | 5 | 0.4992 23 |
| 76 | fiberhome-nanjing-002 | 0.0217 | 151 | 0.0381 | 157 | 0.0874 | 188 | 0.1770 | 192 | 0.0271 | 128 | 0.0351 | 89 | 0.0188 | 84 | 0.0361 | 114 | - |
| 77 | fujitsulab-000 | 0.0123 | 103 | 0.0212 | 110 | 0.0091 | 83 | 0.0133 | 77 | 0.0251 | 123 | 0.4200 | 167 | 0.0360 | 131 | 0.0445 | 134 | - |
| 78 | geo-000 | 0.0543 | 180 | 0.0814 | 178 | 0.1042 | 191 | 0.1592 | 189 | 0.1637 | 184 | 0.8533 | 195 | 0.1800 | 177 | 0.1211 | 178 | - |
| 79 | glory-001 | 0.0902 | 190 | 0.1082 | 187 | 0.1642 | 198 | 0.2065 | 194 | 0.2186 | 191 | 0.2669 | 157 | 0.2089 | 181 | 0.4261 | 208 | 0.8831 74 |
| 80 | glory-002 | 0.0241 | 154 | 0.0311 | 145 | 0.0116 | 111 | 0.0151 | 95 | 0.0157 | 78 | 0.0264 | 63 | 0.0188 | 86 | 0.1265 | 179 | - |
| 81 | gorilla-005 | - | - | - | - | 0.0142 | 131 | 0.0267 | 137 | 0.0228 | 114 | 0.0358 | 90 | 0.0195 | 91 | 0.0307 | 80 | - |
| 82 | gorilla-006 | 0.0105 | 91 | 0.0152 | 79 | 0.0106 | 98 | 0.0203 | 117 | 0.0155 | 74 | 0.0218 | 52 | 0.0136 | 53 | 0.0289 | 47 | - |
| 83 | hik-001 | 0.0096 | 79 | 0.0125 | 67 | 0.0093 | 86 | 0.0164 | 102 | 0.0108 | 53 | 0.0937 | 128 | 0.0127 | 50 | 0.0271 | 2 | - |
| 84 | hr-001 | 0.0044 | 22 | 0.0072 | 27 | 0.0073 | 58 | 0.0108 | 55 | 0.0125 | 58 | 0.0228 | 57 | 0.0145 | 61 | 0.0303 | 73 | 0.5499 33 |
| 85 | hr-002 | 0.0043 | 20 | 0.0059 | 16 | 0.0054 | 28 | 0.0076 | 30 | 0.0076 | 24 | 0.5932 | 174 | 0.0093 | 23 | 0.0338 | 105 | - |
| 86 | id3-004 | 0.0198 | 147 | 0.0344 | 150 | 0.0238 | 158 | 0.0423 | 157 | 0.0289 | 134 | 0.0416 | 99 | 0.0257 | 113 | - | - | - |
| 87 | id3-005 | 0.0104 | 89 | 0.0169 | 90 | 0.0080 | 70 | 0.0133 | 78 | 0.0194 | 102 | 0.0334 | 85 | 0.0262 | 116 | 0.0713 | 159 | - |
| 88 | idemia-005 | 0.0132 | 113 | 0.0216 | 114 | 0.0121 | 117 | 0.0218 | 123 | 0.0215 | 109 | 0.0323 | 78 | 0.0188 | 85 | 0.0294 | 58 | 0.4343 17 |

Table 12: FNMR is the proportion of mated comparisons below a threshold set to achieve the FMR given in the header on the fourth row. FMR is the proportion of impostor comparisons at or above that threshold. The light grey values give rank over all algorithms in that column. The pink columns use only same-sex impostors; others are selected regardless of demographics. The exception, in the green column, uses “matched-covariates” i.e. impostors of the same sex, age group, and country of birth. The second pink column includes effects of extended ageing. Missing entries for border, visa, mugshot and wild images generally mean the algorithm did not run to completion. For child exploitation, missing entries arise because NIST executes those runs only infrequently. The VISA columns compare images described in section 2.2. The MUGSHOT columns compare images described in section 2.5. The VISA-BORDER column compare images described in section 2.3 with those of section 2.4. The BORDER column compares images described in section 2.4. The WILD columns compare images described in section 2.6. The CHILD-EXPLOITATION columns compare images described in section 2.1.

| Algorithm | FALSE NON-MATCH RATE (FNMR) | | | | | | | | | | | |
|--|-----------------------------|--------|--------|---------|---------------|------------|--------|--------|-----------------------------|----------|--------|-----|
| | CONSTRAINED, COOPERATIVE | | | | | | | | LESS CONSTRAINED, NON-COOP. | | | |
| | Name | VISAMC | VISA | MUGSHOT | MUGSHOT12+YRS | VISABORDER | BORDER | BORDER | WILD | CHILDEXP | | |
| FMR | 0.0001 | 1E-06 | 1E-05 | 1E-05 | 1E-06 | 1E-06 | 1E-06 | 1E-05 | 0.0001 | 0.01 | | |
| 89 idemia-006 | 0.0046 | 24 | 0.0062 | 23 | 0.0047 | 22 | 0.0066 | 23 | 0.0073 | 21 | 0.2882 | 159 |
| 90 iit-001 | 0.0104 | 86 | 0.0179 | 95 | 0.0099 | 94 | 0.0142 | 88 | 0.1222 | 181 | 0.2677 | 158 |
| 91 iit-002 | 0.0111 | 94 | 0.0177 | 94 | 0.0085 | 77 | 0.0140 | 86 | 0.0193 | 101 | 0.0332 | 84 |
| 92 imagus-000 | 0.0642 | 184 | 0.0882 | 179 | 0.0497 | 175 | 0.0905 | 173 | 0.0848 | 172 | 0.1026 | 135 |
| 93 imagus-001 | 0.0245 | 157 | 0.0407 | 159 | 0.0257 | 162 | 0.0497 | 166 | 0.0514 | 159 | 0.0656 | 120 |
| 94 imperial-000 | 0.0067 | 52 | 0.0108 | 58 | 0.0080 | 69 | 0.0134 | 82 | 0.0087 | 34 | 0.0581 | 110 |
| 95 imperial-002 | 0.0058 | 37 | 0.0081 | 35 | 0.0055 | 34 | 0.0085 | 35 | 0.0083 | 31 | 0.0157 | 33 |
| 96 incode-006 | 0.0156 | 129 | 0.0273 | 138 | 0.0117 | 112 | 0.0238 | 129 | 0.0202 | 104 | 0.0339 | 87 |
| 97 incode-007 | 0.0109 | 93 | 0.0155 | 84 | 0.0056 | 36 | 0.0099 | 49 | 0.0107 | 52 | 0.0168 | 36 |
| 98 innovativetechnologyltd-001 | 0.0578 | 182 | 0.0938 | 184 | 0.0501 | 176 | 0.0981 | 174 | - | - | 0.0449 | 135 |
| 99 innovativetechnologyltd-002 | 0.0451 | 175 | 0.0716 | 176 | 0.0541 | 178 | 0.1009 | 176 | 0.0506 | 158 | 0.0682 | 121 |
| 100 innovatrics-004 | 0.0194 | 145 | 0.0292 | 141 | 0.0344 | 169 | 0.0617 | 169 | 0.0562 | 162 | 0.0762 | 124 |
| 101 innovatrics-006 | 0.0058 | 40 | 0.0089 | 42 | 0.0061 | 45 | 0.0096 | 47 | 0.0096 | 44 | 0.0165 | 35 |
| 102 intellicloudai-001 | 0.0142 | 120 | 0.0234 | 124 | 0.0092 | 85 | 0.0145 | 90 | 0.0162 | 82 | 0.0371 | 92 |
| 103 intellivision-001 | 0.0072 | 59 | 0.0094 | 47 | 0.0056 | 37 | 0.0085 | 36 | 0.0111 | 55 | 0.0212 | 50 |
| 104 intellivision-002 | 0.0059 | 41 | 0.0077 | 31 | 0.0040 | 19 | 0.0074 | 27 | 0.0085 | 33 | 0.5352 | 171 |
| 105 intellivision-001 | 0.1335 | 195 | 0.2205 | 196 | 0.1090 | 193 | 0.1670 | 190 | 0.1385 | 182 | 0.1676 | 145 |
| 106 intellivision-002 | 0.1000 | 192 | 0.1775 | 191 | 0.0610 | 182 | 0.1009 | 175 | 0.0805 | 171 | 0.1074 | 137 |
| 107 intelresearch-001 | 0.0242 | 155 | 0.0595 | 171 | 0.0129 | 124 | 0.0292 | 142 | 0.0351 | 142 | 0.9993 | 208 |
| 108 intelresearch-002 | 0.0058 | 39 | 0.0082 | 37 | 0.0050 | 27 | 0.0086 | 38 | 0.0136 | 66 | 0.0434 | 100 |
| 109 intsysmsu-001 | 0.9543 | 228 | 0.9888 | 228 | 0.9923 | 223 | - | - | 0.9977 | 215 | 0.9955 | 205 |
| 110 intsysmsu-002 | 0.0130 | 111 | 0.0254 | 133 | 0.0137 | 126 | 0.0267 | 138 | 0.0160 | 79 | 0.0267 | 65 |
| 111 iqface-000 | 0.0091 | 75 | 0.0143 | 73 | 0.0075 | 62 | 0.0110 | 56 | 0.0171 | 89 | 0.2234 | 150 |
| 112 iqface-002 | 0.0057 | 36 | 0.0083 | 39 | 0.0049 | 25 | 0.0058 | 21 | 0.0093 | 40 | 1.0000 | 214 |
| 113 isap-001 | 0.5092 | 217 | 0.6588 | 216 | 0.6899 | 214 | 0.7978 | 211 | 0.7200 | 202 | 0.7253 | 182 |
| 114 isityou-000 | 0.5682 | 219 | 0.7033 | 219 | 1.0000 | 227 | - | - | 1.0000 | 222 | 1.0000 | 218 |
| 115 isystems-001 | 0.0149 | 124 | 0.0245 | 130 | 0.0138 | 128 | 0.0210 | 119 | 0.0209 | 107 | 0.0332 | 83 |
| 116 isystems-002 | 0.0118 | 97 | 0.0182 | 97 | 0.0111 | 105 | 0.0162 | 100 | 0.0166 | 86 | 0.0284 | 68 |
| 117 itmo-006 | 0.0125 | 106 | 0.0220 | 115 | 0.0149 | 139 | 0.0266 | 136 | 0.0233 | 116 | 0.0383 | 94 |
| 118 itmo-007 | 0.0080 | 65 | 0.0125 | 68 | 0.0107 | 99 | 0.0185 | 112 | 0.0167 | 87 | 0.0222 | 54 |
| 119 iws-000 | 0.4824 | 215 | 0.5801 | 213 | 0.6859 | 213 | 0.8155 | 212 | 0.8251 | 207 | 0.7756 | 187 |
| 120 kakao-002 | 0.0625 | 183 | 0.1799 | 192 | 0.0791 | 186 | 0.1381 | 184 | 0.0636 | 168 | 1.0000 | 219 |
| 121 kakao-003 | 0.0130 | 112 | 0.0185 | 101 | 0.0261 | 165 | 0.0464 | 161 | 0.0252 | 124 | 0.2380 | 154 |
| 122 kedacom-000 | 0.0055 | 33 | 0.0081 | 36 | 0.0111 | 107 | 0.0120 | 63 | 0.0415 | 151 | 0.0966 | 133 |
| 123 kneron-003 | 0.0542 | 179 | 0.0902 | 182 | 0.0346 | 170 | 0.0562 | 168 | 0.0919 | 175 | 0.1251 | 141 |
| 124 kneron-005 | 0.0157 | 131 | 0.0259 | 135 | 0.0126 | 123 | 0.0212 | 120 | 0.0406 | 150 | 0.0693 | 122 |
| 125 lookman-002 | 0.0297 | 167 | 0.0547 | 168 | 0.0339 | 168 | 0.0562 | 167 | 0.0614 | 166 | 0.0960 | 132 |
| 126 lookman-004 | 0.0074 | 61 | 0.0099 | 51 | 0.0124 | 120 | 0.0149 | 94 | 0.0430 | 155 | 0.0866 | 126 |
| 127 luxand-000 | 0.2056 | 201 | 0.2814 | 199 | 0.4053 | 205 | 0.5365 | 202 | 0.3497 | 195 | 0.3743 | 162 |
| 128 megvii-001 | 0.0157 | 132 | 0.0244 | 129 | 0.0392 | 173 | 0.0671 | 172 | 0.0168 | 88 | 0.0455 | 101 |
| 129 megvii-002 | 0.0104 | 87 | 0.0145 | 75 | 0.0225 | 155 | 0.0345 | 148 | 0.0099 | 46 | 0.0286 | 69 |
| 130 meiya-001 | 0.0171 | 138 | 0.0275 | 139 | 0.0159 | 142 | 0.0261 | 135 | 0.0311 | 139 | 0.2250 | 151 |
| 131 microfocus-001 | 0.4482 | 213 | 0.5524 | 212 | 0.7256 | 217 | 0.8416 | 214 | 0.7301 | 203 | 0.6926 | 180 |
| 132 microfocus-002 | 0.3605 | 208 | 0.5057 | 209 | 0.5783 | 210 | 0.7223 | 208 | 0.5909 | 200 | 0.5963 | 175 |

Table 13: FNMR is the proportion of mated comparisons below a threshold set to achieve the FMR given in the header on the fourth row. FMR is the proportion of impostor comparisons at or above that threshold. The light grey values give rank over all algorithms in that column. The pink columns use only same-sex impostors; others are selected regardless of demographics. The exception, in the green column, uses "matched-covariates" i.e. impostors of the same sex, age group, and country of birth. The second pink column includes effects of extended ageing. Missing entries for border, visa, mugshot and wild images generally mean the algorithm did not run to completion. For child exploitation, missing entries arise because NIST executes those runs only infrequently. The VISA columns compare images described in section 2.2. The MUGSHOT columns compare images described in section 2.5. The VISA-BORDER column compare images described in section 2.3 with those of section 2.4. The BORDER column compares images described in section 2.4. The WILD columns compare images described in section 2.6. The CHILD-EXPLOITATION columns compare images described in section 2.1.

| Algorithm | FALSE NON-MATCH RATE (FNMR) | | | | | | | | | | | | | | | | | | |
|-----------|-----------------------------|--------|-------|---------|---------------|------------|--------|--------|--------|----------|-----|--------|-----|--------|-----|--------|-----|--------|----|
| | CONSTRAINED, COOPERATIVE | | | | | | | | | | | | | | | | | | |
| | Name | VisAMC | VISA | MUGSHOT | MUGSHOT12+YRS | VisABORDER | BORDER | BORDER | WILD | CHILDEXP | | | | | | | | | |
| FMR | 0.0001 | 1E-06 | 1E-05 | 1E-05 | 1E-06 | 1E-06 | 1E-06 | 1E-05 | 0.0001 | 0.01 | | | | | | | | | |
| 133 | mt-000 | 0.0100 | 81 | 0.0170 | 91 | 0.0074 | 61 | 0.0118 | 61 | 0.0127 | 59 | 0.0197 | 47 | 0.0129 | 51 | 0.0326 | 96 | 0.3773 | 10 |
| 134 | mt-002 | 0.0064 | 47 | 0.0085 | 40 | 0.0054 | 30 | 0.0098 | 48 | 0.0070 | 20 | 0.0108 | 14 | 0.0076 | 10 | 0.0283 | 32 | - | |
| 135 | mvision-001 | 0.0191 | 144 | 0.0233 | 121 | 0.0204 | 151 | 0.0356 | 149 | 0.0198 | 103 | 0.0337 | 86 | 0.0242 | 107 | 0.0431 | 129 | - | |
| 136 | nazhiai-000 | 0.0040 | 15 | 0.0059 | 17 | 0.0036 | 14 | 0.0048 | 14 | 0.0057 | 12 | 0.0125 | 20 | 0.0083 | 16 | 0.0275 | 6 | - | |
| 137 | netbridge-tech-001 | 0.4749 | 214 | 0.6599 | 217 | 0.4438 | 206 | 0.5676 | 204 | 0.4491 | 199 | 1.0000 | 210 | 0.9541 | 209 | 0.1098 | 174 | - | |
| 138 | netbridge-tech-002 | 0.0101 | 83 | 0.0166 | 87 | 0.0077 | 66 | 0.0127 | 70 | 0.0133 | 65 | 0.8215 | 192 | 0.0523 | 150 | 0.0351 | 111 | - | |
| 139 | neurotechnology-008 | 0.0091 | 74 | 0.0184 | 99 | 0.0076 | 64 | 0.0116 | 60 | 0.0157 | 77 | 0.9973 | 206 | 0.1803 | 178 | 0.0301 | 70 | - | |
| 140 | neurotechnology-009 | 0.0049 | 25 | 0.0087 | 41 | 0.0057 | 40 | 0.0094 | 44 | 0.0079 | 27 | 1.0000 | 212 | 0.0101 | 29 | 0.0300 | 67 | - | |
| 141 | nodeflux-002 | 0.0186 | 143 | 0.0340 | 149 | 0.0261 | 164 | 0.0451 | 159 | 0.0548 | 161 | 1.0000 | 216 | 1.0000 | 218 | 0.0299 | 65 | - | |
| 142 | notiontag-000 | 0.6669 | 220 | 0.7885 | 220 | 0.3715 | 203 | 0.4978 | 201 | 0.8571 | 208 | 0.8102 | 190 | 0.6460 | 202 | 0.1807 | 186 | 0.6479 | 44 |
| 143 | ntechlab-007 | 0.0056 | 35 | 0.0076 | 30 | 0.0073 | 59 | 0.0128 | 74 | 0.0079 | 26 | 0.0144 | 30 | 0.0102 | 30 | 0.0276 | 8 | 0.3316 | 5 |
| 144 | ntechlab-008 | 0.0041 | 19 | 0.0061 | 18 | 0.0056 | 35 | 0.0108 | 53 | 0.0042 | 2 | 0.0080 | 4 | 0.0063 | 3 | 0.0289 | 52 | - | |
| 145 | oz-001 | 0.0133 | 114 | 0.0215 | 113 | 0.0109 | 103 | 0.0160 | 98 | 0.0235 | 118 | 1.0000 | 220 | 1.0000 | 221 | 0.0417 | 126 | - | |
| 146 | paravision-004 | 0.0030 | 8 | 0.0046 | 11 | 0.0030 | 5 | 0.0036 | 5 | 0.0091 | 38 | 0.0188 | 44 | 0.0173 | 77 | 0.0288 | 45 | 0.2467 | 1 |
| 147 | pensees-001 | 0.0087 | 70 | 0.0133 | 70 | 0.0071 | 54 | 0.0122 | 66 | 0.0145 | 71 | 0.0252 | 61 | 0.0195 | 93 | 0.0283 | 30 | - | |
| 148 | pixelall-003 | 0.0074 | 62 | 0.0118 | 64 | 0.0057 | 38 | 0.0079 | 32 | 0.0121 | 57 | 0.0390 | 96 | 0.0170 | 75 | 0.0285 | 40 | - | |
| 149 | pixelall-004 | 0.0040 | 17 | 0.0061 | 20 | 0.0055 | 33 | 0.0069 | 26 | 0.0100 | 47 | 0.5663 | 173 | 0.0371 | 133 | 0.0285 | 37 | - | |
| 150 | psl-003 | 0.0065 | 49 | 0.0099 | 52 | 0.0055 | 31 | 0.0075 | 28 | 1.0000 | 220 | 0.0188 | 45 | 0.0129 | 52 | 0.0296 | 63 | - | |
| 151 | psl-005 | 0.0060 | 43 | 0.0094 | 46 | 0.0034 | 12 | 0.0048 | 13 | 0.0081 | 28 | 0.0140 | 27 | 0.0103 | 36 | 0.0281 | 21 | - | |
| 152 | pxl-001 | 0.0488 | 177 | 0.0752 | 177 | 0.0586 | 180 | 0.1087 | 177 | 0.0946 | 176 | 0.1065 | 136 | 0.0625 | 155 | 0.1088 | 173 | - | |
| 153 | pyramid-000 | 0.0136 | 116 | 0.0233 | 123 | 0.0117 | 113 | 0.0192 | 116 | 0.0185 | 94 | 0.0322 | 77 | 0.0206 | 96 | 0.0304 | 74 | - | |
| 154 | rankone-008 | 0.0124 | 104 | 0.0232 | 120 | 0.0082 | 72 | 0.0107 | 51 | 0.0188 | 98 | 0.0320 | 76 | 0.0244 | 109 | 0.0420 | 127 | - | |
| 155 | rankone-009 | 0.0087 | 69 | 0.0119 | 65 | 0.0065 | 48 | 0.0086 | 39 | 0.0088 | 36 | 0.0161 | 34 | 0.0121 | 48 | 0.0323 | 92 | - | |
| 156 | realnetworks-002 | 0.0248 | 158 | 0.0358 | 152 | 0.0513 | 177 | 0.1127 | 179 | 0.0371 | 146 | 0.0614 | 114 | 0.0316 | 126 | 0.0334 | 102 | - | |
| 157 | realnetworks-003 | 0.0259 | 162 | 0.0372 | 156 | 0.0541 | 179 | 0.1208 | 181 | 0.0378 | 148 | 0.0578 | 109 | 0.0306 | 125 | 0.0335 | 103 | 0.5152 | 26 |
| 158 | remarkai-001 | 0.0144 | 121 | 0.0256 | 134 | 0.0102 | 96 | 0.0159 | 97 | 0.0162 | 83 | 0.0582 | 111 | 0.0185 | 83 | 0.0308 | 82 | - | |
| 159 | remarkai-002 | 0.0151 | 127 | 0.0197 | 104 | 0.0075 | 63 | 0.0108 | 54 | 0.0119 | 56 | 0.0187 | 43 | 0.0127 | 49 | 0.0426 | 128 | - | |
| 160 | rokid-000 | 0.0093 | 77 | 0.0145 | 74 | 0.0073 | 57 | 0.0102 | 50 | 0.0164 | 85 | 0.0280 | 67 | 0.0214 | 98 | 0.0857 | 165 | - | |
| 161 | rokid-001 | 0.0105 | 90 | 0.0162 | 86 | 0.0094 | 87 | 0.0163 | 101 | 0.0181 | 92 | 0.0276 | 66 | 0.0165 | 71 | 0.0325 | 93 | - | |
| 162 | s1-001 | 0.0314 | 170 | 0.0651 | 174 | 0.0252 | 161 | 0.0357 | 150 | 0.0444 | 157 | 0.0653 | 119 | 0.0429 | 139 | 0.8493 | 215 | - | |
| 163 | saffe-001 | 0.4339 | 211 | 0.5261 | 210 | 0.7539 | 219 | 0.8736 | 217 | 0.7977 | 206 | 0.9810 | 200 | 0.7435 | 205 | 0.3887 | 205 | 0.8973 | 76 |
| 164 | saffe-002 | 0.0119 | 101 | 0.0206 | 105 | 0.0107 | 102 | 0.0177 | 108 | 0.0244 | 121 | 0.9998 | 209 | 0.2785 | 187 | 0.0308 | 81 | - | |
| 165 | samtech-001 | 0.0197 | 146 | 0.0365 | 153 | 0.0146 | 136 | 0.0241 | 130 | 0.0238 | 119 | 0.0394 | 97 | 0.0251 | 112 | 0.0337 | 104 | - | |
| 166 | scanovate-001 | 0.0175 | 140 | 0.0331 | 147 | 0.0163 | 143 | 0.0248 | 132 | 0.2476 | 192 | 0.3801 | 163 | 0.3740 | 191 | 0.4060 | 206 | - | |
| 167 | scanovate-002 | 0.0175 | 141 | 0.0355 | 151 | 0.0146 | 134 | 0.0286 | 140 | 0.0269 | 125 | 0.0301 | 70 | 0.0178 | 79 | 0.0301 | 72 | - | |
| 168 | sensetime-002 | 0.0068 | 53 | 0.0098 | 50 | 0.0143 | 132 | - | - | 0.0278 | 132 | 0.0502 | 103 | 0.0502 | 149 | 0.9999 | 222 | 0.5309 | 30 |
| 169 | sensetime-003 | 0.0021 | 4 | 0.0027 | 3 | 0.0027 | 2 | 0.0027 | 1 | 0.0051 | 9 | 0.0100 | 11 | 0.0089 | 21 | 0.0329 | 98 | 0.3683 | 9 |
| 170 | sertis-000 | 0.0118 | 98 | 0.0208 | 106 | 0.0080 | 68 | 0.0127 | 68 | 0.0110 | 54 | 0.0176 | 40 | 0.0114 | 43 | 0.0285 | 38 | - | |
| 171 | sertis-001 | 0.0113 | 95 | 0.0182 | 98 | 0.0204 | 152 | 0.0403 | 154 | 0.0216 | 110 | 0.0763 | 125 | 0.0282 | 118 | 0.0310 | 84 | - | |
| 172 | shaman-000 | 0.9297 | 227 | 0.9774 | 227 | 0.9990 | 226 | - | - | 0.9999 | 217 | 1.0000 | 213 | 0.9999 | 216 | 0.9575 | 219 | 0.9618 | 79 |
| 173 | shaman-001 | 0.3346 | 205 | 0.4616 | 206 | 0.2368 | 200 | 0.3723 | 199 | 0.3574 | 196 | 0.3527 | 161 | 0.2304 | 183 | 0.1498 | 183 | 0.8990 | 77 |
| 174 | shu-002 | - | 6 | 0.0079 | 33 | 0.0146 | 135 | 0.0308 | 144 | 1.0000 | 219 | 0.0183 | 42 | 0.0115 | 44 | 0.0284 | 35 | - | |
| 175 | shu-003 | 0.0028 | 6 | 0.0041 | 8 | 0.0050 | 26 | 0.0088 | 41 | 0.0081 | 29 | 0.0133 | 22 | 0.0094 | 24 | 0.0283 | 33 | - | |
| 176 | siat-002 | 0.0091 | 76 | 0.0126 | 69 | 0.0109 | 104 | 0.0190 | 115 | 0.0276 | 131 | 0.0516 | 104 | 0.0464 | 144 | 0.0520 | 147 | 0.4277 | 15 |

Table 14: FNMR is the proportion of mated comparisons below a threshold set to achieve the FMR given in the header on the fourth row. FMR is the proportion of impostor comparisons at or above that threshold. The light grey values give rank over all algorithms in that column. The pink columns use only same-sex impostors; others are selected regardless of demographics. The exception, in the green column, uses “matched-covariates” i.e. impostors of the same sex, age group, and country of birth. The second pink column includes effects of extended ageing. Missing entries for border, visa, mugshot and wild images generally mean the algorithm did not run to completion. For child exploitation, missing entries arise because NIST executes those runs only infrequently. The VISA columns compare images described in section 2.2. The MUGSHOT columns compare images described in section 2.5. The VISA-BORDER column compare images described in section 2.3 with those of section 2.4. The BORDER column compares images described in section 2.4. The WILD columns compare images described in section 2.6. The CHILD-EXPLOITATION columns compare images described in section 2.1.

| | | FALSE NON-MATCH RATE (FNMR) | | | | | | | | | | | | | | | | | |
|-----|-----------------------|-----------------------------|-------|---------|---------------|------------|--------|--------|--------|-----------------------------|----------|--------|--------|--------|--------|--------|--------|--------|-----|
| | Algorithm | CONSTRAINED, COOPERATIVE | | | | | | | | LESS CONSTRAINED, NON-COOP. | | | | | | | | | |
| | Name | VISAMC | VISA | MUGSHOT | MUGSHOT12+YRS | VISABORDER | BORDER | BORDER | BORDER | WILD | CHILDEXP | | | | | | | | |
| | FMR | 0.0001 | 1E-06 | 1E-05 | 1E-05 | 1E-06 | 1E-06 | 1E-05 | 1E-05 | 0.0001 | 0.01 | | | | | | | | |
| 177 | siat-004 | 0.0067 | 51 | 0.0099 | 53 | 0.0152 | 140 | - | 0.0275 | 129 | 0.4823 | 169 | 0.4823 | 195 | 1.0000 | 223 | - | | |
| 178 | sjtu-001 | 0.0051 | 28 | 0.0080 | 34 | 0.0211 | 153 | 0.0446 | 158 | 0.0131 | 62 | 0.0175 | 38 | 0.0110 | 42 | 0.0289 | 51 | - | |
| 179 | sjtu-002 | 0.0053 | 30 | 0.0078 | 32 | 0.0138 | 127 | 0.0296 | 143 | 0.0084 | 32 | 0.0136 | 24 | 0.0095 | 26 | 0.0284 | 36 | - | |
| 180 | smilart-002 | 0.2440 | 202 | 0.3532 | 201 | - | - | - | 0.3785 | 197 | 0.4145 | 166 | 0.2611 | 186 | - | 0.6999 | 53 | | |
| 181 | smilart-003 | 0.6944 | 221 | 0.8836 | 221 | 0.0695 | 183 | 0.1193 | 180 | 0.0894 | 173 | 0.1221 | 140 | 0.0737 | 160 | 0.1190 | 176 | - | |
| 182 | staqu-000 | 0.0139 | 118 | 0.0208 | 107 | 0.0104 | 97 | 0.0145 | 92 | 0.0156 | 75 | 0.8063 | 188 | 0.1408 | 173 | 0.0332 | 101 | - | |
| 183 | starhybrid-001 | 0.0108 | 92 | 0.0138 | 72 | 0.0081 | 71 | 0.0113 | 58 | 0.0152 | 72 | 0.0265 | 64 | 0.0189 | 87 | 0.0350 | 110 | 0.5584 | 34 |
| 184 | synesis-006 | 0.0070 | 56 | 0.0096 | 48 | 0.0107 | 100 | 0.0166 | 104 | - | 0.0128 | 21 | 0.0089 | 20 | 0.0292 | 55 | - | | |
| 185 | synesis-007 | 0.0050 | 26 | 0.0073 | 28 | 0.0062 | 46 | 0.0076 | 29 | - | 0.0105 | 12 | 0.0080 | 14 | 0.0288 | 43 | - | | |
| 186 | synology-000 | 0.0149 | 123 | 0.0238 | 127 | 0.0148 | 137 | 0.0261 | 134 | 0.0221 | 112 | 0.0331 | 82 | 0.0209 | 97 | 0.0330 | 100 | - | |
| 187 | synology-002 | 0.0104 | 88 | 0.0153 | 81 | 0.0107 | 101 | 0.0184 | 111 | 0.0189 | 99 | 0.2032 | 149 | 0.0180 | 80 | 0.0312 | 85 | - | |
| 188 | tech5-004 | 0.0123 | 102 | 0.0234 | 125 | 0.0086 | 80 | 0.0162 | 99 | 0.0065 | 16 | 0.0112 | 16 | 0.0082 | 15 | 0.0281 | 23 | - | |
| 189 | tech5-005 | 0.0054 | 31 | 0.0072 | 24 | 0.0069 | 51 | 0.0122 | 65 | 0.0060 | 14 | 0.0094 | 9 | 0.0066 | 6 | 0.0349 | 109 | - | |
| 190 | tevian-004 | 0.0228 | 152 | 0.0304 | 143 | 0.0226 | 156 | 0.0478 | 162 | 0.0128 | 60 | 0.0228 | 56 | 0.0138 | 56 | 0.0394 | 122 | - | |
| 191 | tevian-005 | 0.0043 | 21 | 0.0062 | 21 | 0.0057 | 39 | 0.0085 | 37 | 0.0070 | 19 | 0.0135 | 23 | 0.0119 | 47 | 0.0300 | 69 | 0.5625 | 37 |
| 192 | tiger-002 | 0.0658 | 185 | 0.0889 | 180 | 0.1083 | 192 | 0.1766 | 191 | 0.0952 | 177 | 0.1568 | 143 | 0.0661 | 156 | 0.0512 | 144 | 0.7862 | 67 |
| 193 | tiger-003 | 0.0313 | 169 | 0.0602 | 172 | 0.0188 | 148 | 0.0359 | 151 | 0.0344 | 140 | - | - | - | - | 0.0482 | 142 | 0.5610 | 36 |
| 194 | tongyi-005 | 0.0073 | 60 | 0.0146 | 77 | 0.0187 | 147 | 0.0421 | 156 | 0.0161 | 81 | 0.0215 | 51 | 0.0149 | 65 | 0.0399 | 123 | 0.6195 | 43 |
| 195 | toshiba-002 | 0.0134 | 115 | 0.0222 | 117 | 0.0097 | 92 | 0.0154 | 96 | - | 0.0327 | 80 | 0.0158 | 68 | 0.0434 | 131 | 0.7103 | 54 | |
| 196 | toshiba-003 | 0.0125 | 105 | 0.0214 | 111 | 0.0085 | 79 | 0.0131 | 75 | - | 0.0241 | 58 | 0.0151 | 66 | 0.0282 | 24 | - | | |
| 197 | trueface-000 | 0.0249 | 159 | 0.4321 | 205 | 0.0119 | 115 | 0.0180 | 110 | 0.0297 | 137 | 0.7467 | 185 | 0.1602 | 175 | 0.0614 | 154 | - | |
| 198 | trueface-001 | 0.0204 | 149 | 0.0438 | 161 | 0.0095 | 88 | 0.0138 | 84 | 0.0154 | 73 | 0.0253 | 62 | 0.0169 | 74 | 0.0772 | 161 | - | |
| 199 | tuputech-000 | 0.3218 | 204 | 0.3696 | 203 | - | - | - | 0.3237 | 194 | 0.4304 | 168 | 0.2973 | 189 | 0.9415 | 218 | - | | |
| 200 | ulsee-001 | 0.0151 | 126 | 0.0246 | 131 | 0.0113 | 108 | 0.0185 | 113 | 0.0187 | 97 | 0.6766 | 179 | 0.0181 | 81 | 0.0316 | 90 | - | |
| 201 | uluface-002 | 0.0081 | 66 | 0.0123 | 66 | 0.0071 | 53 | 0.0095 | 46 | 0.0107 | 51 | 1.0000 | 225 | 0.0140 | 57 | 0.0444 | 133 | 0.6729 | 47 |
| 202 | uluface-003 | 0.0100 | 82 | 0.0150 | 78 | 0.0079 | 67 | 0.0128 | 72 | - | - | - | - | - | - | 0.0635 | 156 | - | |
| 203 | upc-001 | 0.0234 | 153 | 0.0519 | 165 | 0.0291 | 167 | 0.0490 | 165 | 0.0294 | 135 | 0.2316 | 153 | 0.0389 | 135 | 0.0314 | 88 | 0.4224 | 13 |
| 204 | vcog-002 | 0.7522 | 223 | 0.9033 | 222 | - | - | - | - | - | - | - | - | - | - | - | 0.7523 | 61 | |
| 205 | vd-001 | 0.0243 | 156 | 0.0452 | 162 | 0.0271 | 166 | 0.0402 | 153 | 0.0424 | 154 | - | - | - | - | 0.1389 | 181 | - | |
| 206 | veridas-003 | 0.0557 | 181 | 0.0983 | 186 | 0.0734 | 184 | 0.1267 | 183 | 0.0694 | 170 | 0.0951 | 131 | 0.0480 | 146 | 0.0299 | 64 | 0.5785 | 39 |
| 207 | veridas-004 | 0.0281 | 164 | 0.0467 | 163 | 0.0353 | 171 | 0.0643 | 171 | 0.0424 | 153 | 0.0644 | 118 | 0.0342 | 128 | 0.0291 | 53 | - | |
| 208 | via-000 | 0.0216 | 150 | 0.0365 | 154 | 0.0177 | 145 | 0.0287 | 141 | 0.0296 | 136 | 0.0572 | 107 | 0.0290 | 123 | 0.0349 | 108 | 0.7638 | 62 |
| 209 | via-001 | 0.0149 | 122 | 0.0229 | 119 | 0.0114 | 110 | 0.0177 | 109 | 0.0183 | 93 | 0.4056 | 165 | 0.0176 | 78 | 0.0373 | 118 | - | |
| 210 | videmo-000 | 0.0298 | 168 | 0.0423 | 160 | 0.0155 | 141 | 0.0260 | 133 | 0.0246 | 122 | 0.0397 | 98 | 0.0239 | 104 | 0.0541 | 149 | - | |
| 211 | videonetics-001 | 0.5483 | 218 | 0.6446 | 215 | 0.7517 | 218 | 0.8607 | 215 | 0.8664 | 209 | 0.8255 | 193 | 0.6956 | 204 | 0.2986 | 200 | 0.7297 | 58 |
| 212 | videonetics-002 | 0.4274 | 210 | 0.5329 | 211 | 0.6081 | 211 | 0.7438 | 209 | 0.7775 | 204 | 0.7297 | 183 | 0.5756 | 199 | 0.1976 | 189 | 0.7435 | 60 |
| 213 | vigilantsolutions-007 | 0.0202 | 148 | 0.0307 | 144 | 0.0136 | 125 | 0.0227 | 126 | 0.0356 | 145 | 1.0000 | 230 | 1.0000 | 230 | 0.0306 | 76 | 1.0000 | 207 |
| 214 | vigilantsolutions-008 | 0.0156 | 130 | 0.0233 | 122 | 0.0101 | 95 | 0.0147 | 93 | 0.0355 | 144 | 0.0492 | 102 | 0.0293 | 124 | 0.0285 | 41 | - | |
| 215 | vion-000 | 0.0419 | 173 | 0.0590 | 170 | 0.0422 | 174 | 0.0478 | 163 | 0.0581 | 164 | 0.0968 | 134 | 0.0847 | 163 | 0.2479 | 194 | 0.8765 | 72 |
| 216 | visionbox-000 | 0.0293 | 165 | 0.0541 | 167 | 0.0197 | 150 | 0.0339 | 146 | 0.0349 | 141 | 0.0593 | 112 | 0.0329 | 127 | 0.0476 | 141 | - | |
| 217 | visionbox-001 | 0.0159 | 134 | 0.0270 | 137 | 0.0111 | 106 | 0.0173 | 107 | 0.0190 | 100 | 0.0315 | 72 | 0.0205 | 95 | 0.0389 | 121 | - | |
| 218 | visionlabs-008 | 0.0026 | 5 | 0.0036 | 5 | 0.0031 | 8 | 0.0040 | 6 | 0.0045 | 4 | 0.0079 | 3 | 0.0064 | 4 | 0.0282 | 26 | - | |
| 219 | visionlabs-009 | 0.0018 | 3 | 0.0025 | 1 | 0.0026 | 1 | 0.0029 | 2 | 0.0035 | 1 | 0.0064 | 1 | 0.0054 | 1 | 0.0283 | 29 | - | |
| 220 | visteam-000 | 0.9200 | 226 | 0.9489 | 225 | 0.9959 | 224 | - | 0.9994 | 216 | 0.9978 | 207 | 0.9914 | 213 | 0.8783 | 216 | - | | |

Table 15: FNMR is the proportion of mated comparisons below a threshold set to achieve the FMR given in the header on the fourth row. FMR is the proportion of impostor comparisons at or above that threshold. The light grey values give rank over all algorithms in that column. The pink columns use only same-sex impostors; others are selected regardless of demographics. The exception, in the green column, uses “matched-covariates” i.e. impostors of the same sex, age group, and country of birth. The second pink column includes effects of extended ageing. Missing entries for border, visa, mugshot and wild images generally mean the algorithm did not run to completion. For child exploitation, missing entries arise because NIST executes those runs only infrequently. The VISA columns compare images described in section 2.2. The MUGSHOT columns compare images described in section 2.5. The VISA-BORDER column compare images described in section 2.3 with those of section 2.4. The BORDER column compares images described in section 2.4. The WILD columns compare images described in section 2.6. The CHILD-EXPLOITATION columns compare images described in section 2.1.

| | Algorithm | FALSE NON-MATCH RATE (FNMR) | | | | | | | | | | LESS CONSTRAINED, NON-COOP. | | | |
|-----|------------------|-----------------------------|--------|--------|---------|---------------|------------|--------|--------|--------|----------|-----------------------------|-----|--|--|
| | | CONSTRAINED, COOPERATIVE | | | | | | | | | | | | | |
| | | Name | VISAMC | VISA | MUGSHOT | MUGSHOT12+YRS | VISABORDER | BORDER | BORDER | WILD | CHILDEXP | | | | |
| | FMR | 0.0001 | 1E-06 | 1E-05 | 1E-05 | 1E-06 | 1E-06 | 1E-06 | 1E-05 | 0.0001 | 0.01 | | | | |
| 221 | vocord-007 | 0.0039 | 14 | 0.0053 | 14 | 0.0061 | 43 | 0.0094 | 45 | 0.0520 | 160 | 0.0939 | 129 | | |
| 222 | vocord-008 | 0.0029 | 7 | 0.0038 | 6 | 0.0042 | 21 | 0.0055 | 20 | 0.0045 | 5 | 0.0086 | 7 | | |
| 223 | winsense-000 | 0.0140 | 119 | 0.0228 | 118 | 0.0125 | 122 | 0.0215 | 122 | 0.0226 | 113 | 0.8091 | 189 | | |
| 224 | winsense-001 | 0.0062 | 45 | 0.0099 | 54 | 0.0092 | 84 | 0.0210 | 118 | 0.0093 | 41 | 0.0144 | 31 | | |
| 225 | x-laboratory-000 | 0.0071 | 57 | 0.0106 | 56 | 0.0123 | 119 | 0.0138 | 83 | 0.0419 | 152 | 0.5629 | 172 | | |
| 226 | x-laboratory-001 | 0.0059 | 42 | 0.0110 | 60 | 0.0054 | 29 | 0.0078 | 31 | 0.0094 | 43 | 0.0142 | 29 | | |
| 227 | xforwardai-000 | 0.0050 | 27 | 0.0072 | 26 | 0.0036 | 16 | 0.0051 | 18 | 0.0074 | 23 | 0.0136 | 25 | | |
| 228 | yisheng-004 | 0.1988 | 200 | 0.3329 | 200 | 0.1147 | 195 | 0.1849 | 193 | 0.2044 | 188 | - | - | | |
| 229 | yitu-003 | 0.0015 | 1 | 0.0026 | 2 | 0.0066 | 49 | 0.0085 | 34 | 0.0064 | 15 | 0.0114 | 17 | | |
| 230 | voonik-000 | 0.0070 | 54 | 0.0112 | 61 | 0.0074 | 60 | 0.0118 | 62 | 0.0564 | 163 | 0.2013 | 148 | | |
| 231 | yuan-000 | 0.0101 | 84 | 0.0168 | 89 | 0.0077 | 65 | 0.0127 | 69 | 0.0178 | 91 | 0.5189 | 170 | | |

Table 16: FNMR is the proportion of mated comparisons below a threshold set to achieve the FMR given in the header on the fourth row. FMR is the proportion of impostor comparisons at or above that threshold. The light grey values give rank over all algorithms in that column. The pink columns use only same-sex impostors; others are selected regardless of demographics. The exception, in the green column, uses “matched-covariates” i.e. impostors of the same sex, age group, and country of birth. The second pink column includes effects of extended ageing. Missing entries for border, visa, mugshot and wild images generally mean the algorithm did not run to completion. For child exploitation, missing entries arise because NIST executes those runs only infrequently. The VISA columns compare images described in section 2.2. The MUGSHOT columns compare images described in section 2.5. The VISA-BORDER column compare images described in section 2.3 with those of section 2.4. The BORDER column compares images described in section 2.4. The WILD columns compare images described in section 2.6. The CHILD-EXPLOITATION columns compare images described in section 2.1.

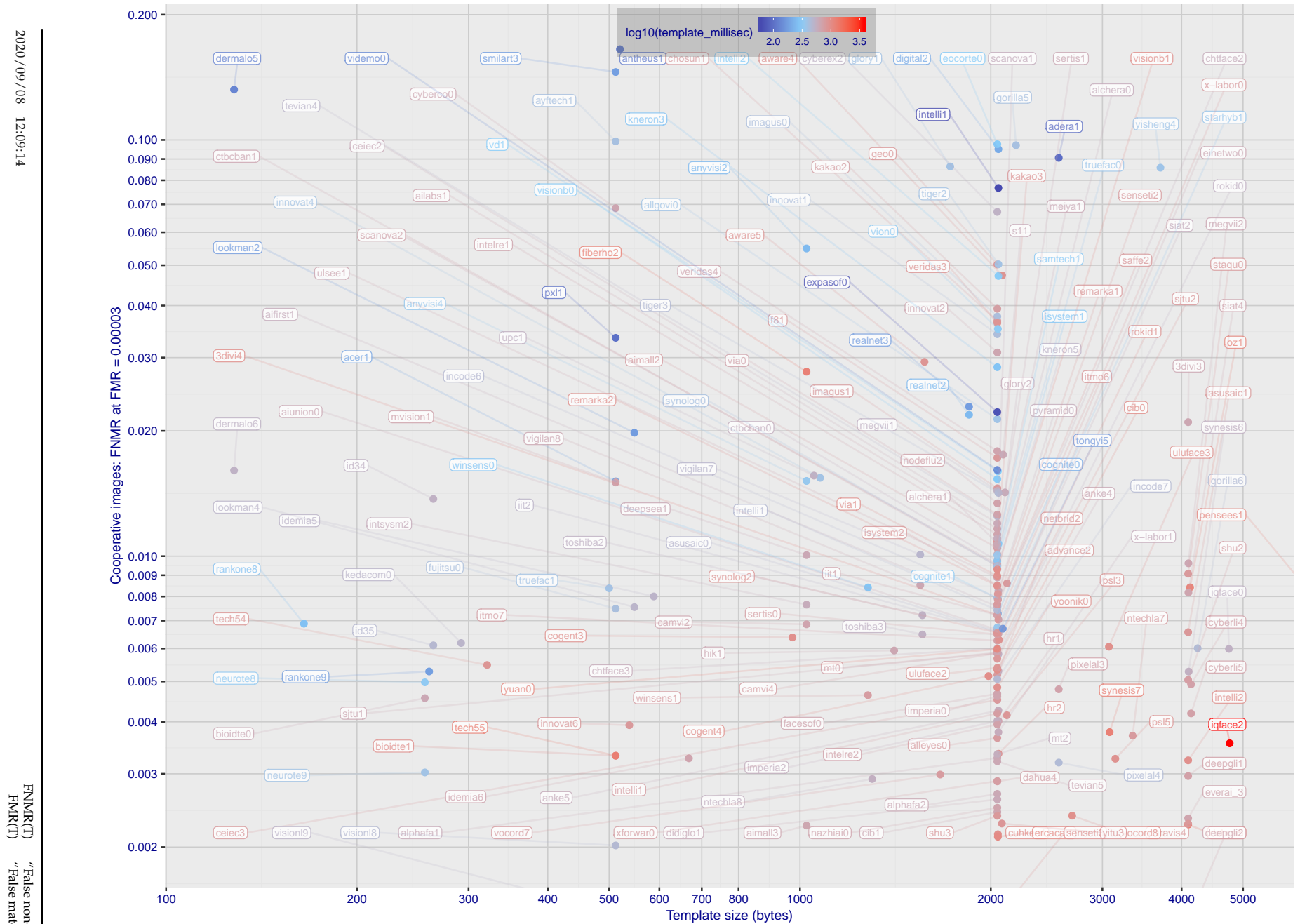


Figure 1: The points show false non-match rates (FNMR) versus the size of the encoded template. FNMR is the geometric mean of FNMR values for visa and mugshot images (from Figs. 37 and 49) at a false match rate (FMR) of 0.0001. The color of the points encodes template generation time - which spans at least one order of magnitude. Durations are measured on a single core of a c. 2016 Intel Xeon CPU E5-2630 v4 running at 2.20GHz. Algorithms with poor FNMR are omitted.

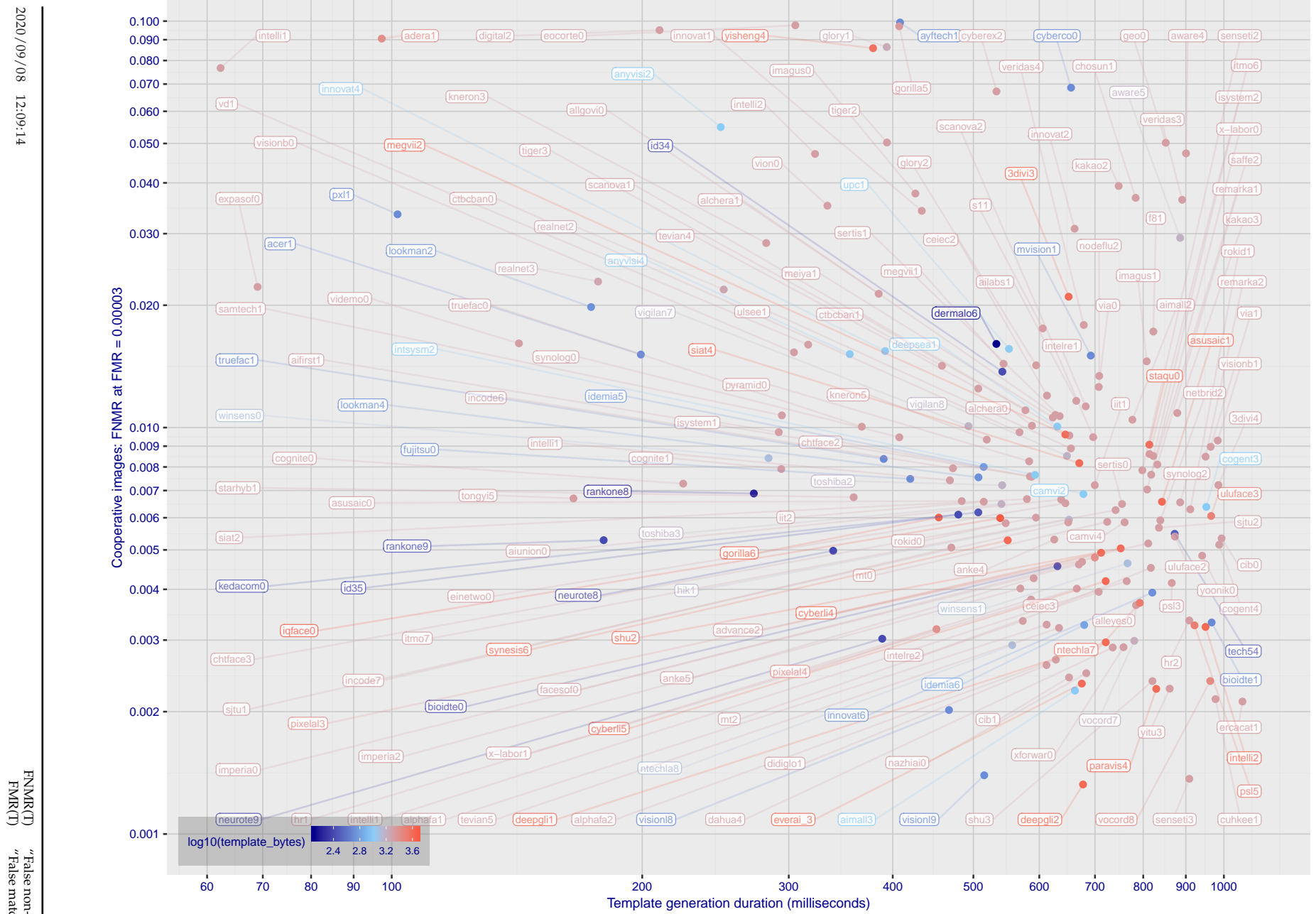


Figure 2: The points show false non-match rates (FNMR) versus the duration of the template generation operation. FNMR is the geometric mean of FNMR values for visa and mugshot images (from Figs. 37 and 49) at a false match rate (FMR) of 0.0001. Template generation time is a median estimated over 640 x 480 pixel portraits. It is measured on a single core of a c. 2016 Intel Xeon CPU E5-2630 v4 running at 2.20GHz. The color of the points encodes template size - which span two orders of magnitude. Algorithms with poor FNMR are omitted.

1 Metrics

1.1 Core accuracy

Given a vector of N genuine scores, u , the false non-match rate (FNMR) is computed as the proportion below some threshold, T:

$$\text{FNMR}(T) = 1 - \frac{1}{N} \sum_{i=1}^N H(u_i - T) \quad (1)$$

where $H(x)$ is the unit step function, and $H(0)$ taken to be 1.

Similarly, given a vector of N impostor scores, v , the false match rate (FMR) is computed as the proportion above T:

$$\text{FMR}(T) = \frac{1}{N} \sum_{i=1}^N H(v_i - T) \quad (2)$$

The threshold, T, can take on any value. We typically generate a set of thresholds from quantiles of the observed impostor scores, v , as follows. Given some interesting false match rate range, $[\text{FMR}_L, \text{FMR}_U]$, we form a vector of K thresholds corresponding to FMR measurements evenly spaced on a logarithmic scale

$$T_k = Q_v(1 - \text{FMR}_k) \quad (3)$$

where Q is the quantile function, and FMR_k comes from

$$\log_{10} \text{FMR}_k = \log_{10} \text{FMR}_L + \frac{k}{K} [\log_{10} \text{FMR}_U - \log_{10} \text{FMR}_L] \quad (4)$$

Error tradeoff characteristics are plots of FNMR(T) vs. FMR(T). These are plotted with $\text{FMR}_U \rightarrow 1$ and FMR_L as low as is sustained by the number of impostor comparisons, N. This is somewhat higher than the “rule of three” limit $3/N$ because samples are not independent, due to re-use of images.

2 Datasets

2.1 Child exploitation images

- ▷ The number of images is on the order of 10^4 .
- ▷ The number of subjects is on the order of 10^3 .
- ▷ The number of subjects with two images on the order of 10^3 .
- ▷ The images are operational. They are taken from ongoing investigations of child exploitation crimes. The images are arbitrarily unconstrained. Pose varies considerably around all three axes, including subject lying down. Resolution varies very widely. Faces can be occluded by other objects, including hair and hands. Lighting varies, although the images are intended for human viewing. Mis-focus is rare. Images are given to the algorithm without any cropping; faces may occupy widely varying areas.
- ▷ The images are usually large from contemporary cameras. The mean interocular distance (IOD) is 70 pixels.
- ▷ The images are of subjects from several countries, due to the global production of this imagery.
- ▷ The images are of children, from infancy to late adolescence.
- ▷ All of the images are live capture, none are scanned. Many have been cropped.
- ▷ When these images are input to the algorithm, they are labelled as being of type "EXPLOITATION" - see Table 4 of the FRVT API.

2.2 Visa images

- ▷ The number of images is on the order of 10^5 .
- ▷ The number of subjects is on the order of 10^5 .
- ▷ The number of subjects with two images is on the order of 10^4 .
- ▷ The images have geometry in reasonable conformance with the ISO/IEC 19794-5 Full Frontal image type. Pose is generally excellent.
- ▷ The images are of size 252x300 pixels. The mean interocular distance (IOD) is 69 pixels.
- ▷ The images are of subjects from greater than 100 countries, with significant imbalance due to visa issuance patterns.
- ▷ The images are of subjects of all ages, including children, again with imbalance due to visa issuance demand.
- ▷ Many of the images are live capture. A substantial number of the images are photographs of paper photographs.
- ▷ When these images are input to the algorithm, they are labelled as being of type "ISO" - see Table 4 of the FRVT API.

2.3 Application images

- ▷ The number of images is on the order of 10^6 .
- ▷ The number of subjects is on the order of 10^6 .
- ▷ The number of subjects with two images is on the order of 10^6 .
- ▷ The images have geometry in good conformance with the ISO/IEC 19794-5 Full Frontal image type. Pose is generally excellent.
- ▷ The images are of size 300x300 pixels. The mean interocular distance (IOD) is 61 pixels.
- ▷ The images are of subjects from greater than 100 countries, with significant imbalance due to population and immigration patterns.

- ▷ The images are of subjects of adults with imbalance due to population and immigration patterns and demand.
- ▷ All of the images are live capture.
- ▷ When these images are input to the algorithm, they are labelled as being of type "ISO" - see Table 4 of the FRVT API.

2.4 Border crossing images

- ▷ The number of images is on the order of 10^6 .
- ▷ The number of subjects is on the order of 10^6 .
- ▷ The number of subjects with two images is on the order of 10^6 .
- ▷ The images are taken with a camera oriented by an attendant toward a cooperating subject. This is done under time constraints so there are roll, pitch and yaw angle variations. Also background illumination is sometimes strong, so the face is under-exposed. There is some perspective distortion due to close range images. Some faces are partially cropped.
- ▷ The images are of subjects from greater than 100 countries, with significant imbalance due to population and immigration patterns.
- ▷ The images are of subjects of adults with imbalance due to population and immigration patterns and demand.
- ▷ The images have mean IOD of 38 pixels.
- ▷ The images are all live capture.
- ▷ When these images are input to the algorithm, they are labelled as being of type "WILD" - see Table 4 of the FRVT API.

2.5 Mugshot images

- ▷ The number of images is on the order of 10^6 .
- ▷ The number of subjects is on the order of 10^6 .
- ▷ The number of subjects with two images is on the order of 10^6 .
- ▷ The images have geometry in reasonable conformance with the ISO/IEC 19794-5 Full Frontal image type.
- ▷ The images are of variable sizes. The median IOD is 105 pixels. The mean IOD is 113 pixels. The 1-st, 5-th, 10-th, 25-th, 75-th, 90-th and 99-th percentiles are 34, 58, 70, 87, 121, 161 and 297 pixels.
- ▷ The images are of subjects from the United States.
- ▷ The images are of adults.
- ▷ The images are all live capture.
- ▷ When these images are input to the algorithm, they are labelled as being of type "mugshot" - see Table 4 of the FRVT API.

2.6 Wild images

- ▷ The number of images is on the order of 10^5 .
- ▷ The number of subjects is on the order of 10^3 .
- ▷ The number of subjects with two images on the order of 10^3 .
- ▷ The images include many photojournalism-style images. Images are given to the algorithm using a variable but generally tight crop of the head. Resolution varies very widely. The images are very unconstrained, with wide yaw and pitch pose variation. Faces can be occluded, including hair and hands.

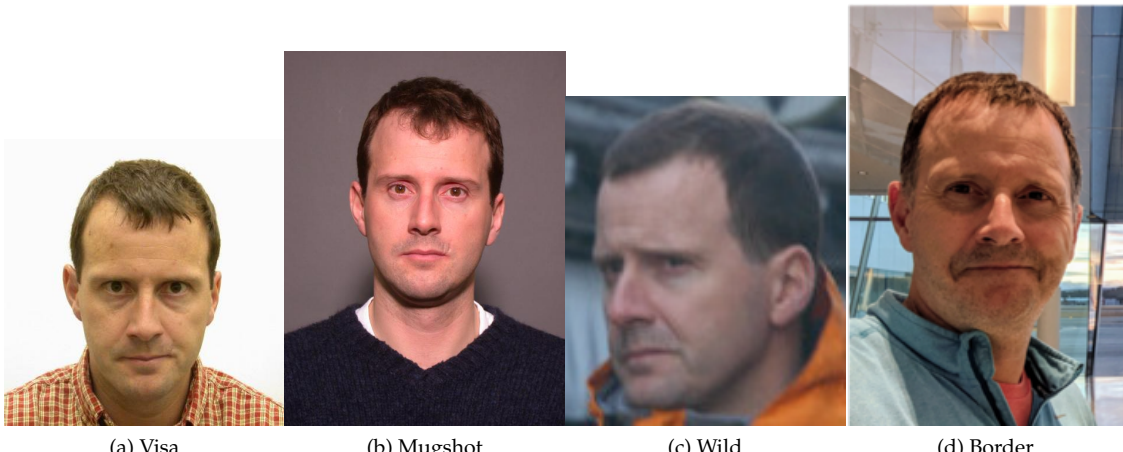


Figure 3: The figure gives simulated samples of image types used in this report.

- ▷ The images are of adults.
 - ▷ All of the images are live capture, none are scanned.
 - ▷ When these images are input to the algorithm, they are labelled as being of type "WILD" - see Table 4 of the FRVT API.

3 Results

3.1 Test goals

- ▷ To state absolute accuracy for different kinds of images, including those with and without subject cooperation.
 - ▷ To state comparative accuracy, across algorithms.

3.2 Test design

Method: For visa images:

- ▷ The comparisons are of visa photos against visa photos.
 - ▷ The number of genuine comparisons is on the order of 10^4 .
 - ▷ The number of impostor comparisons is on the order of 10^{10} .
 - ▷ The comparisons are fully zero-effort, meaning impostors are paired without attention to sex, age or other covariates. However, later analysis is conducted on subsets.
 - ▷ The number of persons is on the order of 10^5 .
 - ▷ The number of images used to make 1 template is 1.
 - ▷ The number of templates used to make each comparison score is two corresponding to simple one-to-one verification.

Method: For mugshot images:

- ▷ The comparisons are of mugshot photos against mugshot photos.

- ▷ The number of genuine comparisons is on the order of 10^6 .
- ▷ The number of impostor comparisons is on the order of 10^8 .
- ▷ The impostors are paired by sex, but not by age or other covariates.
- ▷ The number of persons is on the order of 10^6 .
- ▷ The number of images used to make 1 template is 1.
- ▷ The number of templates used to make each comparison score is two corresponding to simple one-to-one verification.

Method: For visa-border comparisons:

- ▷ The comparisons are of visa-like frontals against border crossing webcam photos.
- ▷ The number of genuine comparisons is on the order of 10^6 .
- ▷ The number of impostor comparisons is on the order of 10^8 .
- ▷ The impostors are paired by sex, but not by age or other covariates.
- ▷ The number of persons is on the order of 10^6 .
- ▷ The number of images used to make 1 template is 1.
- ▷ The number of templates used to make each comparison score is two corresponding to simple one-to-one verification.

Method: For border-border comparisons:

- ▷ The comparisons are of border crossing webcam photos.
- ▷ The number of genuine comparisons is on the order of 10^6 .
- ▷ The number of impostor comparisons is on the order of 10^8 .
- ▷ The impostors are paired by sex, but not by age or other covariates.
- ▷ The number of persons is on the order of 10^6 .
- ▷ The number of images used to make 1 template is 1.
- ▷ The number of templates used to make each comparison score is two corresponding to simple one-to-one verification.

Method: For wild images:

- ▷ The comparisons are of wild photos against wild photos.
- ▷ The number of genuine comparisons is on the order of 10^6 .
- ▷ The number of impostor comparisons is on the order of 10^7 .
- ▷ The comparisons are fully zero-effort, meaning impostors are paired without attention to sex, age or other covariates.
- ▷ The number of persons is on the order of 10^4 .
- ▷ The number of images used to make 1 template is 1.
- ▷ The number of templates used to make each comparison score is two corresponding to simple one-to-one verification.

Method: For child exploitation images:

- ▷ The comparisons are of unconstrained child exploitation photos against others of the same type.

- ▷ The number of genuine comparisons is on the order of 10^4 .
- ▷ The number of impostor comparisons is on the order of 10^7 .
- ▷ The comparisons are fully zero-effort, meaning impostors are paired without attention to sex, age or other covariates.
- ▷ The number of persons is on the order of 10^3 .
- ▷ The number of images used to make 1 template is 1.
- ▷ The number of templates used to make each comparison score is two corresponding to simple one-to-one verification.
- ▷ We produce two performance statements. First, is a DET as used for visa and mugshot images. The second is a cumulative match characteristic (CMC) summarizing a simulated one-to-many search process. This is done as follows.
 - We regard M enrollment templates as items in a gallery.
 - These M templates come from $M > N$ individuals, because multiple images of a subject are present in the gallery under separate identifiers.
 - We regard the verification templates as search templates.
 - For each search we compute the rank of the highest scoring mate.
 - This process should properly be conducted with a 1:N algorithm, such as those tested in NIST IR 8009. We use the 1:1 algorithms in a simulated 1:N mode here to a) better reflect what a child exploitation analyst does, and b) to show algorithm efficacy is better than that revealed in the verification DETs.

3.3 Failure to enroll

| | Algorithm Name | Failure to Enrol Rate ¹ | | | | | | | | | | | |
|----|--------------------|------------------------------------|--------|---------------|---------|--------|------|----------|----------|----------|----------|----------|----------|
| | | APPLICATION | BORDER | CHILD-EXPLOIT | MUGSHOT | VISA | WILD | SEC. 2.3 | SEC. 2.4 | SEC. 2.1 | SEC. 2.5 | SEC. 2.2 | SEC. 2.6 |
| 1 | 3divi-003 | 0.0001 | 192 | 0.0059 | 195 | 0.1806 | 58 | 0.0007 | 180 | 0.0006 | 175 | 0.0294 | 196 |
| 2 | 3divi-004 | 0.0001 | 191 | 0.0059 | 196 | 0.2302 | 64 | 0.0008 | 185 | 0.0006 | 177 | 0.0222 | 189 |
| 3 | acer-000 | 0.0000 | 163 | 0.0024 | 152 | - | 154 | 0.0002 | 132 | 0.0004 | 146 | 0.0008 | 125 |
| 4 | acer-001 | 0.0000 | 128 | 0.0011 | 118 | - | 231 | 0.0001 | 92 | 0.0004 | 127 | 0.0004 | 93 |
| 5 | acisw-003 | 0.0000 | 54 | 0.0000 | 41 | - | 175 | 0.0000 | 40 | 0.0000 | 43 | 0.0001 | 64 |
| 6 | ader-001 | 0.0000 | 162 | 0.0034 | 169 | 0.1928 | 60 | 0.0003 | 147 | 0.0005 | 168 | 0.0505 | 208 |
| 7 | advance-002 | 0.0000 | 89 | 0.0013 | 132 | - | 95 | 0.0000 | 81 | 0.0004 | 125 | 0.0009 | 132 |
| 8 | aifirst-001 | 0.0000 | 3 | 0.0000 | 3 | 0.0000 | 2 | 0.0000 | 3 | 0.0000 | 3 | 0.0000 | 54 |
| 9 | ailabs-001 | 0.0000 | 99 | 0.0090 | 204 | - | 123 | 0.0007 | 184 | 0.0005 | 155 | 0.0016 | 147 |
| 10 | aimall-002 | 0.0000 | 165 | 0.0043 | 179 | - | 167 | 0.0012 | 199 | 0.0005 | 166 | 0.0005 | 110 |
| 11 | aimall-003 | 0.0000 | 151 | 0.0012 | 129 | - | 187 | 0.0004 | 155 | 0.0005 | 153 | 0.0004 | 95 |
| 12 | aiunionface-000 | 0.0000 | 44 | 0.0000 | 33 | - | 161 | 0.0000 | 32 | 0.0000 | 35 | 0.0000 | 57 |
| 13 | alchera-000 | 0.0000 | 185 | 0.0041 | 178 | - | 136 | 0.0004 | 159 | 0.0014 | 207 | 0.0038 | 157 |
| 14 | alchera-001 | 0.0000 | 184 | 0.0041 | 177 | - | 124 | 0.0004 | 158 | 0.0014 | 206 | 0.0038 | 156 |
| 15 | alleyes-000 | 0.0000 | 110 | 0.0010 | 108 | - | 177 | 0.0002 | 123 | 0.0004 | 135 | 0.0004 | 101 |
| 16 | allgovision-000 | 0.0007 | 215 | 0.0062 | 197 | - | 202 | 0.0026 | 213 | 0.0052 | 224 | 0.0131 | 179 |
| 17 | alphaface-001 | 0.0000 | 105 | 0.0012 | 124 | - | 144 | 0.0000 | 84 | 0.0004 | 134 | 0.0004 | 86 |
| 18 | alphaface-002 | 0.0000 | 111 | 0.0012 | 125 | - | 178 | 0.0000 | 85 | 0.0004 | 136 | 0.0004 | 88 |
| 19 | amplifiedgroup-001 | 0.0114 | 225 | 0.1023 | 227 | - | 150 | 0.0189 | 228 | 0.0279 | 230 | 0.1390 | 223 |
| 20 | anke-004 | 0.0000 | 97 | 0.0011 | 117 | 0.0944 | 46 | 0.0001 | 107 | 0.0004 | 137 | 0.0006 | 116 |
| 21 | anke-005 | 0.0000 | 101 | 0.0012 | 126 | 0.1228 | 52 | 0.0001 | 117 | 0.0004 | 145 | 0.0007 | 119 |
| 22 | antheus-000 | 0.0000 | 70 | 0.0000 | 52 | 0.0000 | 26 | 0.0000 | 52 | 0.0000 | 57 | 0.0242 | 190 |
| 23 | antheus-001 | 0.0000 | 82 | 0.0000 | 60 | - | 229 | 0.0000 | 59 | 0.0000 | 64 | 0.0242 | 191 |
| 24 | anyvision-002 | 0.0060 | 222 | 0.0230 | 210 | 0.4866 | 78 | 0.0070 | 224 | 0.0090 | 228 | 0.1146 | 218 |
| 25 | anyvision-004 | 0.0000 | 156 | 0.0017 | 139 | 0.1660 | 55 | 0.0001 | 116 | 0.0004 | 122 | 0.0080 | 166 |
| 26 | asusaics-000 | 0.0000 | 30 | 0.0000 | 25 | - | 140 | 0.0000 | 25 | 0.0000 | 26 | 0.0000 | 21 |
| 27 | asusaics-001 | 0.0000 | 83 | 0.0000 | 61 | - | 232 | 0.0000 | 60 | 0.0000 | 65 | 0.0000 | 51 |
| 28 | aware-004 | 0.0000 | 136 | 0.0023 | 150 | - | 137 | 0.0002 | 126 | 0.0005 | 152 | 0.0014 | 144 |
| 29 | aware-005 | 0.0000 | 141 | 0.0020 | 146 | - | 163 | 0.0001 | 122 | 0.0004 | 140 | 0.0011 | 138 |
| 30 | awiros-001 | 0.0039 | 218 | 0.0369 | 219 | - | 91 | 0.0386 | 229 | 0.0872 | 231 | 0.3415 | 228 |
| 31 | ayftech-001 | 0.0002 | 204 | 0.0046 | 185 | - | 205 | 0.0043 | 218 | 0.0011 | 195 | 0.0091 | 171 |
| 32 | ayonix-000 | 0.0053 | 221 | 0.0341 | 218 | 0.0000 | 19 | 0.0113 | 226 | 0.0137 | 229 | 0.1194 | 219 |
| 33 | boidtechswiss-000 | 0.0000 | 120 | 0.0008 | 96 | - | 200 | 0.0003 | 145 | 0.0004 | 149 | 0.0006 | 111 |
| 34 | boidtechswiss-001 | 0.0000 | 86 | 0.0007 | 90 | - | 87 | 0.0000 | 69 | 0.0004 | 129 | 0.0025 | 152 |
| 35 | bm-001 | 0.0000 | 31 | 0.0000 | 26 | 0.0000 | 12 | 0.0000 | 62 | 0.0000 | 27 | 0.0000 | 22 |
| 36 | bresee-000 | 0.0000 | 98 | 0.0010 | 112 | - | 121 | 0.0002 | 130 | 0.0003 | 79 | 0.0003 | 69 |
| 37 | camvi-002 | 0.0000 | 50 | 0.0000 | 39 | 0.0000 | 20 | 0.0000 | 38 | 0.0000 | 41 | 0.0000 | 33 |
| 38 | camvi-004 | 0.0000 | 59 | 0.0000 | 65 | 0.0000 | 22 | 0.0000 | 44 | 0.0000 | 48 | 0.0000 | 39 |
| 39 | ceiec-002 | 0.0002 | 203 | 0.0056 | 192 | 0.2482 | 67 | 0.0036 | 217 | 0.0031 | 220 | 0.0081 | 167 |
| 40 | ceiec-003 | 0.0000 | 22 | 0.0013 | 133 | - | 125 | 0.0001 | 95 | 0.0004 | 131 | 0.0004 | 83 |
| 41 | chosun-000 | 0.0000 | 17 | 0.0000 | 15 | - | 115 | 0.0000 | 14 | 0.0000 | 15 | 0.0000 | 13 |
| 42 | chosun-001 | 0.0000 | 73 | 0.0000 | 54 | - | 208 | 0.0000 | 54 | 0.0000 | 59 | 0.0000 | 47 |
| 43 | chiface-002 | 0.0000 | 168 | 0.0021 | 148 | - | 149 | 0.0002 | 142 | 0.0007 | 180 | 0.0014 | 143 |
| 44 | chiface-003 | 0.0000 | 161 | 0.0018 | 141 | - | 217 | 0.0001 | 100 | 0.0006 | 174 | 0.0010 | 136 |
| 45 | cib-000 | 0.0000 | 55 | 0.0000 | 42 | - | 176 | 0.0001 | 119 | 0.0000 | 44 | 0.0000 | 35 |
| 46 | cib-001 | 0.0000 | 43 | 0.0000 | 32 | - | 158 | 0.0000 | 31 | 0.0000 | 34 | 0.0000 | 28 |
| 47 | cogent-003 | 0.0000 | 160 | 0.0018 | 142 | - | 191 | 0.0001 | 99 | 0.0004 | 118 | 0.0009 | 135 |
| 48 | cogent-004 | 0.0000 | 7 | 0.0000 | 8 | 0.0000 | 3 | 0.0000 | 7 | 0.0000 | 8 | 0.0000 | 6 |
| 49 | cognitec-000 | 0.0005 | 212 | 0.0112 | 207 | 0.6342 | 82 | 0.0007 | 181 | 0.0007 | 184 | 0.0388 | 204 |
| 50 | cognitec-001 | 0.0003 | 208 | 0.0110 | 206 | - | 166 | 0.0008 | 189 | 0.0010 | 187 | 0.0185 | 185 |
| 51 | ctcbcbank-000 | 0.0001 | 190 | 0.0051 | 188 | 0.3285 | 71 | 0.0011 | 196 | 0.0019 | 211 | 0.0868 | 216 |
| 52 | ctcbcbank-001 | 0.0000 | 169 | 0.0036 | 173 | - | 213 | 0.0005 | 172 | 0.0010 | 188 | 0.0844 | 215 |
| 53 | cuhkee-001 | 0.0000 | 100 | 0.0011 | 121 | - | 128 | 0.0000 | 65 | 0.0004 | 114 | 0.1278 | 220 |
| 54 | cybercore-000 | 0.0000 | 121 | 0.0073 | 199 | - | 201 | 0.0001 | 103 | 0.0005 | 156 | 0.0383 | 203 |
| 55 | cyberextruder-001 | 0.0029 | 217 | 0.0293 | 212 | 0.5338 | 80 | 0.0024 | 210 | 0.0029 | 218 | 0.0597 | 212 |
| 56 | cyberextruder-002 | 0.0013 | 216 | 0.0840 | 226 | 0.2672 | 70 | 0.0027 | 214 | 0.0028 | 217 | 0.0335 | 200 |
| 57 | cyberlink-004 | 0.0000 | 125 | 0.0010 | 116 | - | 222 | 0.0004 | 156 | 0.0003 | 87 | 0.0003 | 75 |
| 58 | cyberlink-005 | 0.0000 | 85 | 0.0009 | 103 | - | 86 | 0.0003 | 151 | 0.0003 | 86 | 0.0003 | 73 |

Table 17: FTE is the proportion of failed template generation attempts. Failures can occur because the software throws an exception, or because the software electively refuses to process the input image. This would typically occur if a face is not detected. FTE is measured as the number of function calls that give EITHER a non-zero error code OR that give a “small” template. This is defined as one whose size is less than 0.3 times the median template size for that algorithm. This second rule is needed because some algorithms incorrectly fail to return a non-zero error code when template generation fails.

¹The effects of FTE are included in the accuracy results of this report by regarding any template comparison involving a failed template to produce a low similarity score. Thus higher FTE results in higher FNMR and lower FMR.

| | Algorithm | Failure to Enrol Rate ¹ | | | | | | | | | | | |
|-----|-----------------------------|------------------------------------|--------|---------------|---------|--------|------|----------|----------|----------|----------|----------|----------|
| | | APPLICATION | BORDER | CHILD-EXPLOIT | MUGSHOT | VISA | WILD | SEC. 2.3 | SEC. 2.4 | SEC. 2.1 | SEC. 2.5 | SEC. 2.2 | SEC. 2.6 |
| 59 | dahua-004 | 0.0000 | 34 | 0.0009 | 106 | - | 145 | 0.0001 | 115 | 0.0003 | 72 | 0.0002 | 65 |
| 60 | dahua-005 | 0.0000 | 72 | 0.0000 | 63 | - | 207 | 0.0000 | 74 | 0.0003 | 80 | 0.0000 | 46 |
| 61 | deepglint-001 | 0.0000 | 33 | 0.0000 | 27 | 0.0000 | 13 | 0.0000 | 26 | 0.0000 | 28 | 0.0000 | 23 |
| 62 | deepglint-002 | 0.0000 | 88 | 0.0004 | 74 | 0.0669 | 40 | 0.0002 | 138 | 0.0004 | 103 | 0.0003 | 74 |
| 63 | deepsea-001 | 0.0000 | 12 | 0.0000 | 12 | 0.0000 | 6 | 0.0000 | 11 | 0.0000 | 12 | 0.0000 | 10 |
| 64 | dermalog-005 | - | 232 | 0.0031 | 161 | 0.1796 | 56 | 0.0013 | 203 | 0.0041 | 221 | 0.0163 | 183 |
| 65 | dermalog-006 | 0.0005 | 213 | 0.0031 | 162 | 0.1797 | 57 | 0.0013 | 202 | 0.0041 | 222 | 0.0163 | 184 |
| 66 | didiglobalface-001 | 0.0000 | 104 | 0.0012 | 123 | 0.2175 | 62 | 0.0000 | 83 | 0.0004 | 133 | 0.0004 | 85 |
| 67 | digitalbarriers-002 | 0.0001 | 195 | 0.0045 | 182 | - | 169 | 0.0028 | 215 | 0.0027 | 216 | 0.0071 | 165 |
| 68 | dsk-000 | 0.0000 | 23 | 0.0000 | 19 | 0.0000 | 9 | 0.0000 | 18 | 0.0000 | 19 | 0.0000 | 17 |
| 69 | einetworks-000 | 0.0000 | 170 | 0.0017 | 138 | - | 216 | 0.0002 | 135 | 0.0005 | 165 | 0.0008 | 128 |
| 70 | ecortex-000 | 0.0095 | 224 | 0.0602 | 223 | - | 116 | 0.0094 | 225 | 0.0059 | 225 | 0.1405 | 224 |
| 71 | ercacat-001 | 0.0000 | 76 | 0.0005 | 80 | - | 219 | 0.0000 | 77 | 0.0003 | 81 | 0.0002 | 66 |
| 72 | everai-paravision-003 | 0.0000 | 137 | 0.0008 | 101 | 0.0705 | 42 | 0.0002 | 125 | 0.0004 | 102 | 0.0004 | 99 |
| 73 | expasoft-000 | 0.0000 | 77 | 0.0000 | 57 | - | 223 | 0.0000 | 56 | 0.0000 | 61 | 0.0000 | 50 |
| 74 | f8-001 | 0.0003 | 207 | 0.0059 | 194 | 0.2026 | 61 | 0.0035 | 216 | 0.0030 | 219 | 0.0087 | 170 |
| 75 | facesoft-000 | 0.0000 | 84 | 0.0000 | 62 | 0.0000 | 28 | 0.0000 | 61 | 0.0000 | 66 | 0.0000 | 52 |
| 76 | fiberhome-nanjing-002 | 0.0000 | 131 | 0.0006 | 85 | - | 96 | 0.0001 | 101 | 0.0004 | 101 | 0.0016 | 146 |
| 77 | fujitsulab-000 | 0.0000 | 179 | 0.0033 | 165 | - | 146 | 0.0005 | 167 | 0.0002 | 69 | 0.0099 | 173 |
| 78 | geo-000 | 0.0000 | 28 | 0.0000 | 23 | - | 138 | 0.0000 | 23 | 0.0000 | 24 | 0.0000 | 19 |
| 79 | glory-001 | 0.0160 | 226 | 0.0314 | 216 | 0.0000 | 25 | 0.0051 | 221 | 0.0010 | 190 | 0.1651 | 225 |
| 80 | glory-002 | 0.0003 | 205 | 0.0045 | 181 | - | 111 | 0.0015 | 205 | 0.0011 | 200 | 0.0557 | 210 |
| 81 | gorilla-005 | 0.0000 | 41 | 0.0008 | 100 | - | 156 | 0.0000 | 72 | 0.0003 | 78 | 0.0004 | 91 |
| 82 | gorilla-006 | 0.0000 | 38 | 0.0006 | 86 | - | 152 | 0.0000 | 68 | 0.0003 | 77 | 0.0003 | 70 |
| 83 | hik-001 | 0.0000 | 63 | 0.0000 | 66 | - | 193 | 0.0000 | 47 | 0.0000 | 51 | 0.0000 | 42 |
| 84 | hr-001 | 0.0000 | 91 | 0.0007 | 93 | 0.1198 | 51 | 0.0001 | 88 | 0.0004 | 108 | 0.0003 | 79 |
| 85 | hr-002 | 0.0000 | 102 | 0.0007 | 92 | - | 135 | 0.0002 | 134 | 0.0004 | 138 | 0.0004 | 84 |
| 86 | id3-004 | 0.0000 | 187 | 0.0052 | 189 | - | 160 | 0.0015 | 207 | 0.0011 | 199 | - | 233 |
| 87 | id3-005 | 0.0000 | 113 | 0.0074 | 201 | - | 183 | 0.0002 | 129 | 0.0005 | 154 | 0.0256 | 194 |
| 88 | idemia-005 | 0.0000 | 10 | 0.0004 | 75 | 0.0239 | 30 | 0.0000 | 66 | 0.0003 | 82 | 0.0003 | 71 |
| 89 | idemia-006 | 0.0000 | 53 | 0.0004 | 76 | - | 174 | 0.0000 | 67 | 0.0003 | 84 | 0.0003 | 72 |
| 90 | iit-001 | 0.0000 | 148 | 0.0806 | 225 | 0.0843 | 45 | 0.0001 | 121 | 0.0004 | 126 | 0.0104 | 174 |
| 91 | iit-002 | 0.0000 | 171 | 0.0021 | 147 | - | 206 | 0.0009 | 192 | 0.0005 | 171 | 0.0443 | 207 |
| 92 | imagus-000 | 0.0002 | 201 | 0.0028 | 157 | 0.1107 | 49 | 0.0010 | 195 | 0.0012 | 202 | 0.0347 | 201 |
| 93 | imagus-001 | 0.0000 | 139 | 0.0030 | 159 | - | 159 | 0.0001 | 108 | 0.0004 | 128 | 0.0396 | 205 |
| 94 | imperial-000 | 0.0000 | 42 | 0.0000 | 31 | - | 157 | 0.0000 | 30 | 0.0000 | 33 | 0.0000 | 27 |
| 95 | imperial-002 | 0.0000 | 11 | 0.0000 | 11 | 0.0000 | 5 | 0.0000 | 10 | 0.0000 | 11 | 0.0000 | 9 |
| 96 | incode-006 | 0.0000 | 95 | 0.0005 | 79 | - | 108 | 0.0001 | 118 | 0.0004 | 89 | 0.0004 | 90 |
| 97 | incode-007 | 0.0000 | 140 | 0.0009 | 104 | - | 162 | 0.0002 | 131 | 0.0004 | 105 | 0.0007 | 124 |
| 98 | innovativetechnologyltd-001 | 0.0001 | 199 | 0.0050 | 187 | - | 172 | 0.0024 | 212 | 0.0025 | 215 | 0.0055 | 163 |
| 99 | innovativetechnologyltd-002 | 0.0000 | 152 | 0.0046 | 184 | - | 189 | 0.0057 | 223 | 0.0005 | 163 | 0.0247 | 193 |
| 100 | innovatrics-004 | 0.0000 | 132 | 0.0017 | 137 | 0.1170 | 50 | 0.0000 | 82 | 0.0004 | 130 | 0.0041 | 159 |
| 101 | innovatrics-006 | 0.0000 | 116 | 0.0009 | 105 | 0.0350 | 33 | 0.0000 | 75 | 0.0004 | 96 | 0.0003 | 82 |
| 102 | intelliloadai-001 | 0.0000 | 80 | 0.0000 | 58 | - | 225 | 0.0000 | 57 | 0.0000 | 62 | 0.0001 | 63 |
| 103 | intellifusion-001 | 0.0000 | 96 | 0.0005 | 81 | 0.0949 | 47 | 0.0001 | 98 | 0.0003 | 85 | 0.0005 | 109 |
| 104 | intellifusion-002 | 0.0000 | 39 | 0.0000 | 64 | - | 155 | 0.0000 | 63 | 0.0000 | 31 | 0.0001 | 62 |
| 105 | intellivision-001 | 0.0042 | 219 | 0.0296 | 213 | 0.5495 | 81 | 0.0048 | 220 | 0.0042 | 223 | 0.1358 | 221 |
| 106 | intellivision-002 | 0.0000 | 186 | 0.0046 | 183 | - | 122 | 0.0012 | 198 | 0.0005 | 172 | 0.0146 | 180 |
| 107 | intelresearch-001 | 0.0000 | 177 | 0.0082 | 203 | - | 182 | 0.0005 | 171 | 0.0010 | 189 | 0.0407 | 206 |
| 108 | intelresearch-002 | 0.0000 | 103 | 0.0022 | 149 | - | 141 | 0.0000 | 78 | 0.0004 | 91 | 0.0003 | 80 |
| 109 | intsysmsu-001 | 0.0000 | 35 | 0.0010 | 110 | - | 147 | 0.0001 | 105 | 0.0004 | 123 | 0.0004 | 96 |
| 110 | intsysmsu-002 | 0.0000 | 60 | 0.0010 | 111 | - | 188 | 0.0001 | 106 | 0.0004 | 124 | 0.0004 | 98 |
| 111 | iqface-000 | 0.0000 | 62 | 0.0000 | 47 | 0.0000 | 23 | 0.0000 | 46 | 0.0000 | 150 | 0.0000 | 41 |
| 112 | iqface-002 | 0.0000 | 5 | 0.0000 | 6 | - | 99 | 0.0000 | 5 | 0.0000 | 6 | 0.0000 | 4 |
| 113 | isap-001 | 0.0000 | 58 | 0.0000 | 45 | - | 185 | 0.0000 | 43 | 0.0000 | 47 | 0.0000 | 38 |
| 114 | isityou-000 | 0.0068 | 223 | 0.0316 | 217 | 0.4714 | 76 | 0.0023 | 208 | 0.0010 | 192 | 0.0663 | 214 |
| 115 | isystems-001 | 0.0000 | 173 | 0.0035 | 170 | 0.1421 | 53 | 0.0010 | 193 | 0.0007 | 181 | 0.0128 | 177 |
| 116 | isystems-002 | 0.0000 | 174 | 0.0035 | 171 | 0.1421 | 54 | 0.0010 | 194 | 0.0007 | 182 | 0.0128 | 178 |

Table 18: FTE is the proportion of failed template generation attempts. Failures can occur because the software throws an exception, or because the software electively refuses to process the input image. This would typically occur if a face is not detected. FTE is measured as the number of function calls that give EITHER a non-zero error code OR that give a “small” template. This is defined as one whose size is less than 0.3 times the median template size for that algorithm. This second rule is needed because some algorithms incorrectly fail to return a non-zero error code when template generation fails.

¹ The effects of FTE are included in the accuracy results of this report by regarding any template comparison involving a failed template to produce a low similarity score. Thus higher FTE results in higher FNMR and lower FMR.

| | Algorithm | Failure to Enrol Rate ¹ | | | | | | | | | | | |
|-----|---------------------|------------------------------------|--------|---------------|---------|--------|------|----------|----------|----------|----------|----------|----------|
| | | APPLICATION | BORDER | CHILD-EXPLOIT | MUGSHOT | VISA | WILD | SEC. 2.3 | SEC. 2.4 | SEC. 2.1 | SEC. 2.5 | SEC. 2.2 | SEC. 2.6 |
| 117 | itmo-006 | 0.0000 | 14 | 0.0015 | 135 | - | 109 | 0.0004 | 162 | 0.0004 | 121 | 0.0006 | 115 |
| 118 | itmo-007 | 0.0000 | 66 | 0.0009 | 102 | - | 197 | 0.0003 | 152 | 0.0000 | 54 | 0.0004 | 92 |
| 119 | iws-000 | 0.0005 | 214 | 0.0650 | 224 | - | 131 | 0.0024 | 211 | 0.0012 | 201 | 0.0936 | 217 |
| 120 | kakao-002 | 0.0000 | 153 | 0.0057 | 193 | 0.2494 | 68 | 0.0002 | 139 | 0.0005 | 159 | 0.0310 | 197 |
| 121 | kakao-003 | 0.0000 | 36 | 0.0000 | 28 | - | 148 | 0.0000 | 27 | 0.0000 | 29 | 0.0000 | 24 |
| 122 | kedacom-000 | 0.0000 | 29 | 0.0000 | 24 | 0.0000 | 11 | 0.0000 | 24 | 0.0000 | 25 | 0.0000 | 20 |
| 123 | kneron-003 | 0.0239 | 228 | 0.0306 | 214 | 0.4883 | 79 | 0.0044 | 219 | 0.0016 | 210 | 0.1823 | 226 |
| 124 | kneron-005 | 0.0000 | 176 | 0.0226 | 209 | - | 110 | 0.0006 | 176 | 0.0005 | 160 | 0.0097 | 172 |
| 125 | lookman-002 | 0.0000 | 57 | 0.0000 | 44 | - | 184 | 0.0000 | 42 | 0.0000 | 46 | 0.0000 | 37 |
| 126 | lookman-004 | 0.0000 | 48 | 0.0000 | 37 | 0.0000 | 18 | 0.0000 | 36 | 0.0000 | 39 | 0.0000 | 31 |
| 127 | luxand-000 | 0.0000 | 16 | 0.0000 | 14 | - | 114 | 0.0000 | 13 | 0.0000 | 14 | 0.0000 | 12 |
| 128 | megvii-001 | 0.0000 | 79 | 0.0006 | 83 | 0.0274 | 32 | 0.0007 | 182 | 0.0004 | 100 | 0.0152 | 181 |
| 129 | megvii-002 | 0.0000 | 78 | 0.0006 | 82 | 0.0274 | 31 | 0.0054 | 222 | 0.0004 | 99 | 0.0126 | 176 |
| 130 | meiya-001 | 0.0000 | 172 | 0.0028 | 158 | - | 221 | 0.0004 | 163 | 0.0010 | 193 | 0.0025 | 151 |
| 131 | microfocus-001 | 0.0001 | 197 | 0.0053 | 191 | 0.0791 | 44 | 0.0008 | 188 | 0.0016 | 209 | 0.0220 | 188 |
| 132 | microfocus-002 | 0.0001 | 196 | 0.0053 | 190 | 0.0791 | 43 | 0.0008 | 187 | 0.0016 | 208 | 0.0220 | 187 |
| 133 | mt-000 | 0.0000 | 106 | 0.0008 | 99 | 0.1043 | 48 | 0.0002 | 136 | 0.0004 | 139 | 0.0004 | 87 |
| 134 | mt-002 | 0.0000 | 92 | 0.0003 | 69 | - | 104 | 0.0001 | 89 | 0.0004 | 93 | 0.0004 | 94 |
| 135 | mvision-001 | 0.0000 | 49 | 0.0000 | 38 | - | 170 | 0.0000 | 37 | 0.0000 | 40 | 0.0000 | 32 |
| 136 | nazhiai-000 | 0.0000 | 56 | 0.0000 | 43 | - | 179 | 0.0000 | 41 | 0.0000 | 45 | 0.0000 | 36 |
| 137 | netbridge-tech-001 | 0.0000 | 9 | 0.0000 | 10 | - | 102 | 0.0000 | 9 | 0.0000 | 10 | 0.0000 | 8 |
| 138 | netbridge-tech-002 | 0.0000 | 26 | 0.0000 | 21 | - | 133 | 0.0000 | 21 | 0.0000 | 22 | 0.0000 | 18 |
| 139 | neurotechnology-008 | 0.0000 | 149 | 0.0006 | 84 | - | 171 | 0.0004 | 157 | 0.0004 | 106 | 0.0018 | 149 |
| 140 | neurotechnology-009 | 0.0000 | 130 | 0.0008 | 98 | - | 88 | 0.0002 | 128 | 0.0004 | 98 | 0.0018 | 148 |
| 141 | nodeflux-002 | 0.0000 | 127 | 0.0261 | 211 | - | 228 | 0.0008 | 186 | 0.0005 | 164 | 0.0008 | 130 |
| 142 | notiontag-000 | 0.0000 | 45 | 0.0000 | 34 | 0.0000 | 16 | 0.0000 | 33 | 0.0000 | 36 | 0.0000 | 29 |
| 143 | ntechlab-007 | 0.0000 | 144 | 0.0019 | 143 | 0.0682 | 41 | 0.0001 | 93 | 0.0004 | 97 | 0.0005 | 108 |
| 144 | ntechlab-008 | 0.0000 | 138 | 0.0005 | 78 | - | 139 | 0.0001 | 96 | 0.0004 | 94 | 0.0005 | 104 |
| 145 | null-000 | - | 231 | - | 231 | - | 97 | - | 232 | - | 233 | - | 231 |
| 146 | null-082 | - | 230 | - | 230 | - | 90 | - | 231 | - | 232 | - | 230 |
| 147 | oz-001 | 0.0000 | 155 | 0.0011 | 122 | - | 126 | 0.0006 | 179 | 0.0004 | 110 | 0.0014 | 142 |
| 148 | paravision-004 | 0.0000 | 154 | 0.0007 | 94 | 0.0570 | 36 | 0.0002 | 133 | 0.0004 | 113 | 0.0008 | 126 |
| 149 | pensees-001 | 0.0000 | 87 | 0.0000 | 4 | - | 92 | 0.0000 | 4 | 0.0000 | 4 | 0.0000 | 2 |
| 150 | pixelall-003 | 0.0000 | 68 | 0.0000 | 50 | - | 199 | 0.0000 | 50 | 0.0000 | 55 | 0.0000 | 44 |
| 151 | pixelall-004 | 0.0000 | 6 | 0.0000 | 7 | - | 100 | 0.0000 | 6 | 0.0000 | 7 | 0.0000 | 5 |
| 152 | psl-003 | 0.0000 | 118 | 0.0007 | 88 | - | 194 | 0.0000 | 79 | 0.0004 | 119 | 0.0003 | 78 |
| 153 | psl-005 | 0.0000 | 90 | 0.0007 | 87 | - | 101 | 0.0000 | 70 | 0.0004 | 107 | 0.0003 | 76 |
| 154 | pxl-001 | 0.0000 | 189 | 0.0044 | 180 | - | 209 | 0.0005 | 169 | 0.0022 | 213 | 0.0323 | 199 |
| 155 | pyramid-000 | 0.0001 | 194 | 0.0041 | 176 | - | 93 | 0.0005 | 168 | 0.0007 | 183 | 0.0015 | 145 |
| 156 | rankone-008 | 0.0000 | 183 | 0.0049 | 186 | - | 89 | 0.0003 | 143 | 0.0004 | 88 | 0.0040 | 158 |
| 157 | rankone-009 | 0.0000 | 81 | 0.0000 | 59 | - | 226 | 0.0000 | 58 | 0.0000 | 63 | 0.0000 | 55 |
| 158 | realnetworks-002 | 0.0000 | 150 | 0.0003 | 72 | - | 181 | 0.0004 | 154 | 0.0003 | 75 | 0.0004 | 97 |
| 159 | realnetworks-003 | 0.0000 | 147 | 0.0003 | 71 | 0.0076 | 29 | 0.0004 | 153 | 0.0003 | 74 | 0.0004 | 100 |
| 160 | remarkai-001 | 0.0000 | 47 | 0.0000 | 36 | - | 164 | 0.0000 | 35 | 0.0000 | 38 | 0.0000 | 58 |
| 161 | remarkai-002 | 0.0000 | 27 | 0.0000 | 22 | - | 134 | 0.0000 | 22 | 0.0000 | 23 | 0.0000 | 56 |
| 162 | rokid-000 | 0.0000 | 74 | 0.0072 | 198 | - | 212 | 0.0001 | 104 | 0.0005 | 161 | 0.0354 | 202 |
| 163 | rokid-001 | 0.0000 | 25 | 0.0013 | 131 | - | 129 | 0.0000 | 20 | 0.0000 | 21 | 0.0007 | 123 |
| 164 | s1-001 | 0.0000 | 188 | 0.0073 | 200 | - | 103 | 0.0013 | 200 | 0.0007 | 179 | 0.0600 | 213 |
| 165 | saffe-001 | 0.0000 | 40 | 0.0000 | 30 | 0.0000 | 15 | 0.0000 | 29 | 0.0000 | 32 | 0.0000 | 26 |
| 166 | saffe-002 | 0.0000 | 71 | 0.0000 | 53 | - | 204 | 0.0000 | 53 | 0.0000 | 58 | 0.0000 | 45 |
| 167 | samtech-001 | 0.0001 | 193 | 0.0032 | 164 | - | 151 | 0.0004 | 161 | 0.0008 | 185 | 0.0013 | 141 |
| 168 | scanovate-001 | 0.0208 | 227 | 0.2388 | 228 | - | 119 | 0.0024 | 209 | 0.0014 | 205 | 0.2751 | 227 |
| 169 | scanovate-002 | 0.0000 | 145 | 0.0018 | 140 | - | 230 | 0.0000 | 86 | 0.0004 | 150 | 0.0008 | 127 |
| 170 | sensetime-002 | 0.0004 | 211 | 0.0082 | 202 | 0.3345 | 72 | 0.0011 | 197 | 0.0005 | 170 | 0.0218 | 186 |
| 171 | sensetime-003 | 0.0000 | 119 | 0.0011 | 120 | 0.0554 | 35 | 0.0000 | 64 | 0.0004 | 115 | 0.0004 | 102 |
| 172 | sertis-000 | 0.0000 | 13 | 0.0007 | 91 | - | 107 | 0.0000 | 87 | 0.0004 | 104 | 0.0004 | 89 |
| 173 | sertis-001 | 0.0000 | 67 | 0.0004 | 77 | - | 198 | 0.0002 | 137 | 0.0005 | 173 | 0.0003 | 81 |
| 174 | shaman-000 | 0.0000 | 51 | 0.0000 | 40 | 0.0000 | 21 | 0.0000 | 39 | 0.0000 | 42 | 0.0000 | 34 |

Table 19: FTE is the proportion of failed template generation attempts. Failures can occur because the software throws an exception, or because the software electively refuses to process the input image. This would typically occur if a face is not detected. FTE is measured as the number of function calls that give EITHER a non-zero error code OR that give a “small” template. This is defined as one whose size is less than 0.3 times the median template size for that algorithm. This second rule is needed because some algorithms incorrectly fail to return a non-zero error code when template generation fails.

¹The effects of FTE are included in the accuracy results of this report by regarding any template comparison involving a failed template to produce a low similarity score. Thus higher FTE results in higher FNMR and lower FMR.

| | Algorithm | Failure to Enrol Rate ¹ | | | | | | | | | | | |
|-----|-----------------------|------------------------------------|----------|----------|----------|---------------|----------|----------|-----|--------|-----|--------|-----|
| | | APPLICATION | | BORDER | | CHILD-EXPLOIT | | MUGSHOT | | | | | |
| | | Name | SEC. 2.3 | SEC. 2.4 | SEC. 2.1 | SEC. 2.5 | SEC. 2.2 | SEC. 2.6 | | | | | |
| 175 | shaman-001 | 0.0000 | 2 | 0.0000 | 2 | 0.0000 | 1 | 0.0000 | 2 | 0.0000 | 2 | 0.0000 | 53 |
| 176 | shu-002 | 0.0000 | 129 | 0.0010 | 113 | - | 84 | 0.0005 | 164 | 0.0004 | 141 | 0.0007 | 120 |
| 177 | shu-003 | 0.0000 | 52 | 0.0007 | 89 | - | 173 | 0.0001 | 91 | 0.0003 | 76 | 0.0004 | 103 |
| 178 | siat-002 | 0.0000 | 123 | 0.0012 | 128 | 0.0616 | 37 | 0.0000 | 76 | 0.0004 | 116 | 0.0048 | 161 |
| 179 | siat-004 | 0.0000 | 108 | 0.0011 | 119 | - | 165 | 0.0000 | 73 | 0.0004 | 112 | 0.0003 | 77 |
| 180 | sjtu-001 | 0.0000 | 133 | 0.0010 | 115 | - | 105 | 0.0005 | 166 | 0.0004 | 148 | 0.0008 | 129 |
| 181 | sjtu-002 | 0.0000 | 142 | 0.0010 | 114 | - | 210 | 0.0005 | 165 | 0.0004 | 144 | 0.0007 | 122 |
| 182 | smilart-002 | 0.0000 | 178 | 0.0036 | 172 | 0.2422 | 66 | 0.0003 | 150 | 0.0011 | 196 | 0.0575 | 211 |
| 183 | smilart-003 | 0.0003 | 206 | 0.0100 | 205 | - | 112 | 0.0014 | 204 | 0.0013 | 204 | 0.0555 | 209 |
| 184 | stachu-000 | 0.0000 | 61 | 0.0000 | 46 | - | 190 | 0.0000 | 45 | 0.0000 | 49 | 0.0000 | 40 |
| 185 | starhybrid-001 | 0.0001 | 198 | 0.0033 | 168 | 0.2340 | 65 | 0.0009 | 191 | 0.0023 | 214 | 0.0044 | 160 |
| 186 | synesis-006 | 0.0000 | 32 | 0.0003 | 73 | - | 143 | 0.0000 | 80 | 0.0003 | 73 | 0.0002 | 68 |
| 187 | synesis-007 | 0.0000 | 126 | 0.0013 | 130 | - | 227 | 0.0002 | 140 | 0.0004 | 117 | 0.0005 | 105 |
| 188 | synology-000 | 0.0000 | 20 | 0.0000 | 17 | - | 120 | 0.0000 | 16 | 0.0000 | 17 | 0.0000 | 15 |
| 189 | synology-002 | 0.0000 | 15 | 0.0000 | 13 | - | 113 | 0.0000 | 12 | 0.0000 | 13 | 0.0000 | 11 |
| 190 | tech5-004 | 0.0000 | 122 | 0.0008 | 97 | - | 211 | 0.0003 | 146 | 0.0004 | 147 | 0.0006 | 112 |
| 191 | tech5-005 | 0.0000 | 107 | 0.0007 | 95 | - | 153 | 0.0000 | 71 | 0.0004 | 132 | 0.0049 | 162 |
| 192 | tevian-004 | 0.0000 | 158 | 0.0024 | 151 | - | 142 | 0.0002 | 127 | 0.0005 | 167 | 0.0057 | 164 |
| 193 | tevian-005 | 0.0001 | 200 | 0.0041 | 175 | 0.3606 | 73 | 0.0006 | 177 | 0.0006 | 178 | 0.0012 | 139 |
| 194 | tiger-002 | 0.0000 | 114 | 0.0010 | 109 | 0.0619 | 39 | 0.0001 | 111 | 0.0004 | 111 | 0.0082 | 169 |
| 195 | tiger-003 | 0.0000 | 93 | - | 232 | 0.0619 | 38 | 0.0001 | 109 | 0.0004 | 109 | 0.0082 | 168 |
| 196 | tongyi-005 | 0.0000 | 8 | 0.0000 | 9 | 0.0000 | 4 | 0.0000 | 8 | 0.0000 | 9 | 0.0000 | 7 |
| 197 | toshiba-002 | 0.0000 | 21 | 0.0000 | 18 | 0.0000 | 8 | 0.0000 | 17 | 0.0000 | 18 | 0.0000 | 16 |
| 198 | toshiba-003 | 0.0000 | 75 | 0.0001 | 67 | - | 215 | 0.0001 | 112 | 0.0001 | 68 | 0.0002 | 67 |
| 199 | trueface-000 | 0.0000 | 124 | 0.0000 | 55 | - | 218 | 0.0000 | 55 | 0.0000 | 60 | 0.0000 | 48 |
| 200 | trueface-001 | 0.0000 | 134 | 0.0038 | 174 | - | 117 | 0.0007 | 183 | 0.0005 | 162 | 0.0277 | 195 |
| 201 | tuputech-000 | 0.0003 | 209 | 0.0116 | 208 | - | 132 | 0.0632 | 230 | 0.0081 | 227 | 0.6383 | 229 |
| 202 | ulsee-001 | 0.0000 | 69 | 0.0000 | 51 | - | 203 | 0.0000 | 51 | 0.0000 | 56 | 0.0001 | 59 |
| 203 | uluface-002 | 0.0000 | 46 | 0.0000 | 35 | 0.0000 | 17 | 0.0000 | 34 | 0.0000 | 37 | 0.0000 | 30 |
| 204 | uluface-003 | 0.0000 | 19 | 0.0001 | 68 | - | 118 | 0.0002 | 124 | 0.0002 | 70 | 0.0244 | 192 |
| 205 | upc-001 | 0.0000 | 167 | 0.0003 | 70 | 0.0450 | 34 | 0.0003 | 144 | 0.0003 | 83 | 0.0011 | 137 |
| 206 | vcog-002 | - | 233 | 0.3719 | 229 | 0.2209 | 63 | - | 233 | 0.0019 | 212 | - | 232 |
| 207 | vd-001 | 0.0000 | 175 | 0.0030 | 160 | - | 130 | 0.0004 | 160 | 0.0009 | 186 | 0.0024 | 150 |
| 208 | veridas-003 | 0.0000 | 164 | 0.0026 | 153 | 0.1893 | 59 | 0.0001 | 110 | 0.0005 | 157 | 0.0006 | 113 |
| 209 | veridas-004 | 0.0000 | 166 | 0.0026 | 154 | - | 233 | 0.0001 | 113 | 0.0005 | 158 | 0.0006 | 114 |
| 210 | via-000 | 0.0000 | 64 | 0.0000 | 48 | 0.0000 | 24 | 0.0000 | 48 | 0.0000 | 52 | 0.0001 | 61 |
| 211 | via-001 | 0.0000 | 24 | 0.0000 | 20 | - | 127 | 0.0000 | 19 | 0.0000 | 20 | 0.0001 | 60 |
| 212 | videmo-000 | 0.0000 | 143 | 0.0019 | 144 | - | 224 | 0.0003 | 148 | 0.0012 | 203 | 0.0158 | 182 |
| 213 | videonetics-001 | 0.0004 | 210 | 0.0309 | 215 | 0.4799 | 77 | 0.0015 | 206 | 0.0010 | 191 | 0.0112 | 175 |
| 214 | videonetics-002 | 0.0000 | 146 | 0.0459 | 221 | 0.4598 | 75 | 0.0006 | 178 | 0.0005 | 169 | 0.0013 | 140 |
| 215 | vigilantsolutions-007 | 0.0000 | 159 | 0.0028 | 156 | 0.2538 | 69 | 0.0001 | 97 | 0.0004 | 95 | 0.0005 | 107 |
| 216 | vigilantsolutions-008 | 0.0000 | 157 | 0.0028 | 155 | - | 94 | 0.0001 | 94 | 0.0004 | 92 | 0.0005 | 106 |
| 217 | vion-000 | 0.0050 | 220 | 0.0392 | 220 | 0.6388 | 83 | 0.0130 | 227 | 0.0078 | 226 | 0.1389 | 222 |
| 218 | visionbox-000 | 0.0000 | 182 | 0.0033 | 167 | - | 220 | 0.0005 | 175 | 0.0011 | 198 | 0.0028 | 155 |
| 219 | visionbox-001 | 0.0000 | 181 | 0.0033 | 166 | - | 195 | 0.0005 | 174 | 0.0011 | 197 | 0.0028 | 154 |
| 220 | visionlabs-008 | 0.0000 | 115 | 0.0015 | 134 | - | 186 | 0.0002 | 141 | 0.0004 | 151 | 0.0009 | 131 |
| 221 | visionlabs-009 | 0.0000 | 94 | 0.0010 | 107 | - | 106 | 0.0001 | 90 | 0.0004 | 120 | 0.0006 | 117 |
| 222 | visteam-000 | 0.0000 | 180 | 0.0031 | 163 | - | 214 | 0.0005 | 170 | 0.0011 | 194 | 0.0026 | 153 |
| 223 | vocord-007 | 0.0000 | 135 | 0.0535 | 222 | 0.0000 | 10 | 0.0001 | 120 | 0.0004 | 90 | 0.0009 | 133 |
| 224 | vocord-008 | 0.0000 | 109 | 0.0015 | 136 | - | 168 | 0.0003 | 149 | 0.0001 | 67 | 0.0007 | 121 |
| 225 | winsense-000 | 0.0000 | 18 | 0.0000 | 16 | 0.0000 | 7 | 0.0000 | 15 | 0.0000 | 16 | 0.0000 | 14 |
| 226 | winsense-001 | 0.0000 | 37 | 0.0000 | 29 | 0.0000 | 14 | 0.0000 | 28 | 0.0000 | 30 | 0.0000 | 25 |
| 227 | x-laboratory-000 | 0.0247 | 229 | 0.0000 | 56 | 0.0000 | 27 | 0.0005 | 173 | 0.0002 | 71 | 0.0000 | 49 |
| 228 | x-laboratory-001 | 0.0000 | 117 | 0.0012 | 127 | - | 192 | 0.0001 | 114 | 0.0004 | 143 | 0.0007 | 118 |
| 229 | xfowardai-000 | 0.0000 | 1 | 0.0000 | 1 | - | 85 | 0.0000 | 1 | 0.0000 | 1 | 0.0000 | 1 |
| 230 | yisheng-004 | 0.0002 | 202 | - | 233 | 0.4279 | 74 | 0.0013 | 201 | 0.0006 | 176 | 0.0321 | 198 |
| 231 | yitu-003 | 0.0000 | 4 | 0.0000 | 5 | - | 98 | 0.0009 | 190 | 0.0000 | 5 | 0.0000 | 3 |
| 232 | yoonik-000 | 0.0000 | 112 | 0.0019 | 145 | - | 180 | 0.0001 | 102 | 0.0004 | 142 | 0.0009 | 134 |

Table 20: FTE is the proportion of failed template generation attempts. Failures can occur because the software throws an exception, or because the software electively refuses to process the input image. This would typically occur if a face is not detected. FTE is measured as the number of function calls that give EITHER a non-zero error code OR that give a “small” template. This is defined as one whose size is less than 0.3 times the median template size for that algorithm. This second rule is needed because some algorithms incorrectly fail to return a non-zero error code when template generation fails.

¹ The effects of FTE are included in the accuracy results of this report by regarding any template comparison involving a failed template to produce a low similarity score. Thus higher FTE results in higher FNMR and lower FMR.

| | | Failure to Enrol Rate ¹ | | | | | | | | | | | |
|-----|----------|------------------------------------|----------|---------------|----------|----------|----------|--------|----|--------|----|--------|----|
| | Name | APPLICATION | BORDER | CHILD-EXPLOIT | MUGSHOT | VISA | WILD | | | | | | |
| | Name | SEC. 2.3 | SEC. 2.4 | SEC. 2.1 | SEC. 2.5 | SEC. 2.2 | SEC. 2.6 | | | | | | |
| 233 | yuan-000 | 0.0000 | 65 | 0.0000 | 49 | - | 196 | 0.0000 | 49 | 0.0000 | 53 | 0.0000 | 43 |

Table 21: FTE is the proportion of failed template generation attempts. Failures can occur because the software throws an exception, or because the software electively refuses to process the input image. This would typically occur if a face is not detected. FTE is measured as the number of function calls that give EITHER a non-zero error code OR that give a “small” template. This is defined as one whose size is less than 0.3 times the median template size for that algorithm. This second rule is needed because some algorithms incorrectly fail to return a non-zero error code when template generation fails.

¹The effects of FTE are included in the accuracy results of this report by regarding any template comparison involving a failed template to produce a low similarity score. Thus higher FTE results in higher FNMR and lower FMR.

3.4 Recognition accuracy

Core algorithm accuracy is stated via:

▷ **Cooperative subjects**

- The summary table of Figure 16;
- The visa image DETs of Figure 37;
- The mugshot DETs of Figure 49;
- The mugshot ageing profiles of Figure 181;
- The human-difficult pairs of Figure 13

▷ **Non-cooperative subjects**

- The photojournalism DET of Figure 59
- The child-exploitation DET of Figure 63;
- The child-exploitation CMC of Figure 67.

Figure 147 shows dependence of false match rate on algorithm score threshold. This allows a deployer to set a threshold to target a particular false match rate appropriate to the security objectives of the application.

Figure 123 likewise shows FMR(T) but for mugshots, and specially four subsets of the population.

Note that in both the mugshot and visa sets false match rates vary with the ethnicity, age, and sex, of the enrollee and impostor. For example figure 80 summarizes FMR for impostors paired from four groups black females, black males, white females, white males.

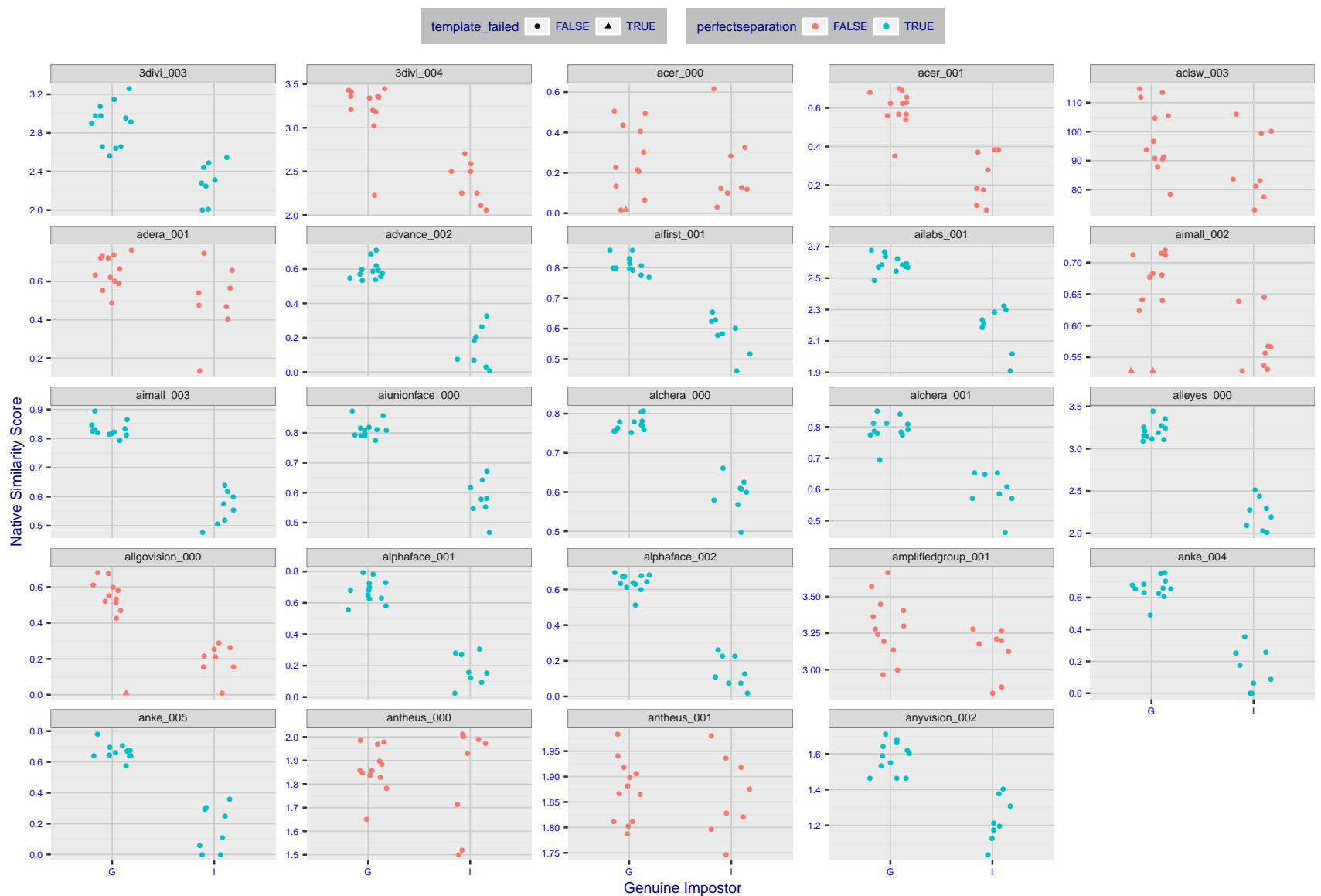


Figure 4: The Figure shows, in blue, algorithms that correctly separate the 12 genuine and 8 impostor pairs used in the May 2018 paper Face recognition accuracy of forensic examiners, superrecognizers, and face recognition algorithms (Phillips et al. [1]). In red are algorithms that are imperfect. Some algorithms fail only because they failed to make a template e.g. due to face detection failure (shown as a triangle). Others fail because the pairs were selected for that study because they had been difficult for three leading algorithms used in FRVT 2006. Caution: Given the small sample size ($n=20$) the figure may change substantially if larger or different sets were used. The images can be downloaded from the [Supplemental Information](#) page provided with that publication.



Figure 5: The Figure shows, in blue, algorithms that correctly separate the 12 genuine and 8 impostor pairs used in the May 2018 paper [Face recognition accuracy of forensic examiners, superrecognizers, and face recognition algorithms](#) (Phillips et al. [1]). In red are algorithms that are imperfect. Some algorithms fail only because they failed to make a template e.g. due to face detection failure (shown as a triangle). Others fail because the pairs were selected for that study because they had been difficult for three leading algorithms used in FRVT 2006. Caution: Given the small sample size ($n=20$) the figure may change substantially if larger or different sets were used. The images can be downloaded from the [Supplemental Information](#) page provided with that publication.



Figure 6: The Figure shows, in blue, algorithms that correctly separate the 12 genuine and 8 impostor pairs used in the May 2018 paper Face recognition accuracy of forensic examiners, superrecognizers, and face recognition algorithms (Phillips et al. [1]). In red are algorithms that are imperfect. Some algorithms fail only because they failed to make a template e.g. due to face detection failure (shown as a triangle). Others fail because the pairs were selected for that study because they had been difficult for three leading algorithms used in FRVT 2006. Caution: Given the small sample size ($n=20$) the figure may change substantially if larger or different sets were used. The images can be downloaded from the [Supplemental Information](#) page provided with that publication.

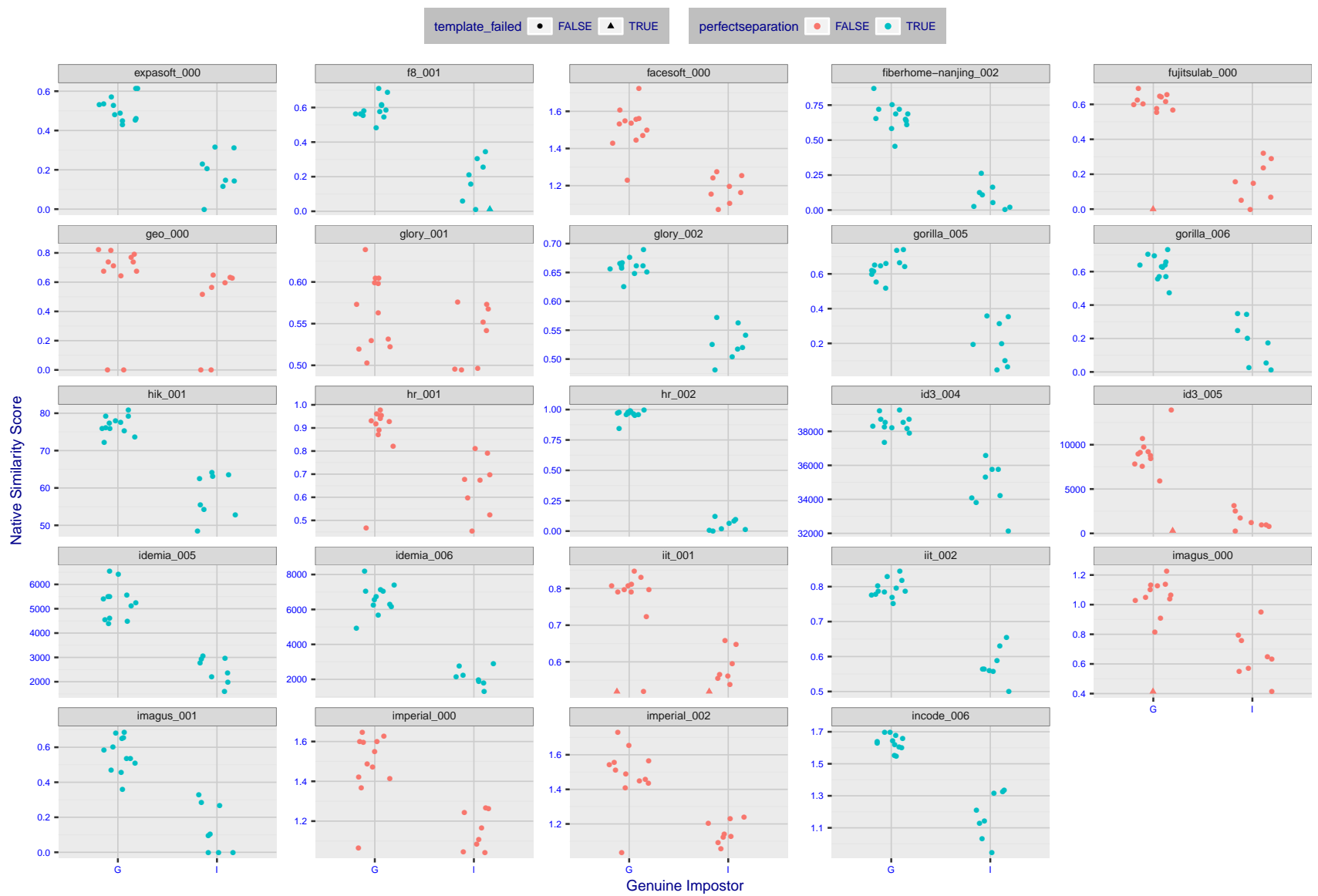


Figure 7: The Figure shows, in blue, algorithms that correctly separate the 12 genuine and 8 impostor pairs used in the May 2018 paper Face recognition accuracy of forensic examiners, superrecognizers, and face recognition algorithms (Phillips et al. [1]). In red are algorithms that are imperfect. Some algorithms fail only because they failed to make a template e.g. due to face detection failure (shown as a triangle). Others fail because the pairs were selected for that study because they had been difficult for three leading algorithms used in FRVT 2006. Caution: Given the small sample size ($n=20$) the figure may change substantially if larger or different sets were used. The images can be downloaded from the [Supplemental Information](#) page provided with that publication.



Figure 8: The Figure shows, in blue, algorithms that correctly separate the 12 genuine and 8 impostor pairs used in the May 2018 paper Face recognition accuracy of forensic examiners, superrecognizers, and face recognition algorithms (Phillips et al. [1]). In red are algorithms that are imperfect. Some algorithms fail only because they failed to make a template e.g. due to face detection failure (shown as a triangle). Others fail because the pairs were selected for that study because they had been difficult for three leading algorithms used in FRVT 2006. Caution: Given the small sample size ($n=20$) the figure may change substantially if larger or different sets were used. The images can be downloaded from the [Supplemental Information](#) page provided with that publication.

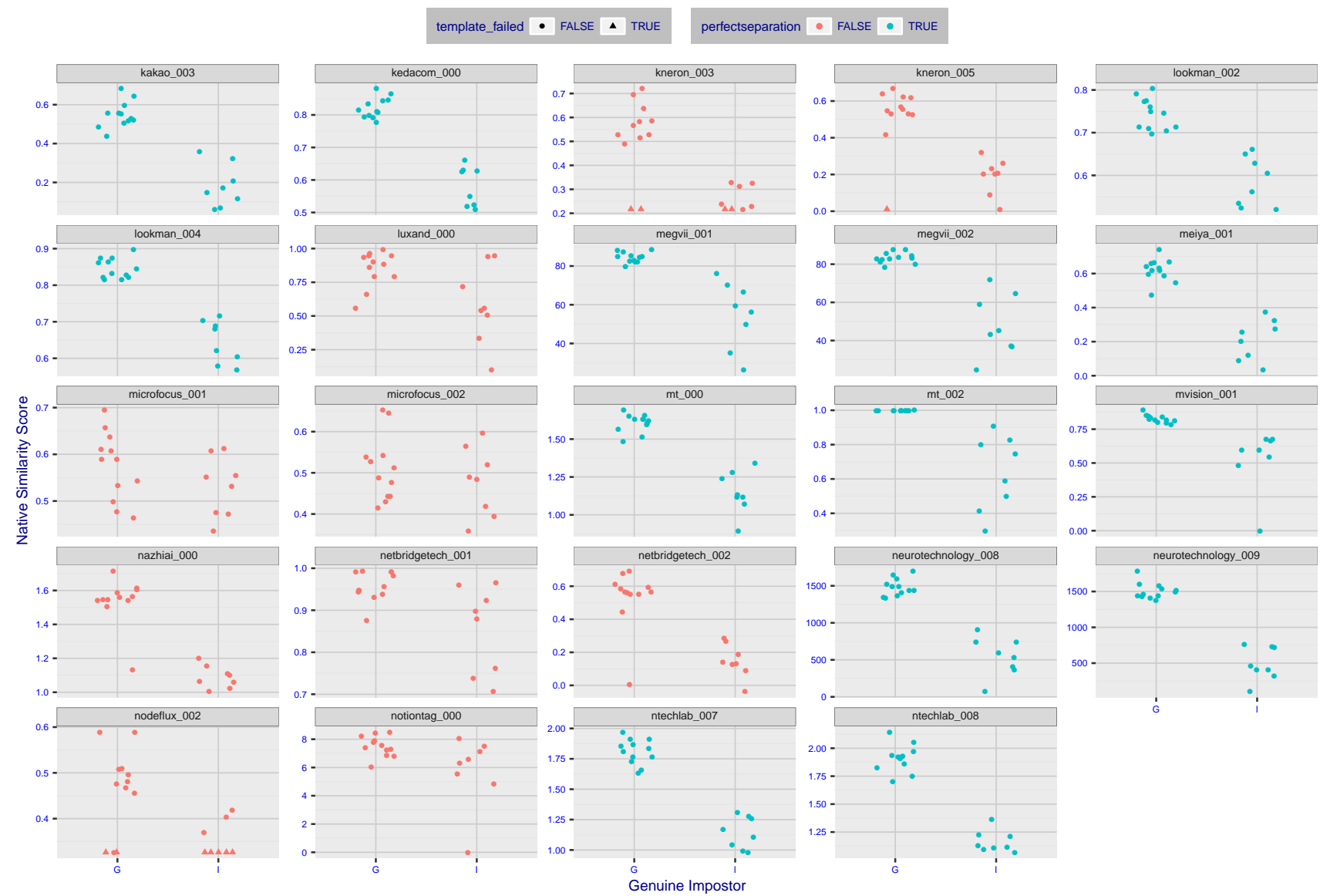


Figure 9: The Figure shows, in blue, algorithms that correctly separate the 12 genuine and 8 impostor pairs used in the May 2018 paper [Face recognition accuracy of forensic examiners, superrecognizers, and face recognition algorithms](#) (Phillips et al. [1]). In red are algorithms that are imperfect. Some algorithms fail only because they failed to make a template e.g. due to face detection failure (shown as a triangle). Others fail because the pairs were selected for that study because they had been difficult for three leading algorithms used in FRVT 2006. Caution: Given the small sample size ($n=20$) the figure may change substantially if larger or different sets were used. The images can be downloaded from the [Supplemental Information](#) page provided with that publication.

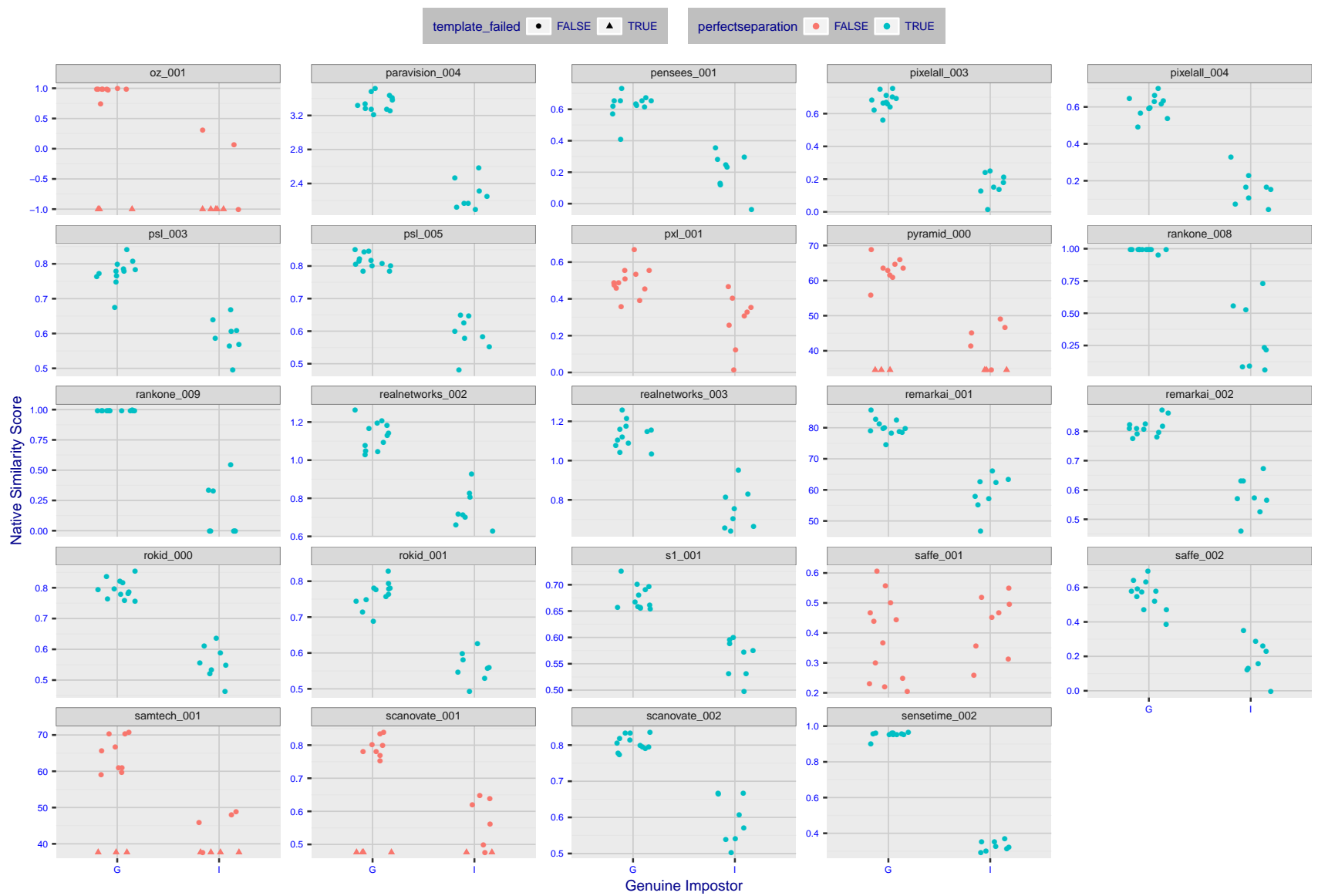


Figure 10: The Figure shows, in blue, algorithms that correctly separate the 12 genuine and 8 impostor pairs used in the May 2018 paper [Face recognition accuracy of forensic examiners, superrecognizers, and face recognition algorithms](#) (Phillips et al. [1]). In red are algorithms that are imperfect. Some algorithms fail only because they failed to make a template e.g. due to face detection failure (shown as a triangle). Others fail because the pairs were selected for that study because they had been difficult for three leading algorithms used in FRVT 2006. Caution: Given the small sample size ($n=20$) the figure may change substantially if larger or different sets were used. The images can be downloaded from the [Supplemental Information](#) page provided with that publication.

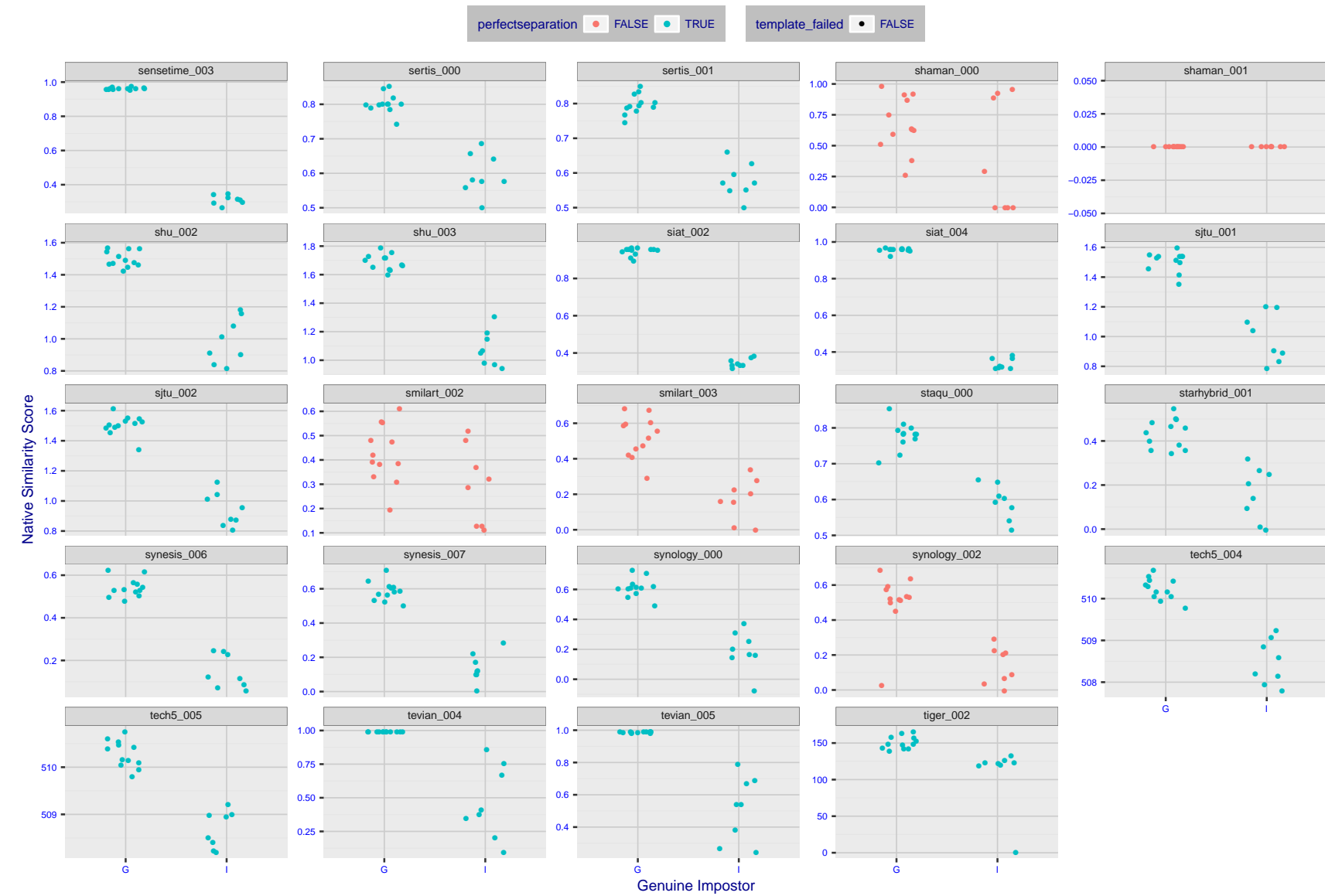


Figure 11: The Figure shows, in blue, algorithms that correctly separate the 12 genuine and 8 impostor pairs used in the May 2018 paper Face recognition accuracy of forensic examiners, superrecognizers, and face recognition algorithms (Phillips et al. [1]). In red are algorithms that are imperfect. Some algorithms fail only because they failed to make a template e.g. due to face detection failure (shown as a triangle). Others fail because the pairs were selected for that study because they had been difficult for three leading algorithms used in FRVT 2006. Caution: Given the small sample size ($n=20$) the figure may change substantially if larger or different sets were used. The images can be downloaded from the [Supplemental Information](#) page provided with that publication.

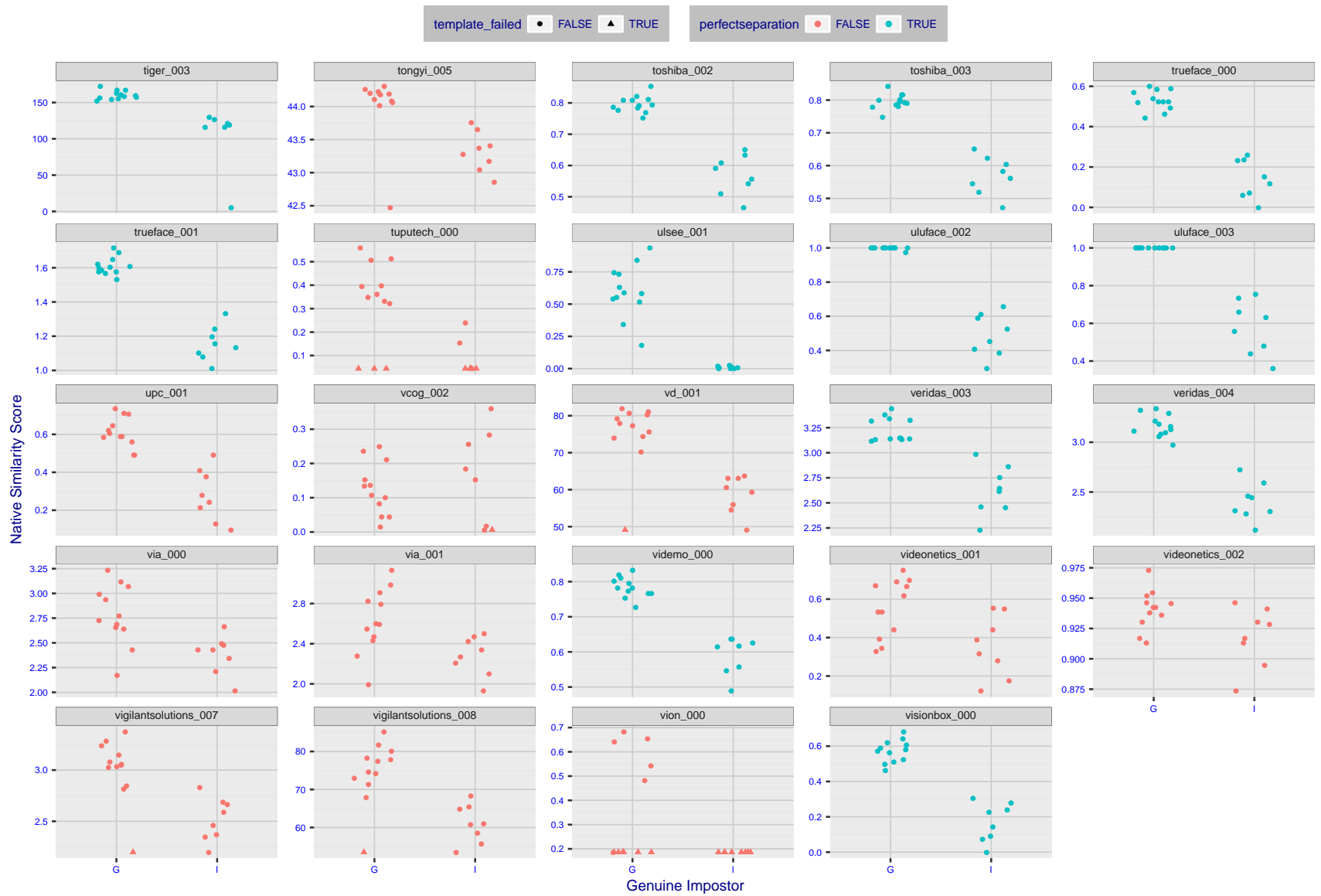


Figure 12: The Figure shows, in blue, algorithms that correctly separate the 12 genuine and 8 impostor pairs used in the May 2018 paper Face recognition accuracy of forensic examiners, superrecognizers, and face recognition algorithms (Phillips et al. [1]). In red are algorithms that are imperfect. Some algorithms fail only because they failed to make a template e.g. due to face detection failure (shown as a triangle). Others fail because the pairs were selected for that study because they had been difficult for three leading algorithms used in FRVT 2006. Caution: Given the small sample size ($n=20$) the figure may change substantially if larger or different sets were used. The images can be downloaded from the [Supplemental Information](#) page provided with that publication.

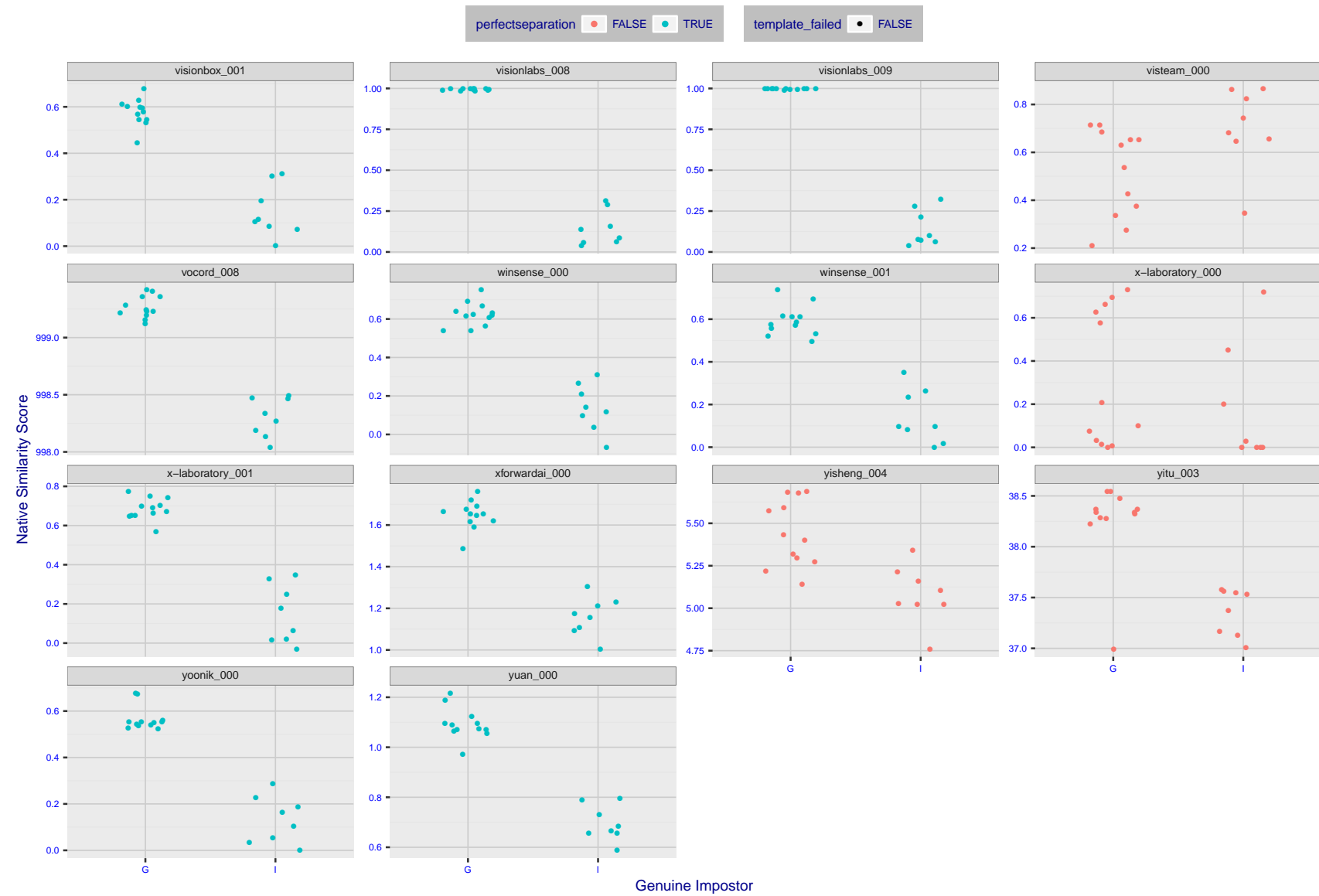


Figure 13: The Figure shows, in blue, algorithms that correctly separate the 12 genuine and 8 impostor pairs used in the May 2018 paper [Face recognition accuracy of forensic examiners, superrecognizers, and face recognition algorithms](#) (Phillips et al. [1]). In red are algorithms that are imperfect. Some algorithms fail only because they failed to make a template e.g. due to face detection failure (shown as a triangle). Others fail because the pairs were selected for that study because they had been difficult for three leading algorithms used in FRVT 2006. Caution: Given the small sample size ($n=20$) the figure may change substantially if larger or different sets were used. The images can be downloaded from the [Supplemental Information](#) page provided with that publication.

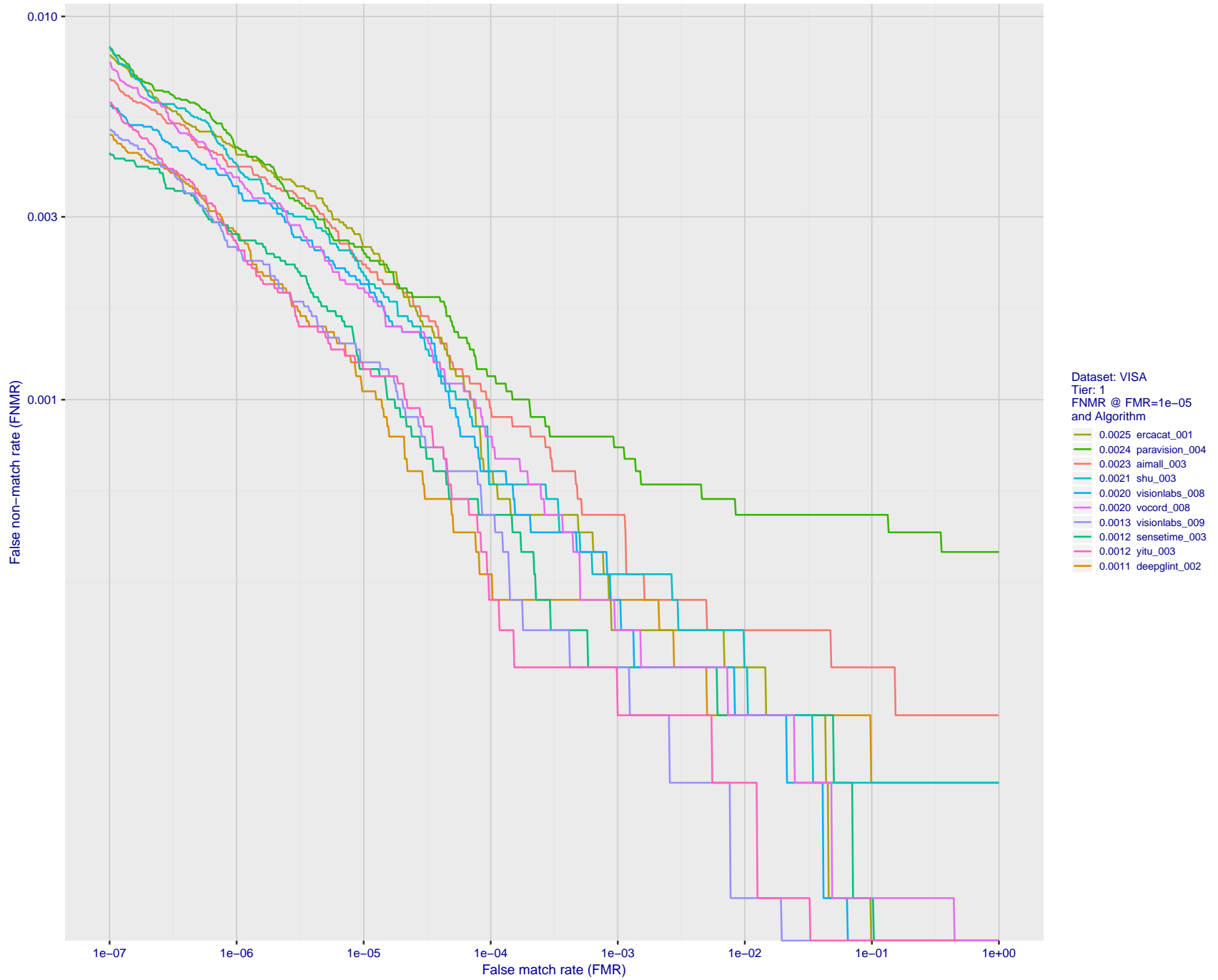


Figure 14: For the visa images, detection error tradeoff (DET) characteristics showing false non-match rate vs. false match rate plotted parametrically on threshold, T . The scales are logarithmic in order to show many decades of FMR.

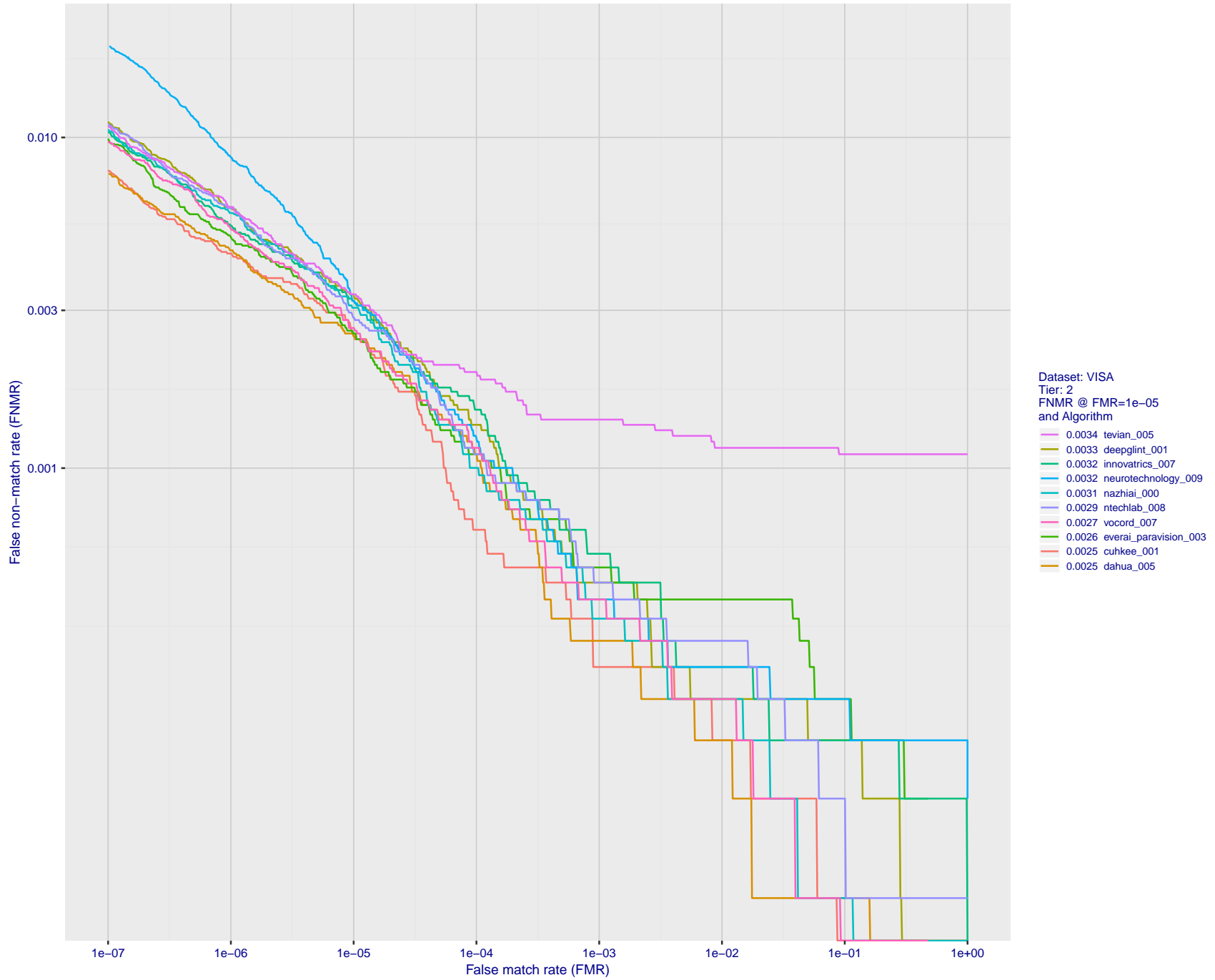


Figure 15: For the visa images, detection error tradeoff (DET) characteristics showing false non-match rate vs. false match rate plotted parametrically on threshold, T . The scales are logarithmic in order to show many decades of FMR.

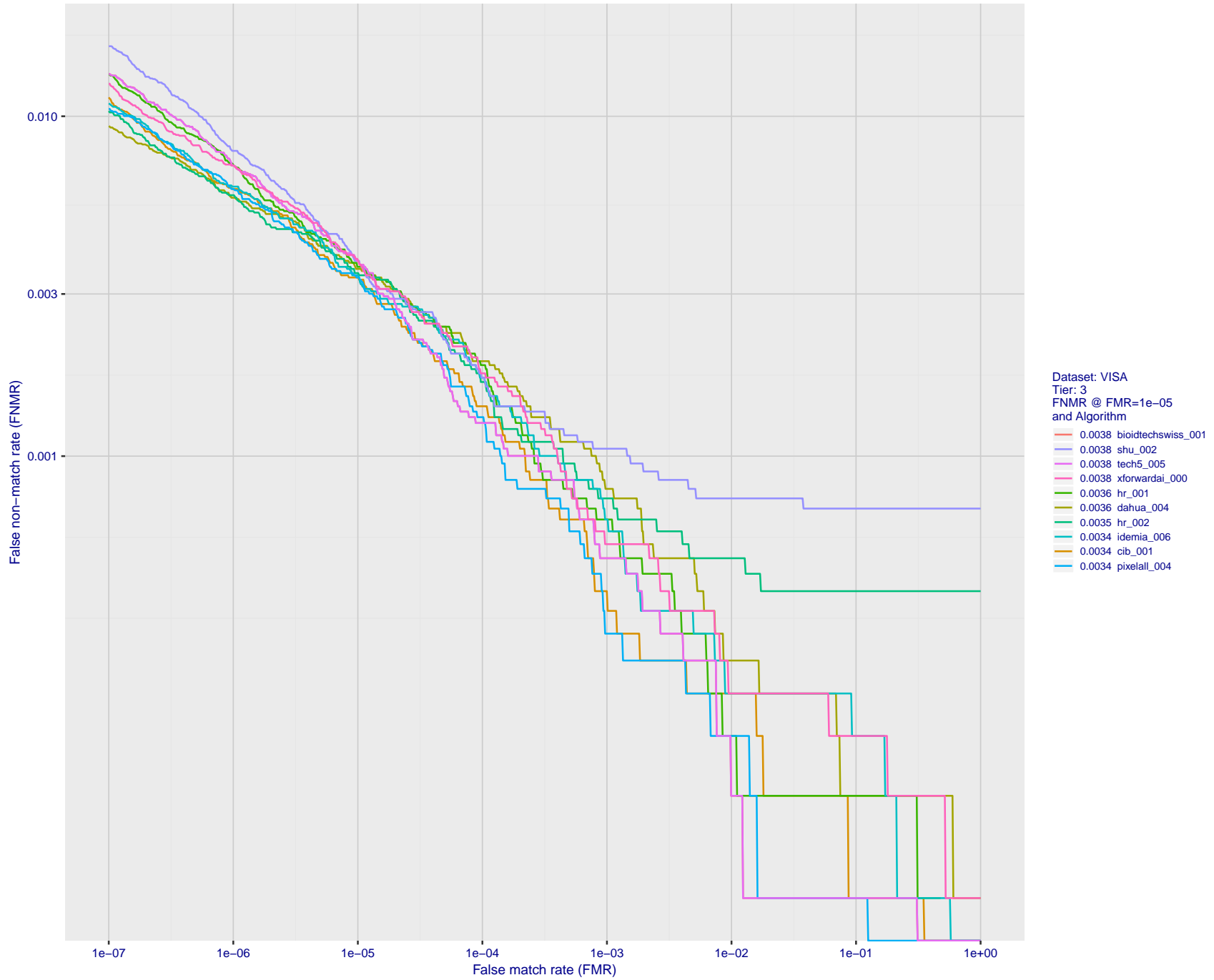


Figure 16: For the visa images, detection error tradeoff (DET) characteristics showing false non-match rate vs. false match rate plotted parametrically on threshold, T . The scales are logarithmic in order to show many decades of FMR.

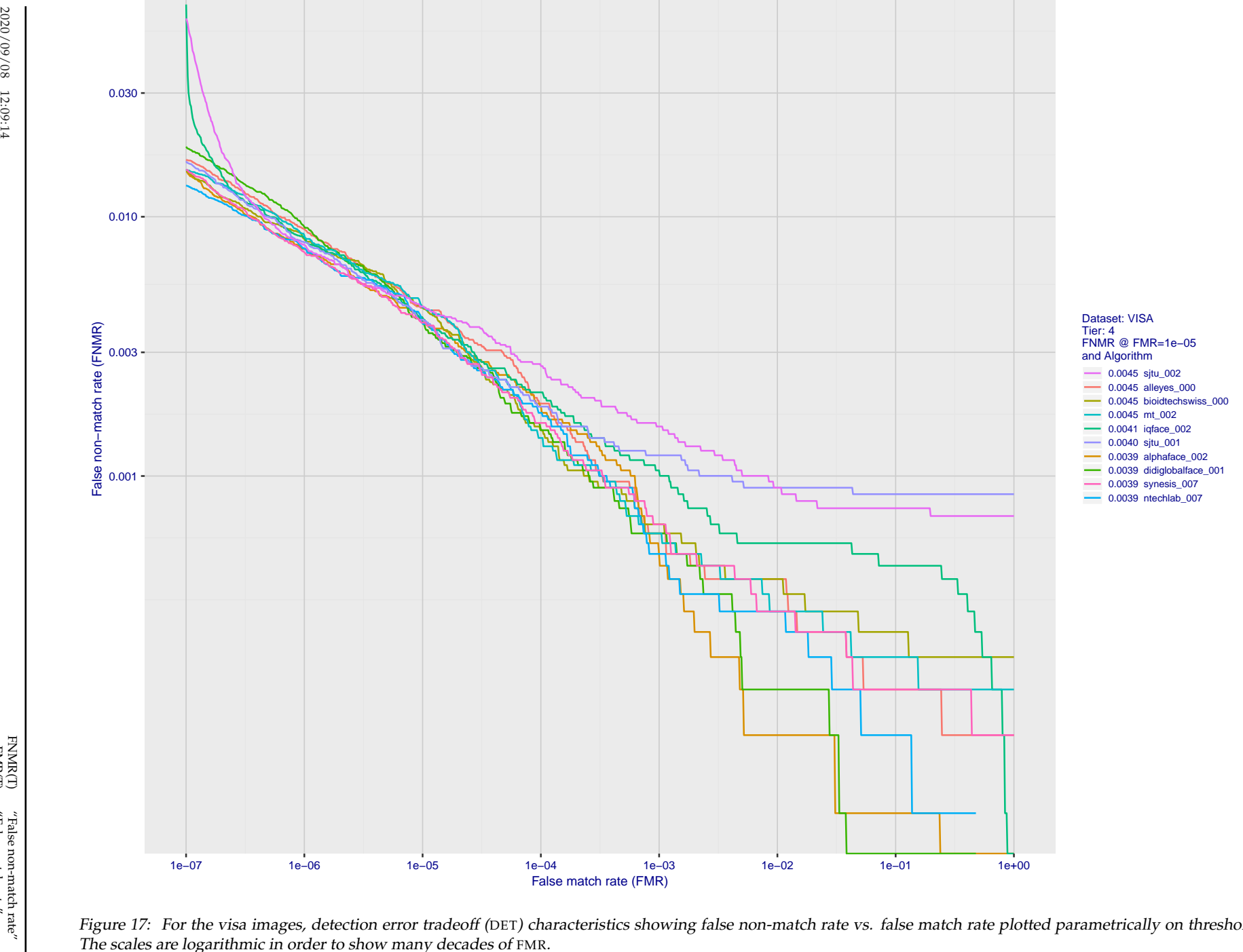


Figure 17: For the visa images, detection error tradeoff (DET) characteristics showing false non-match rate vs. false match rate plotted parametrically on threshold, T . The scales are logarithmic in order to show many decades of FMR.

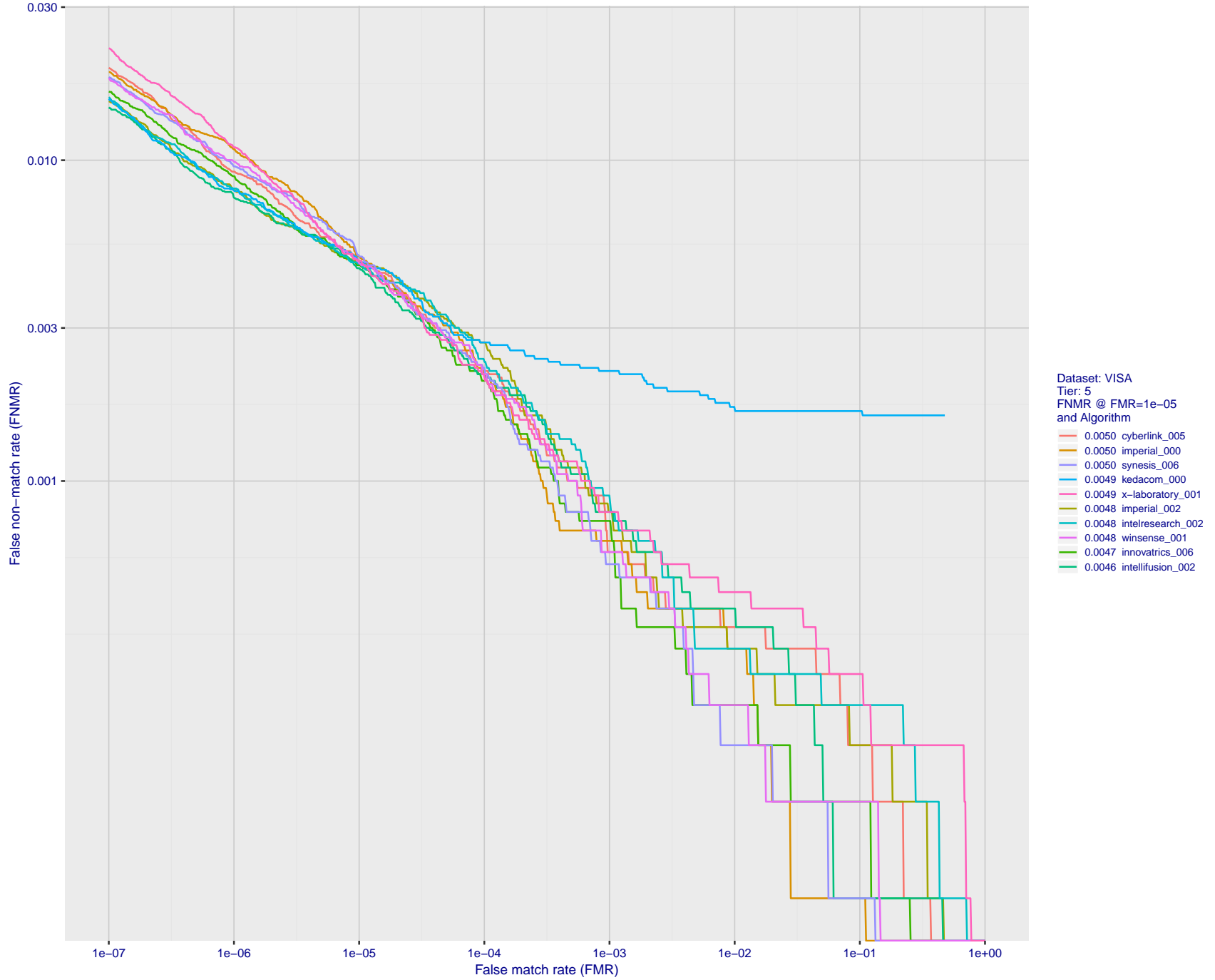


Figure 18: For the visa images, detection error tradeoff (DET) characteristics showing false non-match rate vs. false match rate plotted parametrically on threshold, T . The scales are logarithmic in order to show many decades of FMR.

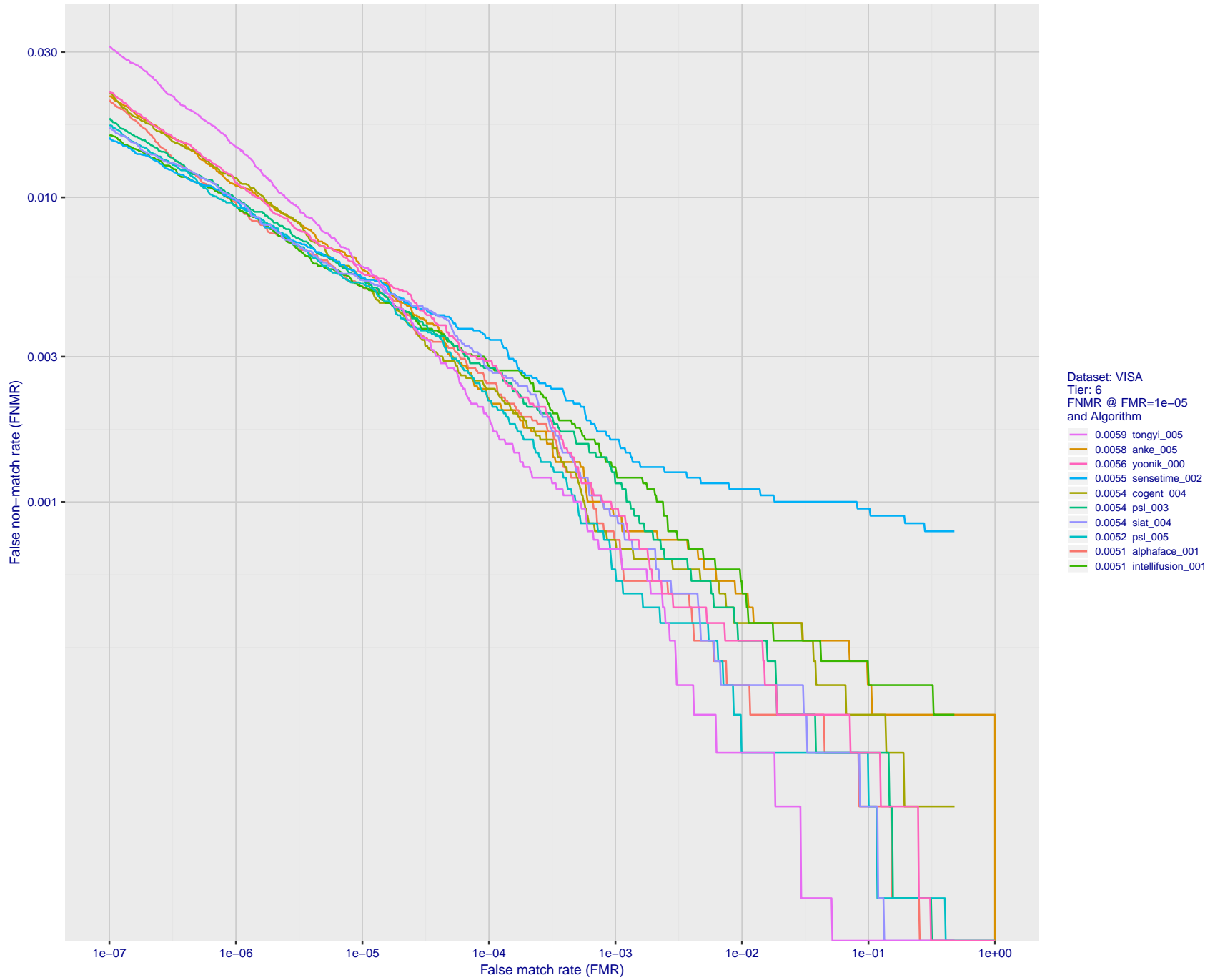


Figure 19: For the visa images, detection error tradeoff (DET) characteristics showing false non-match rate vs. false match rate plotted parametrically on threshold, T . The scales are logarithmic in order to show many decades of FMR.

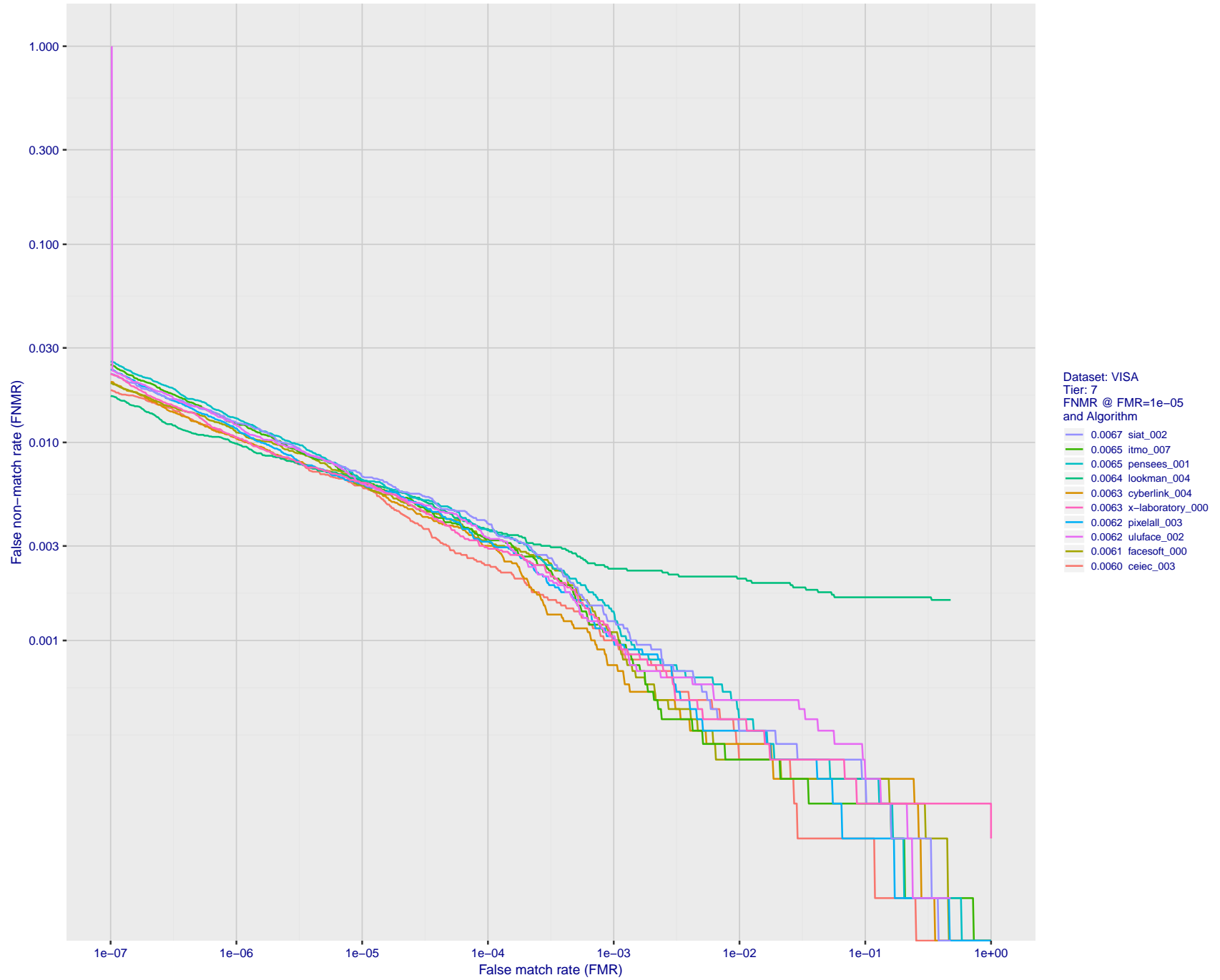


Figure 20: For the visa images, detection error tradeoff (DET) characteristics showing false non-match rate vs. false match rate plotted parametrically on threshold, T . The scales are logarithmic in order to show many decades of FMR.

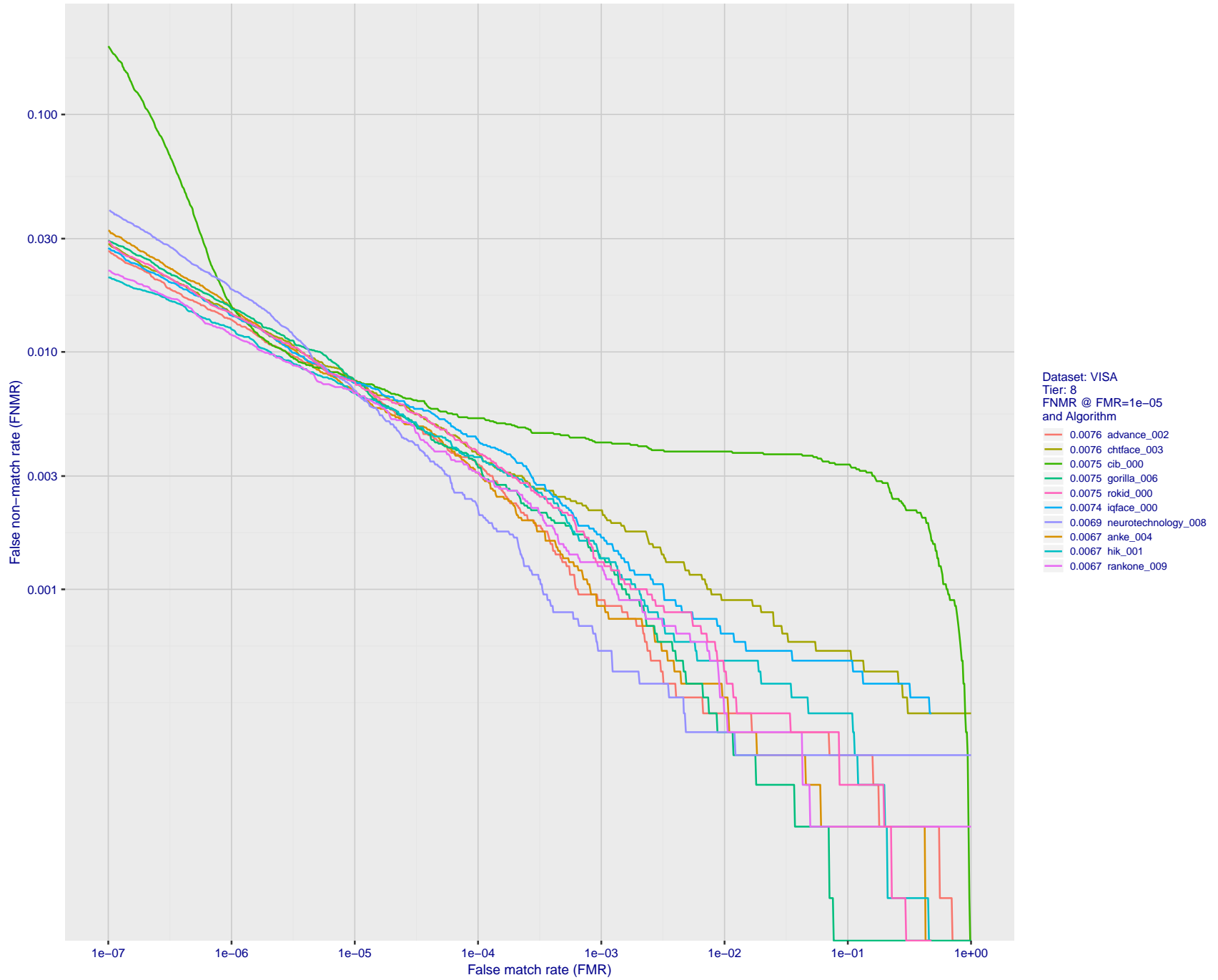


Figure 21: For the visa images, detection error tradeoff (DET) characteristics showing false non-match rate vs. false match rate plotted parametrically on threshold, T . The scales are logarithmic in order to show many decades of FMR.

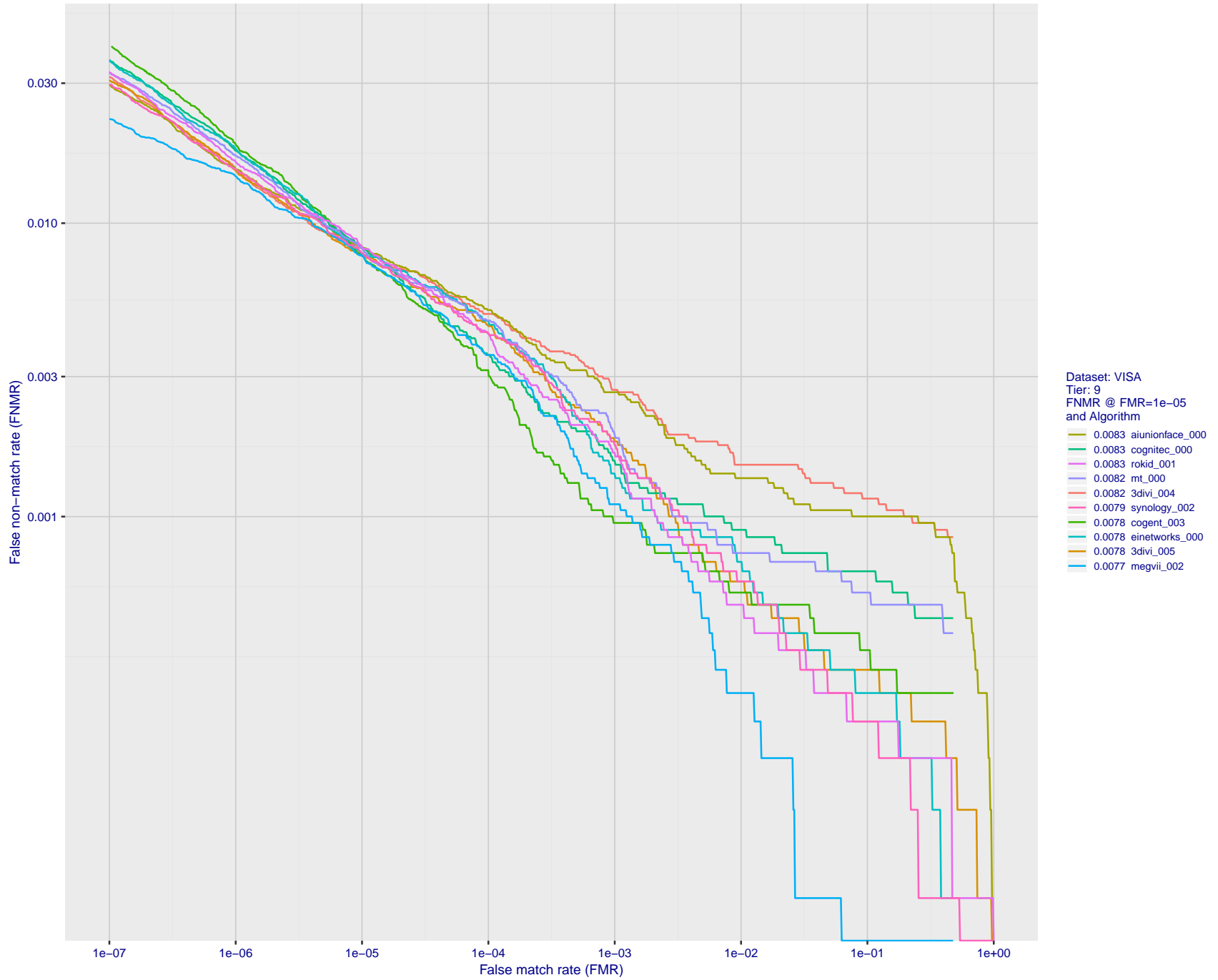


Figure 22: For the visa images, detection error tradeoff (DET) characteristics showing false non-match rate vs. false match rate plotted parametrically on threshold, T . The scales are logarithmic in order to show many decades of FMR.

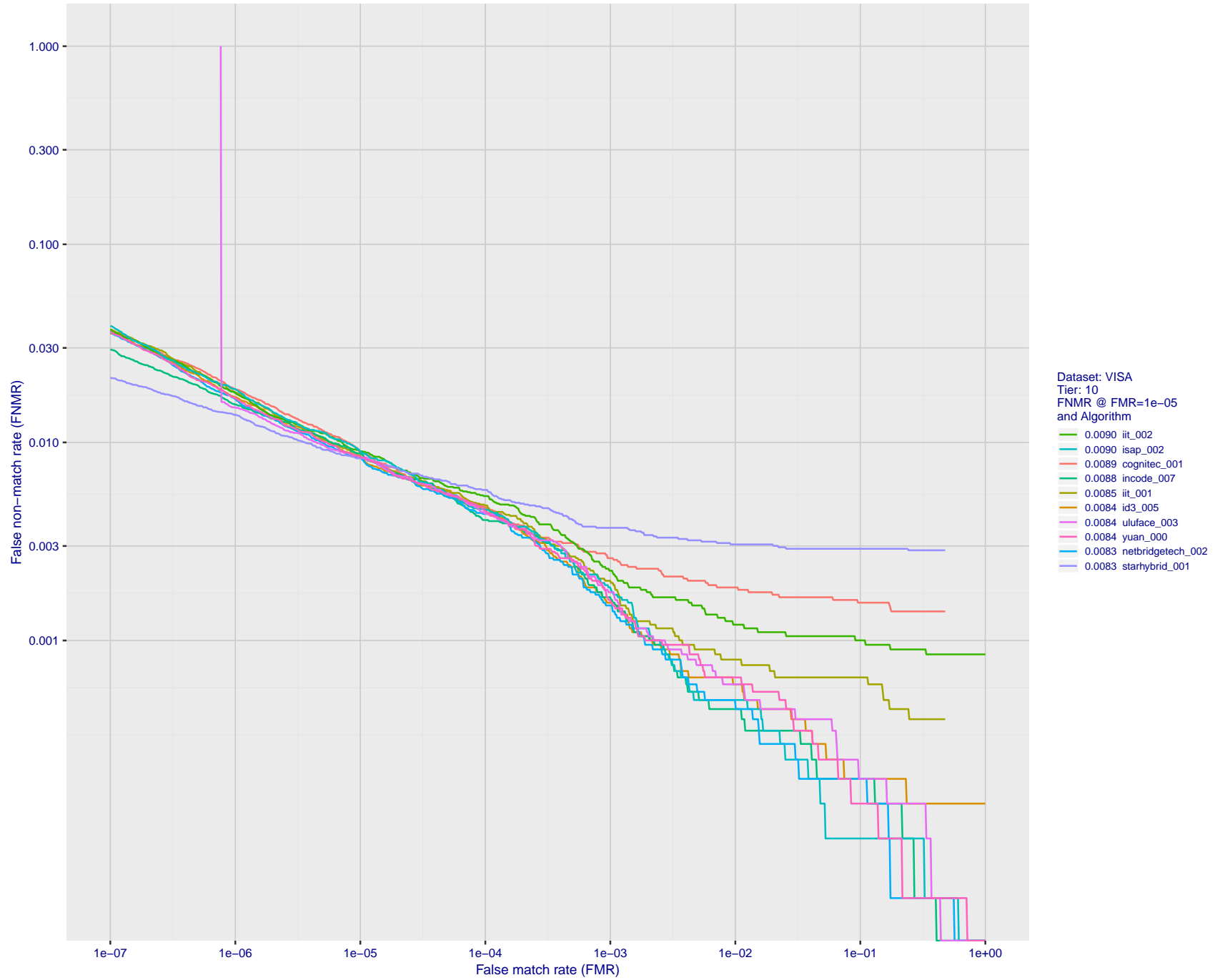


Figure 23: For the visa images, detection error tradeoff (DET) characteristics showing false non-match rate vs. false match rate plotted parametrically on threshold, T . The scales are logarithmic in order to show many decades of FMR.

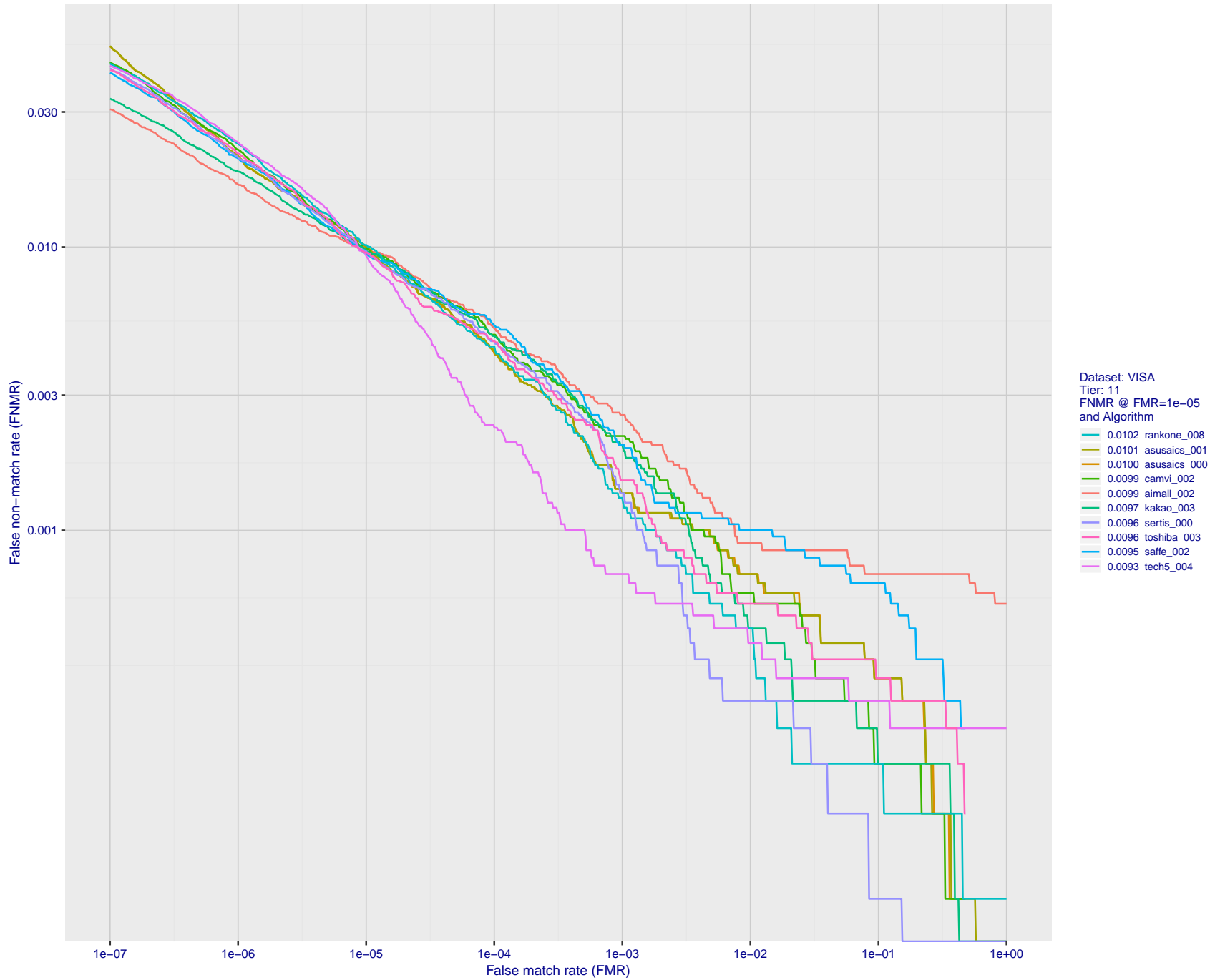


Figure 24: For the visa images, detection error tradeoff (DET) characteristics showing false non-match rate vs. false match rate plotted parametrically on threshold, T . The scales are logarithmic in order to show many decades of FMR.

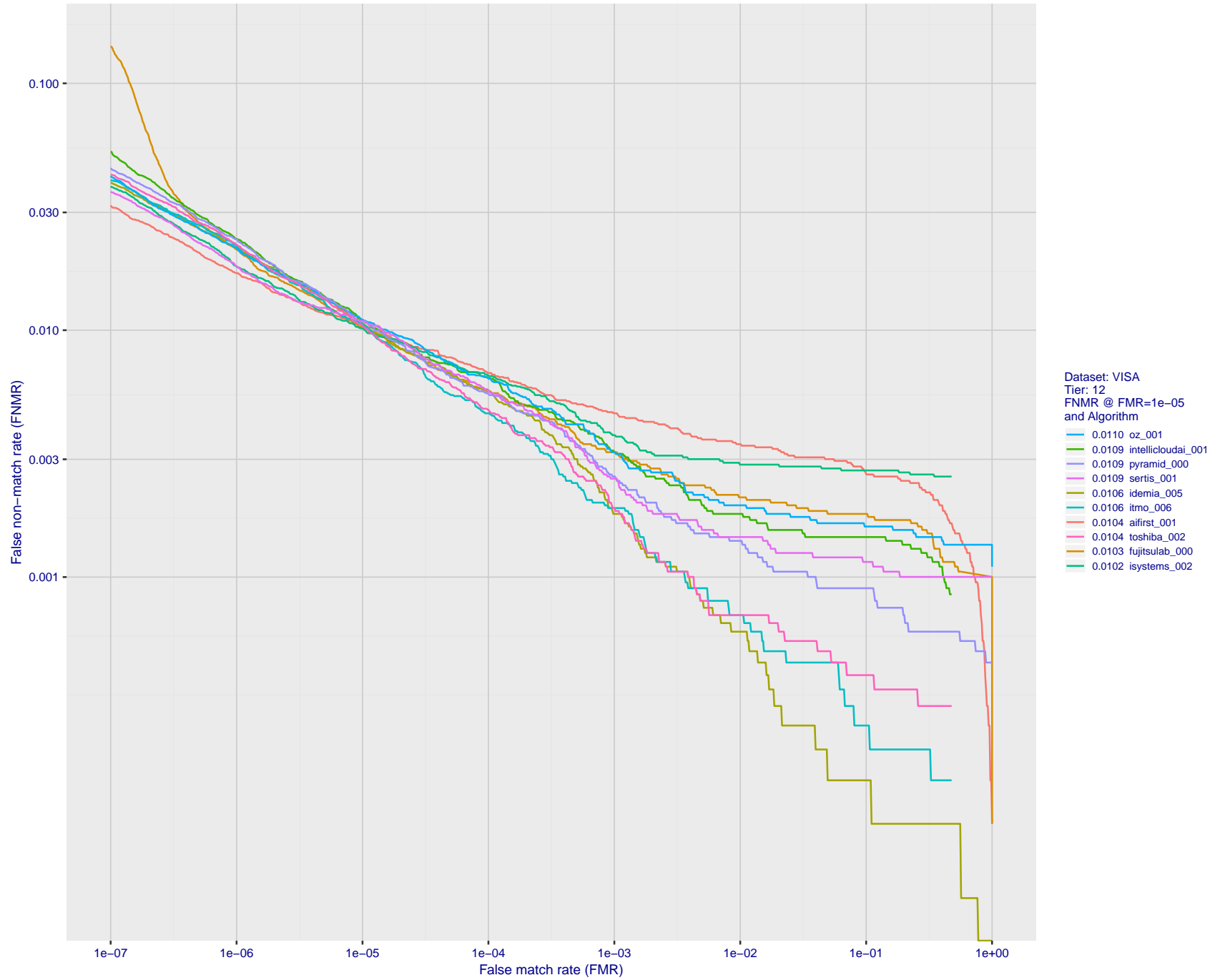


Figure 25: For the visa images, detection error tradeoff (DET) characteristics showing false non-match rate vs. false match rate plotted parametrically on threshold, T . The scales are logarithmic in order to show many decades of FMR.

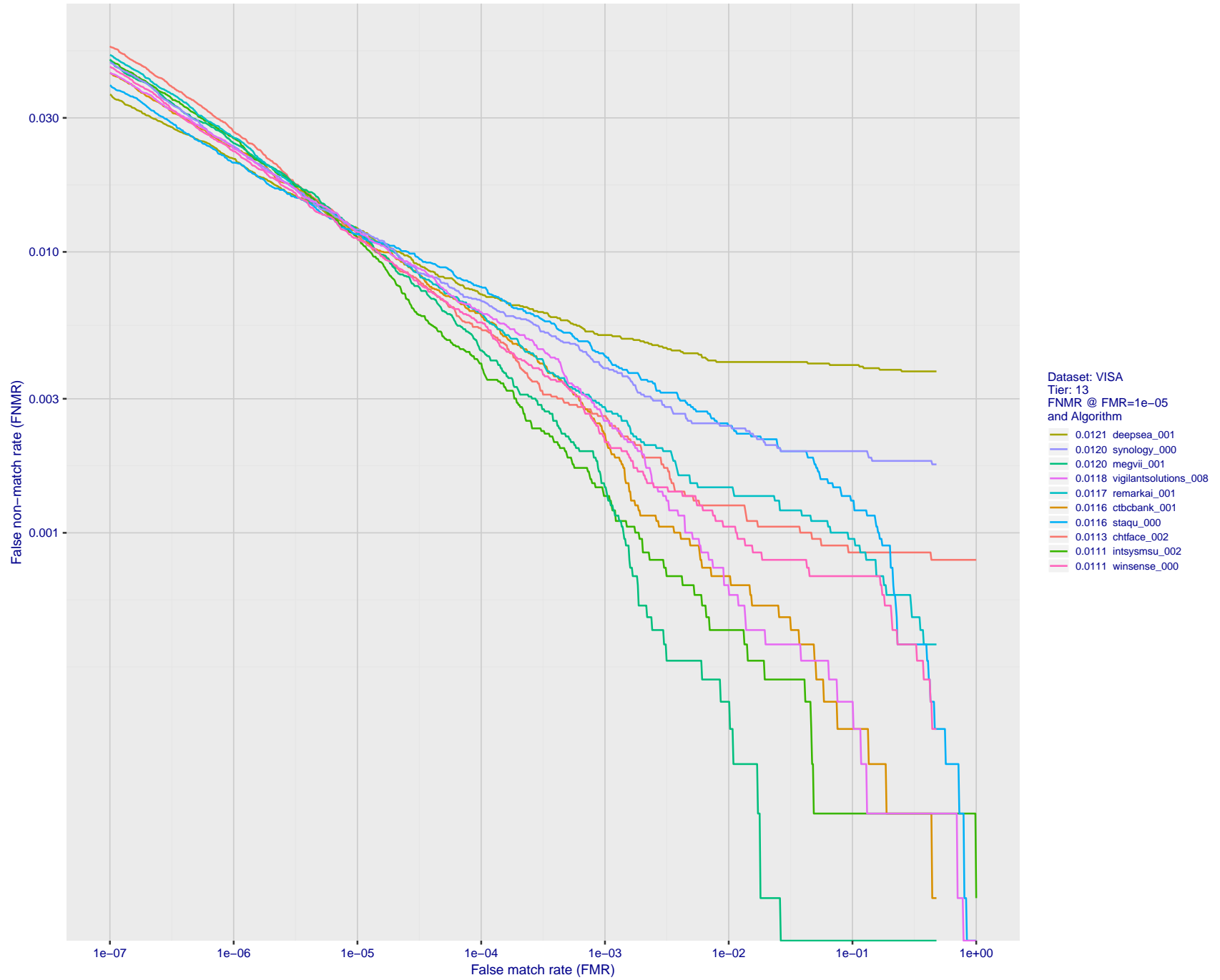


Figure 26: For the visa images, detection error tradeoff (DET) characteristics showing false non-match rate vs. false match rate plotted parametrically on threshold, T . The scales are logarithmic in order to show many decades of FMR.

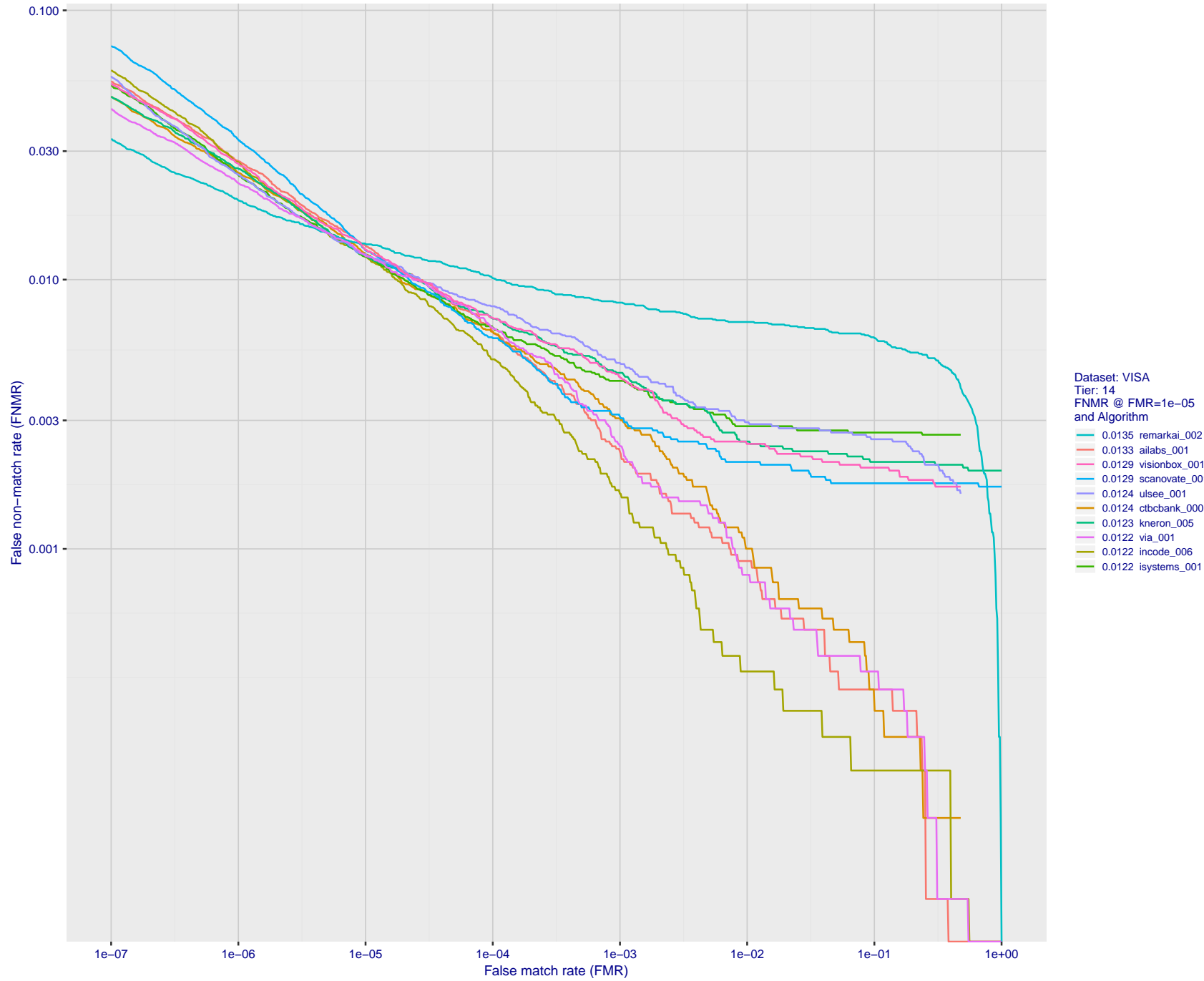


Figure 27: For the visa images, detection error tradeoff (DET) characteristics showing false non-match rate vs. false match rate plotted parametrically on threshold, T . The scales are logarithmic in order to show many decades of FMR.

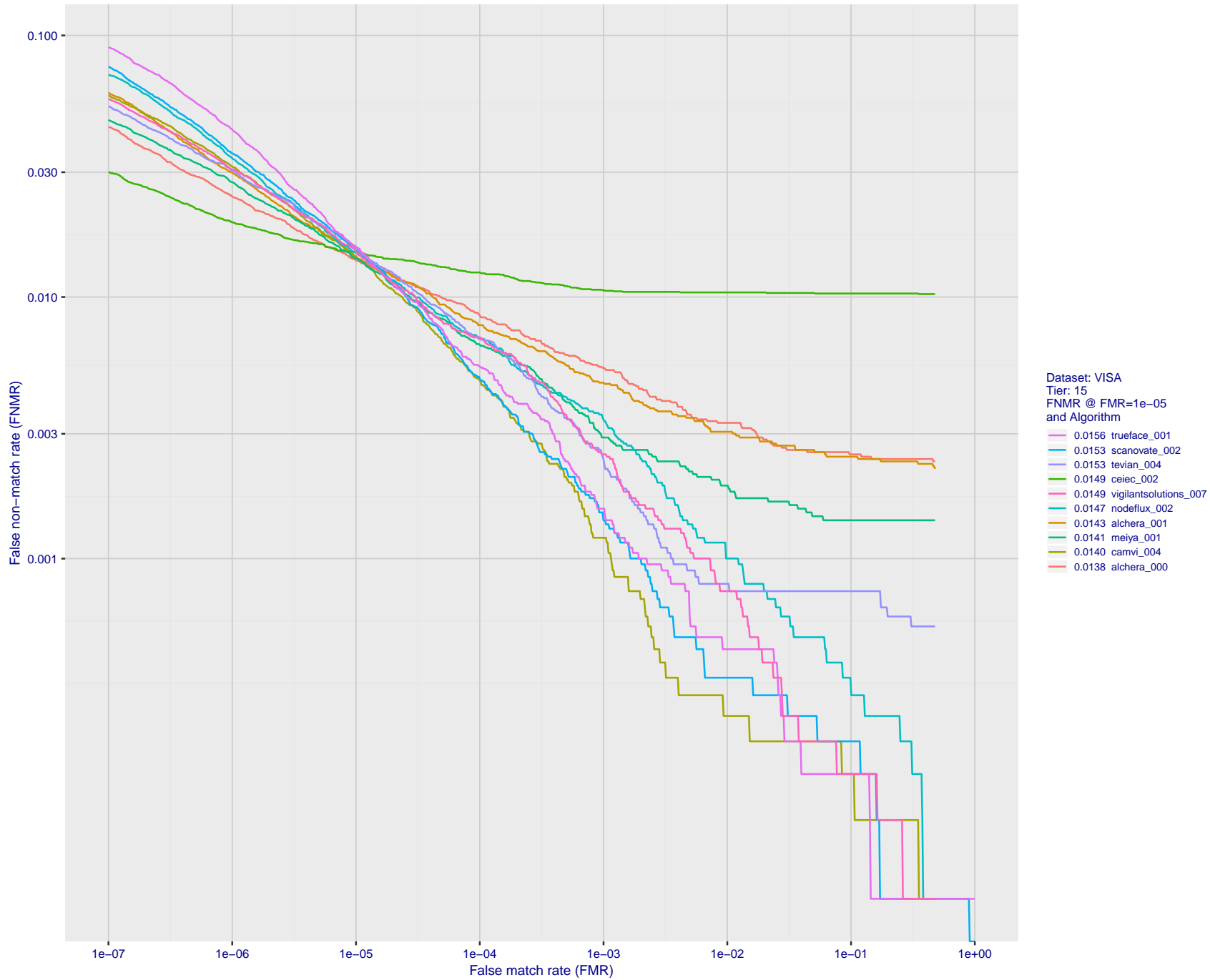


Figure 28: For the visa images, detection error tradeoff (DET) characteristics showing false non-match rate vs. false match rate plotted parametrically on threshold, T . The scales are logarithmic in order to show many decades of FMR.

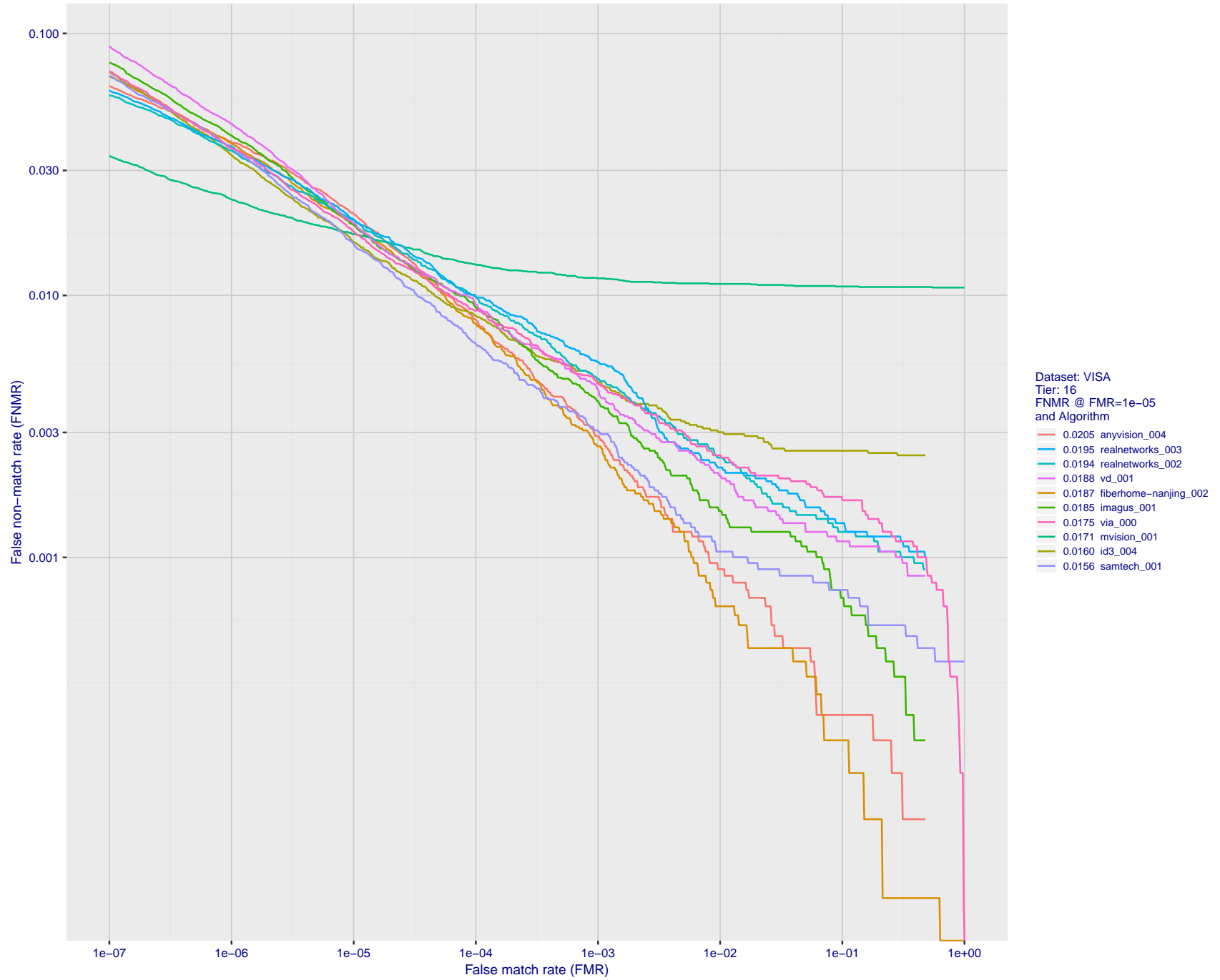


Figure 29: For the visa images, detection error tradeoff (DET) characteristics showing false non-match rate vs. false match rate plotted parametrically on threshold, T . The scales are logarithmic in order to show many decades of FMR.

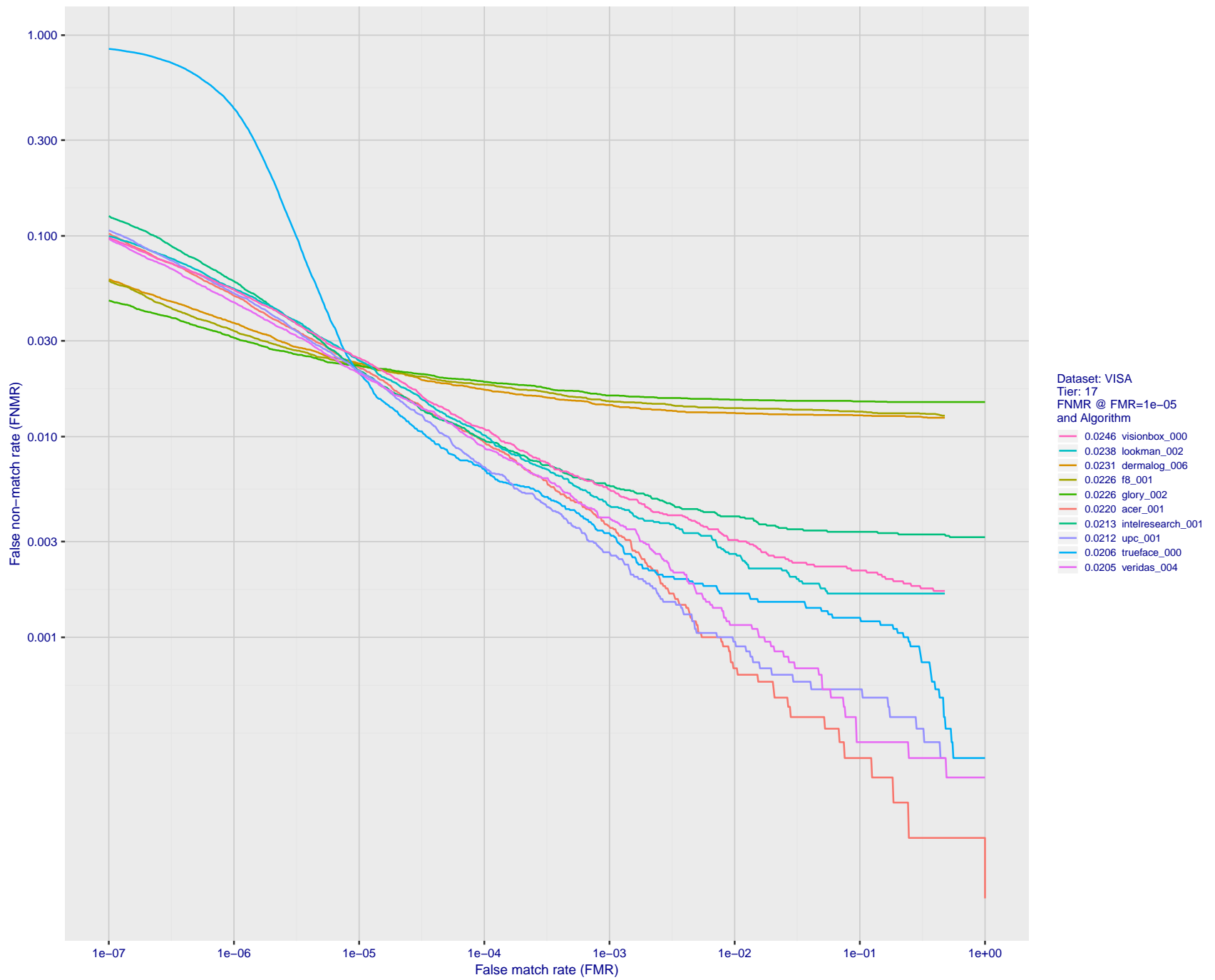


Figure 30: For the visa images, detection error tradeoff (DET) characteristics showing false non-match rate vs. false match rate plotted parametrically on threshold, T . The scales are logarithmic in order to show many decades of FMR.

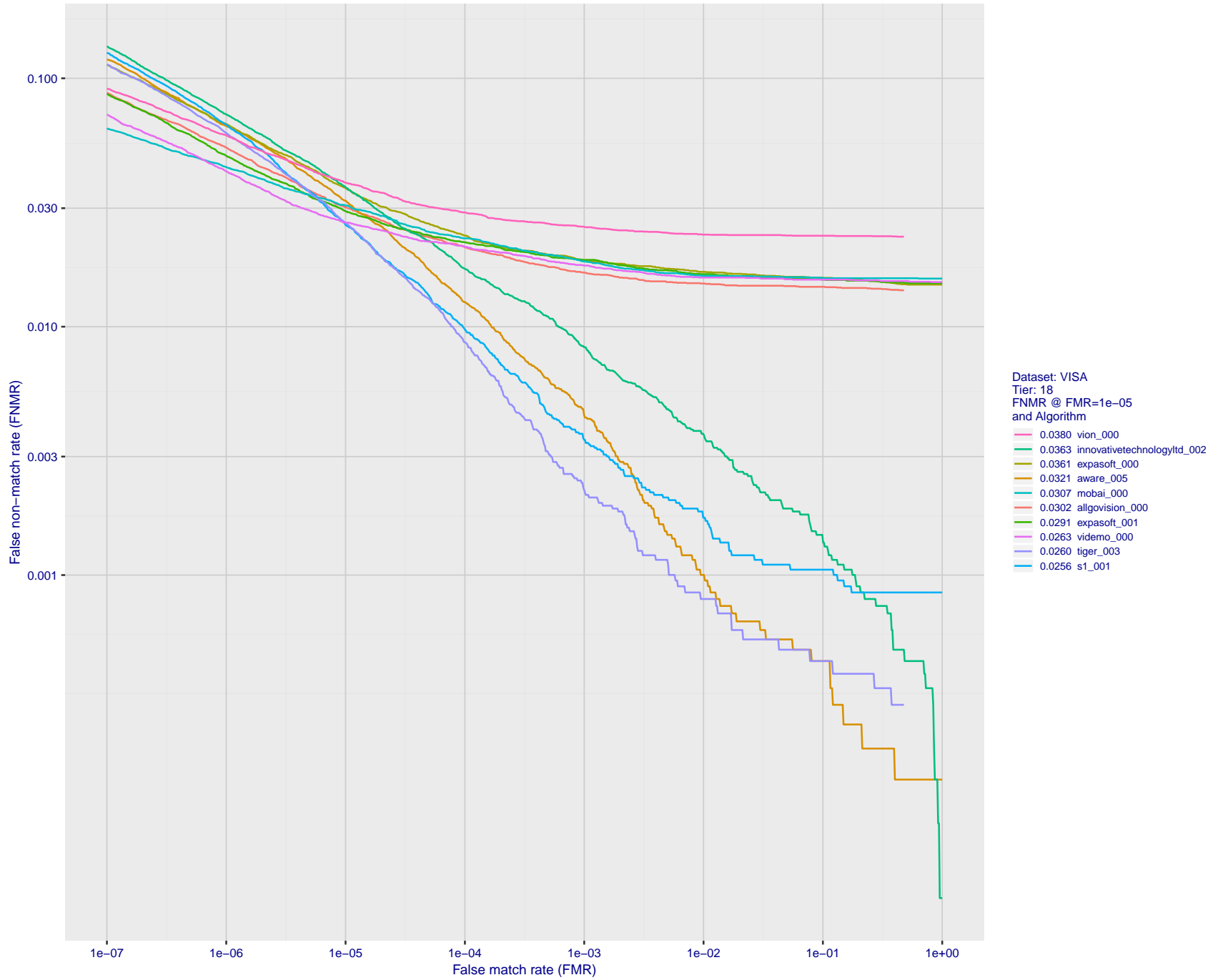


Figure 31: For the visa images, detection error tradeoff (DET) characteristics showing false non-match rate vs. false match rate plotted parametrically on threshold, T . The scales are logarithmic in order to show many decades of FMR.

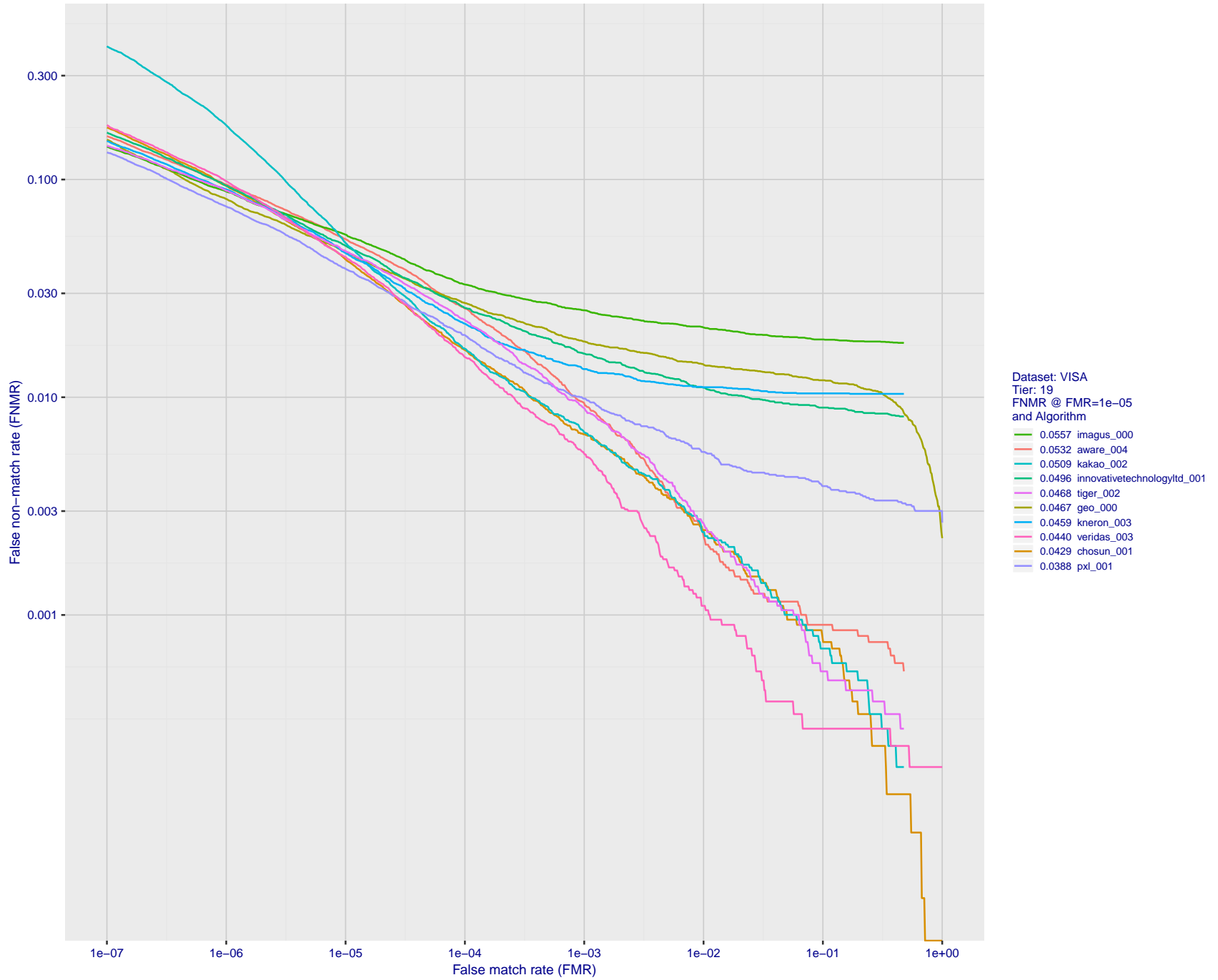


Figure 32: For the visa images, detection error tradeoff (DET) characteristics showing false non-match rate vs. false match rate plotted parametrically on threshold, T . The scales are logarithmic in order to show many decades of FMR.

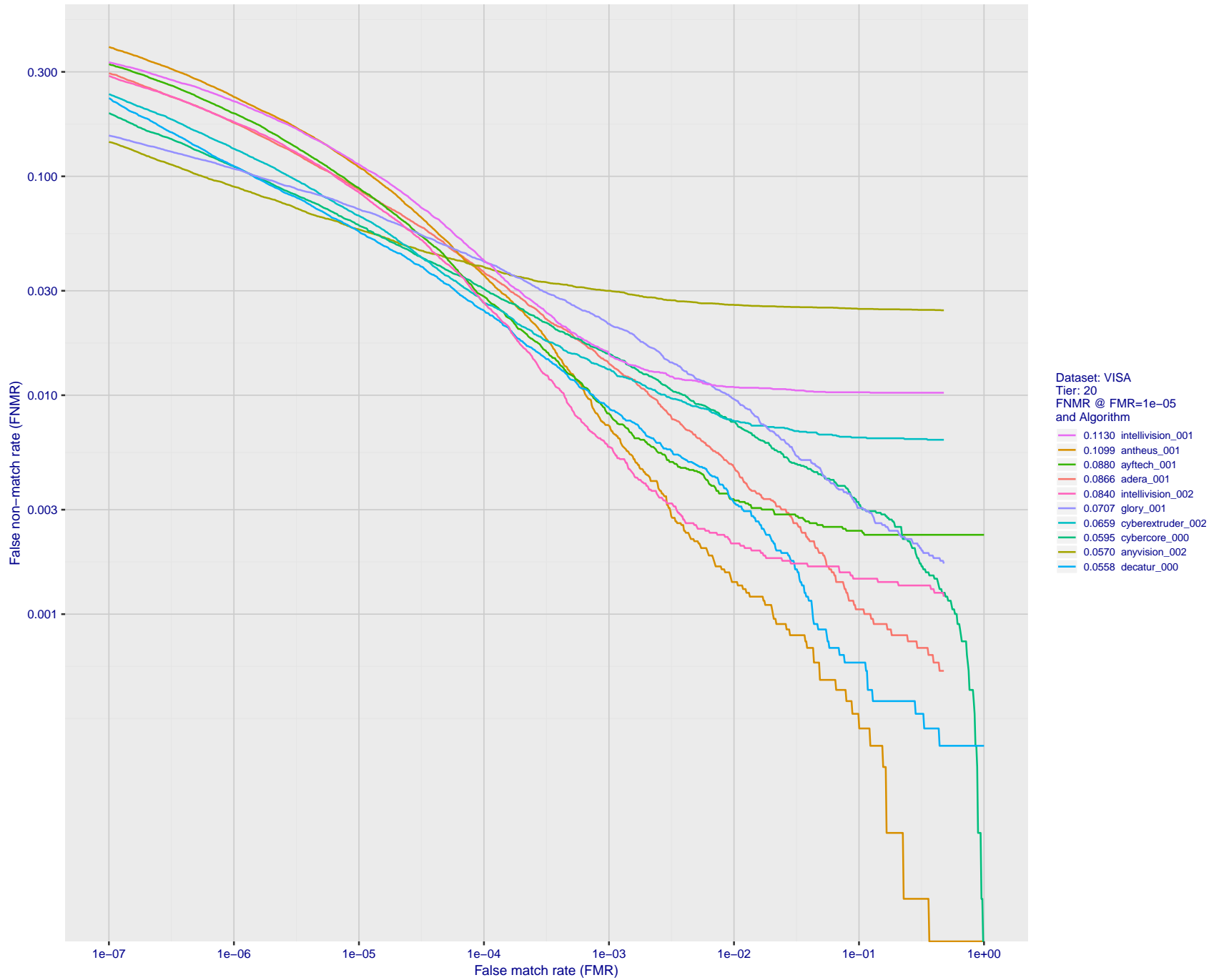


Figure 33: For the visa images, detection error tradeoff (DET) characteristics showing false non-match rate vs. false match rate plotted parametrically on threshold, T . The scales are logarithmic in order to show many decades of FMR.

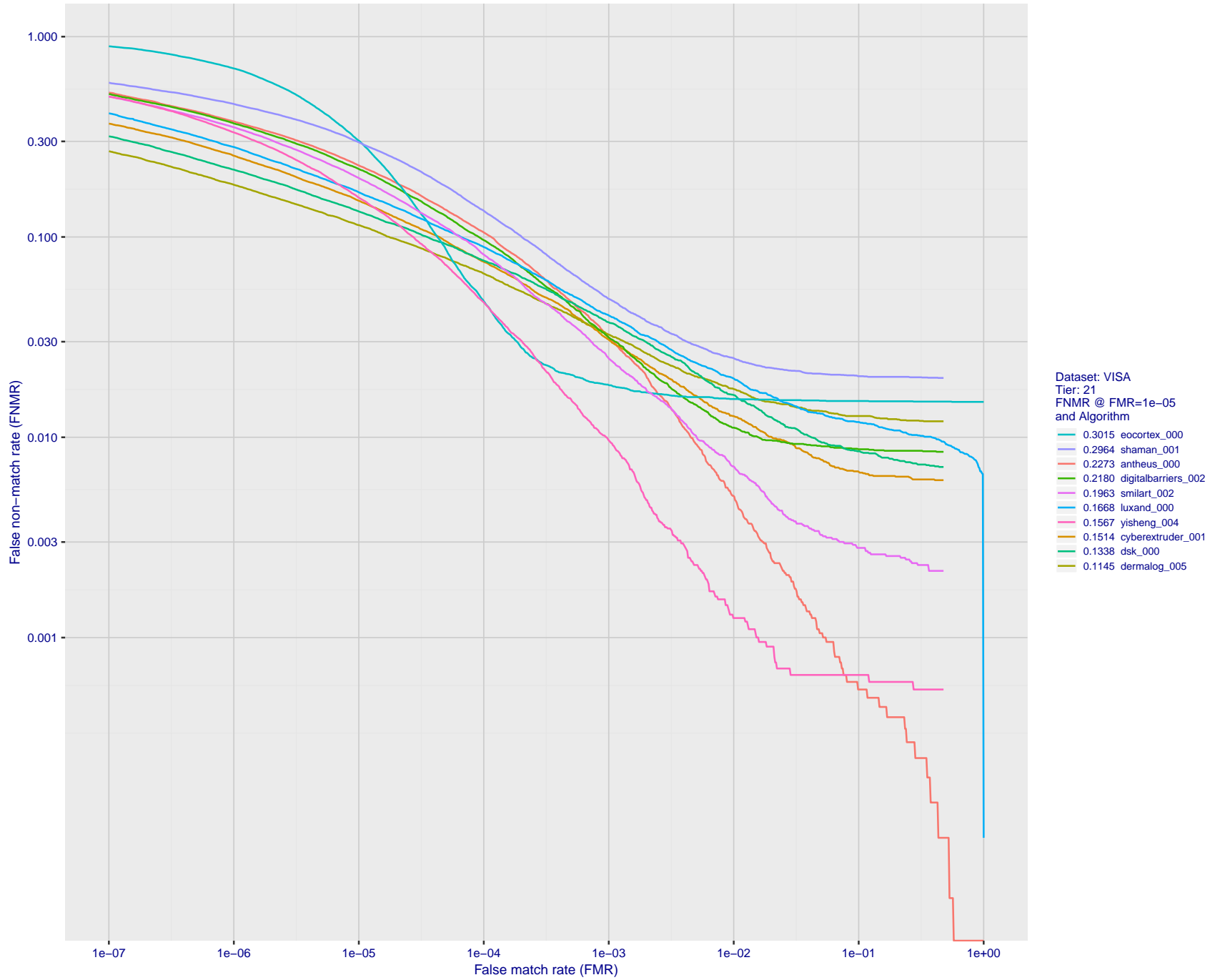


Figure 34: For the visa images, detection error tradeoff (DET) characteristics showing false non-match rate vs. false match rate plotted parametrically on threshold, T . The scales are logarithmic in order to show many decades of FMR.

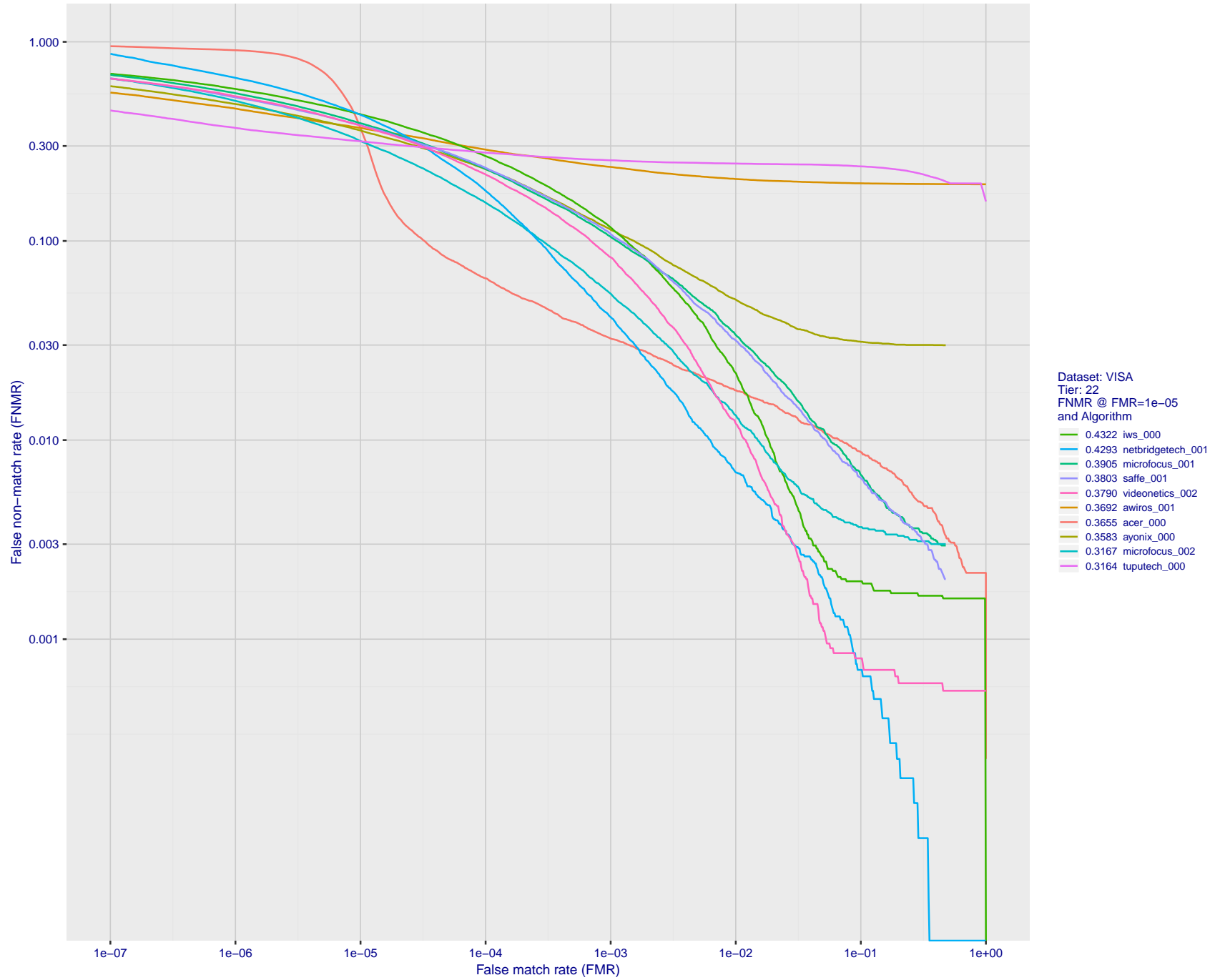


Figure 35: For the visa images, detection error tradeoff (DET) characteristics showing false non-match rate vs. false match rate plotted parametrically on threshold, T . The scales are logarithmic in order to show many decades of FMR.

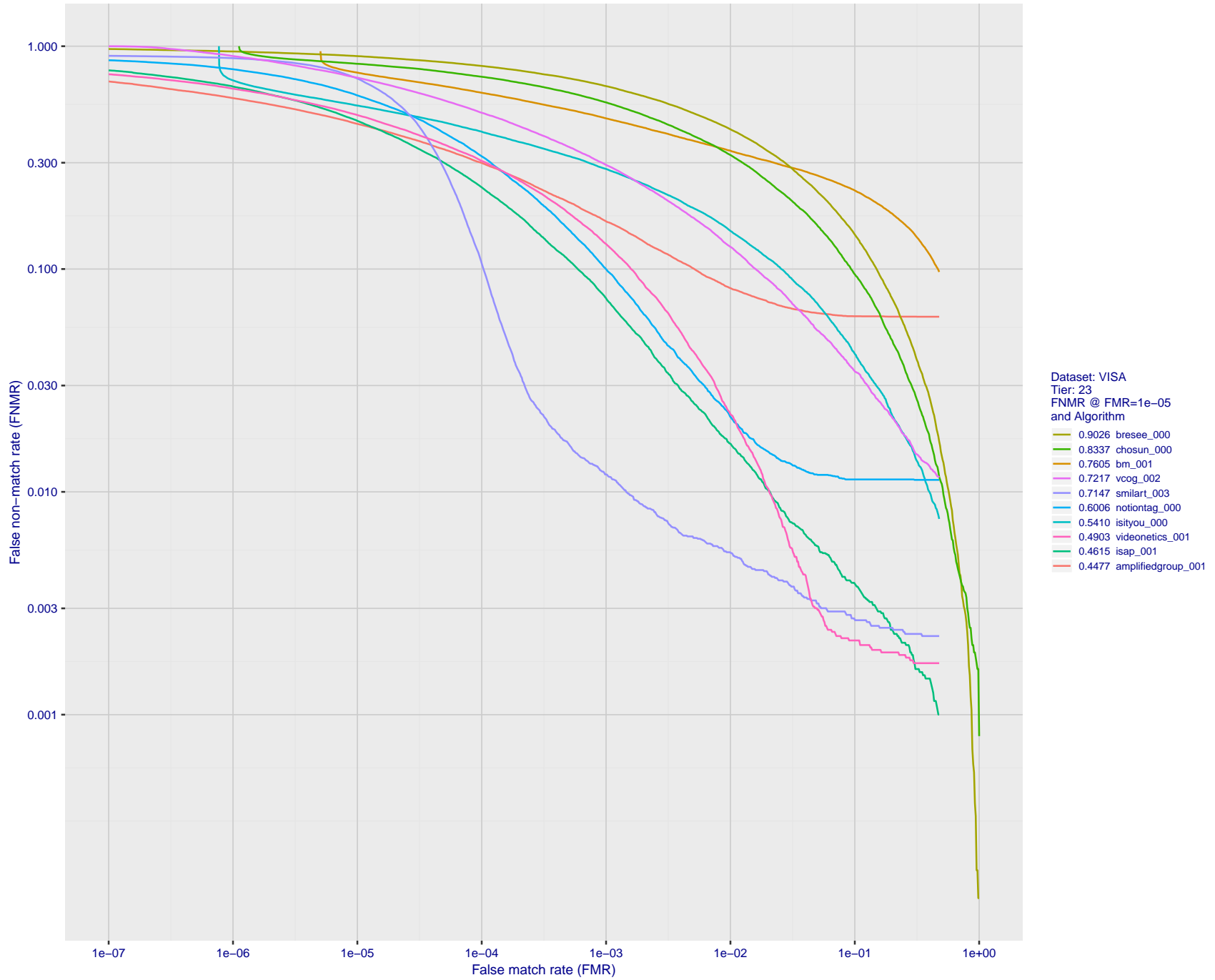


Figure 36: For the visa images, detection error tradeoff (DET) characteristics showing false non-match rate vs. false match rate plotted parametrically on threshold, T . The scales are logarithmic in order to show many decades of FMR.

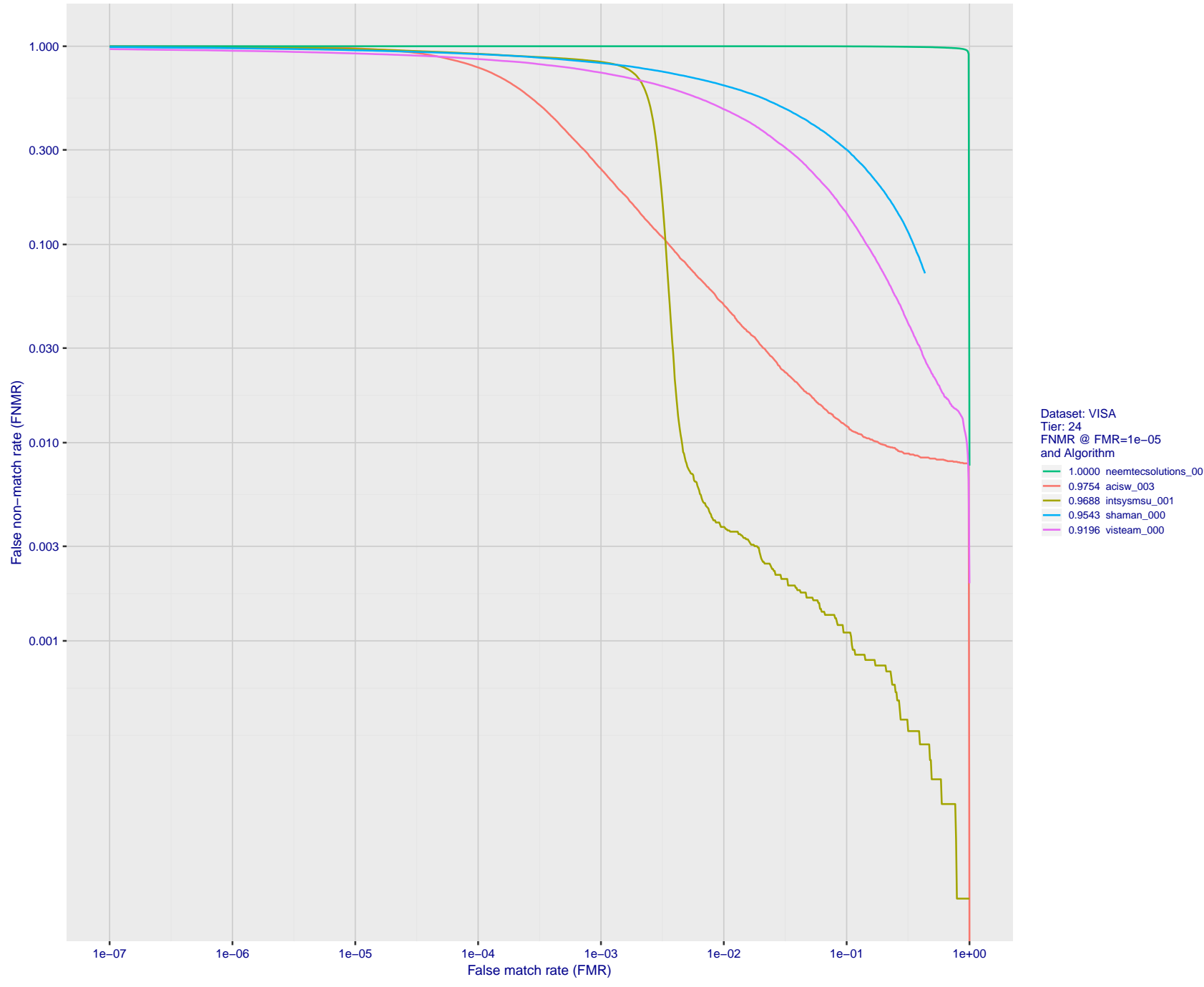


Figure 37: For the visa images, detection error tradeoff (DET) characteristics showing false non-match rate vs. false match rate plotted parametrically on threshold, T . The scales are logarithmic in order to show many decades of FMR.

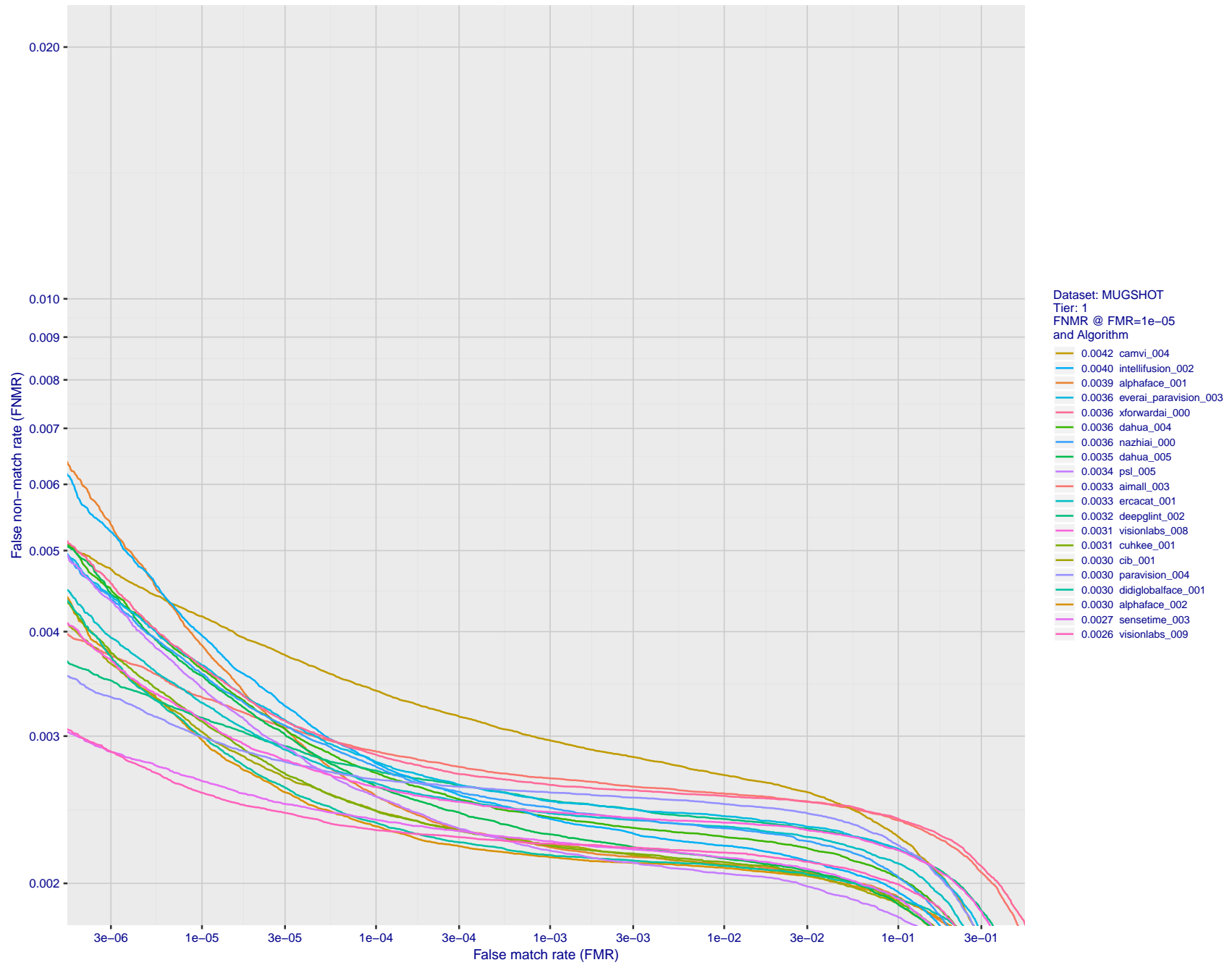
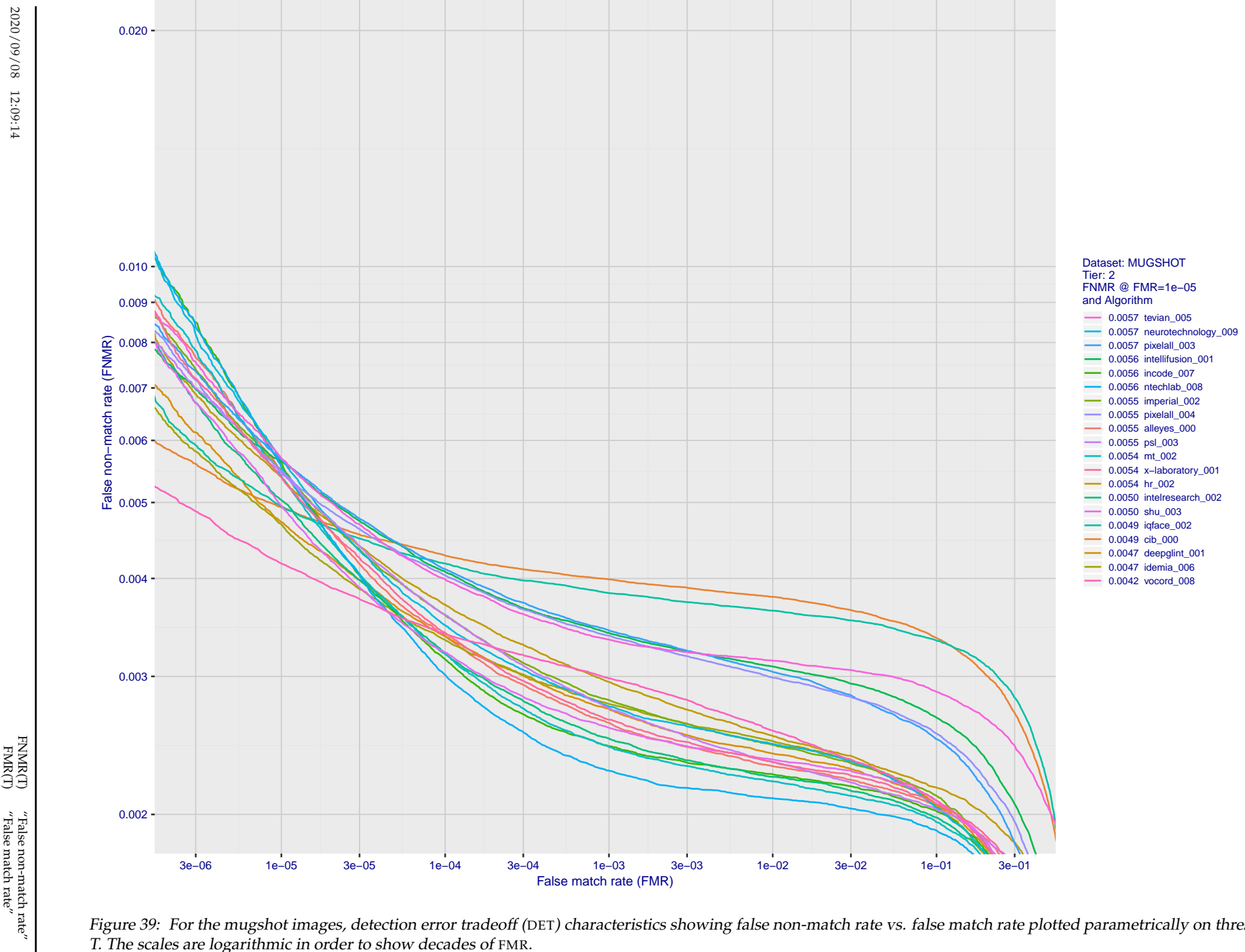


Figure 38: For the mugshot images, detection error tradeoff (DET) characteristics showing false non-match rate vs. false match rate plotted parametrically on threshold, T . The scales are logarithmic in order to show decades of FMR.



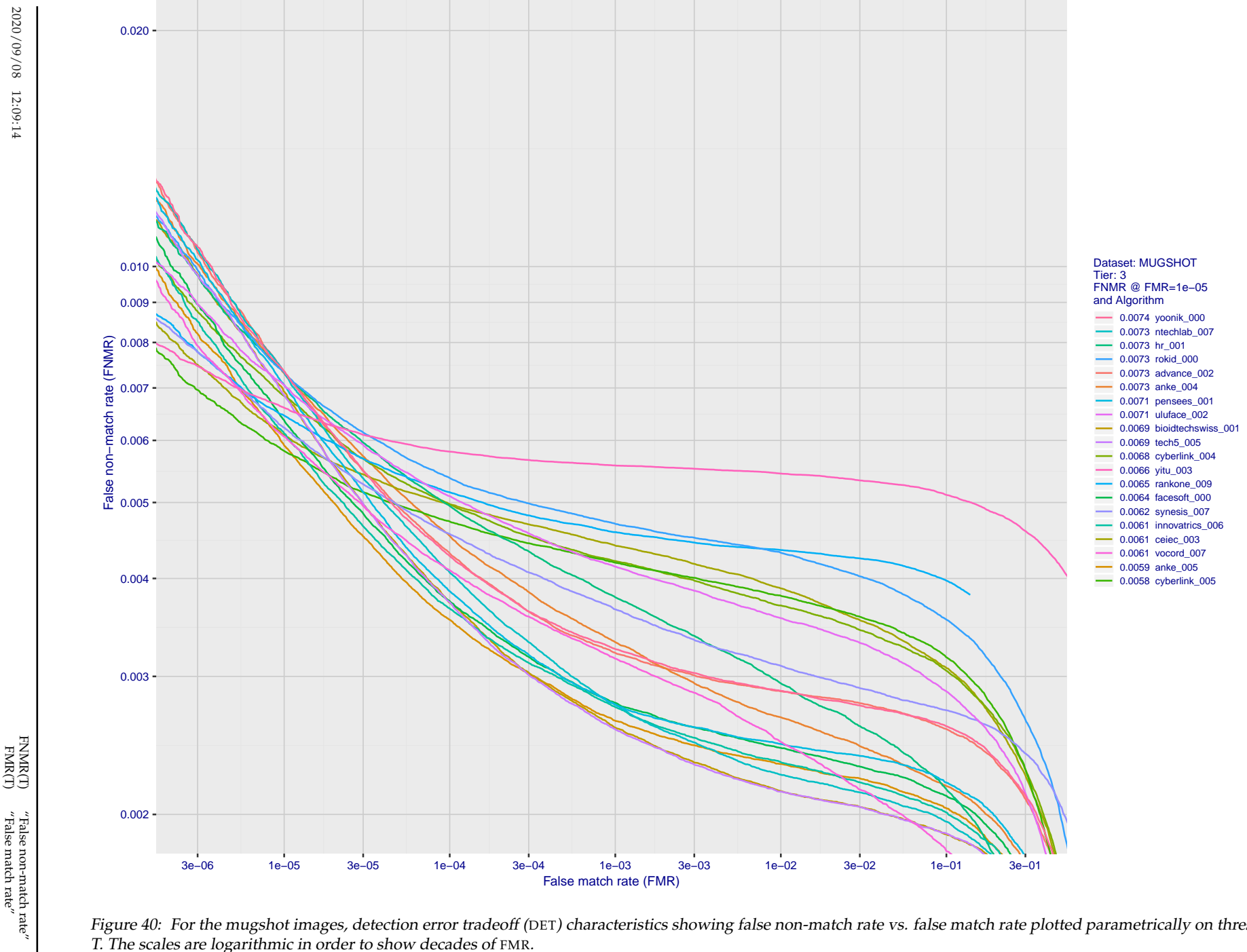


Figure 40: For the mugshot images, detection error tradeoff (DET) characteristics showing false non-match rate vs. false match rate plotted parametrically on threshold, T. The scales are logarithmic in order to show decades of FMR.

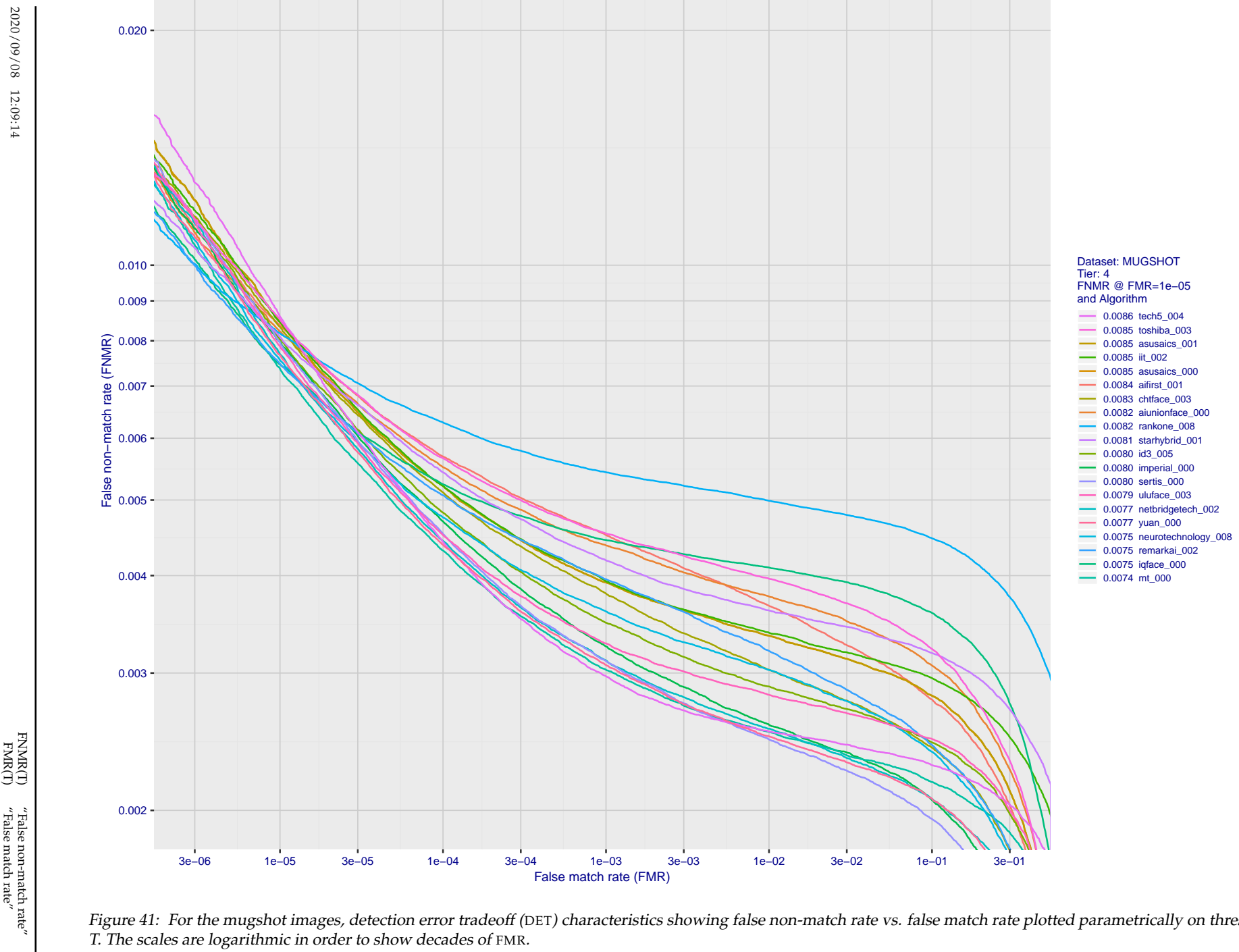


Figure 41: For the mugshot images, detection error tradeoff (DET) characteristics showing false non-match rate vs. false match rate plotted parametrically on threshold, T. The scales are logarithmic in order to show decades of FMR.

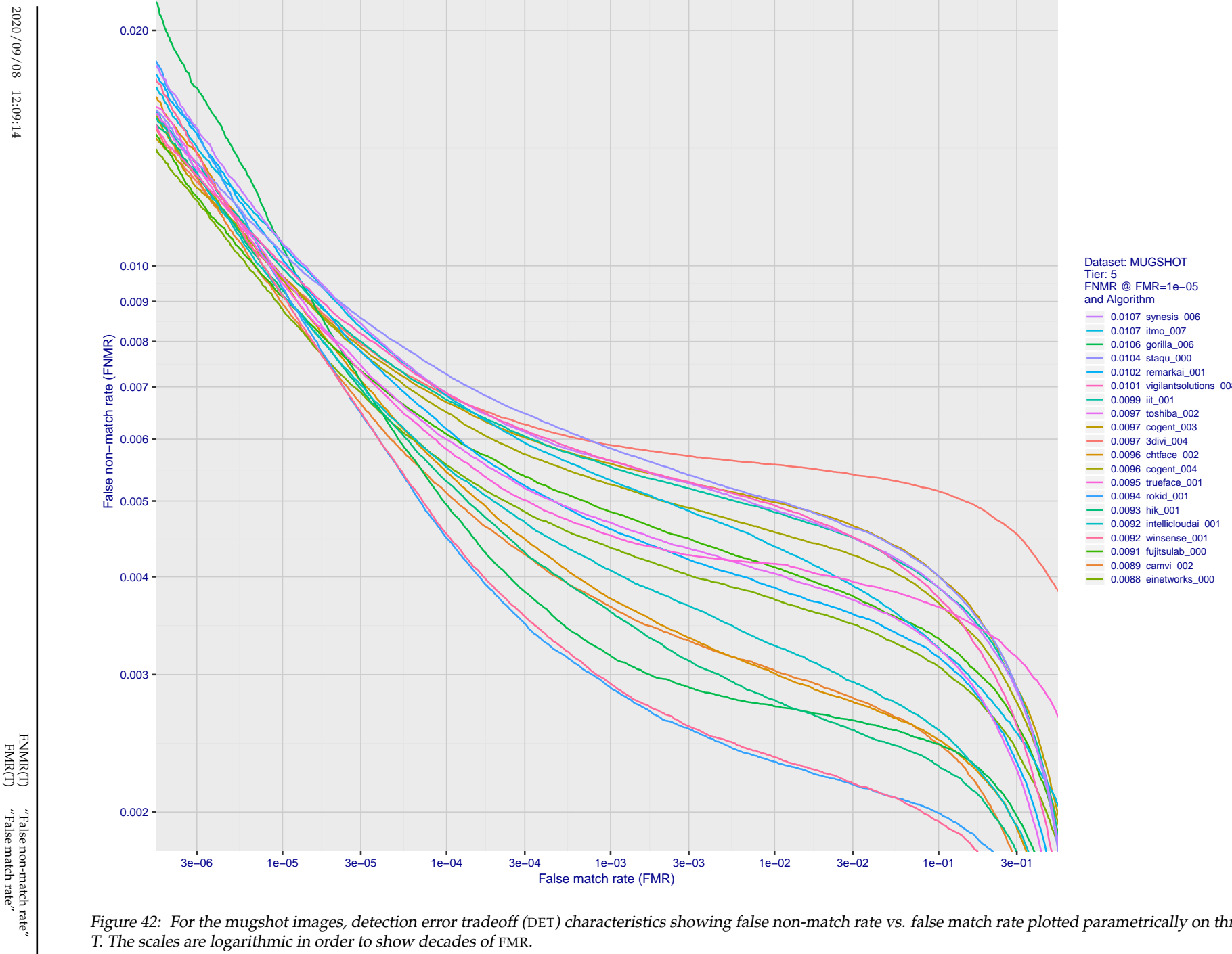


Figure 42: For the mugshot images, detection error tradeoff (DET) characteristics showing false non-match rate vs. false match rate plotted parametrically on threshold, T . The scales are logarithmic in order to show decades of FMR.

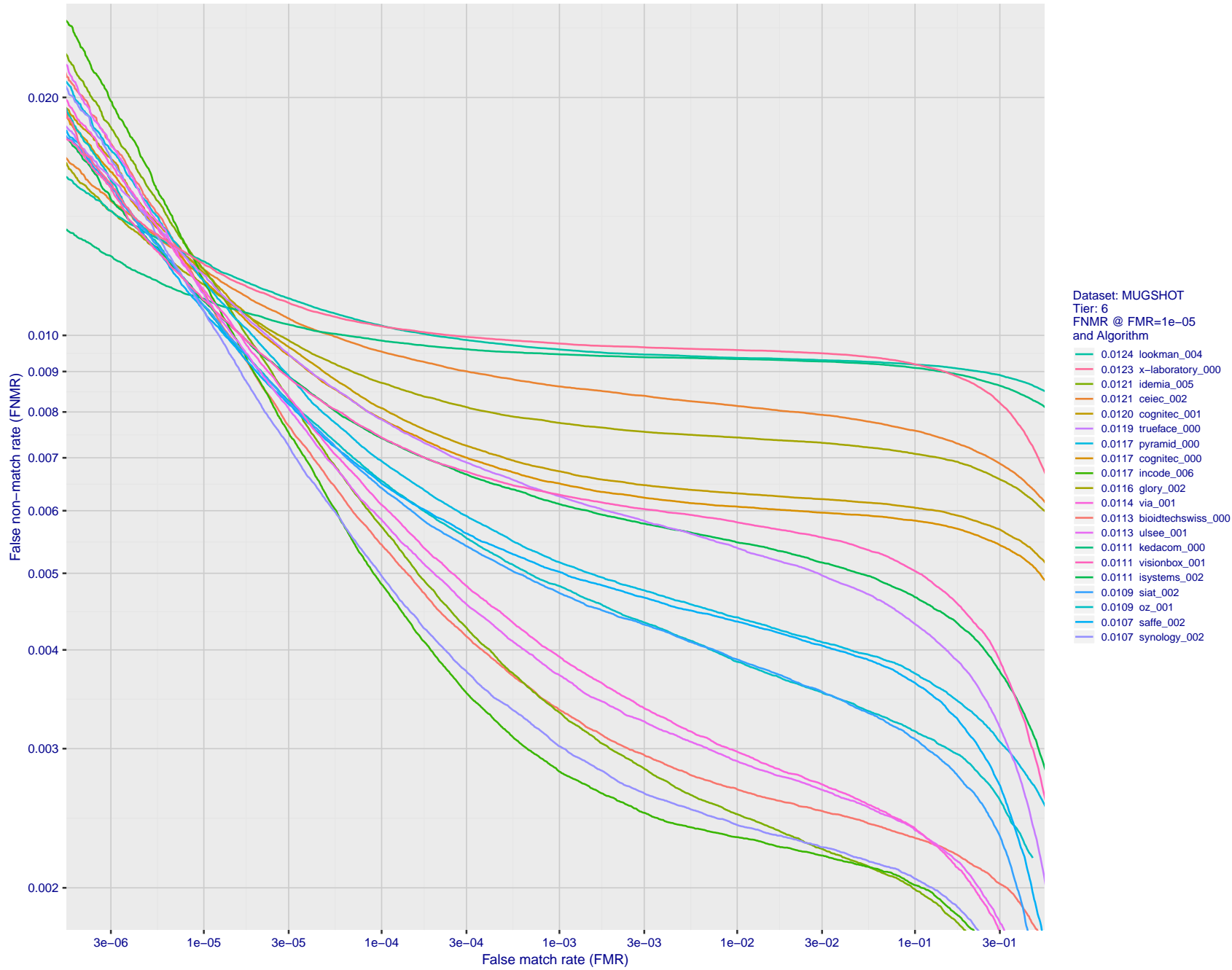


Figure 43: For the mugshot images, detection error tradeoff (DET) characteristics showing false non-match rate vs. false match rate plotted parametrically on threshold, T . The scales are logarithmic in order to show decades of FMR.

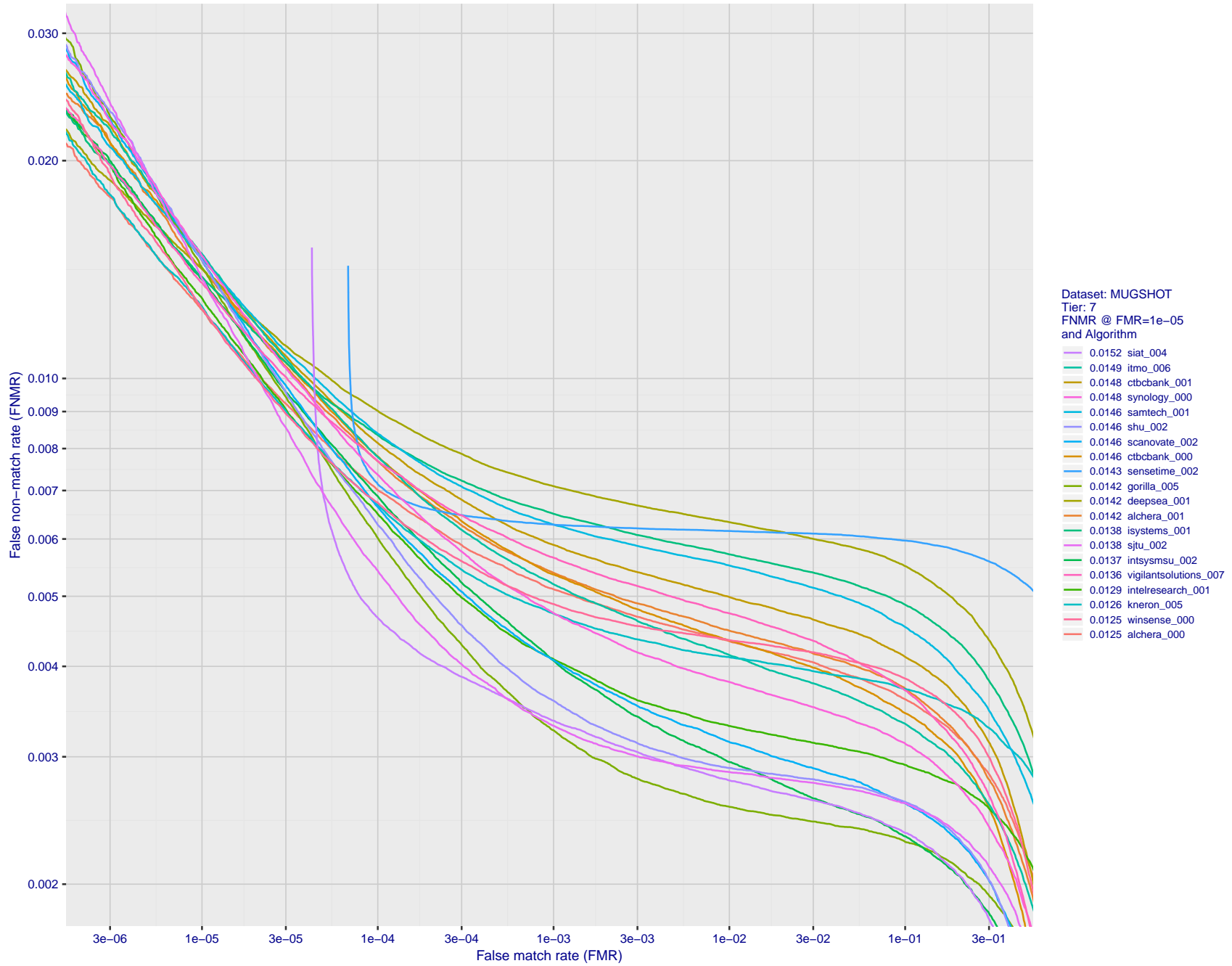


Figure 44: For the mugshot images, detection error tradeoff (DET) characteristics showing false non-match rate vs. false match rate plotted parametrically on threshold, T . The scales are logarithmic in order to show decades of FMR.

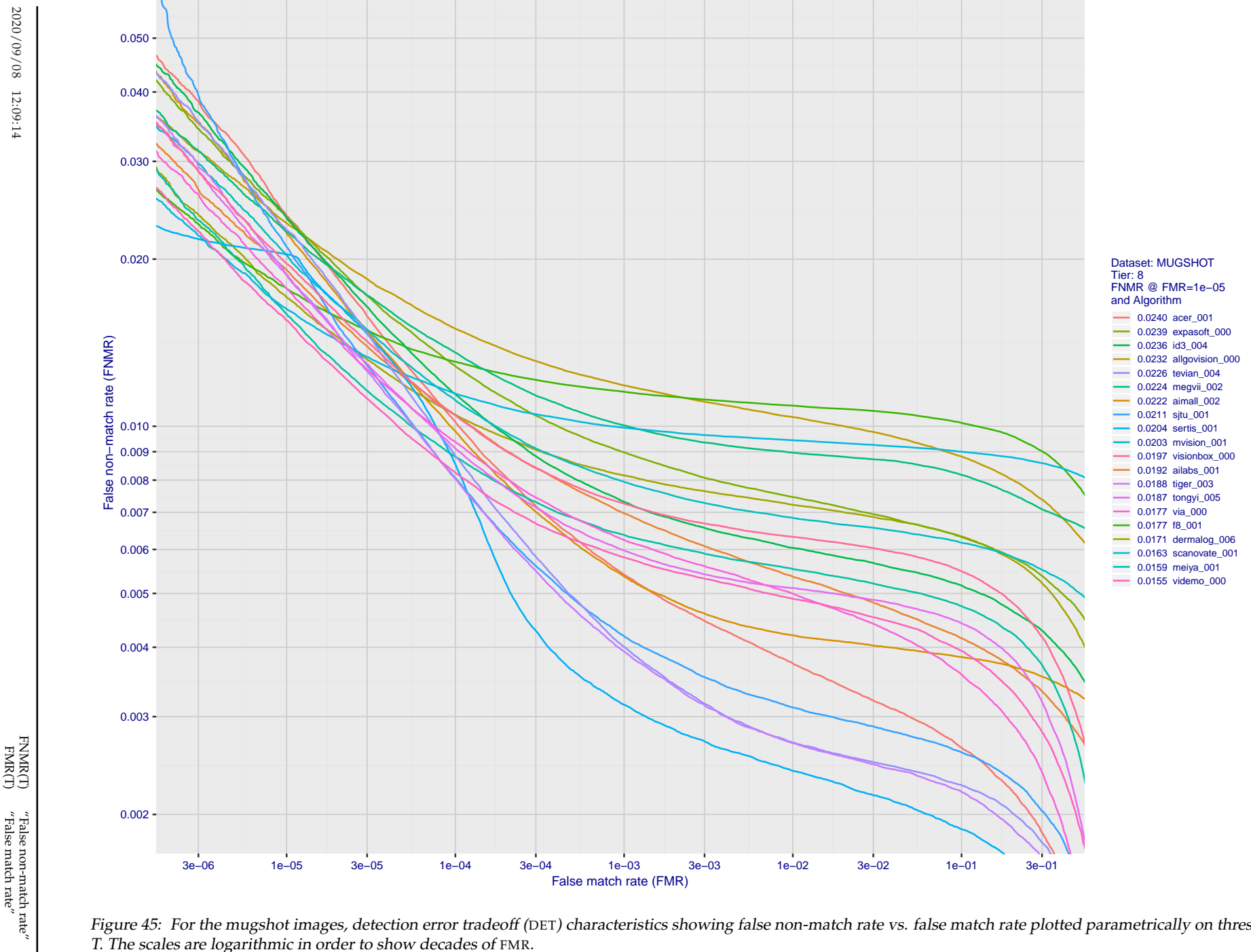


Figure 45: For the mugshot images, detection error tradeoff (DET) characteristics showing false non-match rate vs. false match rate plotted parametrically on threshold, T . The scales are logarithmic in order to show decades of FMR.

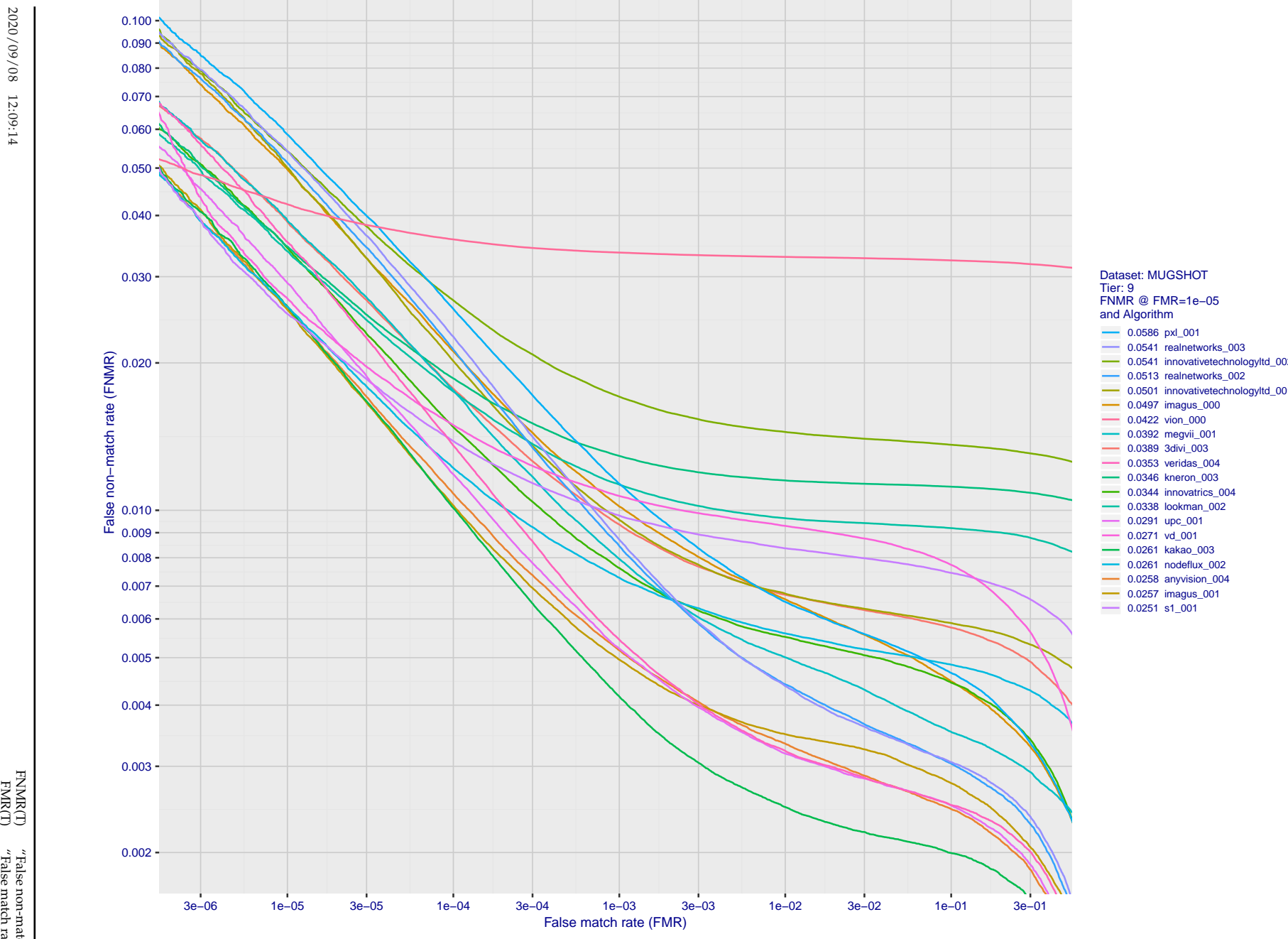


Figure 46: For the mugshot images, detection error tradeoff (DET) characteristics showing false non-match rate vs. false match rate plotted parametrically on threshold, T. The scales are logarithmic in order to show decades of FMR.

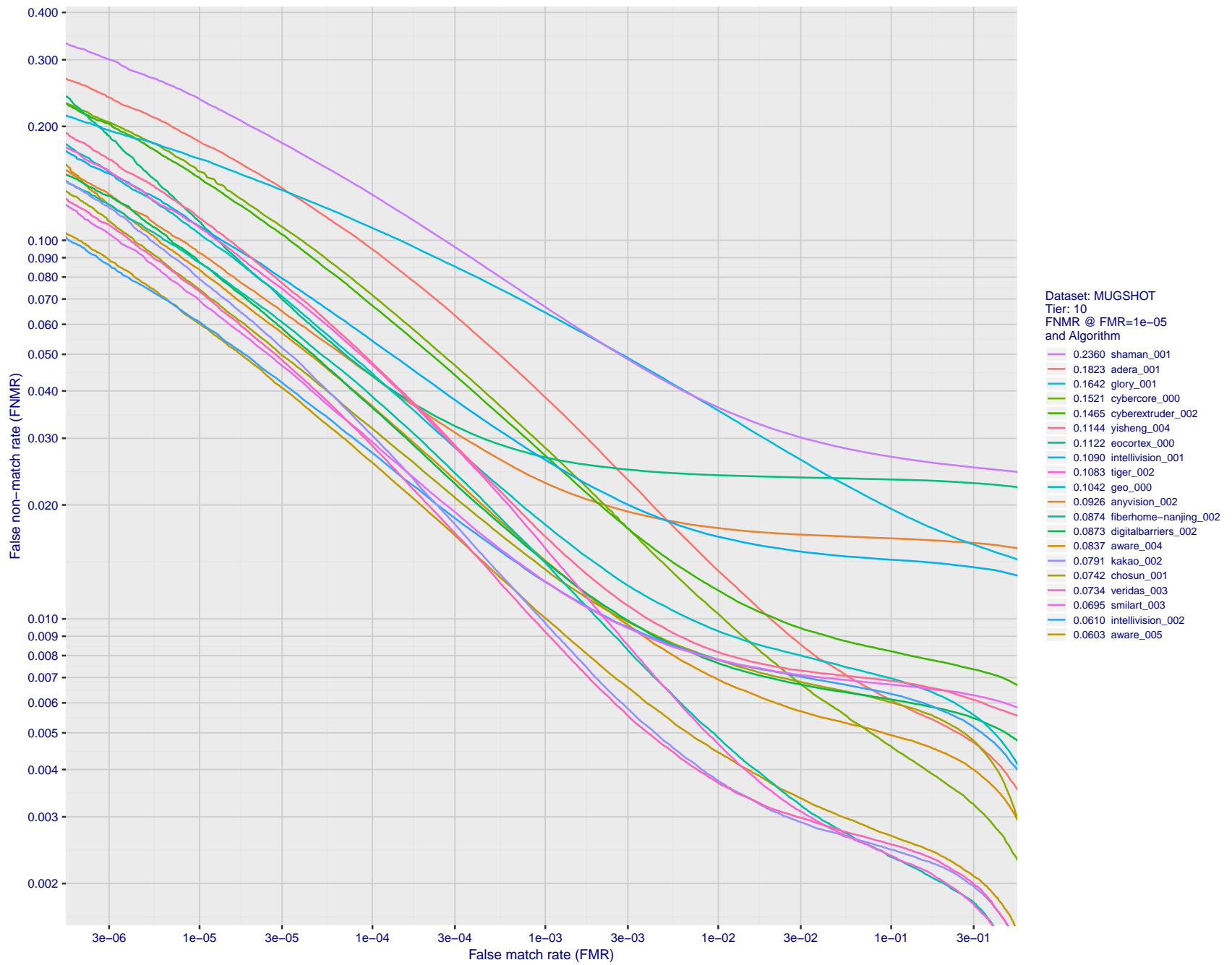


Figure 47: For the mugshot images, detection error tradeoff (DET) characteristics showing false non-match rate vs. false match rate plotted parametrically on threshold, T . The scales are logarithmic in order to show decades of FMR.

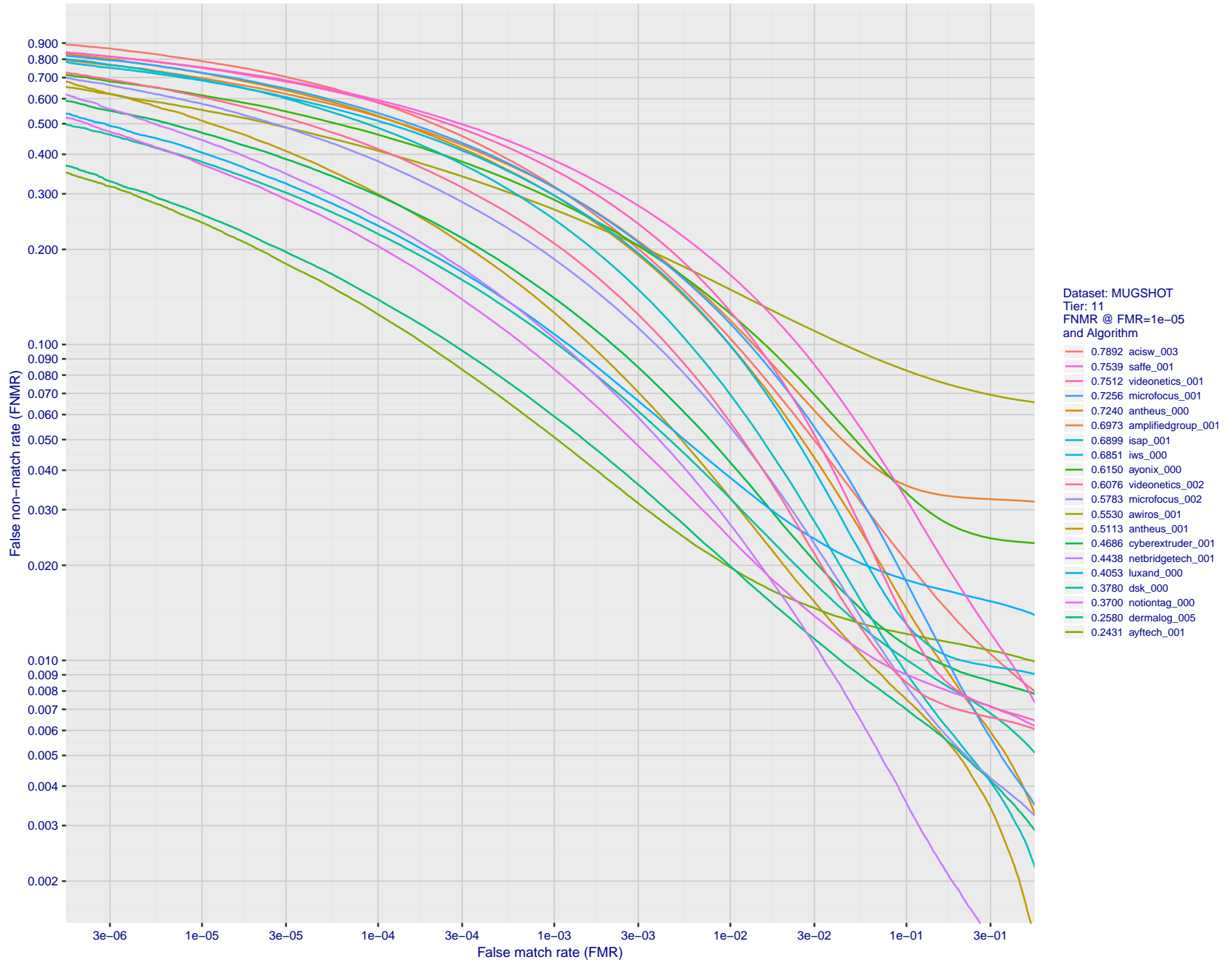


Figure 48: For the mugshot images, detection error tradeoff (DET) characteristics showing false non-match rate vs. false match rate plotted parametrically on threshold, T . The scales are logarithmic in order to show decades of FMR.

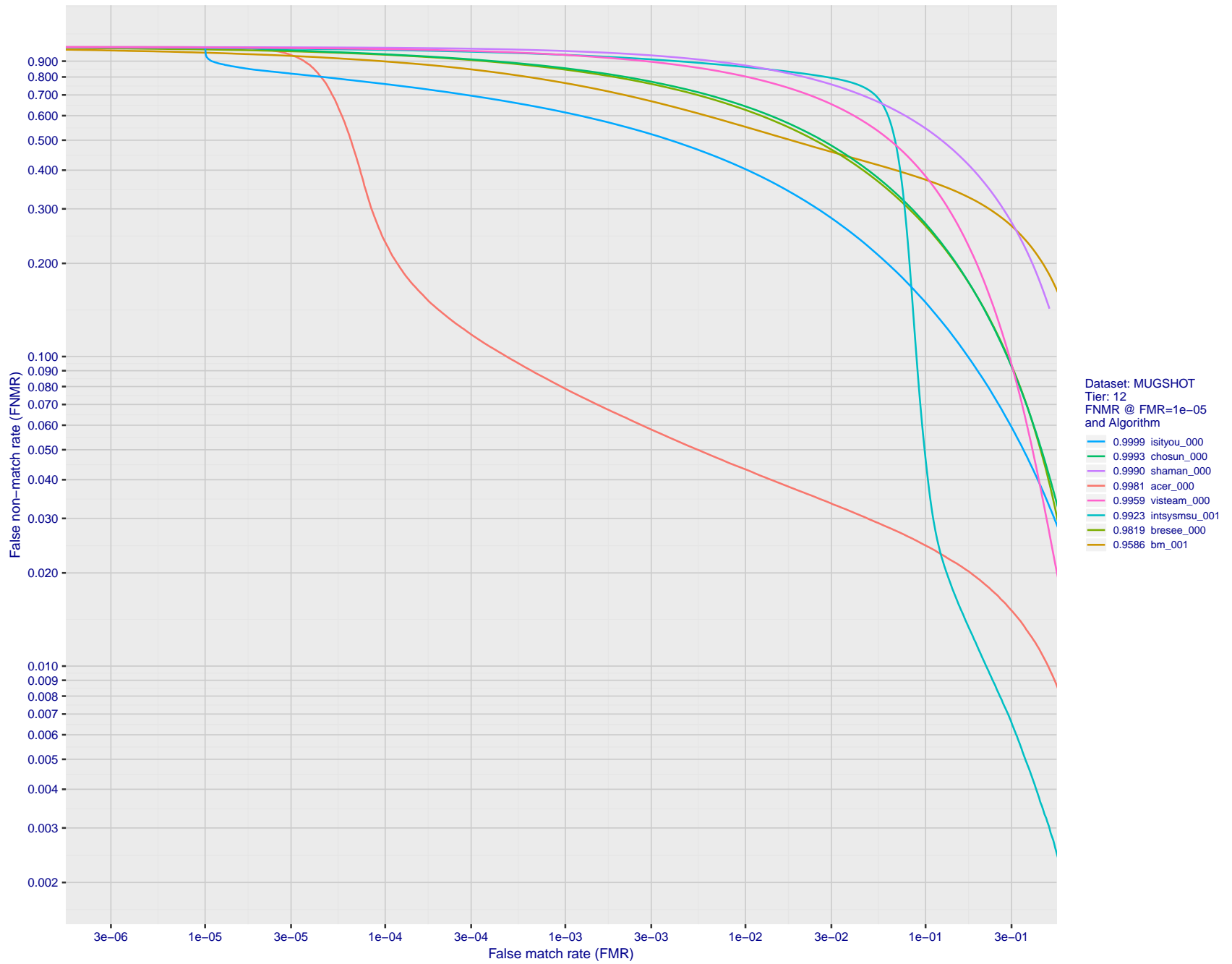


Figure 49: For the mugshot images, detection error tradeoff (DET) characteristics showing false non-match rate vs. false match rate plotted parametrically on threshold, T . The scales are logarithmic in order to show decades of FMR.

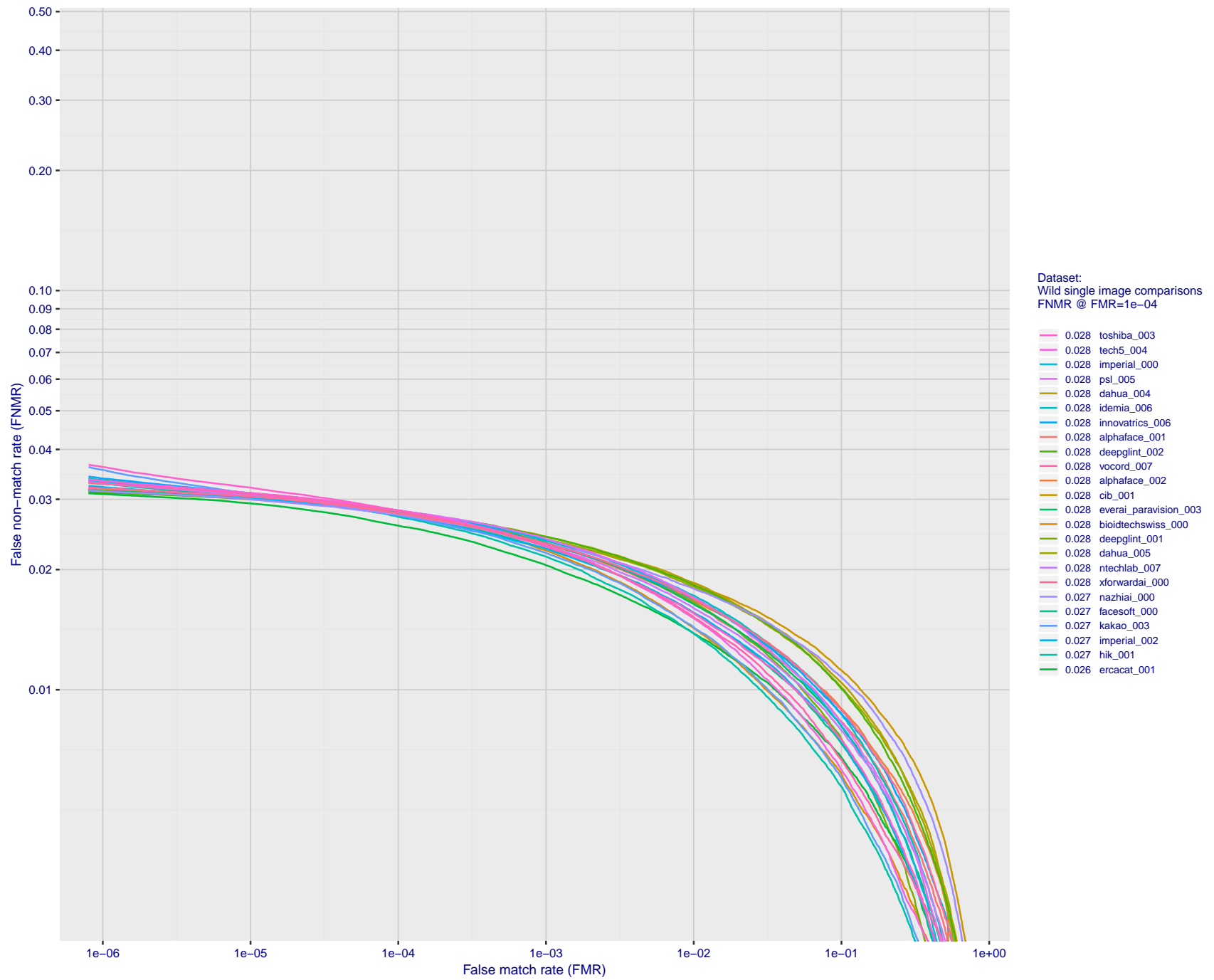


Figure 50: For the 2018 wild image comparisons, detection error tradeoff (DET) characteristics showing false non-match rate vs. false match rate plotted parametrically on threshold, T . The scales are logarithmic in order to show several decades of FMR.

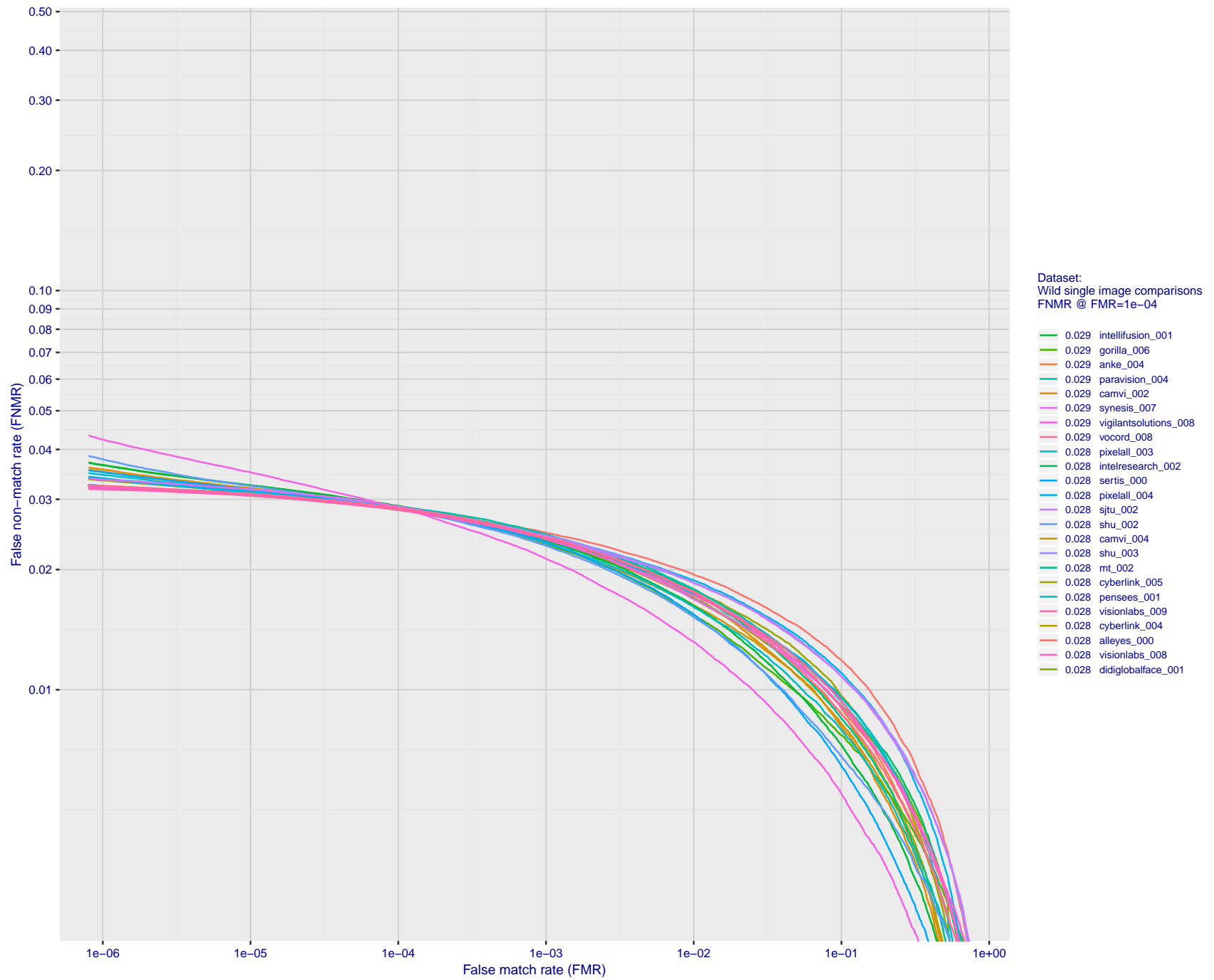


Figure 51: For the 2018 wild image comparisons, detection error tradeoff (DET) characteristics showing false non-match rate vs. false match rate plotted parametrically on threshold, T . The scales are logarithmic in order to show several decades of FMR.

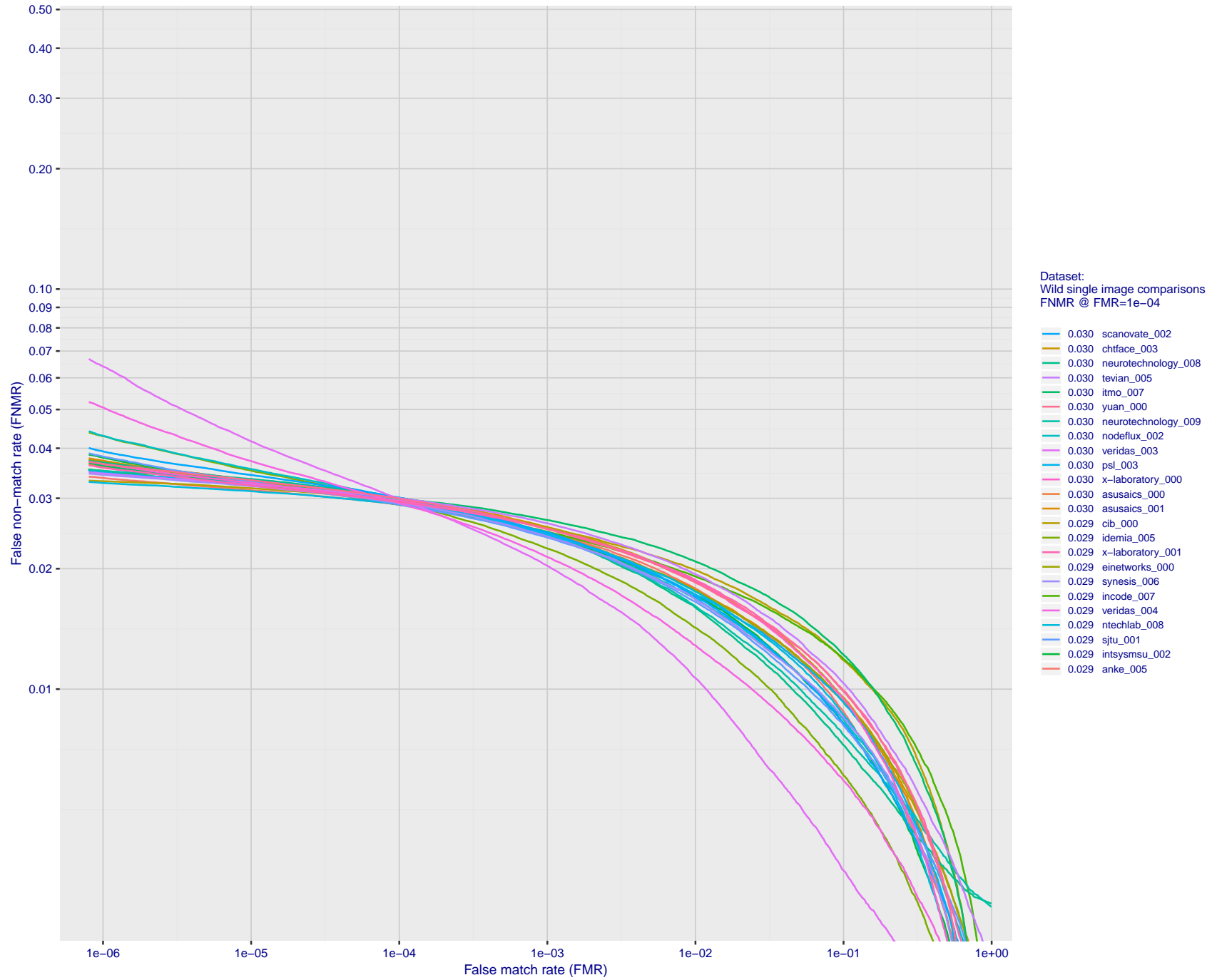


Figure 52: For the 2018 wild image comparisons, detection error tradeoff (DET) characteristics showing false non-match rate vs. false match rate plotted parametrically on threshold, T . The scales are logarithmic in order to show several decades of FMR.

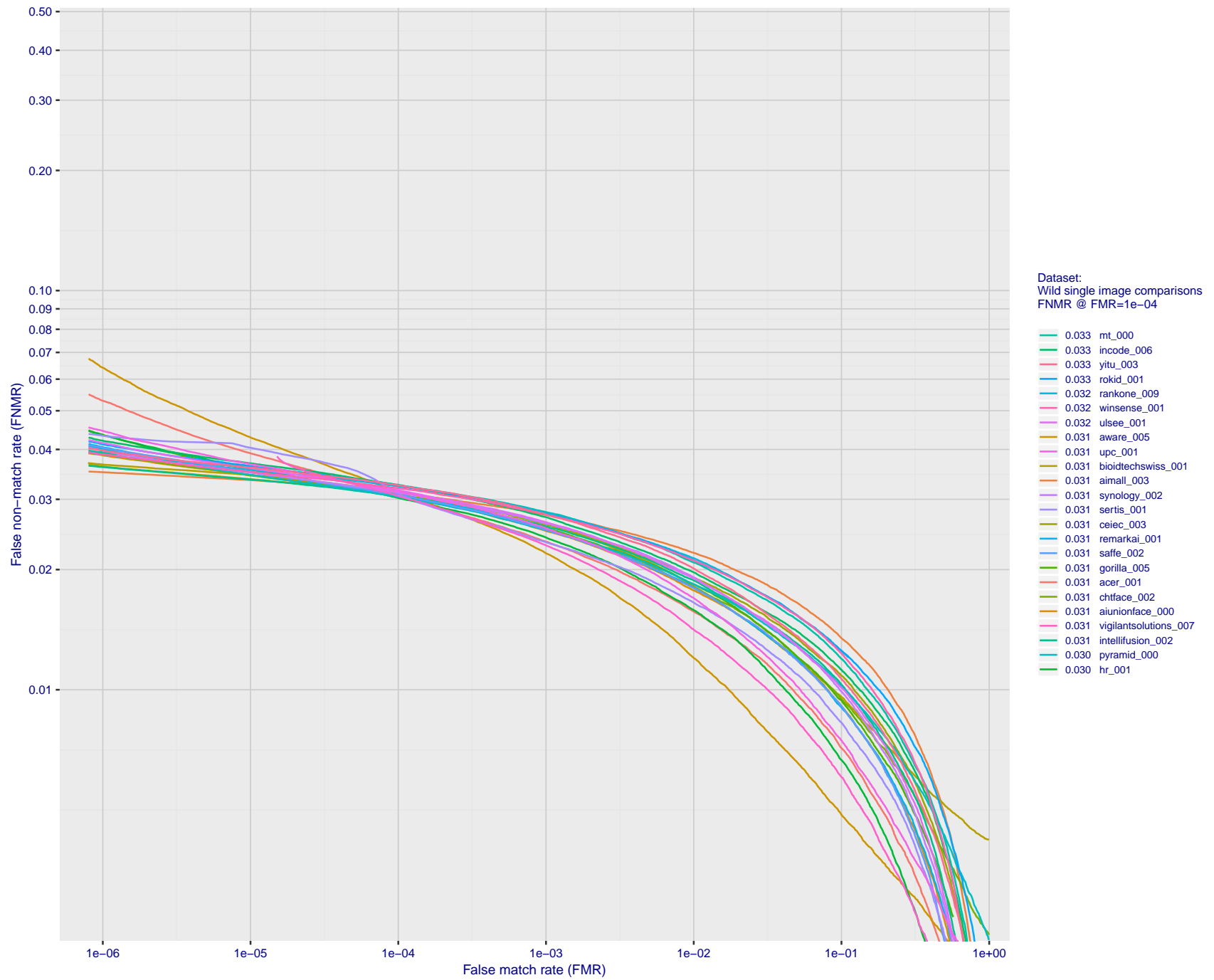


Figure 53: For the 2018 wild image comparisons, detection error tradeoff (DET) characteristics showing false non-match rate vs. false match rate plotted parametrically on threshold, T . The scales are logarithmic in order to show several decades of FMR.

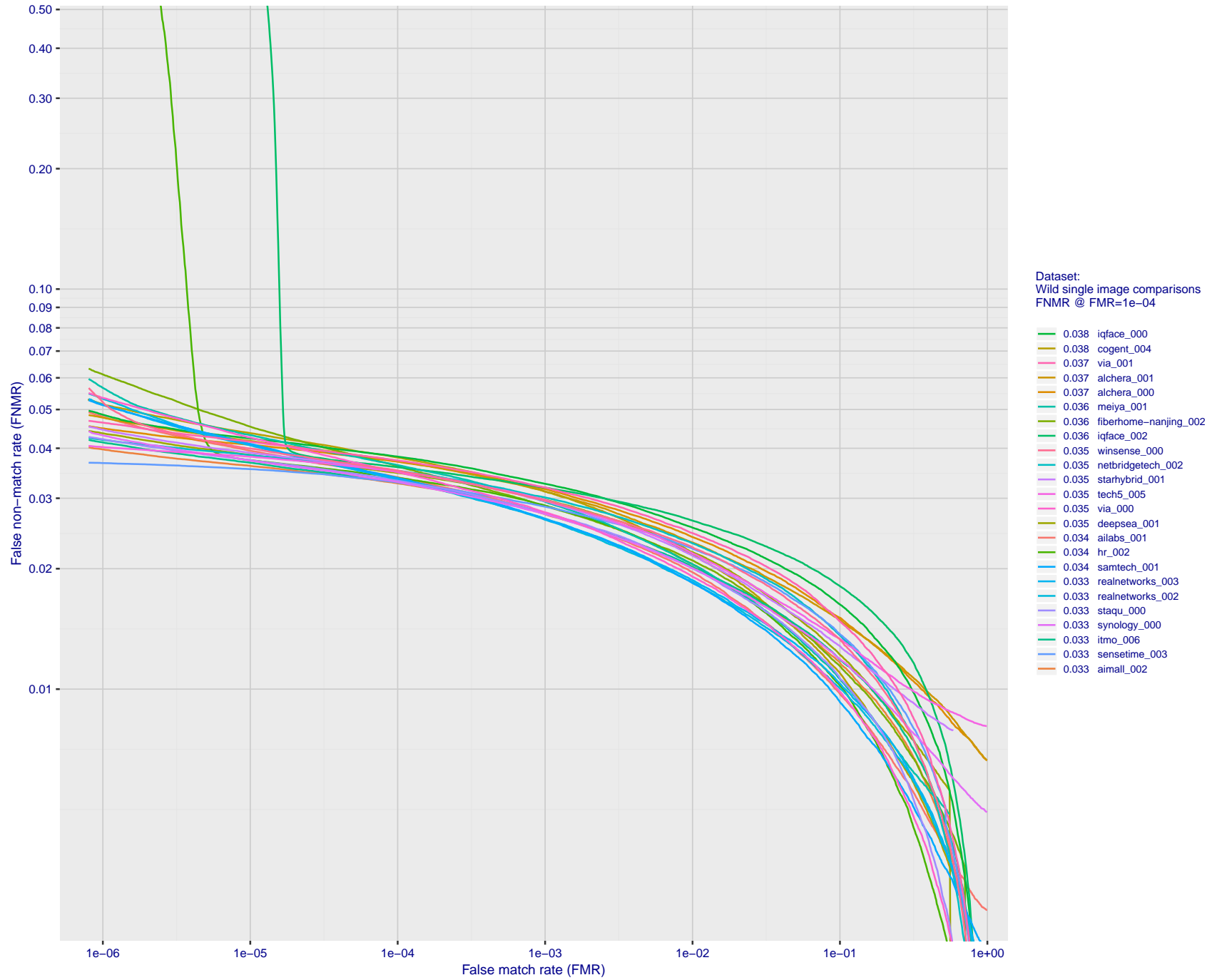


Figure 54: For the 2018 wild image comparisons, detection error tradeoff (DET) characteristics showing false non-match rate vs. false match rate plotted parametrically on threshold, T . The scales are logarithmic in order to show several decades of FMR.

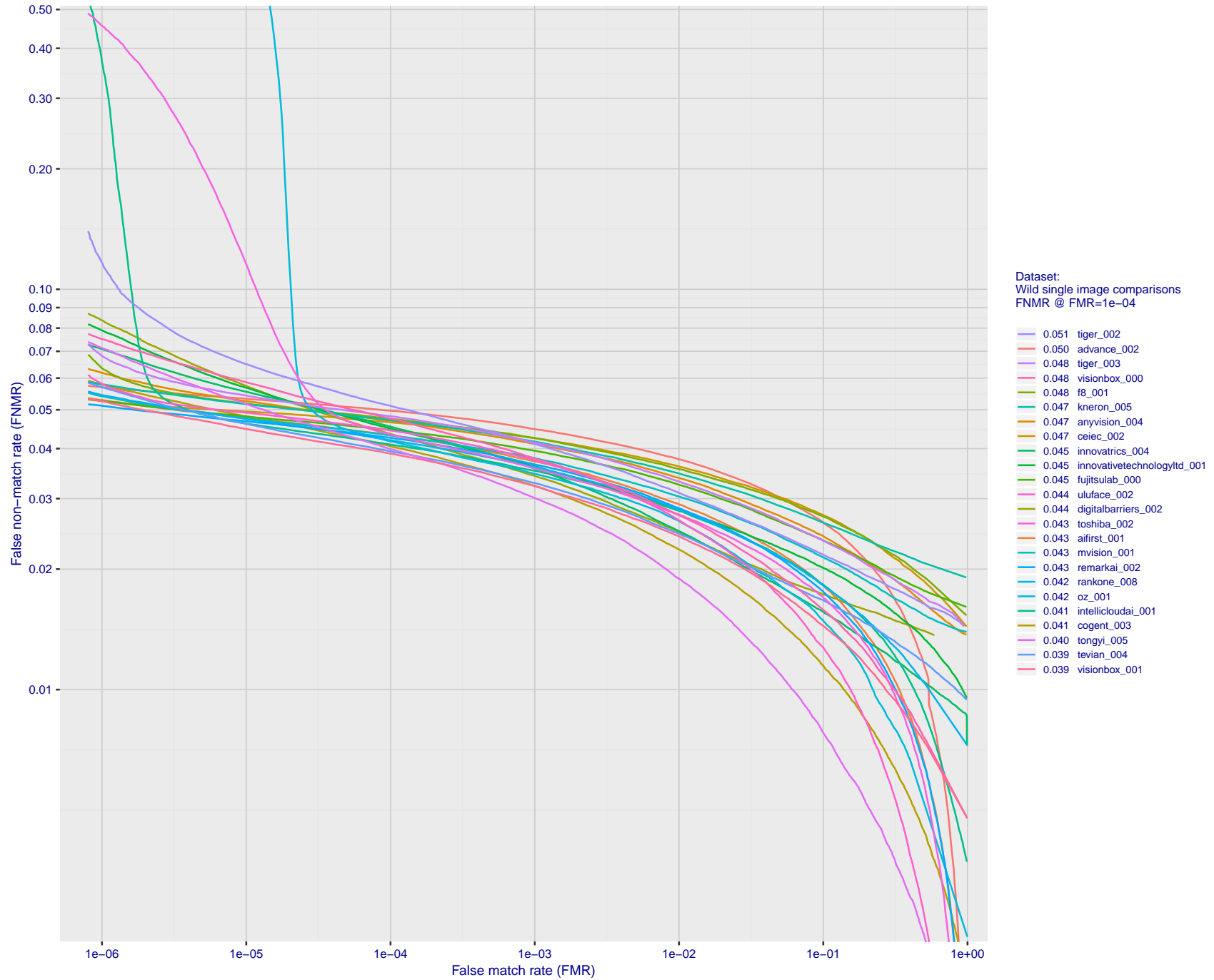


Figure 55: For the 2018 wild image comparisons, detection error tradeoff (DET) characteristics showing false non-match rate vs. false match rate plotted parametrically on threshold, T. The scales are logarithmic in order to show several decades of FMR.

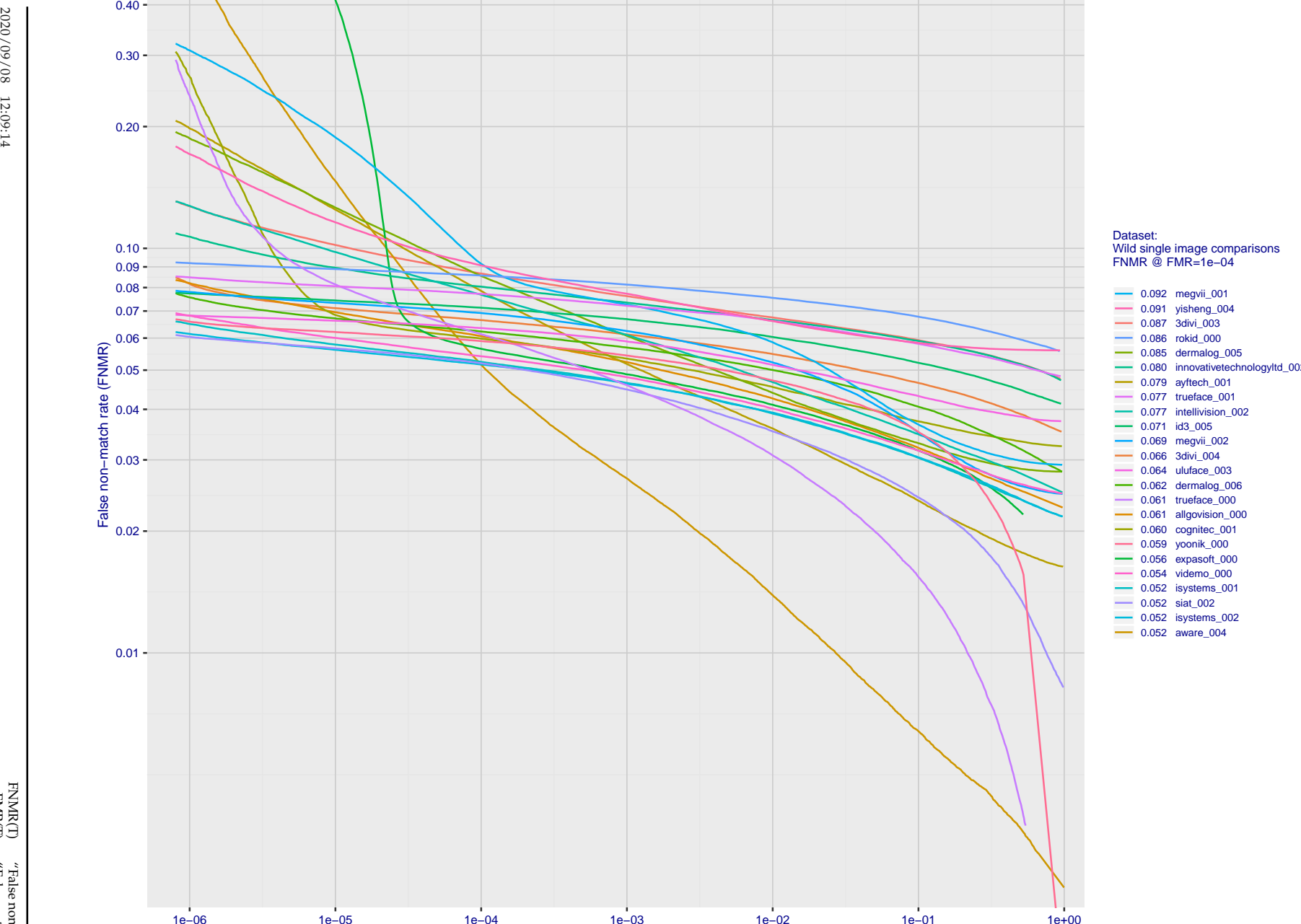
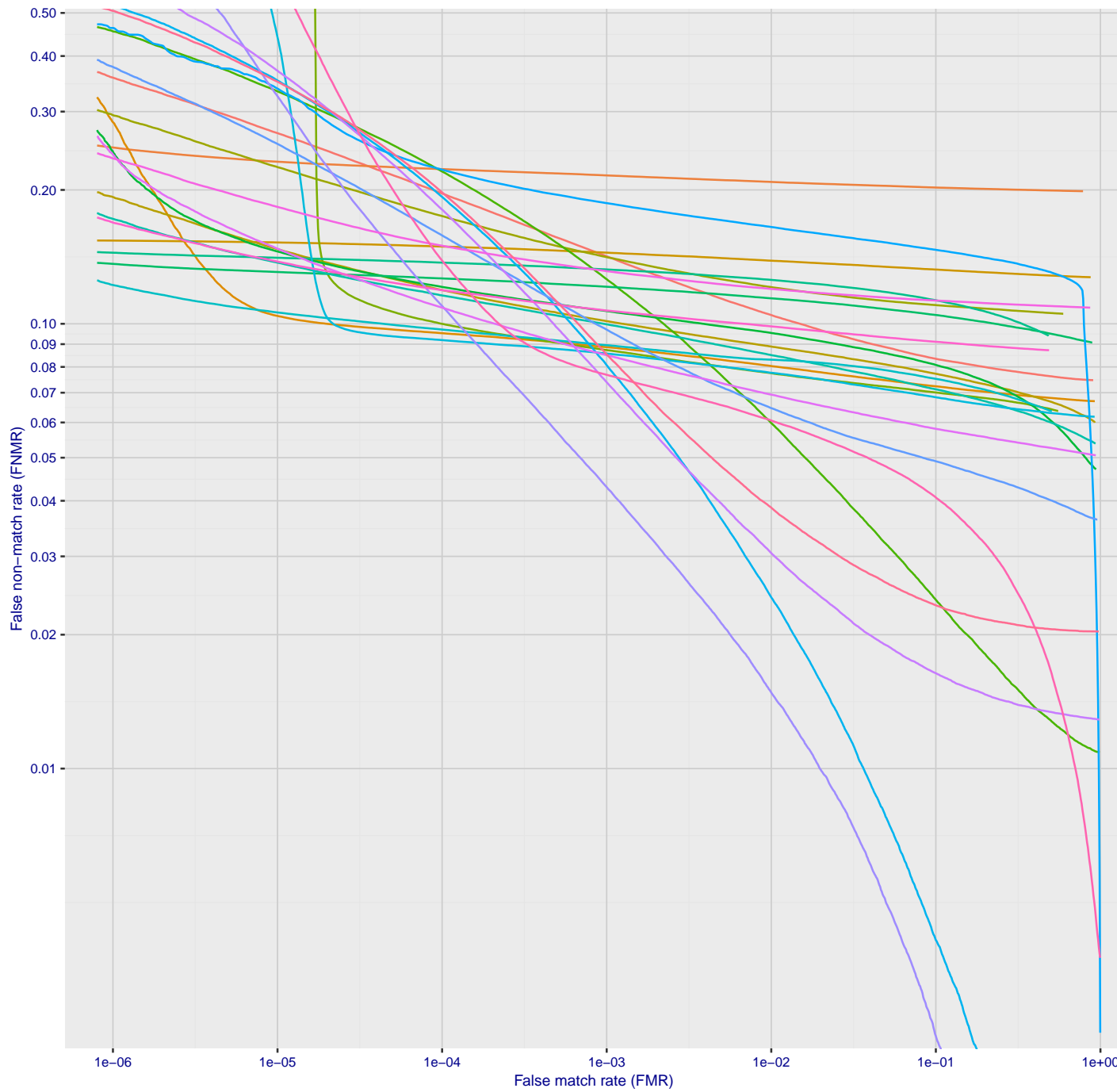


Figure 56: For the 2018 wild image comparisons, detection error tradeoff (DET) characteristics showing false non-match rate vs. false match rate plotted parametrically on threshold, T. The scales are logarithmic in order to show several decades of FMR.

2020/09/08 12:09:14



Dataset:
Wild single image comparisons
FNMR @ FMR=1e-04

Figure 57: For the 2018 wild image comparisons, detection error tradeoff (DET) characteristics showing false non-match rate vs. false match rate plotted parametrically on threshold, T. The scales are logarithmic in order to show several decades of FMR.

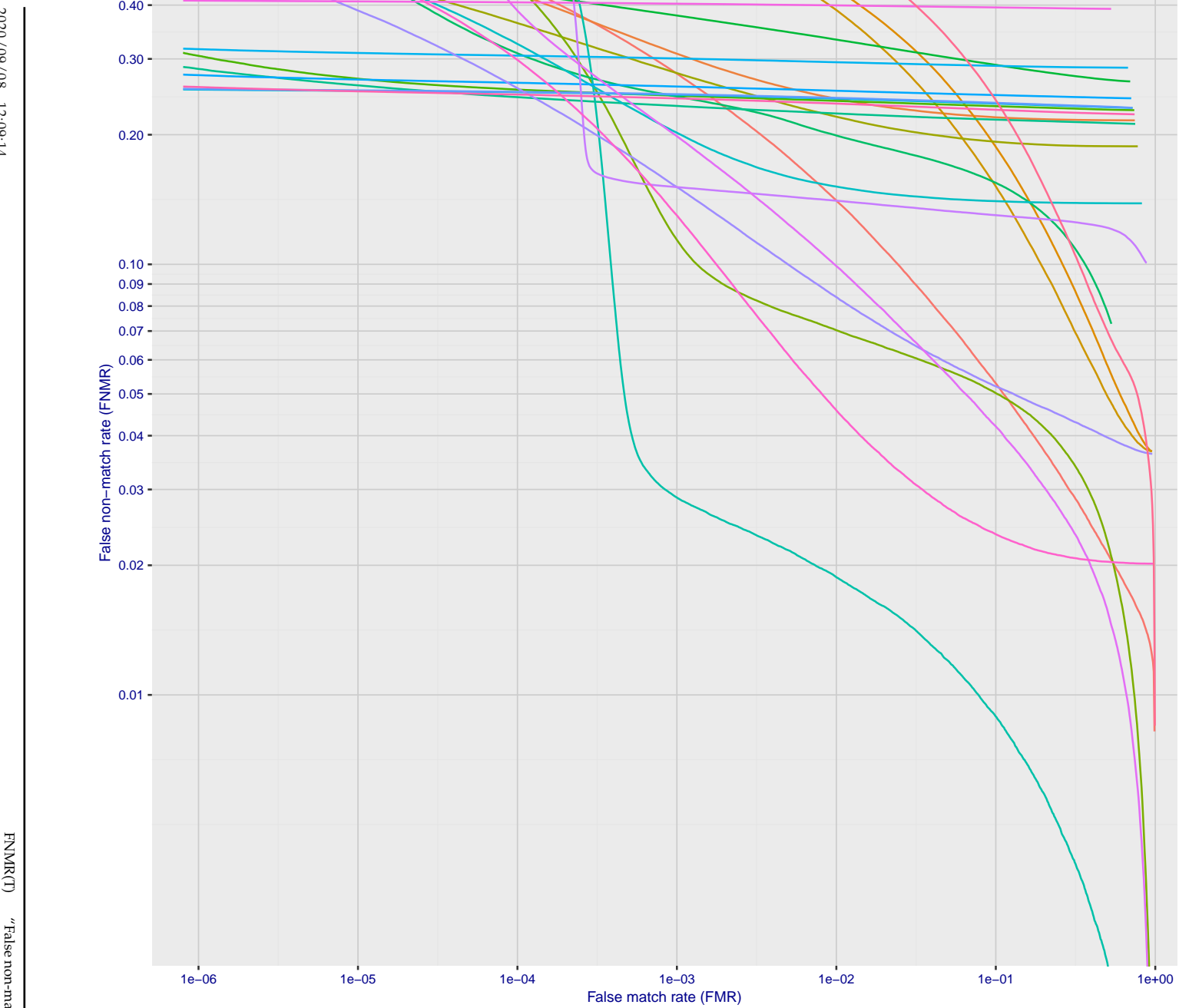


Figure 58: For the 2018 wild image comparisons, detection error tradeoff (DET) characteristics showing false non-match rate vs. false match rate plotted parametrically on threshold, T . The scales are logarithmic in order to show several decades of FMR.

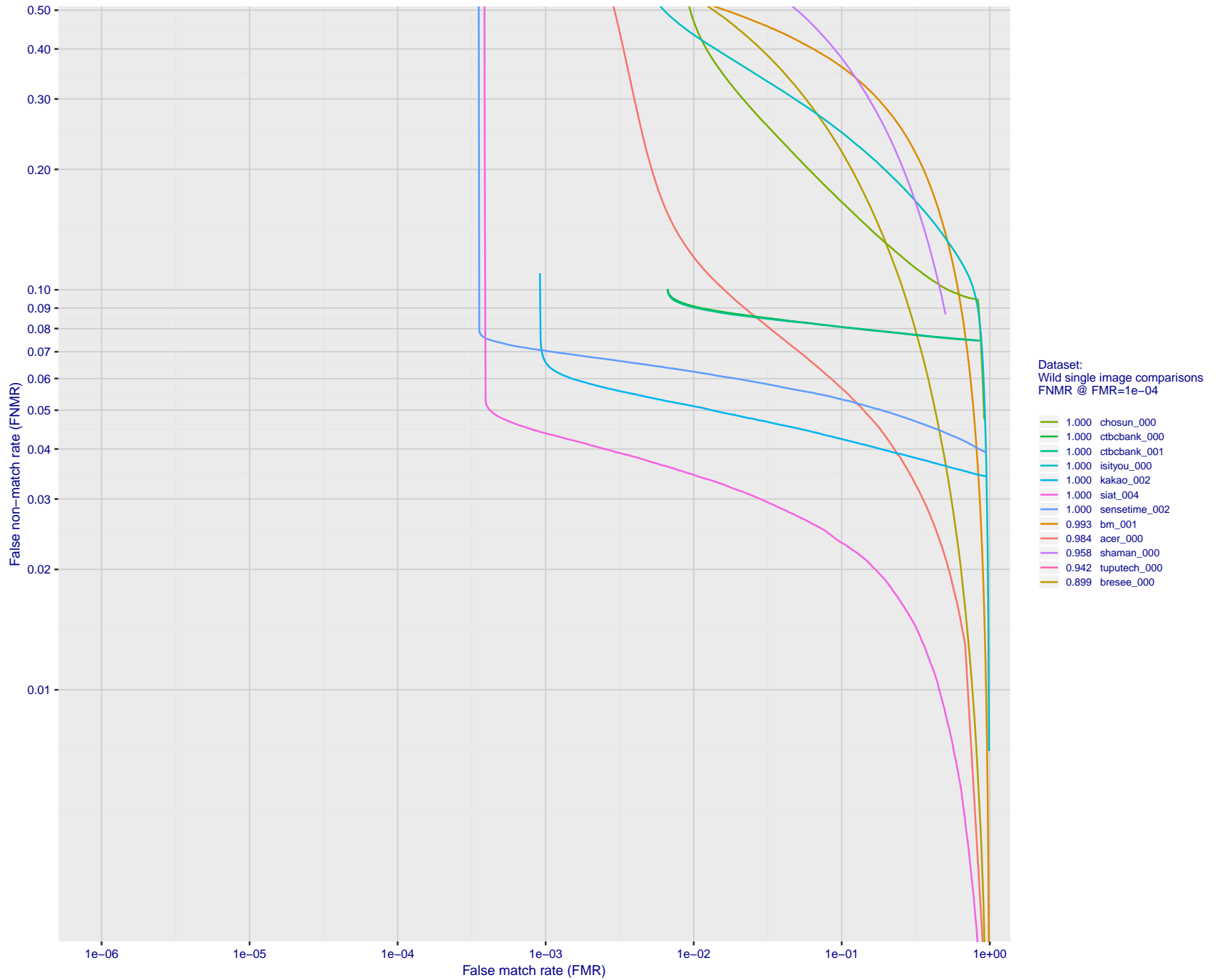


Figure 59: For the 2018 wild image comparisons, detection error tradeoff (DET) characteristics showing false non-match rate vs. false match rate plotted parametrically on threshold, T . The scales are logarithmic in order to show several decades of FMR.

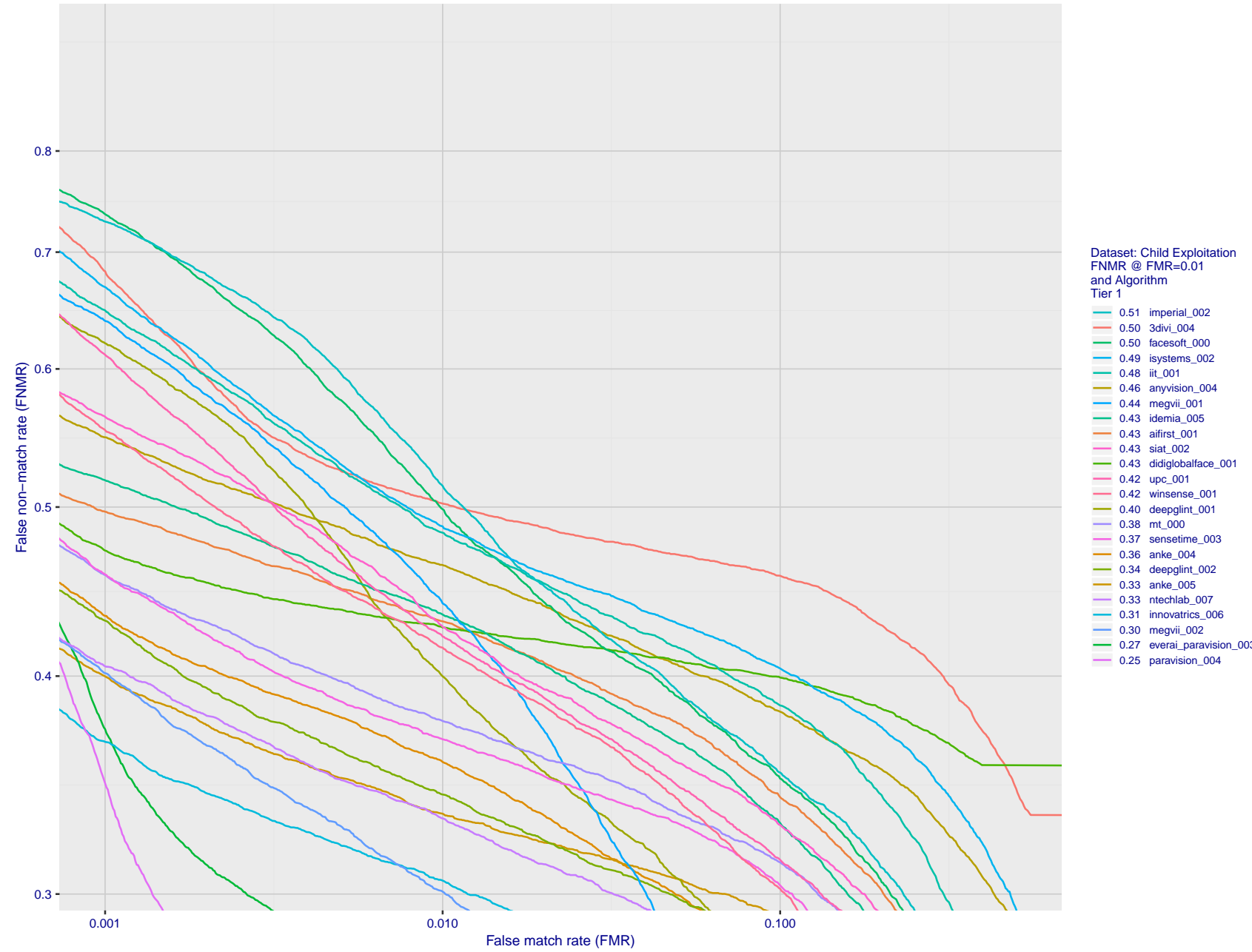


Figure 60: For child exploitation images, detection error tradeoff (DET) characteristics showing false non-match rate vs. false match rate plotted parametrically on threshold, T . The scales are logarithmic in order to show many decades of FMR. Accuracy is poor because many images have adverse quality characteristics, and because detection and enrollment fails.

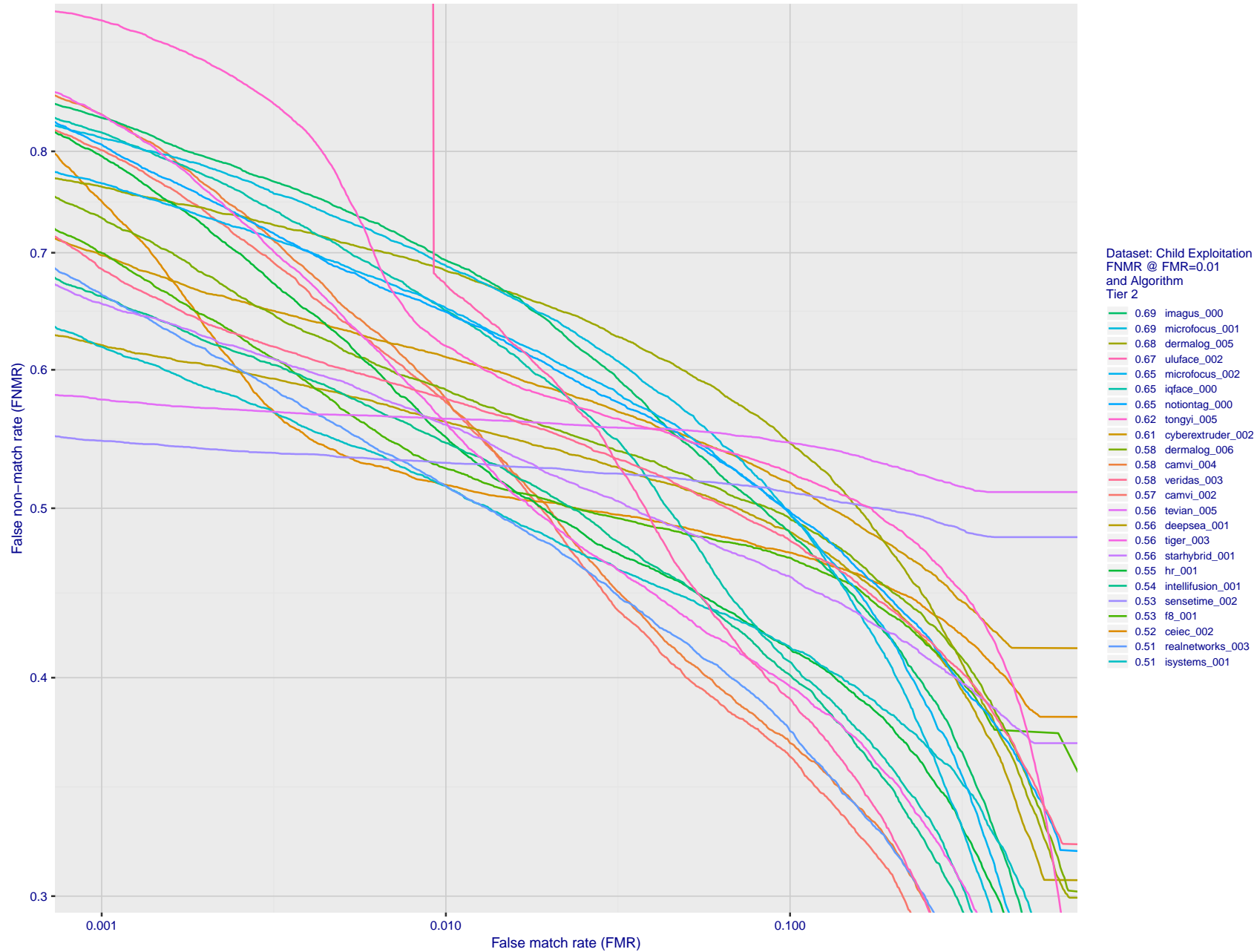


Figure 61: For child exploitation images, detection error tradeoff (DET) characteristics showing false non-match rate vs. false match rate plotted parametrically on threshold, T. The scales are logarithmic in order to show many decades of FMR. Accuracy is poor because many images have adverse quality characteristics, and because detection and enrollment fails.

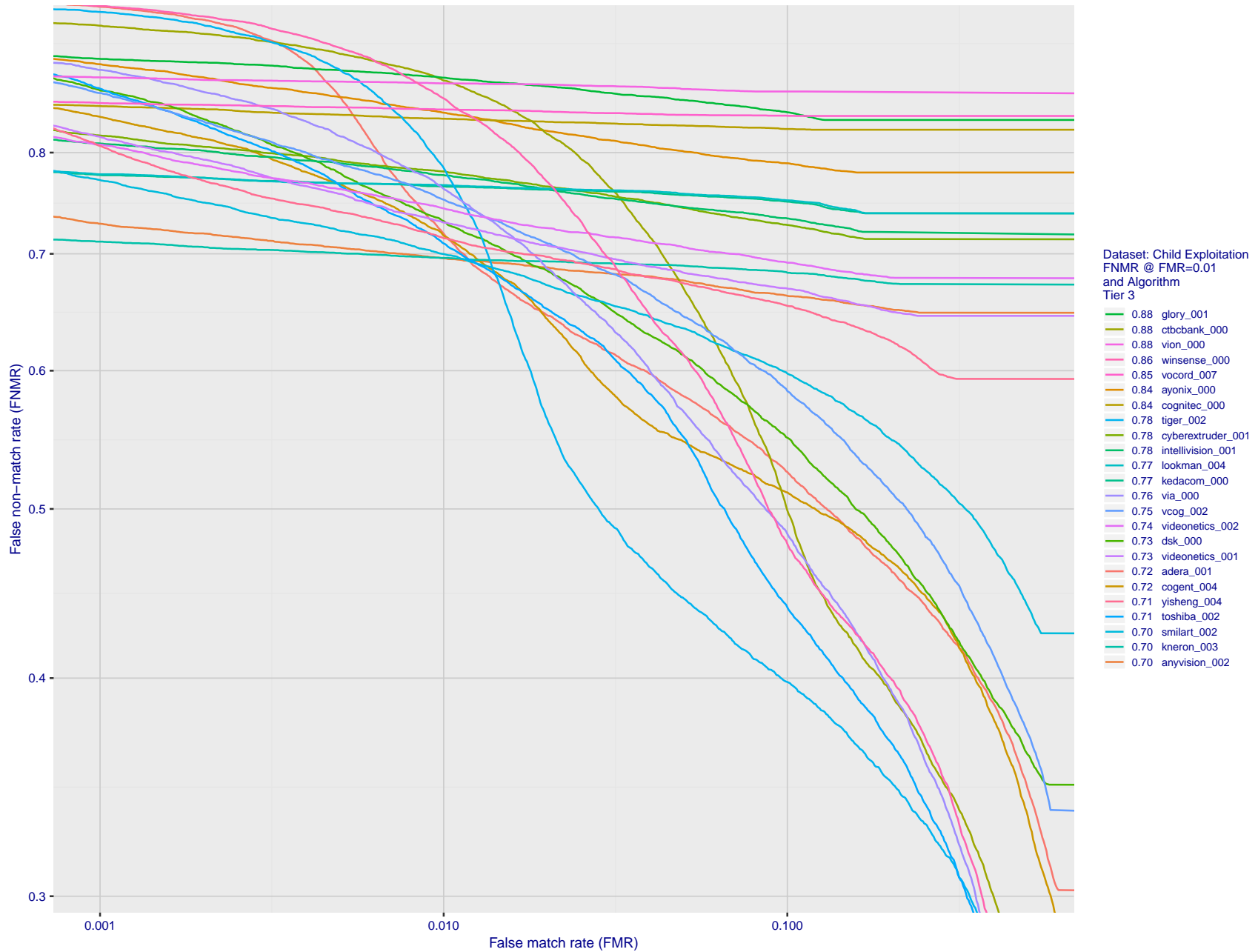


Figure 62: For child exploitation images, detection error tradeoff (DET) characteristics showing false non-match rate vs. false match rate plotted parametrically on threshold, T . The scales are logarithmic in order to show many decades of FMR. Accuracy is poor because many images have adverse quality characteristics, and because detection and enrollment fails.

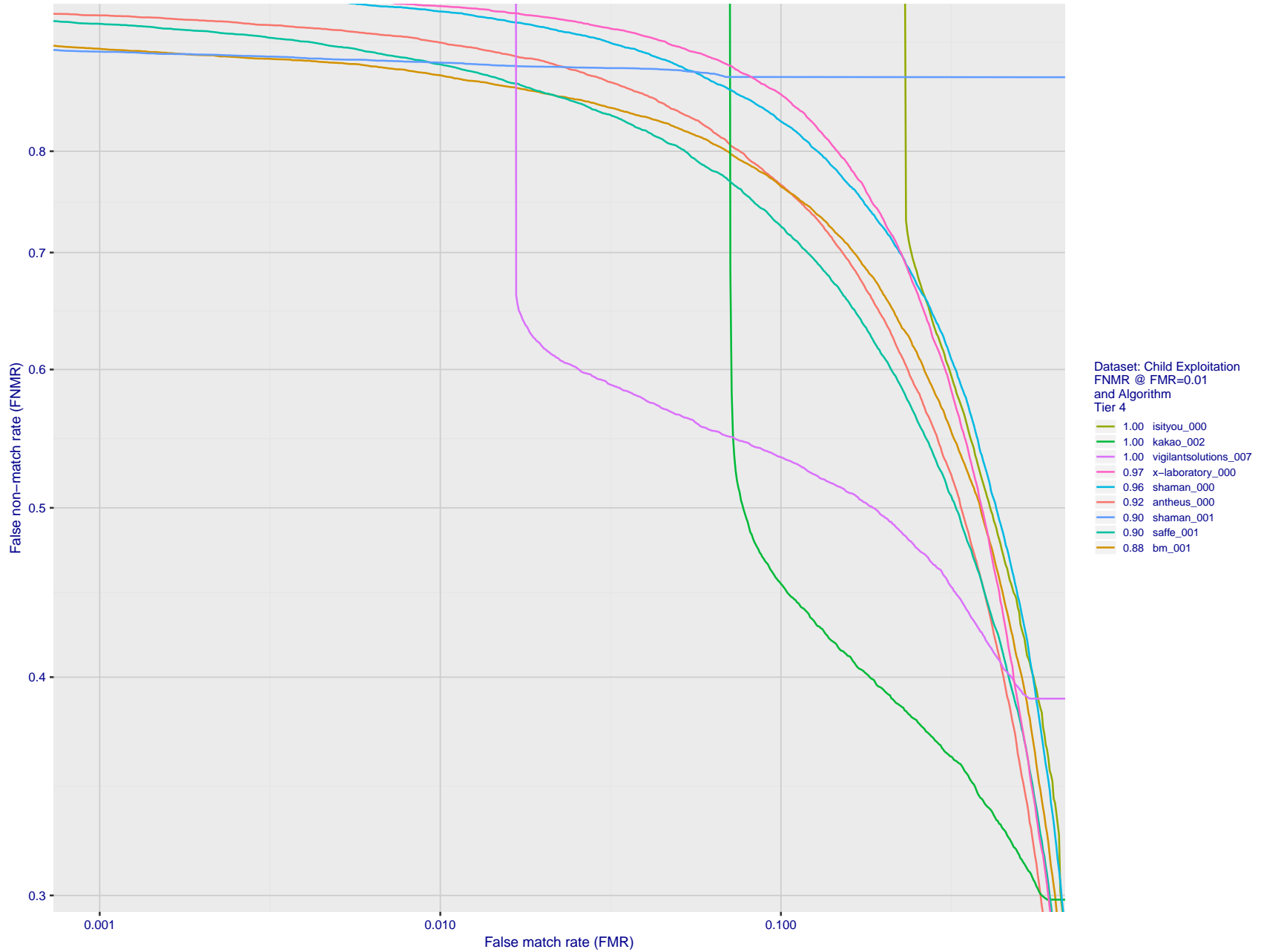


Figure 63: For child exploitation images, detection error tradeoff (DET) characteristics showing false non-match rate vs. false match rate plotted parametrically on threshold, T . The scales are logarithmic in order to show many decades of FMR. Accuracy is poor because many images have adverse quality characteristics, and because detection and enrollment fails.

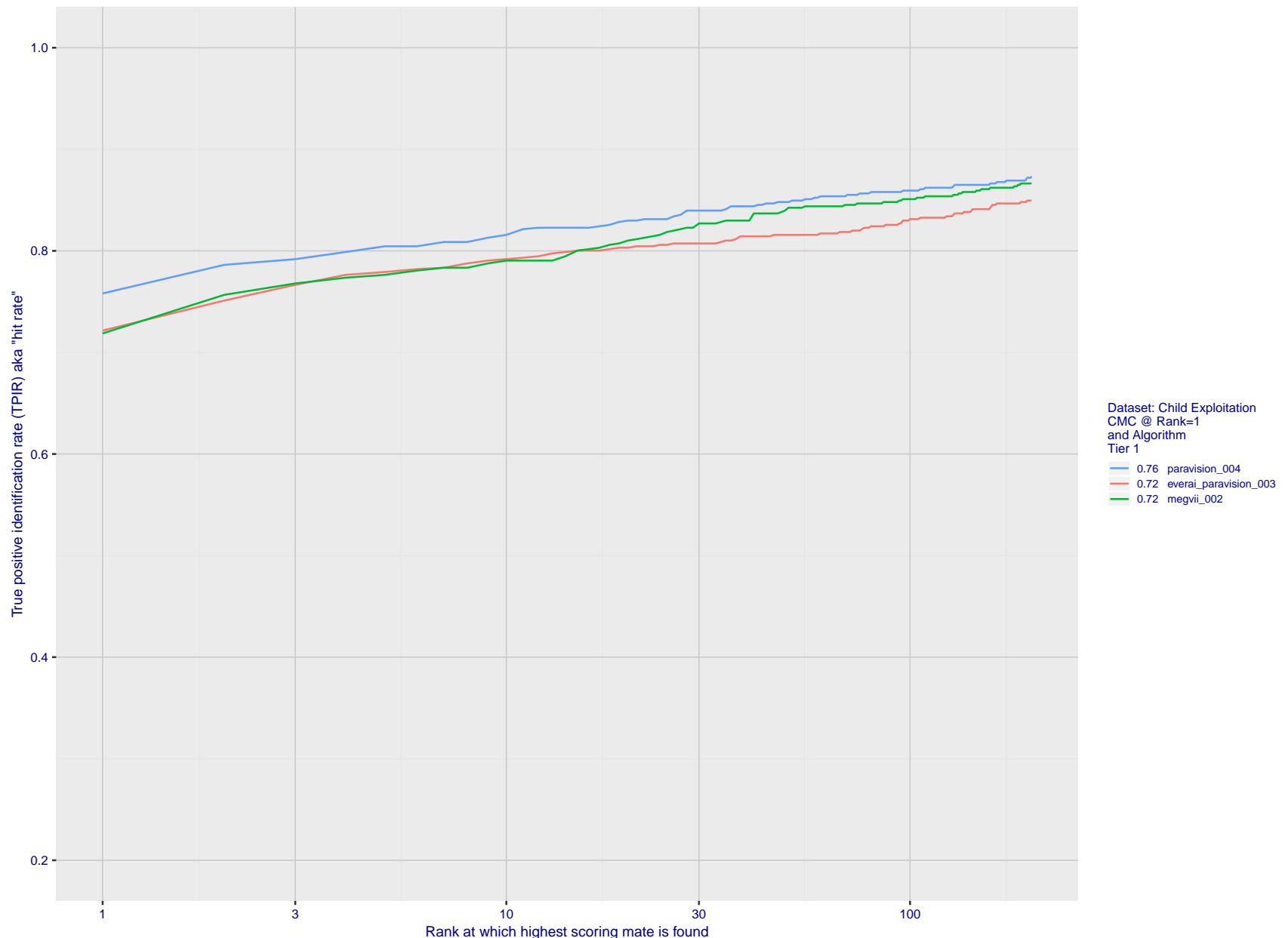


Figure 64: For child exploitation images, cumulative match characteristics (CMC) showing true positive identification rate vs. rank. This is simulation of a one-to-many search experiment - see discussion in section 3.2. The scales are logarithmic in order to show the effect of long candidate lists. Accuracy is poor but much improved relative to the 1:1 DETs of Fig. 63 because a search can succeed if any of a subject's several enrolled images matches the search image with a high score.

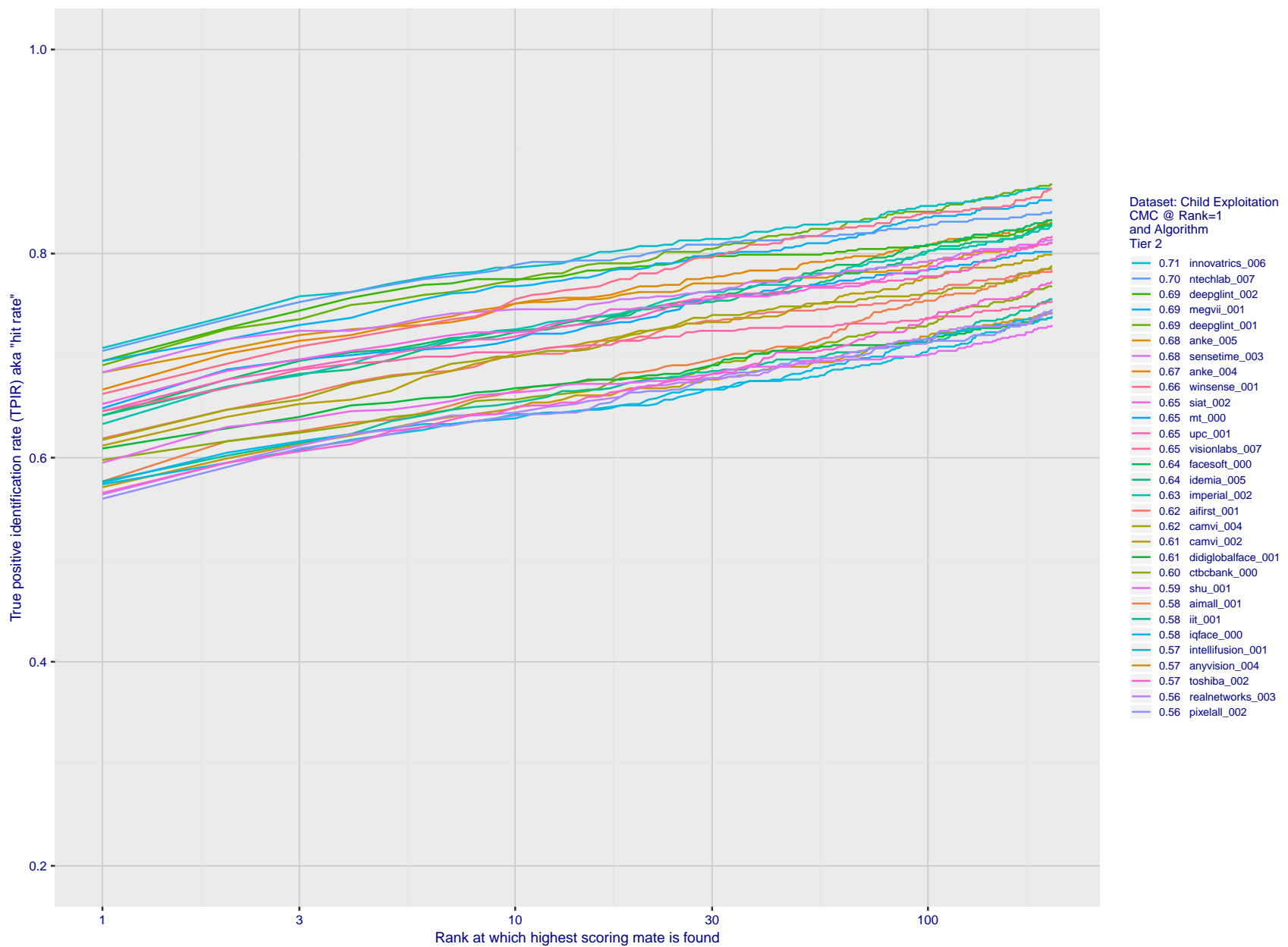


Figure 65: For child exploitation images, cumulative match characteristics (CMC) showing true positive identification rate vs. rank. This is simulation of a one-to-many search experiment - see discussion in section 3.2. The scales are logarithmic in order to show the effect of long candidate lists. Accuracy is poor but much improved relative to the 1:1 DETs of Fig. 63 because a search can succeed if any of a subject's several enrolled images matches the search image with a high score.

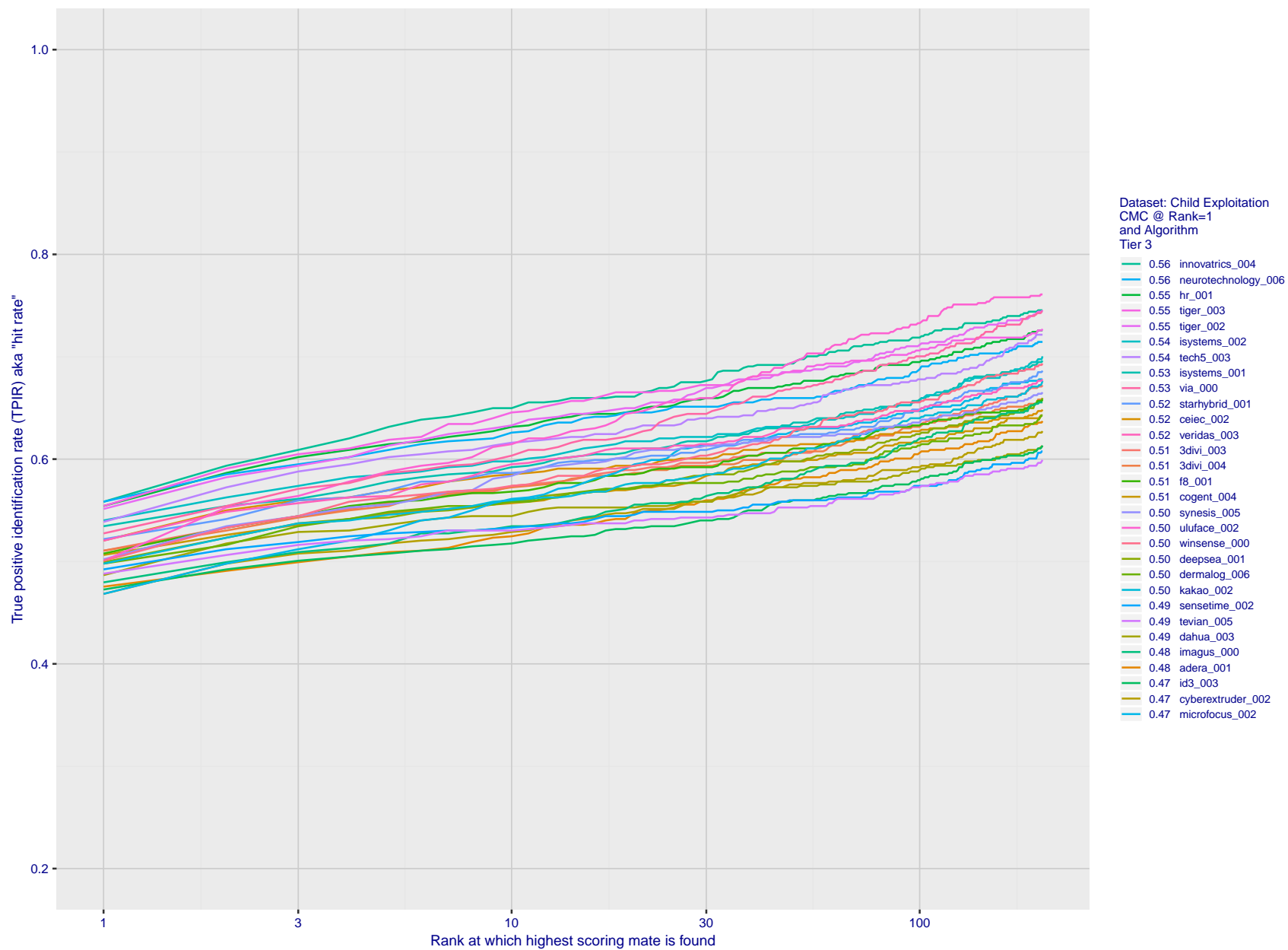


Figure 66: For child exploitation images, cumulative match characteristics (CMC) showing true positive identification rate vs. rank. This is simulation of a one-to-many search experiment - see discussion in section 3.2. The scales are logarithmic in order to show the effect of long candidate lists. Accuracy is poor but much improved relative to the 1:1 DETs of Fig. 63 because a search can succeed if any of a subject's several enrolled images matches the search image with a high score.

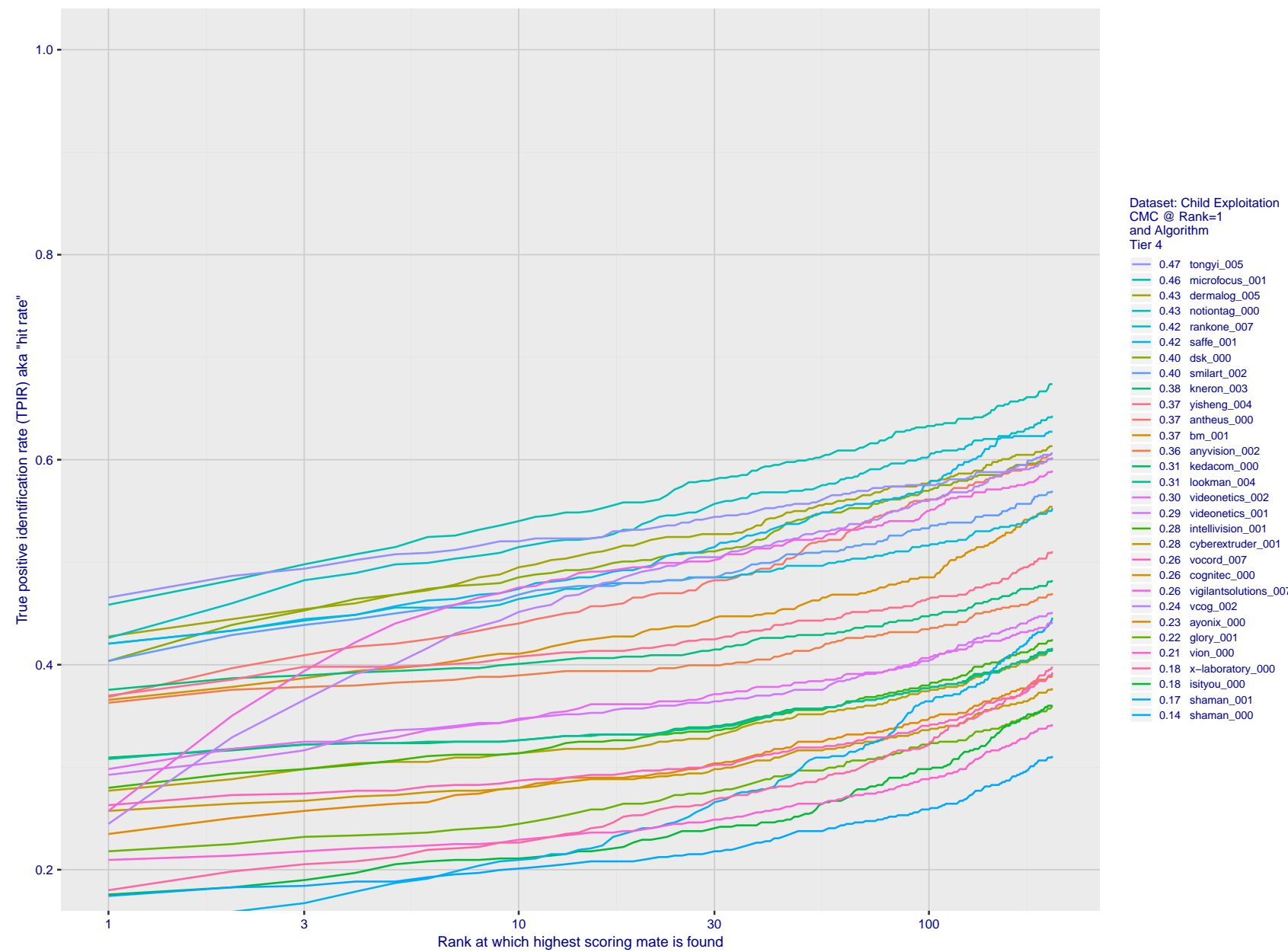


Figure 67: For child exploitation images, cumulative match characteristics (CMC) showing true positive identification rate vs. rank. This is simulation of a one-to-many search experiment - see discussion in section 3.2. The scales are logarithmic in order to show the effect of long candidate lists. Accuracy is poor but much improved relative to the 1:1 DETs of Fig. 63 because a search can succeed if any of a subject's several enrolled images matches the search image with a high score.

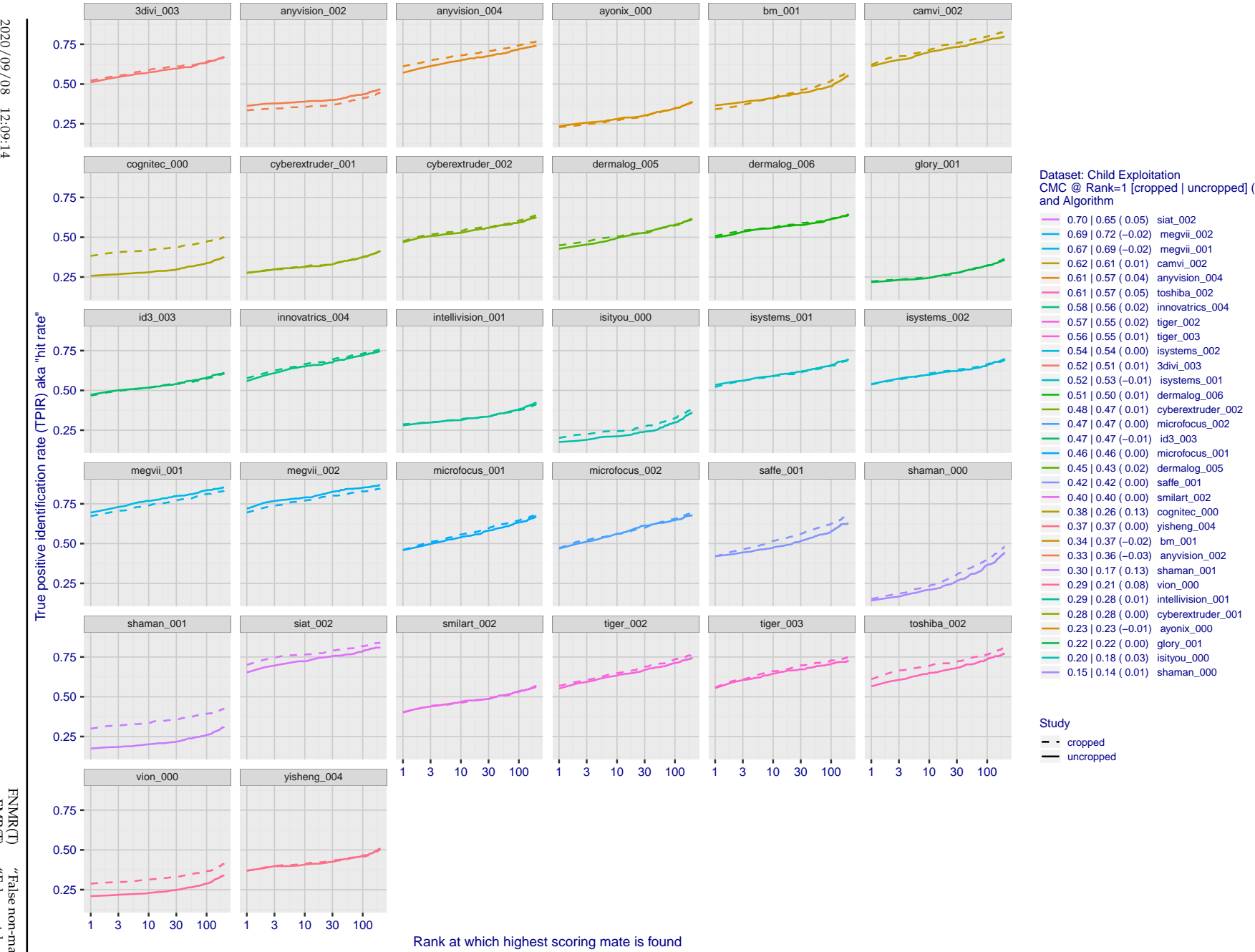


Figure 68: For child exploitation images, cumulative match characteristics (CMC) showing true positive identification rate vs. rank for two cases: 1. Whole image provided to the algorithm; 2. Human annotated rectangular region, cropped and provided to the algorithm. The difference between the traces is associated with detection of difficult faces, and fine localization.

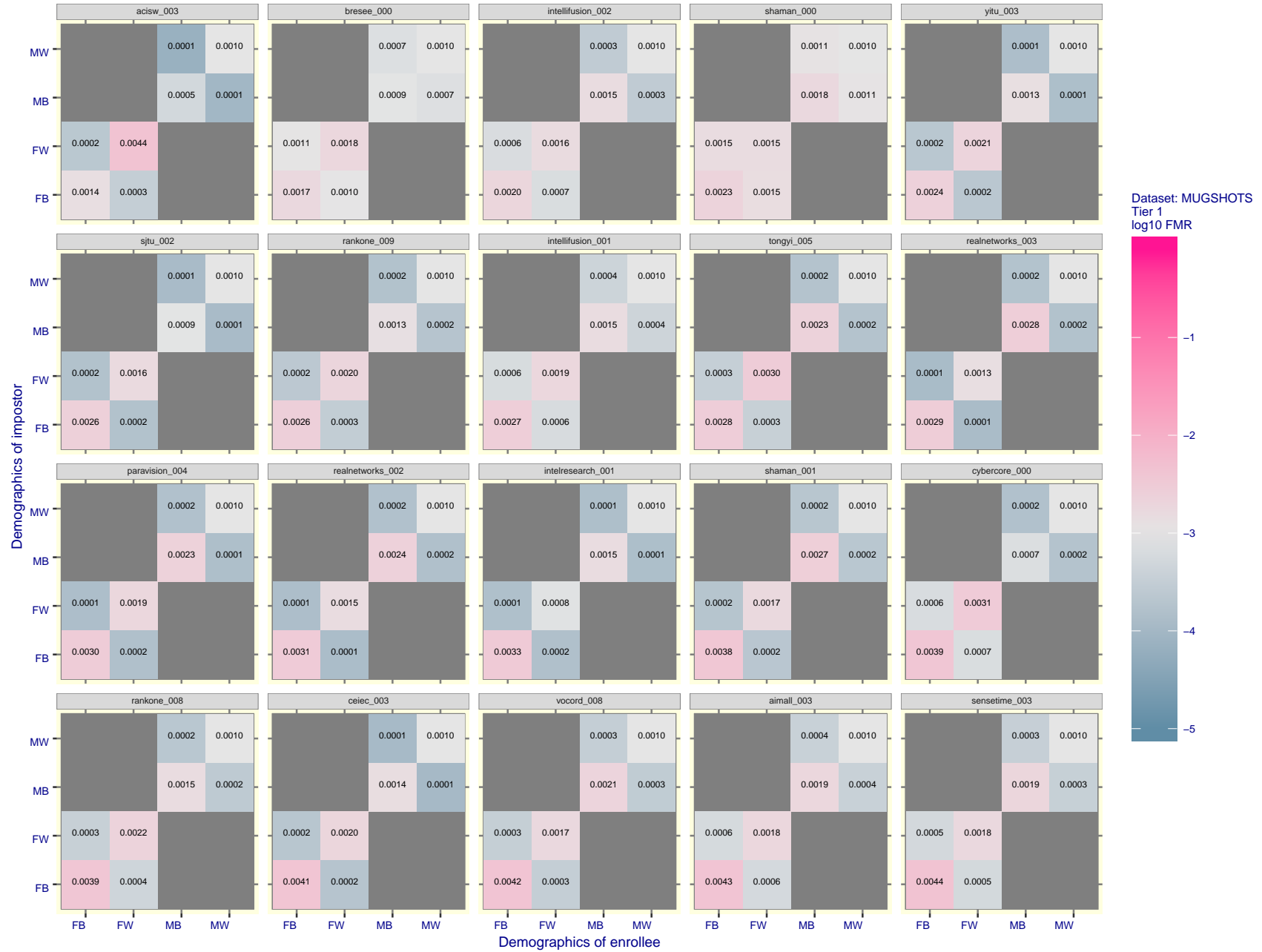


Figure 69: For the mugshot images, FMR for same-sex impostor pairs of images annotated with codes for black female, black male, white female, white male. The threshold is set for each algorithm to give $FMR = 0.001$ for white males which is the demographic that usually gives the lowest FMR. This means the top right box is the same color in all panels. The panels are sorted over multiple pages in order of FMR on black females, which is the demographic that usually gives the highest FMR.

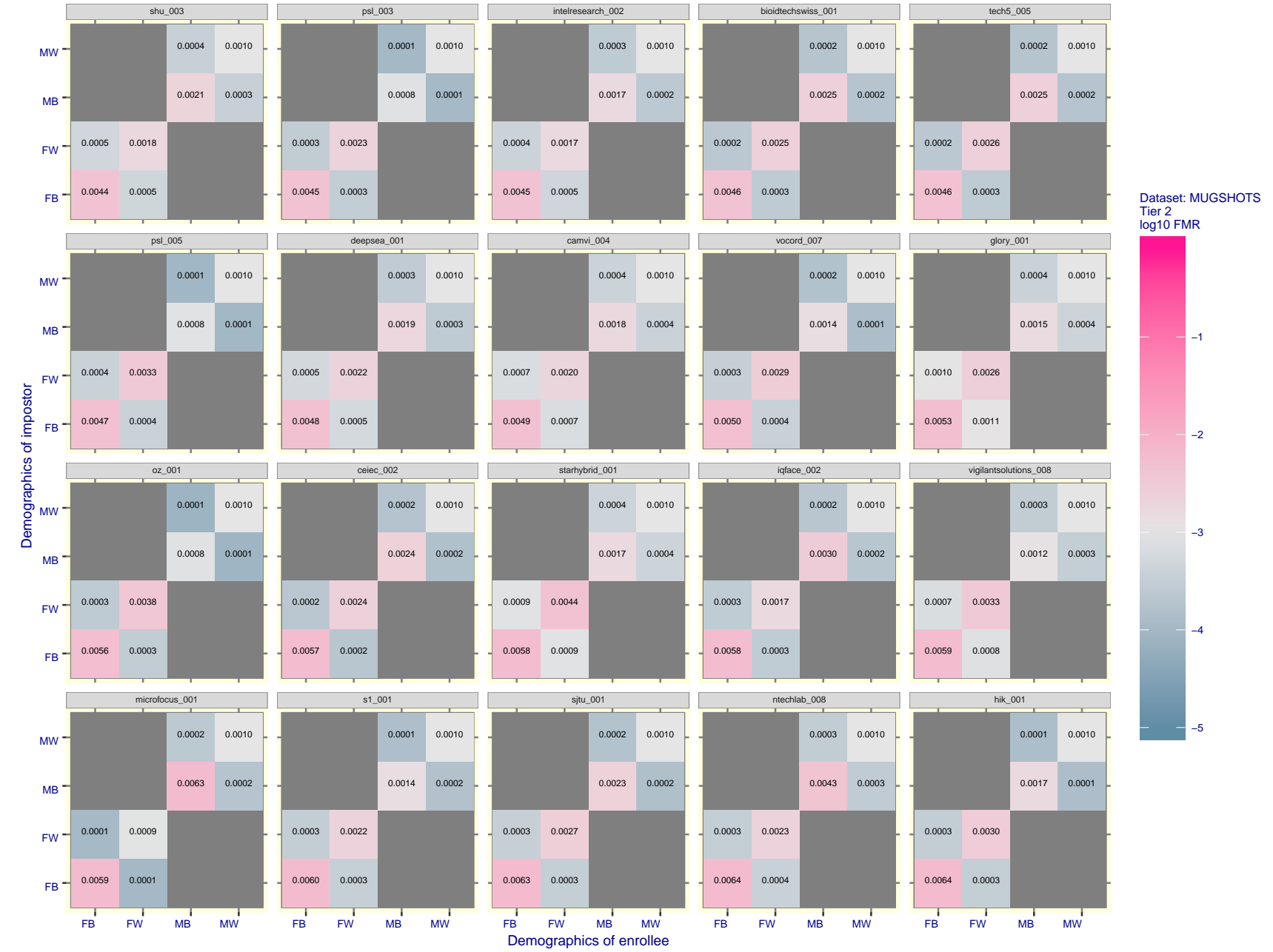


Figure 70: For the mugshot images, FMR for same-sex impostor pairs of images annotated with codes for black female, black male, white female, white male. The threshold is set for each algorithm to give $FMR = 0.001$ for white males which is the demographic that usually gives the lowest FMR. This means the top right box is the same color in all panels. The panels are sorted over multiple pages in order of FMR on black females, which is the demographic that usually gives the highest FMR.

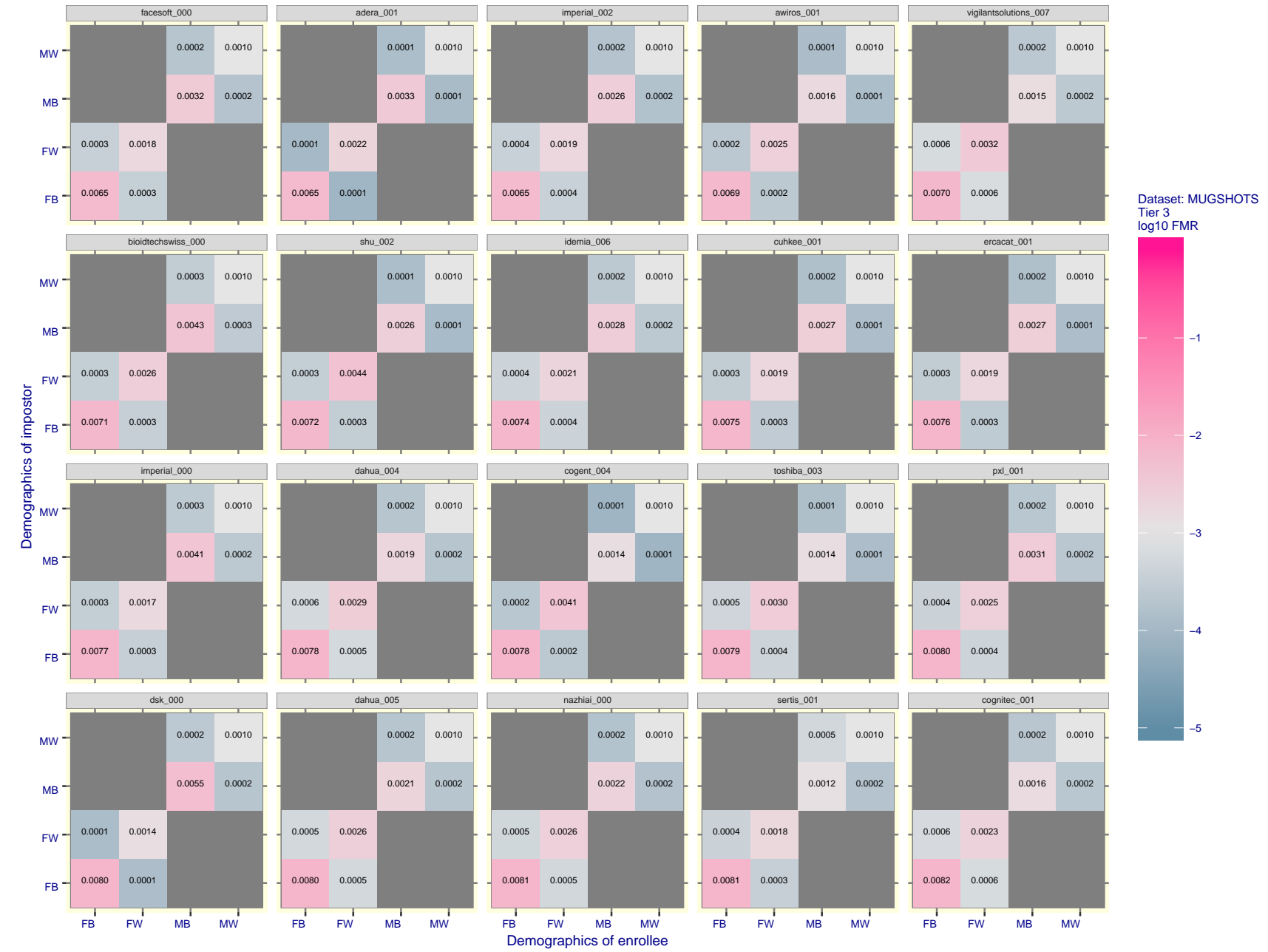


Figure 71: For the mugshot images, FMR for same-sex impostor pairs of images annotated with codes for black female, black male, white female, white male. The threshold is set for each algorithm to give $FMR = 0.001$ for white males which is the demographic that usually gives the lowest FMR. This means the top right box is the same color in all panels. The panels are sorted over multiple pages in order of FMR on black females, which is the demographic that usually gives the highest FMR.

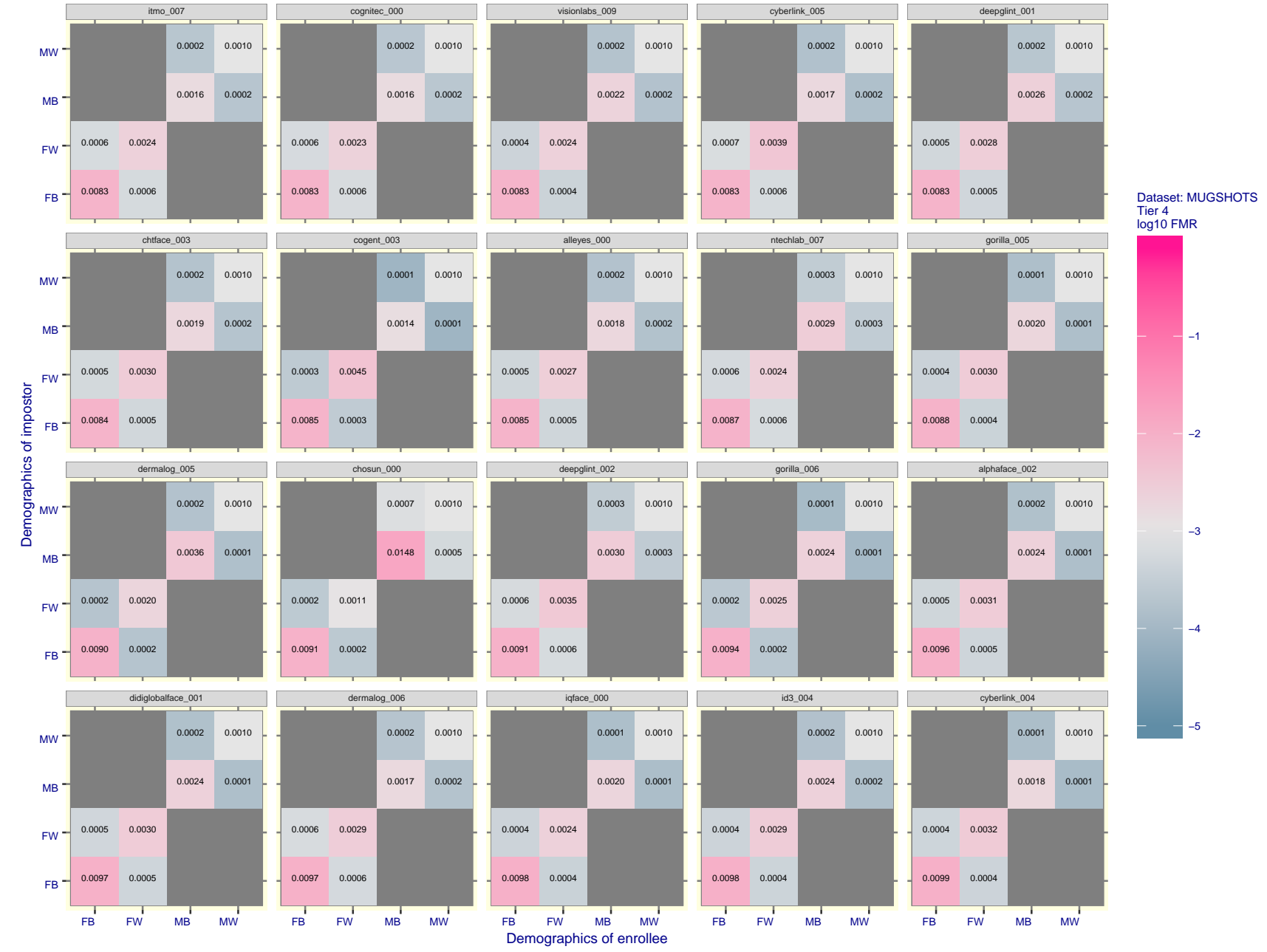


Figure 72: For the mugshot images, FMR for same-sex impostor pairs of images annotated with codes for black female, black male, white female, white male. The threshold is set for each algorithm to give FMR = 0.001 for white males which is the demographic that usually gives the lowest FMR. This means the top right box is the same color in all panels. The panels are sorted over multiple pages in order of FMR on black females, which is the demographic that usually gives the highest FMR.

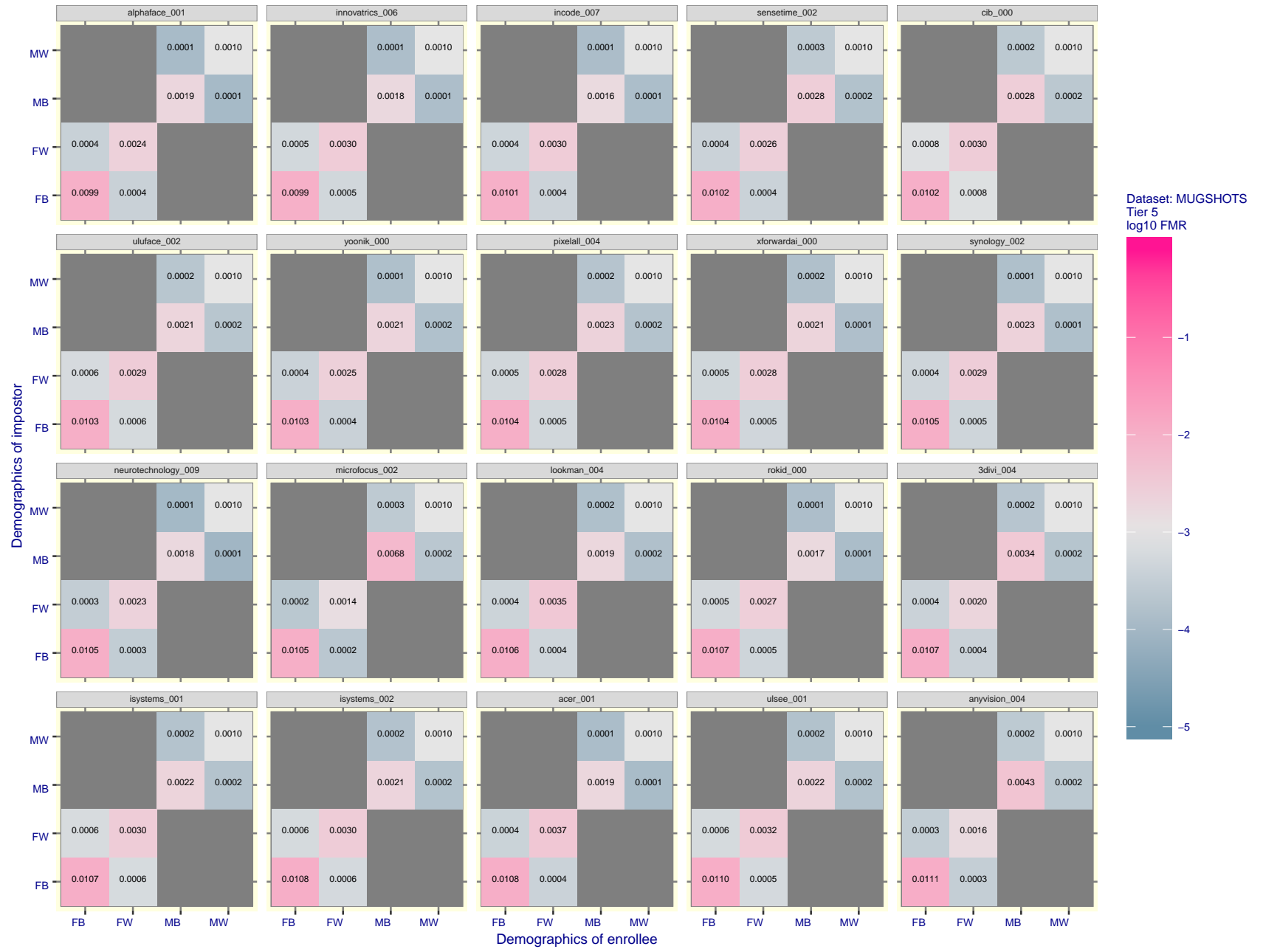


Figure 73: For the mugshot images, FMR for same-sex impostor pairs of images annotated with codes for black female, black male, white female, white male. The threshold is set for each algorithm to give $FMR = 0.001$ for white males which is the demographic that usually gives the lowest FMR. This means the top right box is the same color in all panels. The panels are sorted over multiple pages in order of FMR on black females, which is the demographic that usually gives the highest FMR.

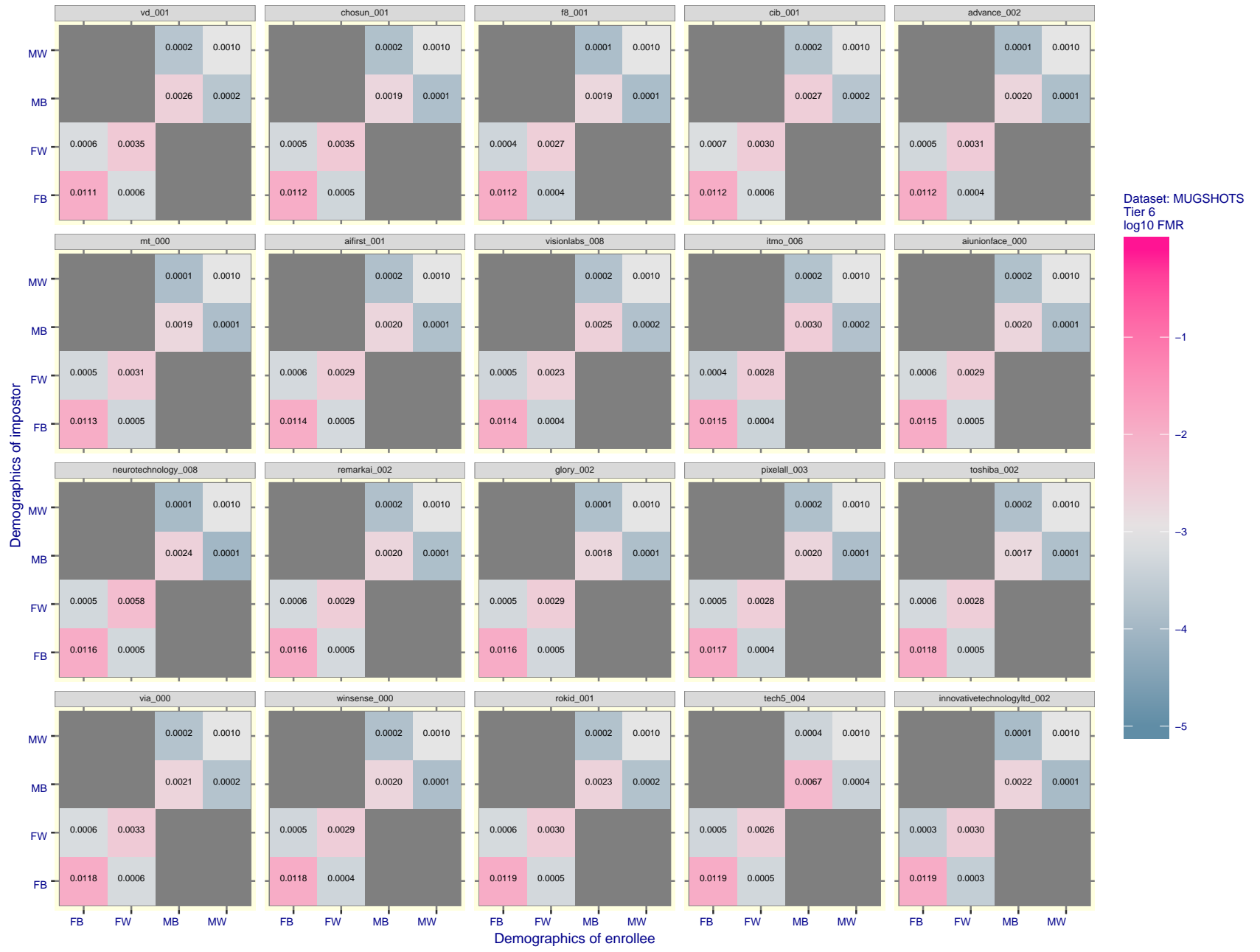


Figure 74: For the mugshot images, FMR for same-sex impostor pairs of images annotated with codes for black female, black male, white female, white male. The threshold is set for each algorithm to give $FMR = 0.001$ for white males which is the demographic that usually gives the lowest FMR. This means the top right box is the same color in all panels. The panels are sorted over multiple pages in order of FMR on black females, which is the demographic that usually gives the highest FMR.

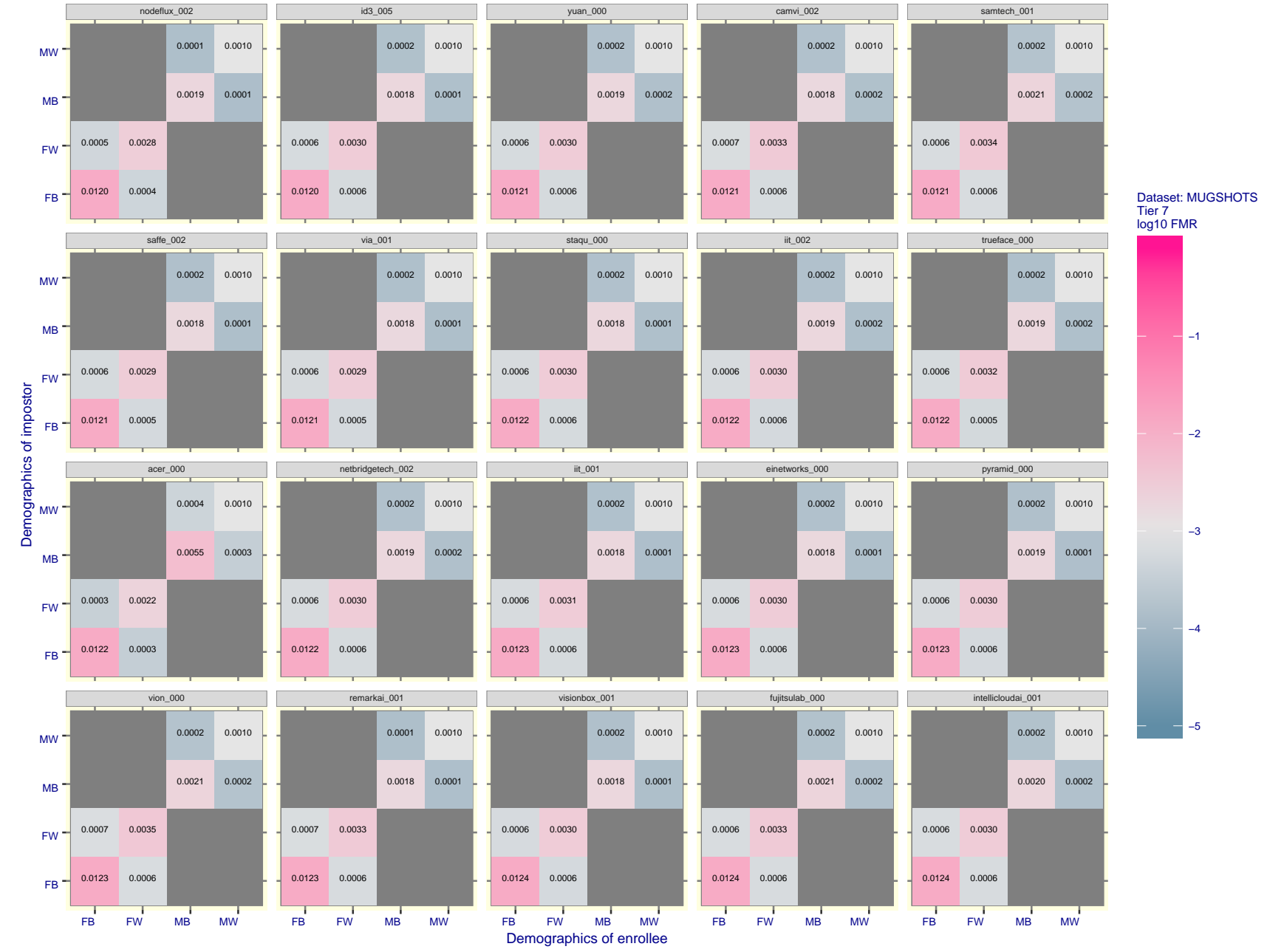


Figure 75: For the mugshot images, FMR for same-sex impostor pairs of images annotated with codes for black female, black male, white female, white male. The threshold is set for each algorithm to give $\text{FMR} = 0.001$ for white males which is the demographic that usually gives the lowest FMR. This means the top right box is the same color in all panels. The panels are sorted over multiple pages in order of FMR on black females, which is the demographic that usually gives the highest FMR.

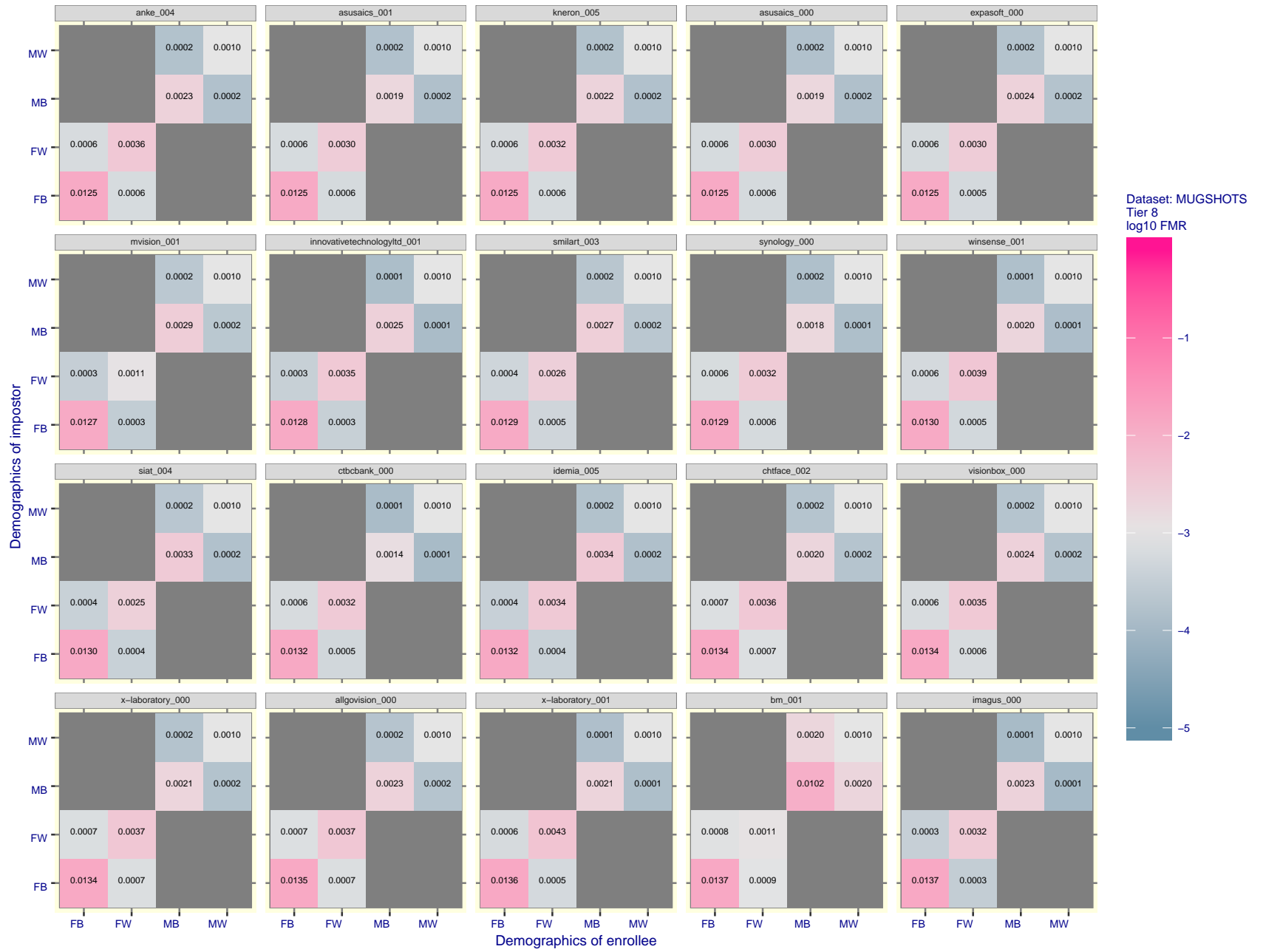


Figure 76: For the mugshot images, FMR for same-sex impostor pairs of images annotated with codes for black female, black male, white female, white male. The threshold is set for each algorithm to give $FMR = 0.001$ for white males which is the demographic that usually gives the lowest FMR. This means the top right box is the same color in all panels. The panels are sorted over multiple pages in order of FMR on black females, which is the demographic that usually gives the highest FMR.

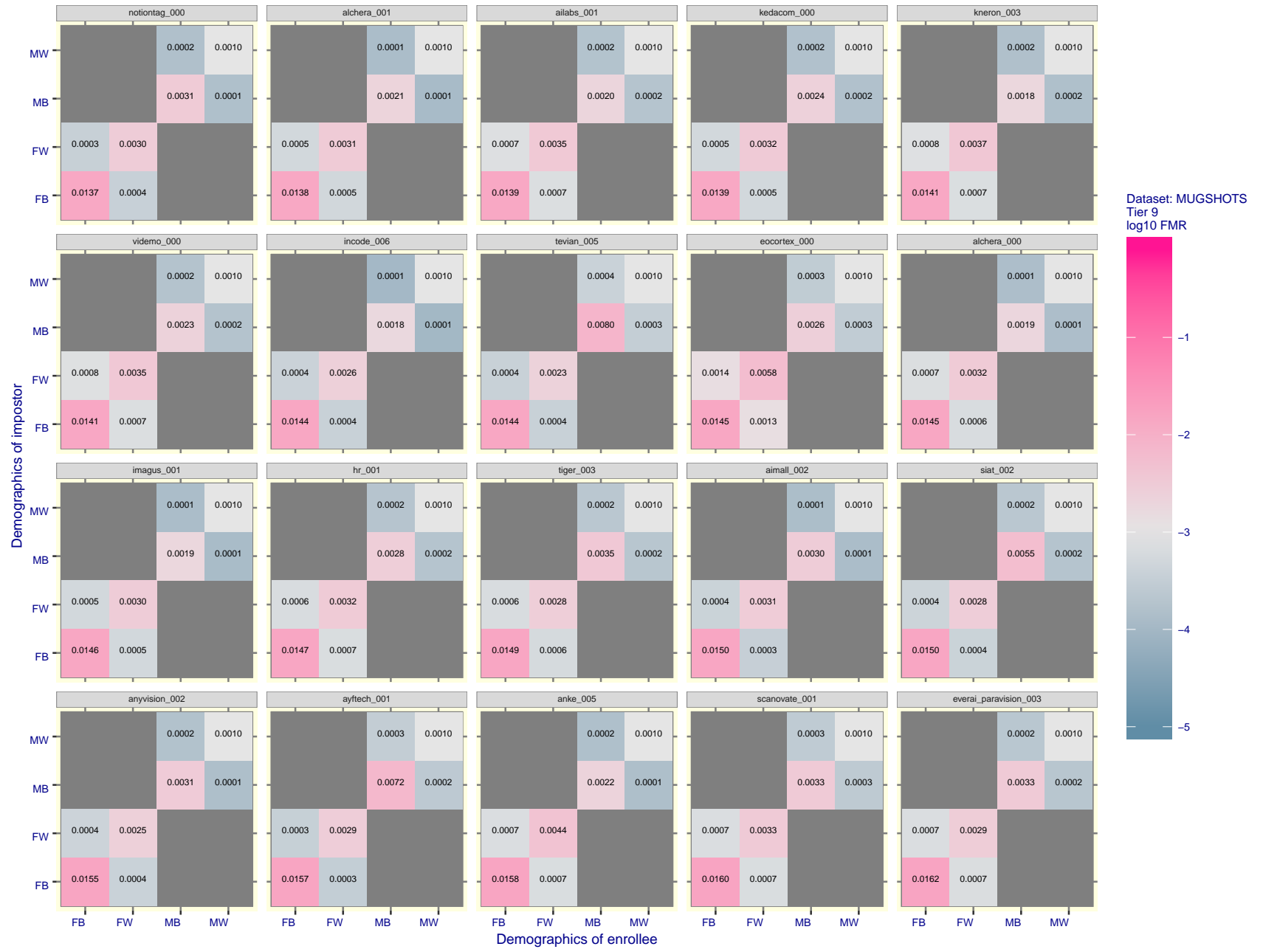


Figure 77: For the mugshot images, FMR for same-sex impostor pairs of images annotated with codes for black female, black male, white female, white male. The threshold is set for each algorithm to give $FMR = 0.001$ for white males which is the demographic that usually gives the lowest FMR. This means the top right box is the same color in all panels. The panels are sorted over multiple pages in order of FMR on black females, which is the demographic that usually gives the highest FMR.

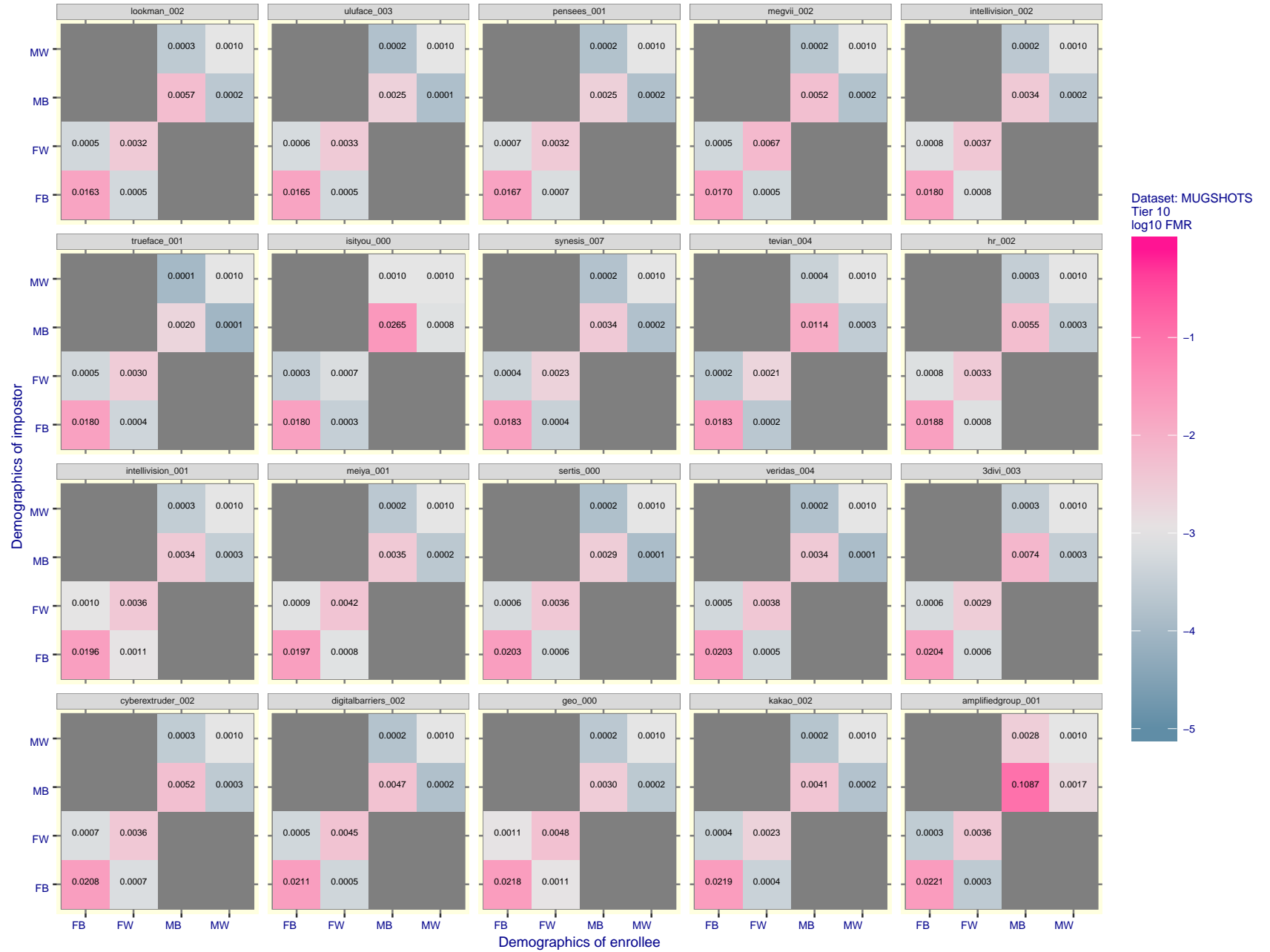


Figure 78: For the mugshot images, FMR for same-sex impostor pairs of images annotated with codes for black female, black male, white female, white male. The threshold is set for each algorithm to give $FMR = 0.001$ for white males which is the demographic that usually gives the lowest FMR. This means the top right box is the same color in all panels. The panels are sorted over multiple pages in order of FMR on black females, which is the demographic that usually gives the highest FMR.

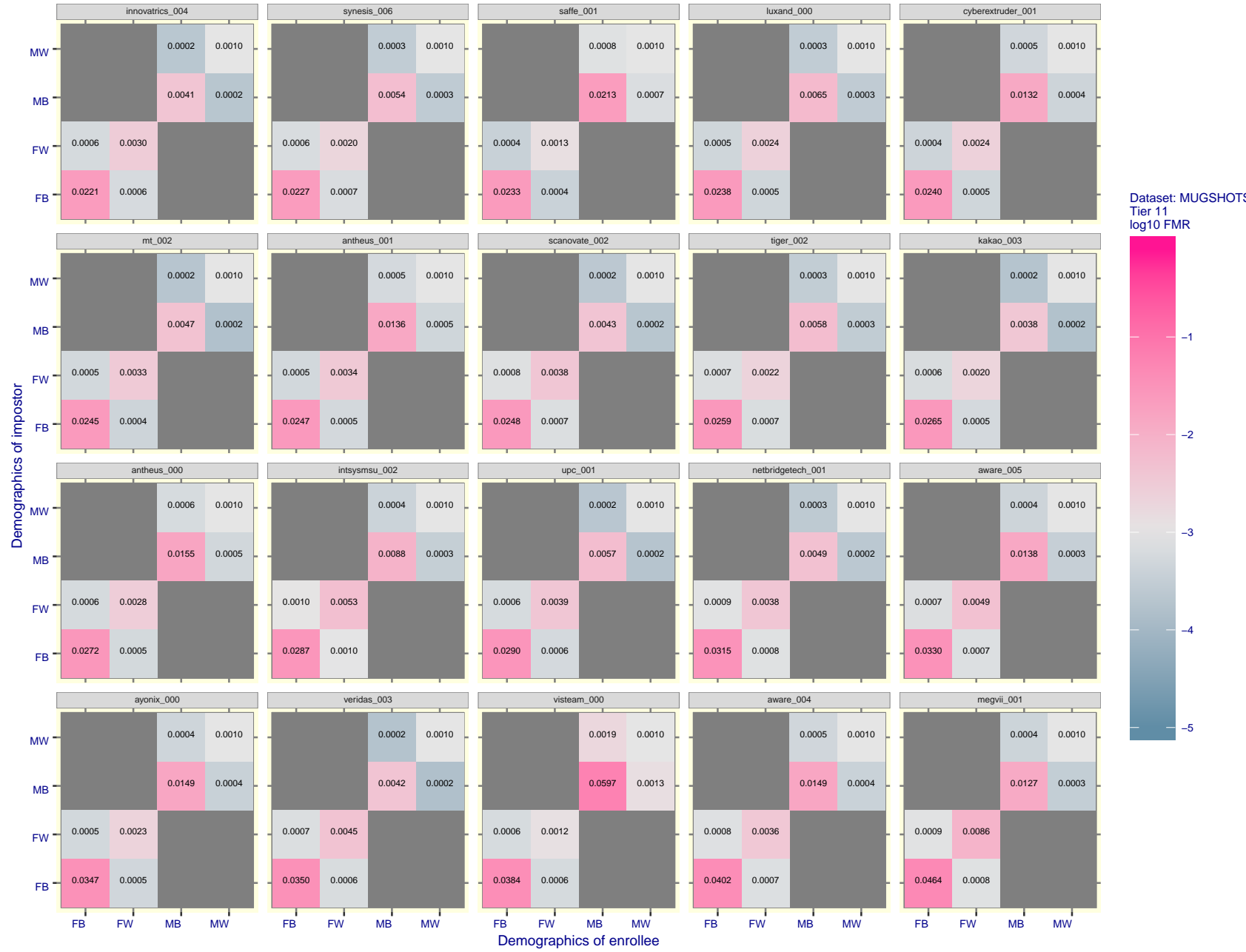


Figure 79: For the mugshot images, FMR for same-sex impostor pairs of images annotated with codes for black female, black male, white female, white male. The threshold is set for each algorithm to give $FMR = 0.001$ for white males which is the demographic that usually gives the lowest FMR. This means the top right box is the same color in all panels. The panels are sorted over multiple pages in order of FMR on black females, which is the demographic that usually gives the highest FMR.



Figure 80: For the mugshot images, FMR for same-sex impostor pairs of images annotated with codes for black female, black male, white female, white male. The threshold is set for each algorithm to give $\text{FMR} = 0.001$ for white males which is the demographic that usually gives the lowest FMR. This means the top right box is the same color in all panels. The panels are sorted over multiple pages in order of FMR on black females, which is the demographic that usually gives the highest FMR.

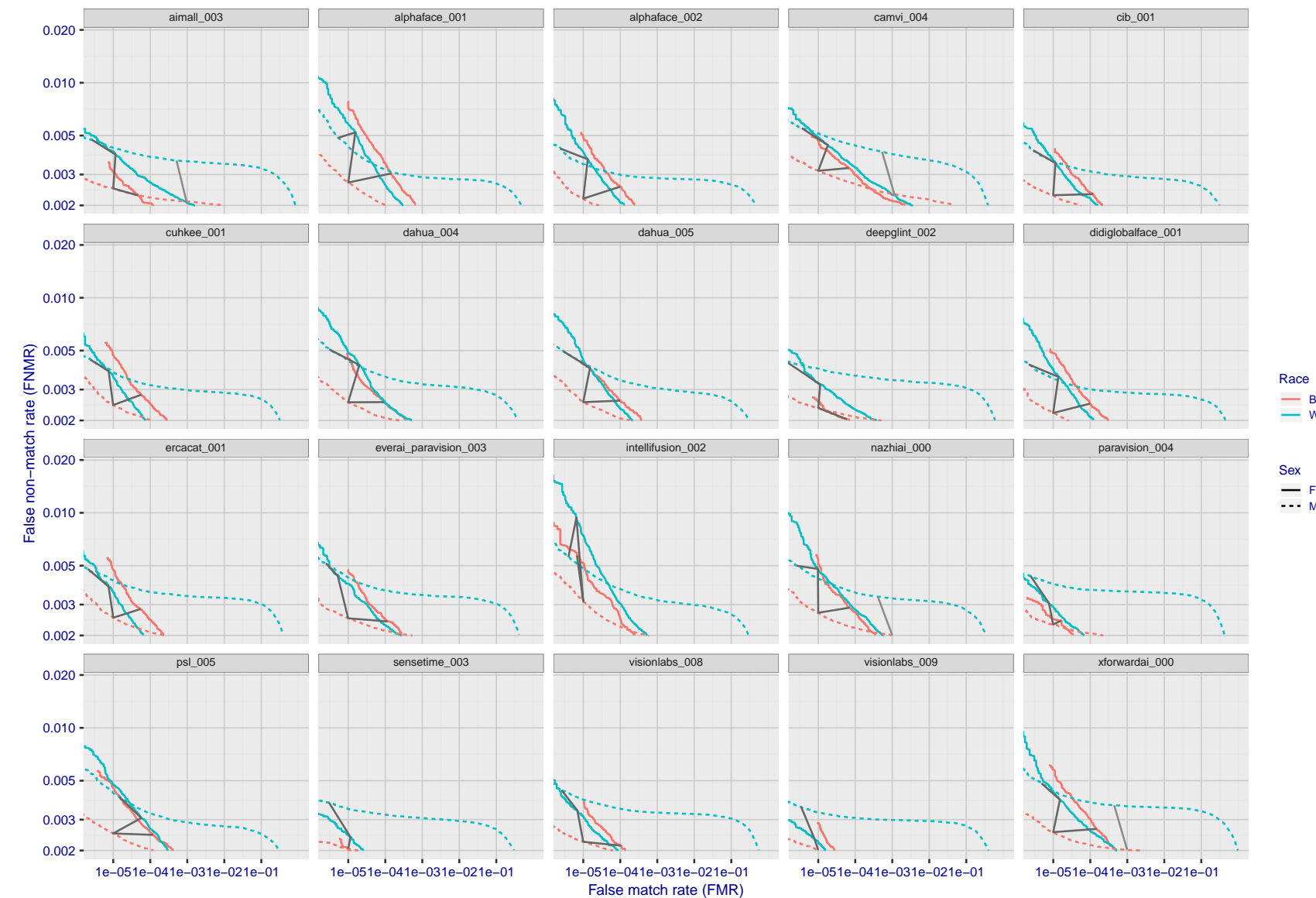


Figure 81: For the mugshot images, error tradeoff characteristics for white females, black females, black males and white males. The Z-shaped grey lines correspond to fixed thresholds, showing both FNMR and FMR vary at one T value. Note: Many of the plots will naively be read as saying women gives worse error rates than men because the solid traces lie above the dotted ones. However, this is misleading and incomplete: The grey lines show the traces reveal horizontal shifts. Thus for the cogent-003 algorithm FNMR for men is higher than for women at a fixed threshold but, at the same time, FMR is higher for women - see Figure 123. As access control systems almost always operate at a fixed threshold, the naive interpretation is incorrect.

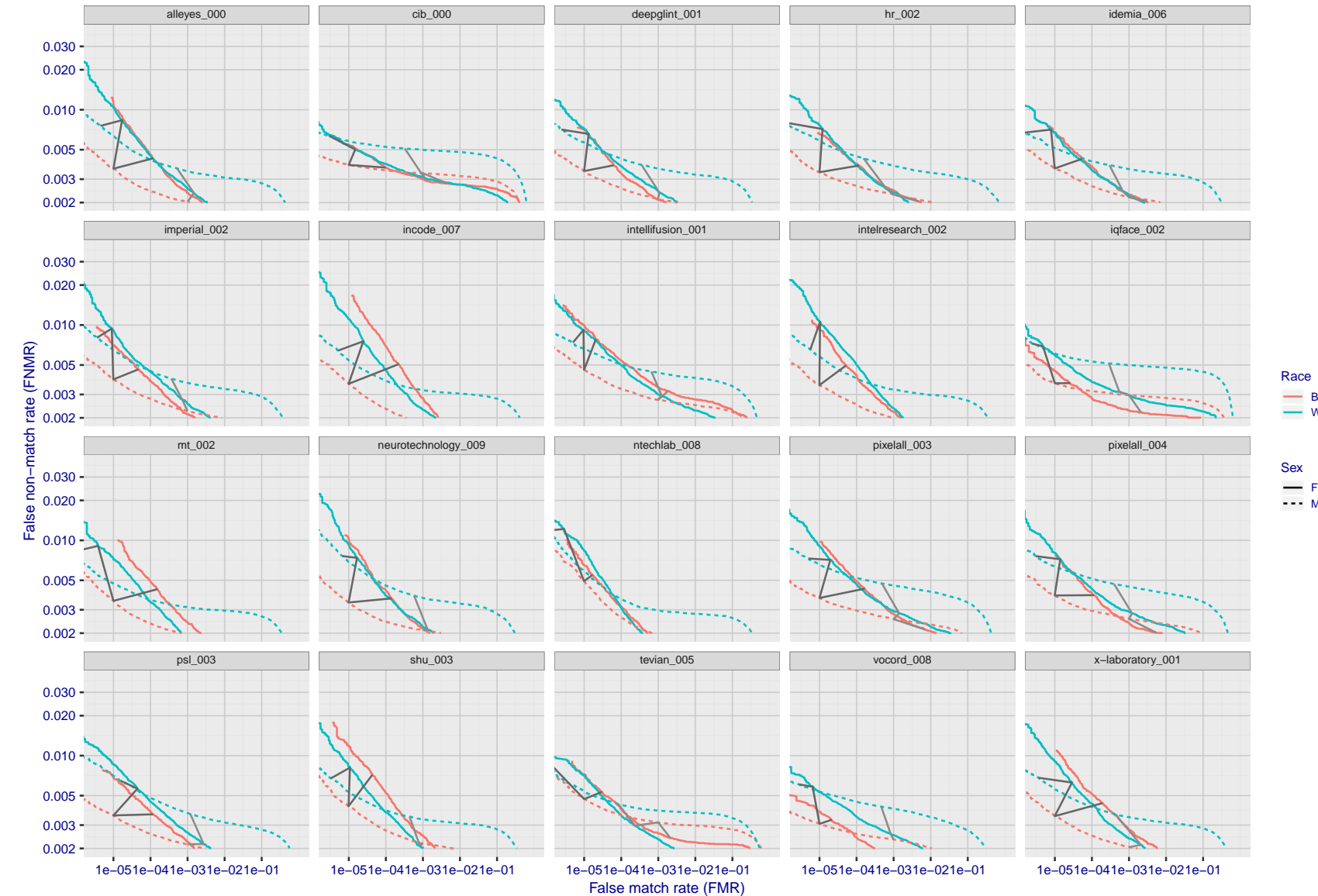


Figure 82: For the mugshot images, error tradeoff characteristics for white females, black females, black males and white males. The Z-shaped grey lines correspond to fixed thresholds, showing both FNMR and FMR vary at one T value. Note: Many of the plots will naively be read as saying women gives worse error rates than men because the solid traces lie above the dotted ones. However, this is misleading and incomplete: The grey lines show the traces reveal horizontal shifts. Thus for the cogent-003 algorithm FNMR for men is higher than for women at a fixed threshold but, at the same time, FMR is higher for women - see Figure 123. As access control systems almost always operate at a fixed threshold, the naive interpretation is incorrect.

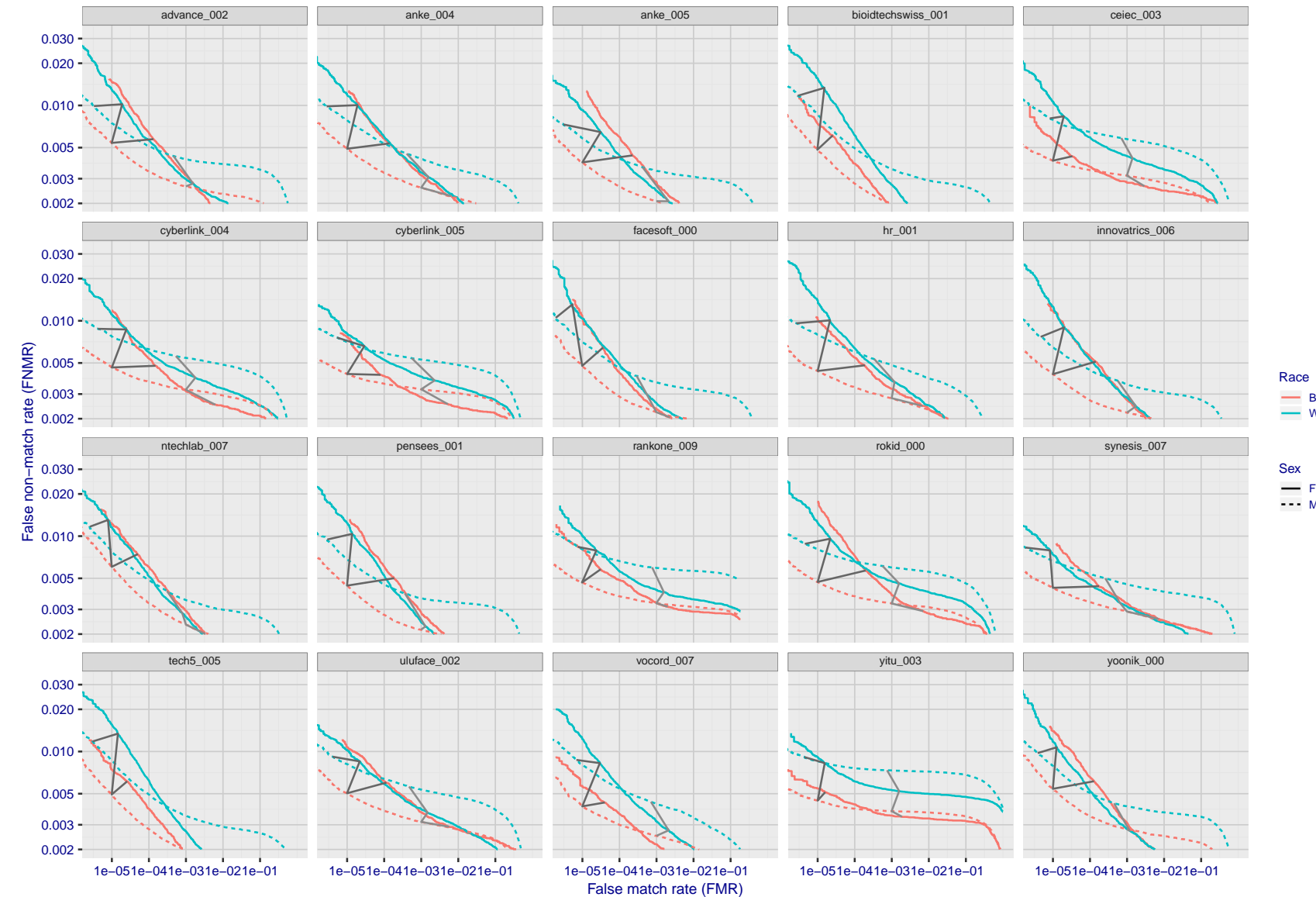


Figure 83: For the mugshot images, error tradeoff characteristics for white females, black females, black males and white males. The Z-shaped grey lines correspond to fixed thresholds, showing both FNMR and FMR vary at one T value. Note: Many of the plots will naively be read as saying women gives worse error rates than men because the solid traces lie above the dotted ones. However, this is misleading and incomplete: The grey lines show the traces reveal horizontal shifts. Thus for the cogent-003 algorithm FNMR for men is higher than for women at a fixed threshold but, at the same time, FMR is higher for women - see Figure 123. As access control systems almost always operate at a fixed threshold, the naive interpretation is incorrect.

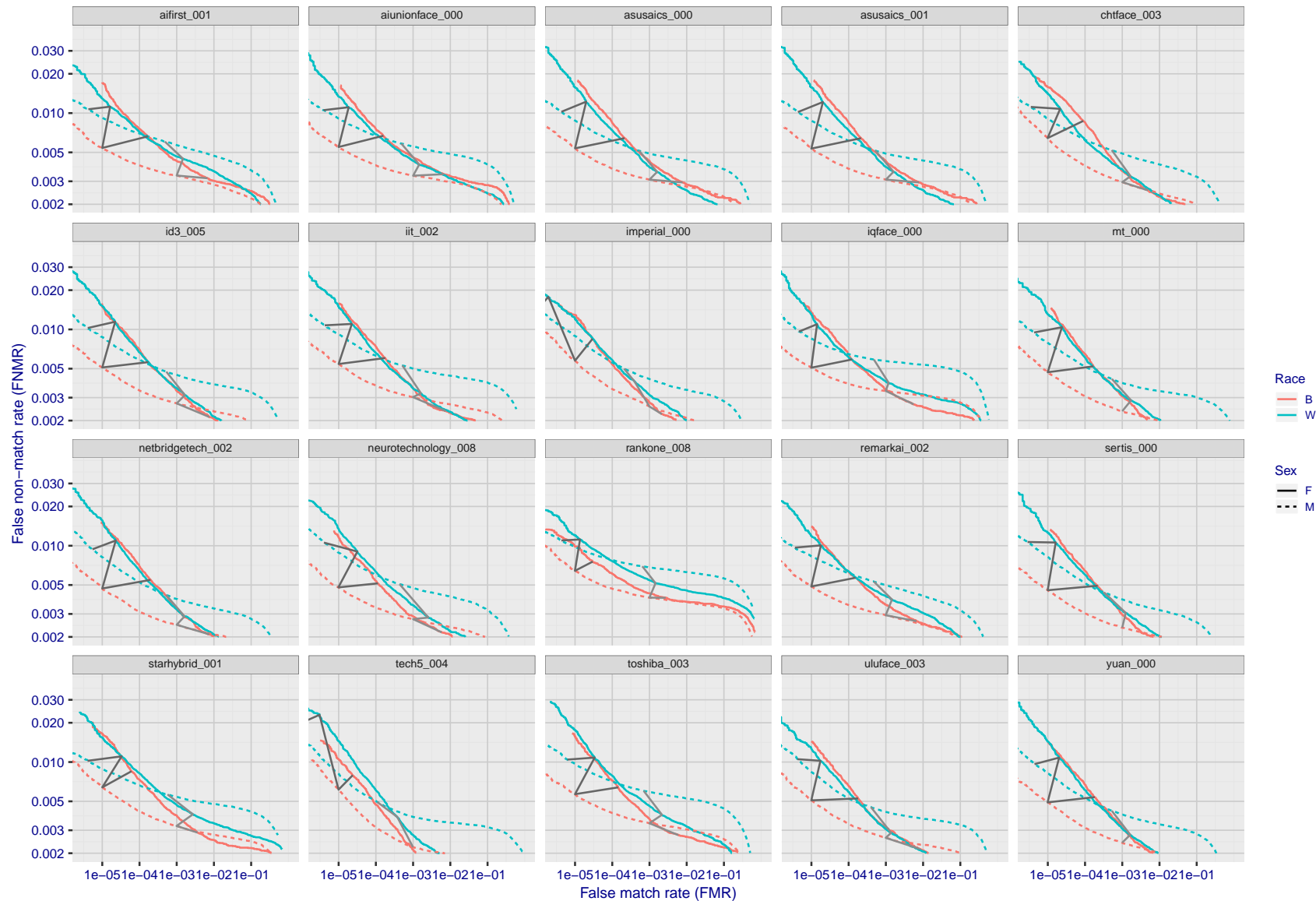
2020/09/08
12:09:14

Figure 84: For the mugshot images, error tradeoff characteristics for white females, black females, black males and white males. The Z-shaped grey lines correspond to fixed thresholds, showing both FNMR and FMR vary at one T value. Note: Many of the plots will naively be read as saying women gives worse error rates than men because the solid traces lie above the dotted ones. However, this is misleading and incomplete: The grey lines show the traces reveal horizontal shifts. Thus for the cogent-003 algorithm FNMR for men is higher than for women at a fixed threshold but, at the same time, FMR is higher for women - see Figure 123. As access control systems almost always operate at a fixed threshold, the naive interpretation is incorrect.

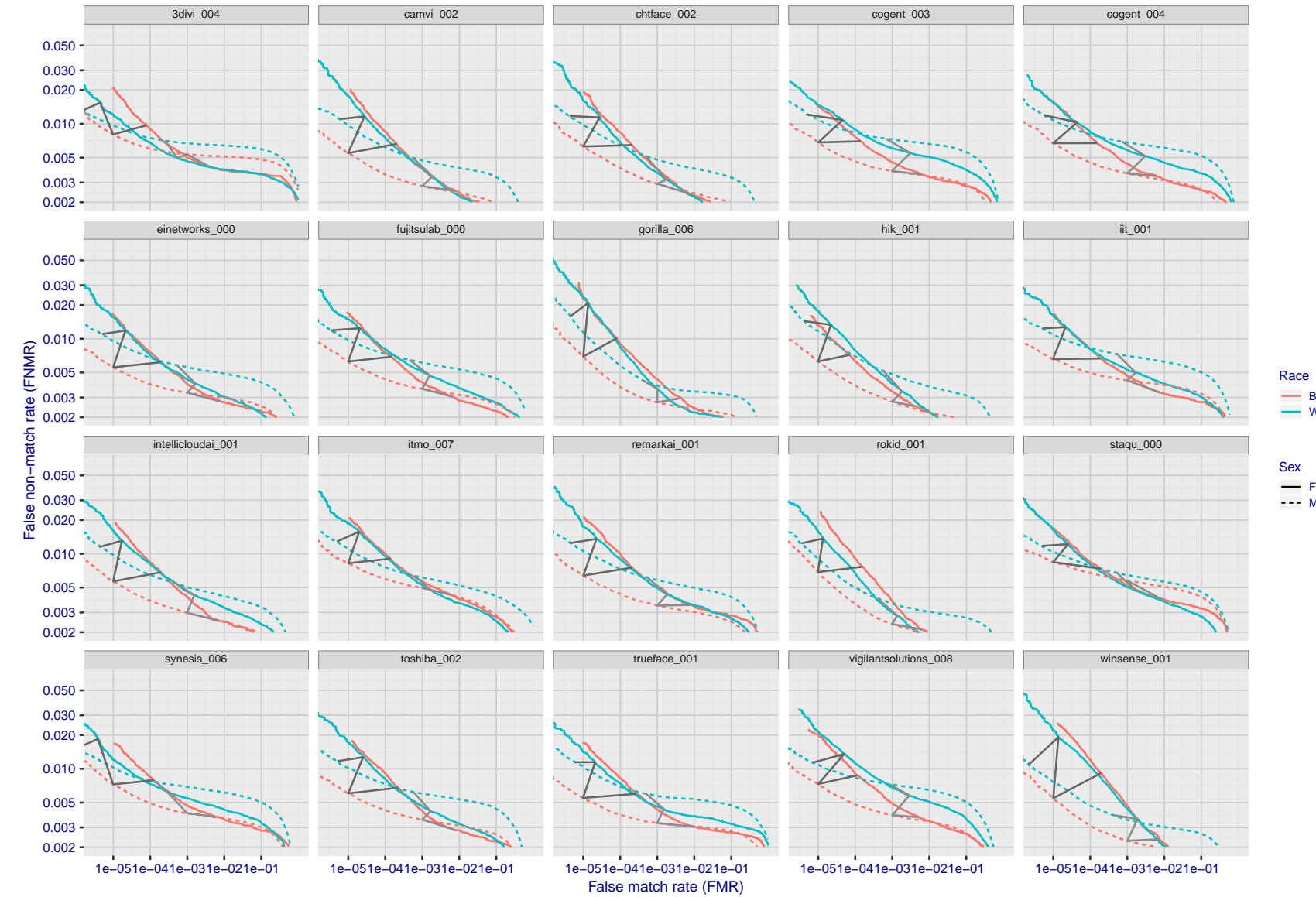


Figure 85: For the mugshot images, error tradeoff characteristics for white females, black females, black males and white males. The Z-shaped grey lines correspond to fixed thresholds, showing both FNMR and FMR vary at one T value. Note: Many of the plots will naively be read as saying women gives worse error rates than men because the solid traces lie above the dotted ones. However, this is misleading and incomplete: The grey lines show the traces reveal horizontal shifts. Thus for the cogent-003 algorithm FNMR for men is higher than for women at a fixed threshold but, at the same time, FMR is higher for women - see Figure 123. As access control systems almost always operate at a fixed threshold, the naive interpretation is incorrect.

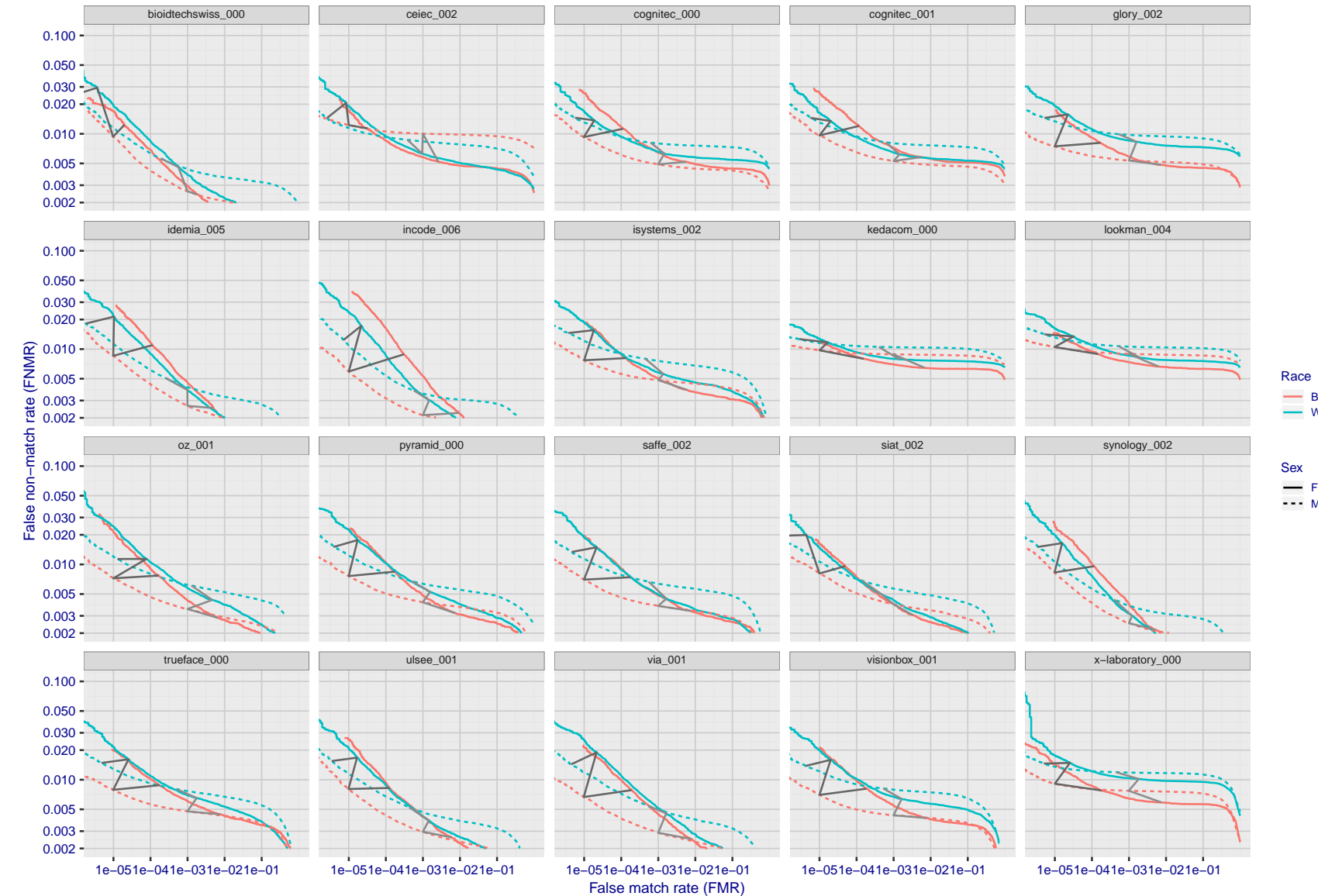


Figure 86: For the mugshot images, error tradeoff characteristics for white females, black females, black males and white males. The Z-shaped grey lines correspond to fixed thresholds, showing both FNMR and FMR vary at one T value. Note: Many of the plots will naively be read as saying women gives worse error rates than men because the solid traces lie above the dotted ones. However, this is misleading and incomplete: The grey lines show the traces reveal horizontal shifts. Thus for the cogent-003 algorithm FNMR for men is higher than for women at a fixed threshold but, at the same time, FMR is higher for women - see Figure 123. As access control systems almost always operate at a fixed threshold, the naive interpretation is incorrect.

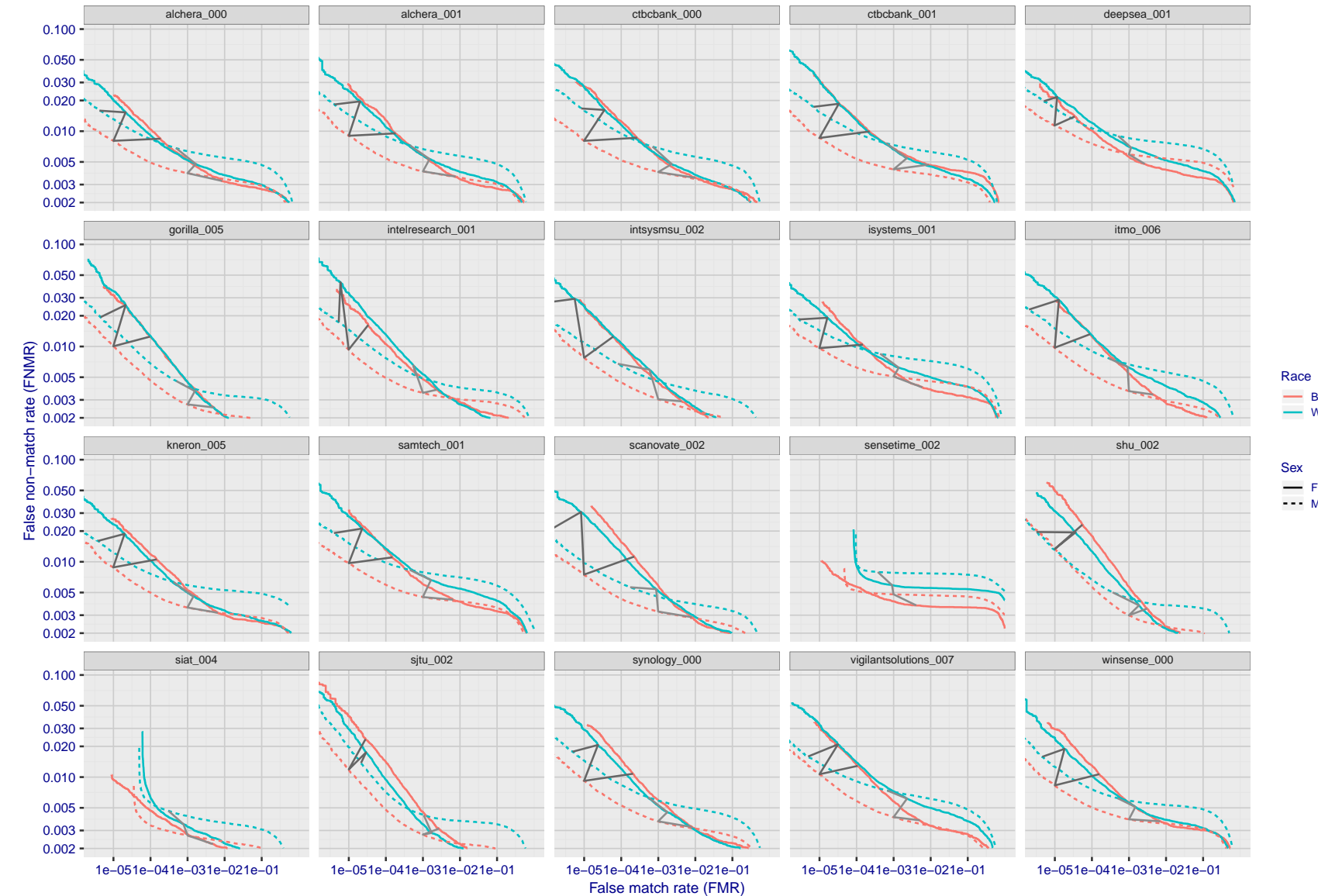


Figure 87: For the mugshot images, error tradeoff characteristics for white females, black females, black males and white males. The Z-shaped grey lines correspond to fixed thresholds, showing both FNMR and FMR vary at one T value. Note: Many of the plots will naively be read as saying women gives worse error rates than men because the solid traces lie above the dotted ones. However, this is misleading and incomplete: The grey lines show the traces reveal horizontal shifts. Thus for the cogent-003 algorithm FNMR for men is higher than for women at a fixed threshold but, at the same time, FMR is higher for women - see Figure 123. As access control systems almost always operate at a fixed threshold, the naive interpretation is incorrect.

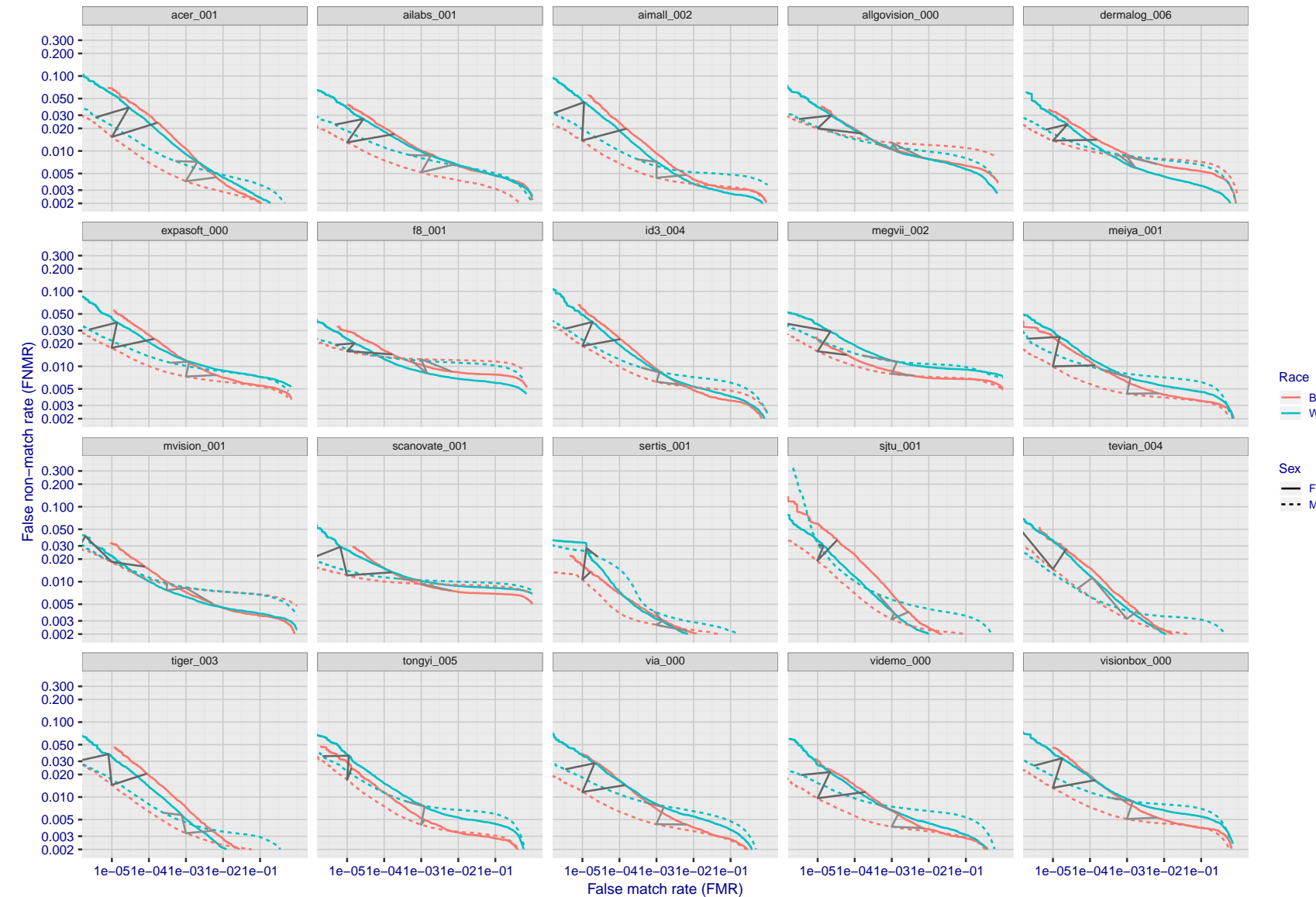


Figure 88: For the mugshot images, error tradeoff characteristics for white females, black females, black males and white males. The Z-shaped grey lines correspond to fixed thresholds, showing both FNMR and FMR vary at one T value. Note: Many of the plots will naively be read as saying women gives worse error rates than men because the solid traces lie above the dotted ones. However, this is misleading and incomplete: The grey lines show the traces reveal horizontal shifts. Thus for the cogent-003 algorithm FNMR for men is higher than for women at a fixed threshold but, at the same time, FMR is higher for women - see Figure 123. As access control systems almost always operate at a fixed threshold, the naive interpretation is incorrect.

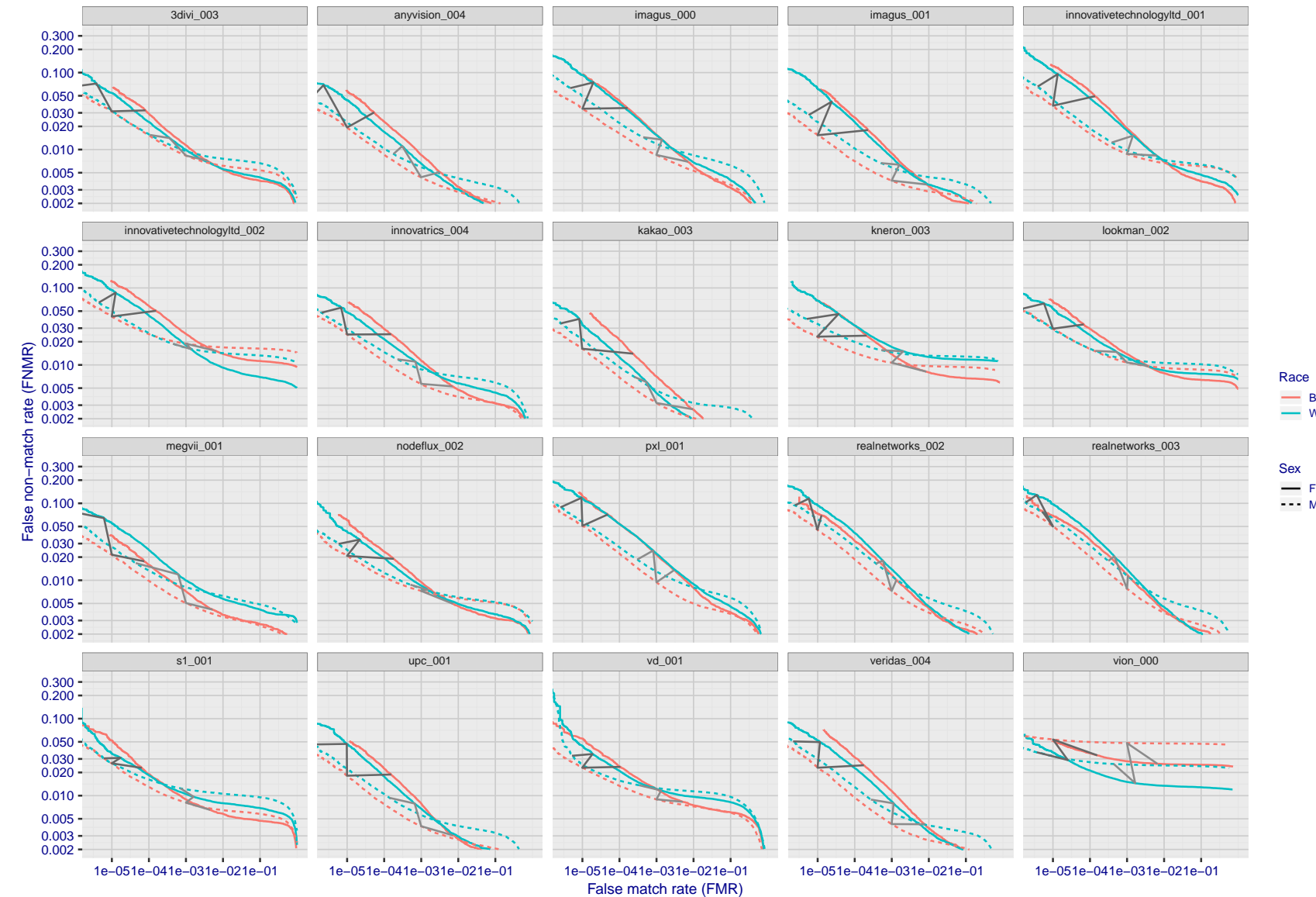


Figure 89: For the mugshot images, error tradeoff characteristics for white females, black females, black males and white males. The Z-shaped grey lines correspond to fixed thresholds, showing both FNMR and FMR vary at one T value. Note: Many of the plots will naively be read as saying women gives worse error rates than men because the solid traces lie above the dotted ones. However, this is misleading and incomplete: The grey lines show the traces reveal horizontal shifts. Thus for the cogent-003 algorithm FNMR for men is higher than for women at a fixed threshold but, at the same time, FMR is higher for women - see Figure 123. As access control systems almost always operate at a fixed threshold, the naive interpretation is incorrect.

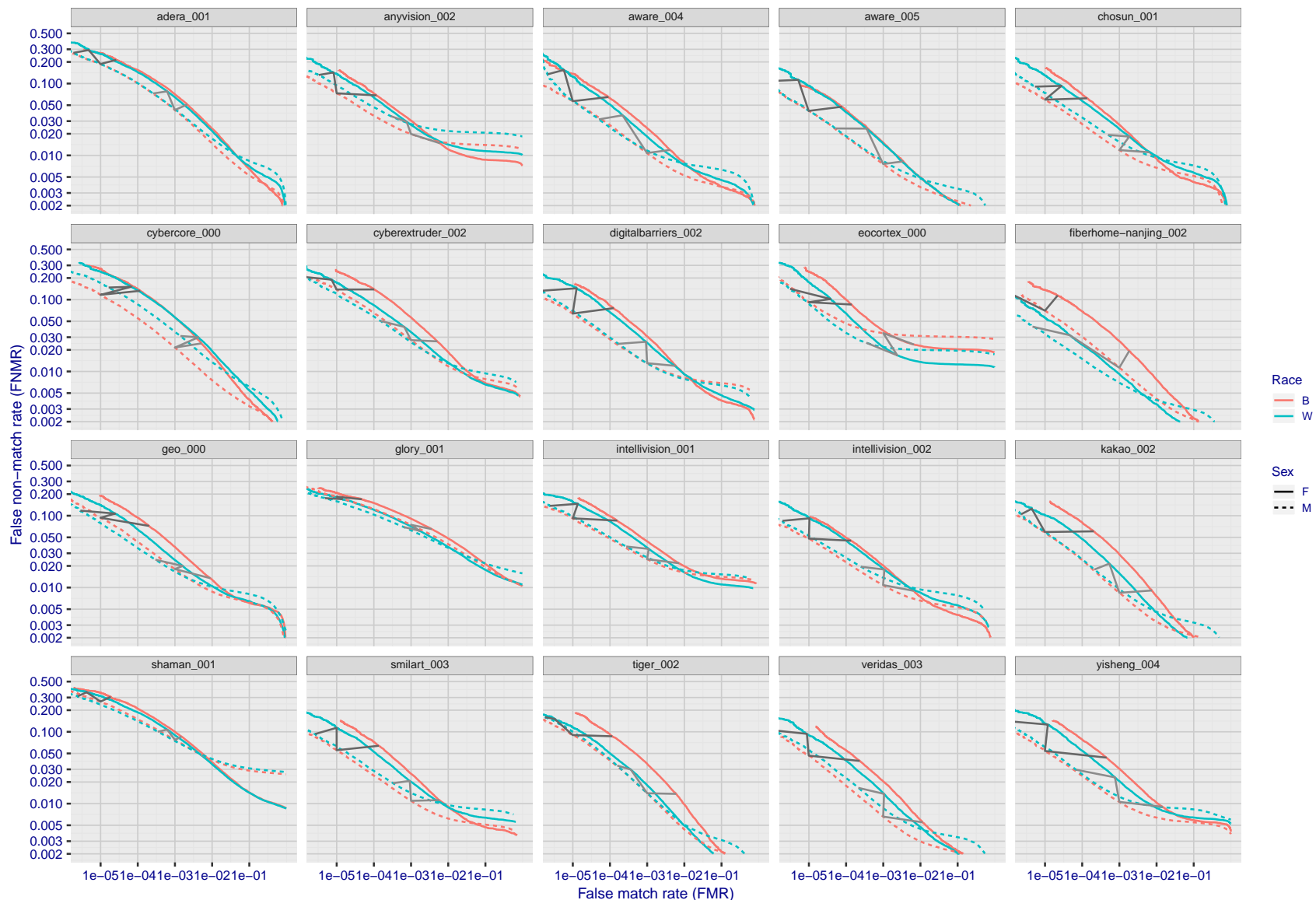


Figure 90: For the mugshot images, error tradeoff characteristics for white females, black females, black males and white males. The Z-shaped grey lines correspond to fixed thresholds, showing both FNMR and FMR vary at one T value. Note: Many of the plots will naively be read as saying women gives worse error rates than men because the solid traces lie above the dotted ones. However, this is misleading and incomplete: The grey lines show the traces reveal horizontal shifts. Thus for the cogent-003 algorithm FNMR for men is higher than for women at a fixed threshold but, at the same time, FMR is higher for women - see Figure 123. As access control systems almost always operate at a fixed threshold, the naive interpretation is incorrect.

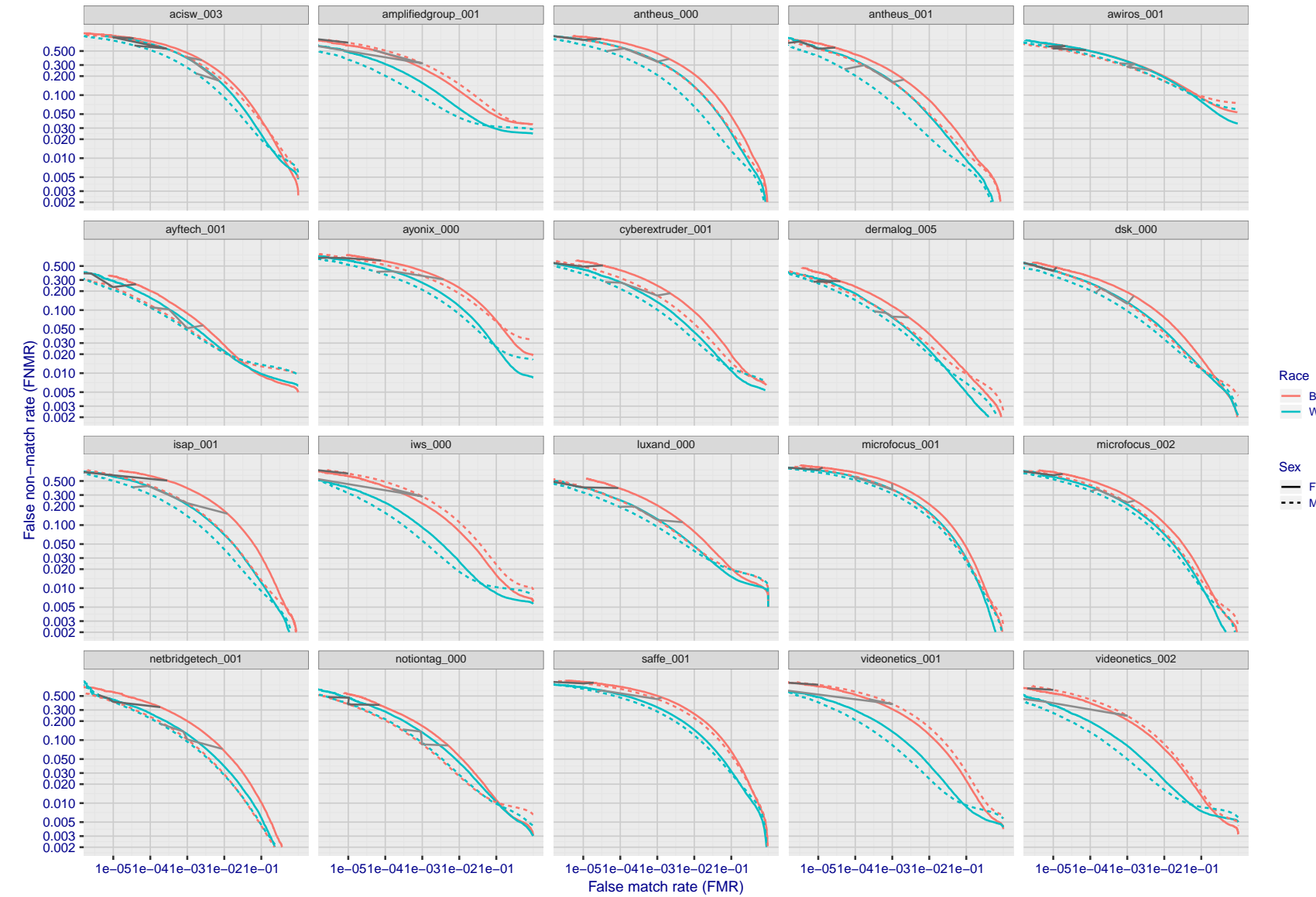


Figure 91: For the mugshot images, error tradeoff characteristics for white females, black females, black males and white males. The Z-shaped grey lines correspond to fixed thresholds, showing both FNMR and FMR vary at one T value. Note: Many of the plots will naively be read as saying women gives worse error rates than men because the solid traces lie above the dotted ones. However, this is misleading and incomplete: The grey lines show the traces reveal horizontal shifts. Thus for the cogent-003 algorithm FNMR for men is higher than for women at a fixed threshold but, at the same time, FMR is higher for women - see Figure 123. As access control systems almost always operate at a fixed threshold, the naive interpretation is incorrect.

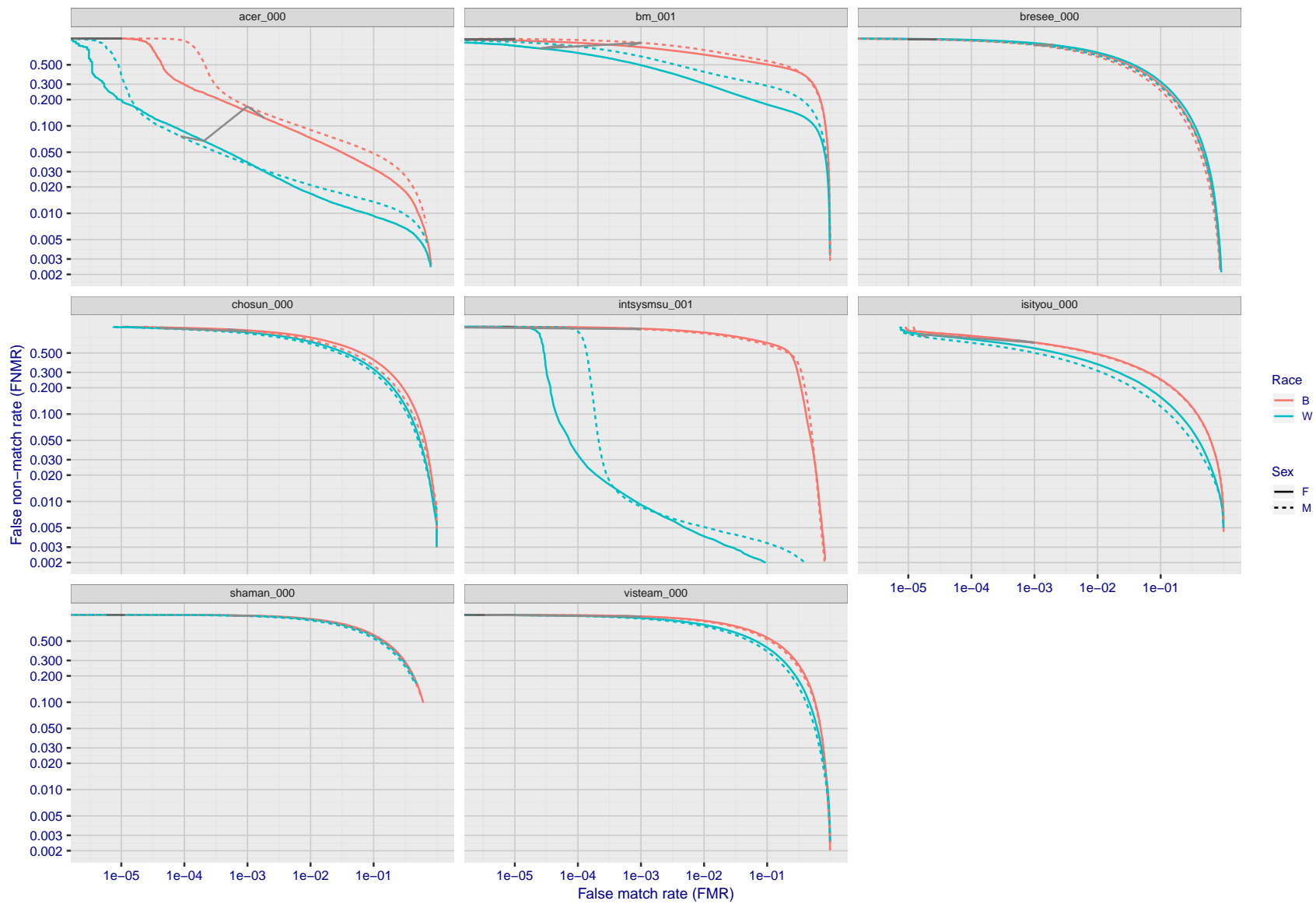


Figure 92: For the mugshot images, error tradeoff characteristics for white females, black females, black males and white males. The Z-shaped grey lines correspond to fixed thresholds, showing both FNMR and FMR vary at one T value. Note: Many of the plots will naively be read as saying women gives worse error rates than men because the solid traces lie above the dotted ones. However, this is misleading and incomplete: The grey lines show the traces reveal horizontal shifts. Thus for the cogent-003 algorithm FNMR for men is higher than for women at a fixed threshold but, at the same time, FMR is higher for women - see Figure 123. As access control systems almost always operate at a fixed threshold, the naive interpretation is incorrect.

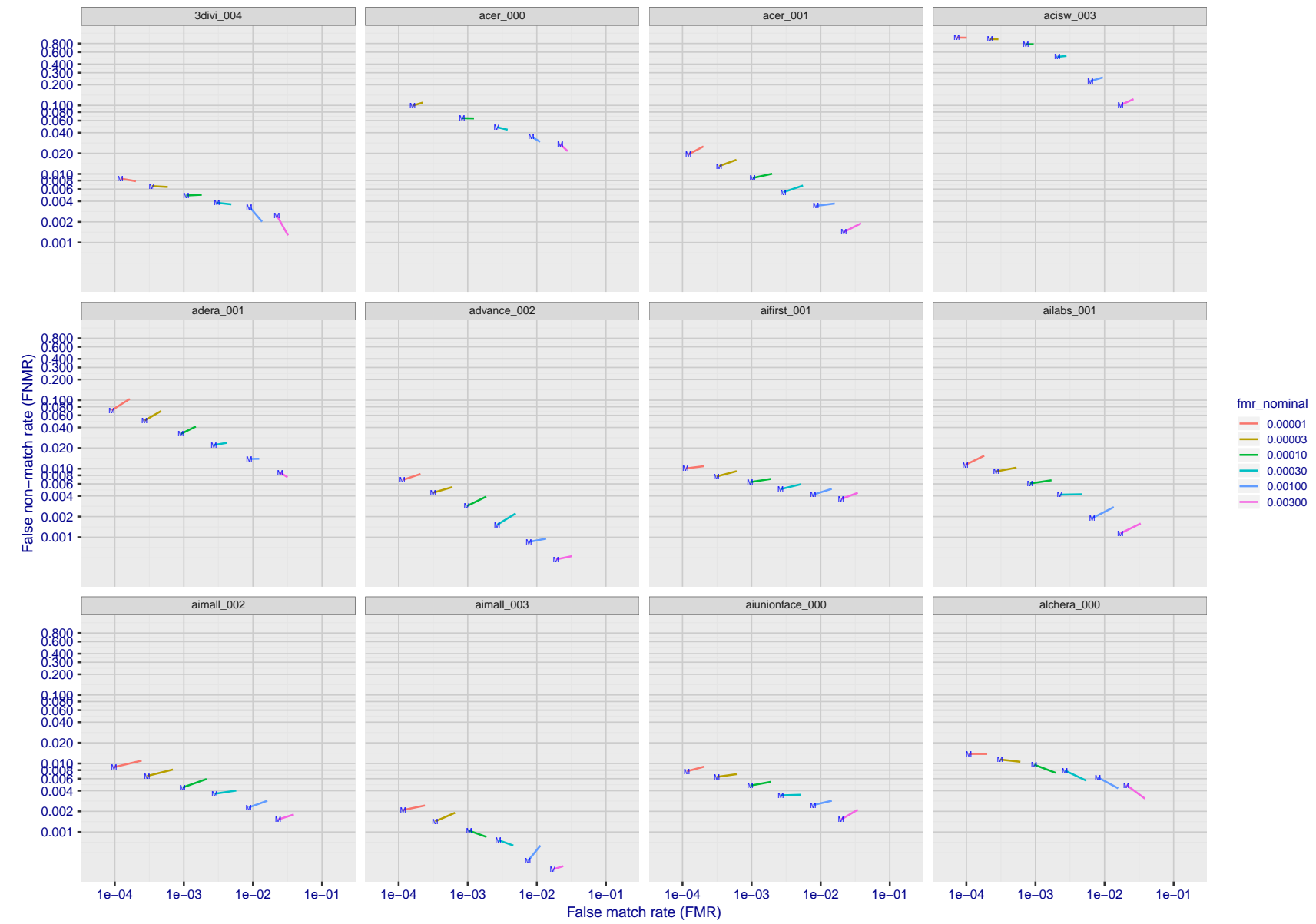


Figure 93: For the visa images, FNMR and FMR at six operating points along the DET characteristic. At each point a line is drawn between $(FMR, FNMR)_{MALE}$ and $(FMR, FNMR)_{FEMALE}$ showing how which sex has lower FMR and/or FNMR. The "M" label denotes male, the other end of the line corresponds to female. The six operating thresholds are selected to give the nominal false match rates given in the legend, and are computed over all impostor pairs regardless of age, sex, and place of birth. The plotted FMR values are broadly an order of magnitude larger than the nominal rates because FMR is computed over demographically-matched impostor pairs i.e individuals of the same sex, from the same geographic region (see section 3.6.1), and the same age group (see section 3.6.2).

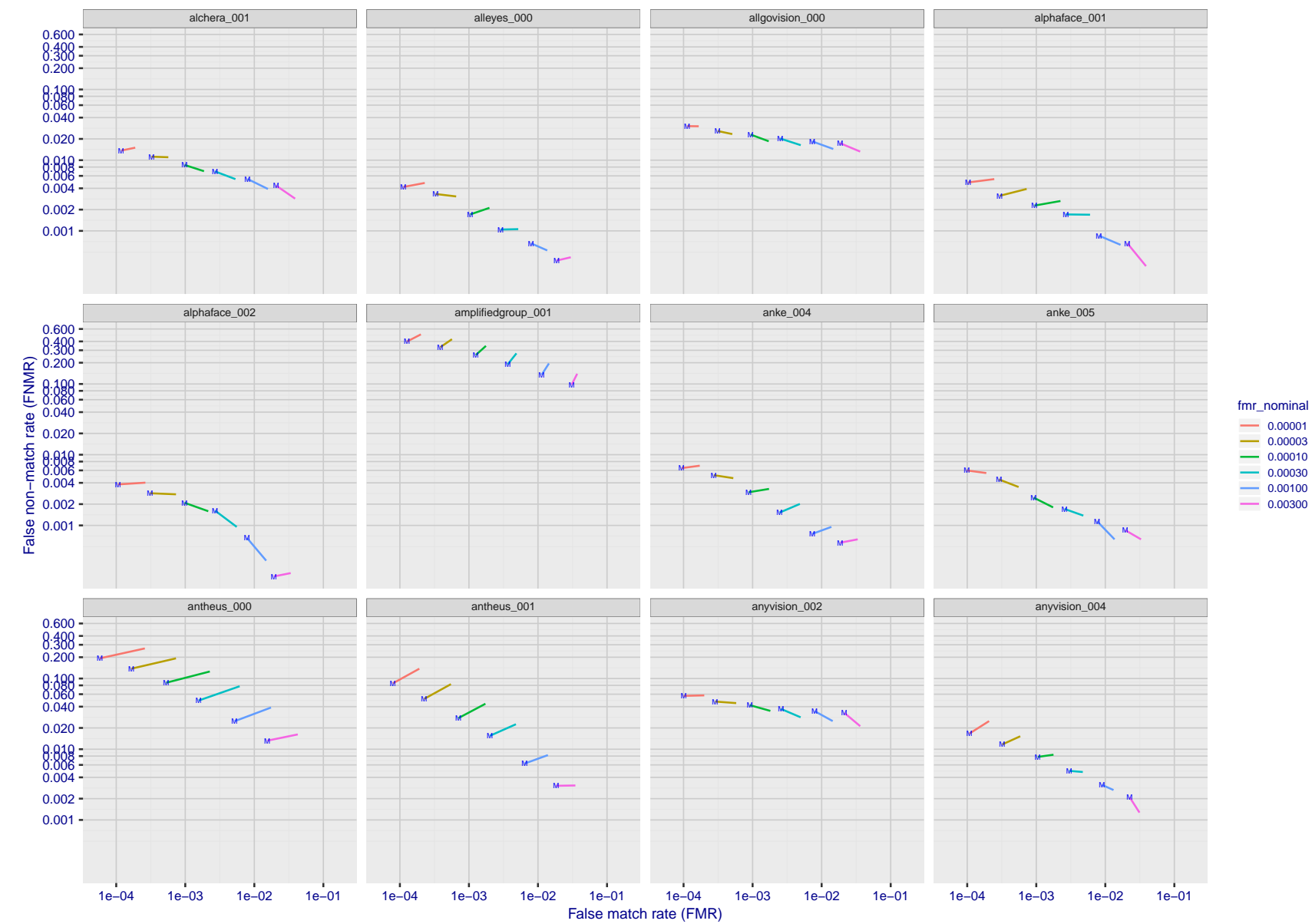


Figure 94: For the visa images, FNMR and FMR at six operating points along the DET characteristic. At each point a line is drawn between $(FMR, FNMR)_{MALE}$ and $(FMR, FNMR)_{FEMALE}$ showing how which sex has lower FMR and/or FNMR. The "M" label denotes male, the other end of the line corresponds to female. The six operating thresholds are selected to give the nominal false match rates given in the legend, and are computed over all impostor pairs regardless of age, sex, and place of birth. The plotted FMR values are broadly an order of magnitude larger than the nominal rates because FMR is computed over demographically-matched impostor pairs i.e individuals of the same sex, from the same geographic region (see section 3.6.1), and the same age group (see section 3.6.2).

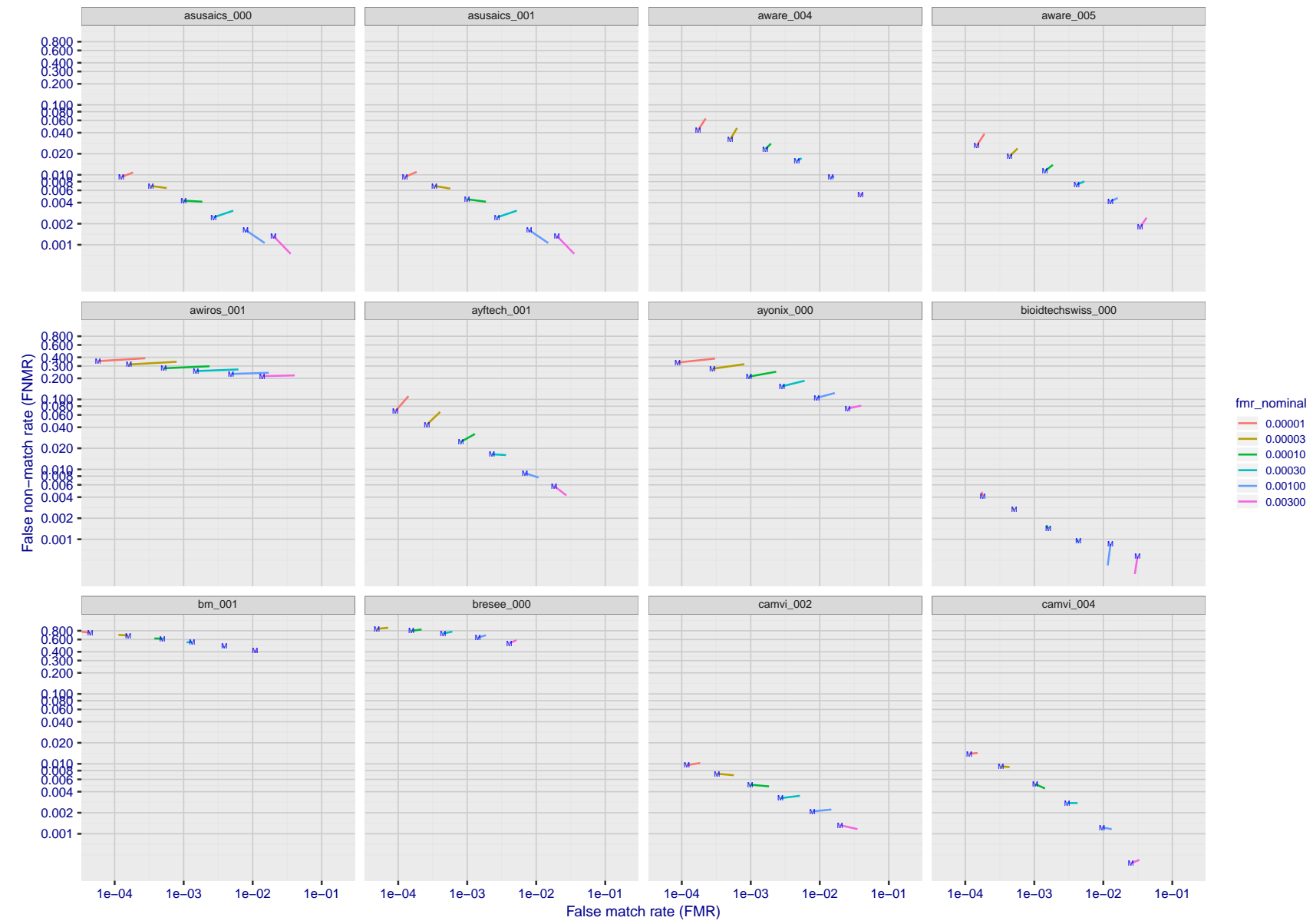


Figure 95: For the visa images, FNMR and FMR at six operating points along the DET characteristic. At each point a line is drawn between $(FMR, FNMR)_{MALE}$ and $(FMR, FNMR)_{FEMALE}$ showing how which sex has lower FMR and/or FNMR. The "M" label denotes male, the other end of the line corresponds to female. The six operating thresholds are selected to give the nominal false match rates given in the legend, and are computed over all impostor pairs regardless of age, sex, and place of birth. The plotted FMR values are broadly an order of magnitude larger than the nominal rates because FMR is computed over demographically-matched impostor pairs i.e individuals of the same sex, from the same geographic region (see section 3.6.1), and the same age group (see section 3.6.2).

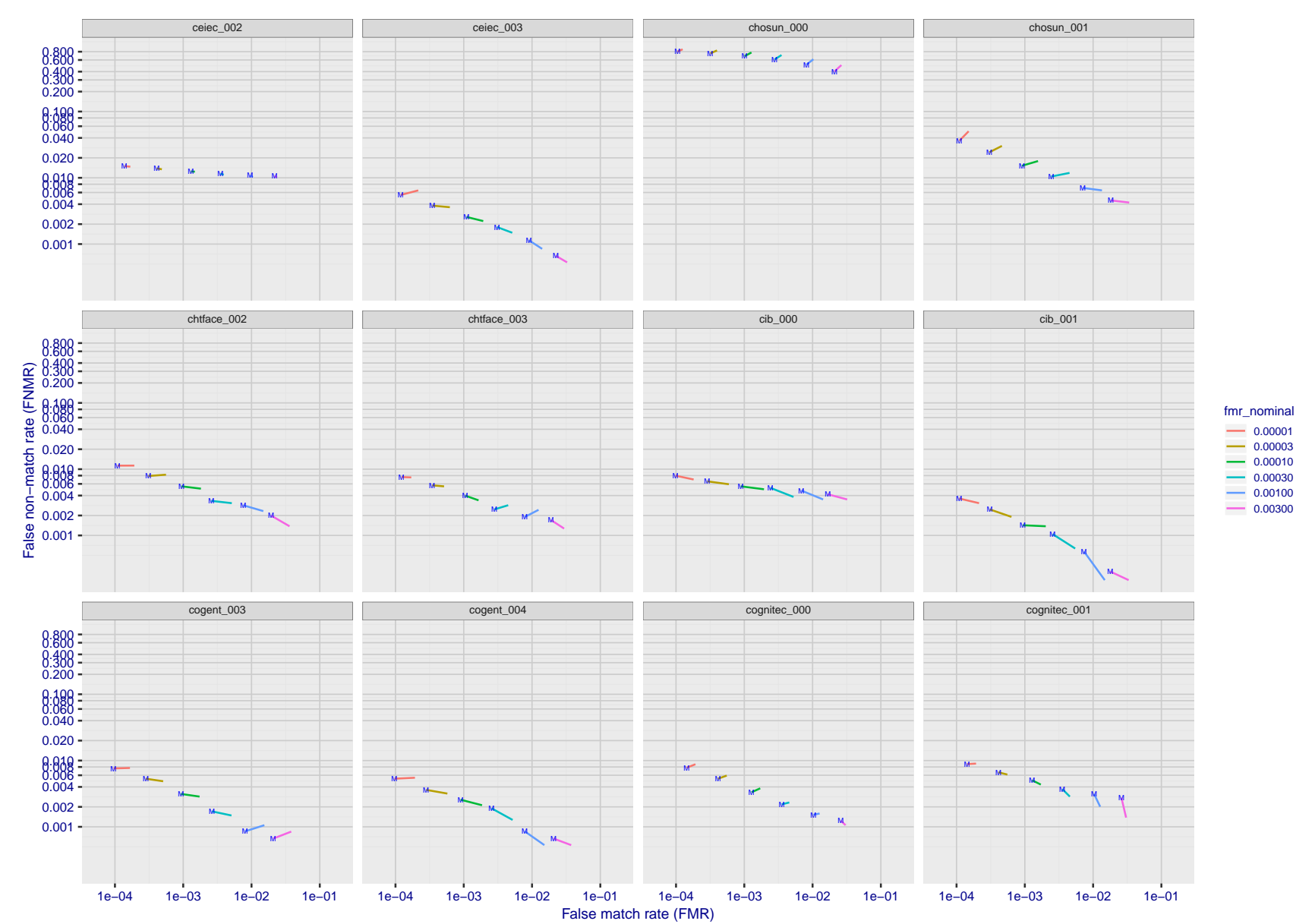


Figure 96: For the visa images, FNMR and FMR at six operating points along the DET characteristic. At each point a line is drawn between $(FMR, FNMR)_{MALE}$ and $(FMR, FNMR)_{FEMALE}$ showing how which sex has lower FMR and/or FNMR. The "M" label denotes male, the other end of the line corresponds to female. The six operating thresholds are selected to give the nominal false match rates given in the legend, and are computed over all impostor pairs regardless of age, sex, and place of birth. The plotted FMR values are broadly an order of magnitude larger than the nominal rates because FMR is computed over demographically-matched impostor pairs i.e individuals of the same sex, from the same geographic region (see section 3.6.1), and the same age group (see section 3.6.2).

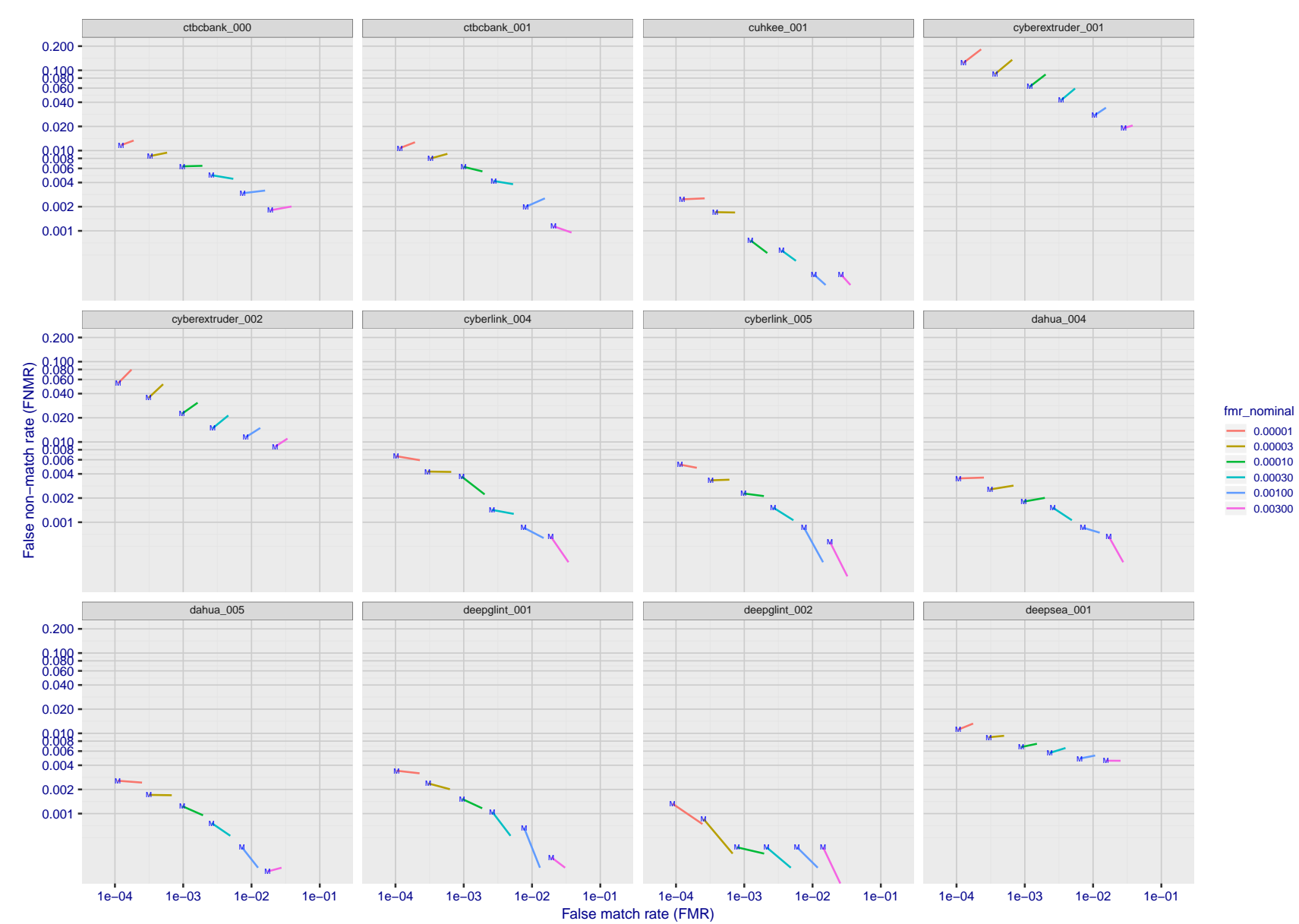


Figure 97: For the visa images, FNMR and FMR at six operating points along the DET characteristic. At each point a line is drawn between $(FMR, FNMR)_{MALE}$ and $(FMR, FNMR)_{FEMALE}$ showing how which sex has lower FMR and/or FNMR. The "M" label denotes male, the other end of the line corresponds to female. The six operating thresholds are selected to give the nominal false match rates given in the legend, and are computed over all impostor pairs regardless of age, sex, and place of birth. The plotted FMR values are broadly an order of magnitude larger than the nominal rates because FMR is computed over demographically-matched impostor pairs i.e individuals of the same sex, from the same geographic region (see section 3.6.1), and the same age group (see section 3.6.2).

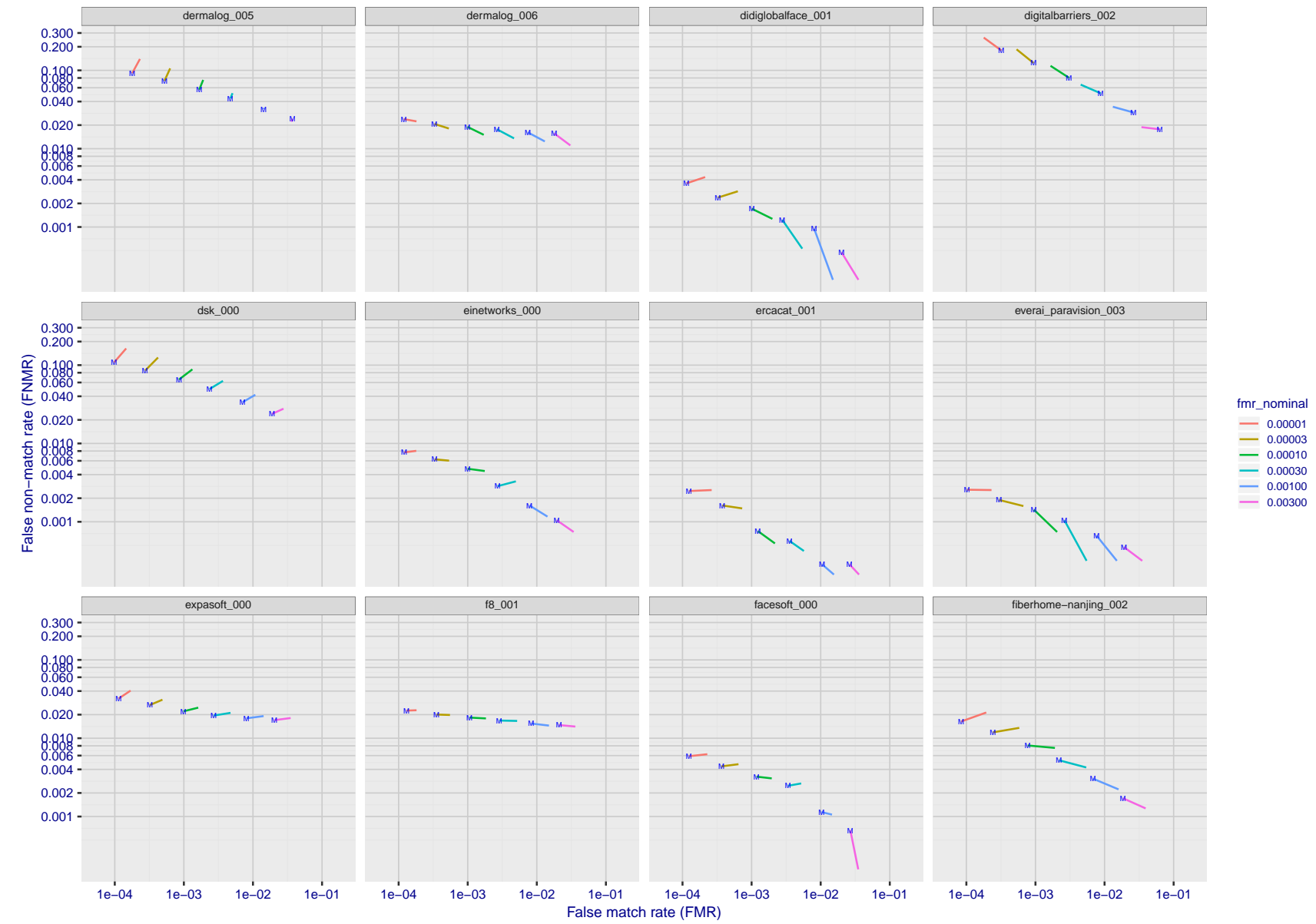


Figure 98: For the visa images, FNMR and FMR at six operating points along the DET characteristic. At each point a line is drawn between $(FMR, FNMR)_{MALE}$ and $(FMR, FNMR)_{FEMALE}$ showing how which sex has lower FMR and/or FNMR. The "M" label denotes male, the other end of the line corresponds to female. The six operating thresholds are selected to give the nominal false match rates given in the legend, and are computed over all impostor pairs regardless of age, sex, and place of birth. The plotted FMR values are broadly an order of magnitude larger than the nominal rates because FMR is computed over demographically-matched impostor pairs i.e individuals of the same sex, from the same geographic region (see section 3.6.1), and the same age group (see section 3.6.2).

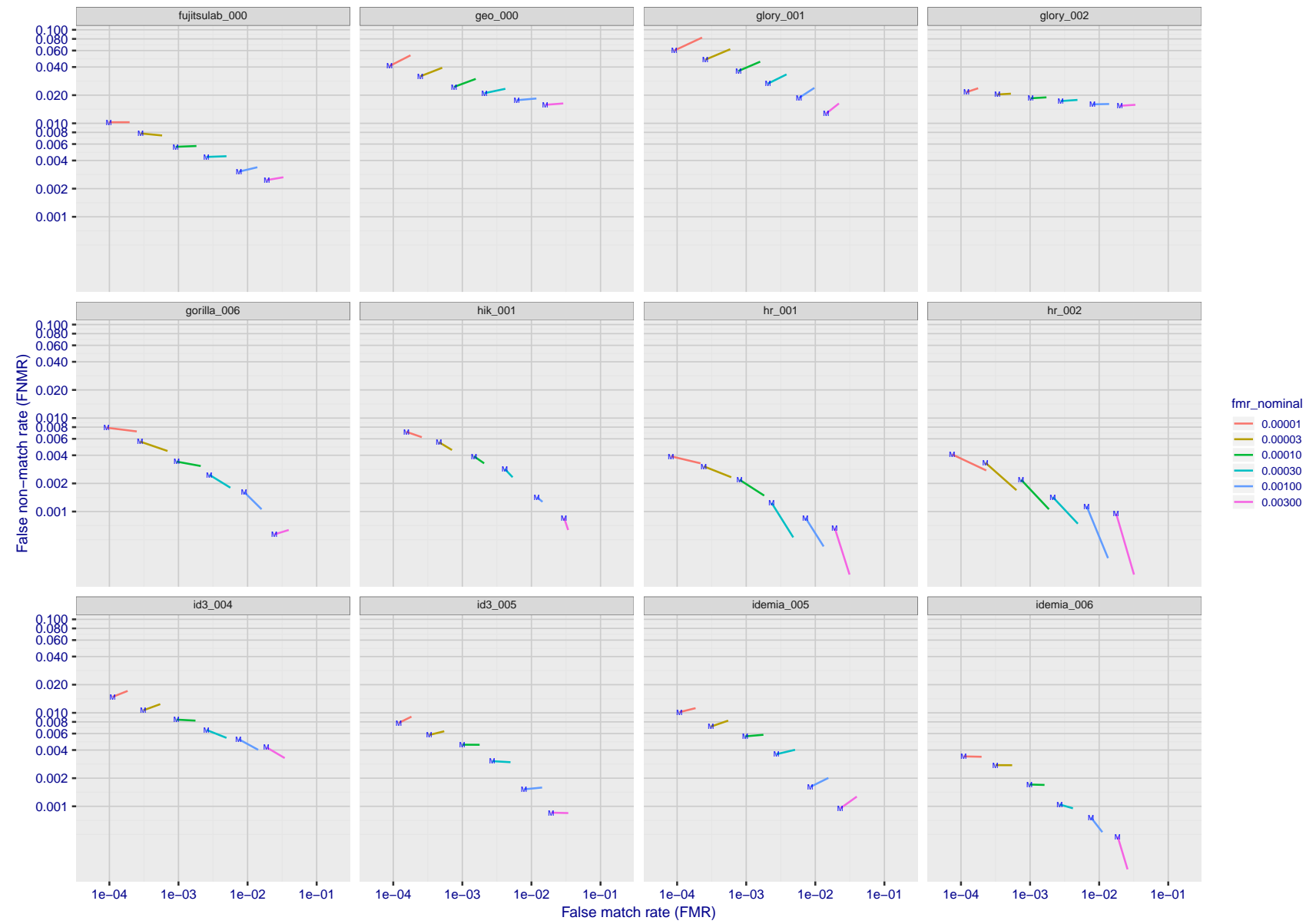


Figure 99: For the visa images, FNMR and FMR at six operating points along the DET characteristic. At each point a line is drawn between $(FMR, FNMR)_{MALE}$ and $(FMR, FNMR)_{FEMALE}$ showing how which sex has lower FMR and/or FNMR. The "M" label denotes male, the other end of the line corresponds to female. The six operating thresholds are selected to give the nominal false match rates given in the legend, and are computed over all impostor pairs regardless of age, sex, and place of birth. The plotted FMR values are broadly an order of magnitude larger than the nominal rates because FMR is computed over demographically-matched impostor pairs i.e individuals of the same sex, from the same geographic region (see section 3.6.1), and the same age group (see section 3.6.2).

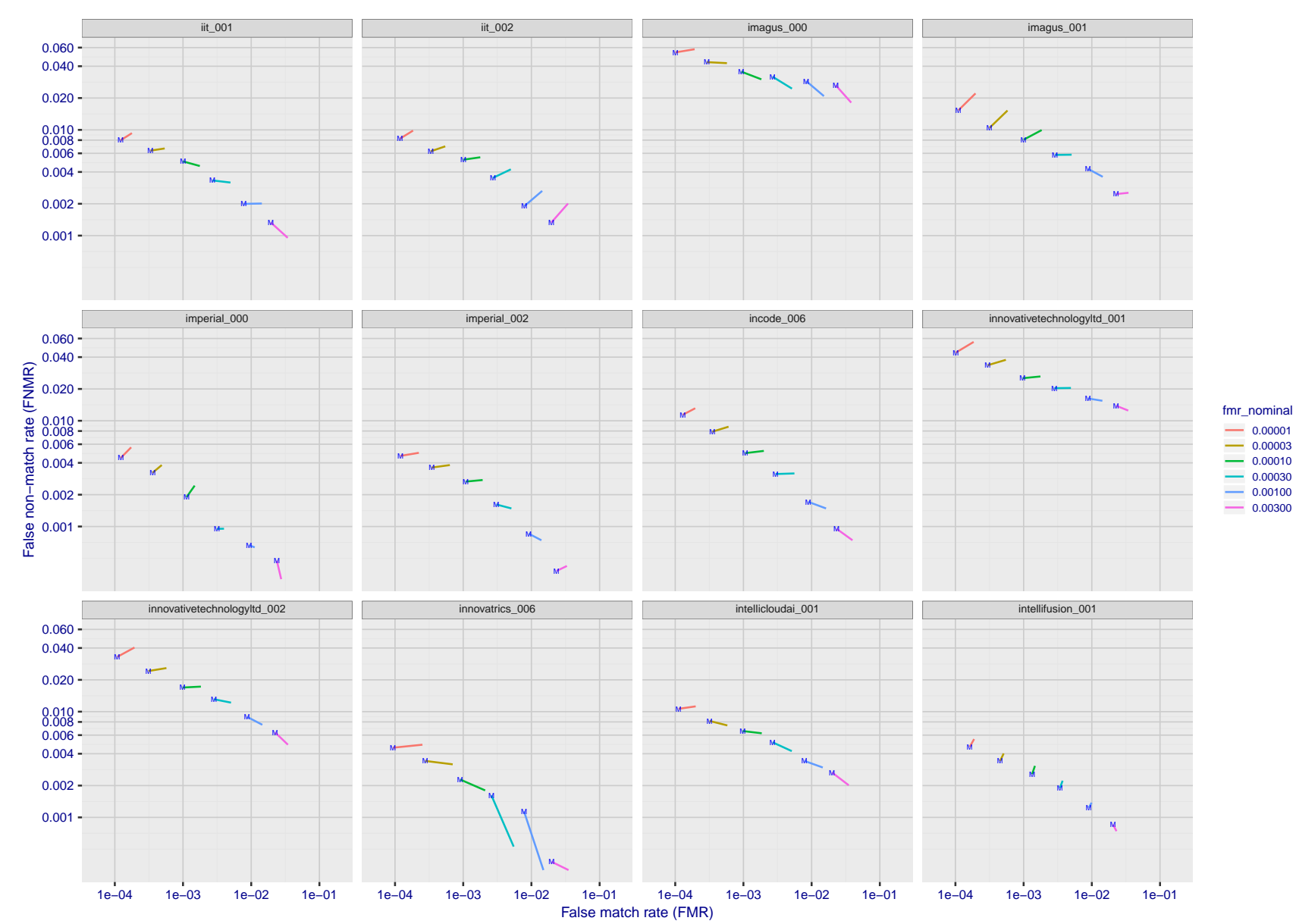


Figure 100: For the visa images, FNMR and FMR at six operating points along the DET characteristic. At each point a line is drawn between $(FMR, FNMR)_{MALE}$ and $(FMR, FNMR)_{FEMALE}$ showing how which sex has lower FMR and/or FNMR. The "M" label denotes male, the other end of the line corresponds to female. The six operating thresholds are selected to give the nominal false match rates given in the legend, and are computed over all impostor pairs regardless of age, sex, and place of birth. The plotted FMR values are broadly an order of magnitude larger than the nominal rates because FMR is computed over demographically-matched impostor pairs i.e individuals of the same sex, from the same geographic region (see section 3.6.1), and the same age group (see section 3.6.2).

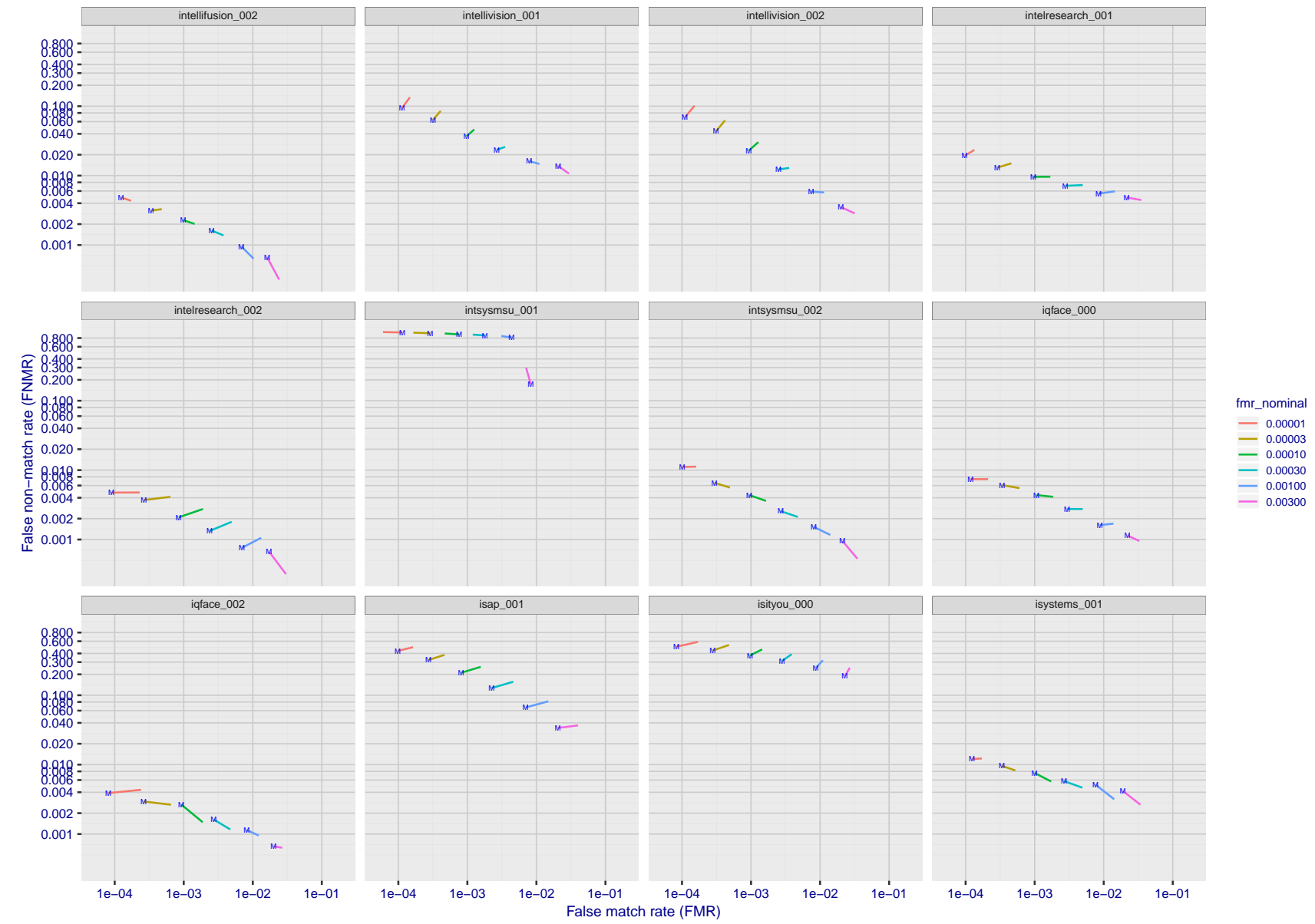


Figure 101: For the visa images, FNMR and FMR at six operating points along the DET characteristic. At each point a line is drawn between $(FMR, FNMR)_{MALE}$ and $(FMR, FNMR)_{FEMALE}$ showing how which sex has lower FMR and/or FNMR. The "M" label denotes male, the other end of the line corresponds to female. The six operating thresholds are selected to give the nominal false match rates given in the legend, and are computed over all impostor pairs regardless of age, sex, and place of birth. The plotted FMR values are broadly an order of magnitude larger than the nominal rates because FMR is computed over demographically-matched impostor pairs i.e individuals of the same sex, from the same geographic region (see section 3.6.1), and the same age group (see section 3.6.2).

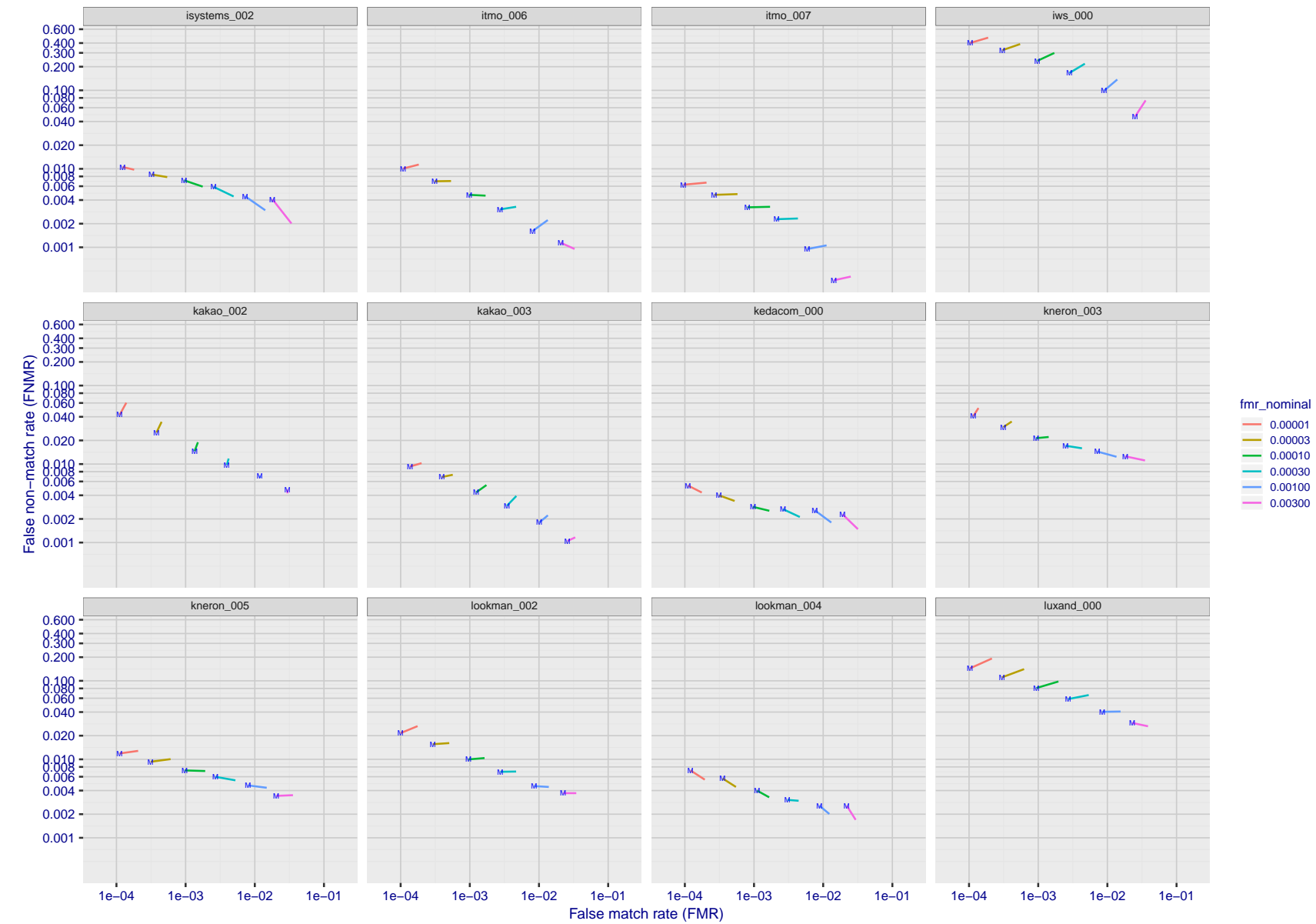


Figure 102: For the visa images, FNMR and FMR at six operating points along the DET characteristic. At each point a line is drawn between $(FMR, FNMR)_{MALE}$ and $(FMR, FNMR)_{FEMALE}$ showing how which sex has lower FMR and/or FNMR. The "M" label denotes male, the other end of the line corresponds to female. The six operating thresholds are selected to give the nominal false match rates given in the legend, and are computed over all impostor pairs regardless of age, sex, and place of birth. The plotted FMR values are broadly an order of magnitude larger than the nominal rates because FMR is computed over demographically-matched impostor pairs i.e individuals of the same sex, from the same geographic region (see section 3.6.1), and the same age group (see section 3.6.2).

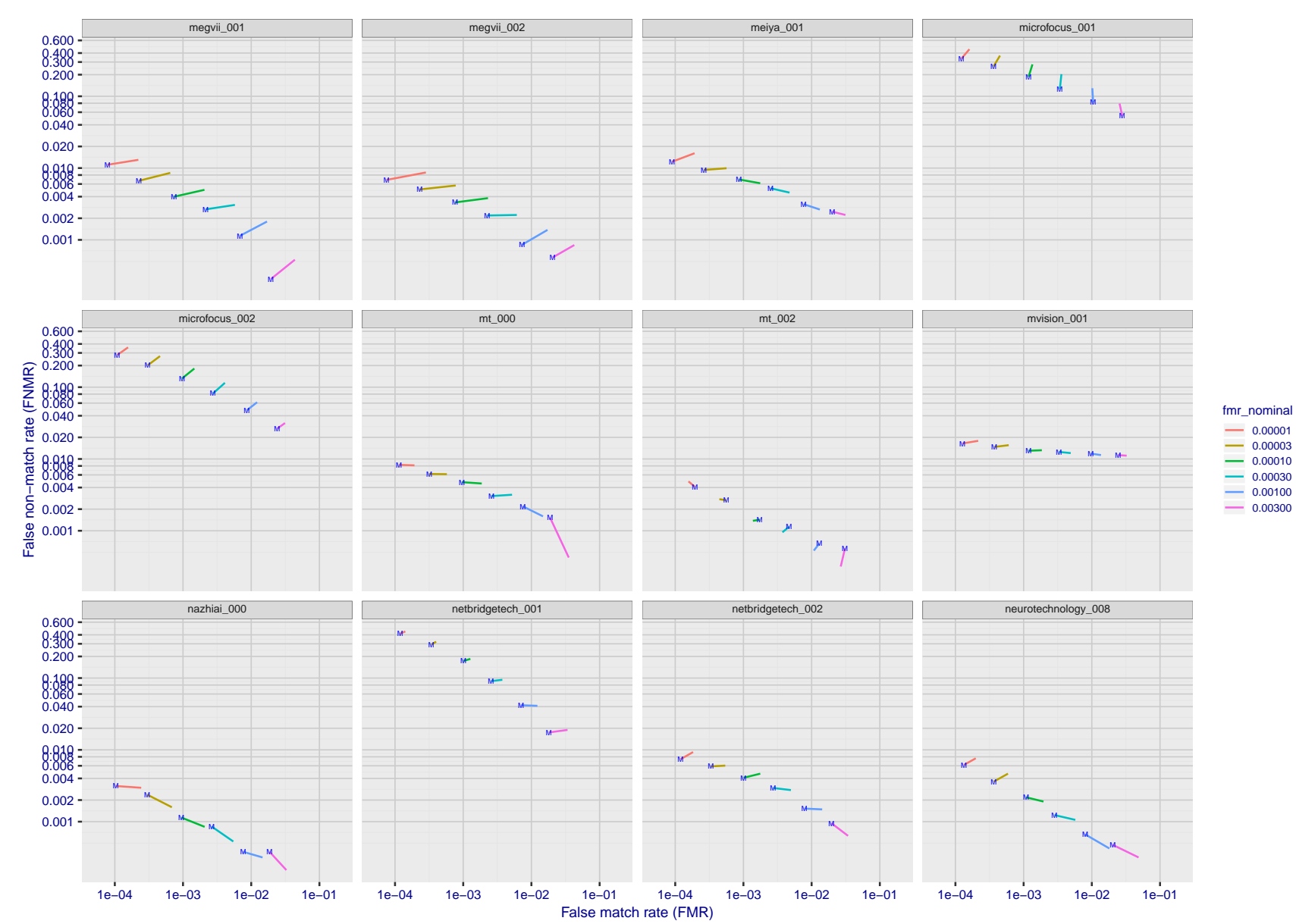


Figure 103: For the visa images, FNMR and FMR at six operating points along the DET characteristic. At each point a line is drawn between $(FMR, FNMR)_{MALE}$ and $(FMR, FNMR)_{FEMALE}$ showing how which sex has lower FMR and/or FNMR. The "M" label denotes male, the other end of the line corresponds to female. The six operating thresholds are selected to give the nominal false match rates given in the legend, and are computed over all impostor pairs regardless of age, sex, and place of birth. The plotted FMR values are broadly an order of magnitude larger than the nominal rates because FMR is computed over demographically-matched impostor pairs i.e individuals of the same sex, from the same geographic region (see section 3.6.1), and the same age group (see section 3.6.2).

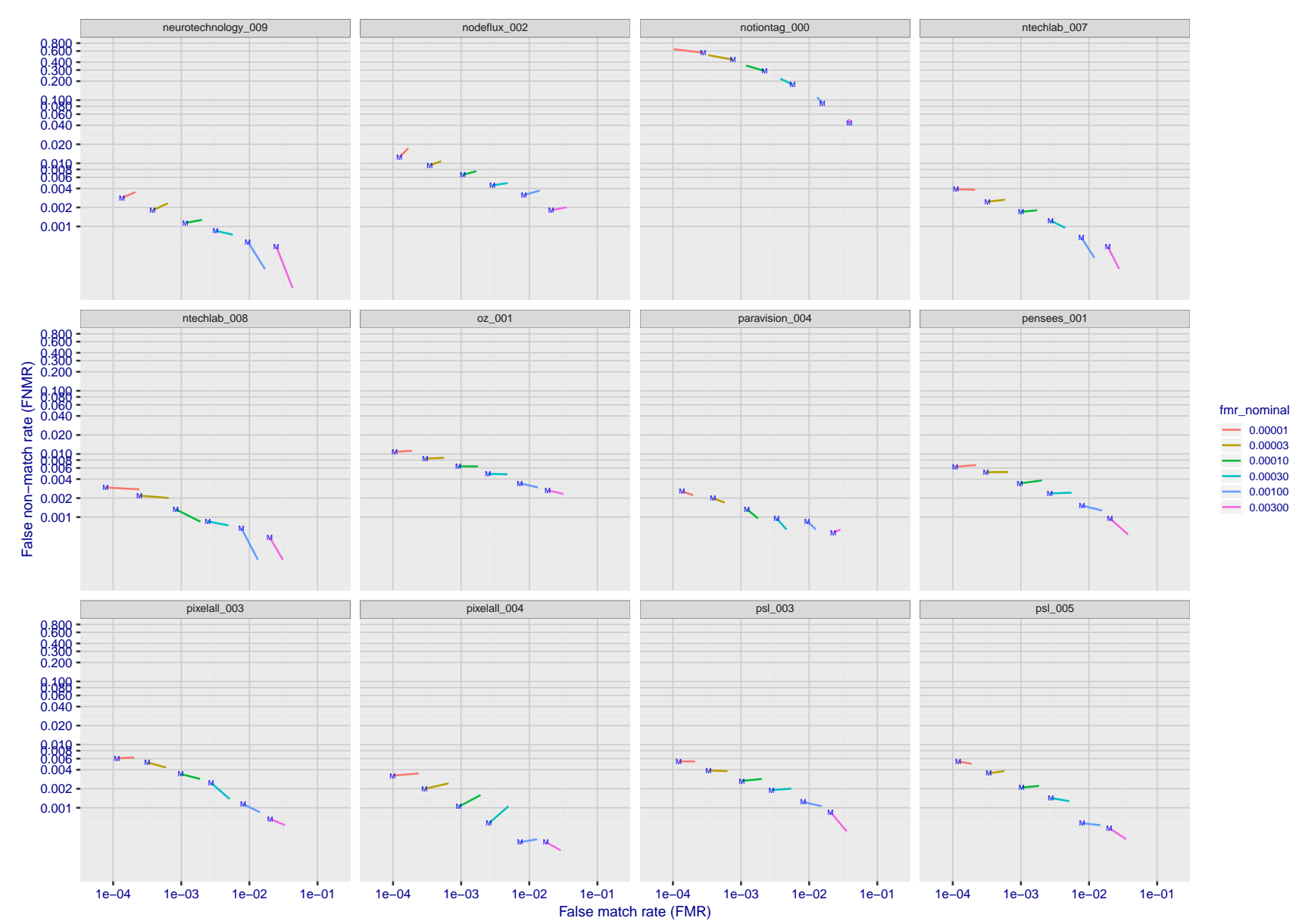


Figure 104: For the visa images, FNMR and FMR at six operating points along the DET characteristic. At each point a line is drawn between $(FMR, FNMR)_{MALE}$ and $(FMR, FNMR)_{FEMALE}$ showing how which sex has lower FMR and/or FNMR. The "M" label denotes male, the other end of the line corresponds to female. The six operating thresholds are selected to give the nominal false match rates given in the legend, and are computed over all impostor pairs regardless of age, sex, and place of birth. The plotted FMR values are broadly an order of magnitude larger than the nominal rates because FMR is computed over demographically-matched impostor pairs i.e individuals of the same sex, from the same geographic region (see section 3.6.1), and the same age group (see section 3.6.2).

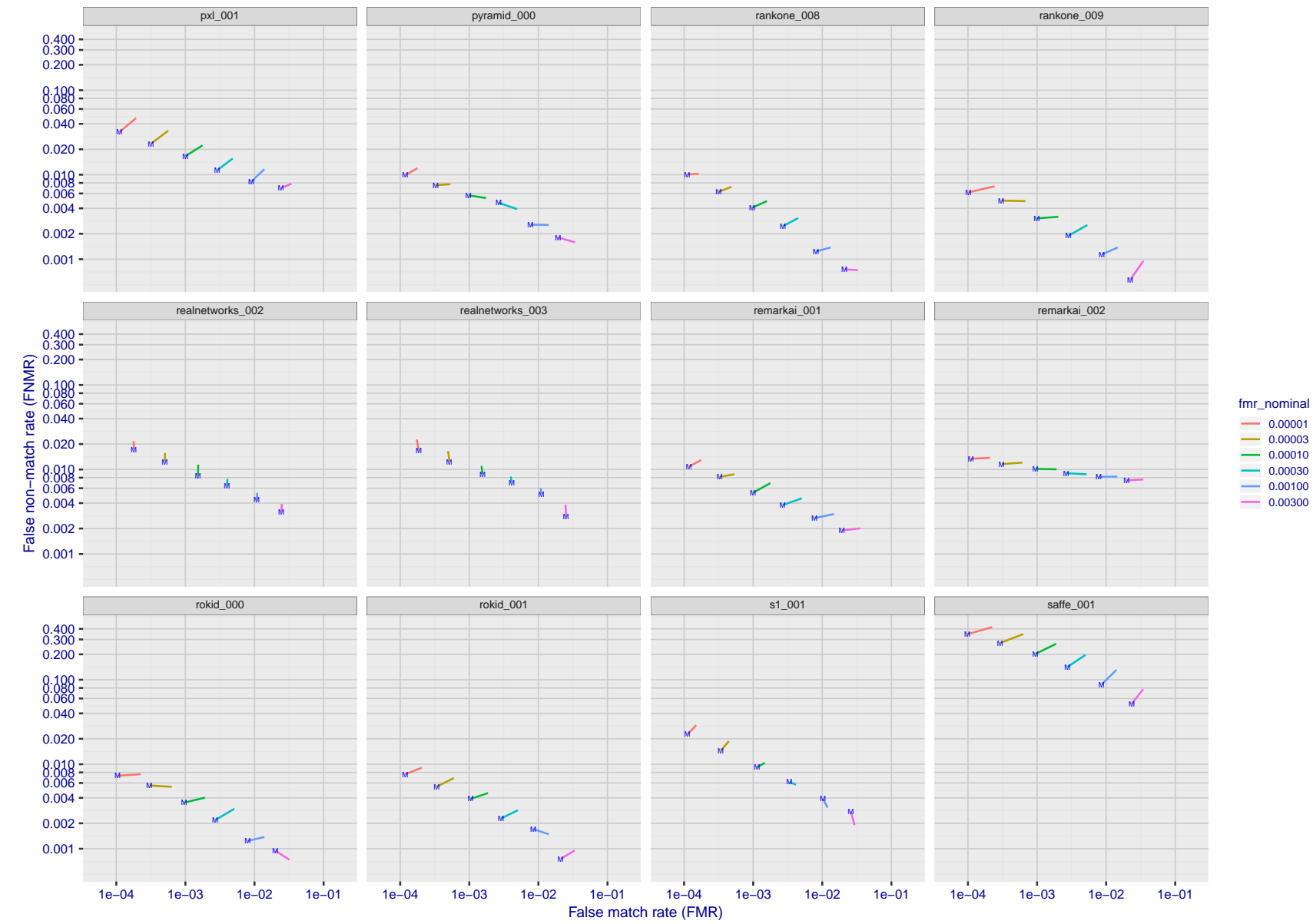


Figure 105: For the visa images, FNMR and FMR at six operating points along the DET characteristic. At each point a line is drawn between $(FMR, FNMR)_{MALE}$ and $(FMR, FNMR)_{FEMALE}$ showing how which sex has lower FMR and/or FNMR. The "M" label denotes male, the other end of the line corresponds to female. The six operating thresholds are selected to give the nominal false match rates given in the legend, and are computed over all impostor pairs regardless of age, sex, and place of birth. The plotted FMR values are broadly an order of magnitude larger than the nominal rates because FMR is computed over demographically-matched impostor pairs i.e individuals of the same sex, from the same geographic region (see section 3.6.1), and the same age group (see section 3.6.2).

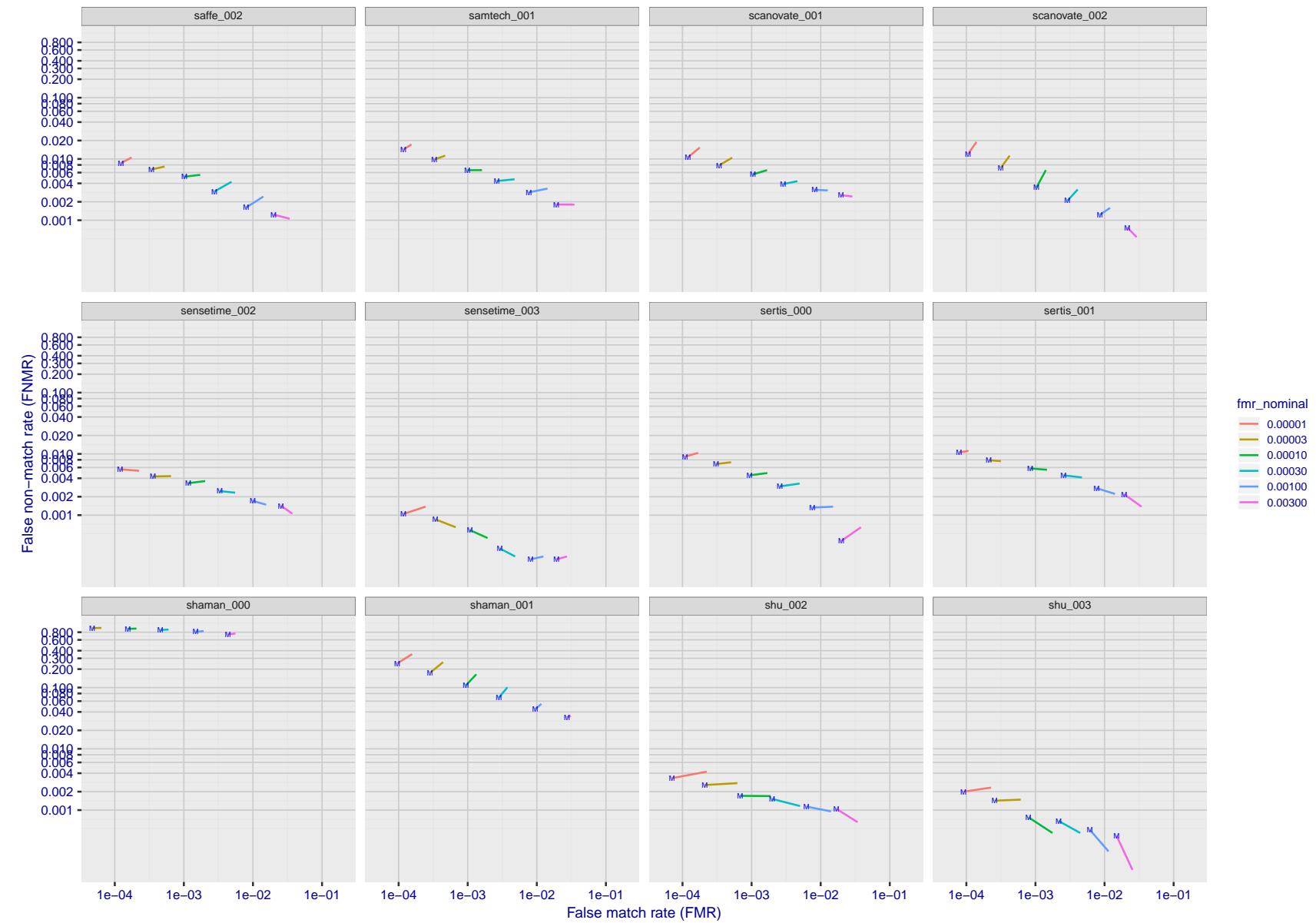


Figure 106: For the visa images, FNMR and FMR at six operating points along the DET characteristic. At each point a line is drawn between $(FMR, FNMR)_{MALE}$ and $(FMR, FNMR)_{FEMALE}$ showing how which sex has lower FMR and/or FNMR. The "M" label denotes male, the other end of the line corresponds to female. The six operating thresholds are selected to give the nominal false match rates given in the legend, and are computed over all impostor pairs regardless of age, sex, and place of birth. The plotted FMR values are broadly an order of magnitude larger than the nominal rates because FMR is computed over demographically-matched impostor pairs i.e individuals of the same sex, from the same geographic region (see section 3.6.1), and the same age group (see section 3.6.2).

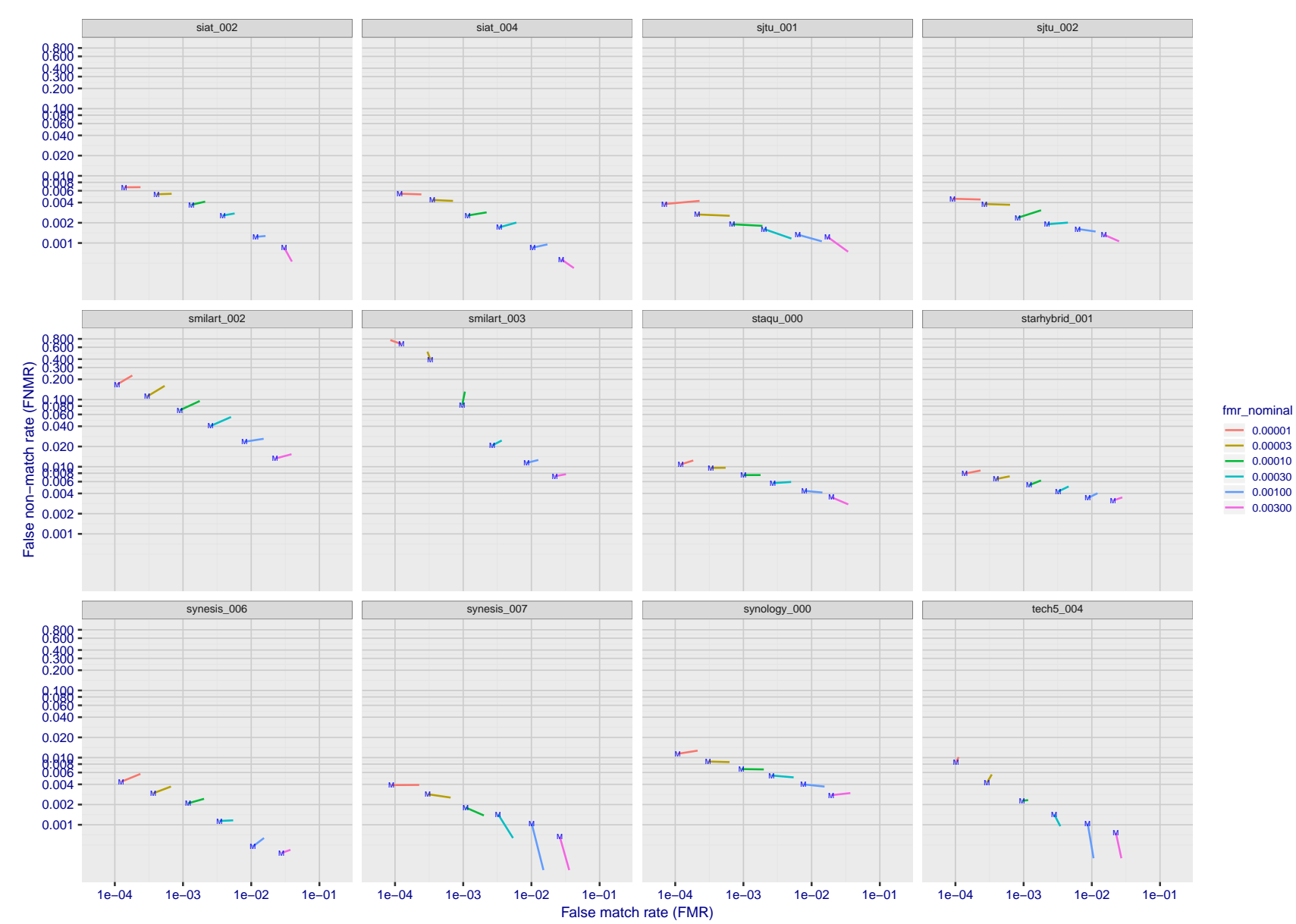


Figure 107: For the visa images, FNMR and FMR at six operating points along the DET characteristic. At each point a line is drawn between $(FMR, FNMR)_{MALE}$ and $(FMR, FNMR)_{FEMALE}$ showing how which sex has lower FMR and/or FNMR. The "M" label denotes male, the other end of the line corresponds to female. The six operating thresholds are selected to give the nominal false match rates given in the legend, and are computed over all impostor pairs regardless of age, sex, and place of birth. The plotted FMR values are broadly an order of magnitude larger than the nominal rates because FMR is computed over demographically-matched impostor pairs i.e individuals of the same sex, from the same geographic region (see section 3.6.1), and the same age group (see section 3.6.2).

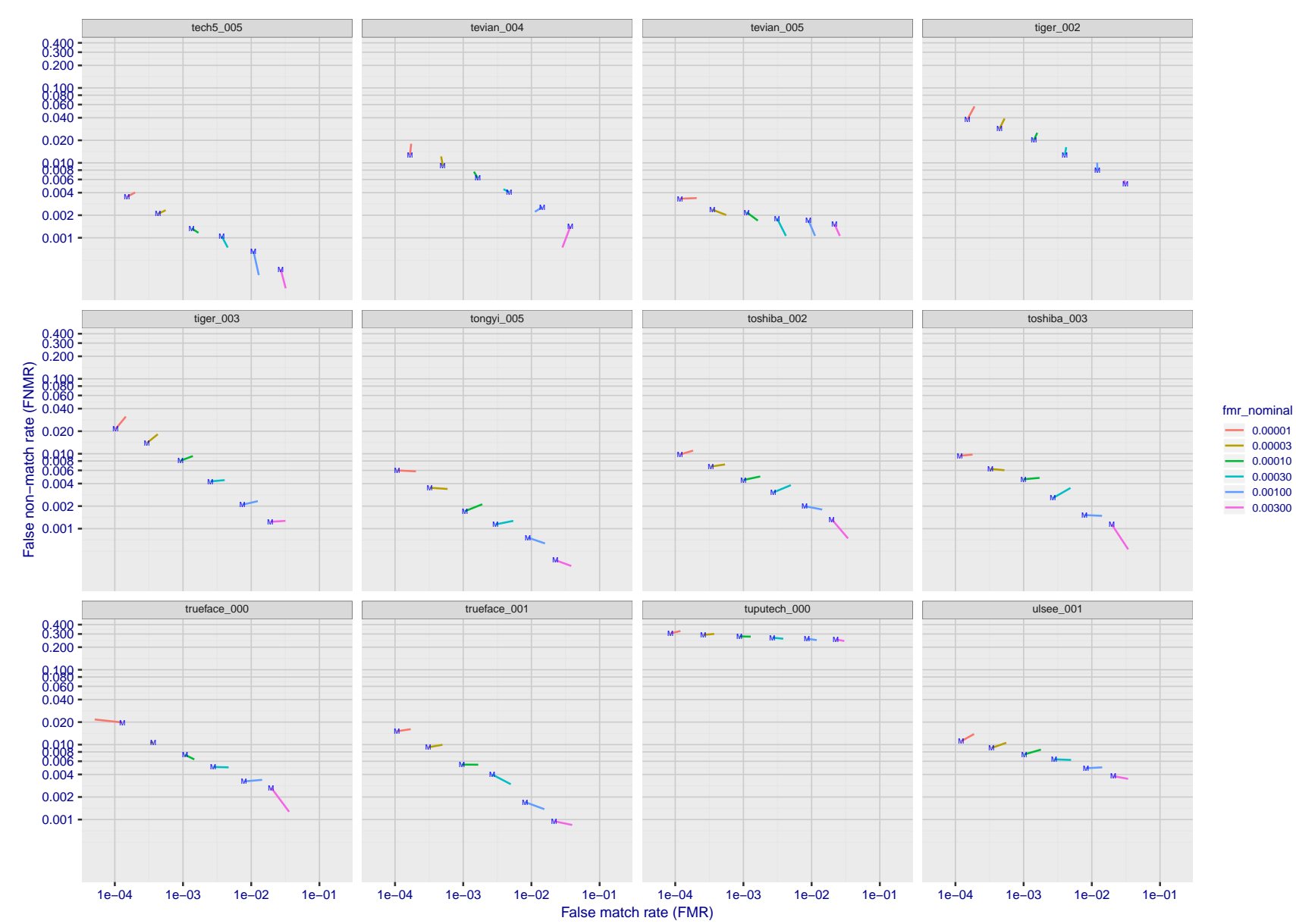


Figure 108: For the visa images, FNMR and FMR at six operating points along the DET characteristic. At each point a line is drawn between $(FMR, FNMR)_{MALE}$ and $(FMR, FNMR)_{FEMALE}$ showing how which sex has lower FMR and/or FNMR. The "M" label denotes male, the other end of the line corresponds to female. The six operating thresholds are selected to give the nominal false match rates given in the legend, and are computed over all impostor pairs regardless of age, sex, and place of birth. The plotted FMR values are broadly an order of magnitude larger than the nominal rates because FMR is computed over demographically-matched impostor pairs i.e individuals of the same sex, from the same geographic region (see section 3.6.1), and the same age group (see section 3.6.2).

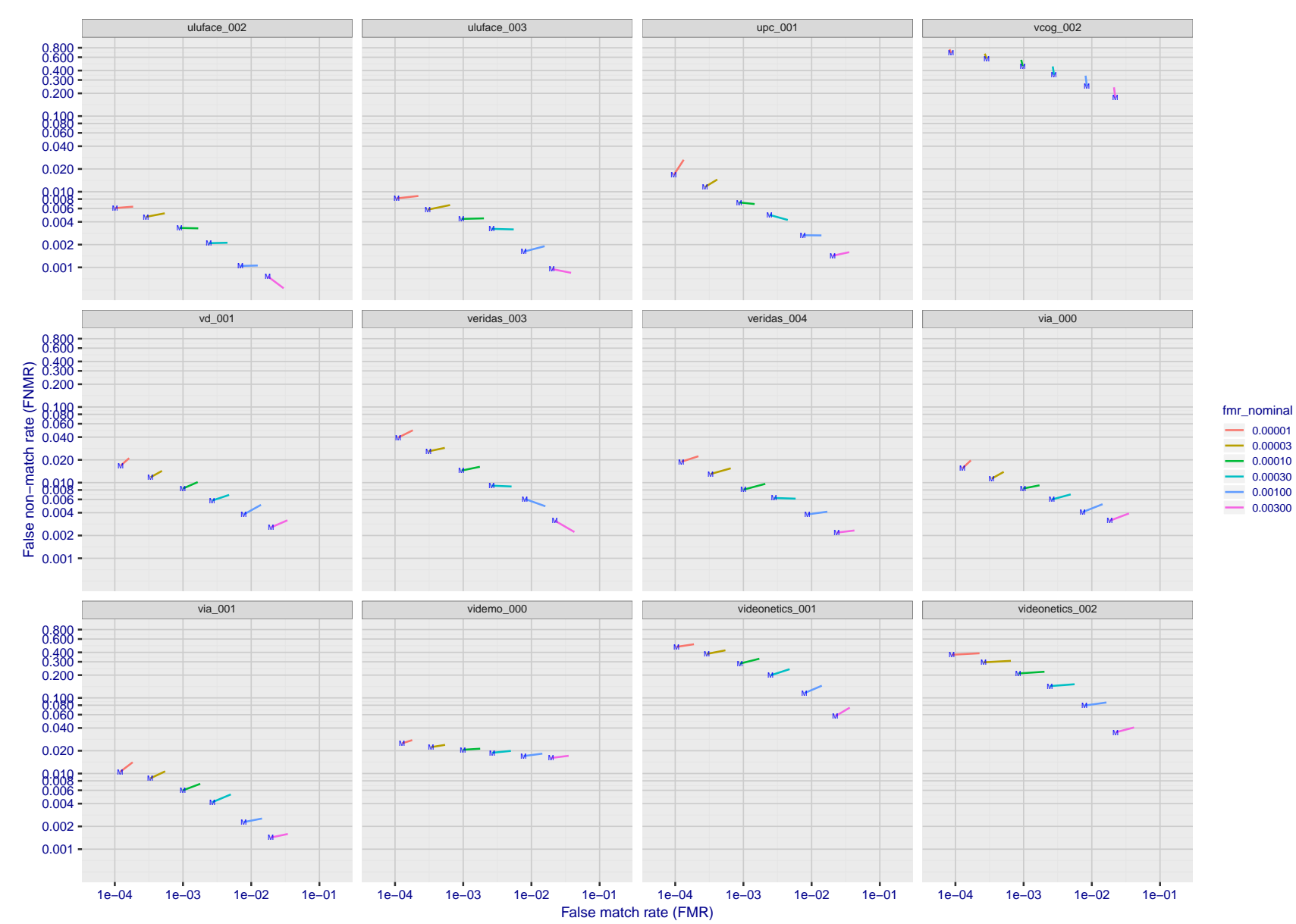


Figure 109: For the visa images, FNMR and FMR at six operating points along the DET characteristic. At each point a line is drawn between $(FMR, FNMR)_{MALE}$ and $(FMR, FNMR)_{FEMALE}$ showing how which sex has lower FMR and/or FNMR. The "M" label denotes male, the other end of the line corresponds to female. The six operating thresholds are selected to give the nominal false match rates given in the legend, and are computed over all impostor pairs regardless of age, sex, and place of birth. The plotted FMR values are broadly an order of magnitude larger than the nominal rates because FMR is computed over demographically-matched impostor pairs i.e individuals of the same sex, from the same geographic region (see section 3.6.1), and the same age group (see section 3.6.2).

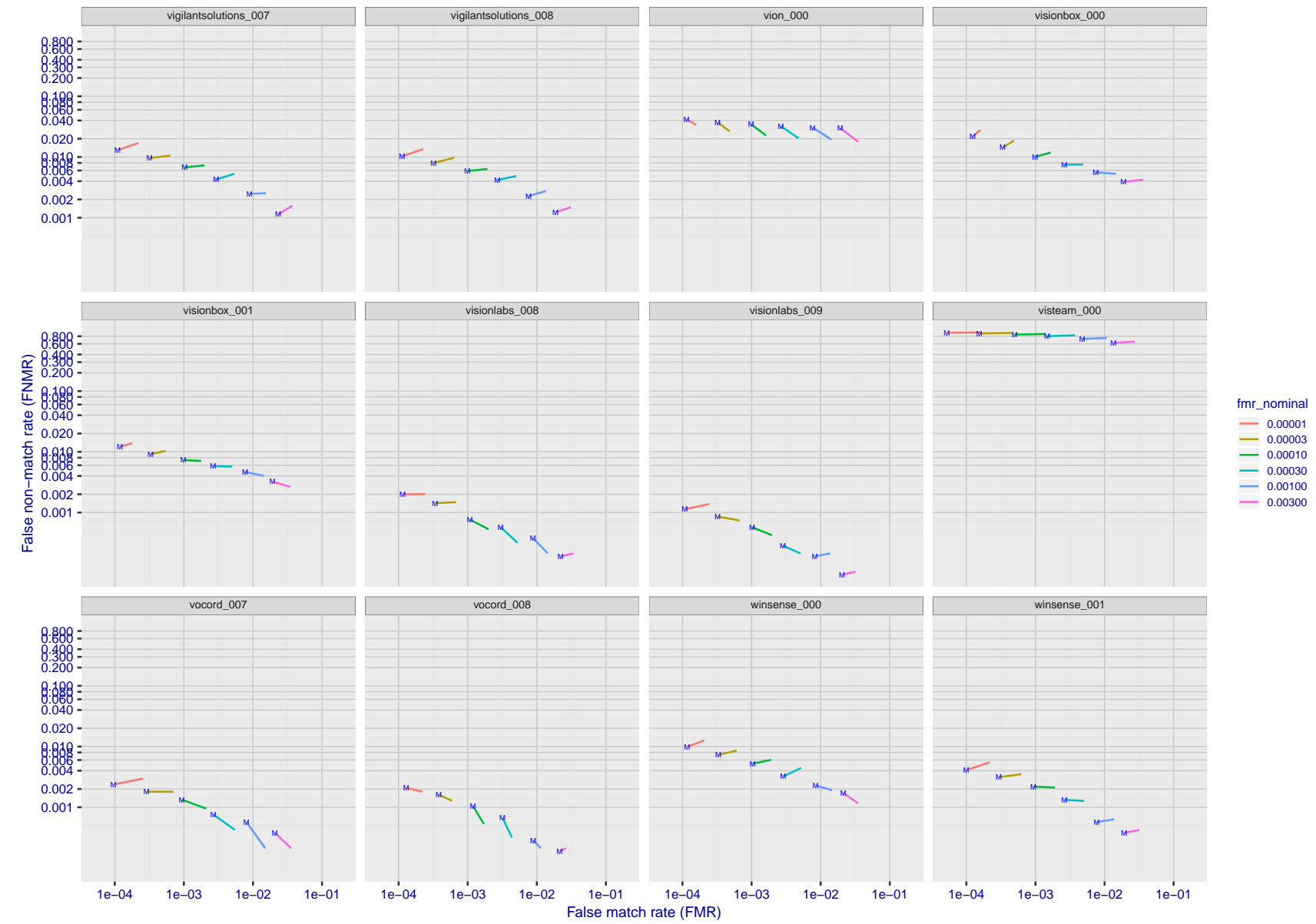


Figure 110: For the visa images, FNMR and FMR at six operating points along the DET characteristic. At each point a line is drawn between $(FMR, FNMR)_{MALE}$ and $(FMR, FNMR)_{FEMALE}$ showing how which sex has lower FMR and/or FNMR. The "M" label denotes male, the other end of the line corresponds to female. The six operating thresholds are selected to give the nominal false match rates given in the legend, and are computed over all impostor pairs regardless of age, sex, and place of birth. The plotted FMR values are broadly an order of magnitude larger than the nominal rates because FMR is computed over demographically-matched impostor pairs i.e individuals of the same sex, from the same geographic region (see section 3.6.1), and the same age group (see section 3.6.2).

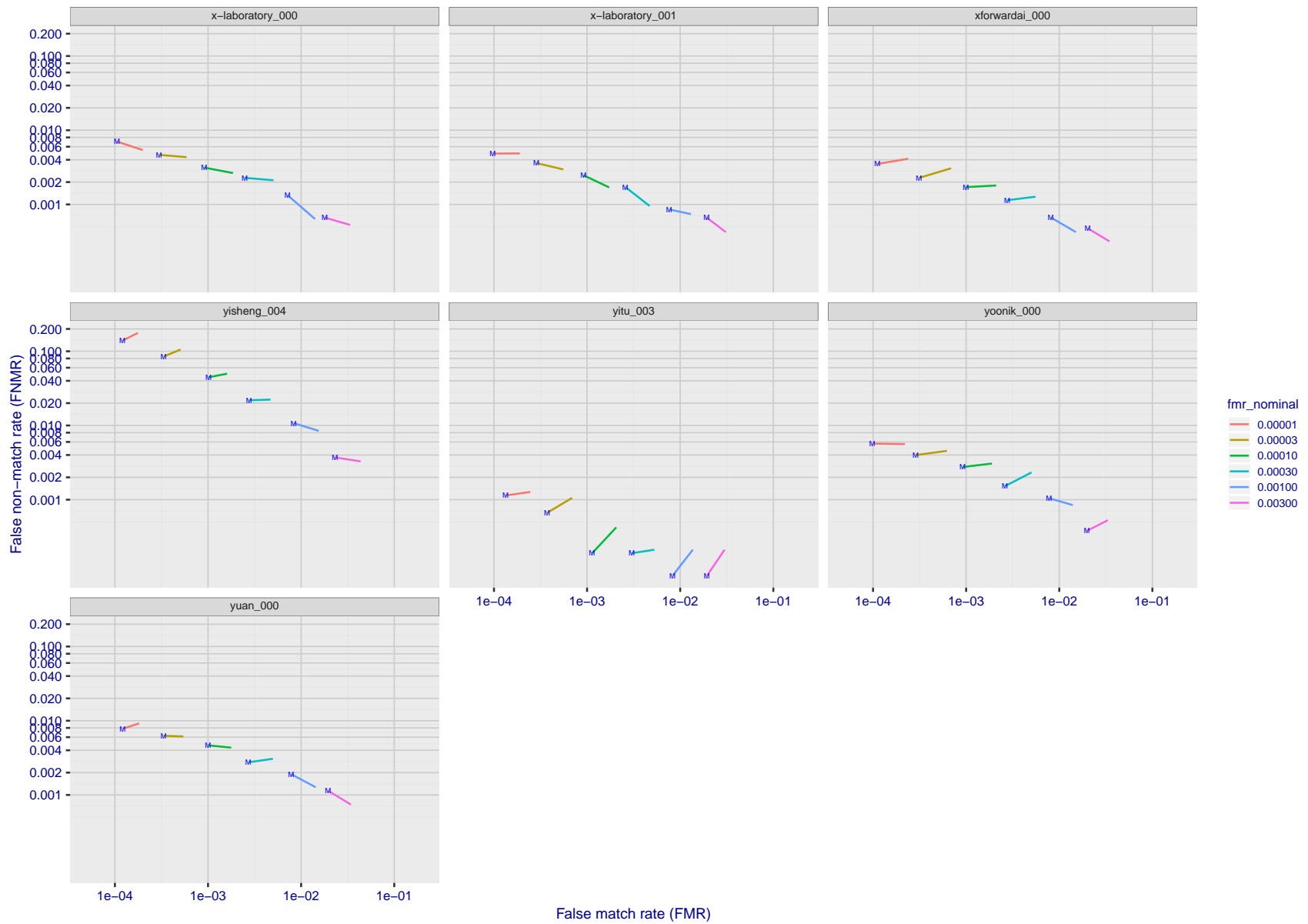


Figure 111: For the visa images, FNMR and FMR at six operating points along the DET characteristic. At each point a line is drawn between $(FMR, FNMR)_{MALE}$ and $(FMR, FNMR)_{FEMALE}$ showing how which sex has lower FMR and/or FNMR. The "M" label denotes male, the other end of the line corresponds to female. The six operating thresholds are selected to give the nominal false match rates given in the legend, and are computed over all impostor pairs regardless of age, sex, and place of birth. The plotted FMR values are broadly an order of magnitude larger than the nominal rates because FMR is computed over demographically-matched impostor pairs i.e individuals of the same sex, from the same geographic region (see section 3.6.1), and the same age group (see section 3.6.2).

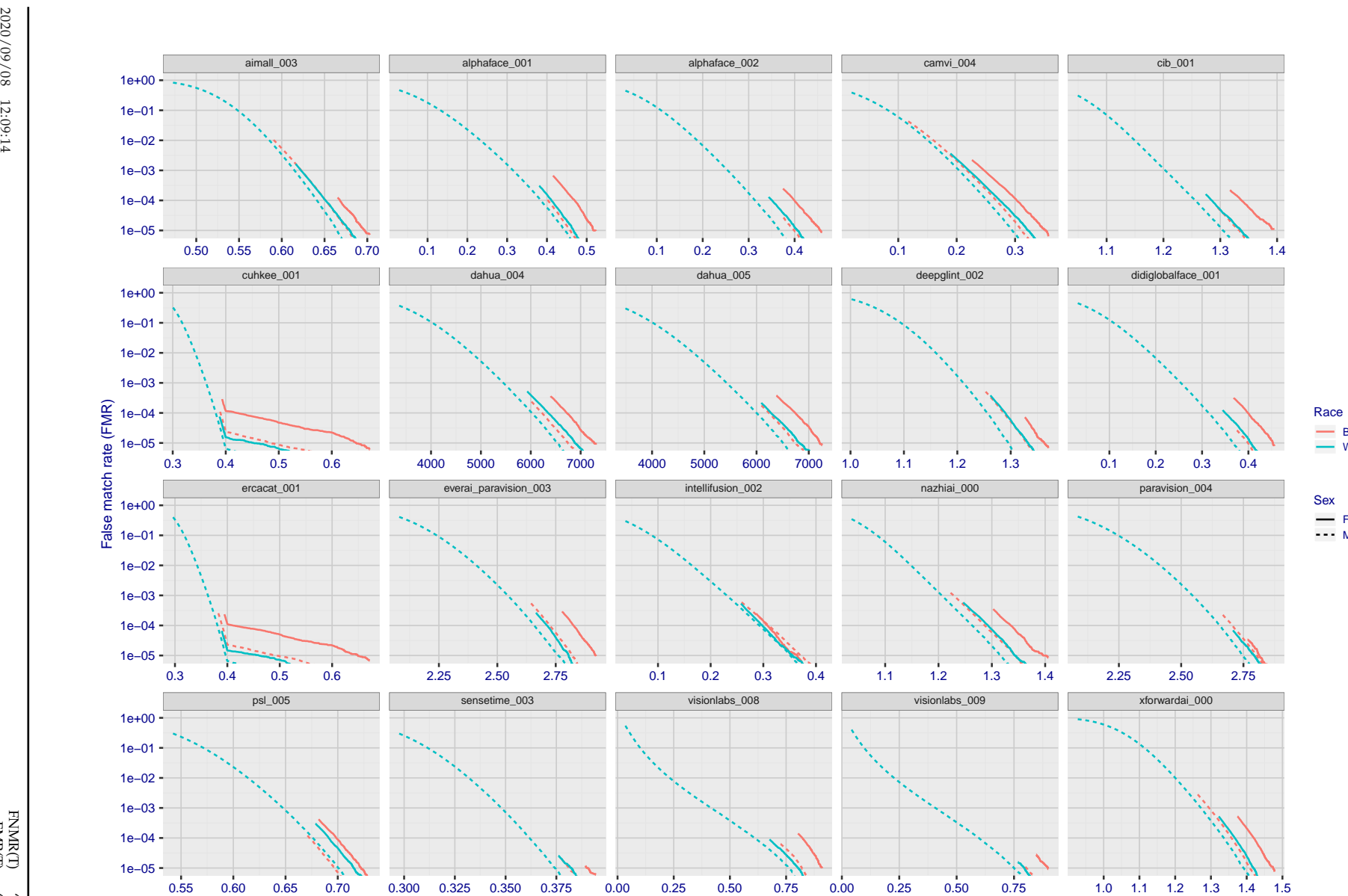


Figure 112: For the mugshot images, the false match calibration curves show false match rate vs. threshold. Separate curves appear for white females, black females, black males and white males.

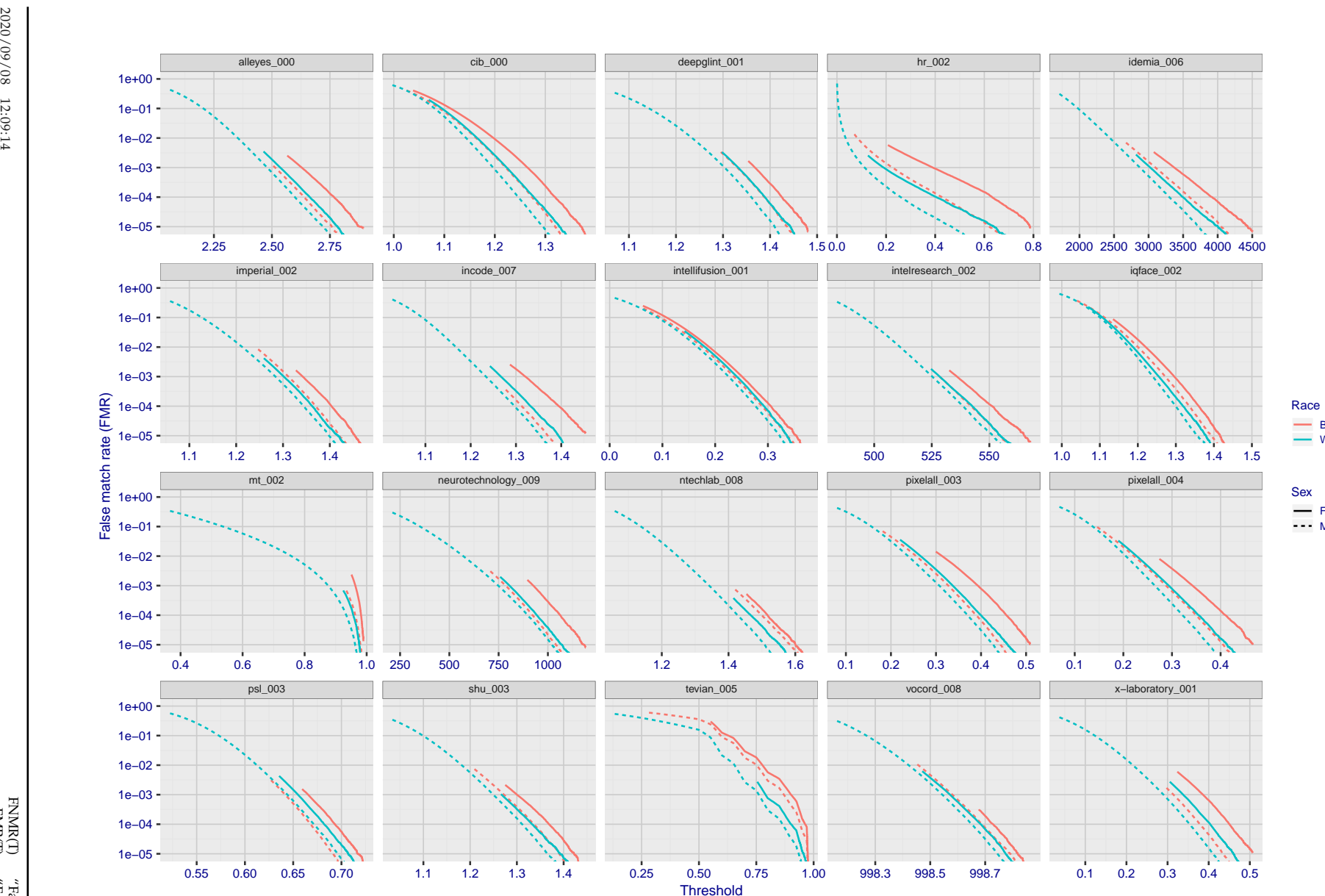


Figure 113: For the mugshot images, the false match calibration curves show false match rate vs. threshold. Separate curves appear for white females, black females, black males and white males.

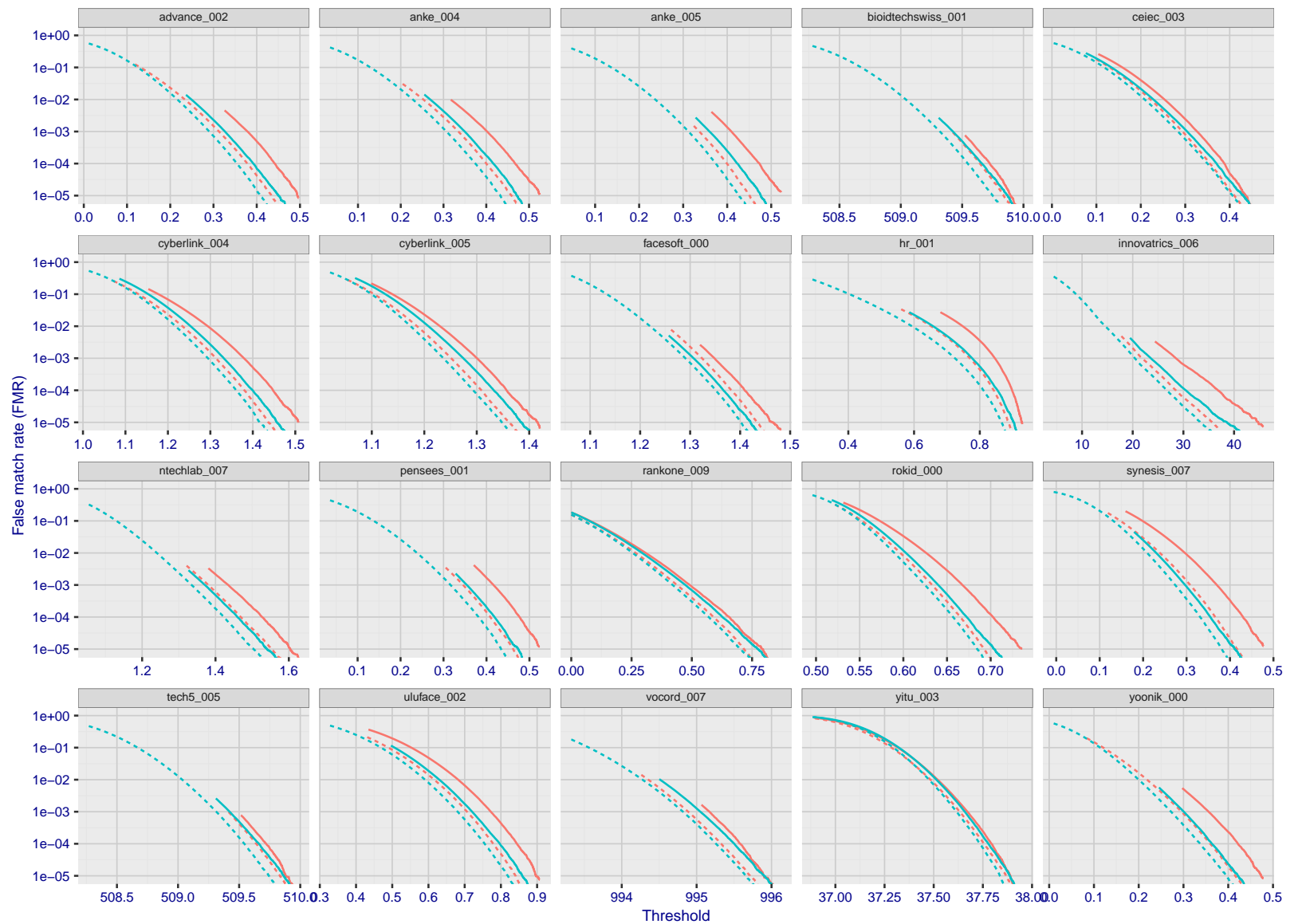
2020/09/08
12:09:14

Figure 114: For the mugshot images, the false match calibration curves show false match rate vs. threshold. Separate curves appear for white females, black females, black males and white males.

FNMR(T)
"False non-match rate"
"False match rate"

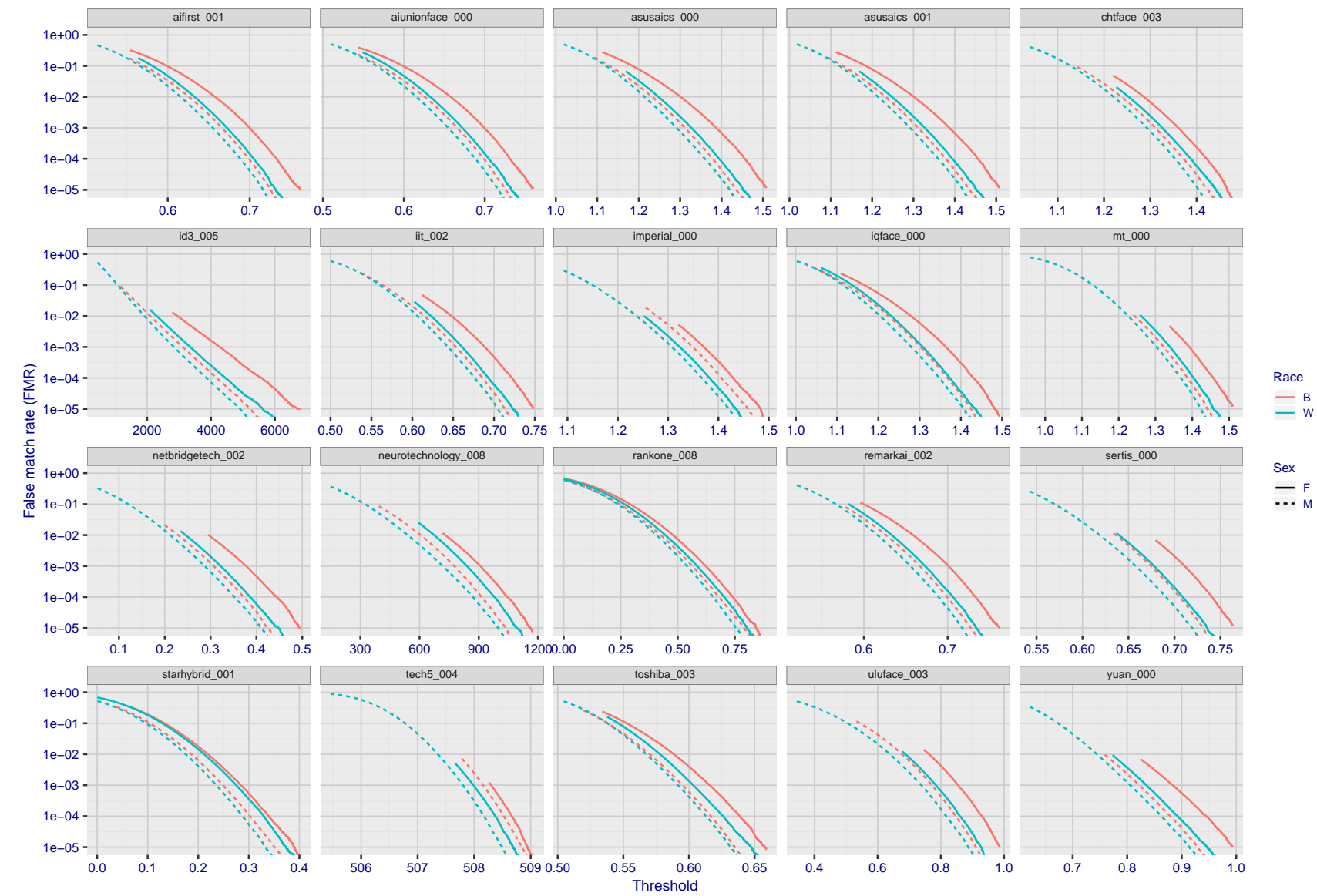


Figure 115: For the mugshot images, the false match calibration curves show false match rate vs. threshold. Separate curves appear for white females, black females, black males and white males.

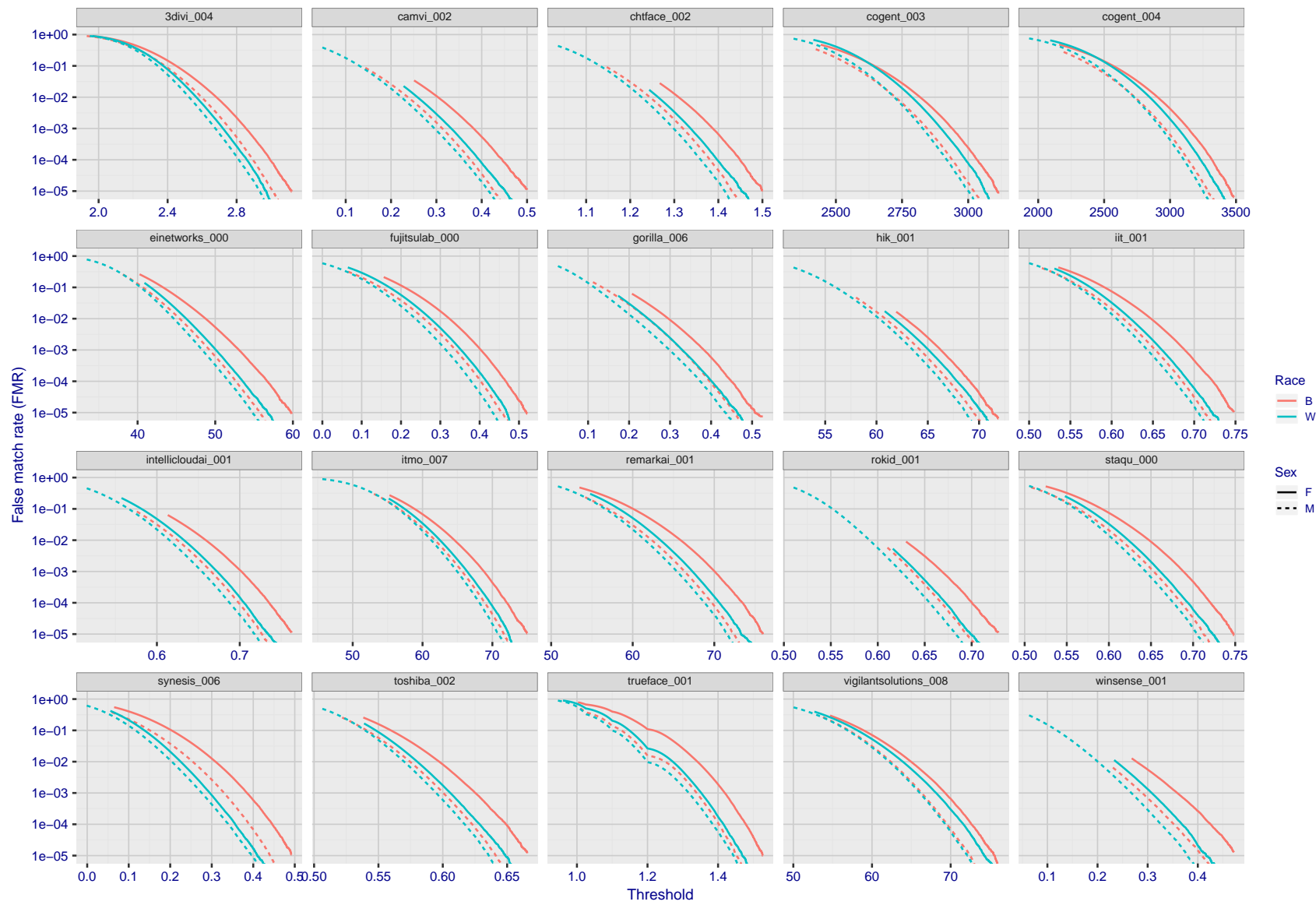
2020/09/08
12:09:14

Figure 116: For the mugshot images, the false match calibration curves show false match rate vs. threshold. Separate curves appear for white females, black females, black males and white males.

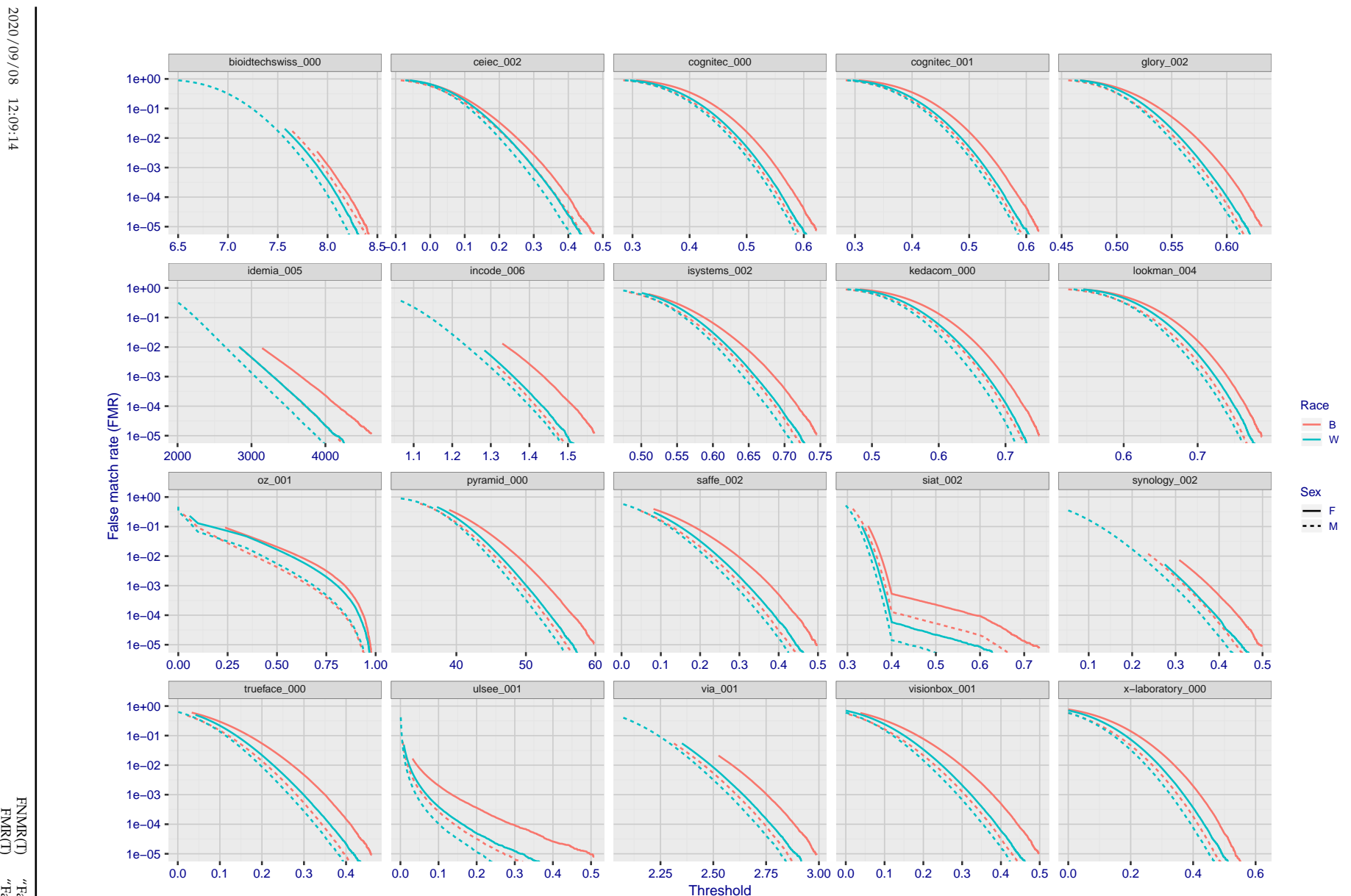


Figure 117: For the mugshot images, the false match calibration curves show false match rate vs. threshold. Separate curves appear for white females, black females, black males and white males.

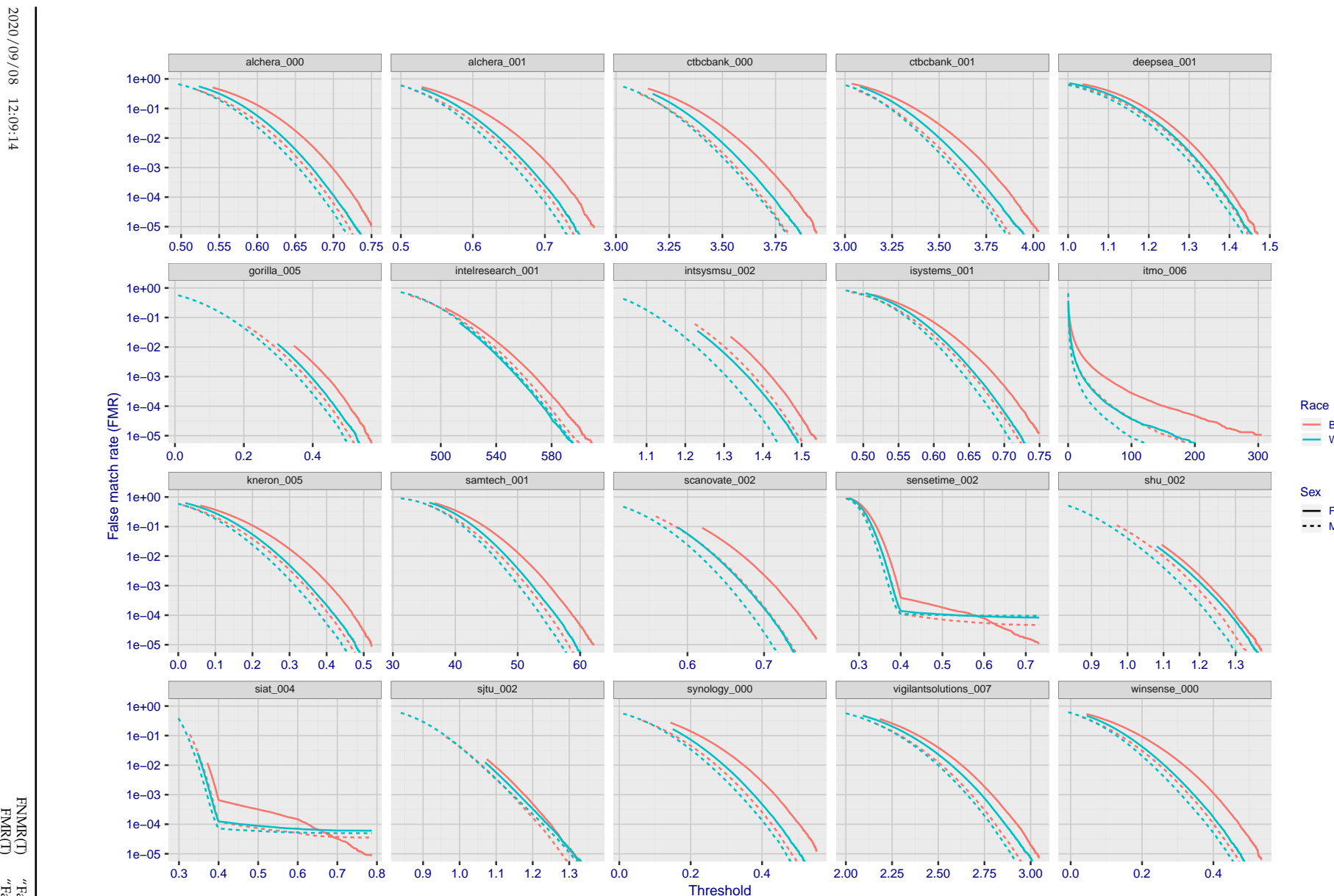


Figure 118: For the mugshot images, the false match calibration curves show false match rate vs. threshold. Separate curves appear for white females, black females, black males and white males.

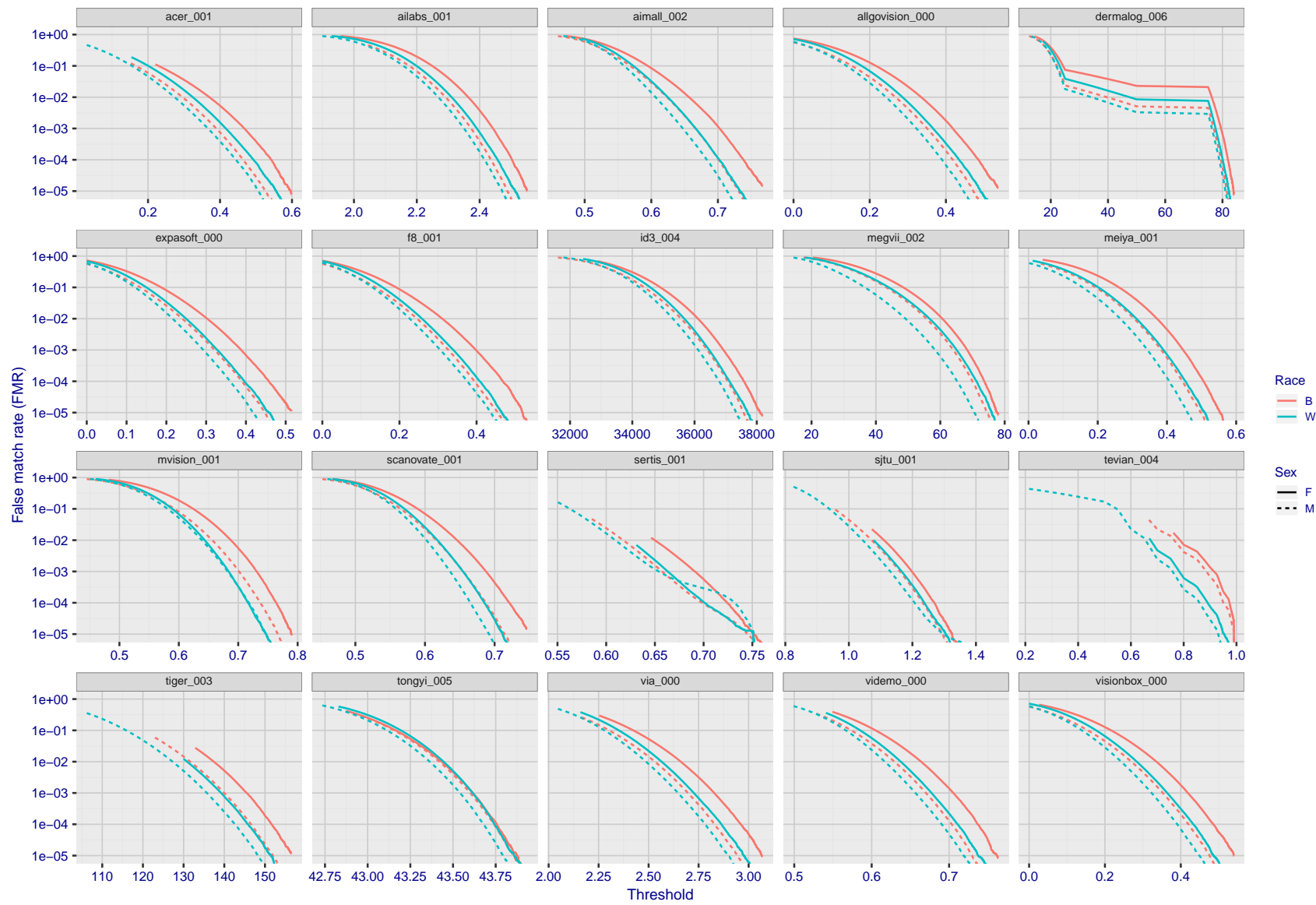
2020/09/08
12:09:14

Figure 119: For the mugshot images, the false match calibration curves show false match rate vs. threshold. Separate curves appear for white females, black females, black males and white males.

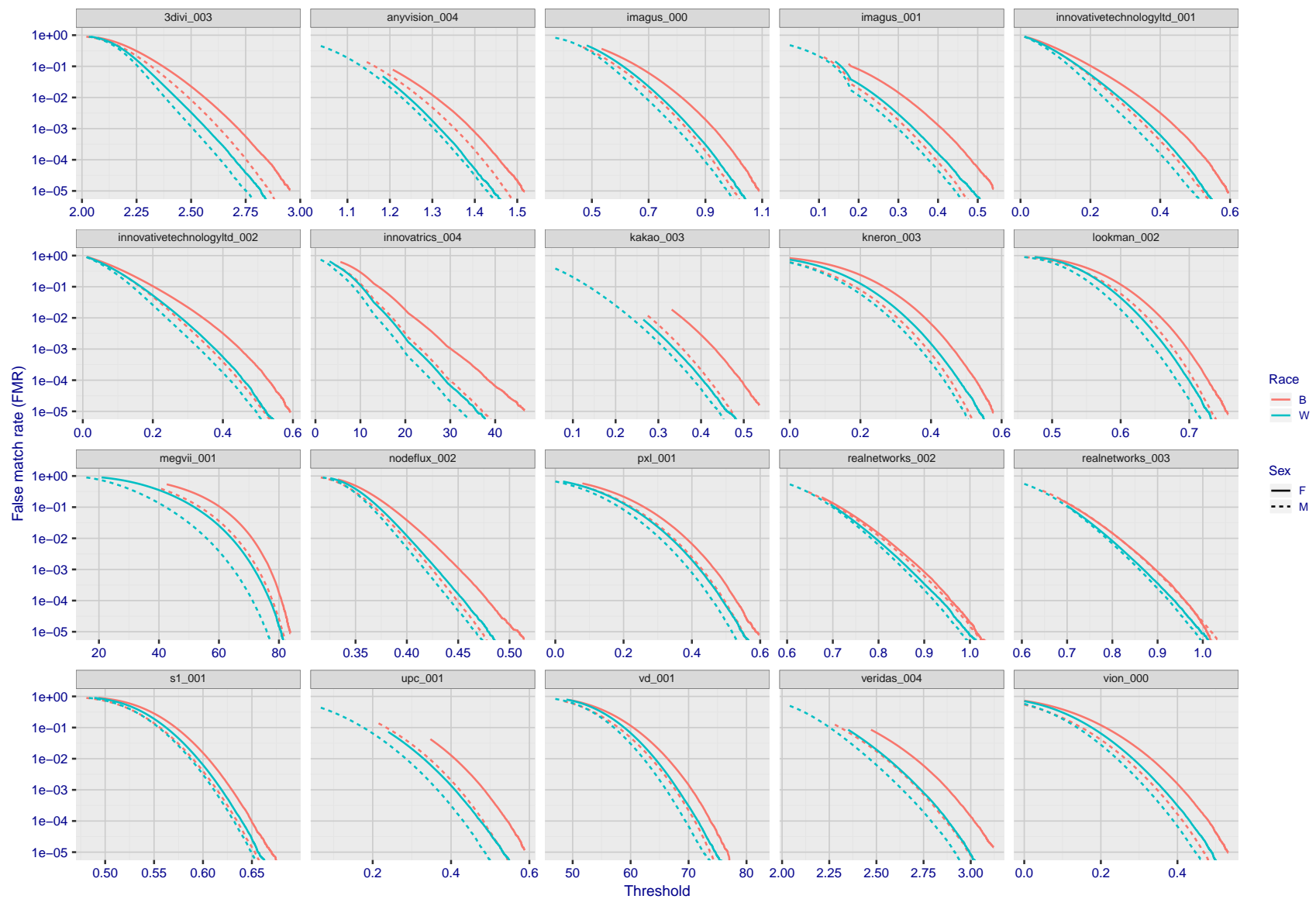


Figure 120: For the mugshot images, the false match calibration curves show false match rate vs. threshold. Separate curves appear for white females, black females, black males and white males.

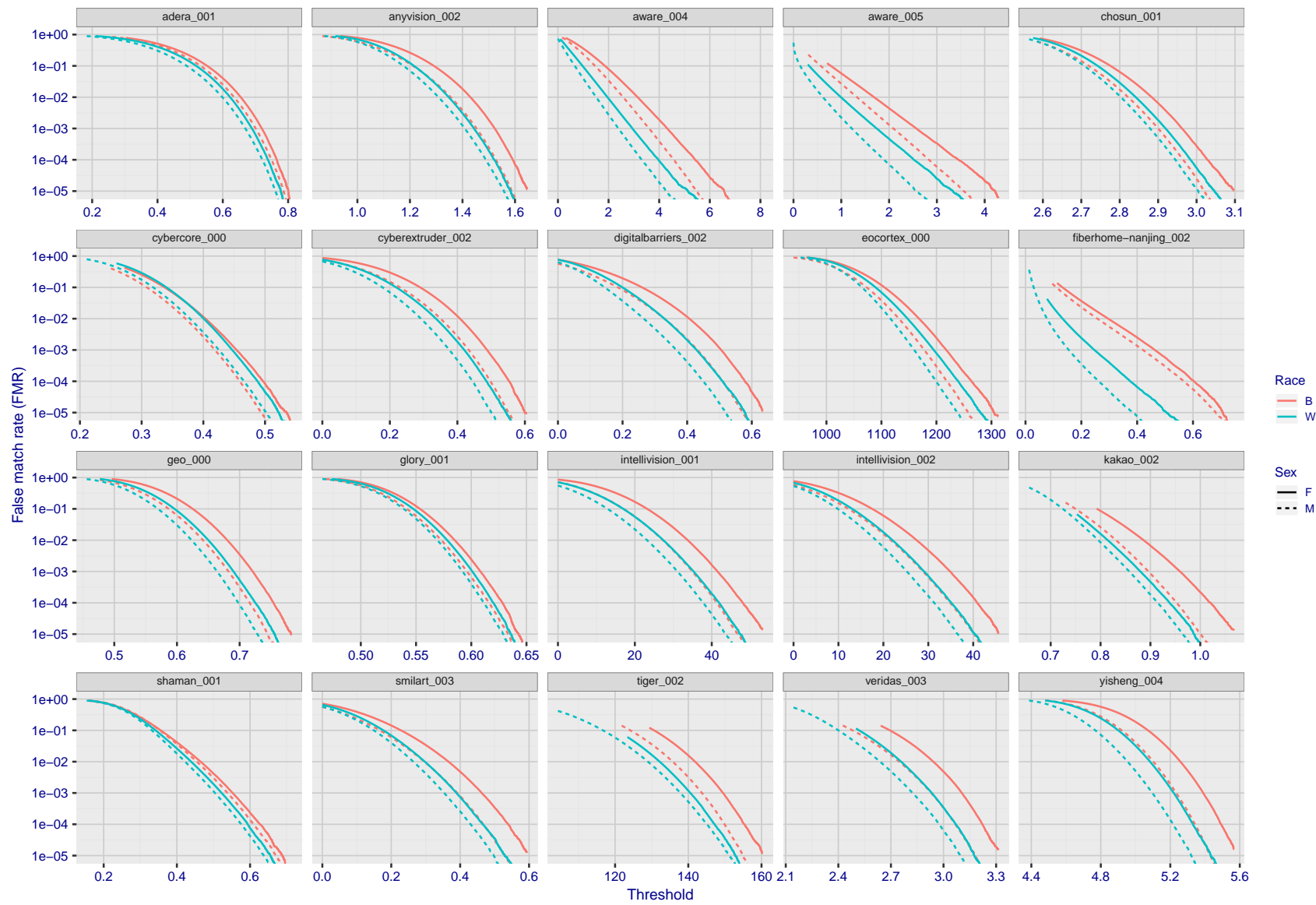
2020/09/08
12:09:14

Figure 121: For the mugshot images, the false match calibration curves show false match rate vs. threshold. Separate curves appear for white females, black females, black males and white males.

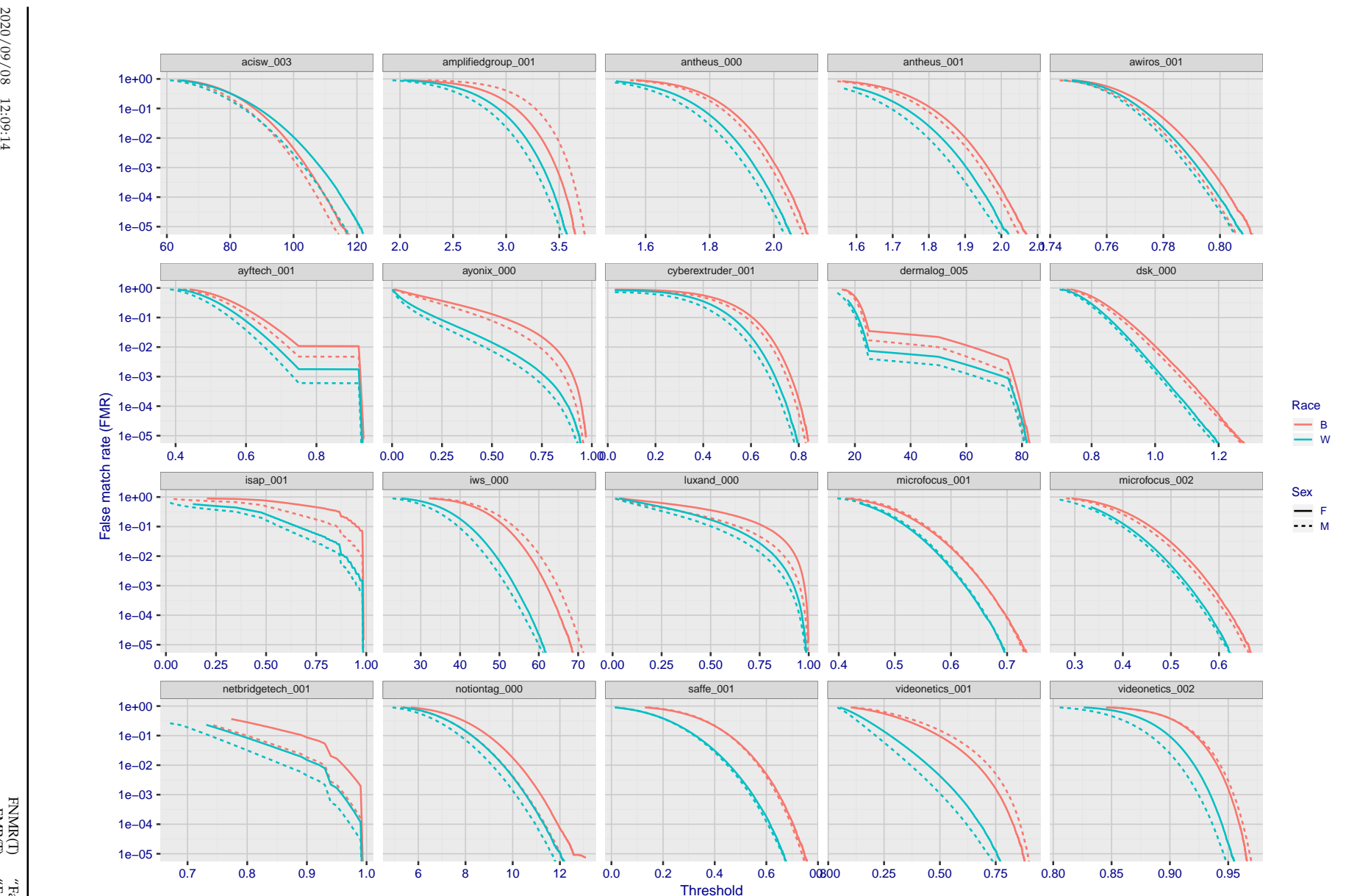


Figure 122: For the mugshot images, the false match calibration curves show false match rate vs. threshold. Separate curves appear for white females, black females, black males and white males.

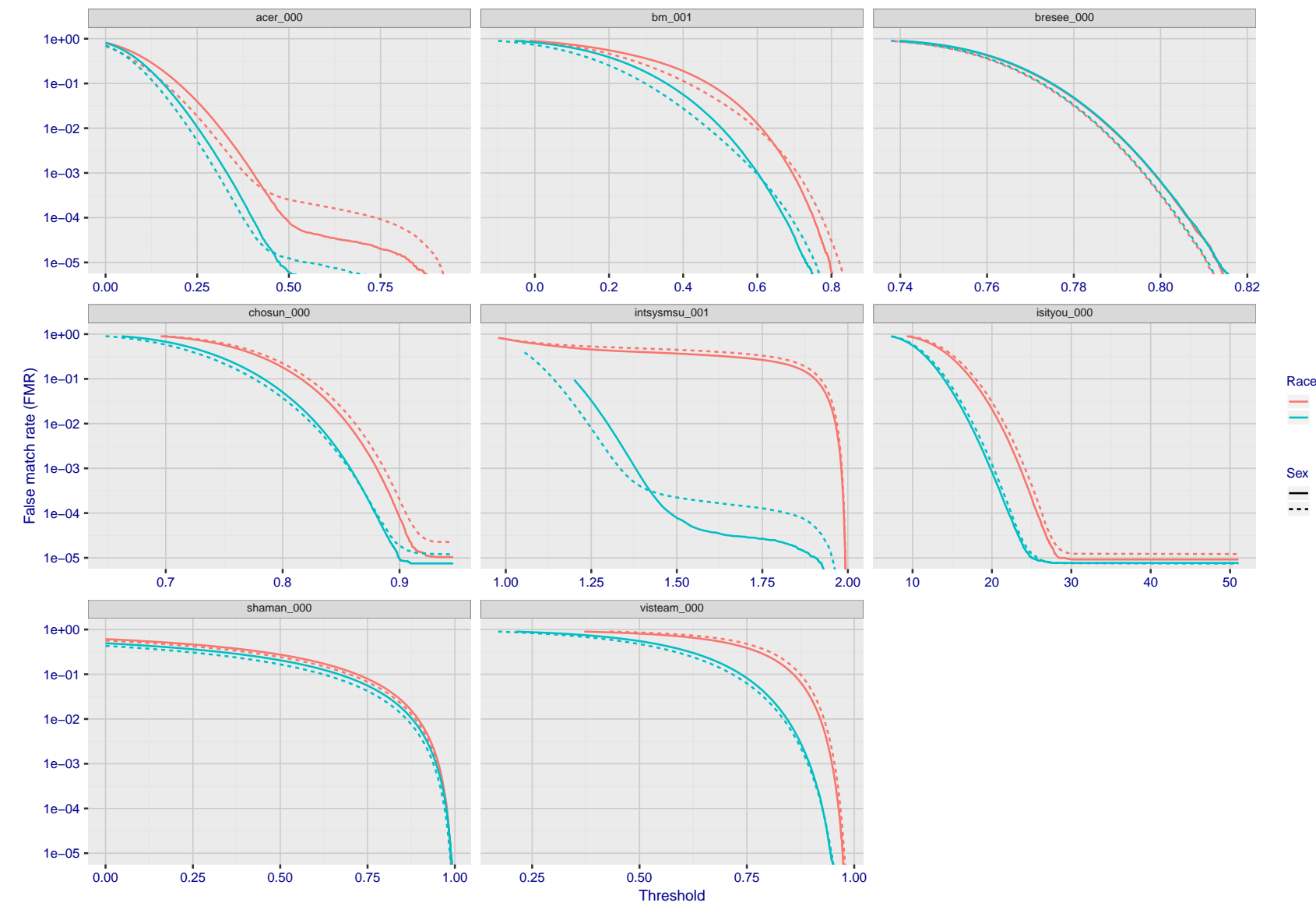


Figure 123: For the mugshot images, the false match calibration curves show false match rate vs. threshold. Separate curves appear for white females, black females, black males and white males.

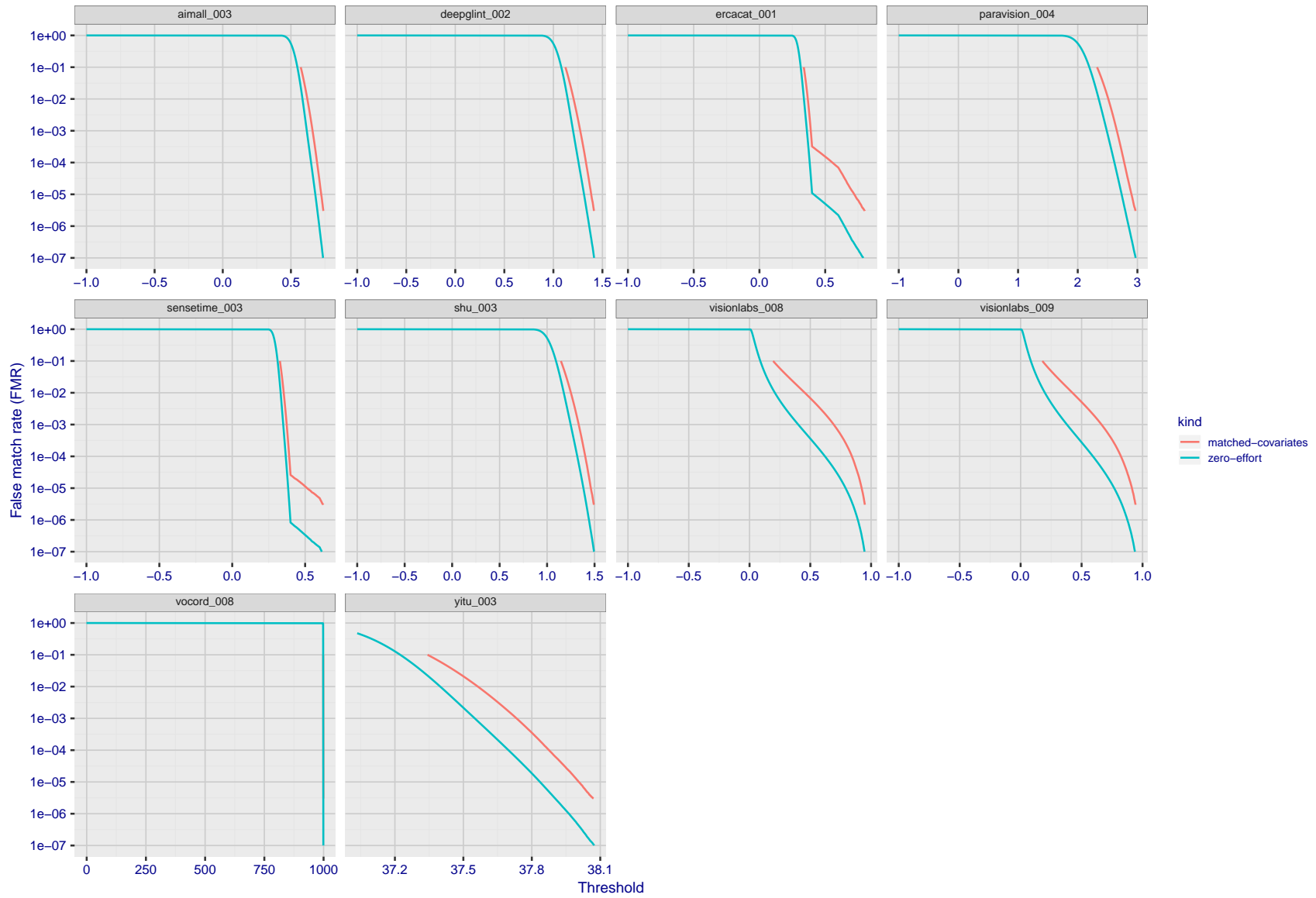


Figure 124: For the visa images, the false match calibration curves show FMR vs. threshold, T . The blue (lower) curves are for zero-effort impostors (i.e. comparing all images against all). The red (upper) curves are for persons of the same-sex, same-age, and same national-origin. This shows that FMR is underestimated (by a factor of 10 or more) by using a zero-effort impostor calculation to calibrate T . As shown later (sec. 3.6), FMR is higher for demographic-matched impostors.

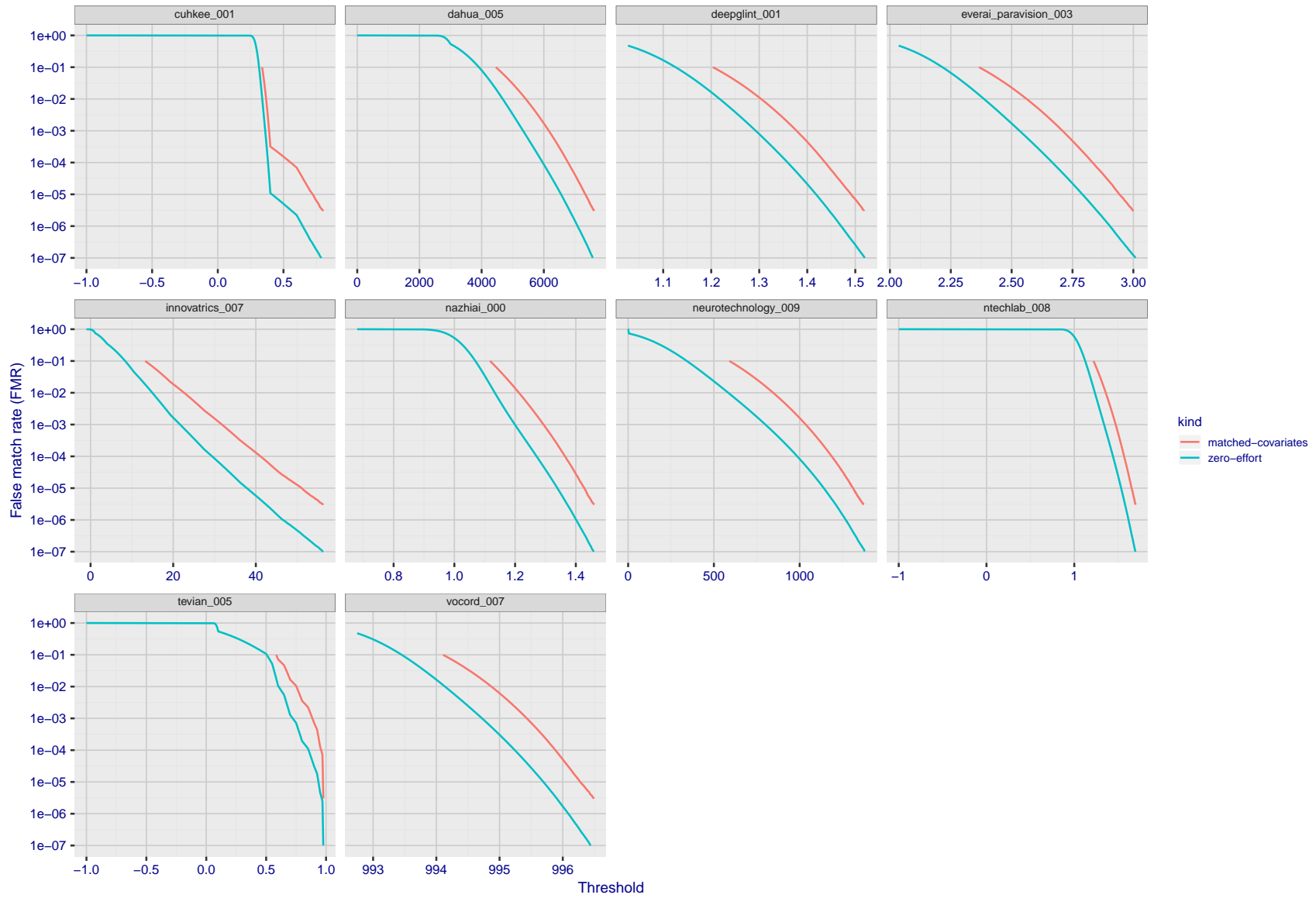


Figure 125: For the visa images, the false match calibration curves show FMR vs. threshold, T . The blue (lower) curves are for zero-effort impostors (i.e. comparing all images against all). The red (upper) curves are for persons of the same-sex, same-age, and same national-origin. This shows that FMR is underestimated (by a factor of 10 or more) by using a zero-effort impostor calculation to calibrate T . As shown later (sec. 3.6), FMR is higher for demographic-matched impostors.

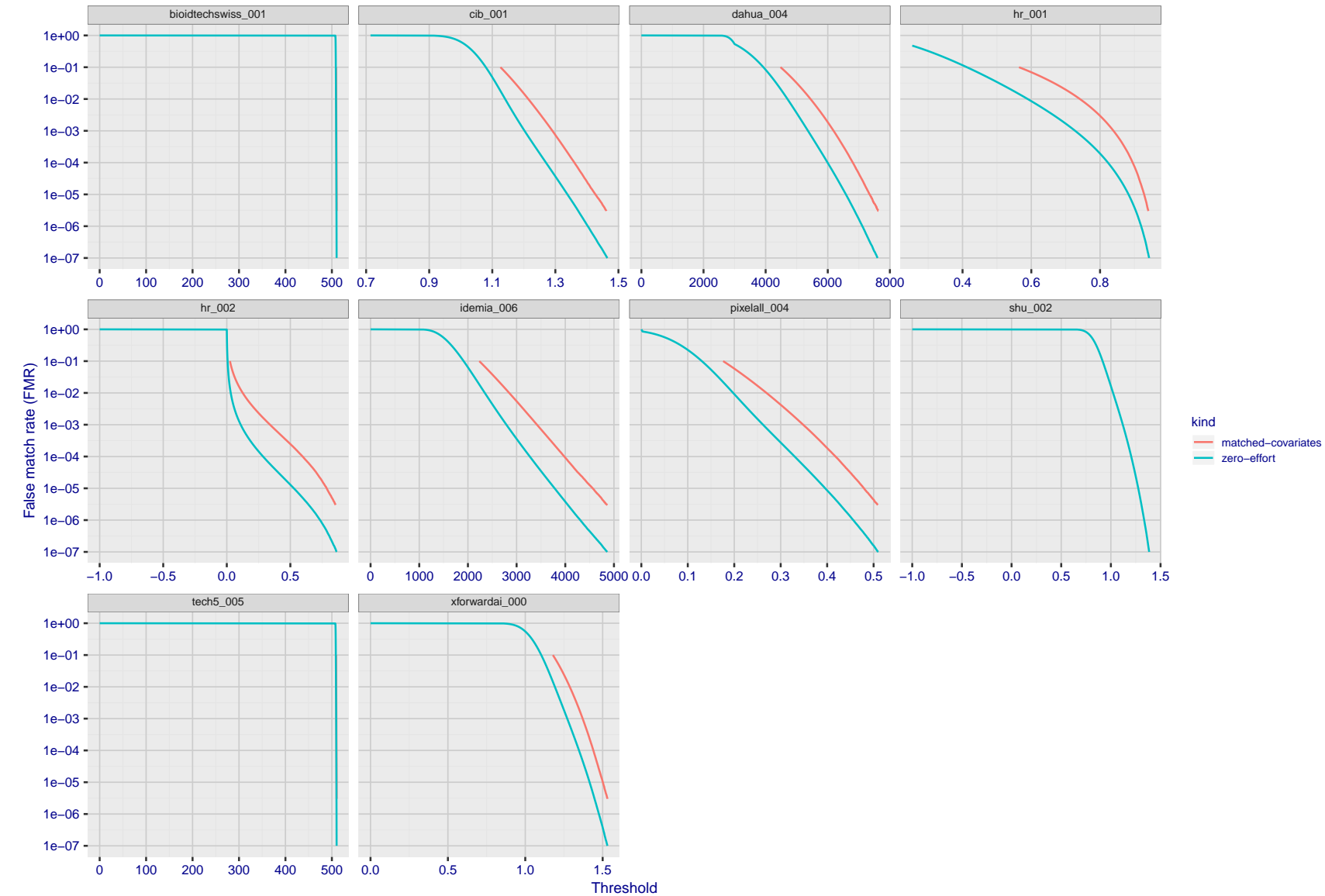


Figure 126: For the visa images, the false match calibration curves show FMR vs. threshold, T . The blue (lower) curves are for zero-effort impostors (i.e. comparing all images against all). The red (upper) curves are for persons of the same-sex, same-age, and same national-origin. This shows that FMR is underestimated (by a factor of 10 or more) by using a zero-effort impostor calculation to calibrate T . As shown later (sec. 3.6), FMR is higher for demographic-matched impostors.

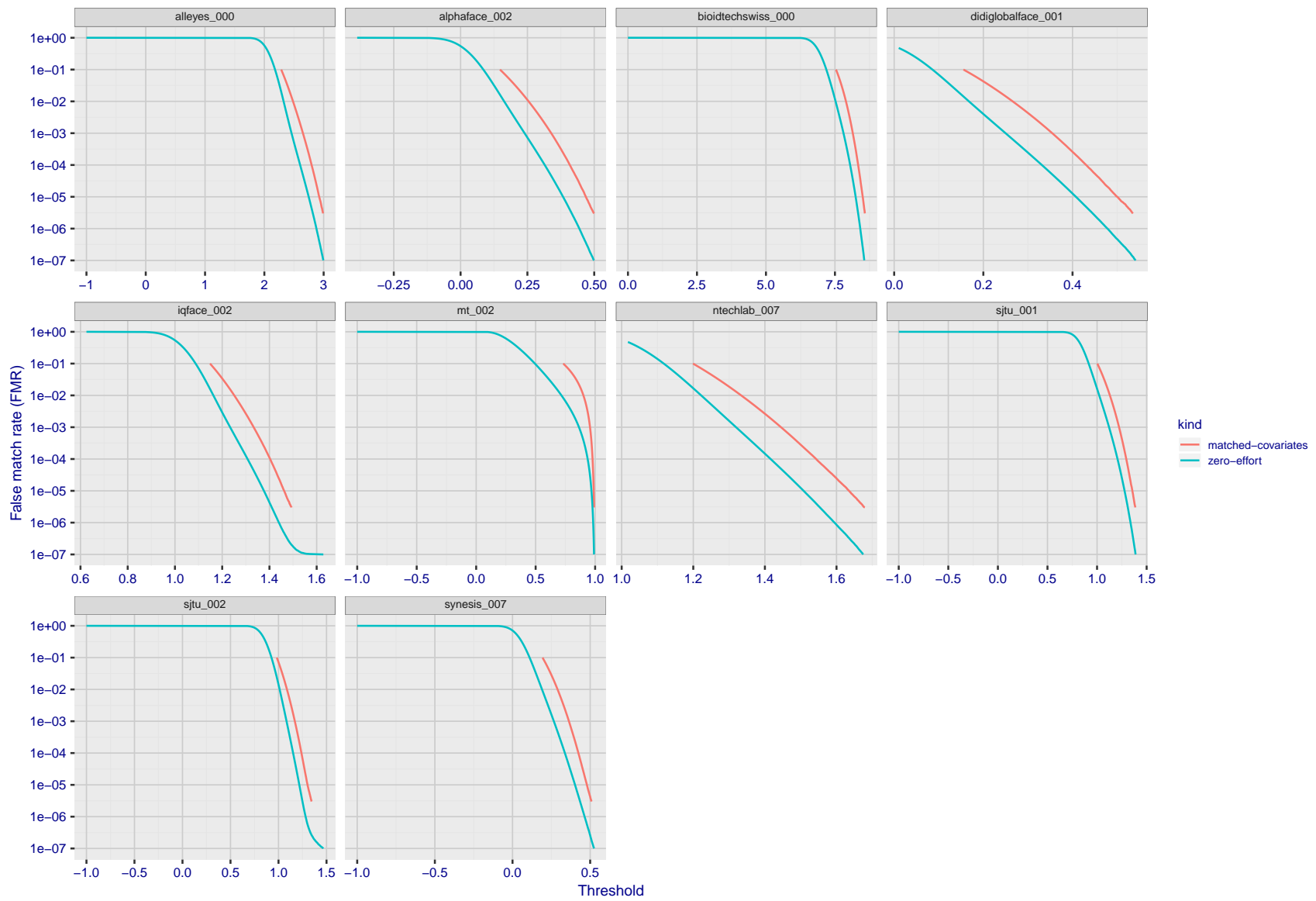


Figure 127: For the visa images, the false match calibration curves show FMR vs. threshold, T . The blue (lower) curves are for zero-effort impostors (i.e. comparing all images against all). The red (upper) curves are for persons of the same-sex, same-age, and same national-origin. This shows that FMR is underestimated (by a factor of 10 or more) by using a zero-effort impostor calculation to calibrate T . As shown later (sec. 3.6), FMR is higher for demographic-matched impostors.

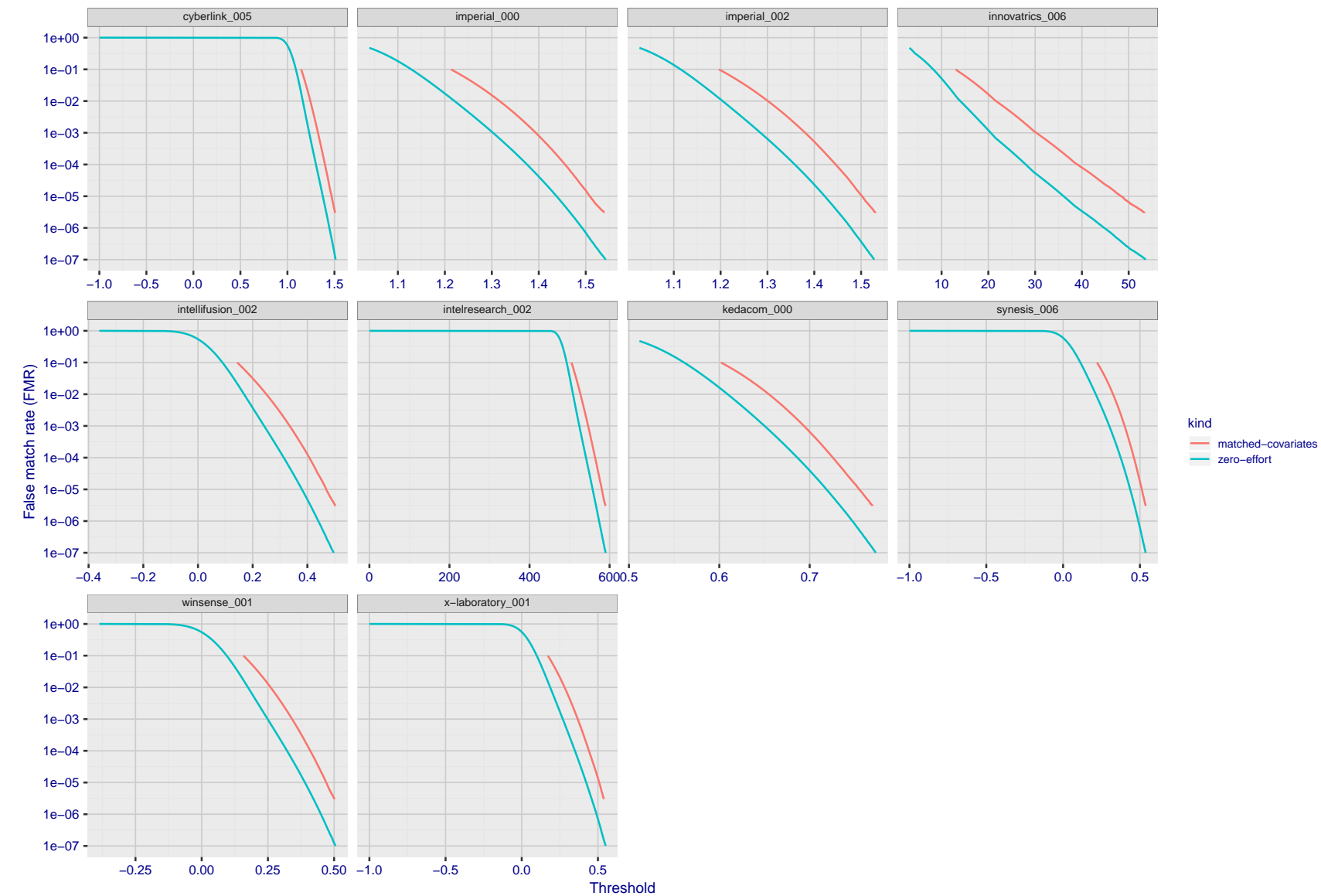


Figure 128: For the visa images, the false match calibration curves show FMR vs. threshold, T . The blue (lower) curves are for zero-effort impostors (i.e. comparing all images against all). The red (upper) curves are for persons of the same-sex, same-age, and same national-origin. This shows that FMR is underestimated (by a factor of 10 or more) by using a zero-effort impostor calculation to calibrate T . As shown later (sec. 3.6), FMR is higher for demographic-matched impostors.

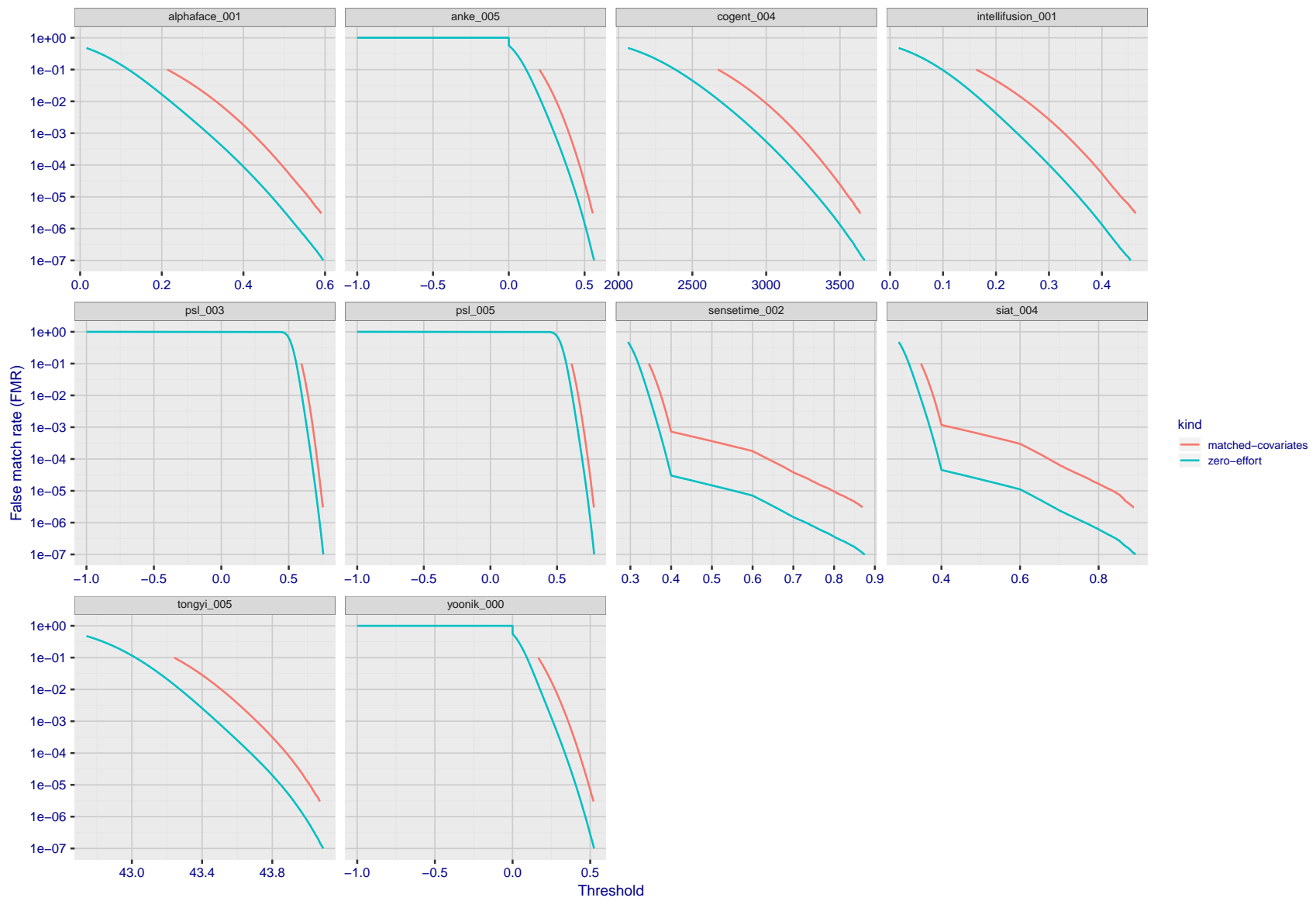


Figure 129: For the visa images, the false match calibration curves show FMR vs. threshold, T . The blue (lower) curves are for zero-effort impostors (i.e. comparing all images against all). The red (upper) curves are for persons of the same-sex, same-age, and same national-origin. This shows that FMR is underestimated (by a factor of 10 or more) by using a zero-effort impostor calculation to calibrate T . As shown later (sec. 3.6), FMR is higher for demographic-matched impostors.

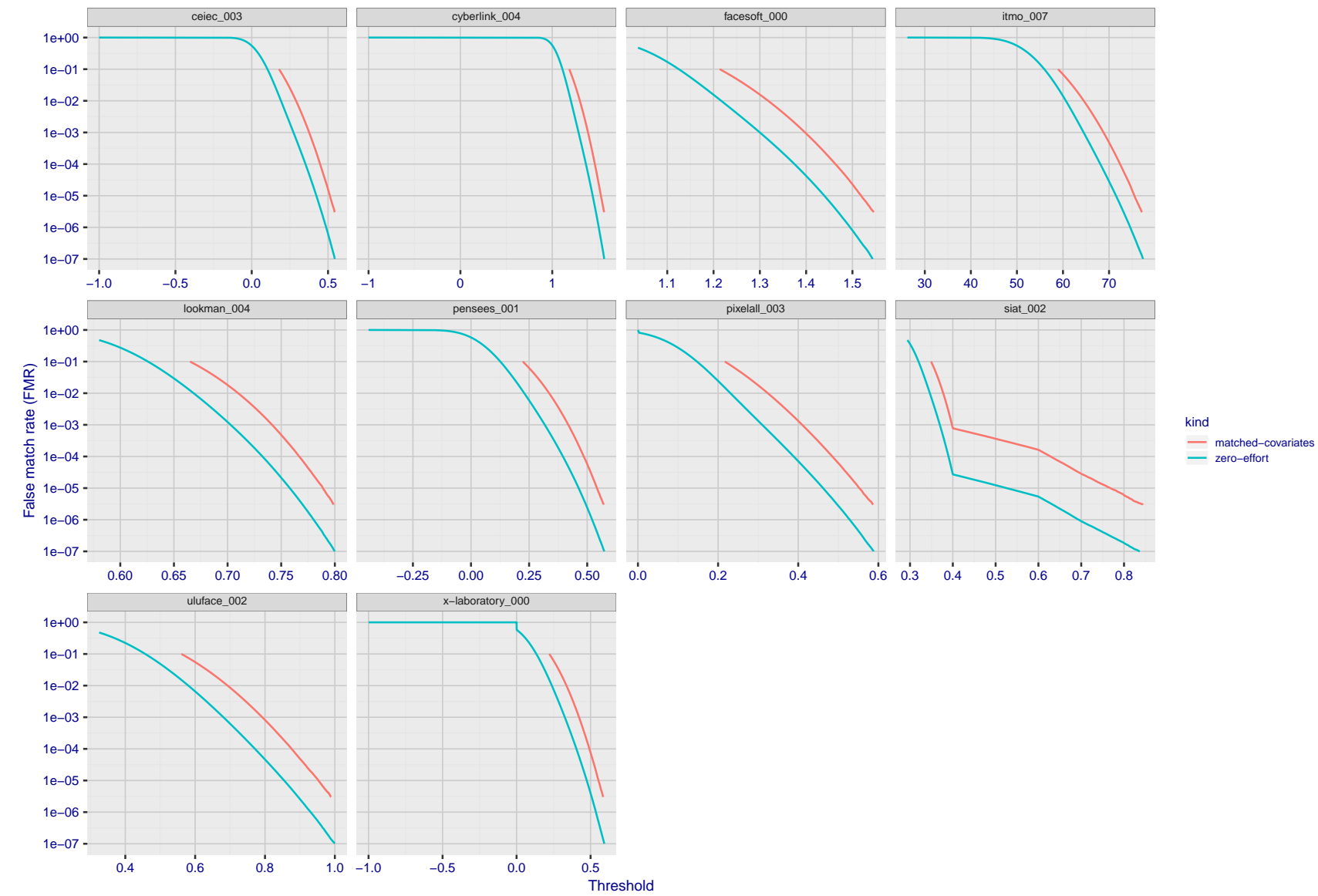


Figure 130: For the visa images, the false match calibration curves show FMR vs. threshold, T . The blue (lower) curves are for zero-effort impostors (i.e. comparing all images against all). The red (upper) curves are for persons of the same-sex, same-age, and same national-origin. This shows that FMR is underestimated (by a factor of 10 or more) by using a zero-effort impostor calculation to calibrate T . As shown later (sec. 3.6), FMR is higher for demographic-matched impostors.

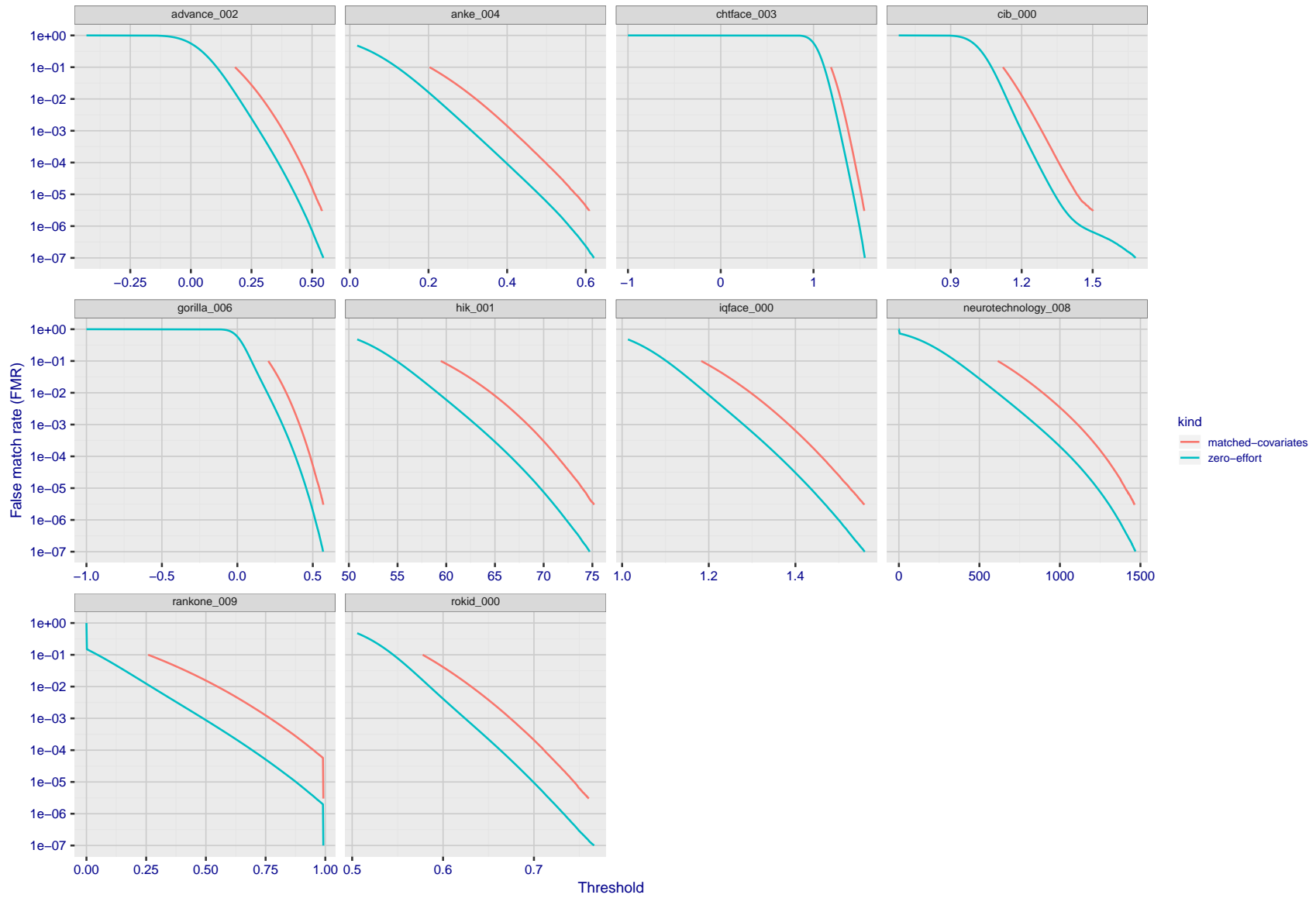


Figure 131: For the visa images, the false match calibration curves show FMR vs. threshold, T . The blue (lower) curves are for zero-effort impostors (i.e. comparing all images against all). The red (upper) curves are for persons of the same-sex, same-age, and same national-origin. This shows that FMR is underestimated (by a factor of 10 or more) by using a zero-effort impostor calculation to calibrate T . As shown later (sec. 3.6), FMR is higher for demographic-matched impostors.

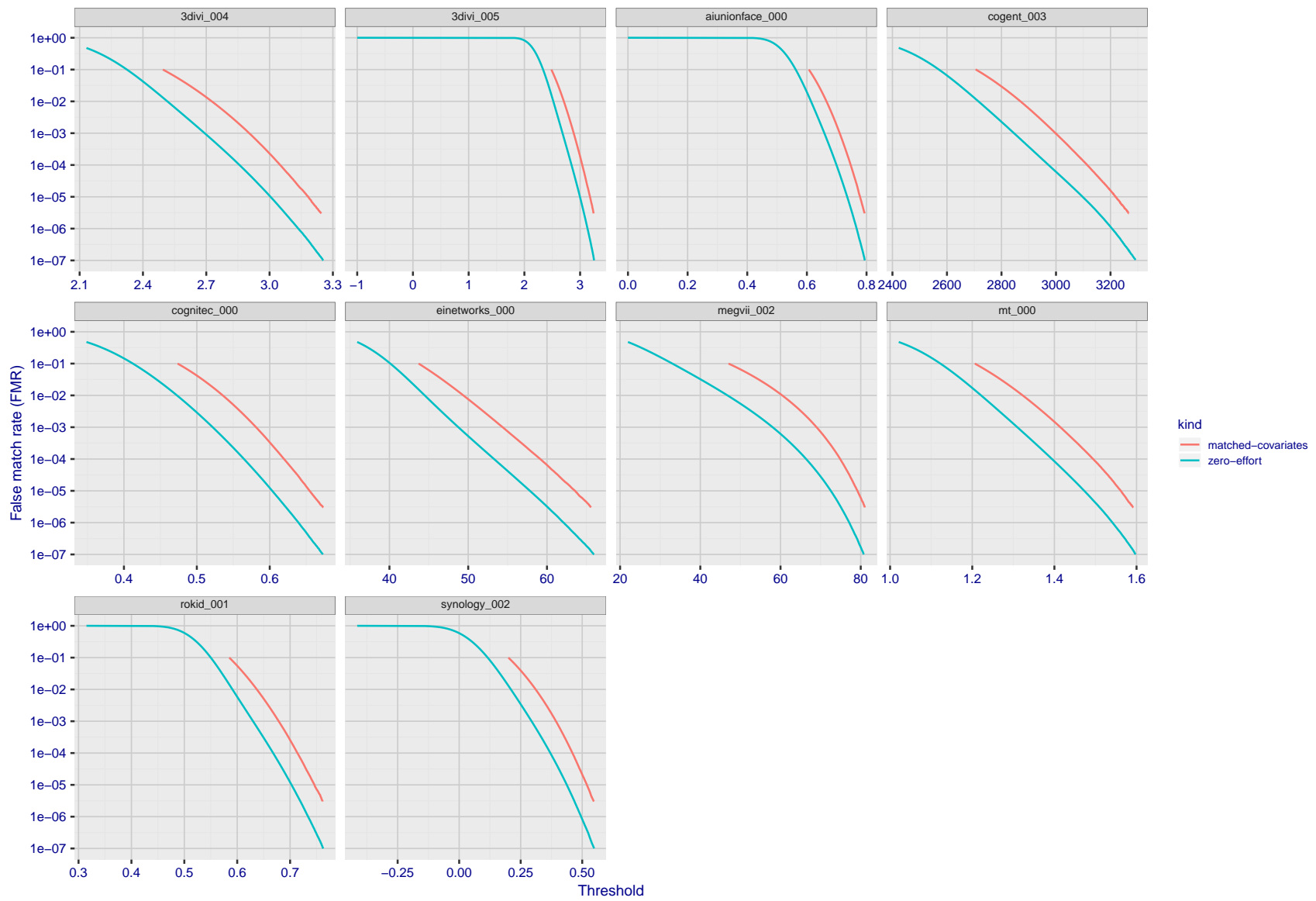


Figure 132: For the visa images, the false match calibration curves show FMR vs. threshold, T . The blue (lower) curves are for zero-effort impostors (i.e. comparing all images against all). The red (upper) curves are for persons of the same-sex, same-age, and same national-origin. This shows that FMR is underestimated (by a factor of 10 or more) by using a zero-effort impostor calculation to calibrate T . As shown later (sec. 3.6), FMR is higher for demographic-matched impostors.

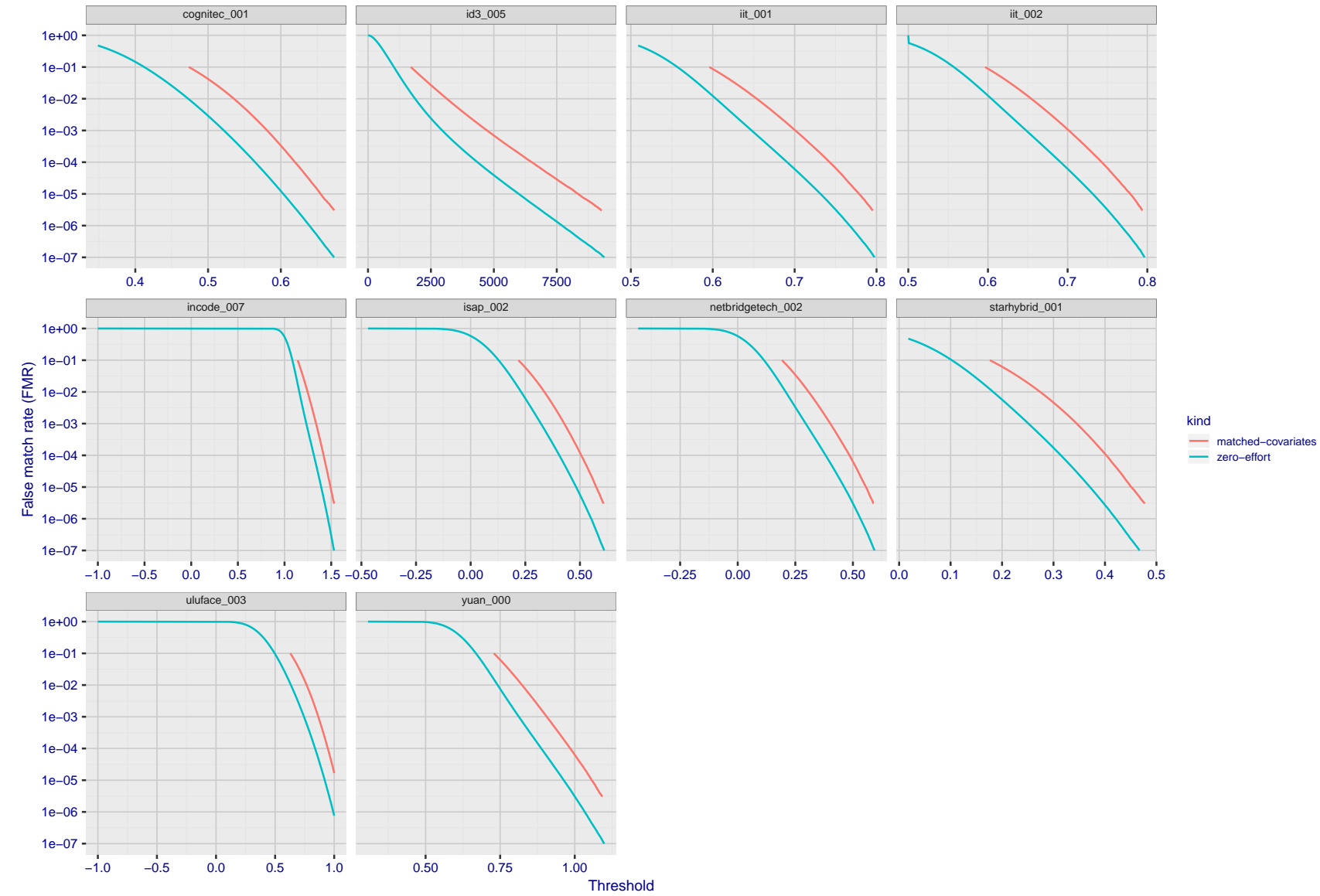


Figure 133: For the visa images, the false match calibration curves show FMR vs. threshold, T . The blue (lower) curves are for zero-effort impostors (i.e. comparing all images against all). The red (upper) curves are for persons of the same-sex, same-age, and same national-origin. This shows that FMR is underestimated (by a factor of 10 or more) by using a zero-effort impostor calculation to calibrate T . As shown later (sec. 3.6), FMR is higher for demographic-matched impostors.

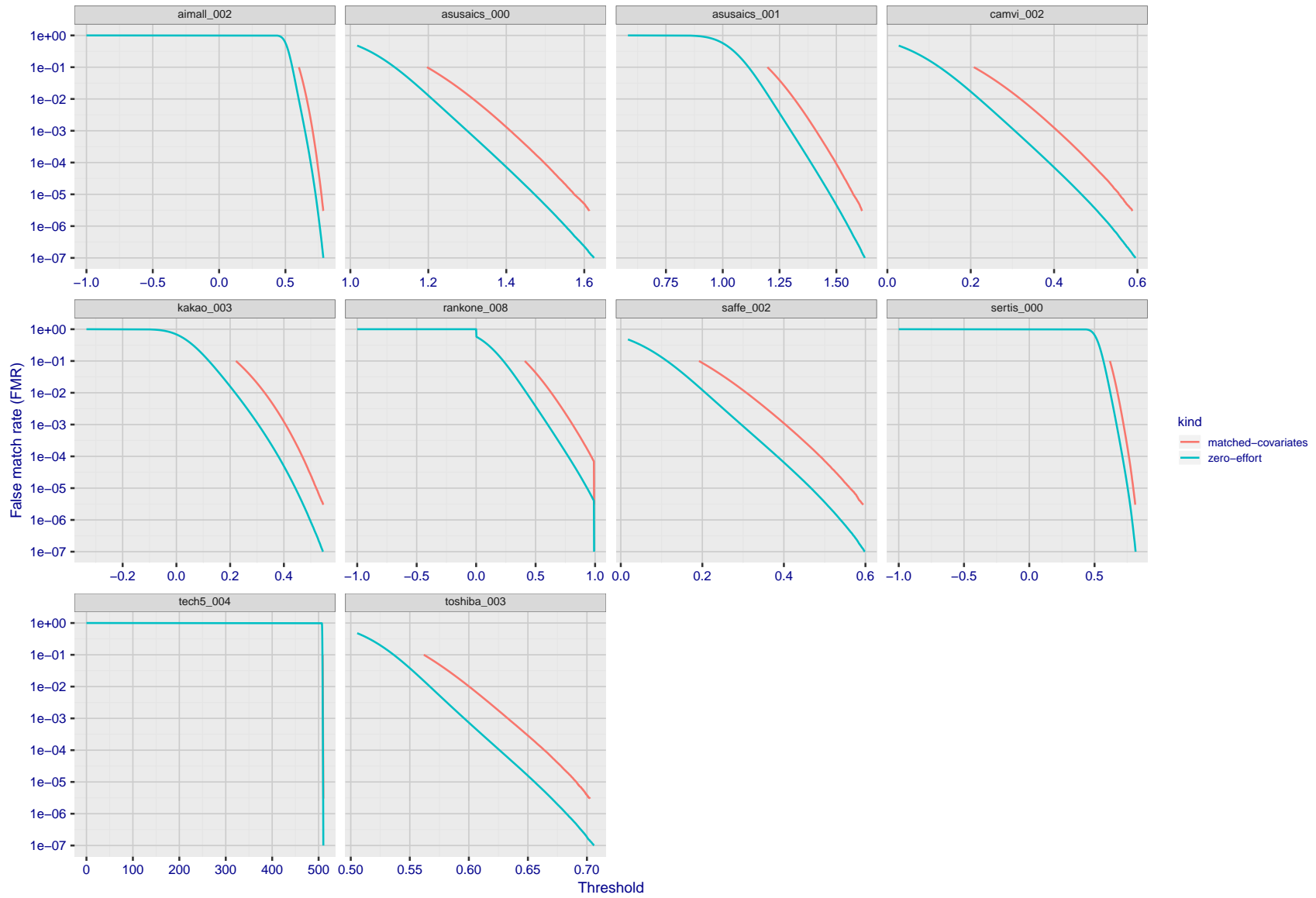


Figure 134: For the visa images, the false match calibration curves show FMR vs. threshold, T . The blue (lower) curves are for zero-effort impostors (i.e. comparing all images against all). The red (upper) curves are for persons of the same-sex, same-age, and same national-origin. This shows that FMR is underestimated (by a factor of 10 or more) by using a zero-effort impostor calculation to calibrate T . As shown later (sec. 3.6), FMR is higher for demographic-matched impostors.

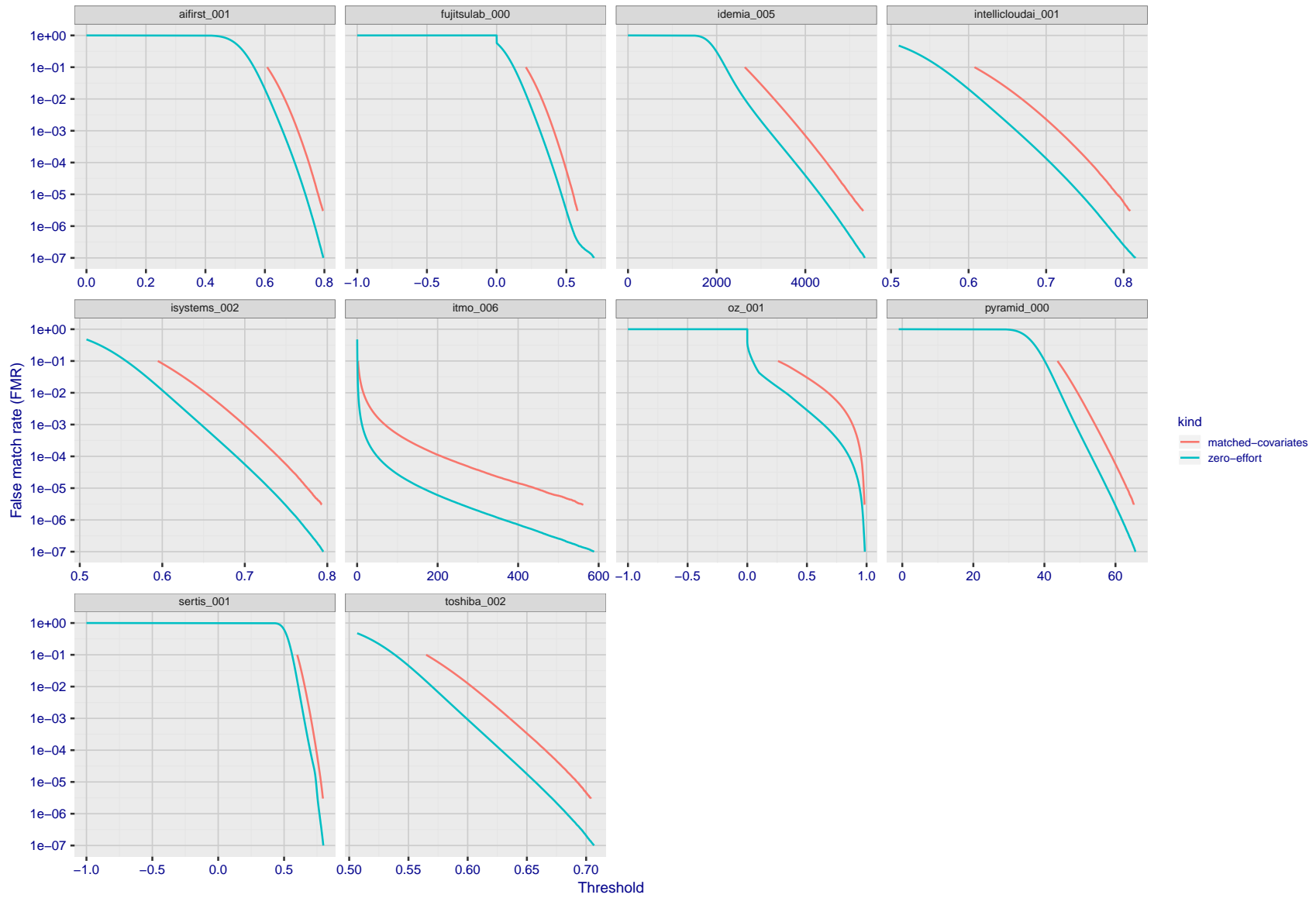


Figure 135: For the visa images, the false match calibration curves show FMR vs. threshold, T . The blue (lower) curves are for zero-effort impostors (i.e. comparing all images against all). The red (upper) curves are for persons of the same-sex, same-age, and same national-origin. This shows that FMR is underestimated (by a factor of 10 or more) by using a zero-effort impostor calculation to calibrate T . As shown later (sec. 3.6), FMR is higher for demographic-matched impostors.

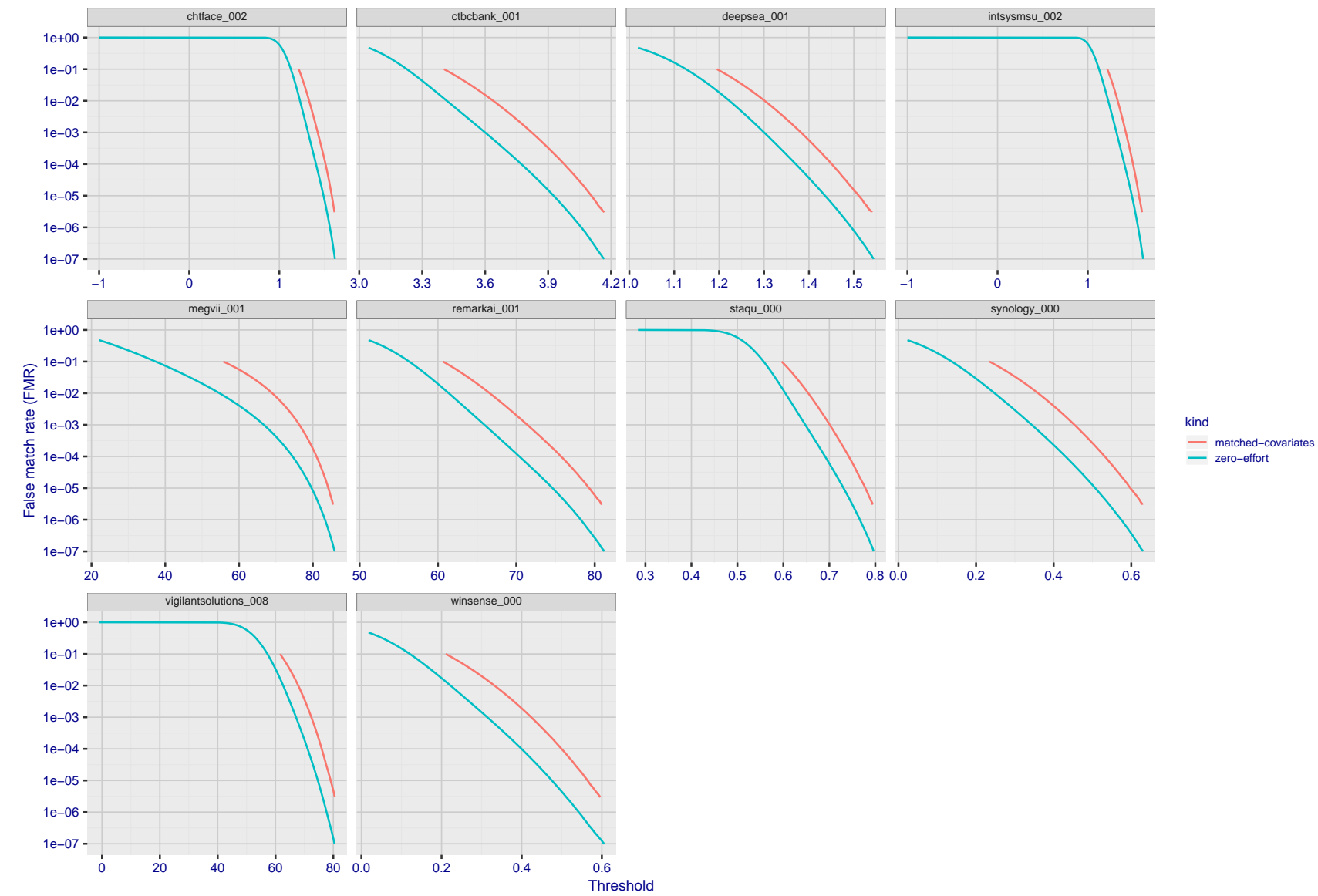


Figure 136: For the visa images, the false match calibration curves show FMR vs. threshold, T . The blue (lower) curves are for zero-effort impostors (i.e. comparing all images against all). The red (upper) curves are for persons of the same-sex, same-age, and same national-origin. This shows that FMR is underestimated (by a factor of 10 or more) by using a zero-effort impostor calculation to calibrate T . As shown later (sec. 3.6), FMR is higher for demographic-matched impostors.

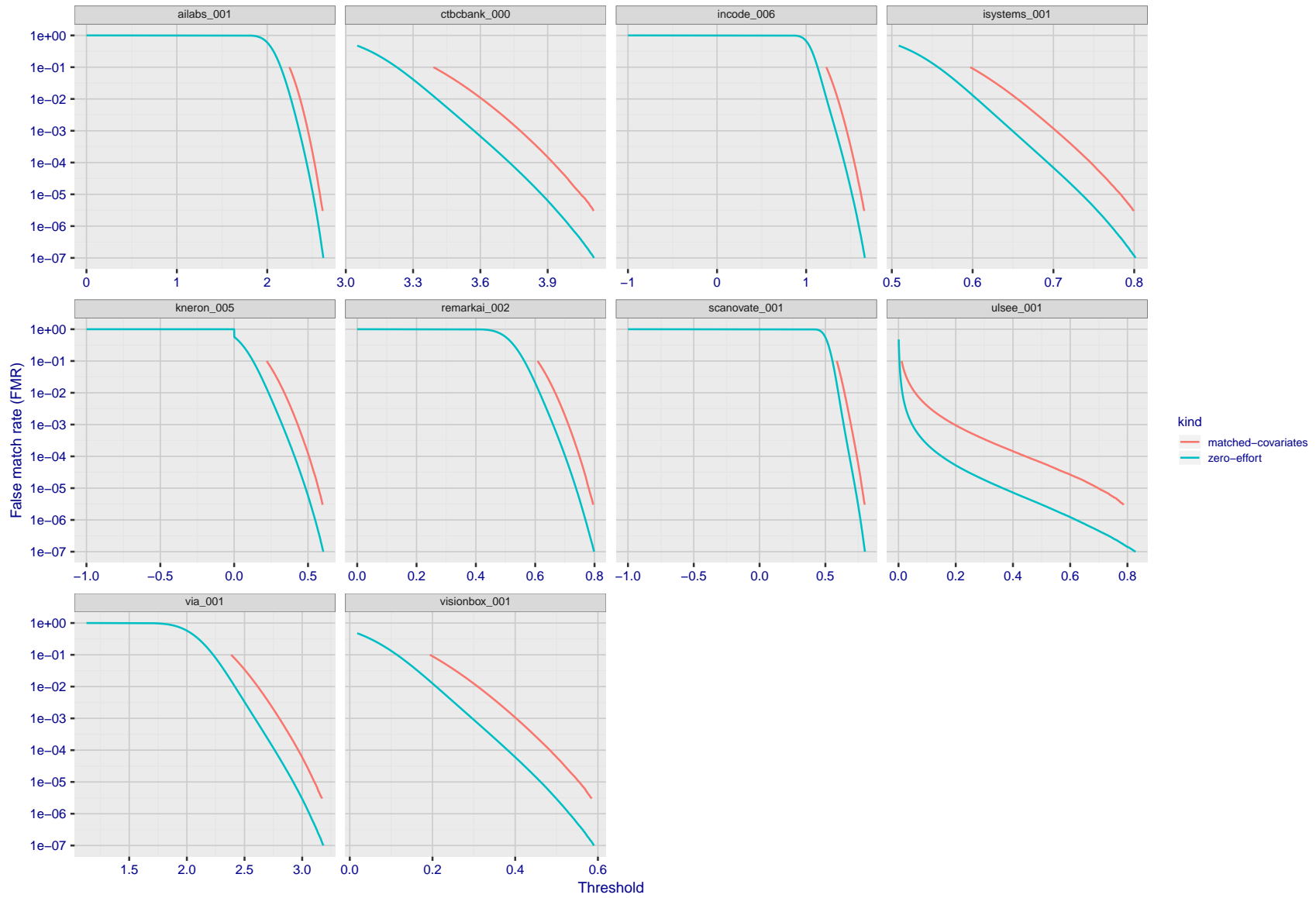
2020/09/08
12:09:14

Figure 137: For the visa images, the false match calibration curves show FMR vs. threshold, T . The blue (lower) curves are for zero-effort impostors (i.e. comparing all images against all). The red (upper) curves are for persons of the same-sex, same-age, and same national-origin. This shows that FMR is underestimated (by a factor of 10 or more) by using a zero-effort impostor calculation to calibrate T . As shown later (sec. 3.6), FMR is higher for demographic-matched impostors.

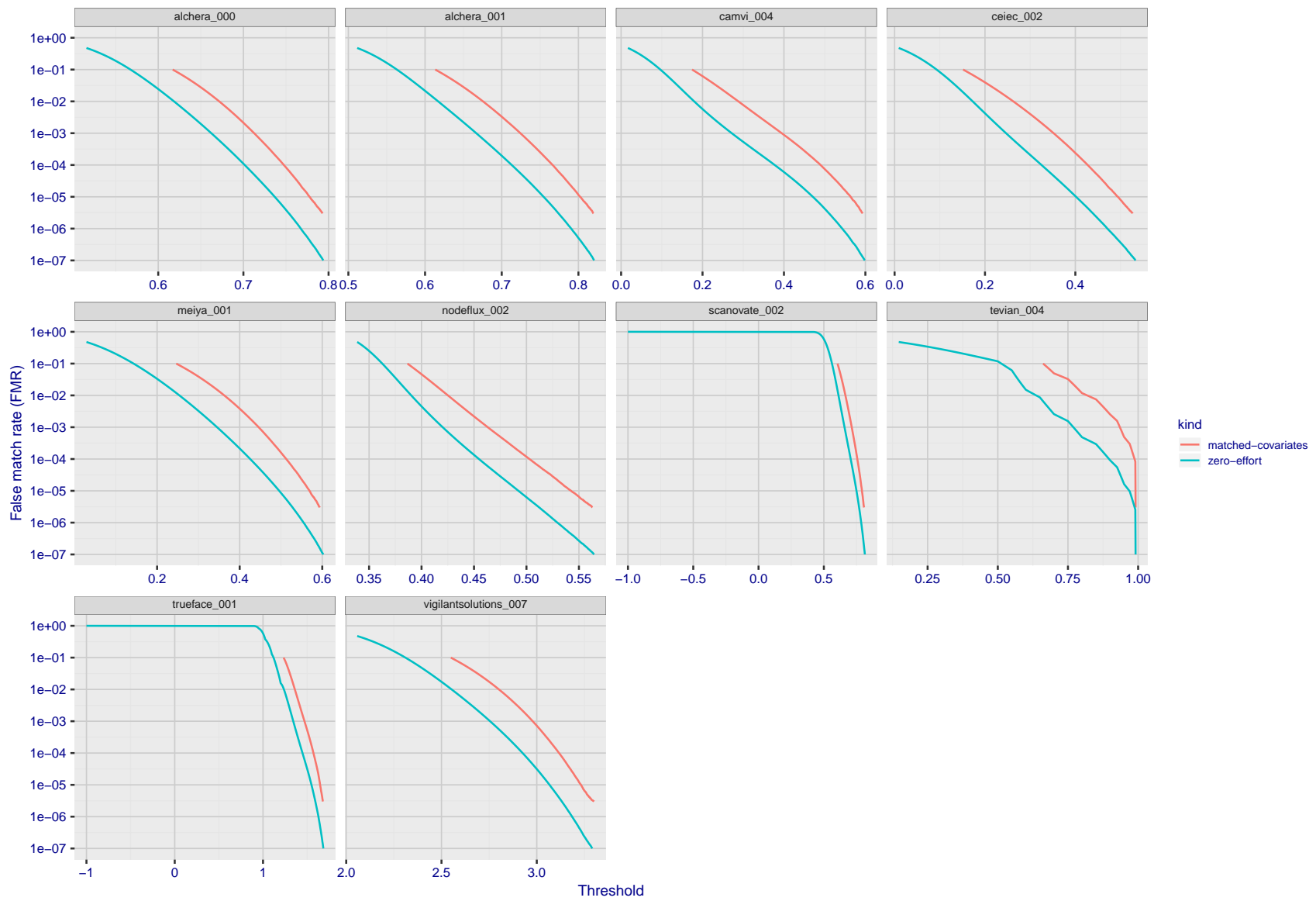


Figure 138: For the visa images, the false match calibration curves show FMR vs. threshold, T . The blue (lower) curves are for zero-effort impostors (i.e. comparing all images against all). The red (upper) curves are for persons of the same-sex, same-age, and same national-origin. This shows that FMR is underestimated (by a factor of 10 or more) by using a zero-effort impostor calculation to calibrate T . As shown later (sec. 3.6), FMR is higher for demographic-matched impostors.

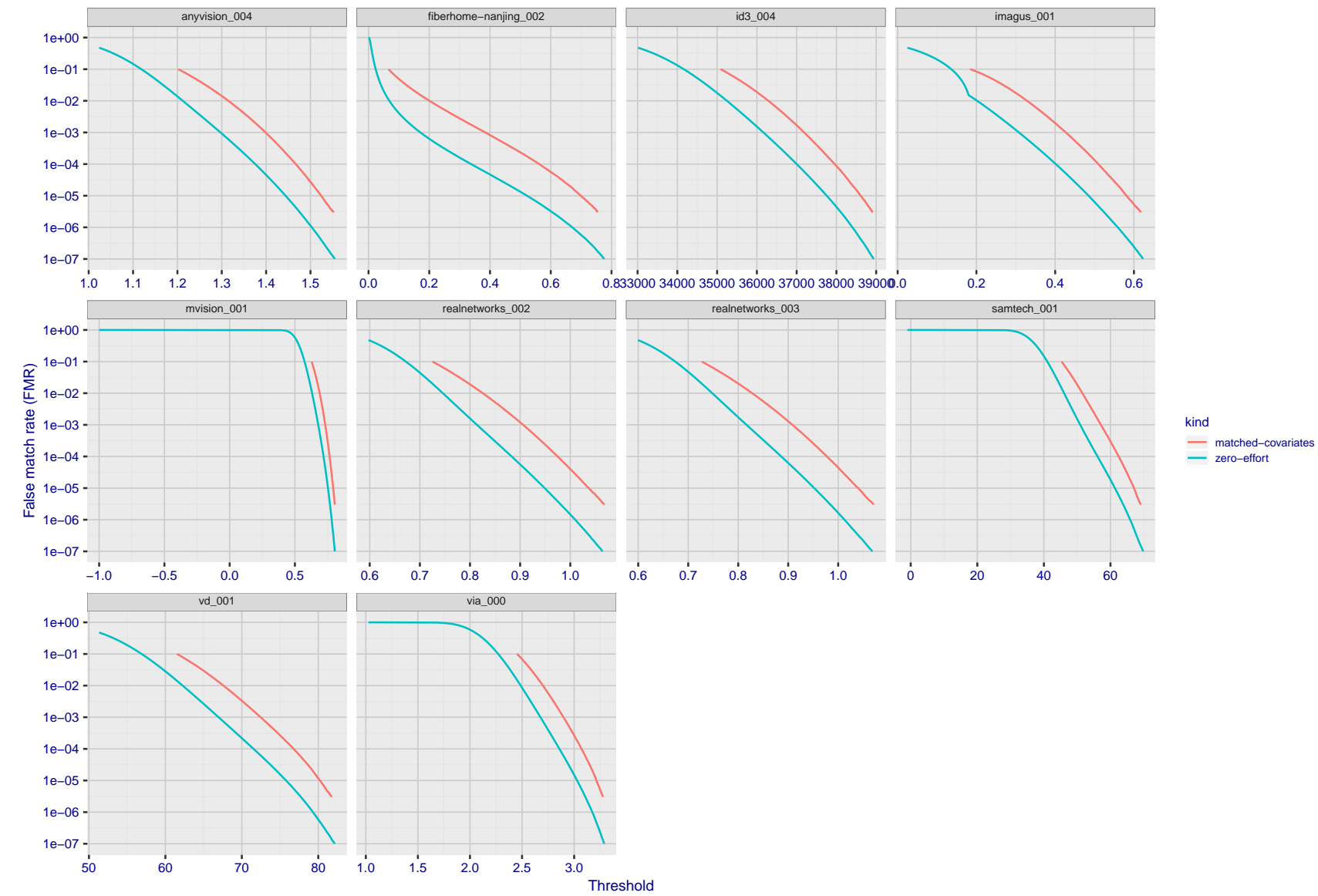


Figure 139: For the visa images, the false match calibration curves show FMR vs. threshold, T . The blue (lower) curves are for zero-effort impostors (i.e. comparing all images against all). The red (upper) curves are for persons of the same-sex, same-age, and same national-origin. This shows that FMR is underestimated (by a factor of 10 or more) by using a zero-effort impostor calculation to calibrate T . As shown later (sec. 3.6), FMR is higher for demographic-matched impostors.

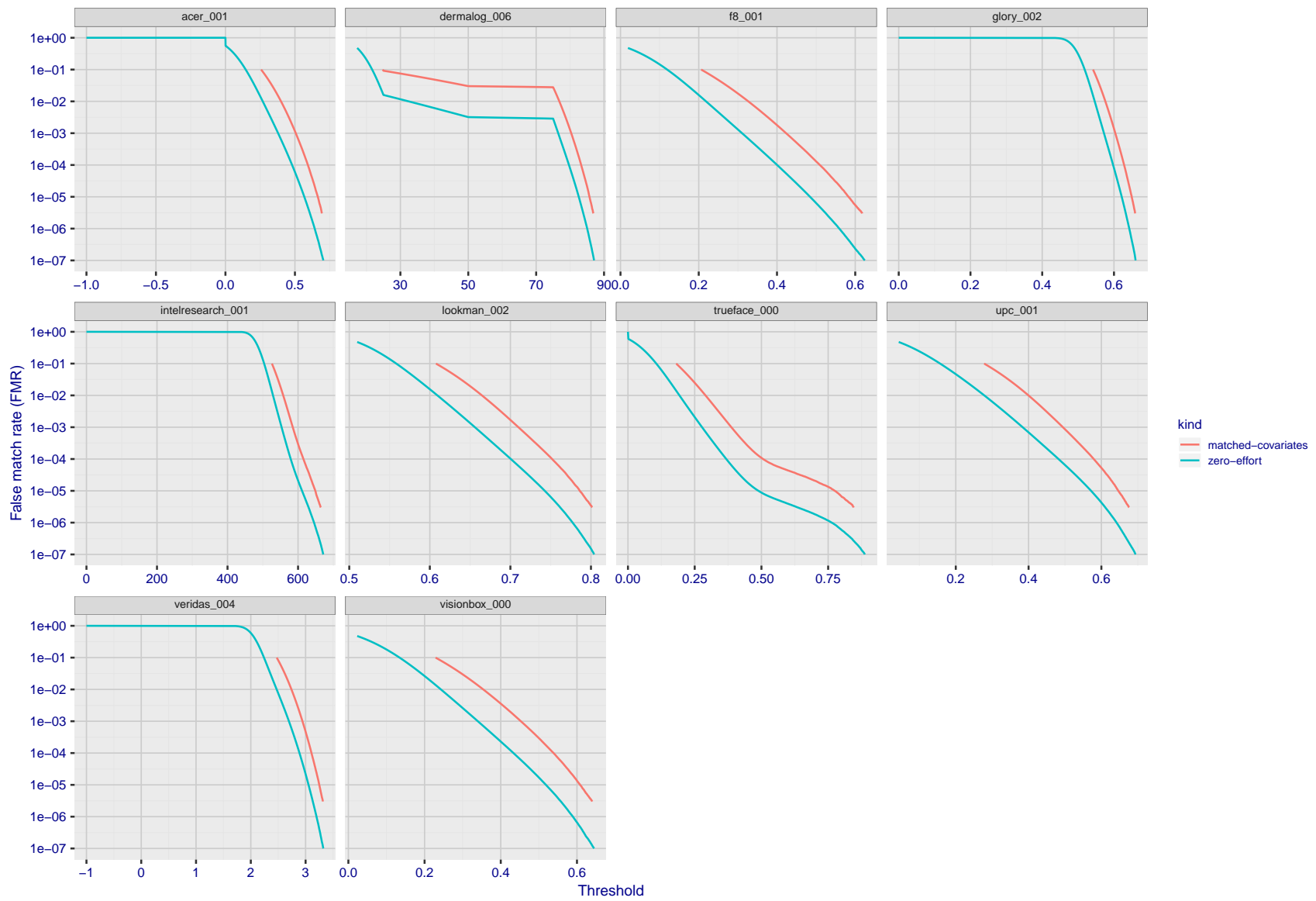


Figure 140: For the visa images, the false match calibration curves show FMR vs. threshold, T . The blue (lower) curves are for zero-effort impostors (i.e. comparing all images against all). The red (upper) curves are for persons of the same-sex, same-age, and same national-origin. This shows that FMR is underestimated (by a factor of 10 or more) by using a zero-effort impostor calculation to calibrate T . As shown later (sec. 3.6), FMR is higher for demographic-matched impostors.

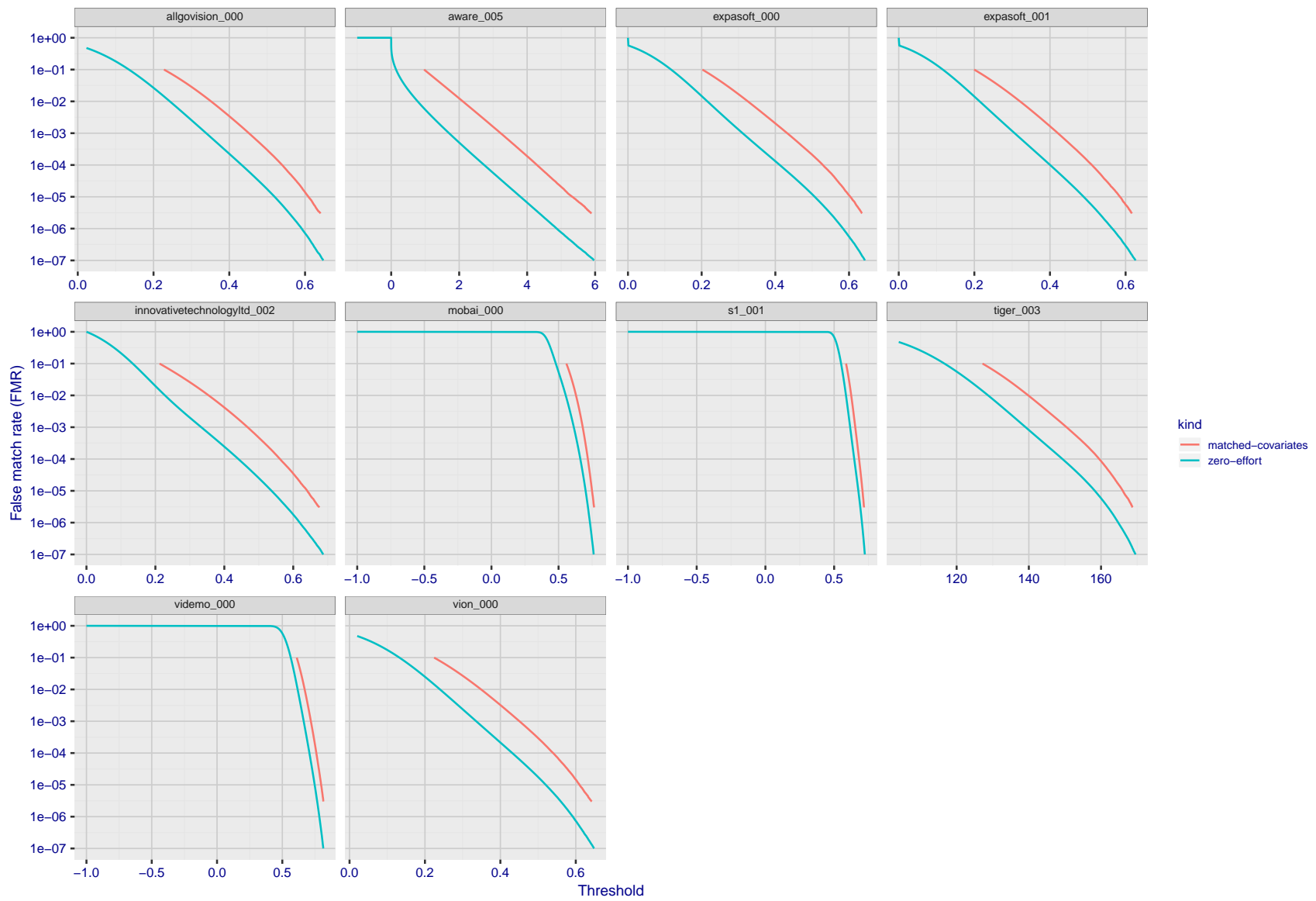


Figure 141: For the visa images, the false match calibration curves show FMR vs. threshold, T . The blue (lower) curves are for zero-effort impostors (i.e. comparing all images against all). The red (upper) curves are for persons of the same-sex, same-age, and same national-origin. This shows that FMR is underestimated (by a factor of 10 or more) by using a zero-effort impostor calculation to calibrate T . As shown later (sec. 3.6), FMR is higher for demographic-matched impostors.

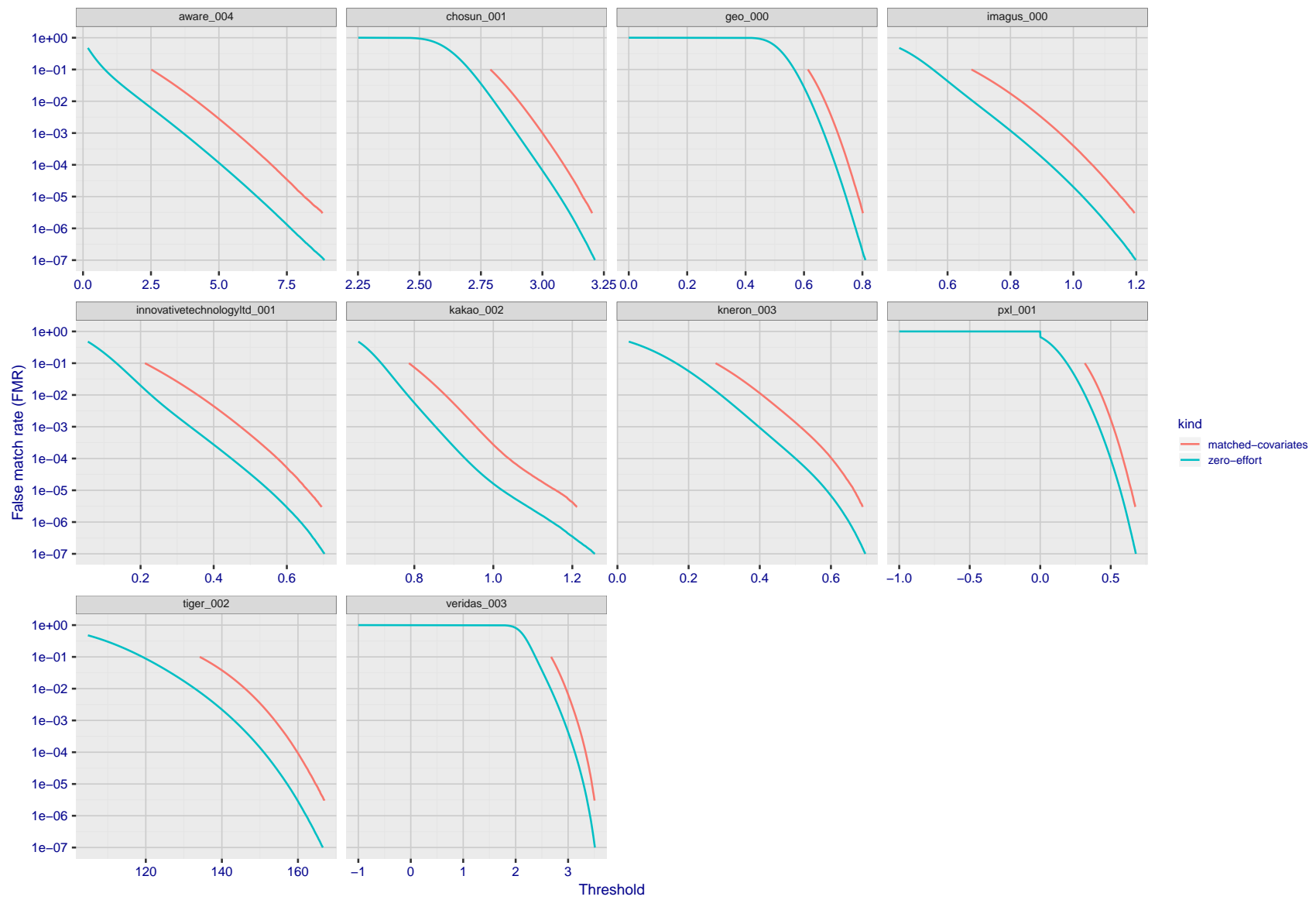


Figure 142: For the visa images, the false match calibration curves show FMR vs. threshold, T . The blue (lower) curves are for zero-effort impostors (i.e. comparing all images against all). The red (upper) curves are for persons of the same-sex, same-age, and same national-origin. This shows that FMR is underestimated (by a factor of 10 or more) by using a zero-effort impostor calculation to calibrate T . As shown later (sec. 3.6), FMR is higher for demographic-matched impostors.

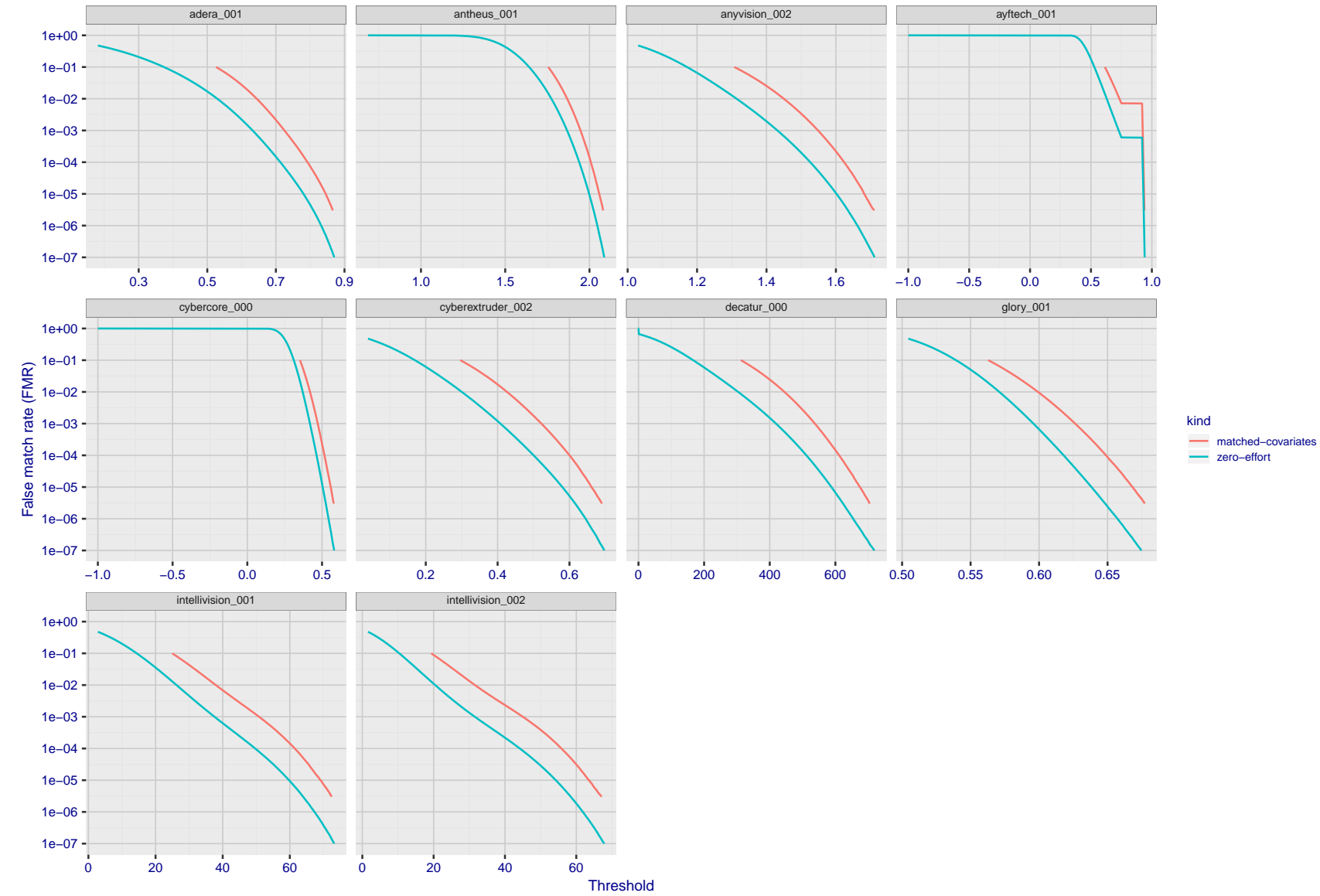


Figure 143: For the visa images, the false match calibration curves show FMR vs. threshold, T . The blue (lower) curves are for zero-effort impostors (i.e. comparing all images against all). The red (upper) curves are for persons of the same-sex, same-age, and same national-origin. This shows that FMR is underestimated (by a factor of 10 or more) by using a zero-effort impostor calculation to calibrate T . As shown later (sec. 3.6), FMR is higher for demographic-matched impostors.

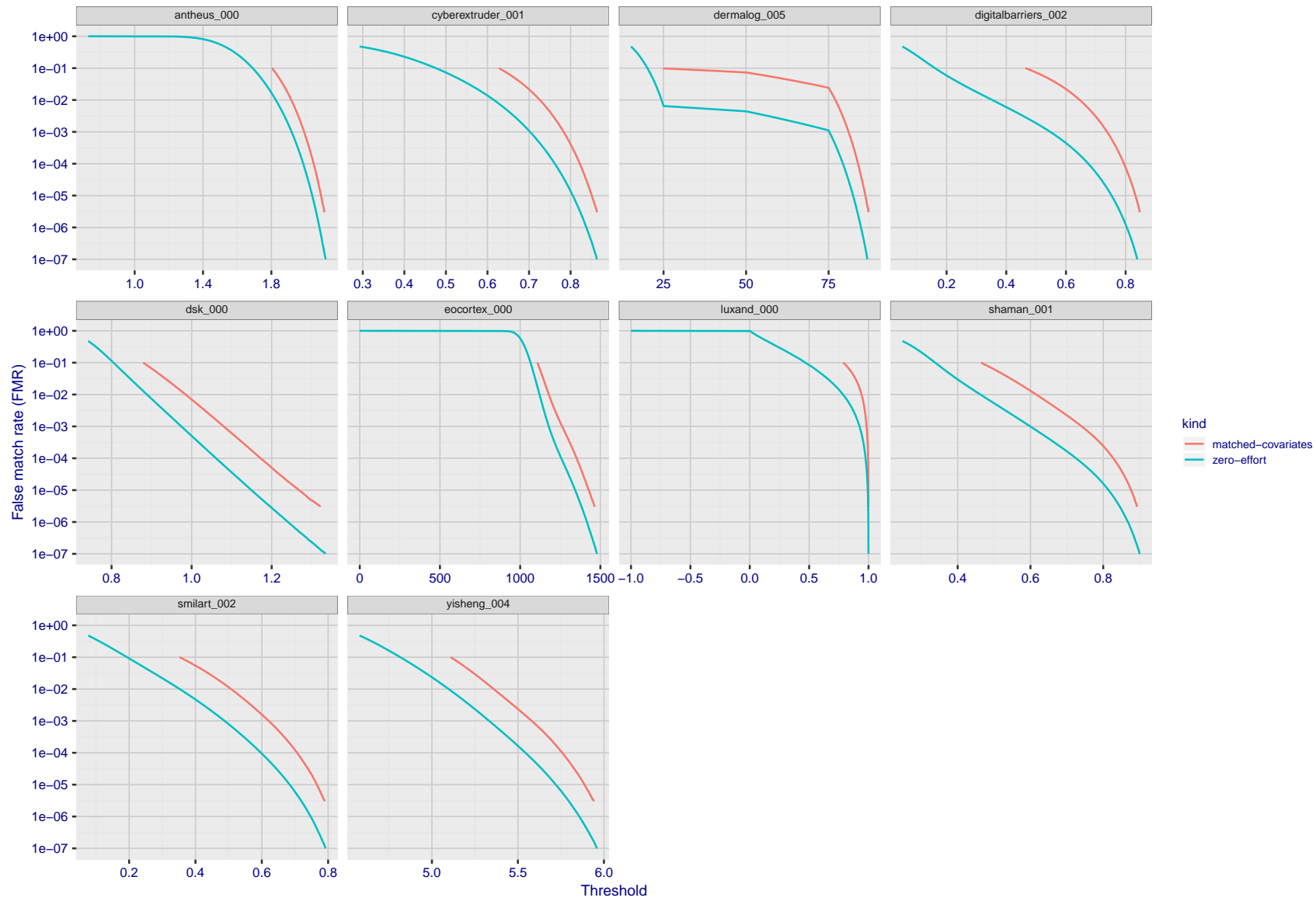
2020/09/08
12:09:14

Figure 144: For the visa images, the false match calibration curves show FMR vs. threshold, T . The blue (lower) curves are for zero-effort impostors (i.e. comparing all images against all). The red (upper) curves are for persons of the same-sex, same-age, and same national-origin. This shows that FMR is underestimated (by a factor of 10 or more) by using a zero-effort impostor calculation to calibrate T . As shown later (sec. 3.6), FMR is higher for demographic-matched impostors.

FNMR(T)
"False non-match rate"
"False match rate"

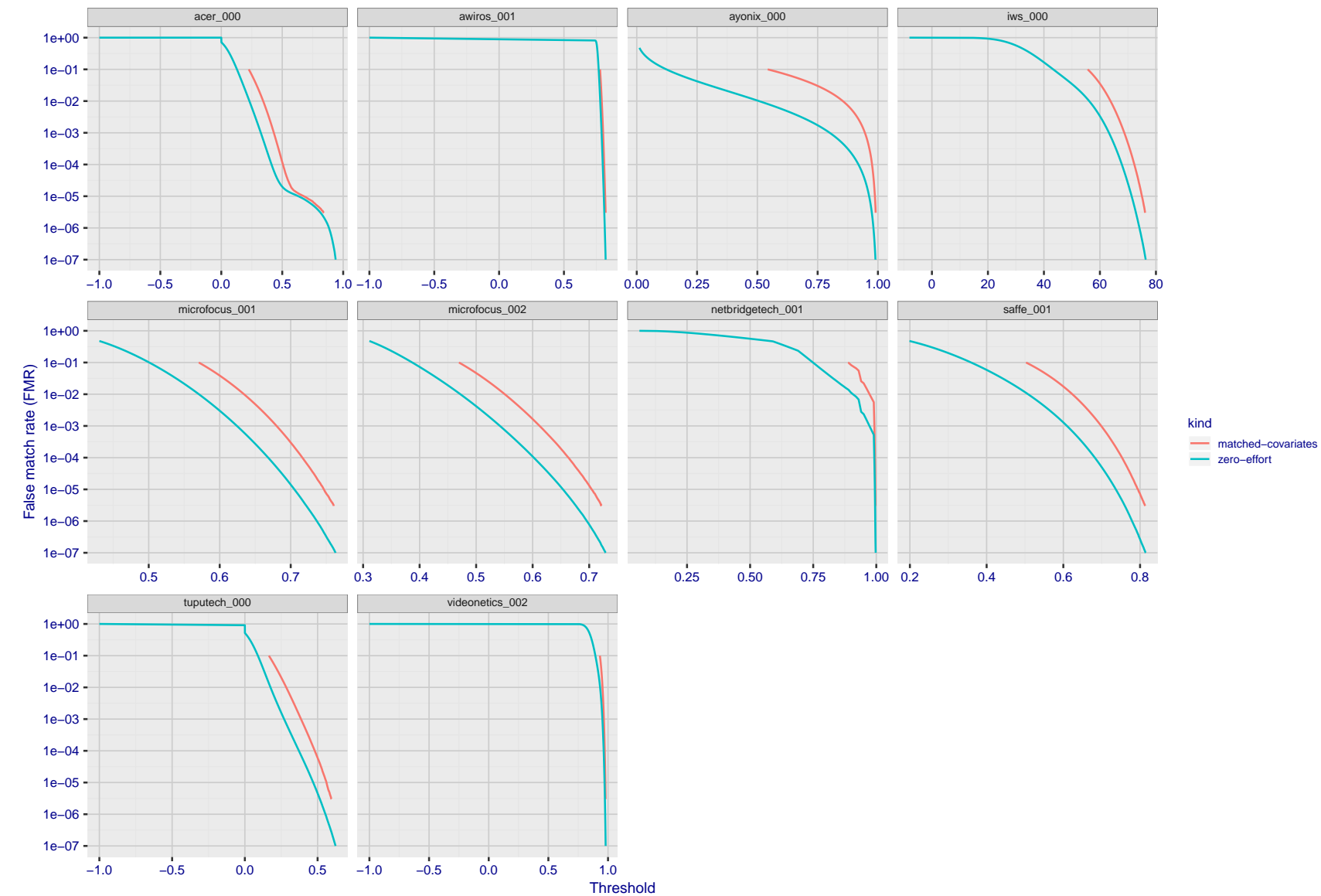


Figure 145: For the visa images, the false match calibration curves show FMR vs. threshold, T . The blue (lower) curves are for zero-effort impostors (i.e. comparing all images against all). The red (upper) curves are for persons of the same-sex, same-age, and same national-origin. This shows that FMR is underestimated (by a factor of 10 or more) by using a zero-effort impostor calculation to calibrate T . As shown later (sec. 3.6), FMR is higher for demographic-matched impostors.

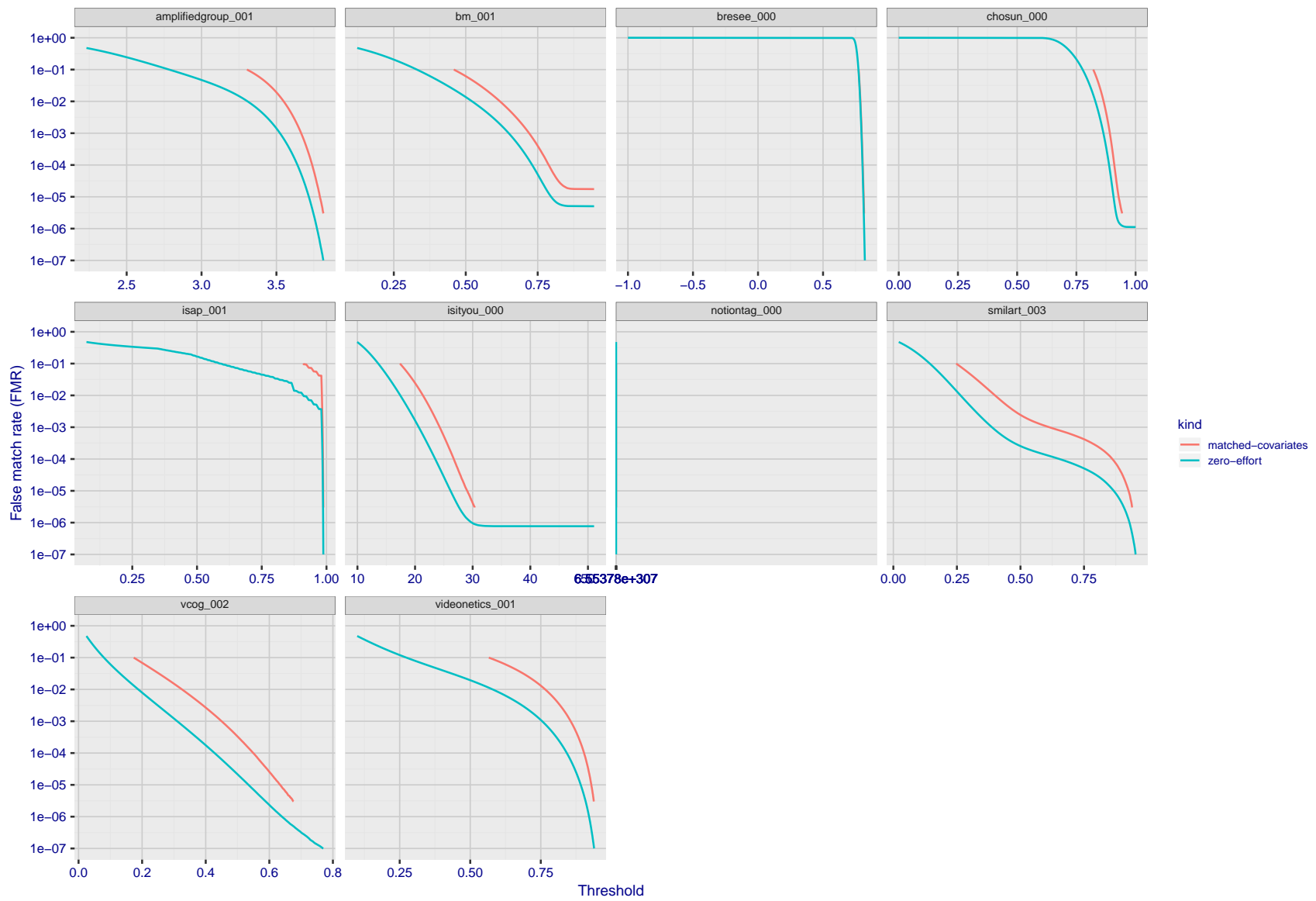


Figure 146: For the visa images, the false match calibration curves show FMR vs. threshold, T . The blue (lower) curves are for zero-effort impostors (i.e. comparing all images against all). The red (upper) curves are for persons of the same-sex, same-age, and same national-origin. This shows that FMR is underestimated (by a factor of 10 or more) by using a zero-effort impostor calculation to calibrate T . As shown later (sec. 3.6), FMR is higher for demographic-matched impostors.

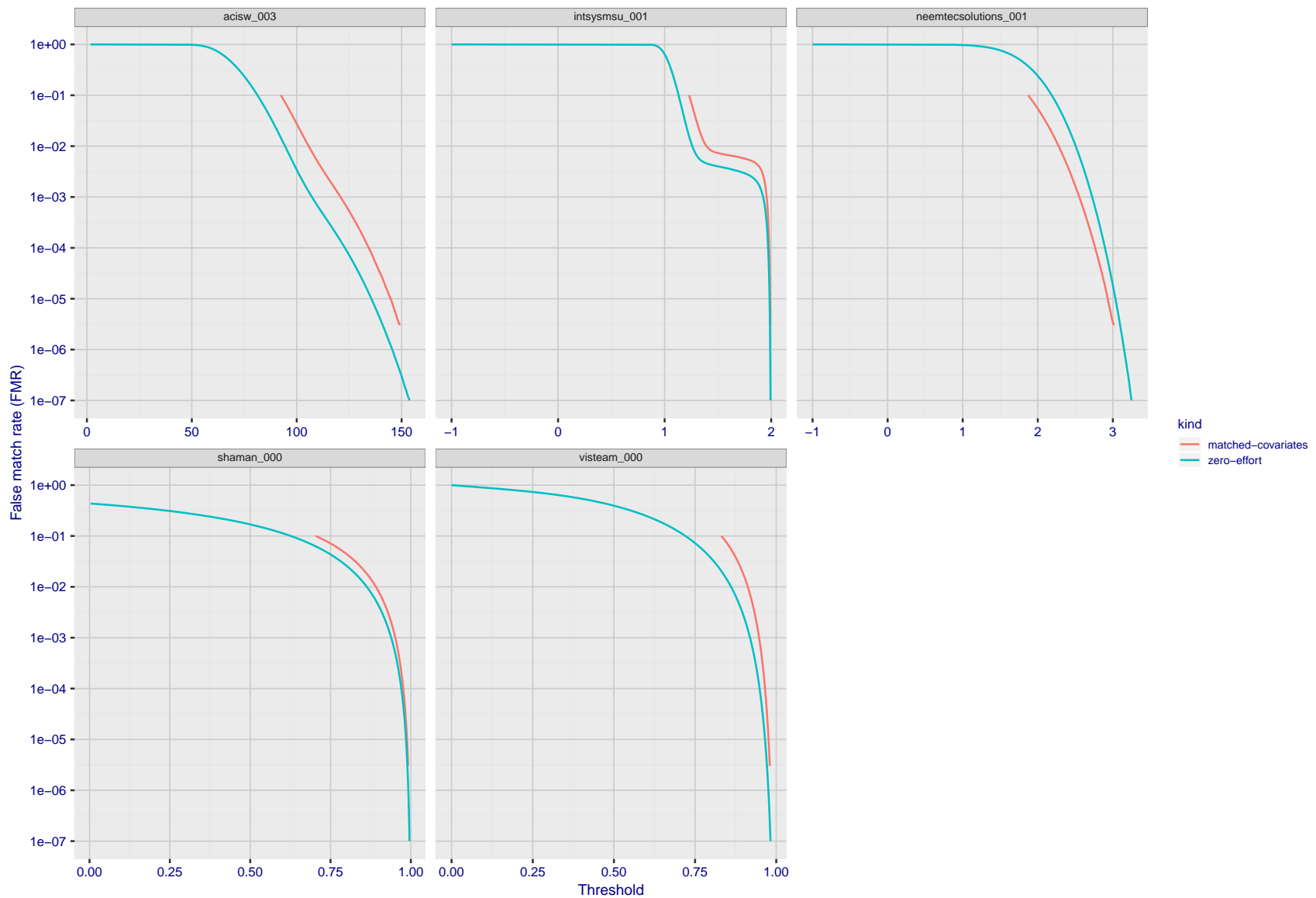


Figure 147: For the visa images, the false match calibration curves show FMR vs. threshold, T . The blue (lower) curves are for zero-effort impostors (i.e. comparing all images against all). The red (upper) curves are for persons of the same-sex, same-age, and same national-origin. This shows that FMR is underestimated (by a factor of 10 or more) by using a zero-effort impostor calculation to calibrate T . As shown later (sec. 3.6), FMR is higher for demographic-matched impostors.

3.5 Genuine distribution stability

3.5.1 Effect of birth place on the genuine distribution

Background: Both skin tone and bone structure vary geographically. Prior studies have reported variations in FNMR and FMR.

Goal: To measure false non-match rate (FNMR) variation with country of birth.

Methods: Thresholds are determined that give $FMR = \{0.001, 0.0001\}$ over the entire impostor set. Then FNMR is measured over 1000 bootstrap replications of the genuine scores. Only those countries with at least 140 individuals are included in the analysis.

Results: Figure 167 shows FNMR by country of birth for the two thresholds.

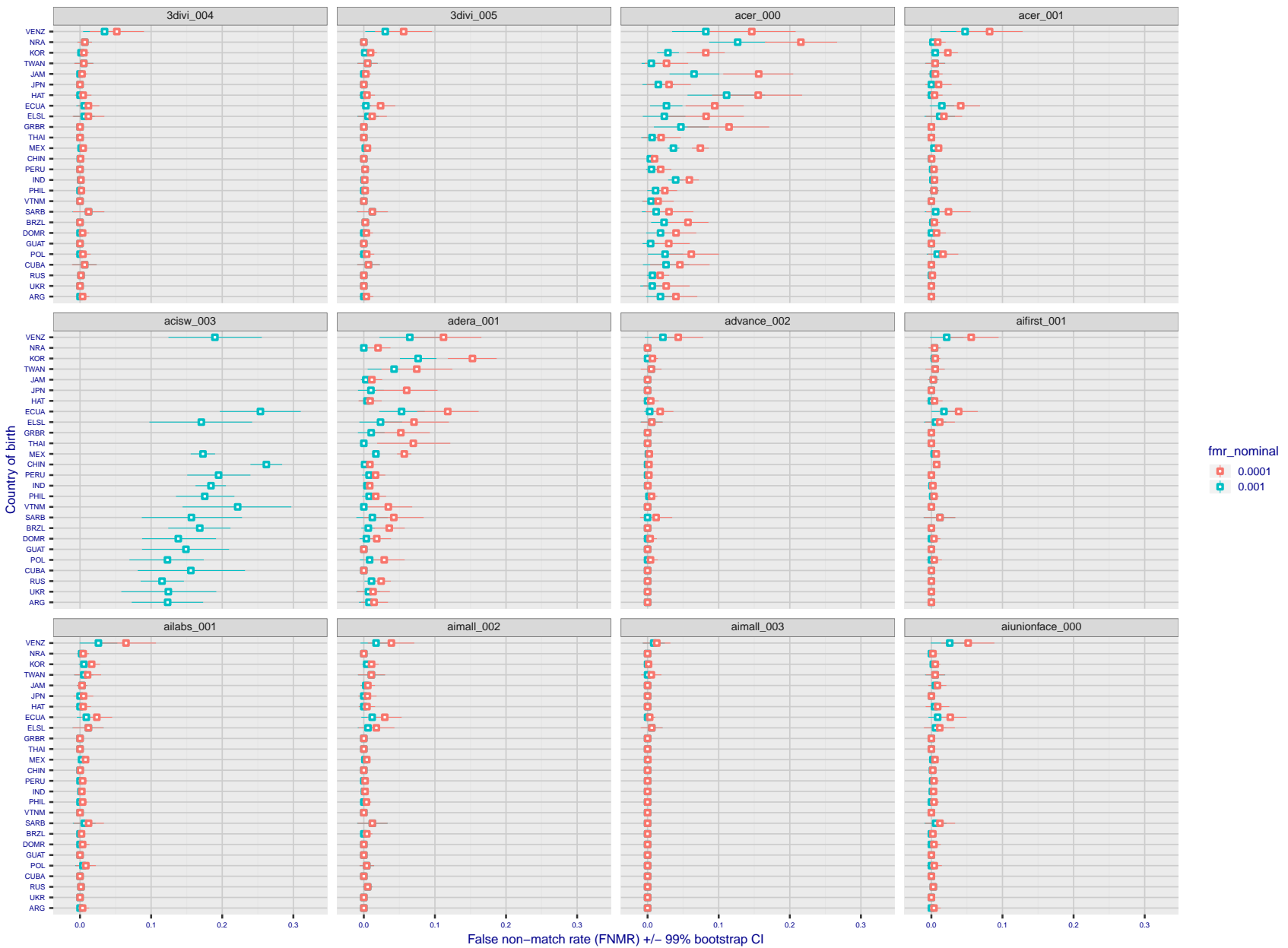


Figure 148: For the visa images, the dots show FNMR by country of birth for two globally set operating thresholds corresponding to $FMR = \{0.001, 0.0001\}$ computed over all on the order of 10^{10} impostor scores. The FMR in each bin will vary also - see subsequent impostor heatmaps in sec. 3.6.1. The figures shows an order of magnitude variation in FNMR across country of birth; these effects are likely due quality variations, then demographics like age and race. The error rates in some cases are zero, and in others the DET is flat so the error rates at the two thresholds are identical. The lines span 1% and 99% of bootstrap replicated FNMR estimates.

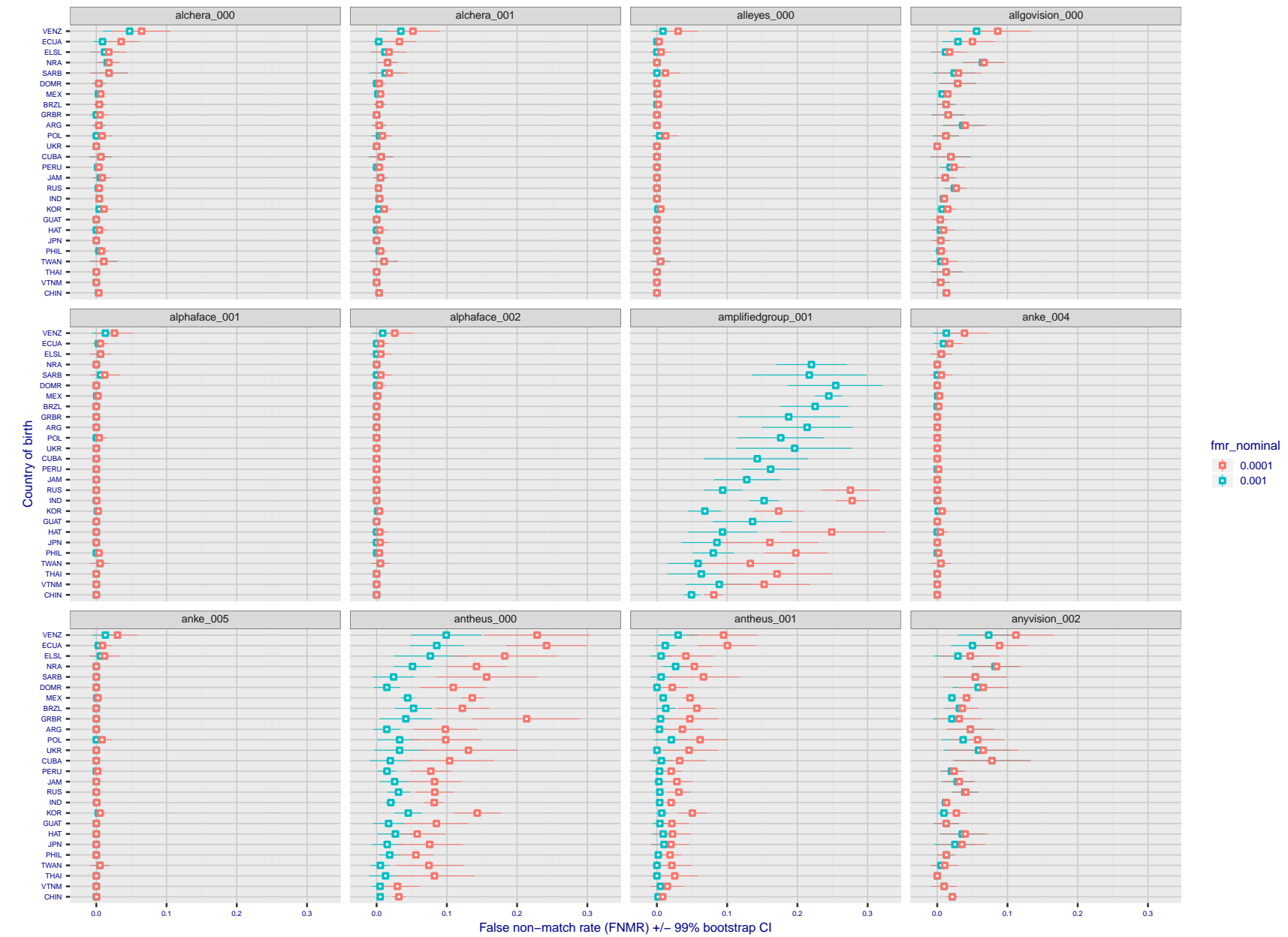


Figure 149: For the visa images, the dots show FNMR by country of birth for two globally set operating thresholds corresponding to $FMR = \{0.001, 0.0001\}$ computed over all on the order of 10^{10} impostor scores. The FMR in each bin will vary also - see subsequent impostor heatmaps in sec. 3.6.1. The figures shows an order of magnitude variation in FNMR across country of birth; these effects are likely due quality variations, then demographics like age and race. The error rates in some cases are zero, and in others the DET is flat so the error rates at the two thresholds are identical. The lines span 1% and 99% of bootstrap replicated FNMR estimates.

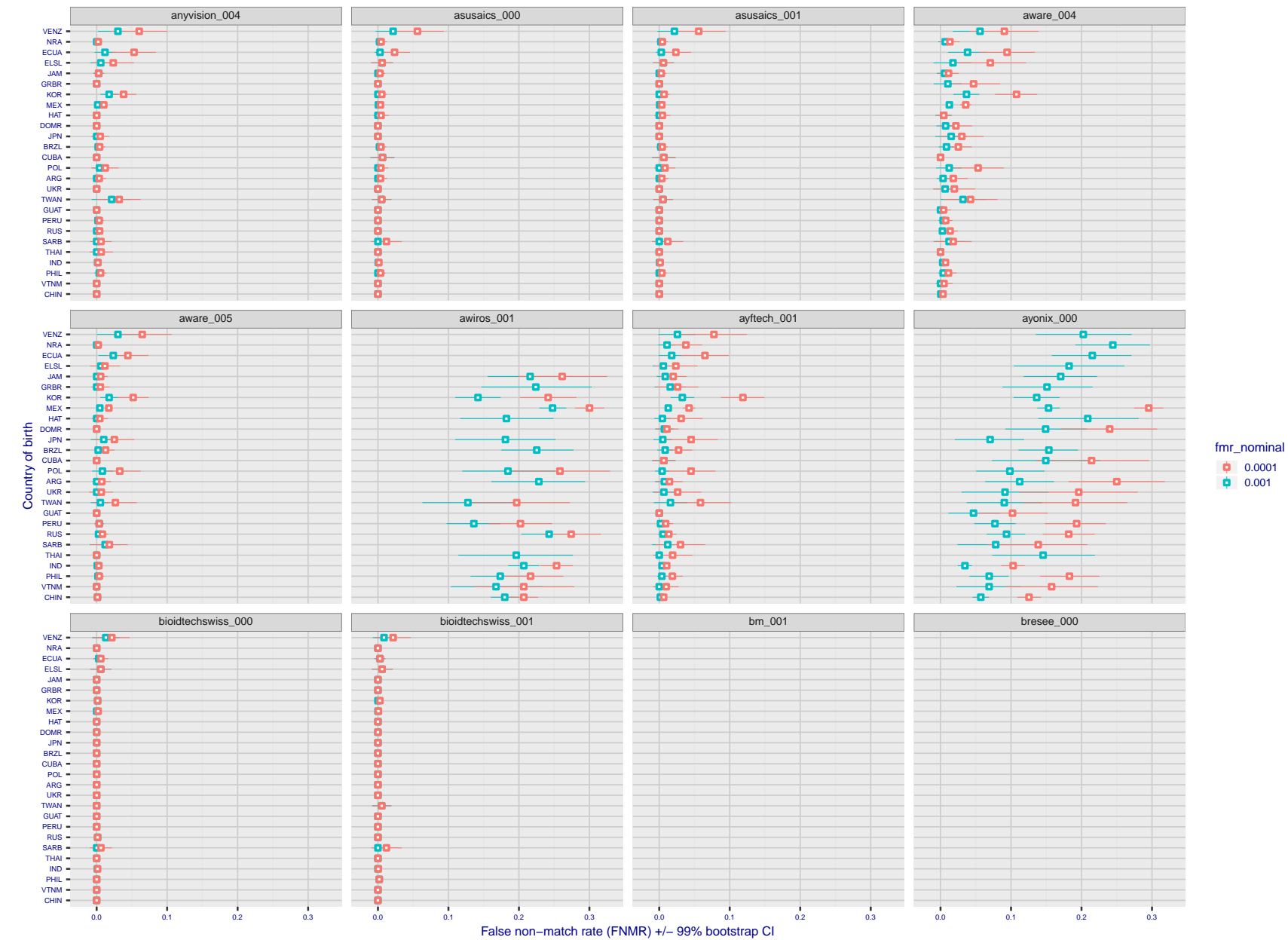


Figure 150: For the visa images, the dots show FNMR by country of birth for two globally set operating thresholds corresponding to $FMR = \{0.001, 0.0001\}$ computed over all on the order of 10^{10} impostor scores. The FMR in each bin will vary also - see subsequent impostor heatmaps in sec. 3.6.1. The figures shows an order of magnitude variation in FNMR across country of birth; these effects are likely due quality variations, then demographics like age and race. The error rates in some cases are zero, and in others the DET is flat so the error rates at the two thresholds are identical. The lines span 1% and 99% of bootstrap replicated FNMR estimates.

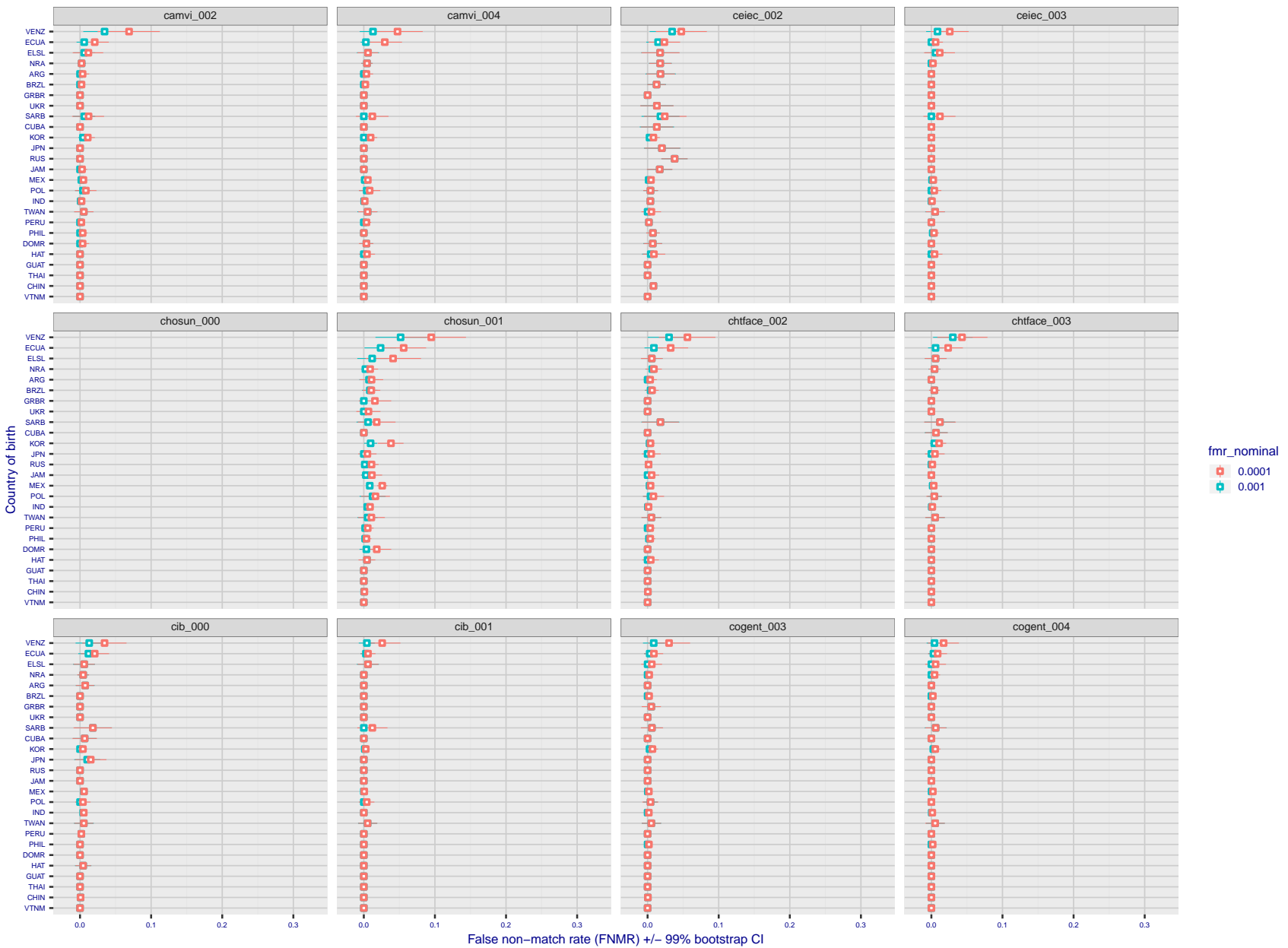


Figure 151: For the visa images, the dots show FNMR by country of birth for two globally set operating thresholds corresponding to $FMR = \{0.001, 0.0001\}$ computed over all on the order of 10^{10} impostor scores. The FMR in each bin will vary also - see subsequent impostor heatmaps in sec. 3.6.1. The figures shows an order of magnitude variation in FNMR across country of birth; these effects are likely due quality variations, then demographics like age and race. The error rates in some cases are zero, and in others the DET is flat so the error rates at the two thresholds are identical. The lines span 1% and 99% of bootstrap replicated FNMR estimates.

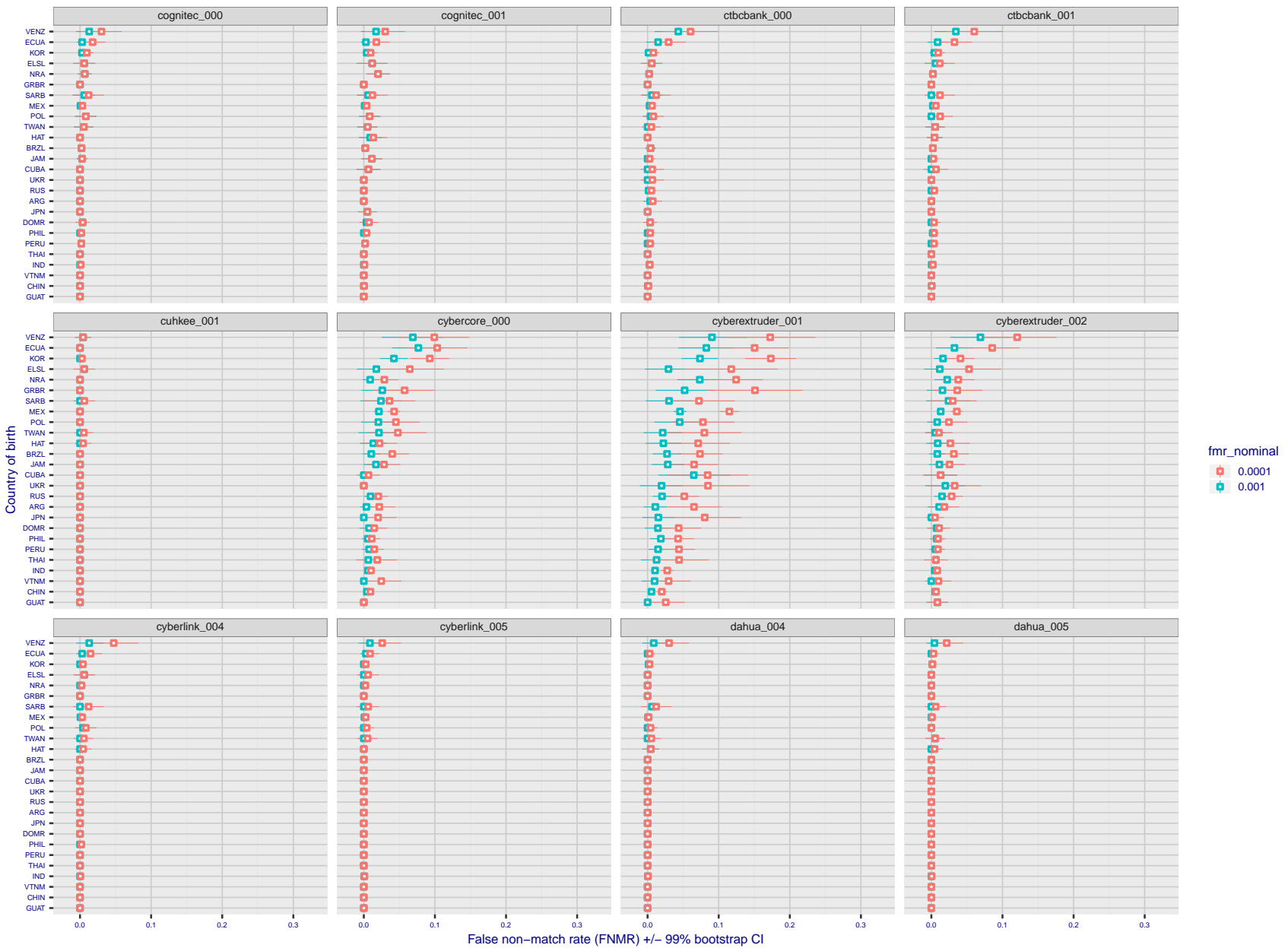


Figure 152: For the visa images, the dots show FNMR by country of birth for two globally set operating thresholds corresponding to $FMR = \{0.001, 0.0001\}$ computed over all on the order of 10^{10} impostor scores. The FMR in each bin will vary also - see subsequent impostor heatmaps in sec. 3.6.1. The figures shows an order of magnitude variation in FNMR across country of birth; these effects are likely due quality variations, then demographics like age and race. The error rates in some cases are zero, and in others the DET is flat so the error rates at the two thresholds are identical. The lines span 1% and 99% of bootstrap replicated FNMR estimates.

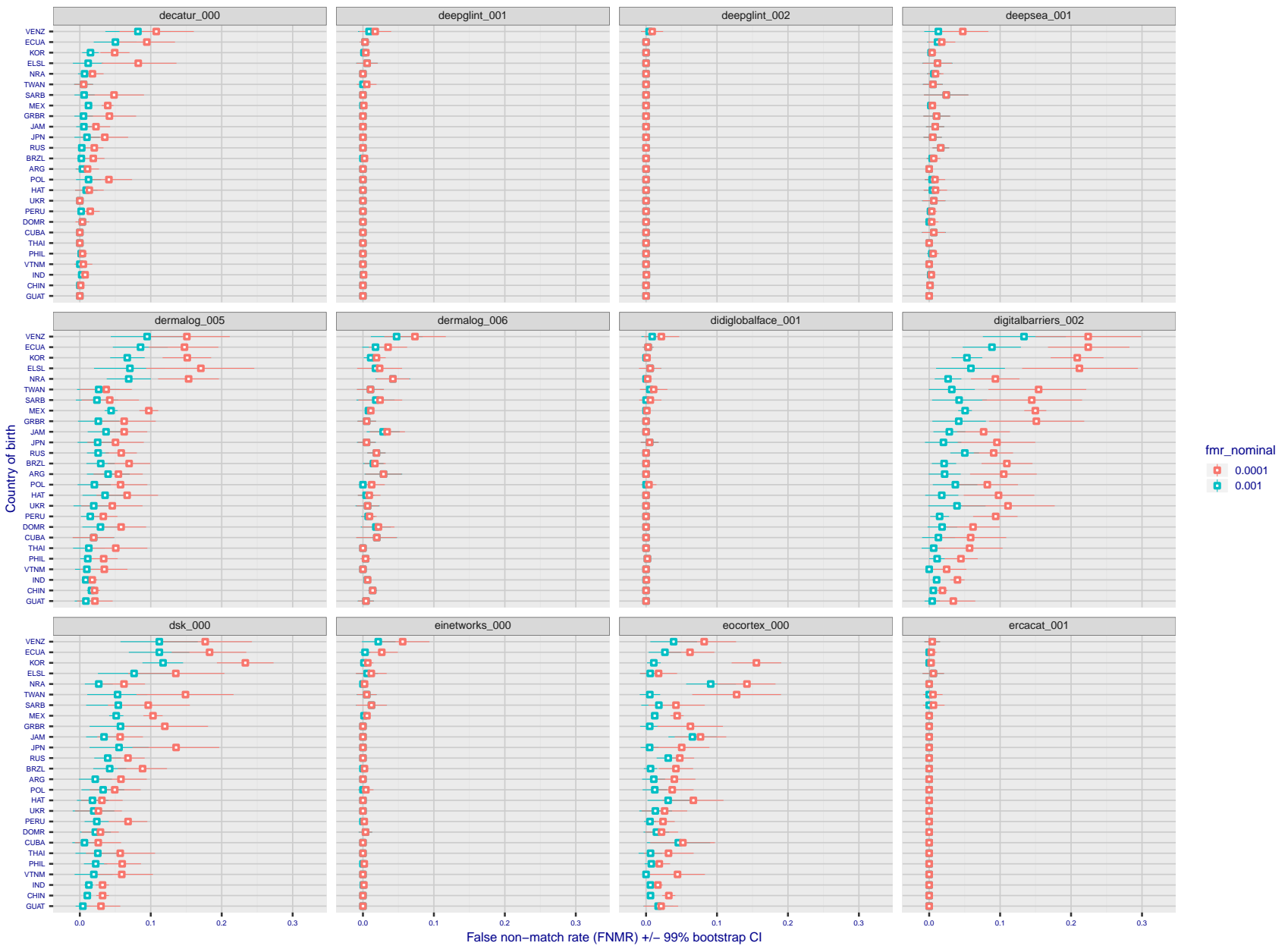


Figure 153: For the visa images, the dots show FNMR by country of birth for two globally set operating thresholds corresponding to $FMR = \{0.001, 0.0001\}$ computed over all on the order of 10^{10} impostor scores. The FMR in each bin will vary also - see subsequent impostor heatmaps in sec. 3.6.1. The figures shows an order of magnitude variation in FNMR across country of birth; these effects are likely due quality variations, then demographics like age and race. The error rates in some cases are zero, and in others the DET is flat so the error rates at the two thresholds are identical. The lines span 1% and 99% of bootstrap replicated FNMR estimates.

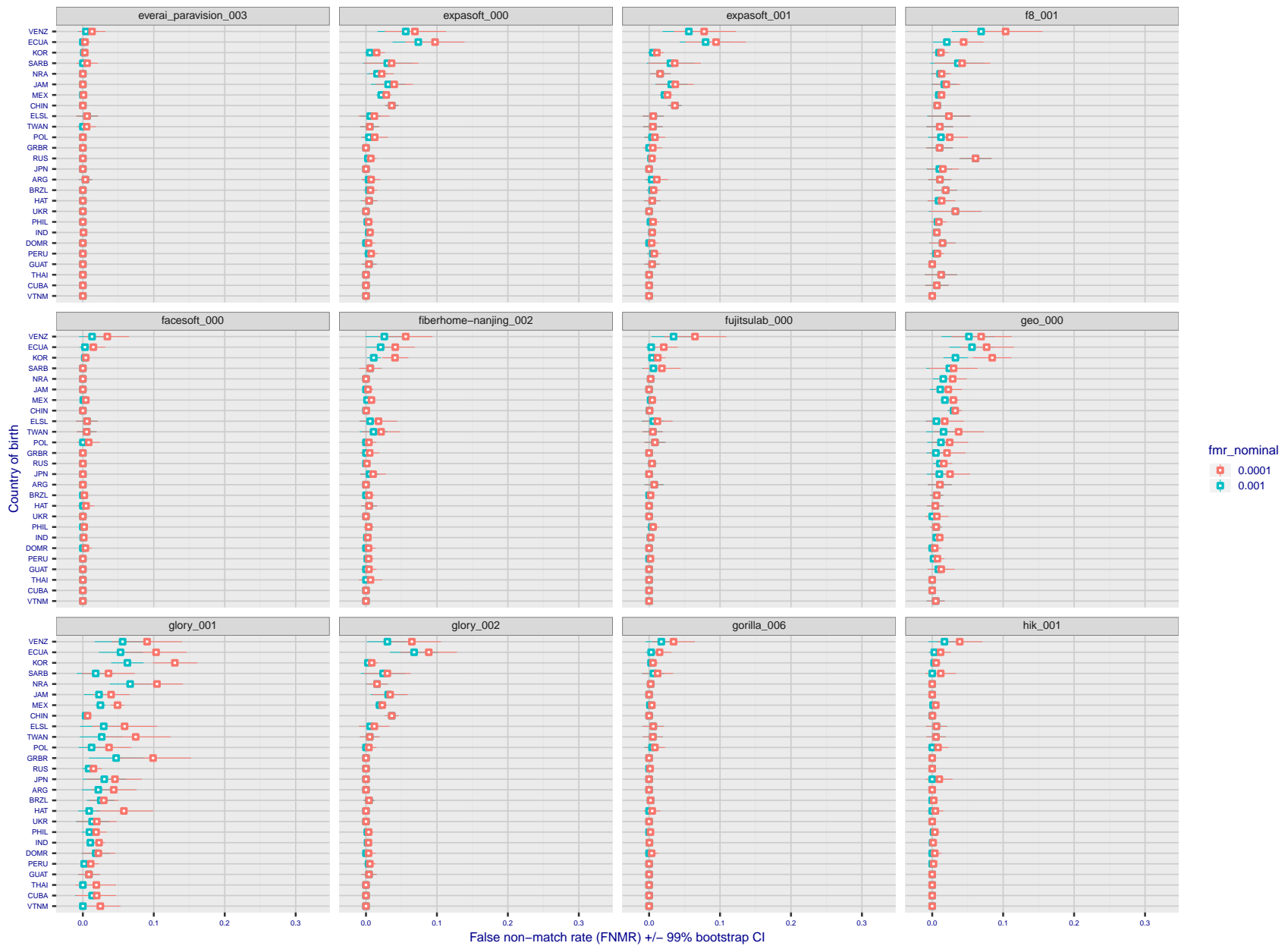


Figure 154: For the visa images, the dots show FNMR by country of birth for two globally set operating thresholds corresponding to $FMR = \{0.001, 0.0001\}$ computed over all on the order of 10^{10} impostor scores. The FMR in each bin will vary also - see subsequent impostor heatmaps in sec. 3.6.1. The figures shows an order of magnitude variation in FNMR across country of birth; these effects are likely due quality variations, then demographics like age and race. The error rates in some cases are zero, and in others the DET is flat so the error rates at the two thresholds are identical. The lines span 1% and 99% of bootstrap replicated FNMR estimates.

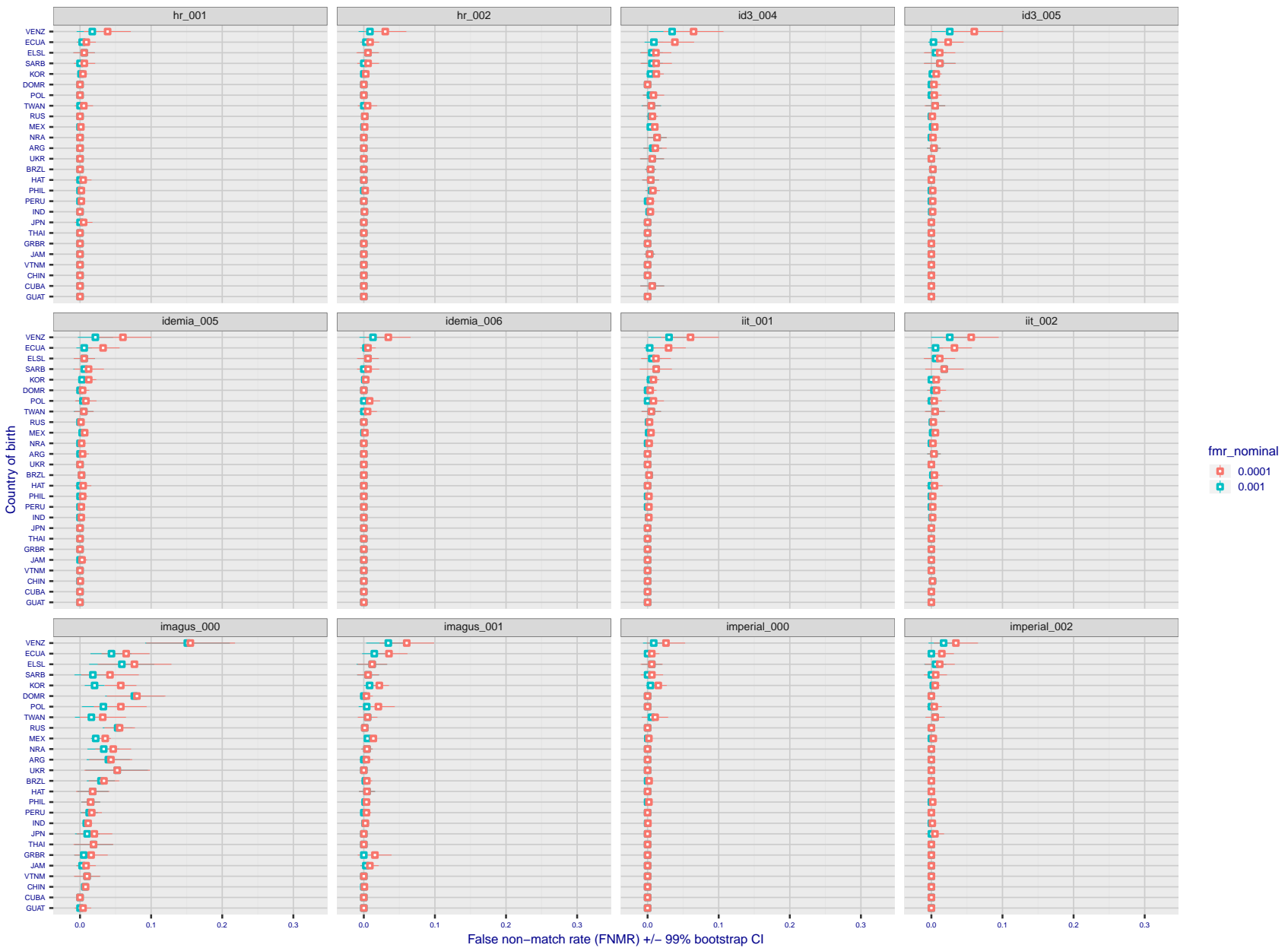


Figure 155: For the visa images, the dots show FNMR by country of birth for two globally set operating thresholds corresponding to $FMR = \{0.0001, 0.00001\}$ computed over all on the order of 10^{10} impostor scores. The FMR in each bin will vary also - see subsequent impostor heatmaps in sec. 3.6.1. The figures shows an order of magnitude variation in FNMR across country of birth; these effects are likely due quality variations, then demographics like age and race. The error rates in some cases are zero, and in others the DET is flat so the error rates at the two thresholds are identical. The lines span 1% and 99% of bootstrap replicated FNMR estimates.

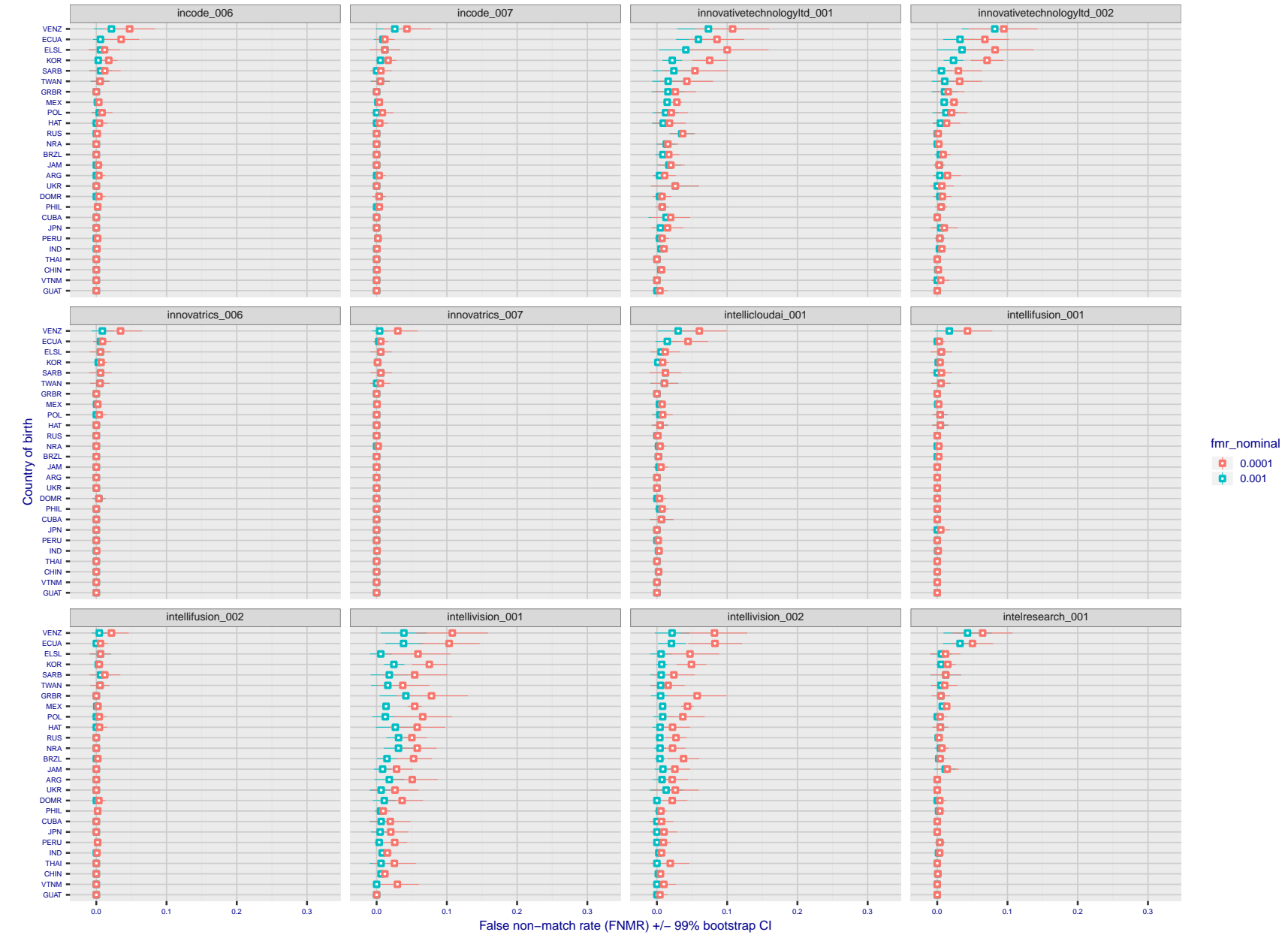


Figure 156: For the visa images, the dots show FNMR by country of birth for two globally set operating thresholds corresponding to $FMR = \{0.001, 0.0001\}$ computed over all on the order of 10^{10} impostor scores. The FMR in each bin will vary also - see subsequent impostor heatmaps in sec. 3.6.1. The figures shows an order of magnitude variation in FNMR across country of birth; these effects are likely due quality variations, then demographics like age and race. The error rates in some cases are zero, and in others the DET is flat so the error rates at the two thresholds are identical. The lines span 1% and 99% of bootstrap replicated FNMR estimates.

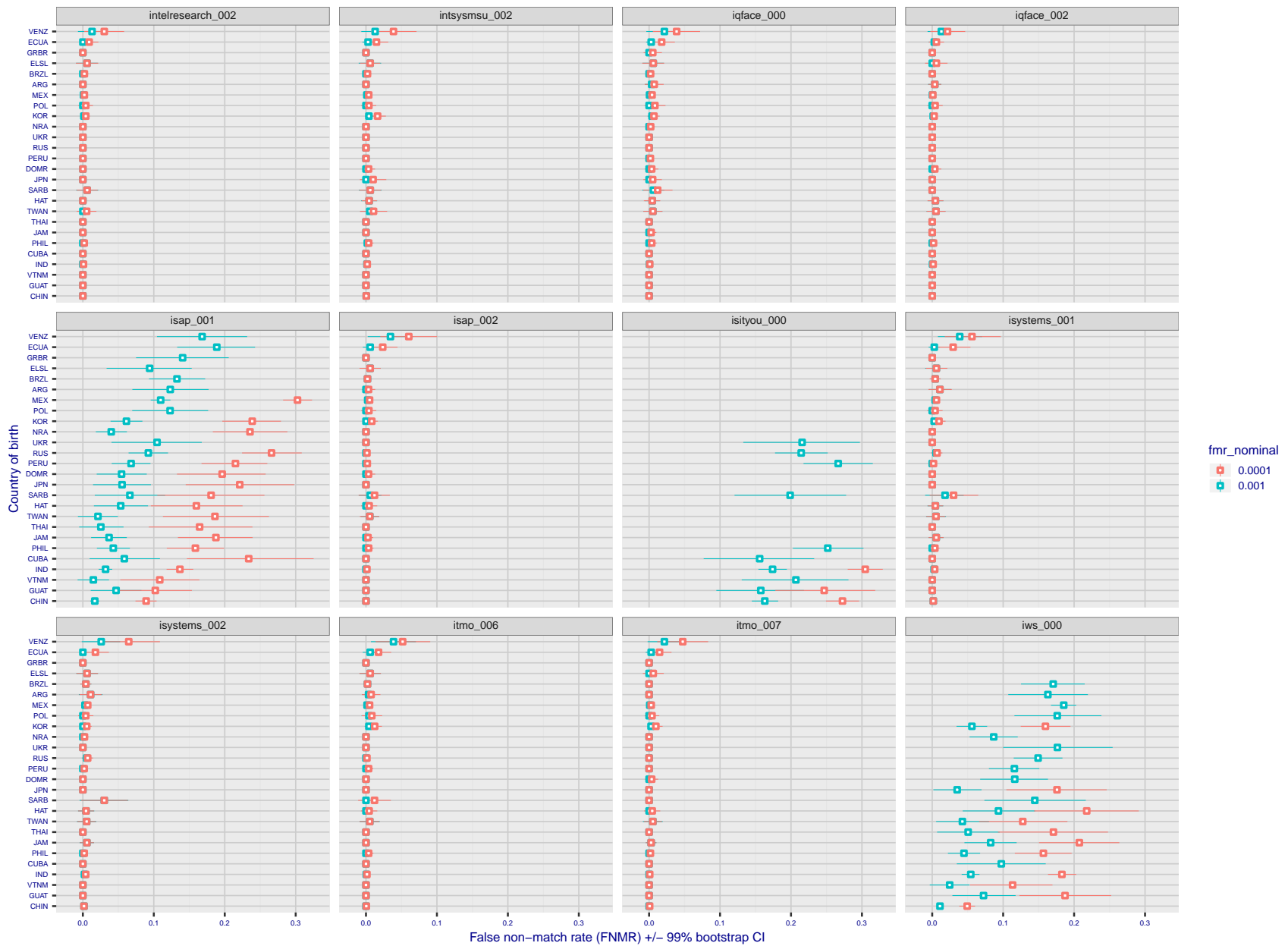


Figure 157: For the visa images, the dots show FNMR by country of birth for two globally set operating thresholds corresponding to $FMR = \{0.001, 0.0001\}$ computed over all on the order of 10^{10} impostor scores. The FMR in each bin will vary also - see subsequent impostor heatmaps in sec. 3.6.1. The figures shows an order of magnitude variation in FNMR across country of birth; these effects are likely due quality variations, then demographics like age and race. The error rates in some cases are zero, and in others the DET is flat so the error rates at the two thresholds are identical. The lines span 1% and 99% of bootstrap replicated FNMR estimates.

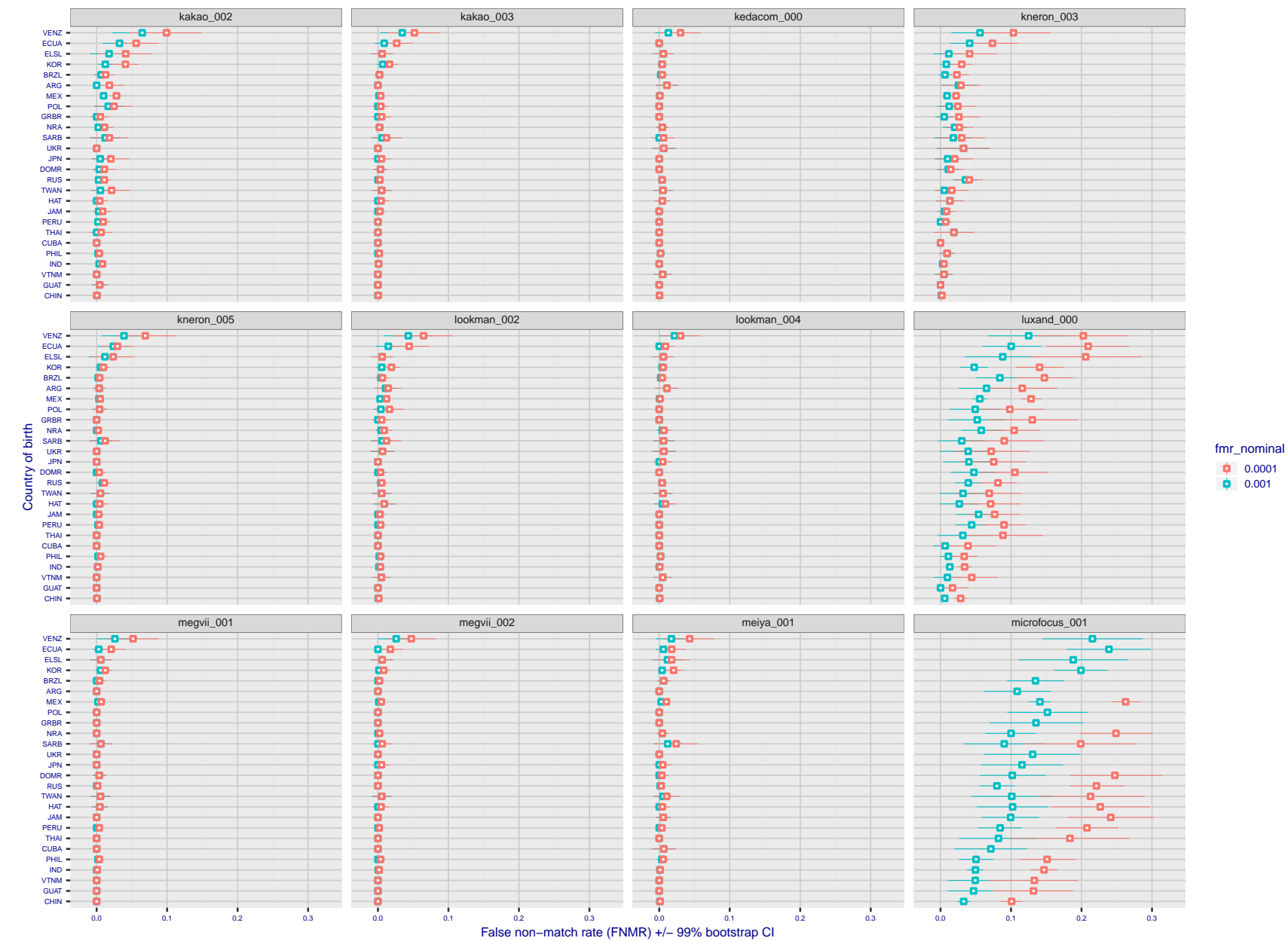


Figure 158: For the visa images, the dots show FNMR by country of birth for two globally set operating thresholds corresponding to $FMR = \{0.001, 0.0001\}$ computed over all on the order of 10^{10} impostor scores. The FMR in each bin will vary also - see subsequent impostor heatmaps in sec. 3.6.1. The figures shows an order of magnitude variation in FNMR across country of birth; these effects are likely due quality variations, then demographics like age and race. The error rates in some cases are zero, and in others the DET is flat so the error rates at the two thresholds are identical. The lines span 1% and 99% of bootstrap replicated FNMR estimates.

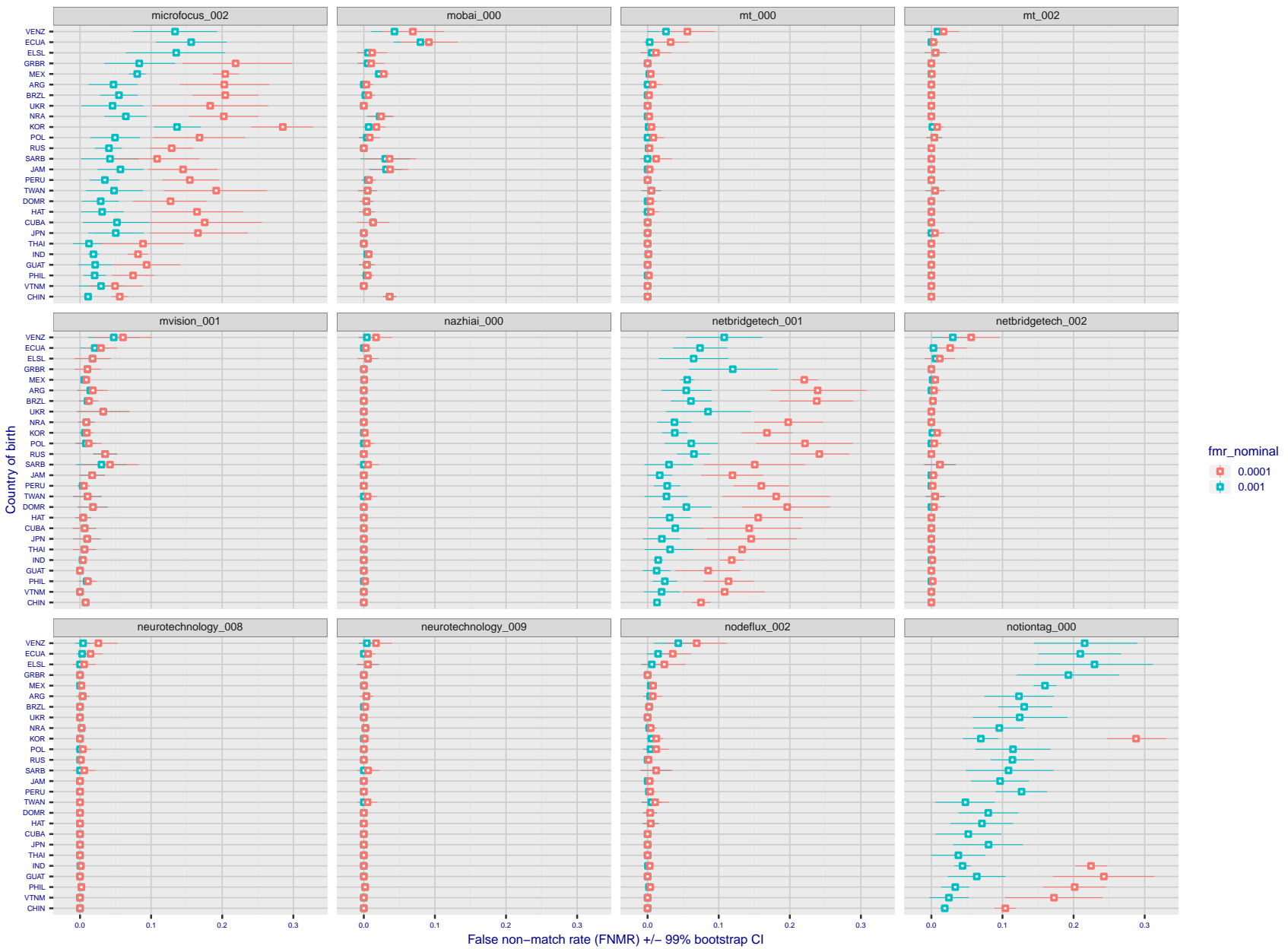


Figure 159: For the visa images, the dots show FNMR by country of birth for two globally set operating thresholds corresponding to $FMR = \{0.001, 0.0001\}$ computed over all on the order of 10^{10} impostor scores. The FMR in each bin will vary also - see subsequent impostor heatmaps in sec. 3.6.1. The figures shows an order of magnitude variation in FNMR across country of birth; these effects are likely due quality variations, then demographics like age and race. The error rates in some cases are zero, and in others the DET is flat so the error rates at the two thresholds are identical. The lines span 1% and 99% of bootstrap replicated FNMR estimates.

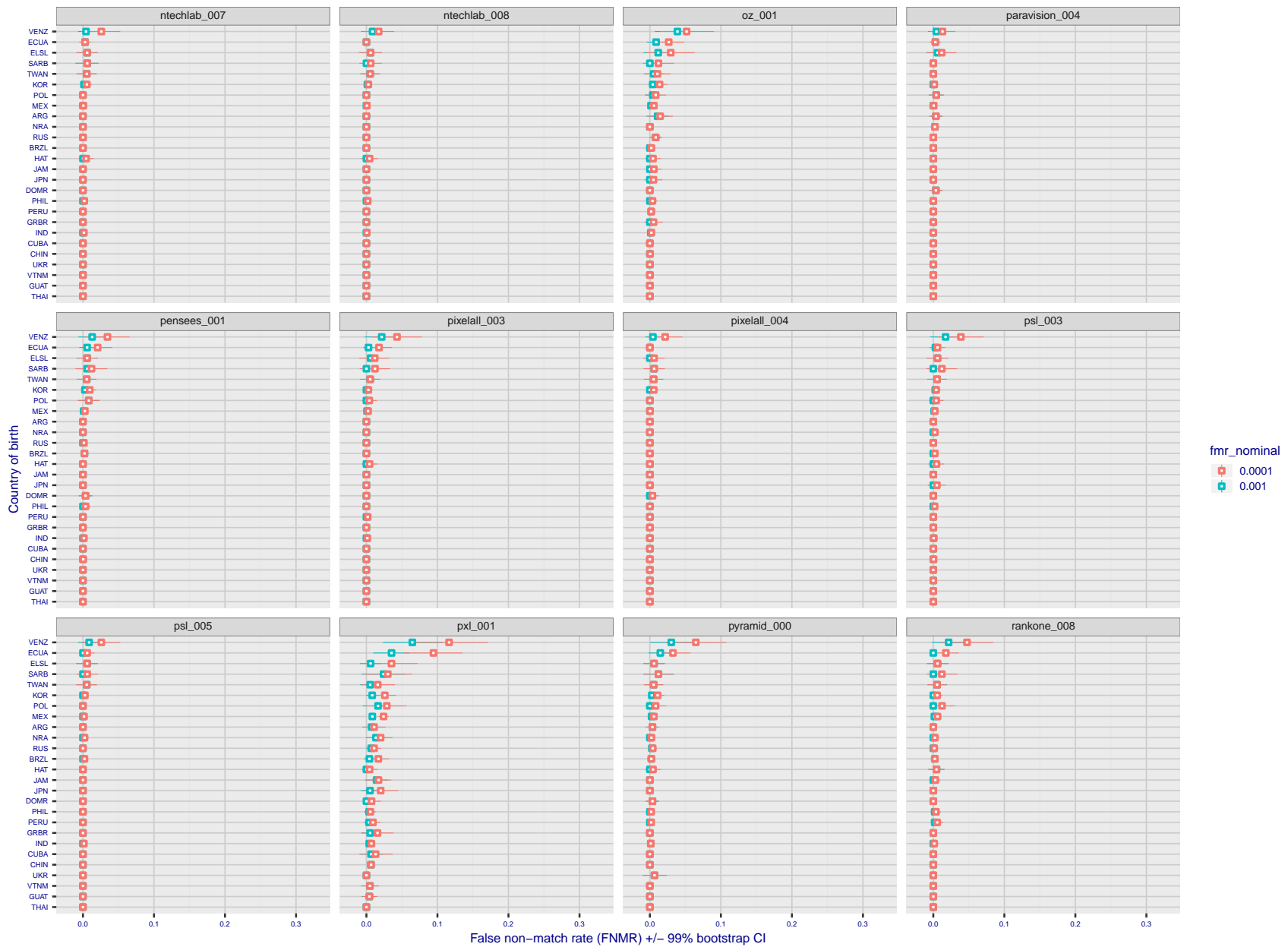


Figure 160: For the visa images, the dots show FNMR by country of birth for two globally set operating thresholds corresponding to $FMR = \{0.001, 0.0001\}$ computed over all on the order of 10^{10} impostor scores. The FMR in each bin will vary also - see subsequent impostor heatmaps in sec. 3.6.1. The figures shows an order of magnitude variation in FNMR across country of birth; these effects are likely due quality variations, then demographics like age and race. The error rates in some cases are zero, and in others the DET is flat so the error rates at the two thresholds are identical. The lines span 1% and 99% of bootstrap replicated FNMR estimates.

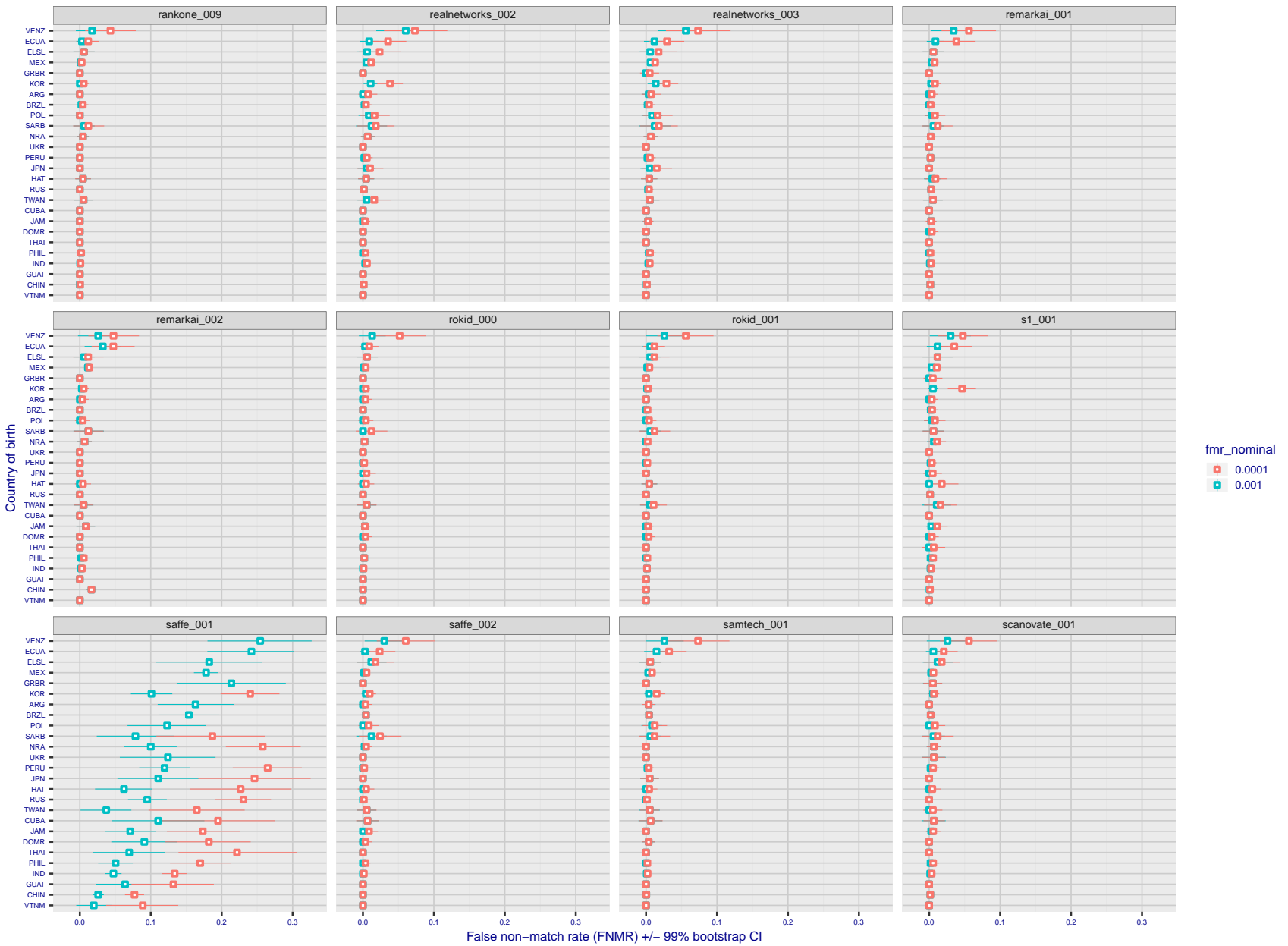


Figure 161: For the visa images, the dots show FNMR by country of birth for two globally set operating thresholds corresponding to $FMR = \{0.001, 0.0001\}$ computed over all on the order of 10^{10} impostor scores. The FMR in each bin will vary also - see subsequent impostor heatmaps in sec. 3.6.1. The figures shows an order of magnitude variation in FNMR across country of birth; these effects are likely due quality variations, then demographics like age and race. The error rates in some cases are zero, and in others the DET is flat so the error rates at the two thresholds are identical. The lines span 1% and 99% of bootstrap replicated FNMR estimates.

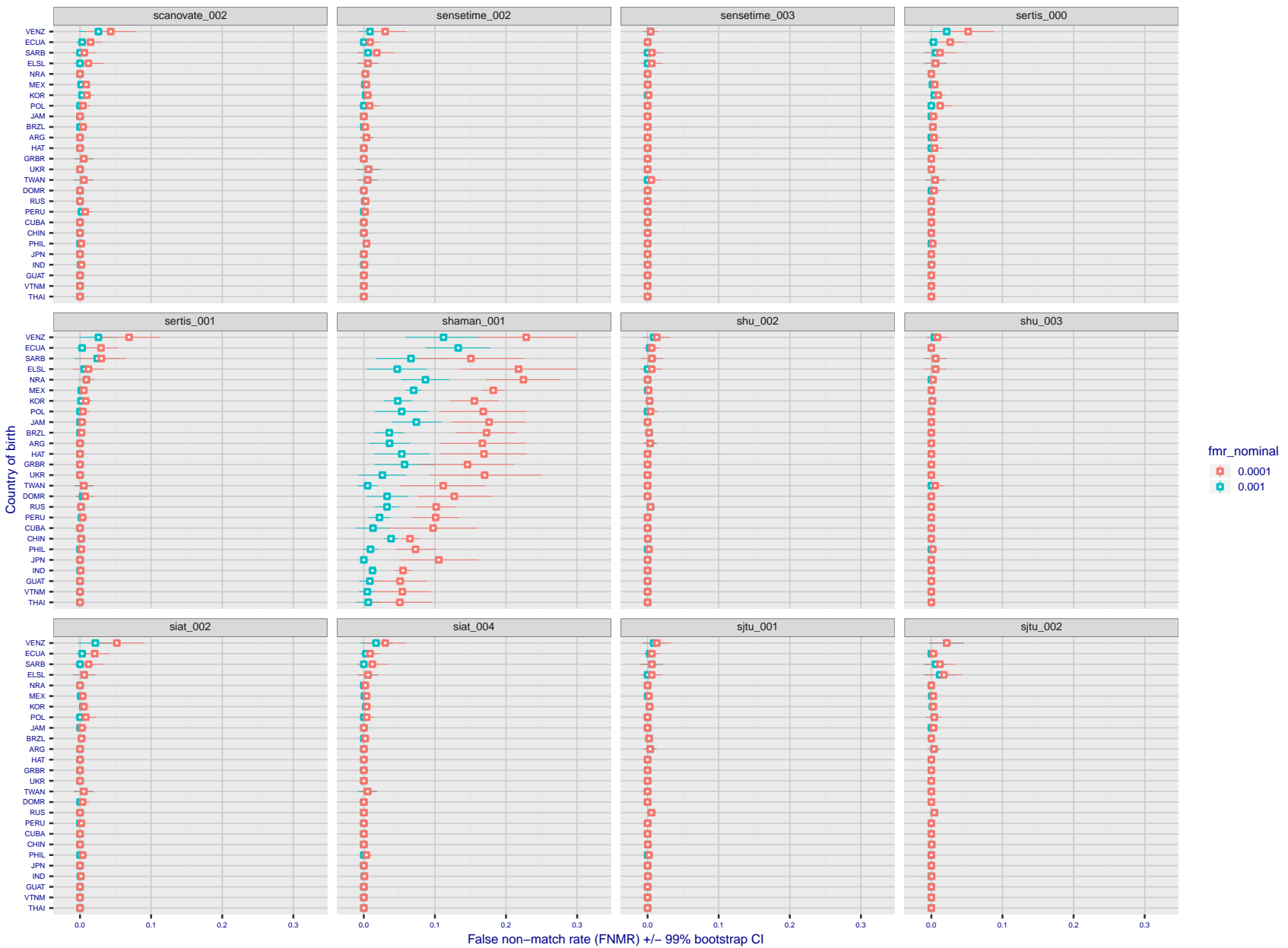


Figure 162: For the visa images, the dots show FNMR by country of birth for two globally set operating thresholds corresponding to $FMR = \{0.001, 0.0001\}$ computed over all on the order of 10^{10} impostor scores. The FMR in each bin will vary also - see subsequent impostor heatmaps in sec. 3.6.1. The figures shows an order of magnitude variation in FNMR across country of birth; these effects are likely due quality variations, then demographics like age and race. The error rates in some cases are zero, and in others the DET is flat so the error rates at the two thresholds are identical. The lines span 1% and 99% of bootstrap replicated FNMR estimates.

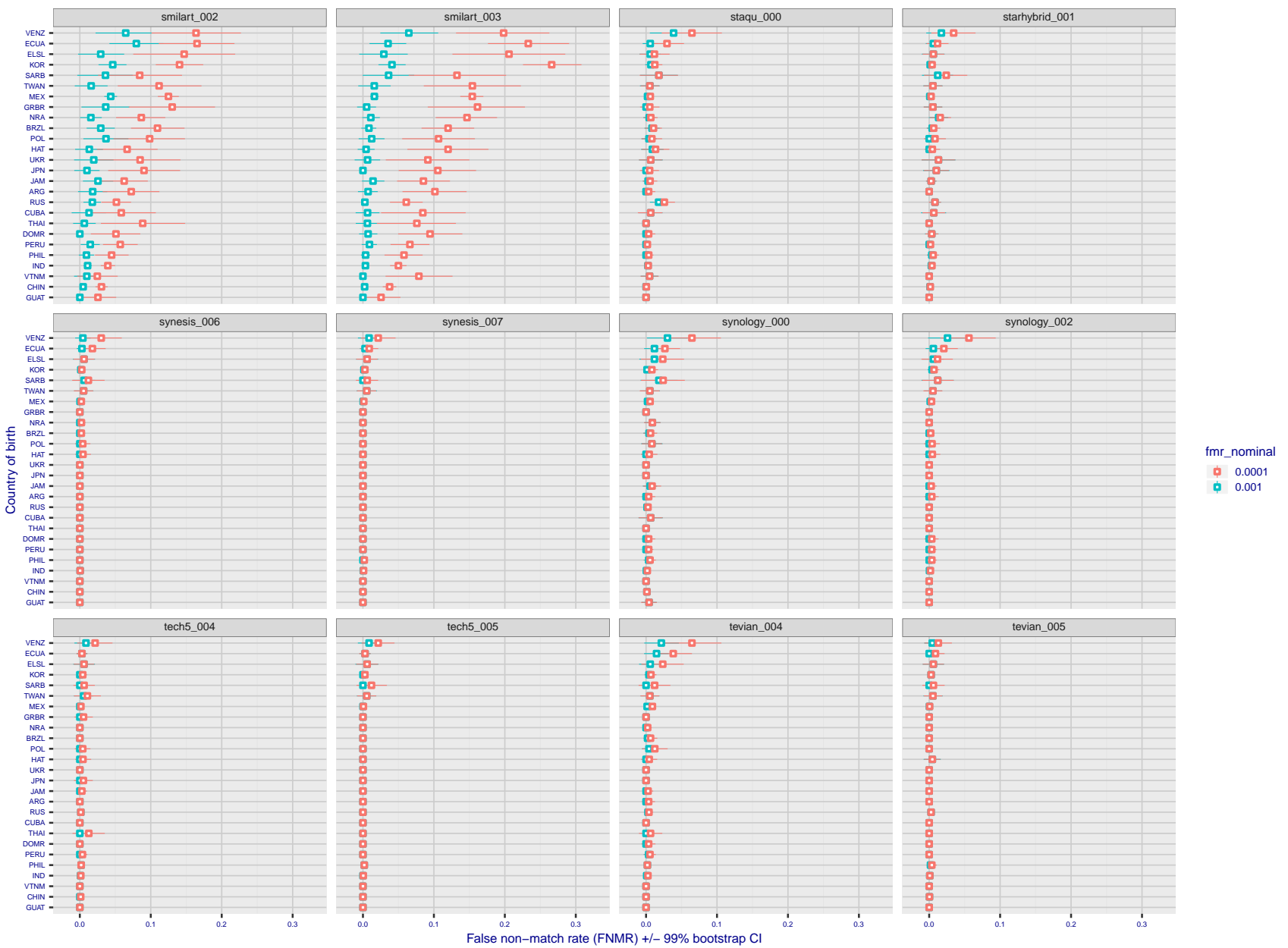


Figure 163: For the visa images, the dots show FNMR by country of birth for two globally set operating thresholds corresponding to $FMR = \{0.001, 0.0001\}$ computed over all on the order of 10^{10} impostor scores. The FMR in each bin will vary also - see subsequent impostor heatmaps in sec. 3.6.1. The figures shows an order of magnitude variation in FNMR across country of birth; these effects are likely due quality variations, then demographics like age and race. The error rates in some cases are zero, and in others the DET is flat so the error rates at the two thresholds are identical. The lines span 1% and 99% of bootstrap replicated FNMR estimates.

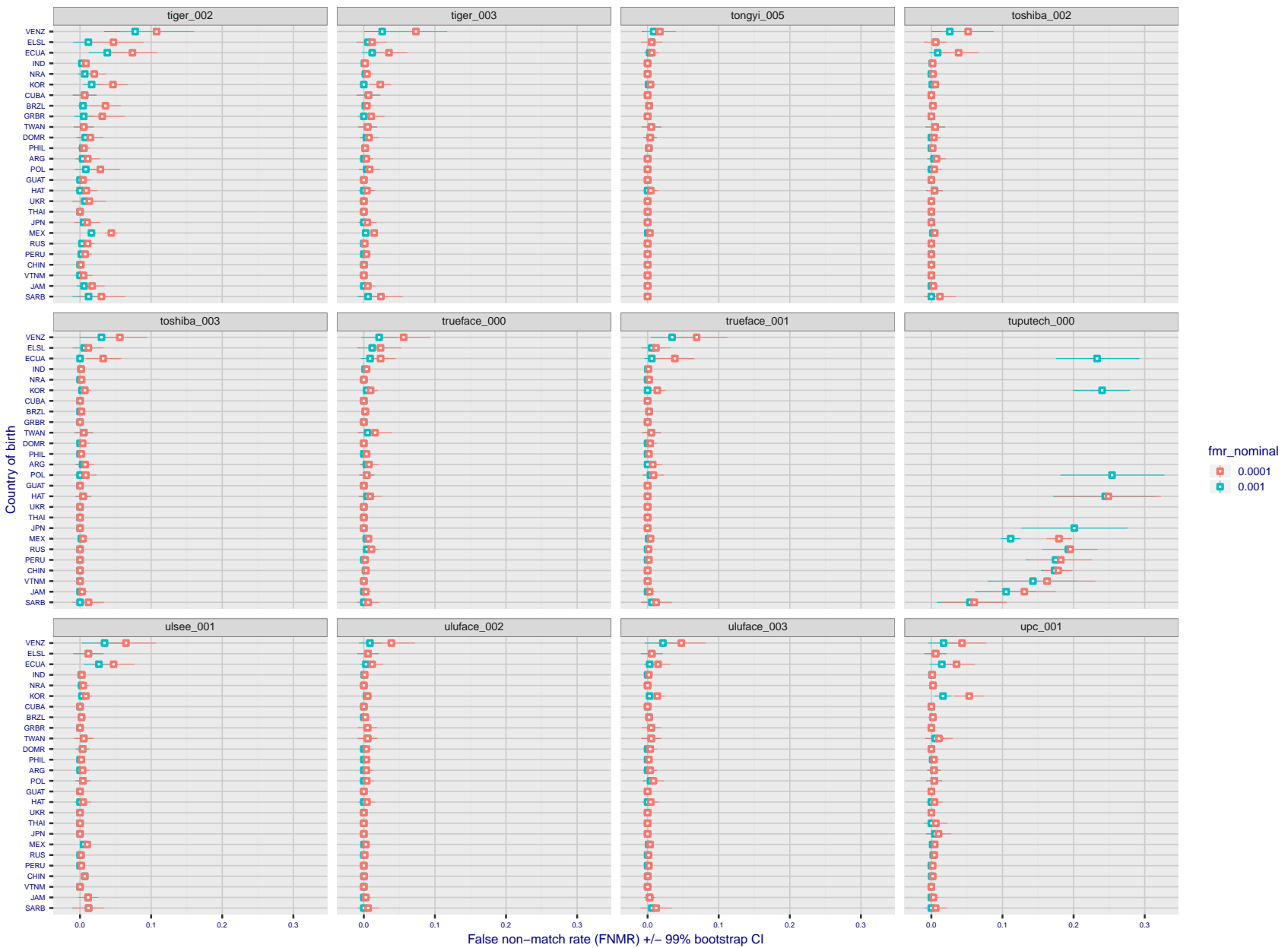


Figure 164: For the visa images, the dots show FNMR by country of birth for two globally set operating thresholds corresponding to $FMR = \{0.001, 0.0001\}$ computed over all on the order of 10^{10} impostor scores. The FMR in each bin will vary also - see subsequent impostor heatmaps in sec. 3.6.1. The figures shows an order of magnitude variation in FNMR across country of birth; these effects are likely due quality variations, then demographics like age and race. The error rates in some cases are zero, and in others the DET is flat so the error rates at the two thresholds are identical. The lines span 1% and 99% of bootstrap replicated FNMR estimates.

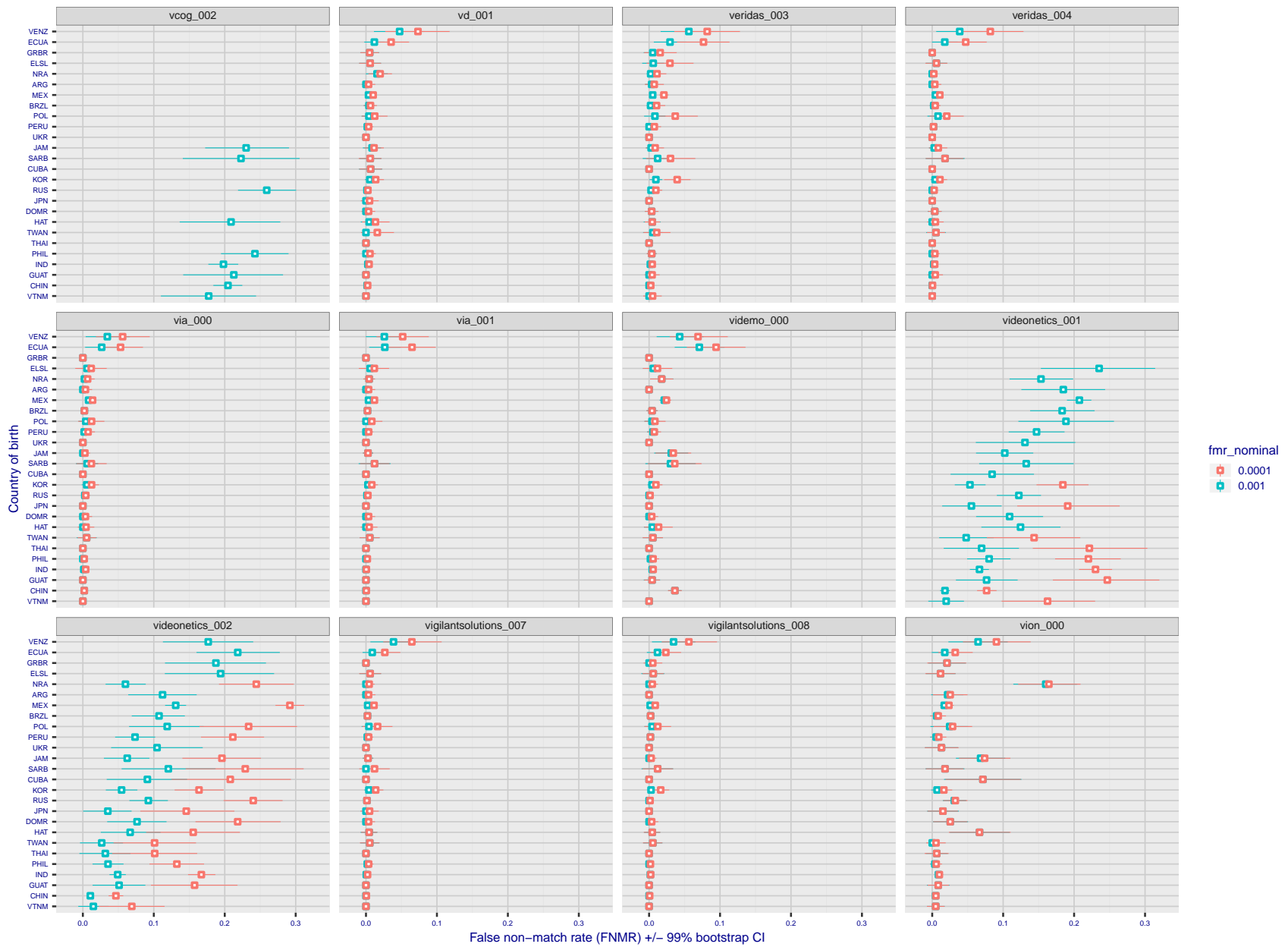


Figure 165: For the visa images, the dots show FNMR by country of birth for two globally set operating thresholds corresponding to $FMR = \{0.001, 0.0001\}$ computed over all on the order of 10^{10} impostor scores. The FMR in each bin will vary also - see subsequent impostor heatmaps in sec. 3.6.1. The figures shows an order of magnitude variation in FNMR across country of birth; these effects are likely due quality variations, then demographics like age and race. The error rates in some cases are zero, and in others the DET is flat so the error rates at the two thresholds are identical. The lines span 1% and 99% of bootstrap replicated FNMR estimates.

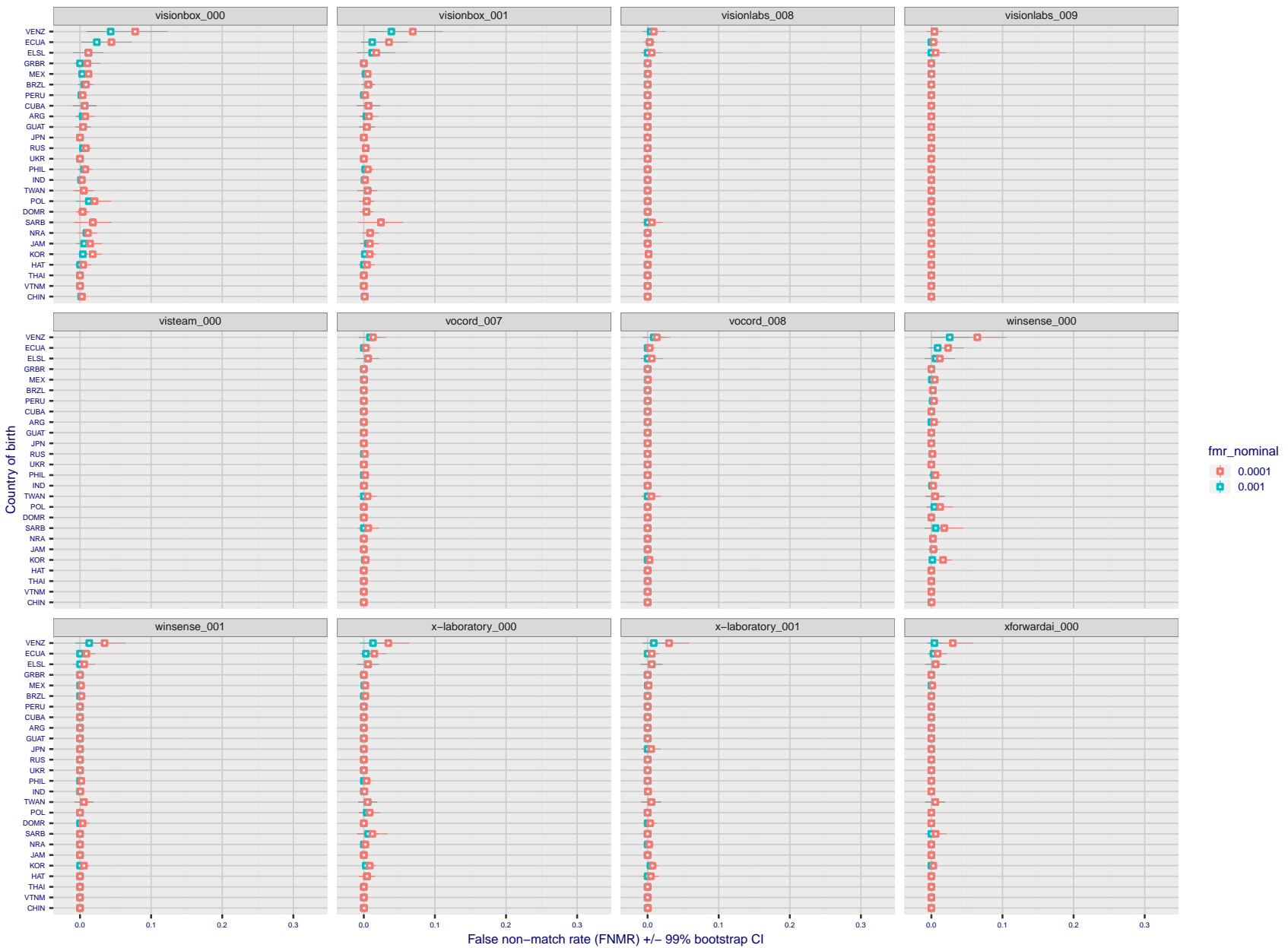


Figure 166: For the visa images, the dots show FNMR by country of birth for two globally set operating thresholds corresponding to $FMR = \{0.001, 0.0001\}$ computed over all on the order of 10^{10} impostor scores. The FMR in each bin will vary also - see subsequent impostor heatmaps in sec. 3.6.1. The figures shows an order of magnitude variation in FNMR across country of birth; these effects are likely due quality variations, then demographics like age and race. The error rates in some cases are zero, and in others the DET is flat so the error rates at the two thresholds are identical. The lines span 1% and 99% of bootstrap replicated FNMR estimates.



Figure 167: For the visa images, the dots show FNMR by country of birth for two globally set operating thresholds corresponding to $FMR = \{0.001, 0.0001\}$ computed over all on the order of 10^{10} impostor scores. The FMR in each bin will vary also - see subsequent impostor heatmaps in sec. 3.6.1. The figures shows an order of magnitude variation in FNMR across country of birth; these effects are likely due quality variations, then demographics like age and race. The error rates in some cases are zero, and in others the DET is flat so the error rates at the two thresholds are identical. The lines span 1% and 99% of bootstrap replicated FNMR estimates.

Caveats: The results may not relate to subject-specific properties. Instead they could reflect image-specific quality differences, which could occur due to collection protocol or software processing variations.

3.5.2 Effect of ageing

Background: Faces change appearance throughout life. This change gradually reduces similarity of a new image to an earlier image. Face recognition algorithms give reduced similarity scores and more frequent false rejections.

Goal: To quantify false non-match rates (FNMR) as a function of elapsed time in an adult population.

Methods: Using the mugshot images, a threshold is set to give FMR = 0.00001 over the entire impostor set. Then FNMR is measured over 1000 bootstrap replications of the genuine scores.

Results: For the visa images, Figure 181 shows how false non-match rates for genuine users, as a function of age group.

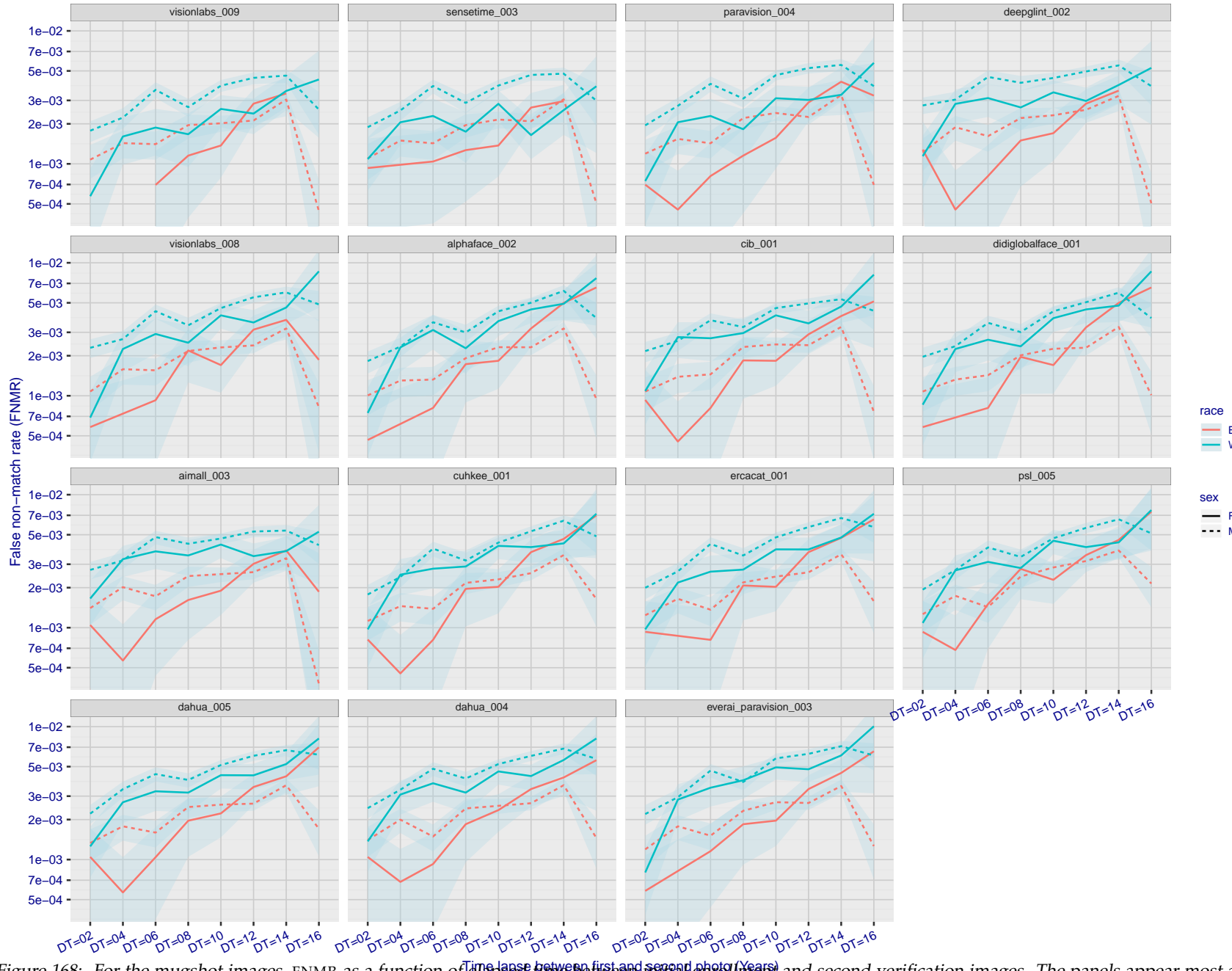


Figure 168: For the mugshot images, FNMR as a function of elapsed time between initial enrollment and second verification images. The panels appear most accurate first, and vertical scale changes on each page. The four traces correspond to images annotated with codes for black female, black male, white female, white male. The threshold is fixed for each algorithm to give FMR = 0.00001 over all (10^8) impostor comparisons. For short time-lapses, the most accurate algorithms give very few errors (FNMR < 0.001) so that the uncertainty estimates are high.

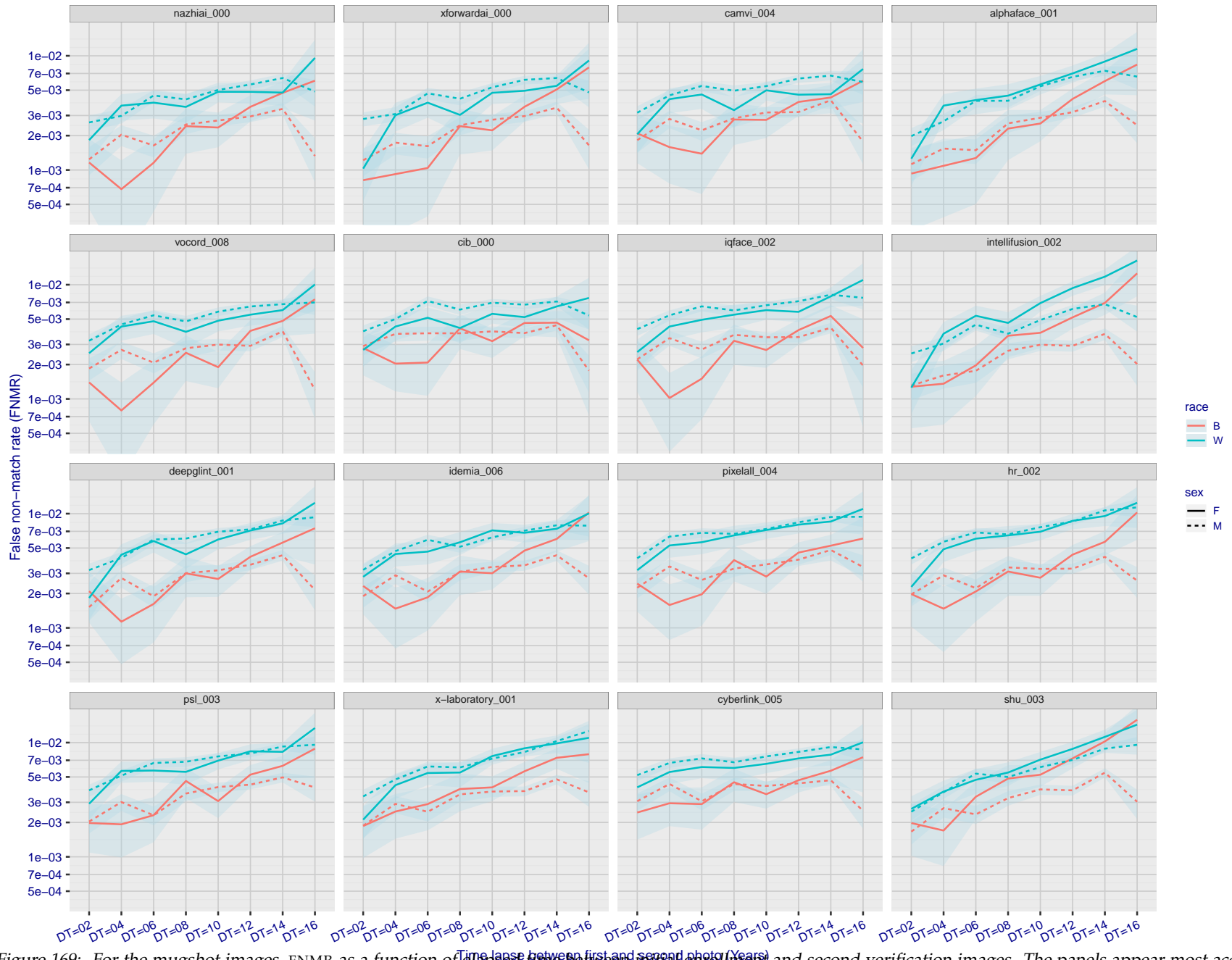


Figure 169: For the mugshot images, FNMR as a function of elapsed time between initial enrollment and second verification images. The panels appear most accurate first, and vertical scale changes on each page. The four traces correspond to images annotated with codes for black female, black male, white female, white male. The threshold is fixed for each algorithm to give FMR = 0.00001 over all (10^8) impostor comparisons. For short time-lapses, the most accurate algorithms give very few errors (FNMR < 0.001) so that the uncertainty estimates are high.

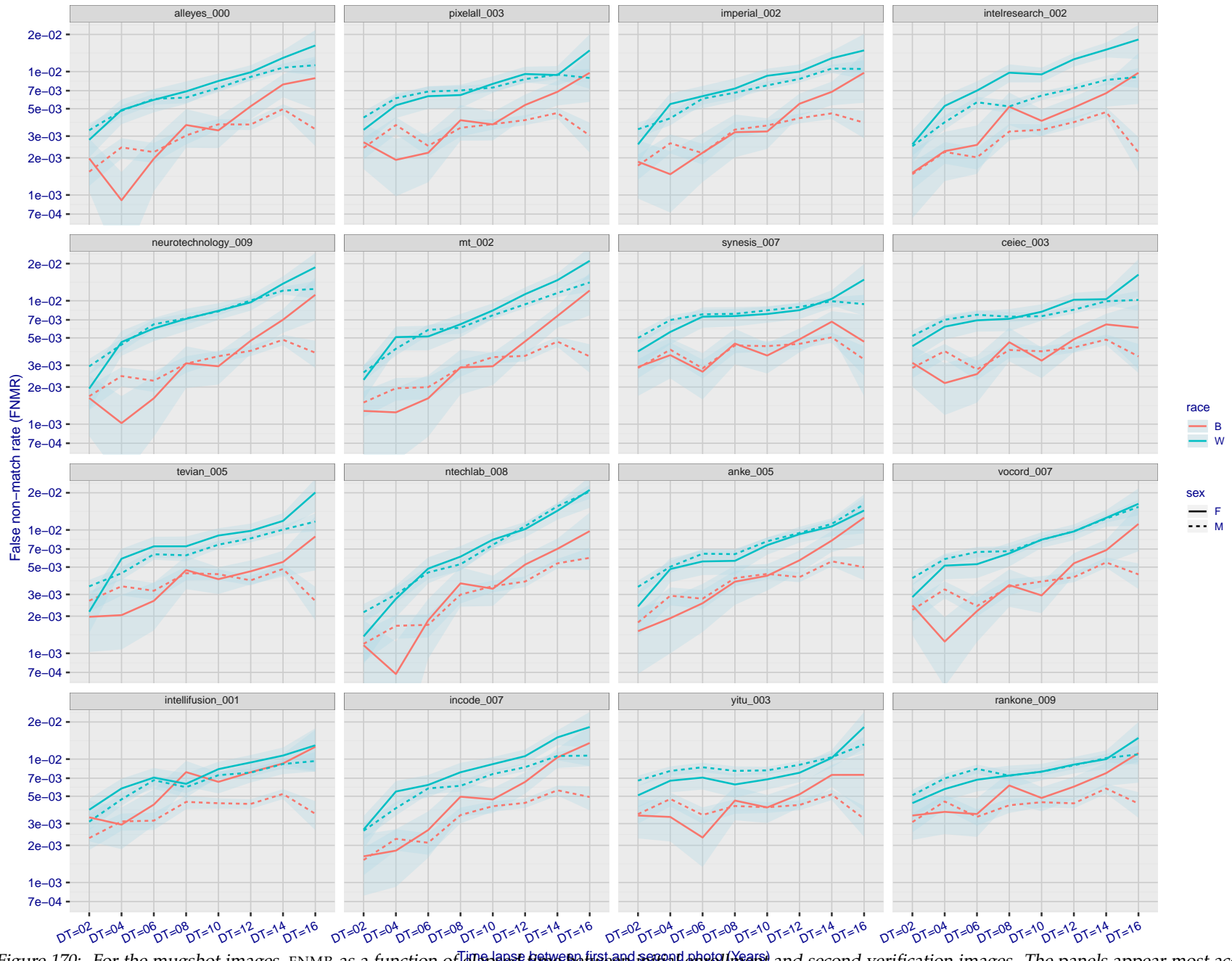


Figure 170: For the mugshot images, FNMR as a function of elapsed time between initial enrollment and second verification images. The panels appear most accurate first, and vertical scale changes on each page. The four traces correspond to images annotated with codes for black female, black male, white female, white male. The threshold is fixed for each algorithm to give FMR = 0.00001 over all (10^8) impostor comparisons. For short time-lapses, the most accurate algorithms give very few errors (FNMR < 0.001) so that the uncertainty estimates are high.

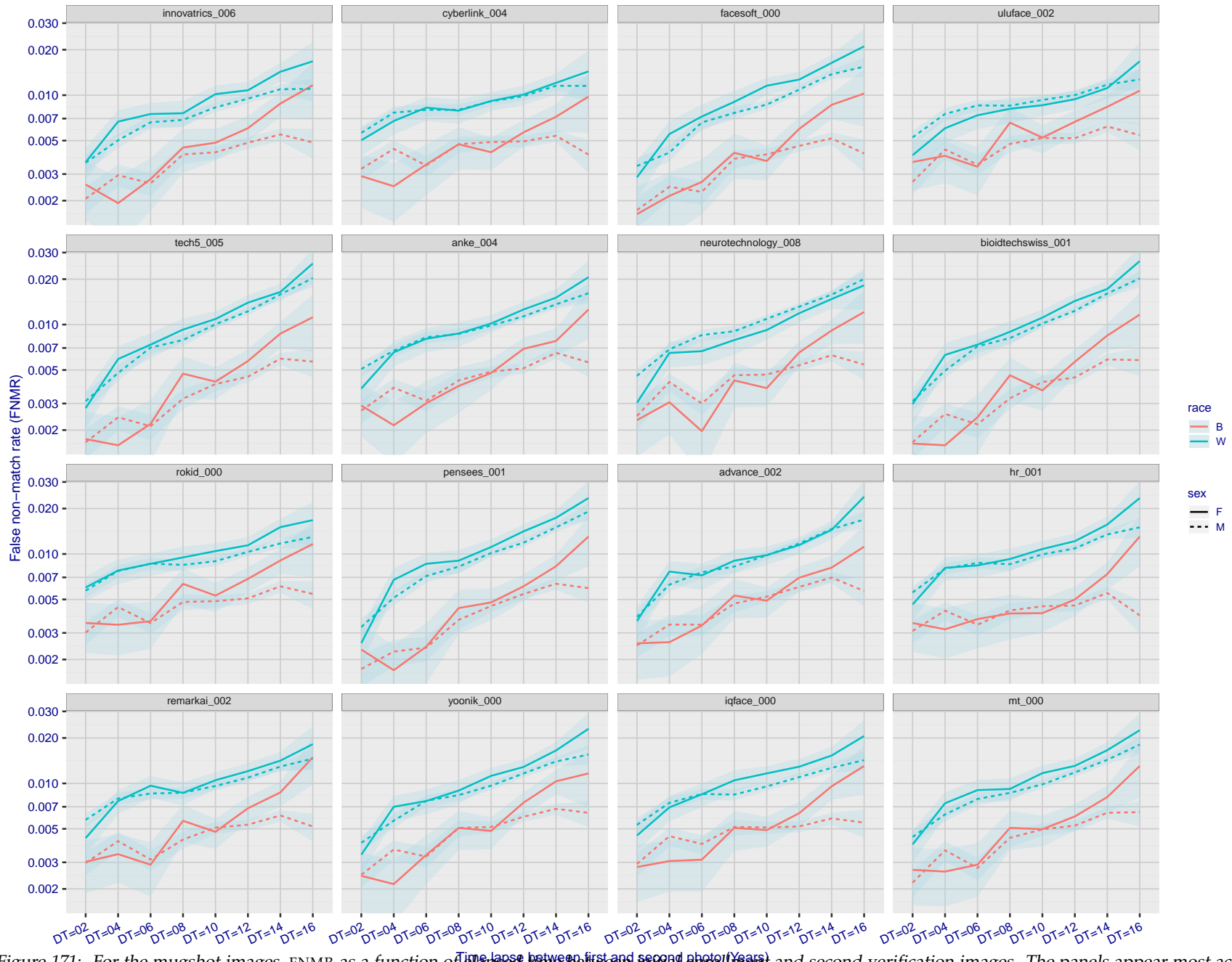


Figure 171: For the mugshot images, FNMR as a function of elapsed time between initial enrollment and second verification images. The panels appear most accurate first, and vertical scale changes on each page. The four traces correspond to images annotated with codes for black female, black male, white female, white male. The threshold is fixed for each algorithm to give FMR = 0.00001 over all (10^8) impostor comparisons. For short time-lapses, the most accurate algorithms give very few errors (FNMR < 0.001) so that the uncertainty estimates are high.

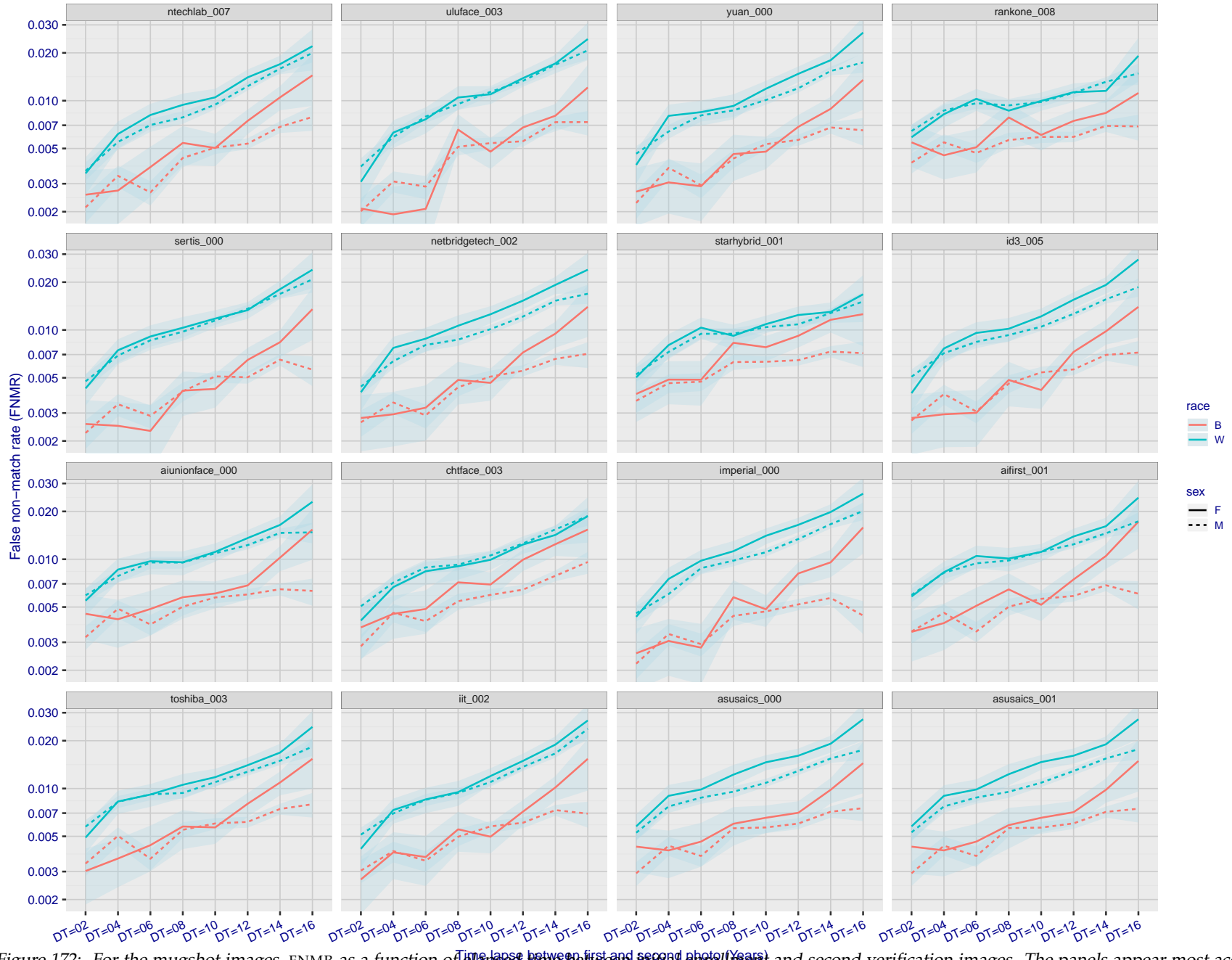


Figure 172: For the mugshot images, FNMR as a function of elapsed time between initial enrollment and second verification images. The panels appear most accurate first, and vertical scale changes on each page. The four traces correspond to images annotated with codes for black female, black male, white female, white male. The threshold is fixed for each algorithm to give FMR = 0.00001 over all (10^8) impostor comparisons. For short time-lapses, the most accurate algorithms give very few errors (FNMR < 0.001) so that the uncertainty estimates are high.

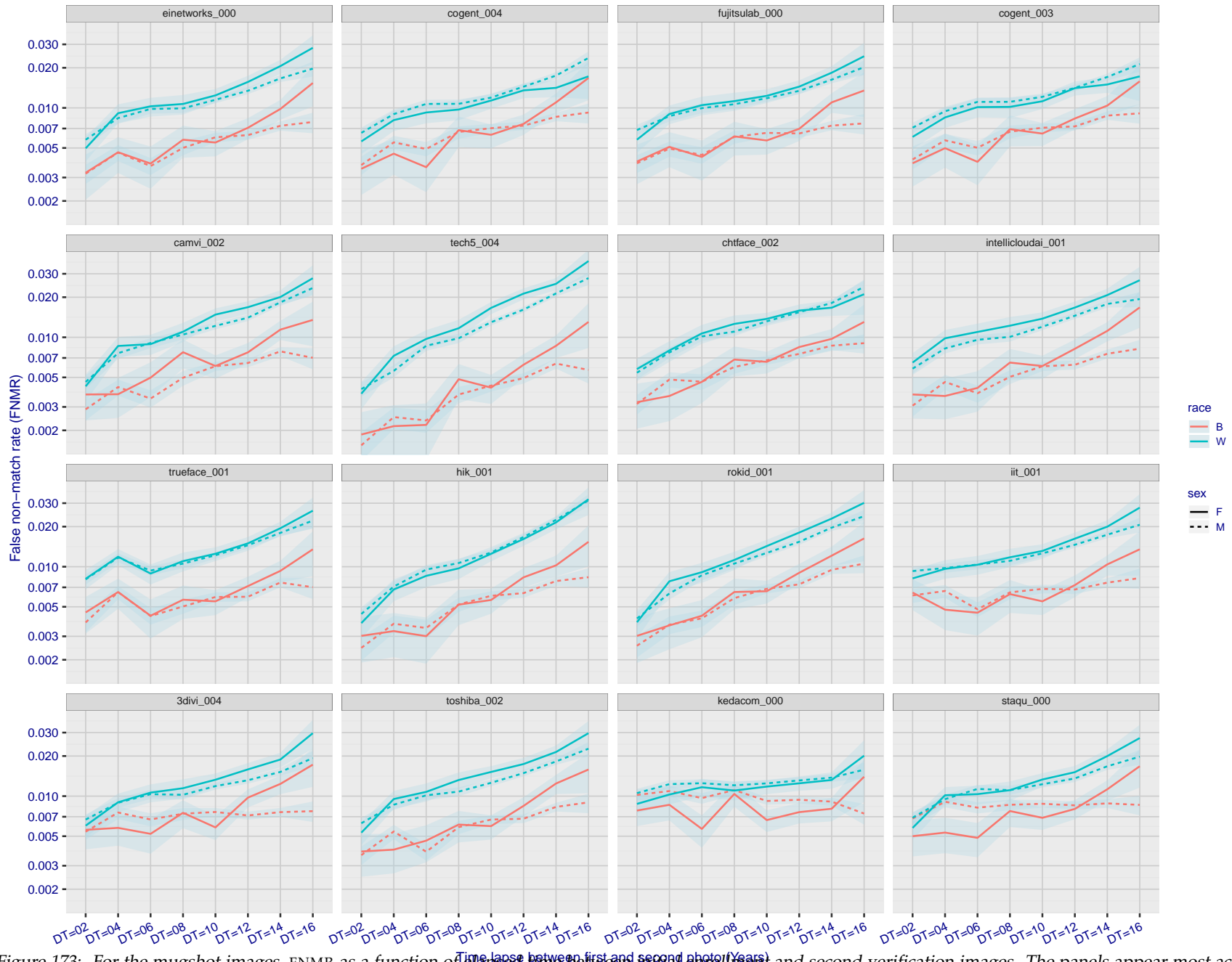


Figure 173: For the mugshot images, FNMR as a function of elapsed time between initial enrollment and second verification images. The panels appear most accurate first, and vertical scale changes on each page. The four traces correspond to images annotated with codes for black female, black male, white female, white male. The threshold is fixed for each algorithm to give FMR = 0.00001 over all (10^8) impostor comparisons. For short time-lapses, the most accurate algorithms give very few errors (FNMR < 0.001) so that the uncertainty estimates are high.

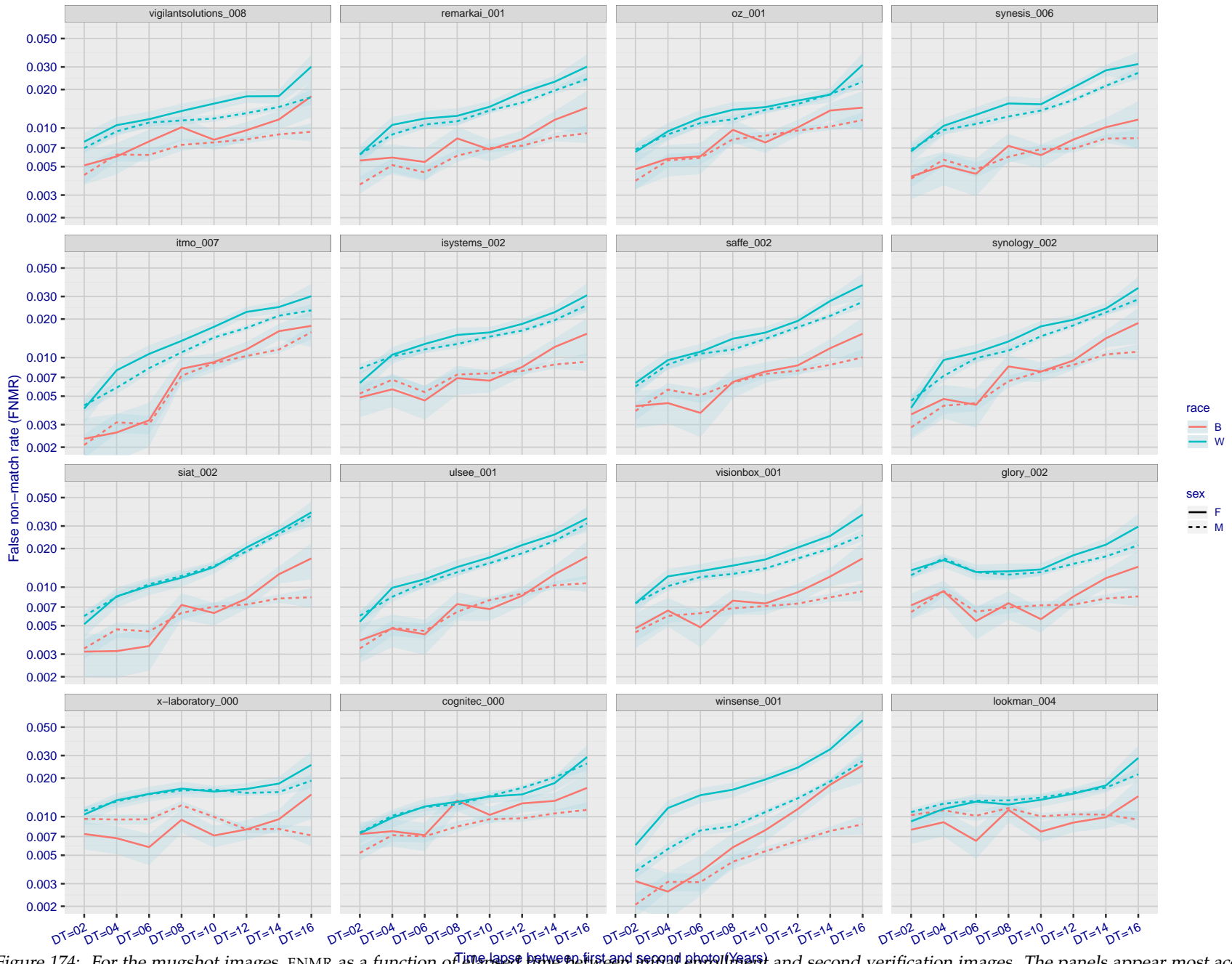


Figure 174: For the mugshot images, FNMR as a function of elapsed time between initial enrollment and second verification images. The panels appear most accurate first, and vertical scale changes on each page. The four traces correspond to images annotated with codes for black female, black male, white female, white male. The threshold is fixed for each algorithm to give FMR = 0.00001 over all (10^8) impostor comparisons. For short time-lapses, the most accurate algorithms give very few errors (FNMR < 0.001) so that the uncertainty estimates are high.

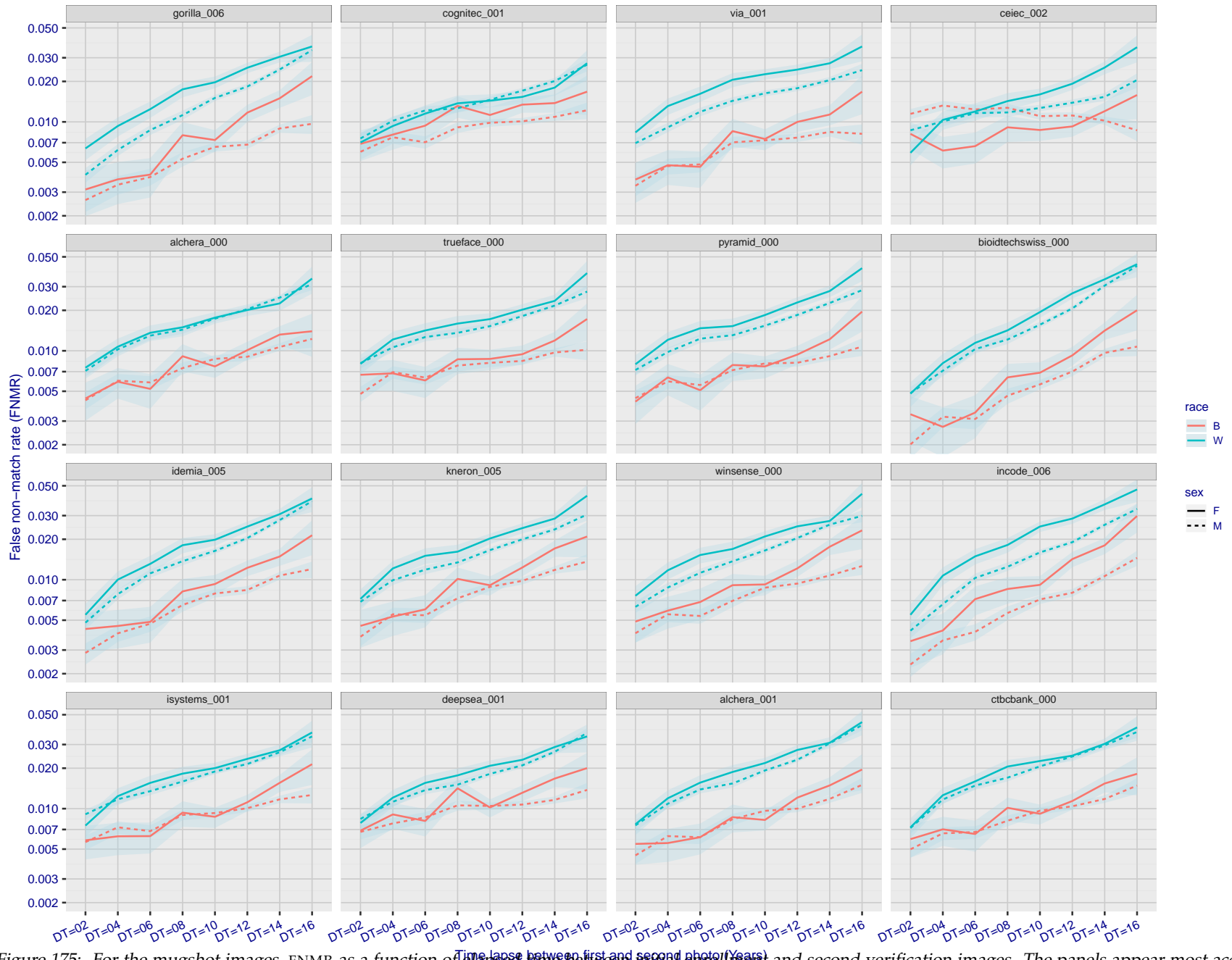


Figure 175: For the mugshot images, FNMR as a function of elapsed time between initial enrollment and second verification images. The panels appear most accurate first, and vertical scale changes on each page. The four traces correspond to images annotated with codes for black female, black male, white female, white male. The threshold is fixed for each algorithm to give FMR = 0.00001 over all (10^8) impostor comparisons. For short time-lapses, the most accurate algorithms give very few errors (FNMR < 0.001) so that the uncertainty estimates are high.

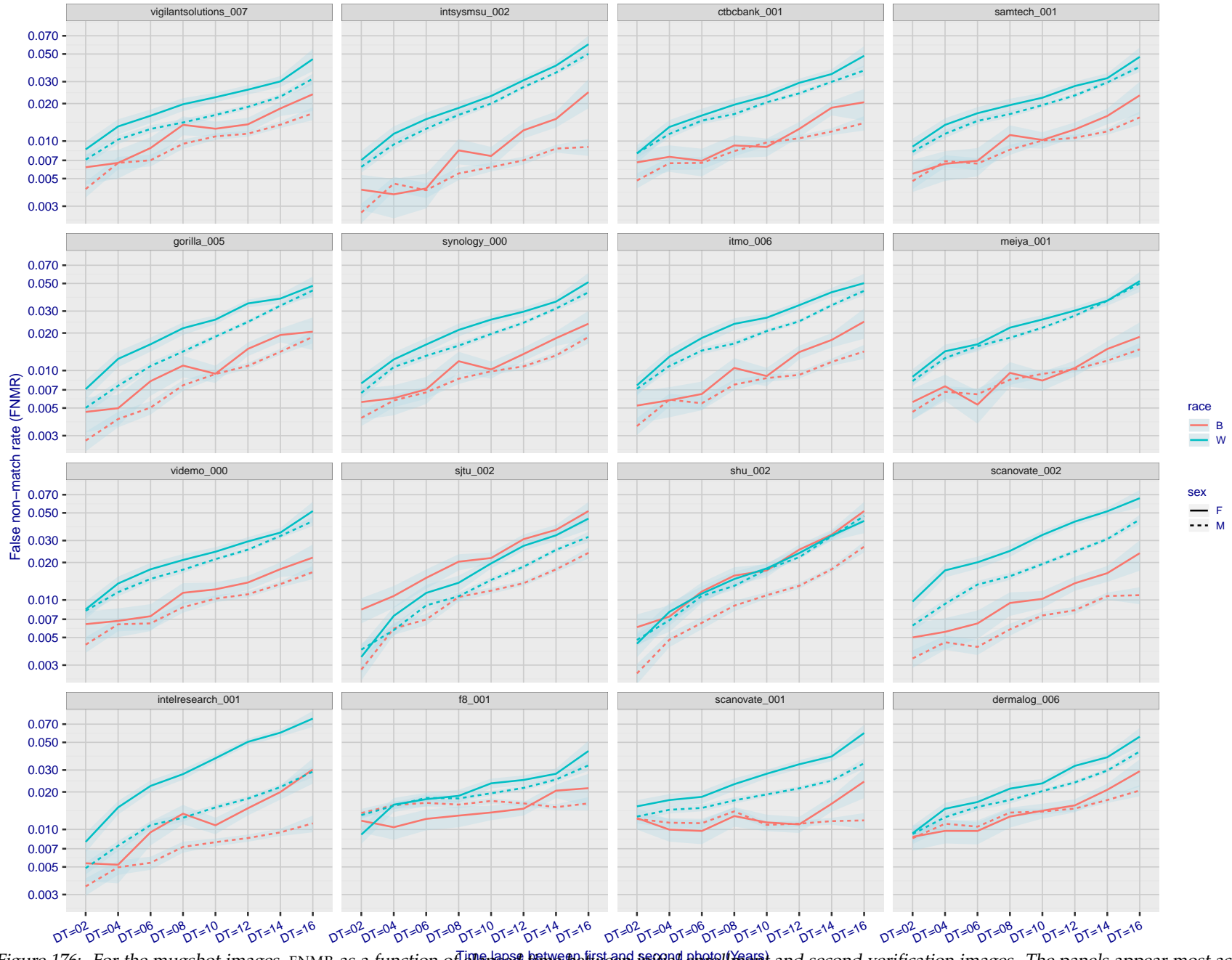


Figure 176: For the mugshot images, FNMR as a function of elapsed time between initial enrollment and second verification images. The panels appear most accurate first, and vertical scale changes on each page. The four traces correspond to images annotated with codes for black female, black male, white female, white male. The threshold is fixed for each algorithm to give FMR = 0.00001 over all (10^8) impostor comparisons. For short time-lapses, the most accurate algorithms give very few errors (FNMR < 0.001) so that the uncertainty estimates are high.

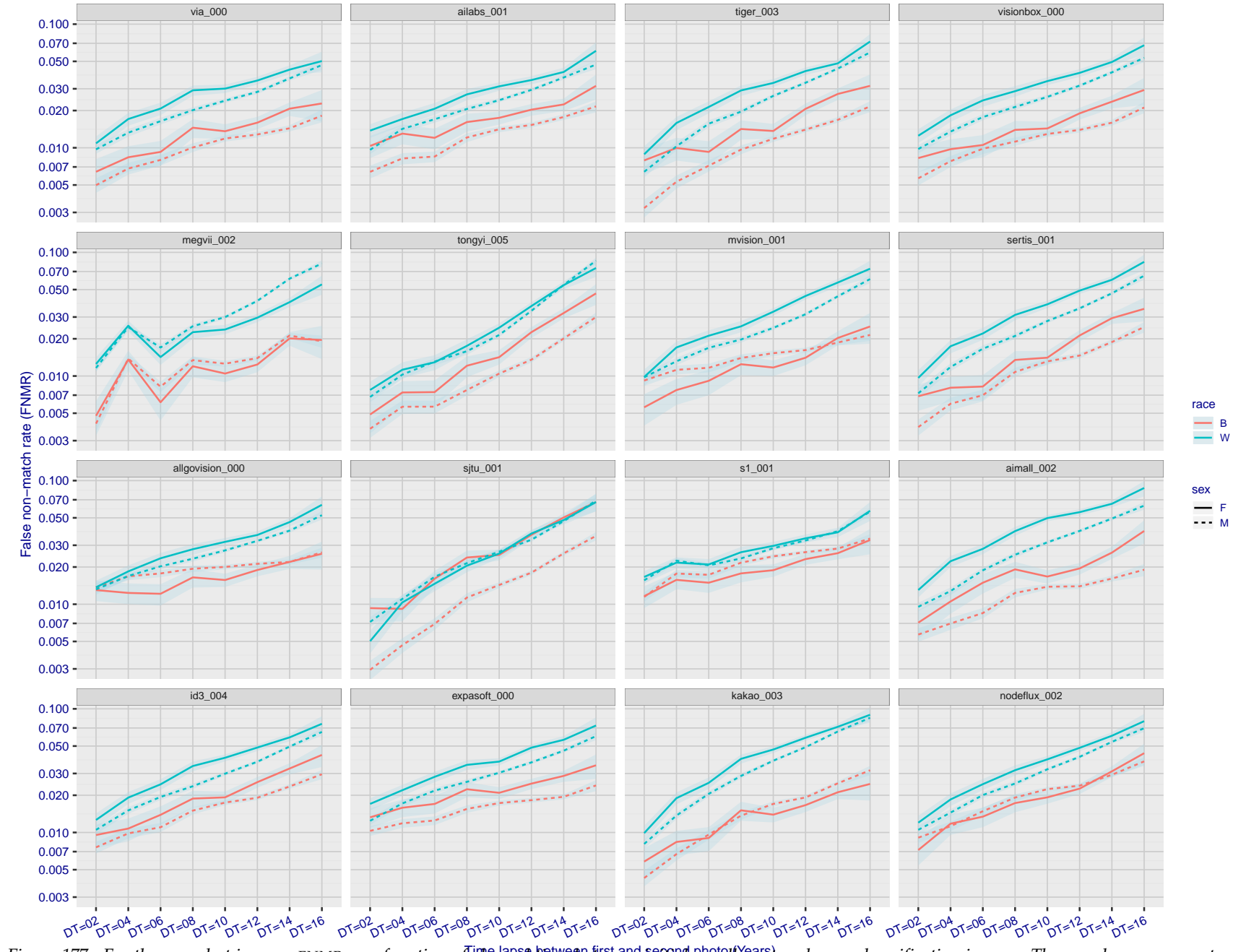


Figure 177: For the mugshot images, FNMR as a function of elapsed time between initial enrollment and second verification images. The panels appear most accurate first, and vertical scale changes on each page. The four traces correspond to images annotated with codes for black female, black male, white female, white male. The threshold is fixed for each algorithm to give FMR = 0.00001 over all (10^8) impostor comparisons. For short time-lapses, the most accurate algorithms give very few errors (FNMR < 0.001) so that the uncertainty estimates are high.

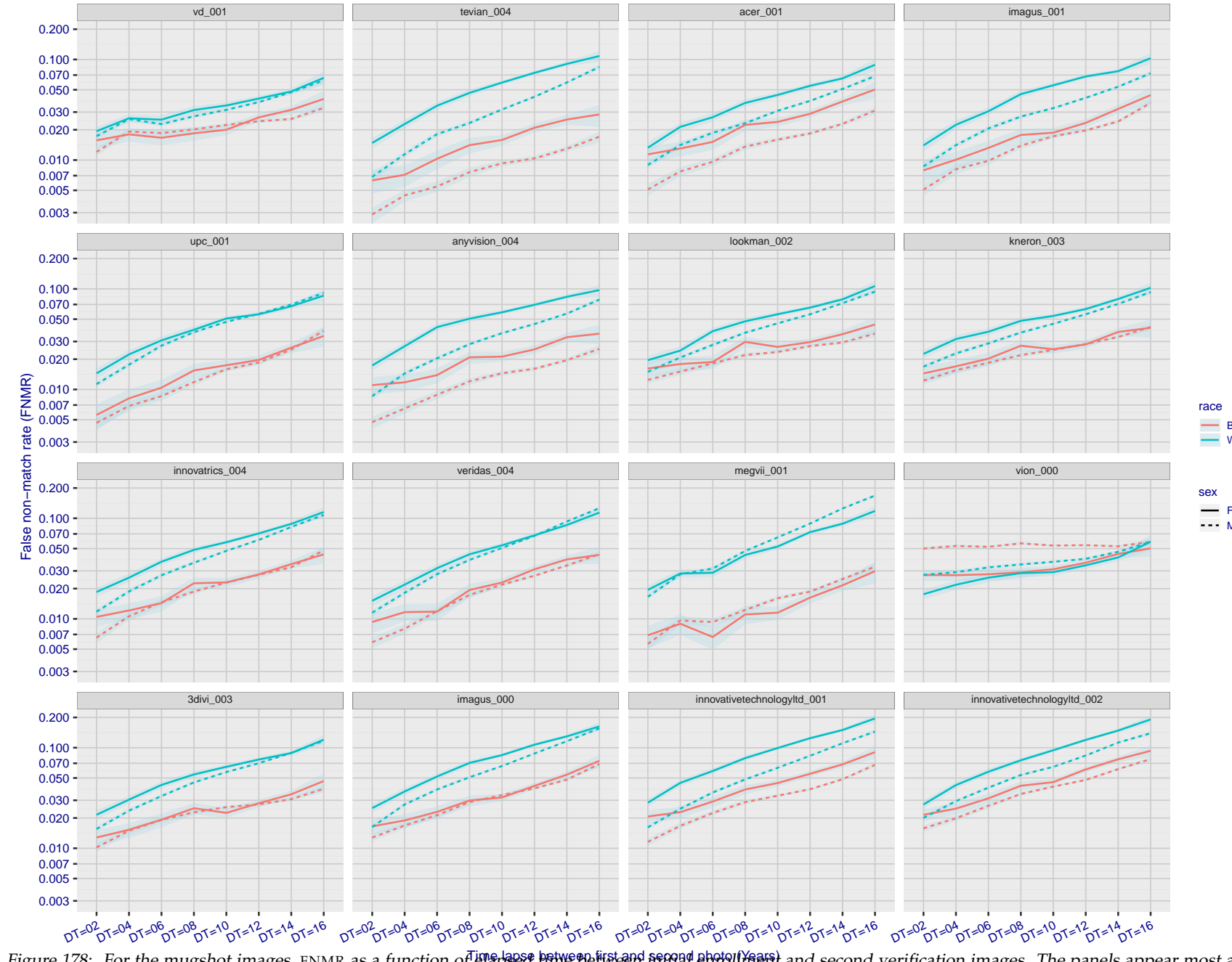


Figure 178: For the mugshot images, FNMR as a function of elapsed time between initial enrollment and second verification images. The panels appear most accurate first, and vertical scale changes on each page. The four traces correspond to images annotated with codes for black female, black male, white female, white male. The threshold is fixed for each algorithm to give FMR = 0.00001 over all (10^8) impostor comparisons. For short time-lapses, the most accurate algorithms give very few errors (FNMR < 0.001) so that the uncertainty estimates are high.

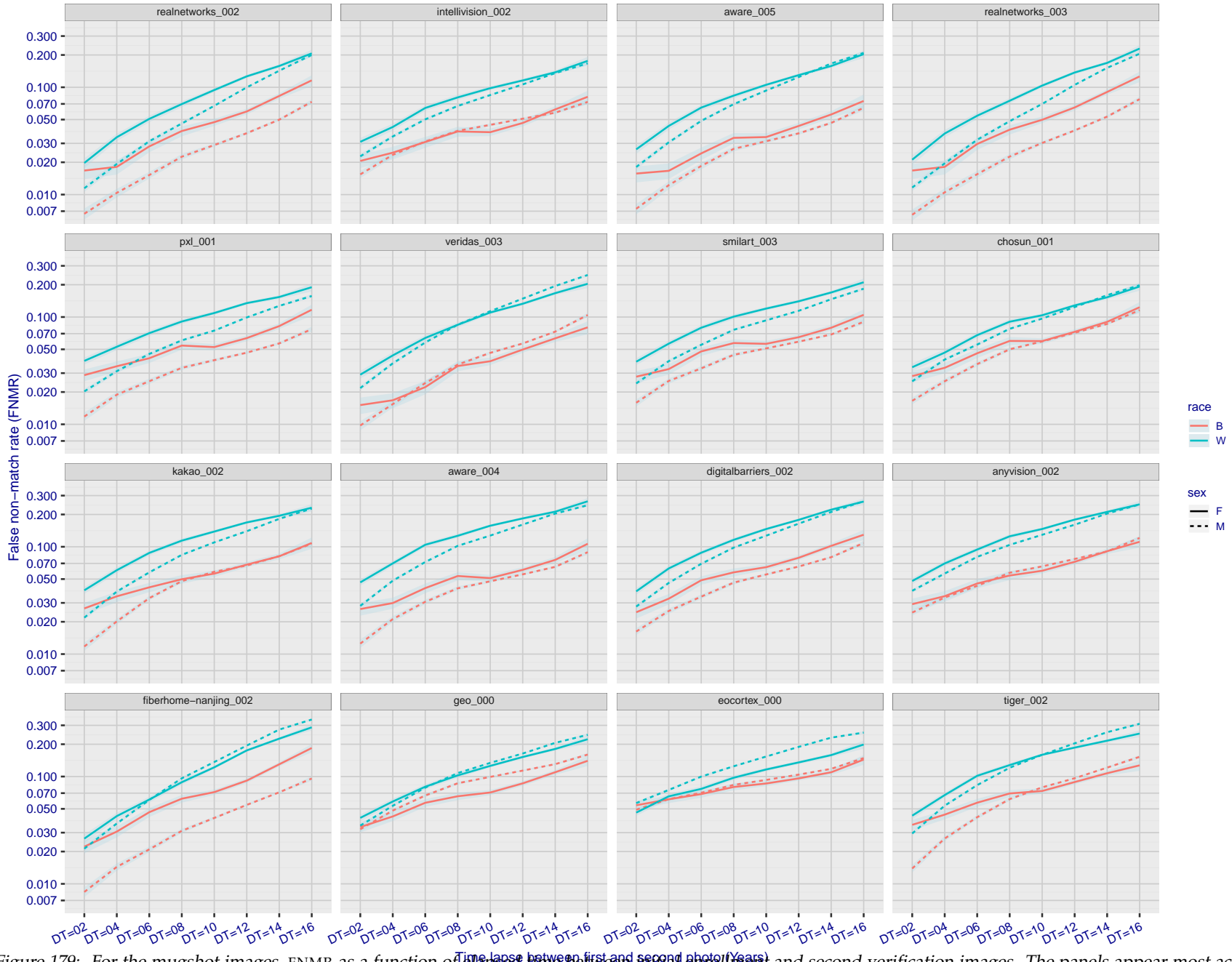


Figure 179: For the mugshot images, FNMR as a function of elapsed time between initial enrollment and second verification images. The panels appear most accurate first, and vertical scale changes on each page. The four traces correspond to images annotated with codes for black female, black male, white female, white male. The threshold is fixed for each algorithm to give FMR = 0.00001 over all (10^8) impostor comparisons. For short time-lapses, the most accurate algorithms give very few errors (FNMR < 0.001) so that the uncertainty estimates are high.

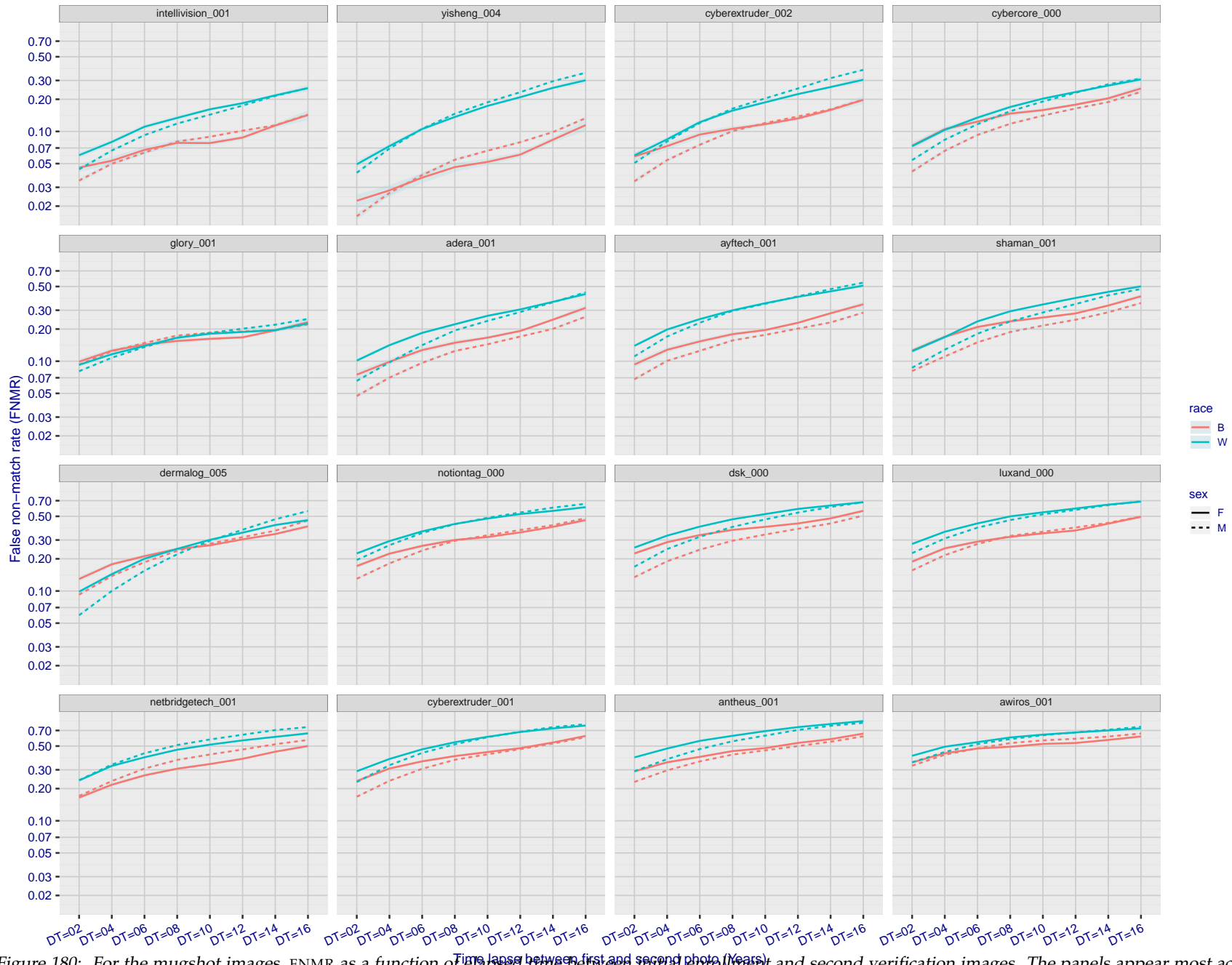


Figure 180: For the mugshot images, FNMR as a function of elapsed time between initial enrollment and second verification images. The panels appear most accurate first, and vertical scale changes on each page. The four traces correspond to images annotated with codes for black female, black male, white female, white male. The threshold is fixed for each algorithm to give FMR = 0.00001 over all (10^8) impostor comparisons. For short time-lapses, the most accurate algorithms give very few errors (FNMR < 0.001) so that the uncertainty estimates are high.

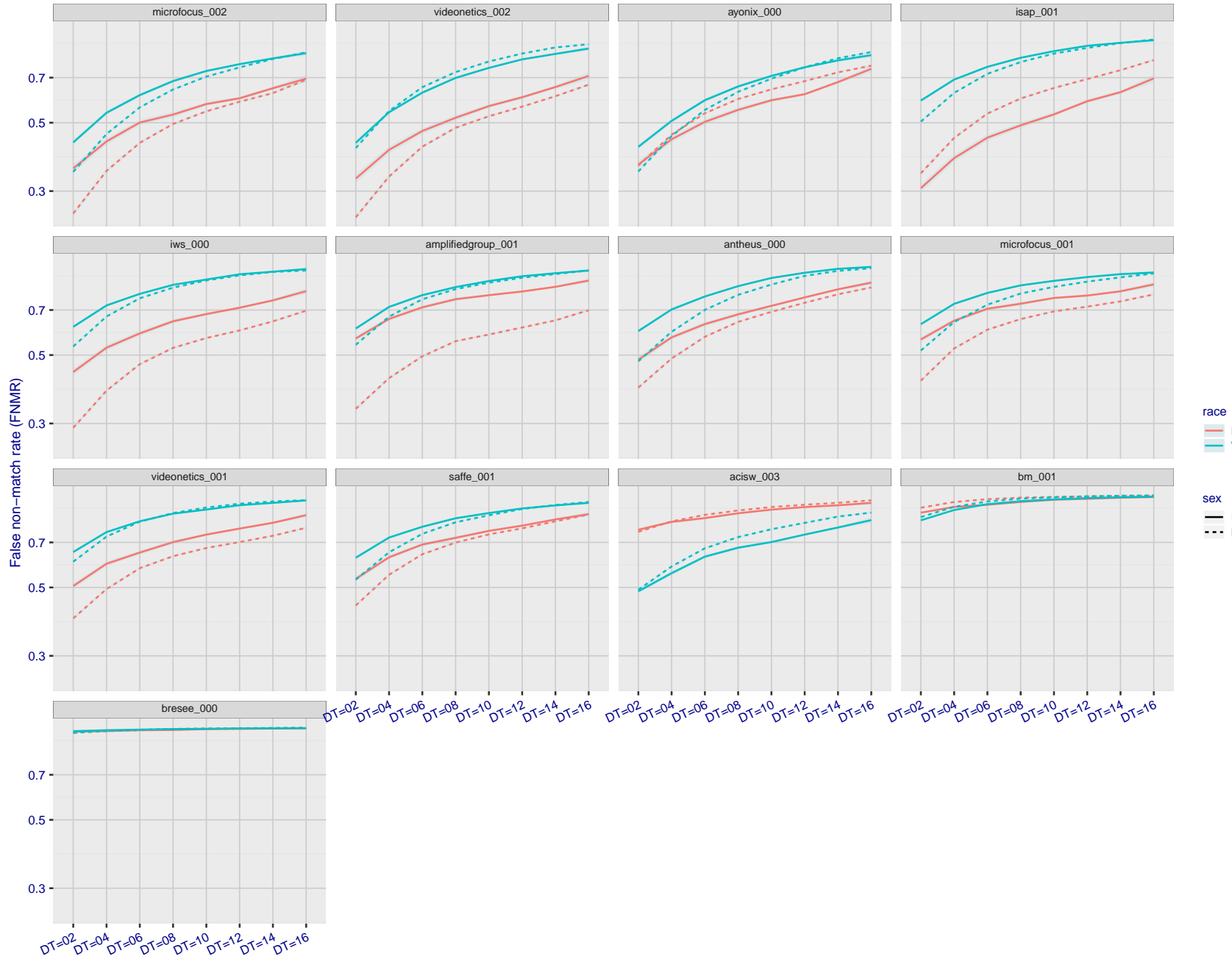


Figure 181: For the mugshot images, FNMR as a function of elapsed time between initial enrollment and second verification images. The panels appear most accurate first, and vertical scale changes on each page. The four traces correspond to images annotated with codes for black female, black male, white female, white male. The threshold is fixed for each algorithm to give $FMR = 0.00001$ over all (10^8) impostor comparisons. For short time-lapses, the most accurate algorithms give very few errors ($FNMR < 0.001$) so that the uncertainty estimates are high.

3.5.3 Effect of age on genuine subjects

Background: Faces change appearance throughout life. Face recognition algorithms have previously been reported to give better accuracy on older individuals (See NIST IR 8009).

Goal: To quantify false non-match rates (FNMR) as a function of age, without an ageing component.

Methods: Using the visa images, which span fewer than five years, thresholds are determined that give FMR = 0.001 and 0.0001 over the entire impostor set. Then FNMR is measured over 1000 bootstrap replications of the genuine scores.

Results: For the visa images, Figure 201 shows how false non-match rates for genuine users, as a function of age group.

The notable aspects are:

- ▷ Younger subjects give considerably higher FNMR. This is likely due to rapid growth and change in facial appearance.
- ▷ FNMR trends down throughout life. The last bin, AGE > 72, contains fewer than 140 mated pairs, and may be affected by small sample size.

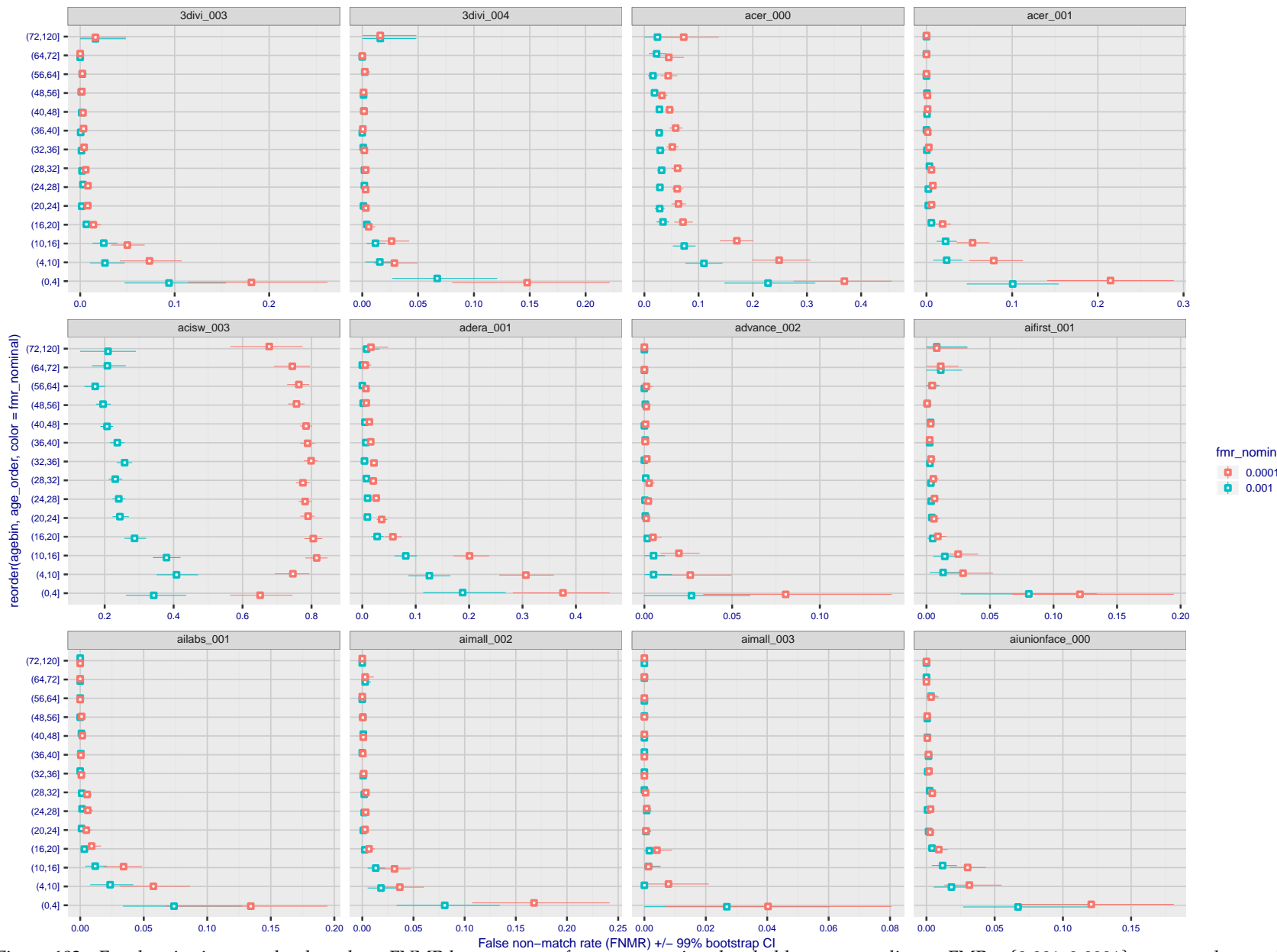
2020/09/08
12:09:14

Figure 182: For the visa images, the dots show FNMR by age group for two operating thresholds corresponding to $FMR = \{0.001, 0.0001\}$ computed over all on the order of 10^{10} impostor scores. The FMR in each bin will vary also - see subsequent impostor heatmaps in sec. 3.6.2. Given a pair of face images taken at different times, we assign the comparison to the bin that is the arithmetic average of the subject's ages. This plot shows only the effect of age, not ageing. The number of comparisons in each bin is generally in the thousands, however the first and last bins are computed over 149 and 124 respectively. The error rates in some (adult) cases are zero, and in others the DET is flat so the error rates at the two thresholds are identical. The lines span 1% and 99% of bootstrap replicated FNMR estimates.

FNMR(T)
FMR(T)
"False non-match rate"
"False match rate"

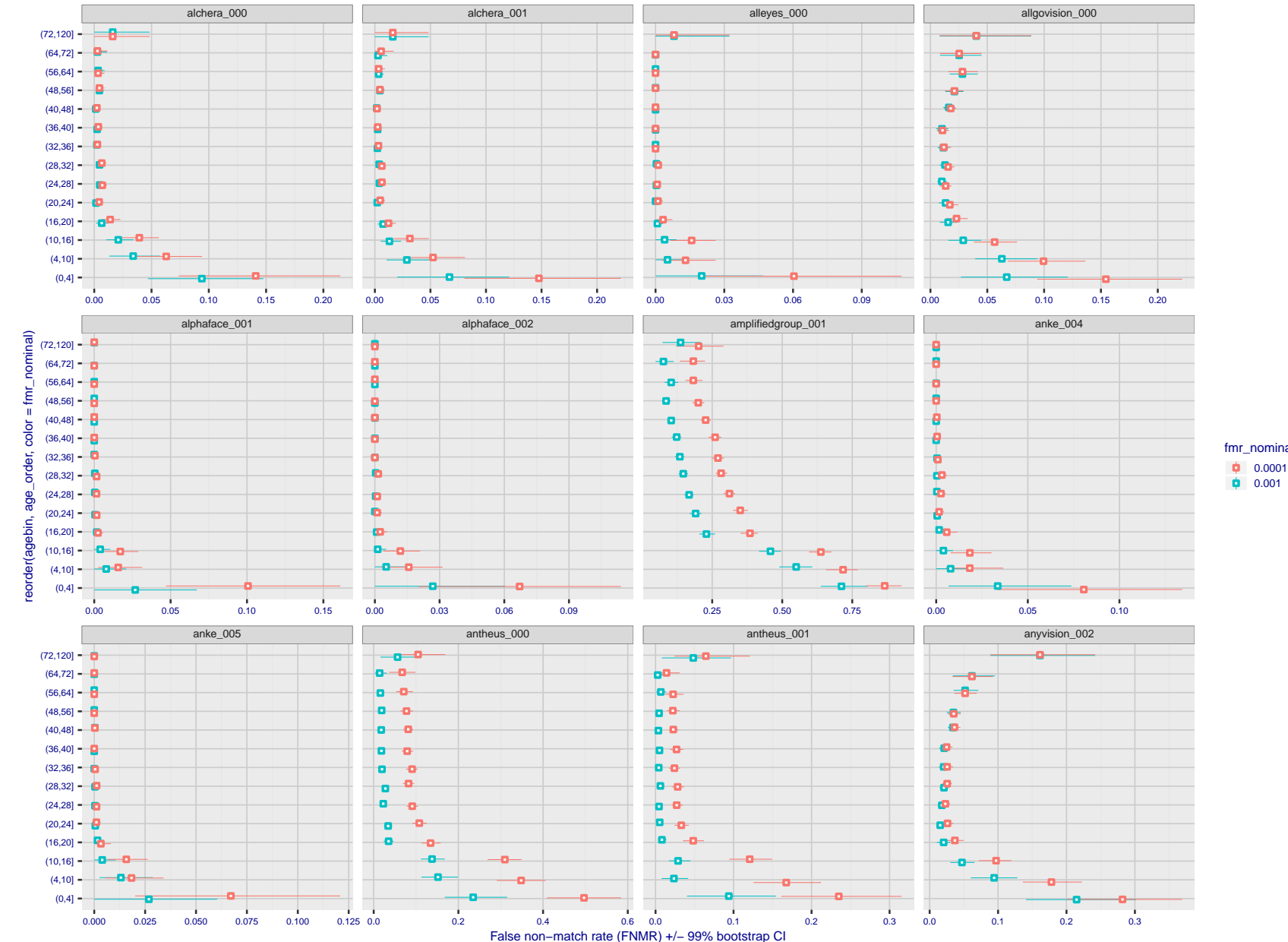


Figure 183: For the visa images, the dots show FNMR by age group for two operating thresholds corresponding to $FMR = \{0.001, 0.0001\}$ computed over all on the order of 10^{10} impostor scores. The FMR in each bin will vary also - see subsequent impostor heatmaps in sec. 3.6.2. Given a pair of face images taken at different times, we assign the comparison to the bin that is the arithmetic average of the subject's ages. This plot shows only the effect of age, not ageing. The number of comparisons in each bin is generally in the thousands, however the first and last bins are computed over 149 and 124 respectively. The error rates in some (adult) cases are zero, and in others the DET is flat so the error rates at the two thresholds are identical. The lines span 1% and 99% of bootstrap replicated FNMR estimates.

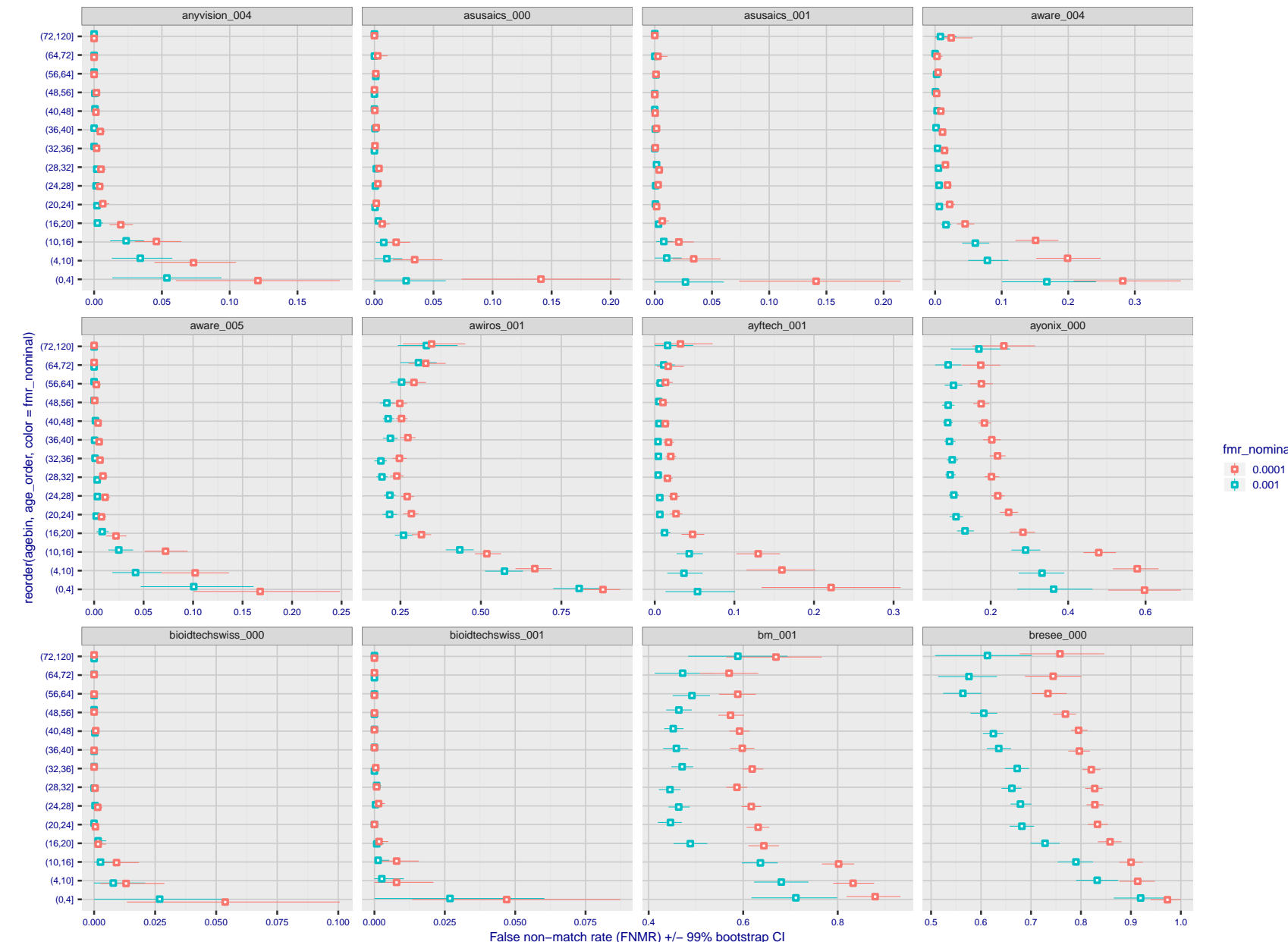


Figure 184: For the visa images, the dots show FNMR by age group for two operating thresholds corresponding to $FMR = \{0.001, 0.0001\}$ computed over all on the order of 10^{10} impostor scores. The FMR in each bin will vary also - see subsequent impostor heatmaps in sec. 3.6.2. Given a pair of face images taken at different times, we assign the comparison to the bin that is the arithmetic average of the subject's ages. This plot shows only the effect of age, not ageing. The number of comparisons in each bin is generally in the thousands, however the first and last bins are computed over 149 and 124 respectively. The error rates in some (adult) cases are zero, and in others the DET is flat so the error rates at the two thresholds are identical. The lines span 1% and 99% of bootstrap replicated FNMR estimates.



Figure 185: For the visa images, the dots show FNMR by age group for two operating thresholds corresponding to $FMR = \{0.001, 0.0001\}$ computed over all on the order of 10^{10} impostor scores. The FMR in each bin will vary also - see subsequent impostor heatmaps in sec. 3.6.2. Given a pair of face images taken at different times, we assign the comparison to the bin that is the arithmetic average of the subject's ages. This plot shows only the effect of age, not ageing. The number of comparisons in each bin is generally in the thousands, however the first and last bins are computed over 149 and 124 respectively. The error rates in some (adult) cases are zero, and in others the DET is flat so the error rates at the two thresholds are identical. The lines span 1% and 99% of bootstrap replicated FNMR estimates.

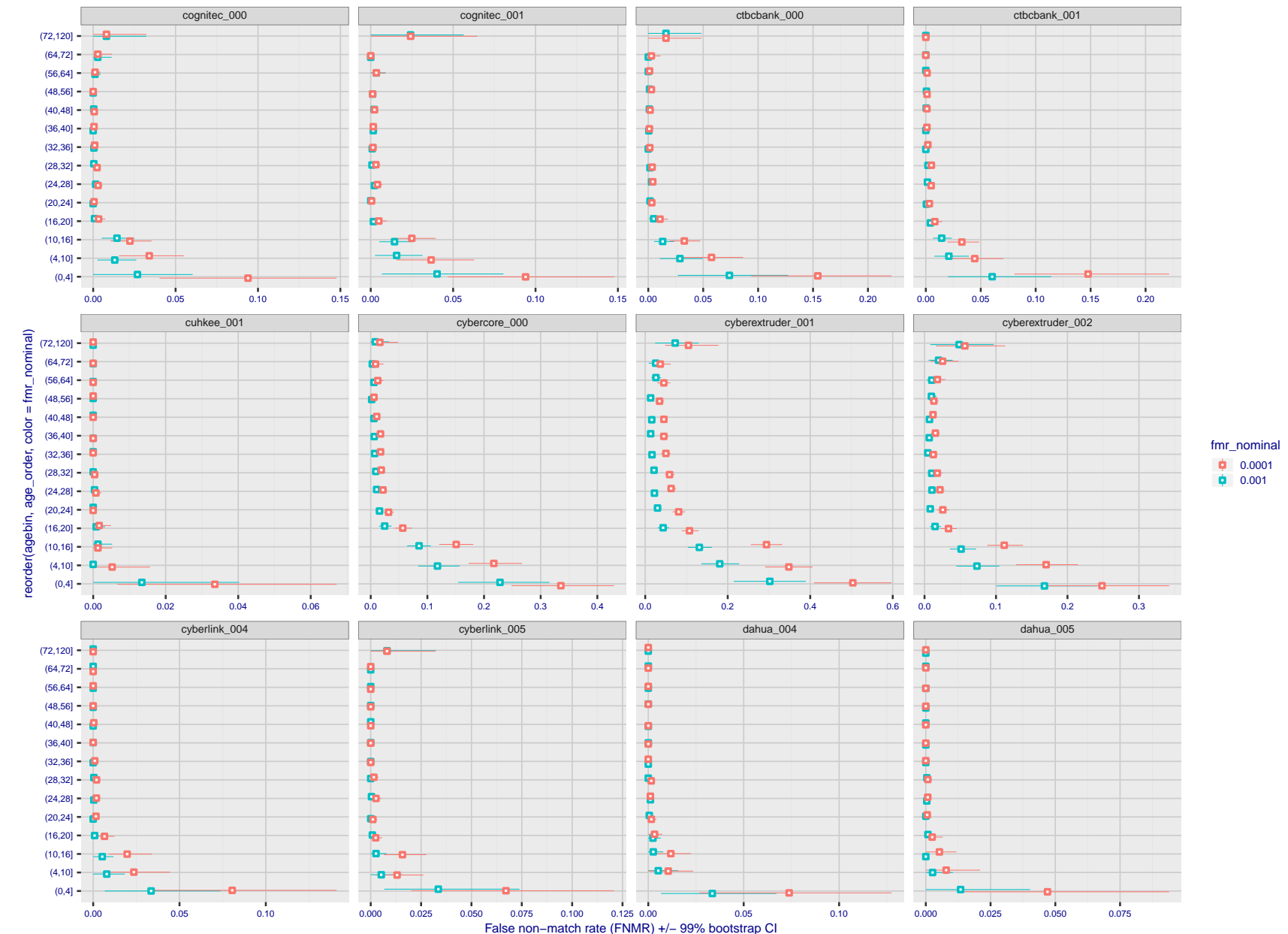


Figure 186: For the visa images, the dots show FNMR by age group for two operating thresholds corresponding to $FMR = \{0.001, 0.0001\}$ computed over all on the order of 10^{10} impostor scores. The FMR in each bin will vary also - see subsequent impostor heatmaps in sec. 3.6.2. Given a pair of face images taken at different times, we assign the comparison to the bin that is the arithmetic average of the subject's ages. This plot shows only the effect of age, not ageing. The number of comparisons in each bin is generally in the thousands, however the first and last bins are computed over 149 and 124 respectively. The error rates in some (adult) cases are zero, and in others the DET is flat so the error rates at the two thresholds are identical. The lines span 1% and 99% of bootstrap replicated FNMR estimates.



Figure 187: For the visa images, the dots show FNMR by age group for two operating thresholds corresponding to $FMR = \{0.001, 0.0001\}$ computed over all on the order of 10^{10} impostor scores. The FMR in each bin will vary also - see subsequent impostor heatmaps in sec. 3.6.2. Given a pair of face images taken at different times, we assign the comparison to the bin that is the arithmetic average of the subject's ages. This plot shows only the effect of age, not ageing. The number of comparisons in each bin is generally in the thousands, however the first and last bins are computed over 149 and 124 respectively. The error rates in some (adult) cases are zero, and in others the DET is flat so the error rates at the two thresholds are identical. The lines span 1% and 99% of bootstrap replicated FNMR estimates.



Figure 188: For the visa images, the dots show FNMR by age group for two operating thresholds corresponding to $FMR = \{0.001, 0.0001\}$ computed over all on the order of 10^{10} impostor scores. The FMR in each bin will vary also - see subsequent impostor heatmaps in sec. 3.6.2. Given a pair of face images taken at different times, we assign the comparison to the bin that is the arithmetic average of the subject's ages. This plot shows only the effect of age, not ageing. The number of comparisons in each bin is generally in the thousands, however the first and last bins are computed over 149 and 124 respectively. The error rates in some (adult) cases are zero, and in others the DET is flat so the error rates at the two thresholds are identical. The lines span 1% and 99% of bootstrap replicated FNMR estimates.

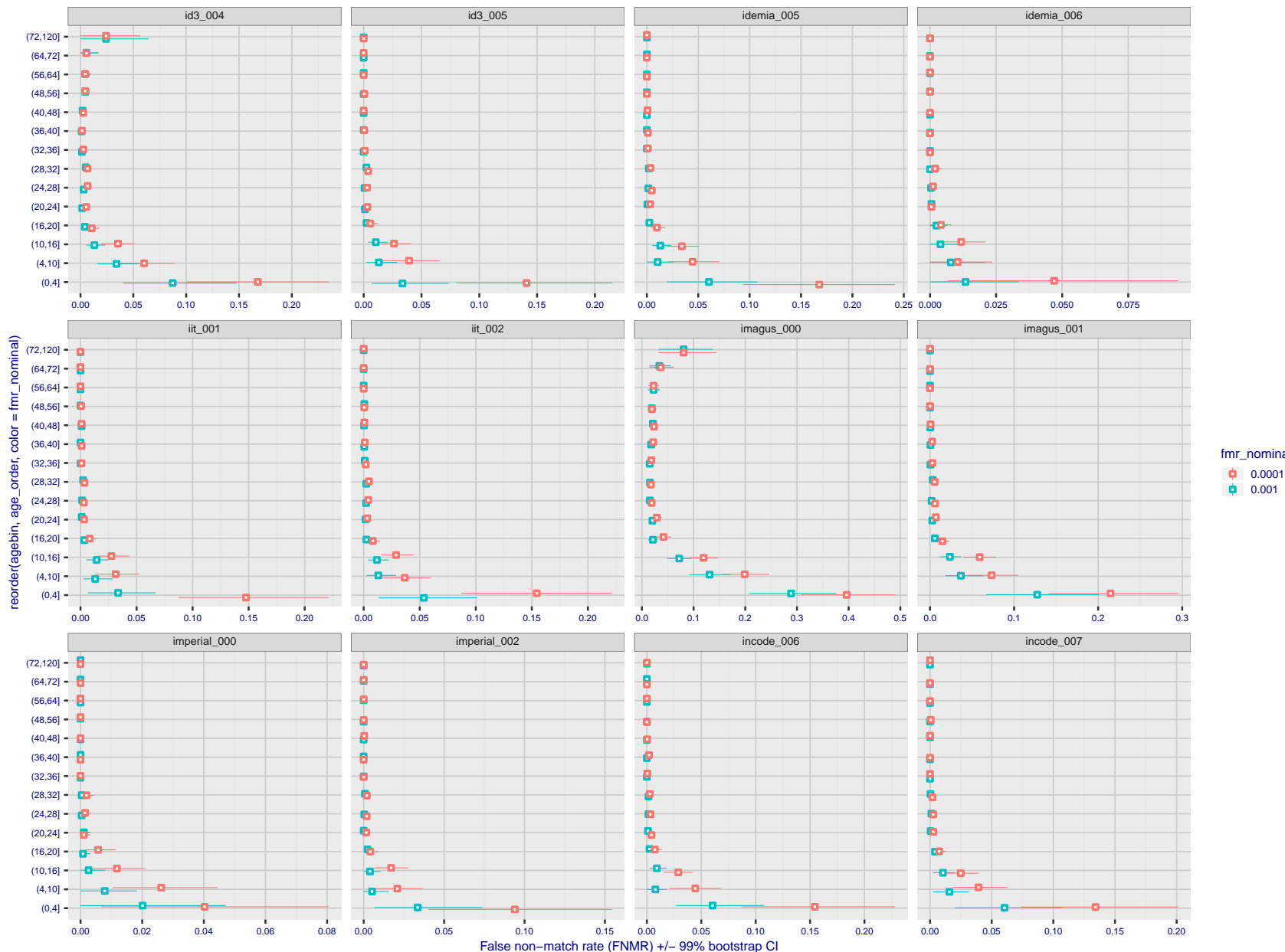
2020/09/08
12:09:14

Figure 189: For the visa images, the dots show FNMR by age group for two operating thresholds corresponding to $FMR = \{0.001, 0.0001\}$ computed over all on the order of 10^{10} impostor scores. The FMR in each bin will vary also - see subsequent impostor heatmaps in sec. 3.6.2. Given a pair of face images taken at different times, we assign the comparison to the bin that is the arithmetic average of the subject's ages. This plot shows only the effect of age, not ageing. The number of comparisons in each bin is generally in the thousands, however the first and last bins are computed over 149 and 124 respectively. The error rates in some (adult) cases are zero, and in others the DET is flat so the error rates at the two thresholds are identical. The lines span 1% and 99% of bootstrap replicated FNMR estimates.

FNMR(T)
FMR(T)
"False non-match rate"
"False match rate"

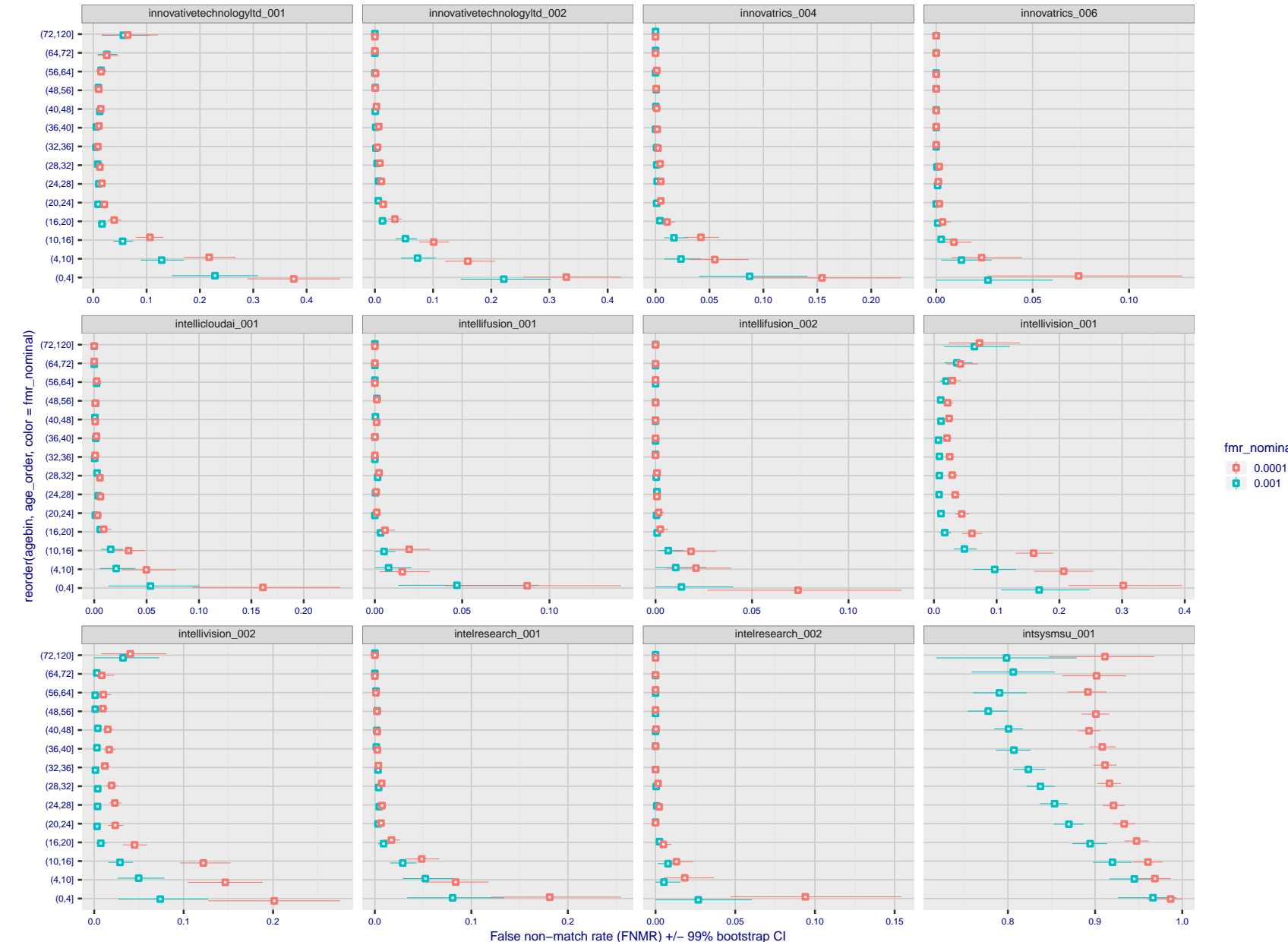


Figure 190: For the visa images, the dots show FNMR by age group for two operating thresholds corresponding to $FMR = \{0.001, 0.0001\}$ computed over all on the order of 10^{10} impostor scores. The FMR in each bin will vary also - see subsequent impostor heatmaps in sec. 3.6.2. Given a pair of face images taken at different times, we assign the comparison to the bin that is the arithmetic average of the subject's ages. This plot shows only the effect of age, not ageing. The number of comparisons in each bin is generally in the thousands, however the first and last bins are computed over 149 and 124 respectively. The error rates in some (adult) cases are zero, and in others the DET is flat so the error rates at the two thresholds are identical. The lines span 1% and 99% of bootstrap replicated FNMR estimates.

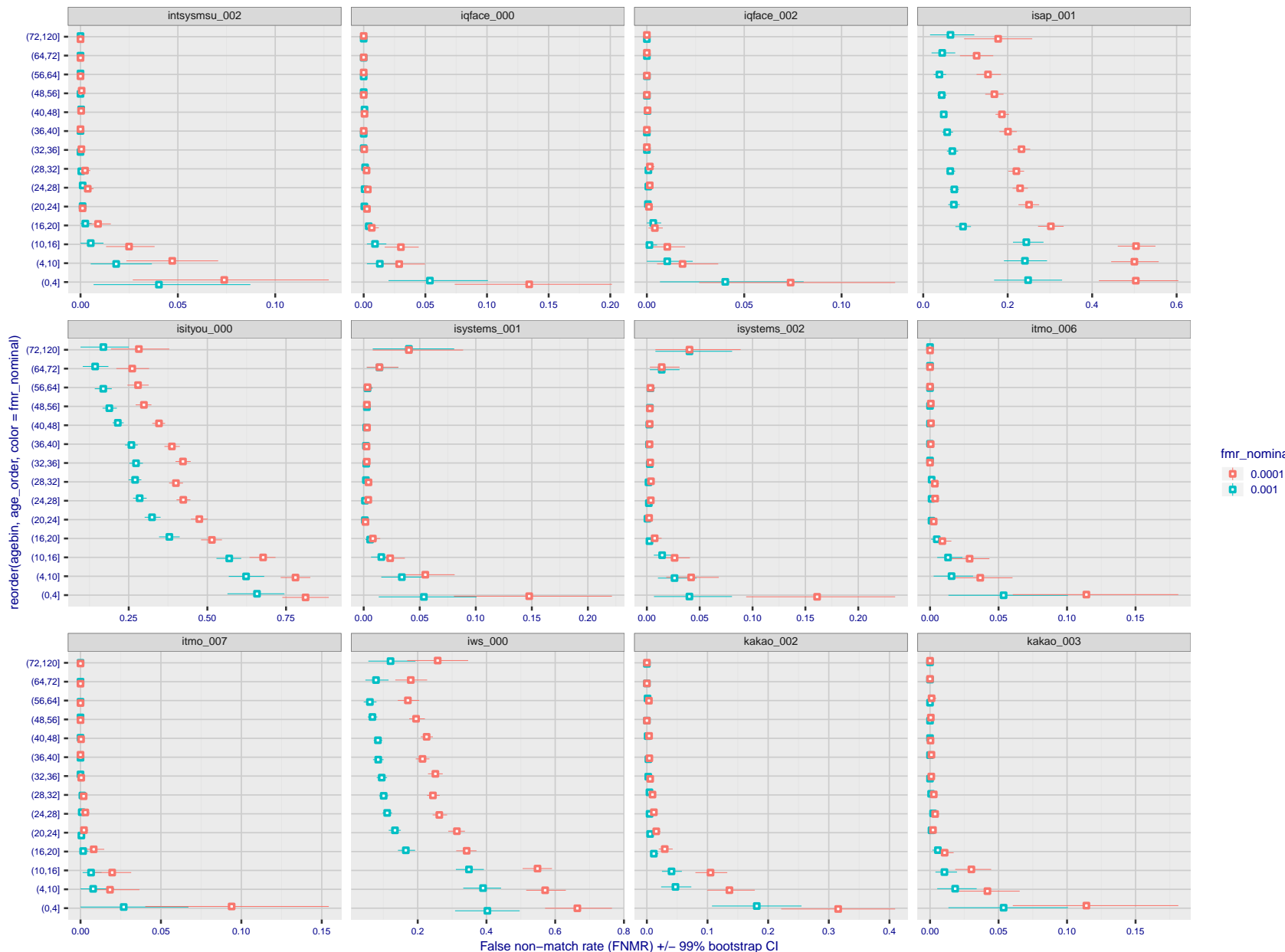
2020/09/08
12:09:14

Figure 191: For the visa images, the dots show FNMR by age group for two operating thresholds corresponding to $FMR = \{0.001, 0.0001\}$ computed over all on the order of 10^{10} impostor scores. The FMR in each bin will vary also - see subsequent impostor heatmaps in sec. 3.6.2. Given a pair of face images taken at different times, we assign the comparison to the bin that is the arithmetic average of the subject's ages. This plot shows only the effect of age, not ageing. The number of comparisons in each bin is generally in the thousands, however the first and last bins are computed over 149 and 124 respectively. The error rates in some (adult) cases are zero, and in others the DET is flat so the error rates at the two thresholds are identical. The lines span 1% and 99% of bootstrap replicated FNMR estimates.

FNMR(T)
FMR(T)
"False non-match rate"
"False match rate"

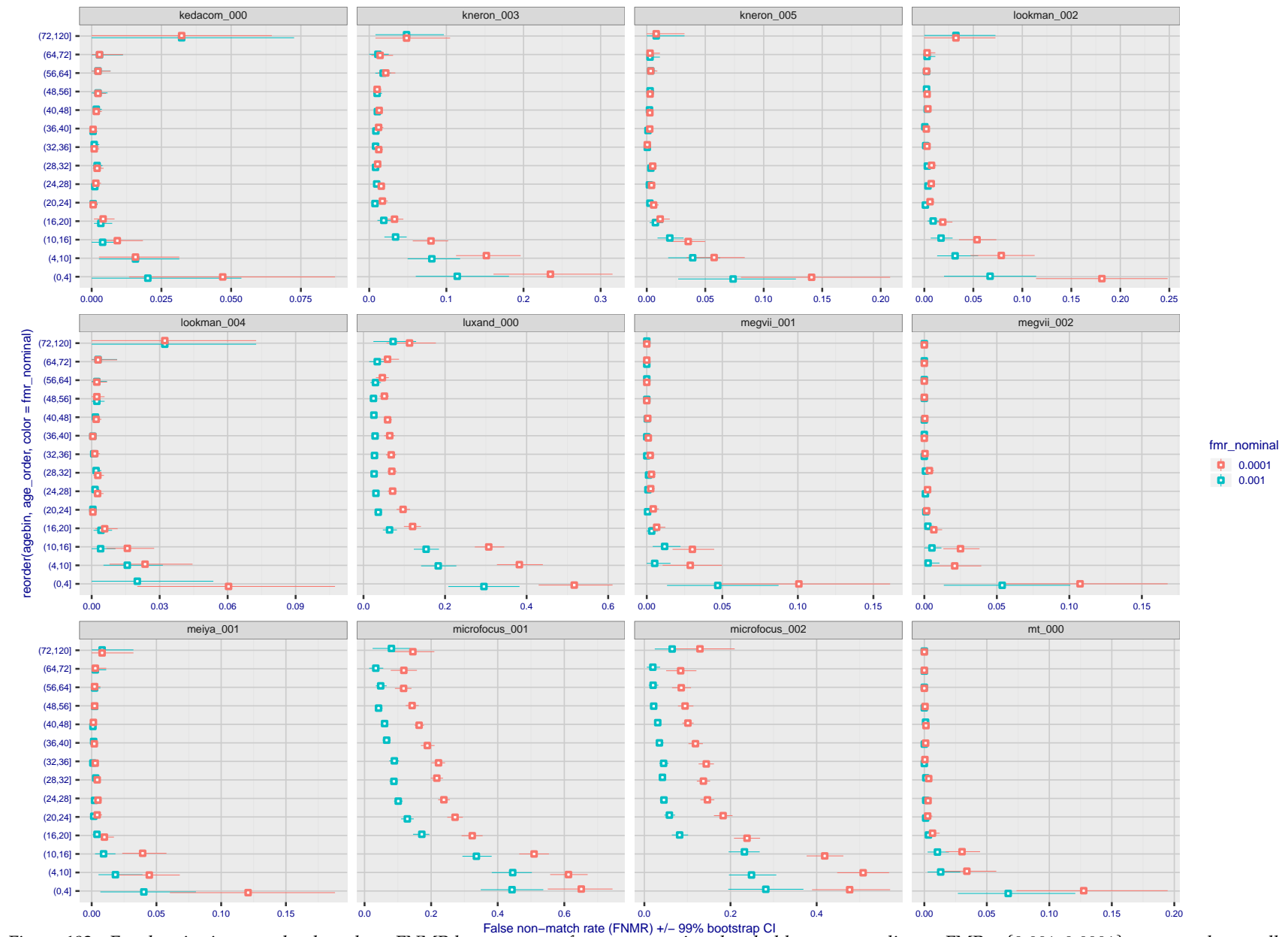


Figure 192: For the visa images, the dots show FNMR by age group for two operating thresholds corresponding to $FMR = \{0.001, 0.0001\}$ computed over all on the order of 10^{10} impostor scores. The FMR in each bin will vary also - see subsequent impostor heatmaps in sec. 3.6.2. Given a pair of face images taken at different times, we assign the comparison to the bin that is the arithmetic average of the subject's ages. This plot shows only the effect of age, not ageing. The number of comparisons in each bin is generally in the thousands, however the first and last bins are computed over 149 and 124 respectively. The error rates in some (adult) cases are zero, and in others the DET is flat so the error rates at the two thresholds are identical. The lines span 1% and 99% of bootstrap replicated FNMR estimates.

2020/09/08
12:09:14

Figure 193: For the visa images, the dots show FNMR by age group for two operating thresholds corresponding to $FMR = \{0.001, 0.0001\}$ computed over all on the order of 10^{10} impostor scores. The FMR in each bin will vary also - see subsequent impostor heatmaps in sec. 3.6.2. Given a pair of face images taken at different times, we assign the comparison to the bin that is the arithmetic average of the subject's ages. This plot shows only the effect of age, not ageing. The number of comparisons in each bin is generally in the thousands, however the first and last bins are computed over 149 and 124 respectively. The error rates in some (adult) cases are zero, and in others the DET is flat so the error rates at the two thresholds are identical. The lines span 1% and 99% of bootstrap replicated FNMR estimates.

FNMR(T)
FMR(T)
"False non-match rate"
"False match rate"

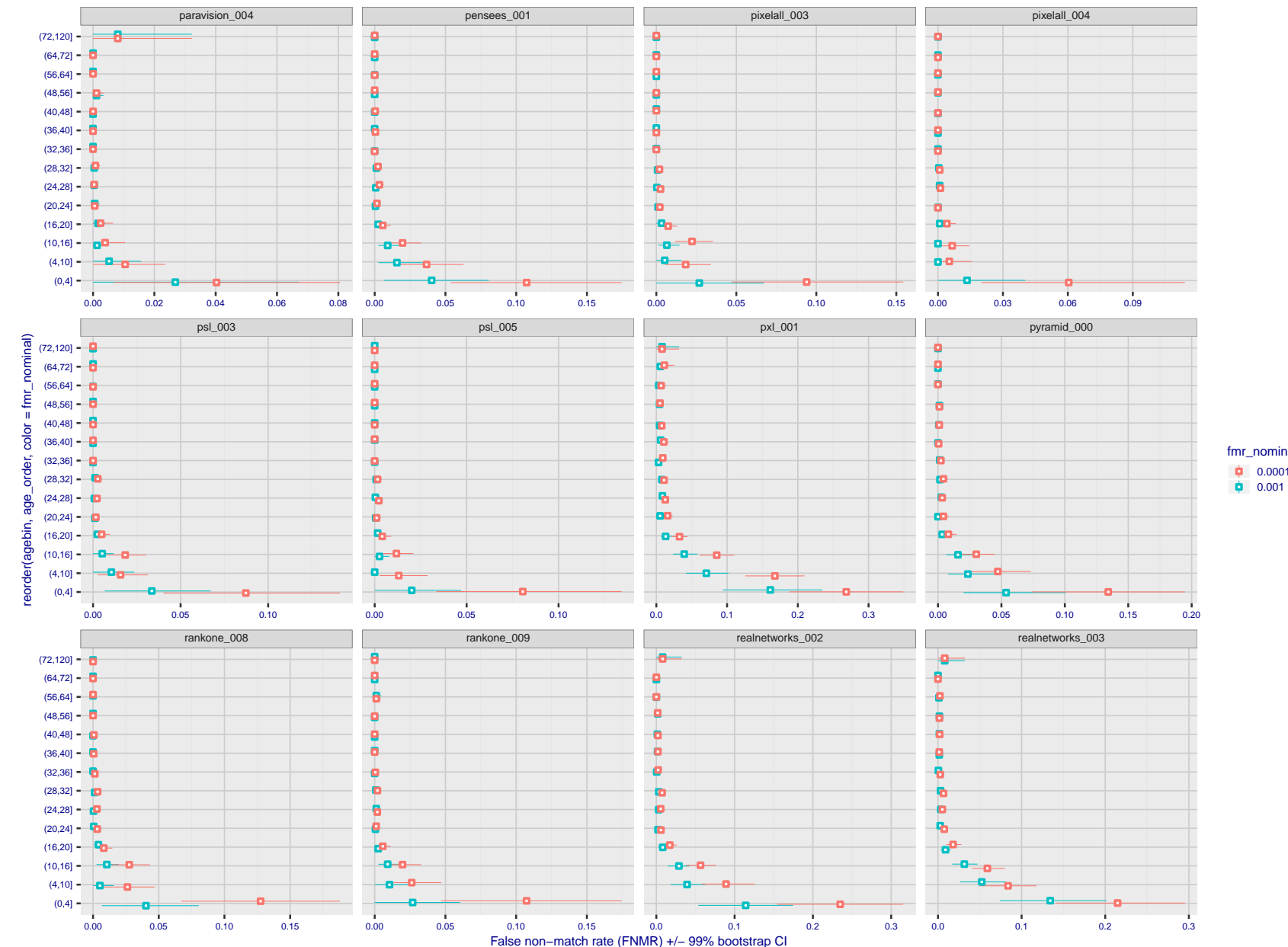


Figure 194: For the visa images, the dots show FNMR by age group for two operating thresholds corresponding to $FMR = \{0.001, 0.0001\}$ computed over all on the order of 10^{10} impostor scores. The FMR in each bin will vary also - see subsequent impostor heatmaps in sec. 3.6.2. Given a pair of face images taken at different times, we assign the comparison to the bin that is the arithmetic average of the subject's ages. This plot shows only the effect of age, not ageing. The number of comparisons in each bin is generally in the thousands, however the first and last bins are computed over 149 and 124 respectively. The error rates in some (adult) cases are zero, and in others the DET is flat so the error rates at the two thresholds are identical. The lines span 1% and 99% of bootstrap replicated FNMR estimates.

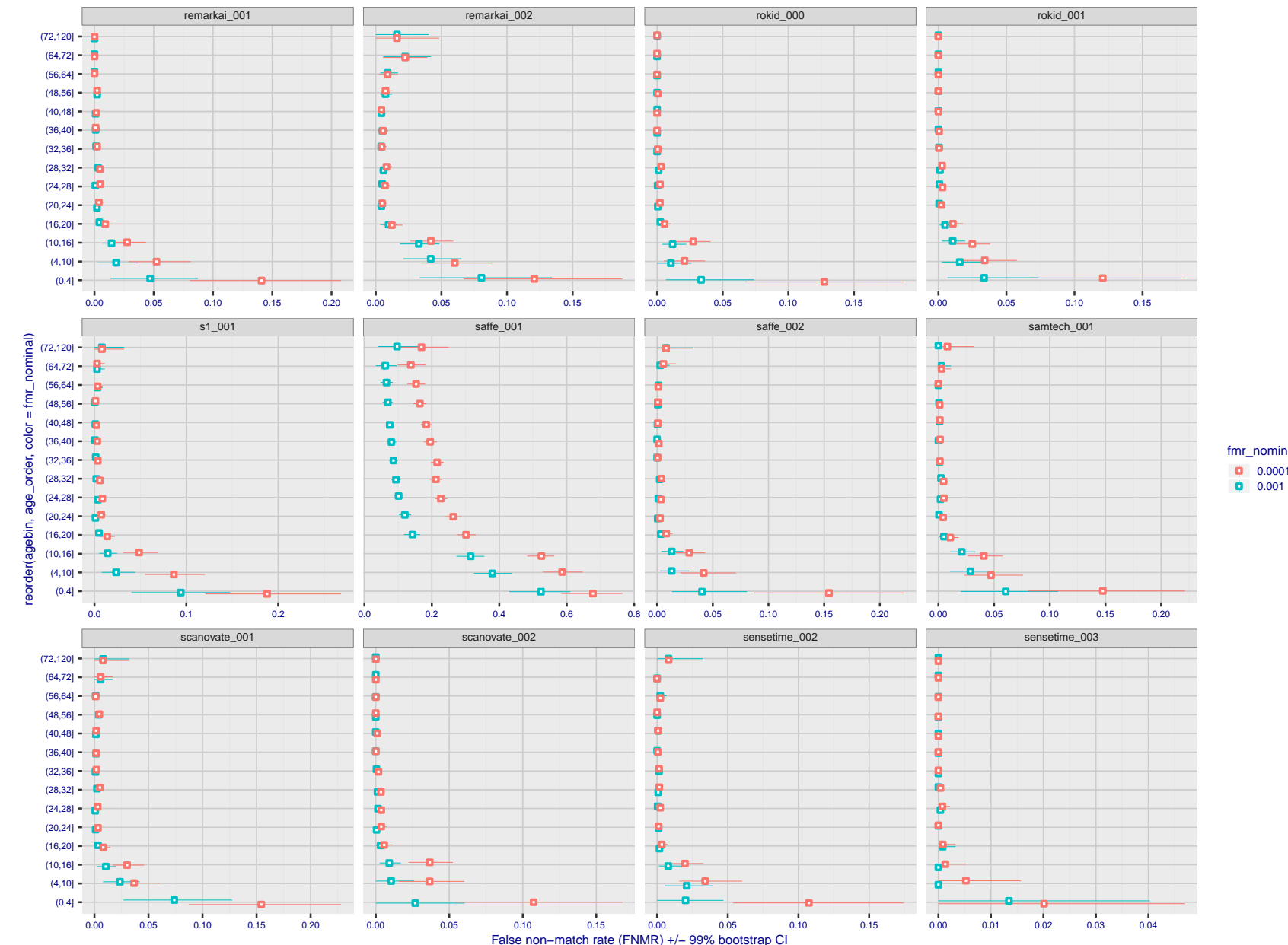


Figure 195: For the visa images, the dots show FNMR by age group for two operating thresholds corresponding to $FMR = \{0.001, 0.0001\}$ computed over all on the order of 10^{10} impostor scores. The FMR in each bin will vary also - see subsequent impostor heatmaps in sec. 3.6.2. Given a pair of face images taken at different times, we assign the comparison to the bin that is the arithmetic average of the subject's ages. This plot shows only the effect of age, not ageing. The number of comparisons in each bin is generally in the thousands, however the first and last bins are computed over 149 and 124 respectively. The error rates in some (adult) cases are zero, and in others the DET is flat so the error rates at the two thresholds are identical. The lines span 1% and 99% of bootstrap replicated FNMR estimates.

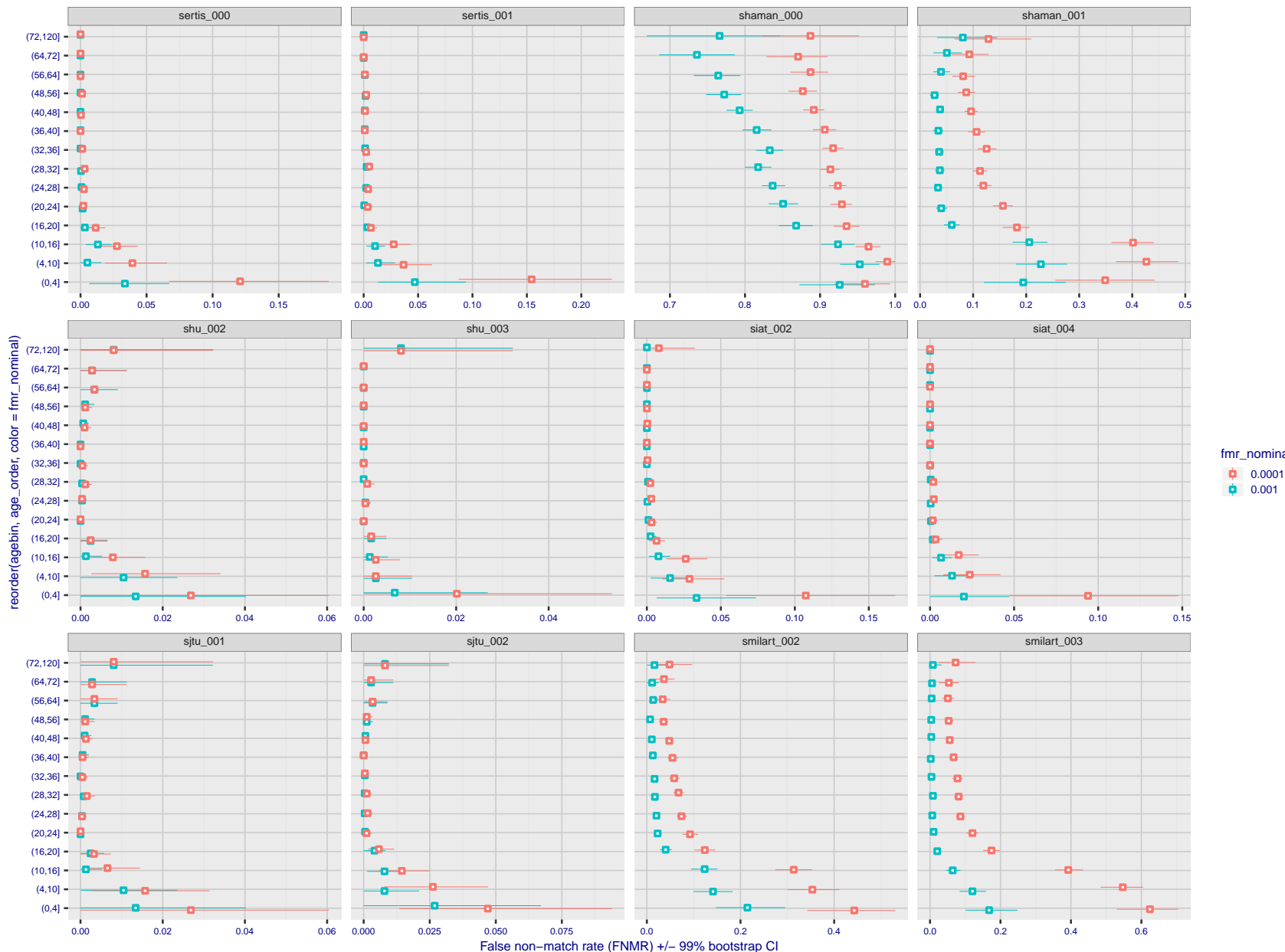


Figure 196: For the visa images, the dots show FNMR by age group for two operating thresholds corresponding to $FMR = \{0.001, 0.0001\}$ computed over all on the order of 10^{10} impostor scores. The FMR in each bin will vary also - see subsequent impostor heatmaps in sec. 3.6.2. Given a pair of face images taken at different times, we assign the comparison to the bin that is the arithmetic average of the subject's ages. This plot shows only the effect of age, not ageing. The number of comparisons in each bin is generally in the thousands, however the first and last bins are computed over 149 and 124 respectively. The error rates in some (adult) cases are zero, and in others the DET is flat so the error rates at the two thresholds are identical. The lines span 1% and 99% of bootstrap replicated FNMR estimates.



Figure 197: For the visa images, the dots show FNMR by age group for two operating thresholds corresponding to $FMR = \{0.001, 0.0001\}$ computed over all on the order of 10^{10} impostor scores. The FMR in each bin will vary also - see subsequent impostor heatmaps in sec. 3.6.2. Given a pair of face images taken at different times, we assign the comparison to the bin that is the arithmetic average of the subject's ages. This plot shows only the effect of age, not ageing. The number of comparisons in each bin is generally in the thousands, however the first and last bins are computed over 149 and 124 respectively. The error rates in some (adult) cases are zero, and in others the DET is flat so the error rates at the two thresholds are identical. The lines span 1% and 99% of bootstrap replicated FNMR estimates.

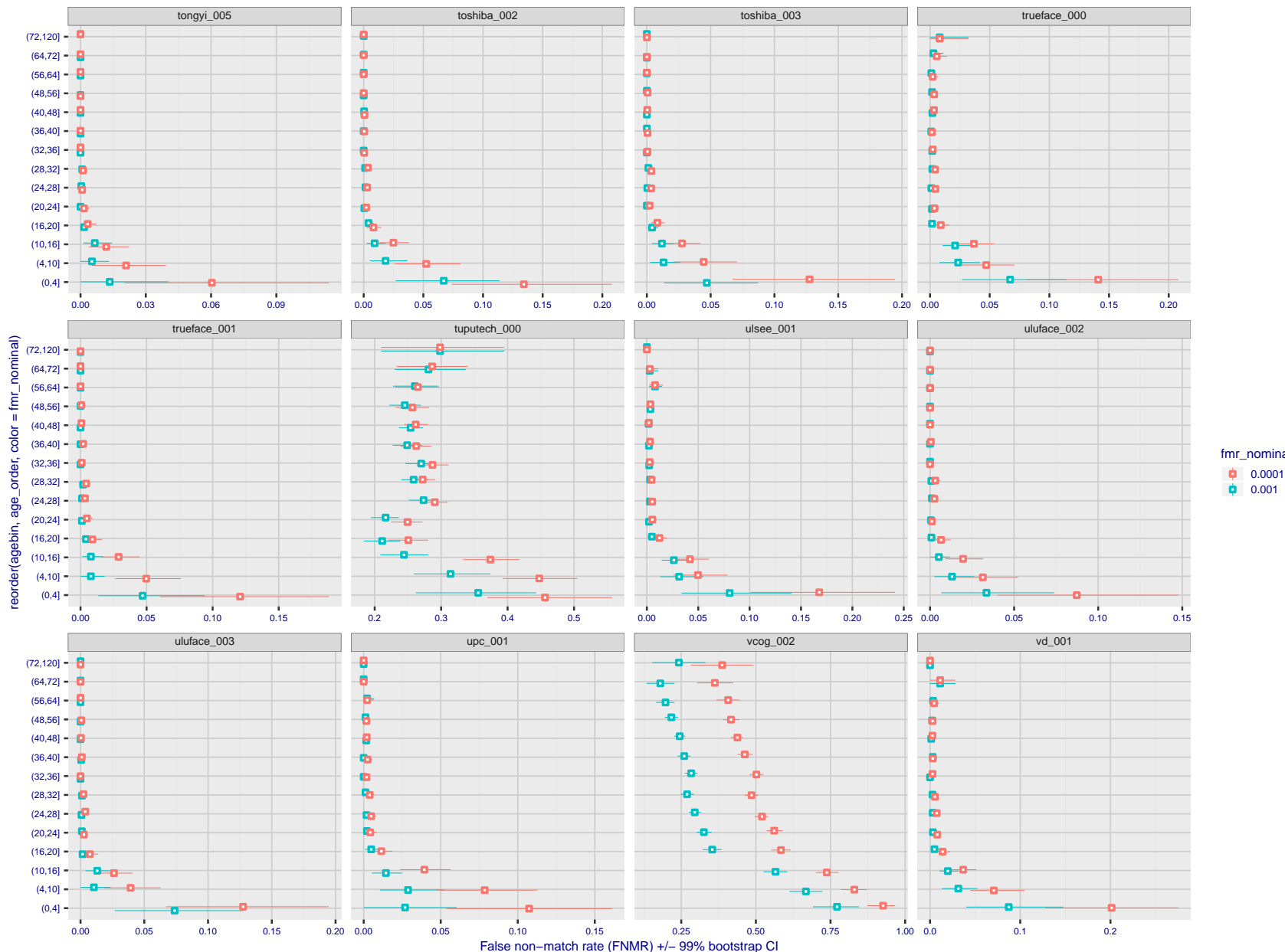


Figure 198: For the visa images, the dots show FNMR by age group for two operating thresholds corresponding to $FMR = \{0.001, 0.0001\}$ computed over all on the order of 10^{10} impostor scores. The FMR in each bin will vary also - see subsequent impostor heatmaps in sec. 3.6.2. Given a pair of face images taken at different times, we assign the comparison to the bin that is the arithmetic average of the subject's ages. This plot shows only the effect of age, not ageing. The number of comparisons in each bin is generally in the thousands, however the first and last bins are computed over 149 and 124 respectively. The error rates in some (adult) cases are zero, and in others the DET is flat so the error rates at the two thresholds are identical. The lines span 1% and 99% of bootstrap replicated FNMR estimates.

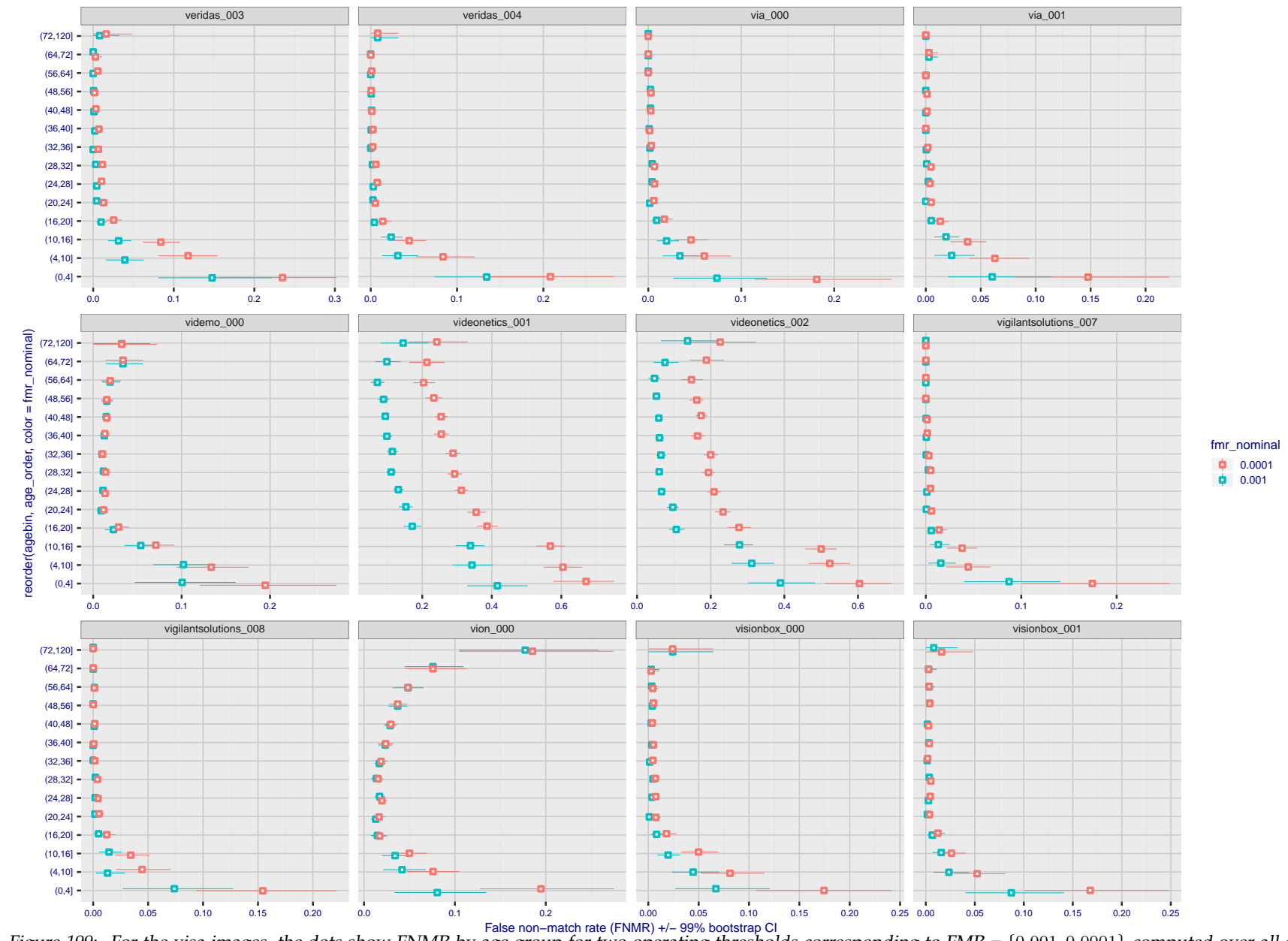


Figure 199: For the visa images, the dots show FNMR by age group for two operating thresholds corresponding to $FMR = \{0.001, 0.0001\}$ computed over all on the order of 10^{10} impostor scores. The FMR in each bin will vary also - see subsequent impostor heatmaps in sec. 3.6.2. Given a pair of face images taken at different times, we assign the comparison to the bin that is the arithmetic average of the subject's ages. This plot shows only the effect of age, not ageing. The number of comparisons in each bin is generally in the thousands, however the first and last bins are computed over 149 and 124 respectively. The error rates in some (adult) cases are zero, and in others the DET is flat so the error rates at the two thresholds are identical. The lines span 1% and 99% of bootstrap replicated FNMR estimates.

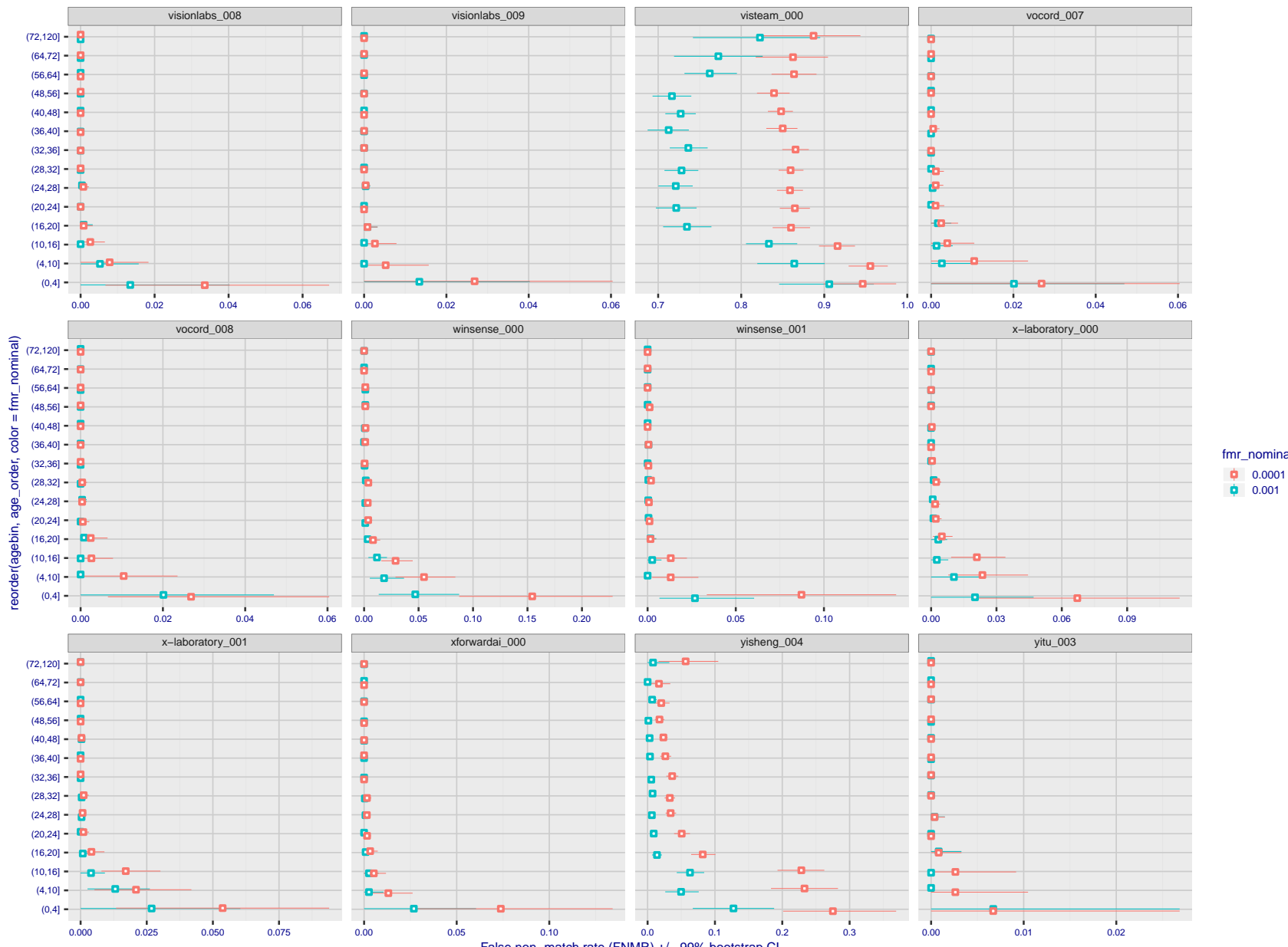


Figure 200: For the visa images, the dots show FNMR by age group for two operating thresholds corresponding to $FMR = \{0.001, 0.0001\}$ computed over all on the order of 10^{10} impostor scores. The FMR in each bin will vary also - see subsequent impostor heatmaps in sec. 3.6.2. Given a pair of face images taken at different times, we assign the comparison to the bin that is the arithmetic average of the subject's ages. This plot shows only the effect of age, not ageing. The number of comparisons in each bin is generally in the thousands, however the first and last bins are computed over 149 and 124 respectively. The error rates in some (adult) cases are zero, and in others the DET is flat so the error rates at the two thresholds are identical. The lines span 1% and 99% of bootstrap replicated FNMR estimates.

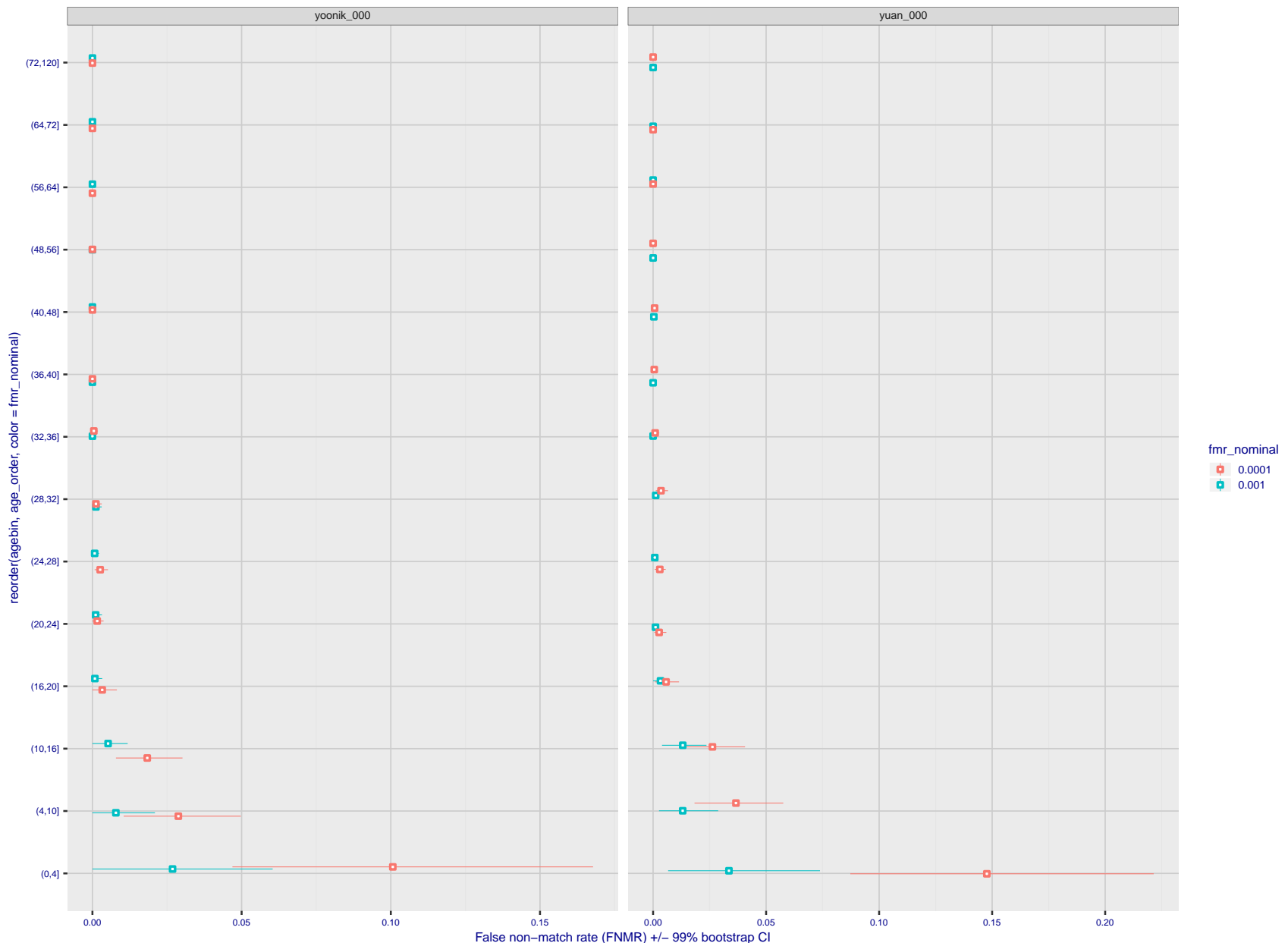


Figure 201: For the visa images, the dots show FNMR by age group for two operating thresholds corresponding to $FMR = \{0.001, 0.0001\}$ computed over all on the order of 10^{10} impostor scores. The FMR in each bin will vary also - see subsequent impostor heatmaps in sec. 3.6.2. Given a pair of face images taken at different times, we assign the comparison to the bin that is the arithmetic average of the subject's ages. This plot shows only the effect of age, not ageing. The number of comparisons in each bin is generally in the thousands, however the first and last bins are computed over 149 and 124 respectively. The error rates in some (adult) cases are zero, and in others the DET is flat so the error rates at the two thresholds are identical. The lines span 1% and 99% of bootstrap replicated FNMR estimates.

Caveats: None.

3.6 Impostor distribution stability

3.6.1 Effect of birth place on the impostor distribution

Background: Facial appearance varies geographically, both in terms of skin tone, cranio-facial structure and size. This section addresses whether false match rates vary intra- and inter-regionally.

Goals:

- ▷ To show the effect of birth region of the impostor and enrollee on false match rates.
- ▷ To determine whether some algorithms give better impostor distribution stability.

Methods:

- ▷ For the visa images, NIST defined 10 regions: Sub-Saharan Africa, South Asia, Polynesia, North Africa, Middle East, Europe, East Asia, Central and South America, Central Asia, and the Caribbean.
- ▷ For the visa images, NIST mapped each country of birth to a region. There is some arbitrariness to this. For example, Egypt could reasonably be assigned to the Middle East instead of North Africa. An alternative methodology could, for example, assign the Philippines to *both* Polynesia and East Asia.
- ▷ FMR is computed for cases where all face images of impostors born in region r_2 are compared with enrolled face images of persons born in region r_1 .

$$\text{FMR}(r_1, r_2, T) = \frac{\sum_{i=1}^{N_{r_1, r_2}} H(s_i - T)}{N_{r_1, r_2}} \quad (5)$$

where the same threshold, T , is used in all cells, and H is the unit step function. The threshold is set to give $\text{FMR}(T) = 0.001$ over the entire set of visa image impostor comparisons.

- ▷ This analysis is then repeated by country-pair, but only for those country pairs where both have at least 1000 images available. The countries¹ appear in the axes of graphs that follow.
- ▷ The mean number of impostor scores in any cross-region bin is 33 million. The smallest number of impostor scores in any bin is 135000, for Central Asia - North Africa. While these counts are large enough to support reasonable significance, the number of individual faces is much smaller, on the order of $N^{0.5}$.
- ▷ The numbers of impostor scores in any cross-country bin is shown in Figure ??.

Results: Subsequent figures show heatmaps that use color to represent the base-10 logarithm of the false match rate. Red colors indicate high (bad) false match rates. Dark colors indicate benign false match rates. There are two series of graphs corresponding to aggregated geographical regions, and to countries. The notable observations are:

- ▷ The on-diagonal elements correspond to within-region impostors. FMR is generally above the nominal value of $\text{FMR} = 0.001$. Particularly there is usually higher FMR in, Sub-Saharan Africa, South Asia, and the Caribbean. Europe and Central Asia, on the other hand, usually give FMR closer to the nominal value.
- ▷ The off-diagonal elements correspond to across-region impostors. The highest FMR is produced between the Caribbean and Sub-Saharan Africa.
- ▷ Algorithms vary.

¹These are Argentina, Australia, Brazil, Chile, China, Costa Rica, Cuba, Czech Republic, Dominican Republic, Ecuador, Egypt, El Salvador, Germany, Ghana, Great Britain, Greece, Guatemala, Haiti, Hong Kong, Honduras, Indonesia, India, Israel, Jamaica, Japan, Kenya, Korea, Lebanon, Mexico, Malaysia, Nepal, Nigeria, Peru, Philippines, Pakistan, Poland, Romania, Russia, South Africa, Saudi Arabia, Thailand, Trinidad, Turkey, Taiwan, Ukraine, Venezuela, and Vietnam.

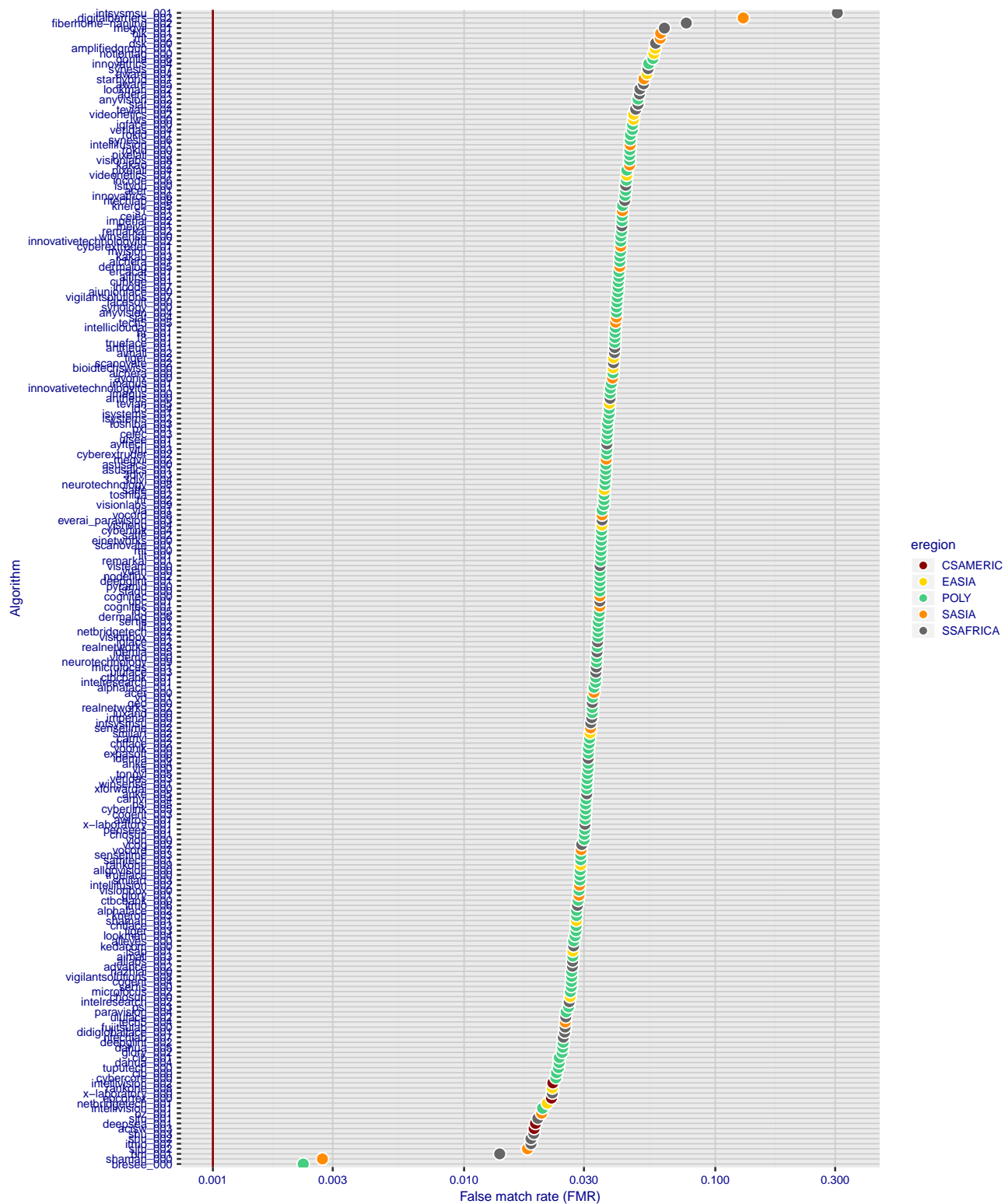


Figure 202: For the visa images, the dots show FMR for impostor comparisons of individuals of the same sex and same age group for the region of the world that gives the worst (highest) FMR when the threshold is set to give $FMR = 0.001$ (red vertical line) over all on the order of 10^{10} impostor scores i.e. zero-effort. The shift of the dots to right shows massive increases in FMR when impostors have the same sex, age, and region of birth. The color code indicates which region gives the worst case FMR. If the observed variation is due to the prevalence of one kind of images in the training imagery, then algorithms developed on one kind of data might be expected to give higher FMR on other kinds.

- ▷ We computed the same quantities for a global FMR = 0.0001. The effects are similar.

Caveats:

- ▷ The effects of variable impostor rates on one-to-many identification systems may well differ from what's implied by these one-to-one verification results. Two reasons for this are a) the enrollment galleries are usually imbalanced across countries of birth, age and sex; b) one-to-many identification algorithms often implement techniques aimed at stabilizing the impostor distribution. Further research is necessary.
- ▷ In principle, the effects seen in this subsection could be due to differences in the image capture process. We consider this unlikely since the effects are maintained across geography - e.g. Caribbean vs. Africa, or Japan vs. China.

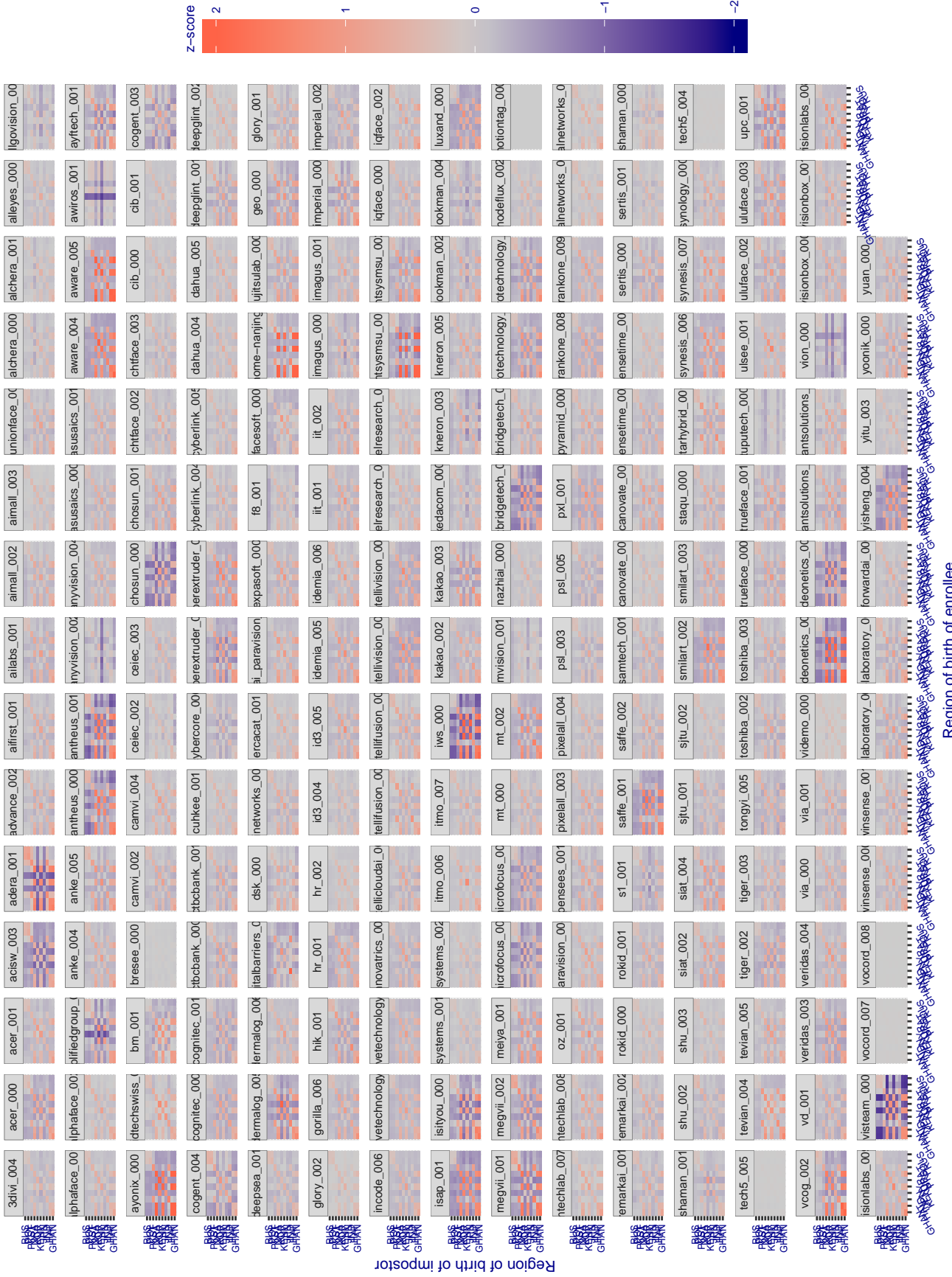


Figure 203: For visa images, the heatmap shows how the mean of the impostor distribution for the country pair (a,b) is shifted relative to the mean of the global impostor distribution, expressed as a number of standard deviations of the global impostor distribution. This statistic is designed to show shifts in the entire impostor distribution, not just tail effects that manifest as the anomalously high (or low) false match rates that appear in the subsequent figures. The countries are chosen to show that skin tone alone does not explain impostor distribution shifts. The reduced shift in Asian populations with the Yitu and Tong YiTrans algorithms, is accompanied by positive shifts in the European populations. This reversal relative to most other algorithms, may derive from use of nationally weighted training sets. The figure is computed from same-sex and same-age impostor pairs.

3.6.2 Effect of age on impostors

Background: This section shows the effect of age on the impostor distribution. The ideal behaviour is that the age of the enrollee and the impostor would not affect impostor scores. This would support FMR stability over sub-populations.

Goals:

- ▷ To show the effect of relative ages of the impostor and enrollee on false match rates.
- ▷ To determine whether some algorithms have better impostor distribution stability.

Methods:

- ▷ Define 14 age group bins, spanning 0 to over 100 years old.
- ▷ Compute FMR over all impostor comparisons for which the subjects in the enrollee and impostor images have ages in two bins.
- ▷ Compute FMR over all impostor comparisons for which the subjects are additionally of the same sex, and born in the same geographic region.

Results:

The notable aspects are:

- ▷ Diagonal dominance: Impostors are more likely to be matched against their same age group.
- ▷ Same sex and same region impostors are more successful. On the diagonal, an impostor is more likely to succeed by posing as someone of the same sex. If $\Delta \log_{10} \text{FMR} = 0.2$, then same-sex same-region FMR exceeds the all-pairs FMR by factor of $10^{0.2} = 1.6$.
- ▷ Young children impostors give elevated FMR against young children. Older adult impostor give elevated FMR against older adults. These effects are quite large, for example if $\Delta \log_{10} \text{FMR} = 1.0$ larger than a 32 year old, then these groups have higher FMR by a factor of $10^1 = 10$. This would imply an FMR above 0.01 for a nominal (global) FMR = 0.001.
- ▷ Algorithms vary.
- ▷ We computed the same quantities for a global FMR = 0.0001. The effects are similar.

Note the calculations in this section include impostors paired across all countries of birth.

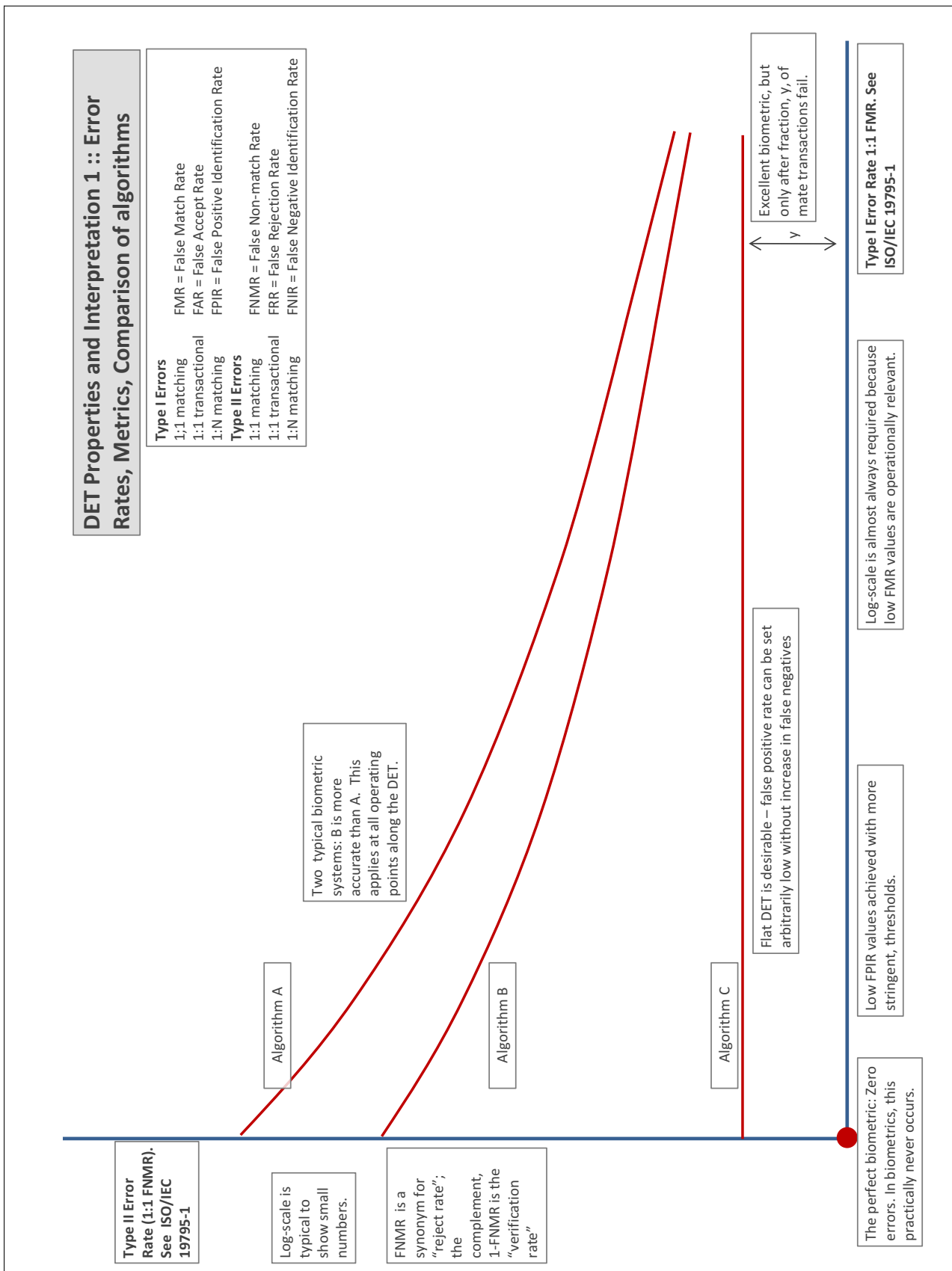
Accuracy Terms + Definitions

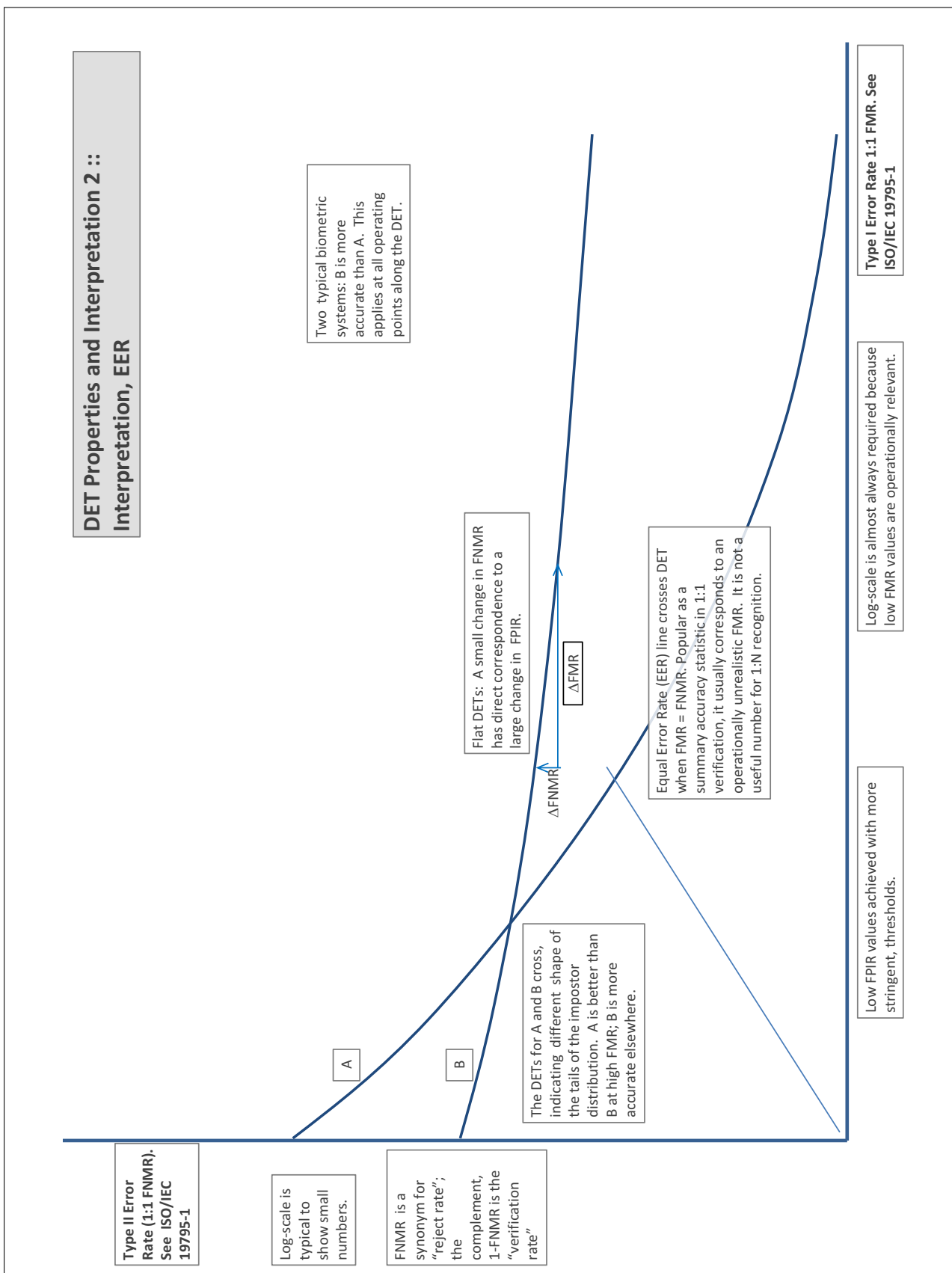
In biometrics, Type II errors occur when two samples of one person do not match – this is called a **false negative**. Correspondingly, Type I errors occur when samples from two persons do match – this is called a **false positive**. Matches are declared by a biometric system when the native comparison score from the recognition algorithm meets some **threshold**. Comparison scores can be either **similarity scores**, in which case higher values indicate that the samples are more likely to come from the same person, or **dissimilarity scores**, in which case higher values indicate different people. Similarity scores are traditionally computed by **fingerprint** and **face** recognition algorithms, while dissimilarities are used in **iris recognition**. In some cases, the dissimilarity score is a distance; this applies only when **metric** properties are obeyed. In any case, scores can be either **mate** scores, coming from a comparison of one person's samples, or **nonmate** scores, coming from comparison of different persons' samples. The words **genuine** or **authentic** are synonyms for mate, and the word **impostor** is used as a synonym for nonmatch. The words mate and nonmatch are traditionally used in identification applications (such as law enforcement search, or background checks) while genuine and impostor are used in verification applications (such as access control).

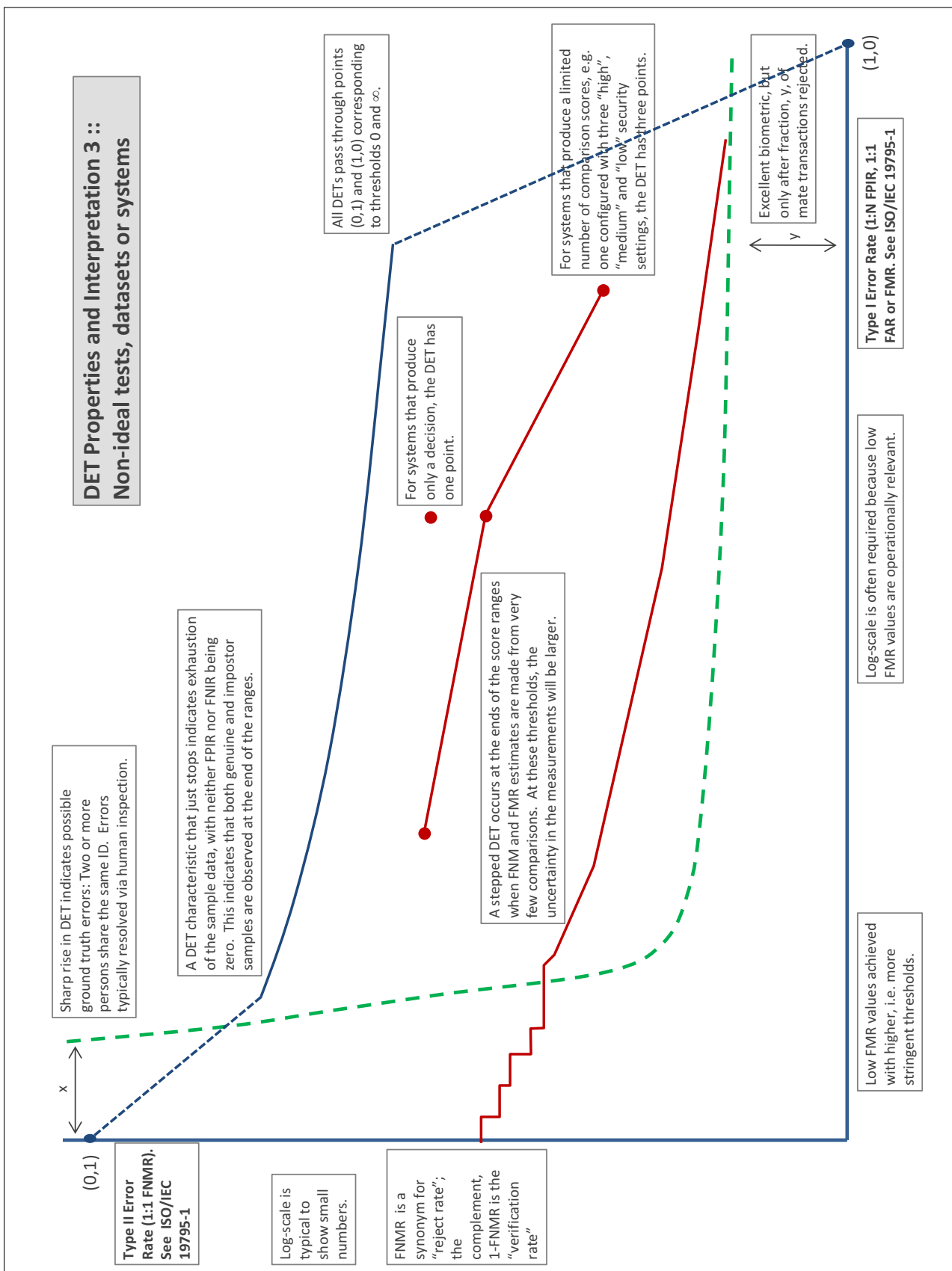
A **error tradeoff** characteristic represents the tradeoff between Type II and Type I classification errors. For verification this plots false non-match rate (FNMR) vs. false match rate (FMR) parametrically with T.

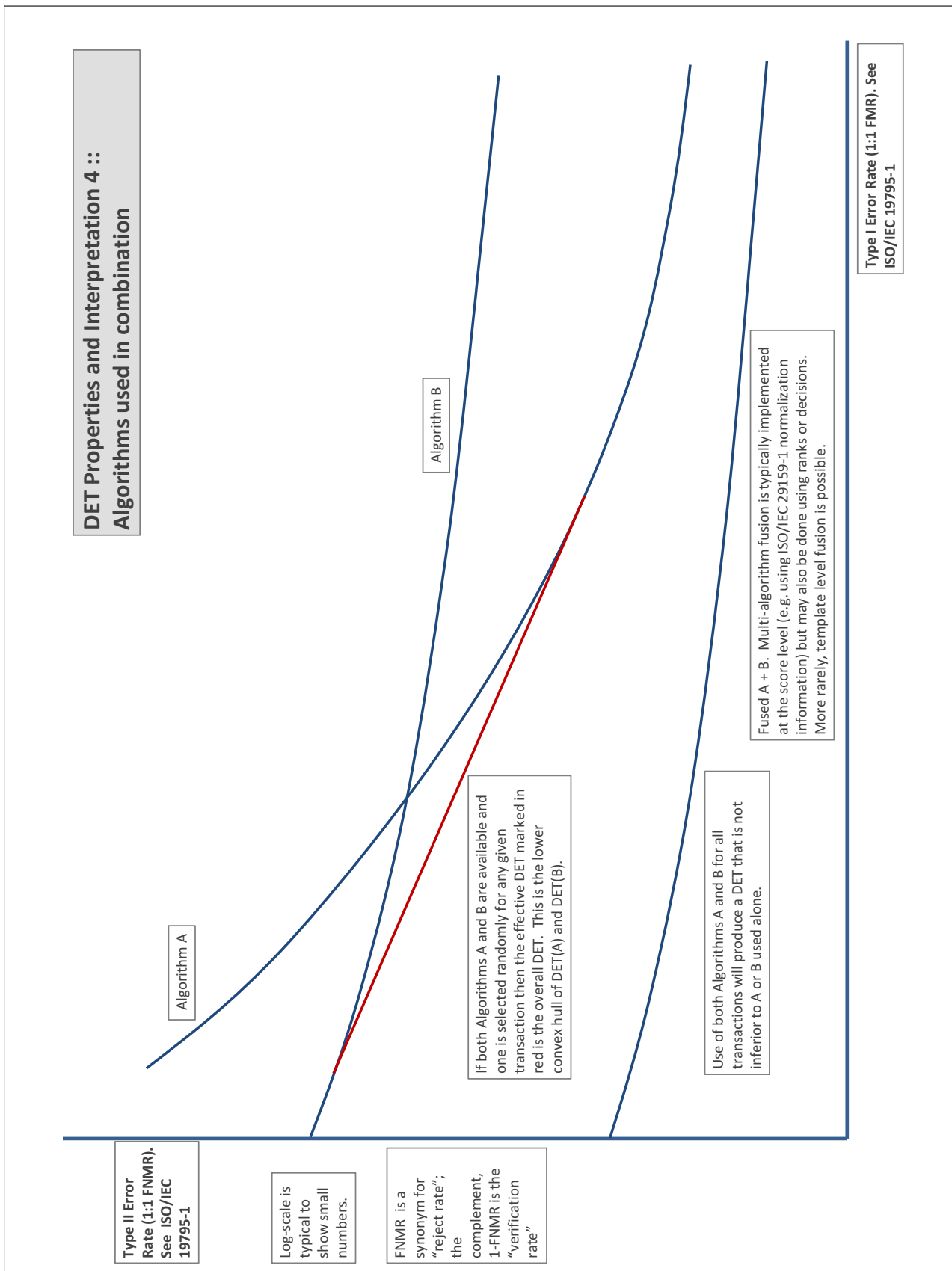
The error tradeoff plots are often called **detection error tradeoff (DET)** characteristics or **receiver operating characteristic (ROC)**. These serve the same function but differ, for example, in plotting the complement of an error rate (e.g., $TMR = 1 - FNMR$) and in transforming the axes most commonly using logarithms, to show multiple decades of FMR. More rarely, the function might be the inverse Gaussian function.

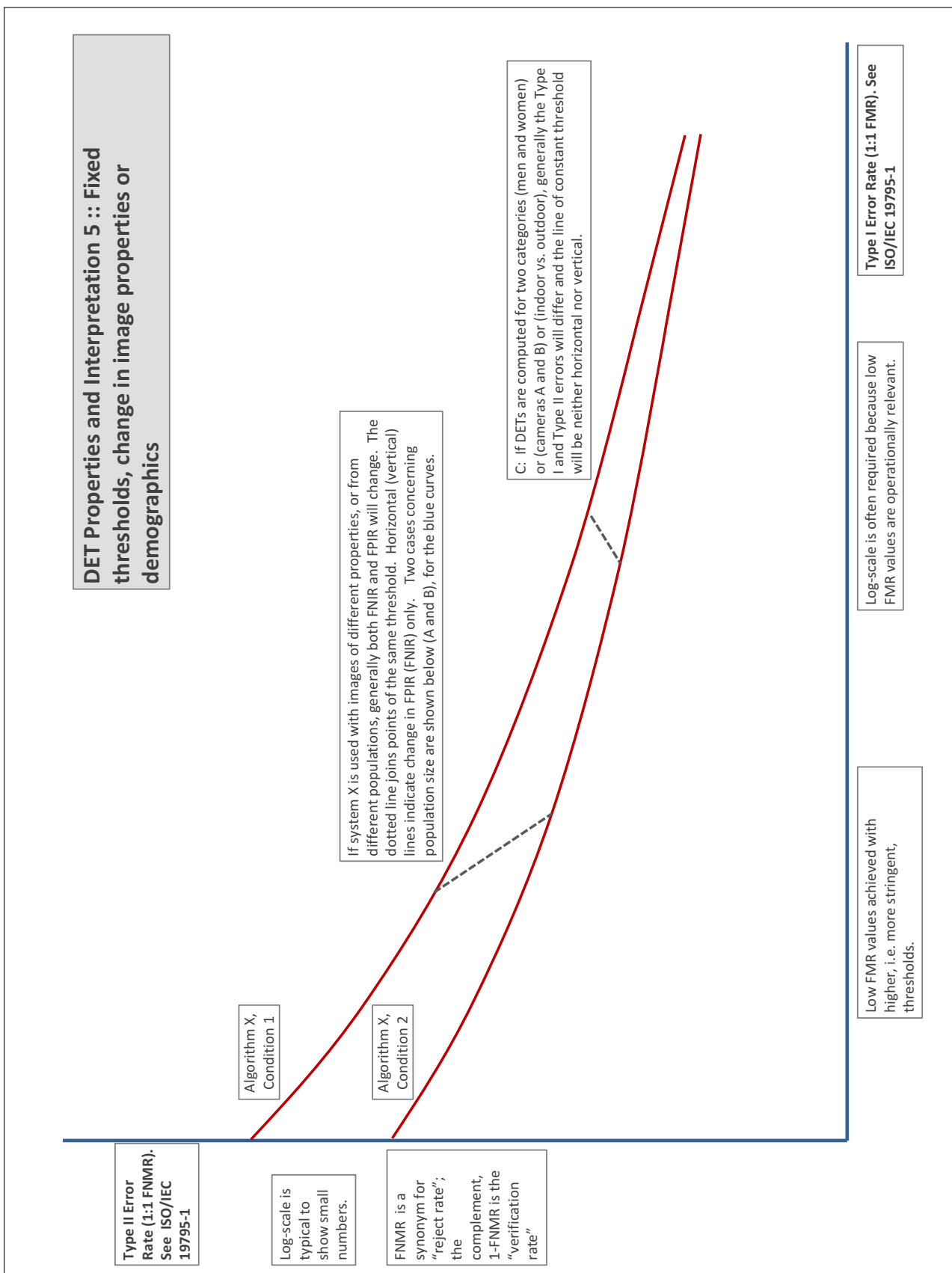
More detail and generality is provided in formal biometrics testing standards, see the various parts of [ISO/IEC 19795 Biometrics Testing and Reporting](#). More terms, including and beyond those to do with accuracy, see [ISO/IEC 2382-37 Information technology -- Vocabulary -- Part 37: Harmonized biometric vocabulary](#)











References

- [1] P. Jonathon Phillips, Amy N. Yates, Ying Hu, Carina A. Hahn, Eilidh Noyes, Kelsey Jackson, Jacqueline G. Cavazos, Géraldine Jeckeln, Rajeev Ranjan, Swami Sankaranarayanan, Jun-Cheng Chen, Carlos D. Castillo, Rama Chellappa, David White, and Alice J. O'Toole. Face recognition accuracy of forensic examiners, superrecognizers, and face recognition algorithms. *Proceedings of the National Academy of Sciences*, 115(24):6171–6176, 2018.